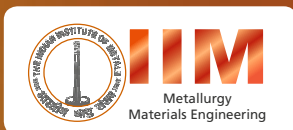


Indian Institute of Metals Series

N. Eswara Prasad
R.J.H. Wanhill
Editors

Aerospace Materials and Material Technologies

Volume 2:
Aerospace Material Technologies



 Springer

Indian Institute of Metals Series

Editors-in-chief

Baldev Raj, National Institute of Advanced Studies, Bangalore, Karnataka, India
U. Kamachi Mudali, Indira Gandhi Centre for Atomic Research, Kalpakkam,
Tamil Nadu, India

More information about this series at <http://www.springer.com/series/15453>

N. Eswara Prasad · R.J.H. Wanhill
Editors

Aerospace Materials and Material Technologies

Volume 2: Aerospace Material Technologies

 Springer

Editors

N. Eswara Prasad
Defence Materials and Stores R&D
Establishment (DMSRDE)
Kanpur, Uttar Pradesh
India

R.J.H. Wanhill
Emmeloord, Flevoland
The Netherlands

ISSN 2509-6400

Indian Institute of Metals Series

ISBN 978-981-10-2142-8

DOI 10.1007/978-981-10-2143-5

ISSN 2509-6419 (electronic)

ISBN 978-981-10-2143-5 (eBook)

Library of Congress Control Number: 2016948239

© Springer Science+Business Media Singapore 2017

This work is subject to copyright. All rights are reserved by the Publisher, whether the whole or part of the material is concerned, specifically the rights of translation, reprinting, reuse of illustrations, recitation, broadcasting, reproduction on microfilms or in any other physical way, and transmission or information storage and retrieval, electronic adaptation, computer software, or by similar or dissimilar methodology now known or hereafter developed.

The use of general descriptive names, registered names, trademarks, service marks, etc. in this publication does not imply, even in the absence of a specific statement, that such names are exempt from the relevant protective laws and regulations and therefore free for general use.

The publisher, the authors and the editors are safe to assume that the advice and information in this book are believed to be true and accurate at the date of publication. Neither the publisher nor the authors or the editors give a warranty, express or implied, with respect to the material contained herein or for any errors or omissions that may have been made.

Printed on acid-free paper

This Springer imprint is published by Springer Nature

The registered company is Springer Nature Singapore Pte Ltd.

The registered company address is: 152 Beach Road, #22-06/08 Gateway East, Singapore 189721, Singapore

*To
our eminent teachers and close associates for
aerospace materials and material
technologies;*

and to

*our partners and families for their support,
notably during 2014–2016, the years in
which these books were prepared.*

N. Eswara Prasad and R.J.H. Wanhill

Foreword by Dr. S. Christopher



First of all, I would like to congratulate all the authors, the editors, Drs. N. Eswara Prasad, R.J.H. Wanhill, and the editor-in-chief, Dr. Baldev Raj, and the Indian Institute of Metals (IIM) and Springer for publishing this two-volume innovative reference work on aerospace materials and materials technologies. I am also extremely happy to write the foreword for this special volume, since I have been associated with Indian Avionics for more than 30 years and have fair knowledge on the present status of the material technologies covered in this second volume. Materials and material technologies are the backbone of any

engineering industry. This is especially so for the aerospace industry, which has provided the impetus to develop many advanced manufacturing and design technologies. The world has seen massive investments in the aerospace industry in a number of developed countries, notably the USA, Europe and Russia, and also in developing nations, including India and China. Still more countries are becoming important players and partners in developing aerospace materials and technologies.

The present volume on aerospace material technologies is a well-devised and considered book encompassing nearly 20 material technologies, including propulsion, refurbishment, stealth, failure analysis, certification and life extension, and more traditional aerospace technologies such as metal and material processing, characterization and property evaluation. This volume also contains a very useful section on structural design, discussing fatigue and fracture requirements and stress corrosion cracking (SCC) criteria. I find that the editors have taken special care to present the book chapters with extremely useful contents and good readability. In this context, I applaud the efforts of Dr. R.J.H. Wanhill for single-handedly reviewing all the chapters and assisting in their revision and the equally daunting editorial work by Dr. Eswara Prasad.

I hope and wish that this kind of book will appear in the international literature from time to time, so that engineering graduates, aerospace and mechanical engineers, and aeronautical designers are provided with essential and state-of-the-art knowledge and databases on aerospace material technologies. Such volumes also aid in finalizing a number of white/approach papers for establishing material technology and production centres. They also point out the future requirements for aerospace development. Every country should identify the gaps in materials development and establish facilities for the production of these materials, especially the advanced materials required for aerospace applications. I feel these two volumes greatly aid in addressing this task. Hence emerging countries like India and South Asia can benefit greatly from these kinds of endeavours.

Finally, being at the helm of DRDO, India, I take special pride in congratulating several of the DRDO authors and Dr. N. Eswara Prasad, for their valuable international contributions. I wish success all around the world in the development of future aerospace material technologies and the production, qualification and certification of aerospace components and subsystems for various aircraft, missiles and spacecraft. If this book volume serves as a basis for such endeavours, it will have amply achieved its purpose.

Dr. S. Christopher, FNAE, FIETE
Former Distinguished Scientist and Director
Centre for Air Borne Systems (CABS), DRDO, Bangalore, India
Presently, the Director General
Defence Research and Development Organisation, and Secretary
Department of Defence R&D, Government of India
New Delhi, India

Foreword by Dr. G. Satheesh Reddy



While materials and materials development are widely acknowledged as core expertise in engineering in any country, the material processing and production technologies and facilities for metal and materials production essentially dictate the actual progress of that country in terms of actual GDP growth. Every country should identify its materials strengths and develop material production around those strengths. India has vast material resources, but it is the lack of large-scale processing and production facilities that limit us in joining the elite members of the developed world. The Indian Institute of Metals has on numerous

occasions tasked its eminent members and researchers to identify technology gaps not only for India but for the whole world, so that corrective measures could be taken for the advancement of new materials and technologies. I am very happy that the present book project, conceived by Dr. Baldev Raj, put in place by the various authors and two able editors, Dr. N. Eswara Prasad and Dr. R.J.H. Wanhill, and brought out in book form by IIM and Springer, notably serves this purpose.

Aerospace materials and their manufacturing are easily the most basic and most important core aerospace/aeronautical technologies. The present Volume 2 on Aerospace Material Technologies of the 2-Volume Source Book Series of IIM/Springer is a rich compilation of various traditional, advanced and futuristic material technologies encompassing nearly 20 major areas. Each of the chapters addresses scientific principles behind production, production details, equipment and facilities for industrial production, and finally aerospace application areas of these material technologies. The authors of these chapters have been pioneers of industrial aerospace material technologies and they are not only from India but from advanced countries like the Netherlands, Australia and the USA. This book has a well-planned layout in 4 parts. Part I deals with primary metal and material processing, including nanomanufacturing. Part II deals with materials

characterization and testing methodologies and technologies. Part III addresses structural design. Finally, several advanced material technologies such as quality assurance, refurbishment, failure analysis, certification, and life extension technologies are covered in Part IV. Some of the very important and advanced topics such as ‘Structural Design by ASIP’, ‘Damage Mechanics-Based Life Prediction and Extension’ and ‘Principles of Structural Health Monitoring’ are dealt with at equal length as the traditional aerospace materials technology topics.

I am happy that some of these chapters bring out the present Indian scenario vis-a-vis international developments, thus providing important scope for identifying gaps in aerospace material technologies in India and South Asia. I am glad that the present volume provides a summary of various aspects of the technologies and serves as a ready reference for all the readers.

Dr. G. Satheesh Reddy
FNAE, FRIN, FAeSI, FIET, FSSWR, FIE, FAPAS, AFAIAA, HFCSI
Scientific Advisor to RakshaMantri (SA to RM)
Min. Defence, Govt. India, New Delhi, India

Series Editors' Preface

The Indian Institute of Metals Series is an institutional partnership series focusing on metallurgy and materials sciences.

About the Indian Institute of Metals

The Indian Institute of Metals (IIM) is a premier professional body (since 1947) representing an eminent and dynamic group of metallurgists and materials scientists from R&D institutions, academia and industry mostly from India. It is a registered professional institute with the primary objective of promoting and advancing the study and practice of the science and technology of metals, alloys and novel materials. The institute is actively engaged in promoting academia–research and institute–industry interactions.

Genesis and History of the Series

The study of metallurgy and materials science is vital for developing advanced materials for diverse applications. In the last decade the progress in this field has been rapid and extensive, giving us a new array of materials, with a wide range of applications and a variety of possibilities for processing and characterizing the materials. In order to make this growing volume of knowledge available, an initiative to publish a series of books in metallurgy and materials science was taken during the Diamond Jubilee year of the Indian Institute of Metals (IIM) in the year 2006. IIM entered into a partnership with Universities Press, Hyderabad, and as part of the IIM Book series 11 books were published, and a number of these have been co-published by CRC Press, USA. The books were authored by eminent professionals in academia, industry and R&D with outstanding background in their respective domains, thus generating unique resources of validated expertise of

interest in metallurgy. The international character of the authors and editors has enabled the books to command national and global readership. This book series includes different categories of publications: textbooks to satisfy the requirements of undergraduates and beginners in the field, monographs on select topics by experts in the field, and proceedings of select international conferences organized by IIM after mandatory peer review. An eminent panel of international and national experts constitute the advisory body in overseeing the selection of topics and important areas to be covered in the books and the selection of contributing authors.

Current Series Information

To increase the readership and to ensure wide dissemination among global readers, this new chapter of the series has been initiated with Springer. The goal is to continue publishing high-value content on metallurgy and materials science, focussing on current trends and applications. Readers interested in writing for the series may contact the undersigned series editor or the Springer publishing editor, Swati Meherishi.

About This Book

The current source book on 'Aerospace Materials and Material Technologies—2 Volumes' with comprehensive coverage in aerospace, materials and technologies is the first and latest book to be published with Springer. This book comprises 2 volumes, with the first volume dedicated to aerospace materials in three parts, a total of 26 chapters covering all types of materials including metallic, composites and special materials. Volume 2, in 25 chapters, is fully dedicated to the recent and advanced material technologies which have emerged in the aerospace industry. This volume consists of four parts covering processing technologies, characterization and testing, structural design and special technologies. As a whole, this source book on 'Aerospace Materials and Technologies' fully covers the important aspects of the materials developments and their technologies in the aerospace industry, and is an update and unique knowledge base. We are confident that the book will help the readers to develop the basic and advanced understanding of the materials and their recent developments that are essential to address significant growth in the aerospace industry. The authors and editors are of the conviction that the book will be a prime source to all those pursuing advanced materials and technologies in aerospace sectors. The students, younger faculty members, and research scholars in academic and R&D institutions, in addition to libraries and knowledge parks, are

the beneficiaries of the dedicated work and efforts by Dr. N. Eswara Prasad and Dr. R.J.H. Wanhill, as editors, and a large number of eminent authors of the 2 volumes of this important book.

We wish you enrichment in knowledge and motivation. Also, we await your feedbacks for improving the book when it goes to the second edition.

Baldev Raj
Editor-in-Chief, and
Director, National Institute of Advanced Studies, Bengaluru

U. Kamachi Mudali
Co-Editor-in-Chief
Outstanding Scientist and Associate Director
Indira Gandhi Centre for Atomic Research, Kalpakkam

Preface

The aerospace industry is at the forefront of materials and technology developments. There are never-ending demands for high-performance aerospace vehicles with lightweight, highly reliable and durable structures. Candidate materials are continually being developed and improved, and their property envelopes expanded. Structural design and certification requirements and inspection and monitoring techniques also evolve to keep pace with these developments.

There are many excellent materials handbooks and source books available, most notably the ASM International series. These offer comprehensive multivolume guides that belong to the libraries of every materials-oriented university and institute. However, they are less suitable, even in e-form, for regular ‘desktop’ consultation. This led us to the concept of a compact and affordable vade mecum that would serve as a ready reference for practicing engineers, and a comprehensive introduction, at an advanced level, for students and faculty members.

It soon became evident that a two-volume series would be appropriate. These have the distinguishing titles ‘Aerospace Materials’ (Volume 1) and ‘Aerospace Material Technologies’ (Volume 2). These volumes are divided into the following main parts:

- Volume 1:
 - Part I: Metallic Materials (Chaps. 1–12)
 - Part II: Composites (Chaps. 13–17)
 - Part III: Special Materials (Chaps. 18–26)
- Volume 2:
 - Part I: Processing Technologies (Chaps. 1–5)
 - Part II: Characterization and Testing Technologies (Chaps. 6–11)
 - Part III: Structural Design (Chaps. 12–19)
 - Part IV: Special Technologies (Chaps. 20–25)

This Volume 2 contains chapters on (i) primary and secondary processing, superplastic forming, welding and nanomanufacturing; (ii) microstructure, texture,

physical and mechanical properties, and non-destructive testing; (iii) primary structures, mechanical systems, aircraft engines, missile propulsion, fatigue (including full-scale testing) and residual strength requirements, and stress corrosion cracking; and (iv) aero stores inspection and quality assurance, life extension, structural health monitoring, failure analysis, airworthiness certification and light-weight ballistic armour.

Kanpur, Uttar Pradesh, India
Emmeloord, Flevoland, The Netherlands

N. Eswara Prasad
R.J.H. Wanhill

Acknowledgements

In 2012, the Indian Institute of Metals (IIM) invited me to prepare a monograph on continuous fibre-reinforced, ceramic-matrix composites (CFCCs) to publish in the IIM series. The outline of that monograph was prepared, and a few chapters took preliminary shape. However, this project could not be completed because the subject was dealt with only in a very few institutions in India, and the processing details were mostly proprietary. In the meantime, several of my colleagues and well-wishers, who have worked with me for several years on a new generation of aluminium alloys based on lithium additions, agreed to contribute comprehensive overview articles to a book on the physical metallurgy, processing, mechanical behaviour and applications of aluminium–lithium alloys—a subject that I have been associated with for nearly 30 years. This book was published in 2014 by Butterworth-Heinemann—An Imprint of Elsevier, UK/USA.

But my quest to write on other aerospace materials (including the CFCCs) and their material technologies still was not fulfilled. This was the time, during one of the discussions with Dr. Baldev Raj, editor-in-chief, IIM Book series, that it was suggested to me that my recent experience on concurrent development and certification of aerospace materials should be used to prepare comprehensive book(s) on aerospace materials and technologies. I gratefully agreed to this suggestion of Dr. Baldev Raj and started almost immediately on an outline of such a compendium. I was most pleased when Dr. Russell Wanhill, formerly of the NLR, the Netherlands (my co-editor for the Aluminum-Lithium Alloys Monograph and an internationally known materials scientist), agreed to co-edit this book series. Within months, by early 2015, the outline of the book series took a definite shape, in the form of a two-volume book series on aerospace materials and technologies—Aerospace Materials (Vol. 1) and Aerospace Material Technologies (Vol. 2). I am profoundly grateful to both Dr. Baldev Raj and Dr. Wanhill for many in-depth subsequent discussions to shape these volumes.

I am very fortunate to have a long association with many outstanding aerospace materials scientists of India and abroad. Four of these most exemplary scientists, Dr. Dipankar Banerjee and Dr. Indranil Manna (for Volume 1 on Aerospace

Materials) and Dr. S. Christopher and Dr. G. Satheesh Reddy (for Volume 2 on Aerospace Material Technologies), have kindly consented to my request to provide the Forewords for this book series.

The present book series comprises a number of overview articles on aerospace materials and aerospace material technologies. The authors of the book chapters have mostly been pooled from Indian aerospace materials institutions encompassing the Defence Research and Development Organisation (DRDO), Council of Scientific and Industrial Research (CSIR), Department of Atomic Energy (DAE), Defence Production, Govt of India (particularly Mishra Dhatu Nigam (MIDHANI) Limited, Hyderabad) and Hindustan Aeronautics Limited (HAL). My own colleagues at the Regional Centre for Military Airworthiness (RCMA (Materials)), CEMILAC and Defence Metallurgical Research Laboratory (DMRL) have contributed magnanimously to this book project. Some of the close associates of Dr. Wanhill have also contributed. Dr. Wanhill and I have also contributed a considerable number of book chapters. I am grateful to each of these principal authors and their co-authors of the chapters for their valuable contributions to this book series.

Dr. Wanhill has further extended his help and guidance to shape the technical contents of these two book series by painstakingly reviewing all the book chapters. Although such an exercise is very arduous and difficult to accomplish, it has resulted in close uniformity in contents and style of the book chapters. I am most grateful and greatly indebted to him.

The book contents provided by the authors were typeset by my book secretariat which consisted of Mr. D.B.A. Sagar, late Mrs. P. Varsha, Ms. S. Hima Bindu and Mr. Vishal Shreyas, who worked nearly full-time on this project. They were also greatly aided by my colleagues Mrs. M. Swarna Bai, Mr. P. Rambabu, Mr. B. Saha, Mr. Abhishek Singh, Ms. Pratibha Singh, Dr. D.S. Bag and Dr. Ashish Dubey. I am very thankful to all these colleagues.

It is an honour for me that Springer has become the principal source of professional support by agreeing to publish these two book volumes. At this juncture, I should acknowledge gratefully the initiative taken by the IIM, particularly Dr. Baldev Raj and Dr. Kamachi Mudali, to conduct a series of discussions with Springer, thereby enabling the publication of these volumes by Springer. I must mention here and express my gratitude for the help and support received from the Springer team, especially to Swati Meherishi, senior editor, and Aparajita Singh, editorial assistant.

N. Eswara Prasad

Contents

Part I Processing Technologies

- 1 Processing of Aerospace Metals and Alloys: Part 1—Special Melting Technologies** 3
M. Chatterjee, A. Patra, R.R. Babu and M. Narayana Rao
- 2 Processing of Aerospace Metals and Alloys: Part 2—Secondary Processing** 25
S. Narahari Prasad, P. Rambabu and N. Eswara Prasad
- 3 Superplastic Forming of Aerospace Materials** 39
K.A. Padmanabhan, S. Balasivanandha Prabu and S. Madhavan
- 4 Welding Technologies in Aerospace Applications** 65
T. Mohandas
- 5 Nanomanufacturing for Aerospace Applications** 85
S. Anandan, Neha Hebalkar, B.V. Sarada and Tata N. Rao

Part II Characterisation and Testing

- 6 Microstructure: An Introduction** 105
C. Suryanarayana
- 7 Texture Effects in Important Aerospace Materials** 125
R.J.H. Wanhill
- 8 Physical Property Significances for Aerospace Structural Materials** 143
R.J.H. Wanhill
- 9 Structural Alloy Testing: Part 1—Ambient Temperature Properties** 159
R.J.H. Wanhill

10	Structural Alloy Testing: Part 2—Creep Deformation and Other High-Temperature Properties.	185
	R.J.H. Wanhill, D.V.V. Satyanarayana and N. Eswara Prasad	
11	Non-destructive Testing and Damage Detection	209
	B. Purna Chandra Rao	
Part III Structural Design		
12	Design of Aircraft Structures: An Overview	231
	S. Kamle, R. Kitey, P.M. Mohite, C.S. Upadhyay, C. Venkatesan and D. Yadav	
13	Aircraft Mechanical Systems	251
	R.V. Huliraj and H.L. Janardhana	
14	Design and Structures of Aircraft Engines	279
	Rajaram Nagappa, Sankarkumar Jeyaraman and C. Kishore Kumar	
15	Missile Propulsion Systems	305
	P. Satyaprasad, M. Pandu Ranga Sharma, Abhishek Richarya, A. Rolex Ranjit and B.S. Subhash Chandran	
16	Fatigue Requirements for Aircraft Structures	331
	R.J.H. Wanhill	
17	Full-Scale Fatigue Testing	353
	R. Sunder	
18	Residual Strength Requirements for Aircraft Structures	373
	R.J.H. Wanhill	
19	Stress Corrosion Cracking in Aircraft Structures	387
	R.J.H. Wanhill and R.T. Byrnes	
Part IV Special Technologies		
20	Aero Stores (Materials) Inspection and Quality Assurance	413
	K.K. Mehta and S. Chawla	
21	Fatigue Life Enhancement for Metallic Airframe Materials	433
	L. Molent and S.A. Barter	
22	Structural Health Monitoring	449
	Prakash D. Mangalgiri and Kota Harinarayana	
23	Failure Analysis and Prevention	479
	K.P. Balan and A. Venugopal Reddy	

- 24 Airworthiness Certification of Metallic and Non-metallic Materials: The Indian Approach and Methodologies 515**
M. Sai Krishna Rao, P. Rambabu, Ch.V.S. Murthy, B. Jana, B. Saha,
N. Eswara Prasad, P. Jayapal and K. Tamilmani
- 25 Lightweight Ballistic Armours for Aero-Vehicle Protection 541**
Arun Kumar Singh, R.J.H. Wanhill and N. Eswara Prasad

Editors and Contributors

About the Editors



Dr. N. Eswara Prasad FIE, FAPAS, FIIM, FAeSI, a B.Tech. (1985) and a Ph.D. (1993) in metallurgical engineering from Indian Institute of Technology (BHU), Varanasi, India, is an innovative and creative researcher and technologist. He is currently serving as a director, Defence Materials and Stores Research and Development Establishment (DMSRDE), DRDO, at Kanpur, India. He has made significant and outstanding contributions to the Indian Defence Research and Development Organisation (DRDO) in the last 30 years in the fields of design, materials development and characterization, and airworthiness certified production

of many advanced aerospace, aeronautical and naval materials and components. The extensive research work conducted by him has resulted in the development and certified production of (i) Al and Al-Li alloys for the LCA, LCH and Indian Space Programme, (ii) aero steels, including maraging and PH Steels for Indian Missile Programmes, (iii) high-strength and high-temperature Ti alloys, including β -Ti alloys for the LCA's slat tracks and landing gear, and (iv) advanced ultrahigh-temperature materials—Mo and Ti intermetallics; monolithic ceramics (structural alumina, graphite and SiC); and carbon-, silica- and SiC-based continuous fibre-reinforced, ceramic-matrix composites (CFCCs) for cutting-edge components, systems and technologies. Application of these materials in DRDO has been complemented by him by extensive fundamental research on tensile deformation, fatigue and fracture, and correlations between chemical composition, processing, microstructure, texture and deformation, leading to first-time scientific explanations on property anisotropy. In the last 6 years, Dr. Prasad has been instrumental in the concurrent development and production of several airworthiness certified materials and components of aero and naval steels, Al alloys, Ni-base

superalloys, Ti sponge and special Ti alloys for Indian Defence, Indian Air Force, Indian Navy and ATVP—the Indian Submarine Programme, which have resulted in realizing defence hardware worth more than Rs. 12 billion, out of which direct materials production of nearly Rs. 6.2 billion through 180 provisional clearances and 11 type approvals of CEMILAC. Dr. Prasad's prolific research resulted in over 170 research articles in peer-reviewed national and international journals and conference proceedings, including 30 written/edited books and book chapters as well as 26 classified and unclassified and also peer-reviewed technical reports and a highly acclaimed first international monograph on Al-Li alloys in 2014. He has also authored nearly 90 confidential reports and more than 260 certification documents for DRDO. In recognition of his original contributions in the fields of metallurgy and materials engineering, Dr. Prasad has received several national and international awards. He has been the recipient of Young Scientist Award (ICSA, 1991), Young Metallurgist (Ministry of Steel, 1994), AvH's Humboldt Research Fellowship (1998–99), Max Planck Institute (Stuttgart)'s visiting scientist (1998–99), Binani Gold Medal (IIM, 2006), Metallurgist of the Year (Ministry of Steel, 2010), AICTE-INAE Distinguished Visiting Professorship at the Andhra University and Mahatma Gandhi Institute of Technology (INAE, 2012-Till Date), IIT-BHU (MET)'s Distinguished Alumnus Award (2013), and the prestigious Dr. V.M. Ghatge Award of AeSI (in 2014). Dr. Prasad is a fellow of the Institute of Engineers (India) [FIE], Indian Institute of Metals [FIIM] and AP Akademi of Sciences [FAPAS].



Dr. R.J.H. Wanhill is an emeritus principal research scientist at the Netherlands Aerospace Centre, formerly the National Aerospace Laboratory NLR, in the Netherlands. He holds two doctorates, one from the University of Manchester (1968) and the second from the Delft University of Technology (1994). He joined the NLR in 1970, and since then he has investigated fatigue and fracture of all classes of aerospace alloys. He is the co-author of the book 'Fracture Mechanics' (1984), which has run into a second edition; co-author with Simon Barter of the monograph 'Fatigue of Beta Processed and Beta Heat-treated Titanium Alloys',

published by Springer in 2012; and co-author and co-editor for the book 'Aluminium—Lithium Alloys: Processing, Properties and Applications', editors N. Eswara Prasad, Amol A. Gokhale and R.J.H. Wanhill, published in 2014. From 1978 to 1996 Dr. Wanhill was the head of the Materials Department of the NLR and in 1979–1980 adjunct professor of materials at the Delft University of Technology. From 1997 to 2008 he was a principal research scientist in the Aerospace Vehicles Division of the NLR. From 2008 to 2015 he has been an emeritus principal research scientist at the NLR. In 2002 the Board of the Foundation NLR awarded Dr. Wanhill the first Dr. ir. B.M. Spee Prize for

outstanding contributions on aerospace materials. In October 2014 he was awarded an honour diploma by the Netherlands Aerospace Fund for his long-term contributions to scientific research and knowledge at the NLR and use of this knowledge for aircraft failure analyses. In recent years, Dr. Wanhill has worked on the analysis of fatigue cracking in GLARE panels from the Airbus 380 MegaLiner Barrel test (presented at ICAF 2009) and in collaboration with Dr. Simon Barter (Defence Science and Technology Group (DSTG), Melbourne). From November 2009 to May 2010 Dr. Wanhill was a visiting academic at the DSTG. The work there included (i) a collaborative report, book chapter and presentation for the Royal Australian Air Force (RAAF) on fatigue life assessment of combat aircraft; (ii) a book chapter on stress corrosion cracking (SCC) in aerospace; (iii) two seminar presentations, on service failures and the MegaLiner Barrel GLARE cracking (see above); and (iv) preparation of a course on failure analysis, held twice at the Auckland Technical University at the beginning of May 2010. This course has been adopted by the RAAF as part of its instruction material. Since 1994 Dr. Wanhill has been investigating the fracture phenomena in ancient silver and iron and has published eight peer-reviewed papers on this topic. The most recent papers have been published in the *Journal of Failure Analysis and Prevention* (2011), *Metallography, Microstructure, and Analysis* (2012), and the leading archaeological scientific journal *Studies in Conservation* (2013). Dr. Wanhill also gives annual lectures on ancient silver for a master's degree course on conservation at the University of Amsterdam. Dr. Wanhill has been an author and speaker on several fatigue and fracture topics and also on fatigue-based design of aircraft structures. In 2012, Dr. Wanhill was a keynote speaker for the International Conference on Engineering Failure Analysis V, held in The Hague. He also had two additional contributions, with co-authors: 'Validation of F-16 wing attachment fitting bolts' and 'Five helicopter accidents with evidence of material and/or design deficiencies'. All three presentations have been published as papers in *Engineering Failure Analysis* in 2013. In 2014 he was a keynote speaker at *Fatigue 2014*, held in Melbourne. In 2015 he gave a public lecture at *Materials Days 2015*, Rostock, with the title 'Materials and structural integrity: Milestone aircraft case histories and continuing developments'. This presentation has also been adopted by the RAAF as instruction material and in written chapter form has been published in 'The Reference Module in Materials Science and Engineering'.

Contributors

S. Anandan Centre for Nanomaterials, ARCI, Hyderabad, India

R.R. Babu Mishra Dhatu Nigam Limited, Kanchanbagh, Hyderabad, India

K.P. Balan DMRL, Hyderabad, India

S. Balasivanandha Prabu Department of Mechanical Engineering, College of Engineering Guindy, Anna University, Chennai, India

S.A. Barter Aerospace Division, Defence Science and Technology Group, Melbourne, Australia

R.T. Byrnes Defence Science and Technology Group, Melbourne, Australia

M. Chatterjee Mishra Dhatu Nigam Limited, Kanchanbagh, Hyderabad, India

S. Chawla DGAQA, New Delhi, India

N. Eswara Prasad DMSRDE, DRDO, Kanpur, India

Kota Harinarayana IIT Bombay, Powai, Mumbai, India

Neha Hebalkar Centre for Nanomaterials, ARCI, Hyderabad, India

R.V. Huliraj ARDC, HAL, Bangalore, India

B. Jana RCMA (Materials), CEMILAC, Hyderabad, India

H.L. Janardhana ARDC, HAL, Bangalore, India

P. Jayapal CEMILAC, Bengaluru, India

Sankarkumar Jeyaraman GTRE, DRDO, Bangalore, India

S. Kamle Department of Aerospace Engineering, Indian Institute of Technology, Kanpur, India

C. Kishore Kumar GTRE, DRDO, Bangalore, India

R. Kitey Department of Aerospace Engineering, Indian Institute of Technology, Kanpur, India

S. Madhavan Department of Mechanical Engineering, IIT Madras, Chennai, India

Prakash D. Mangalgi Aeronautical Development Agency, Bangalore, India

K.K. Mehta DGAQA (GW & M), Hyderabad, India

T. Mohandas Nalla Malla Reddy Engineering College, Hyderabad, India; Formerly with Defence Metallurgical Research Laboratory, DRDO, Hyderabad, India

P.M. Mohite Department of Aerospace Engineering, Indian Institute of Technology, Kanpur, India

L. Molent Aerospace Division, Defence Science and Technology Group, Melbourne, Australia

Ch.V.S. Murthy RCMA (Materials), CEMILAC, Hyderabad, India

Rajaram Nagappa NIAS, Bangalore, India

S. Narahari Prasad Mishra Dhatu Nigam Limited, Hyderabad, India

M. Narayana Rao Mishra Dhatu Nigam Limited, Kanchanbagh, Hyderabad, India

K.A. Padmanabhan Department of Mechanical Engineering, Anna University, Chennai, India

M. Pandu Ranga Sharma Defence Research and Development Laboratory, PO Kanchanbagh, Kanchanbagh, Hyderabad, India

A. Patra Mishra Dhatu Nigam Limited, Kanchanbagh, Hyderabad, India

B. Purna Chandra Rao IGCAR, Kalpakkam, India

P. Rambabu RCMA (Materials), CEMILAC, DRDO, Hyderabad, India

Tata N. Rao Centre for Nanomaterials, ARCI, Hyderabad, India; Centre for Solar Energy Materials, ARCI, Hyderabad, India

Abhishek Richarya DRDL, DRDO, Hyderabad, India

A. Rolex Ranjit DRDL, DRDO, Hyderabad, India

B. Saha RCMA (Materials), CEMILAC, Hyderabad, India

M. Sai Krishna Rao RCMA (Materials), CEMILAC, Hyderabad, India

B.V. Sarada Centre for Solar Energy Materials, ARCI, Hyderabad, India

D.V.V. Satyanarayana DMRL, DRDO, Hyderabad, India

P. Satyaprasad DRDL, DRDO, Hyderabad, India

Arun Kumar Singh DMSRDE, DRDO, Kanpur, India

B.S. Subhash Chandran DRDL, DRDO, Hyderabad, India

R. Sunder BISS, Bengaluru, India

C. Suryanarayana Department of Mechanical and Aerospace Engineering, University of Central Florida, Orlando, FL, USA

K. Tamilmani Office of DG (Aero), DARE, Bengaluru, India

C.S. Upadhyay Department of Aerospace Engineering, Indian Institute of Technology, Kanpur, India

C. Venkatesan Department of Aerospace Engineering, Indian Institute of Technology, Kanpur, India

A. Venugopal Reddy ARCI, Hyderabad, India

R.J.H. Wanhil NLR, Emmeloord, The Netherlands

D. Yadav Department of Aerospace Engineering, Indian Institute of Technology,
Kanpur, India

Part I
Processing Technologies

Chapter 1

Processing of Aerospace Metals and Alloys: Part 1—Special Melting Technologies

M. Chatterjee, A. Patra, R.R. Babu and M. Narayana Rao

Abstract This chapter discusses in detail the special melting technologies adopted for worldwide commercial scale manufacture of aerospace metals and alloys. Some case studies have been included to illustrate the role of these melting technologies in the production of premium-quality products for critical aerospace applications.

Keywords Primary processing · Melting technologies · Steels · Titanium alloys · Nickel superalloys

1.1 Introduction

Reliable performance of the metals and alloys in critical aerospace applications depends on their meeting stringent requirements and specifications. There is thus a continuing demand for high-quality alloys with closely controlled chemistries, cleanliness, homogeneity, and heat-to-heat reproducibility. This has compelled alloy producers all over the world to use advanced melting technologies for ingot metallurgy (IM) production of these materials.

The choice of melting processes is primarily governed by the characteristics of the alloys to be manufactured, the specification requirements, and the service conditions in which they are to be used. For example, materials subjected to long-term high-temperature exposures and extreme thermal stresses are invariably processed via high end-vacuum melting technologies.

Metallurgical benefits derived from vacuum melting, coupled with technological advances in vacuum investment casting, are widely used to manufacture various types of premium-quality near-net-shaped aeroengine components. Remelting processes such as electroslag remelting (ESR) or vacuum arc remelting (VAR) or their combination are extensively used to enhance the quality of primary melted materials with respect to their homogeneity, solidification structure, soundness, and cleanliness. In recent years the

M. Chatterjee (✉) · A. Patra · R.R. Babu · M. Narayana Rao
Mishra Dhatu Nigam Limited, Kanchanbagh, Hyderabad, India
e-mail: mrinal_chatterjee54@yahoo.com

international metallurgical fraternity has seen massive growth in the installation of new melting, remelting, and casting equipment using a vacuum environment. This is mainly driven by the need for premium-quality high-performance materials in the aerospace and power turbine industries.

This chapter provides a critical assessment of the specialized melting technologies for processing critical aerospace alloys, together with specific case studies. The chapter concludes with an overview of the titanium melting process, which owing to titanium's high reactivity and affinity for oxygen is carried out exclusively in water-cooled copper crucibles under vacuum.

1.2 Vacuum Induction Melting (VIM)

Materials for aerospace application should possess a high degree of integrity and reliability in service and accordingly require the use of sophisticated and controlled melting processes. Success in overcoming these challenges owes much to the development of vacuum induction melting (VIM). This process first became important in the 1950s, when superalloy components containing large amounts of reactive elements were found to have superior service life when melted under vacuum. Since then, VIM has become an indispensable melting strategy for manufacturing high-performance alloys, owing to its ability to produce high-quality materials in a reproducible manner.

1.2.1 *Functional Principle*

Melting of a solid charge is done in a refractory-lined crucible and takes place owing to electromagnetic induction from a high-frequency AC current flow in an induction coil. The electromagnetic forces cause a stirring effect in the molten metal that aids in producing chemically and thermally homogeneous melts. Figure 1.1 gives a schematic for a VIM furnace and its ancillary equipment [1]. VIM processing involves melting, refining, and composition adjustment under controlled conditions. For example, Fig. 1.2 shows the furnace pressure variations during the different stages of melting [1].

1.2.2 *Melting Process*

The initial charge normally contains all the non-reactive elements and sufficient carbon to facilitate an active carbon–oxygen reaction during melting. The progress of refining is monitored by periodical checks of the hot leak rate (a measure of outgassing) and visual observations of gas bubble formation from the liquid metal.

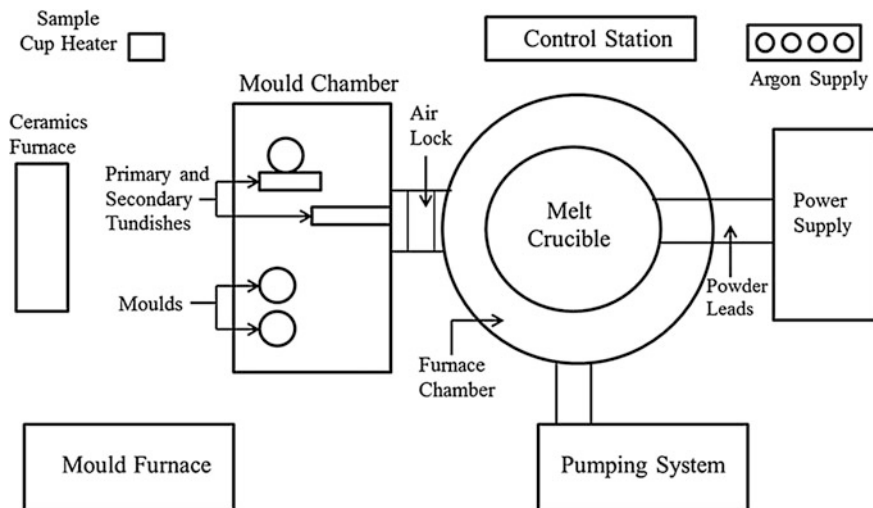


Fig. 1.1 Schematic layout of VIM system [1]

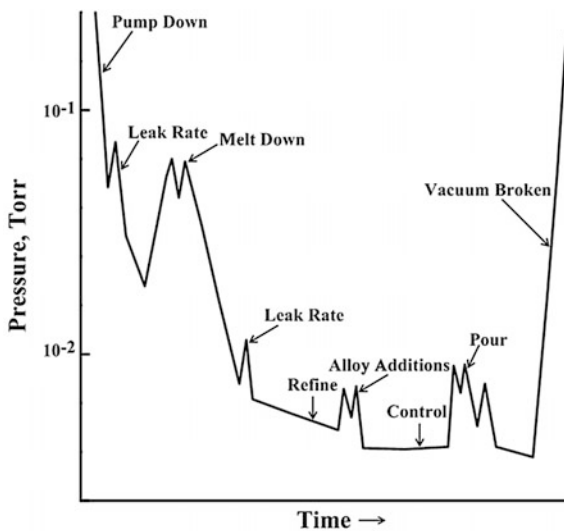


Fig. 1.2 Schematic variation of furnace pressure at different stages of melting [1]

After refining, the reactive elements are added along with other alloying adjustments. At this stage the power input is precisely adjusted to control the liquid metal temperature in order to minimize the formation of inclusions by refractory–metal interactions. Just before tapping, the final microadditions of specific alloying elements are done. This all takes place under controlled temperature and reduced pressure to ensure reproducibility.

1.2.3 Process Benefits

VIM has been extensively used for primary melting of a variety of aerospace alloys because of the following process benefits:

Degassing Reduced pressure during vacuum melting helps to remove dissolved gases such as H_2 and N_2 , owing to reduction in their solubility in the liquid metal. However, nitrogen removal is ineffective in the presence of strong nitride formers (Ti, Nb, Hf, Al, etc.), since the formation of stable nitrides reduces nitrogen activity in the liquid metal.

Decarburization VIM melting helps in achieving extremely low levels of carbon as well as oxygen, since the carbon–oxygen decarburization reaction (Eq. 1.1) is favoured by a reduced partial pressure of carbon monoxide above the liquid metal bath, as represented in Fig. 1.3 [2].



where

K_{CO} Equilibrium constant,

p_{CO} Partial pressure of CO,

a_C Activity of C in melt, and

a_O Activity of O in liquid bath.

This phenomenon is effectively utilized to achieve extremely low levels of carbon (< 50 ppm) as well as gas levels (< 30 ppm O_2 and N_2), during manufacture

Fig. 1.3 Activity of C and O in an Fe–C–O system at different reduced pressures [2]

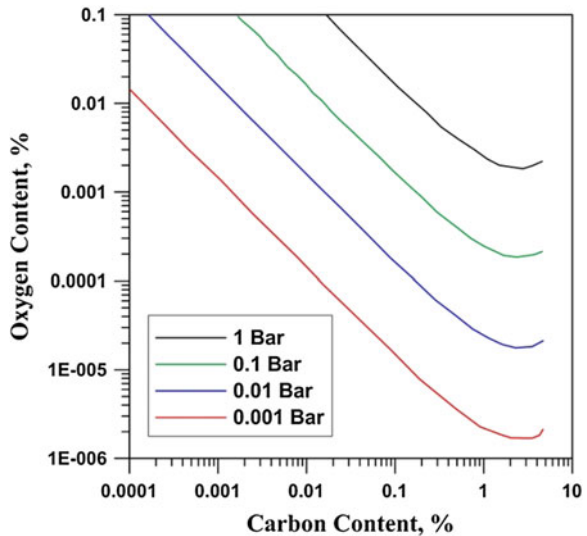
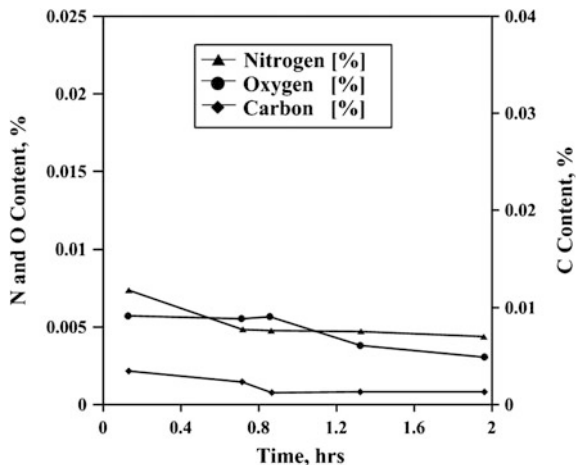


Fig. 1.4 Extent of lowering N, O, and C contents in a maraging steel melt with progressive refining time [2]



of maraging and precipitation-hardened stainless steels meant for critical aerospace structural applications.

Figure 1.4 shows the progress of removal of N, O, and C from a steel melt during refining [2]. However, as before it should be noted that pressure-dependent removals are ineffective in the presence of strong nitride, oxide, or carbide formers, since the conditions prevailing during vacuum induction melting do not favour their dissociation.

Tramp Element Removal Some of the detrimental and volatile elements (elements with high vapour pressure) are readily removed by distillation under vacuum. A study of evaporation of a wide range of elements at the level of 0.1 % from an 80Ni20Cr baseline alloy at 1565 °C showed that Te, Pb, Bi, Se, and Cu were volatilized, but Sb, Sn, and As were not, owing to deviation of the solid solution from ideality. Figure 1.5 summarizes these results, showing that very low levels of some tramp elements (Te, Pb, Bi) can be achieved during VIM refining [3].

Melt Cleanliness Melting under vacuum under controlled conditions yields clean liquid metal, since contamination due to atmospheric oxidation or refractory–metal interactions can be avoided. Cleanliness of liquid metal can be further controlled by (i) pulse stirring and argon purging during refining and (ii) the use of specially designed tundishes (with multiple gates and ceramic filters) during liquid metal teeming.

Precise Chemistry Control Precise chemistry control is extremely important to achieve the targeted microstructure and properties in the final product as well as to ensure microstructural stability during long-term service exposure. One of the biggest benefits of VIM is the precise chemistry control within desirable limits, thus ensuring reproducibility. The degree to which the precise control of chemistry can be achieved is illustrated in Table 1.1 for 123 batches of the nickel-base superalloy Udimet 720 [4].

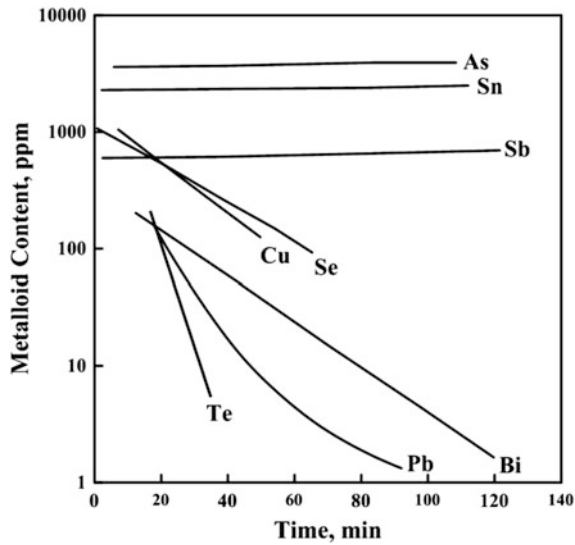


Fig. 1.5 Removal of metalloids during refining [3]

Table 1.1 Consistency of the chemistry of 123 heats of Udimet 720 [4]

Element	Max in the range (wt%)	Min in the range (wt%)	Average in the range (wt %)
Al	4.45	4.29	4.36
Ti	3.55	3.42	3.47
B	0.032	0.026	0.029
C	0.08	0.06	0.07
Cr	15.85	14.83	15.32
Mo	5.32	5.0	5.14
Co	19.05	18.23	18.70
Fe	0.33	0.11	0.15
Ni	Balance	Balance	Balance

Sulphur and Phosphorus Control Desulphurisation and dephosphorization reactions are limited by the absence of slag–metal reactions due to characteristic bath movement, whereby slag moves and solidifies on the crucible wall. These limitations have been overcome primarily by careful selection of raw materials. Controlled additions of desulphurising agents such as Ca, Mg, and Ce can also be carried out to achieve both desulphurization and control of inclusion shapes. However, since these elements are also potential deoxidizers, effective deoxidation must precede desulphurization.

1.2.4 Post-VIM Processing Technologies

VIM has become indispensable in the manufacture of high-performance aerospace materials and is regarded as the central core of every vacuum refining operation. Incorporation of sophisticated computer control during processing provides excellent reproducibility between melts.

The liquid metal produced by VIM can be further processed by different routes, depending on the nature of the material or products [5]. This has been schematically represented in Fig. 1.6. Practical examples are presented below to further illustrate this point:

- (i) Several high-performance alloys such as Fe–Ni/Fe–Co–Ni soft magnetic and controlled expansion alloys, and Ni–Ti shape memory alloys (which are not segregation prone but require a high degree of cleanliness and precision chemistry control) are directly cast into ingots after VIM and then processed further by hot working.
- (ii) Highly alloyed superalloys and steels which are hot workable but segregation prone, for example alloys 718, 617, 625 and 17-4PH steel, are cast into electrodes and again melted by ESR or VAR before further hot processing.
- (iii) High-performance alloys, which are not only segregation prone but also virtually unworkable, and are required in the form of complex profiled near-net-shape components (e.g. IN 738 and CM247 turbine blades), are further processed via vacuum investment casting (VIM-IC) or powder metallurgy (PM) routes.

A specific case study with respect to manufacture of Ni-base superalloy vacuum investment castings is discussed in Sect. 1.2.5 to bring out the role of VIM in the manufacture of critical gas turbine components.

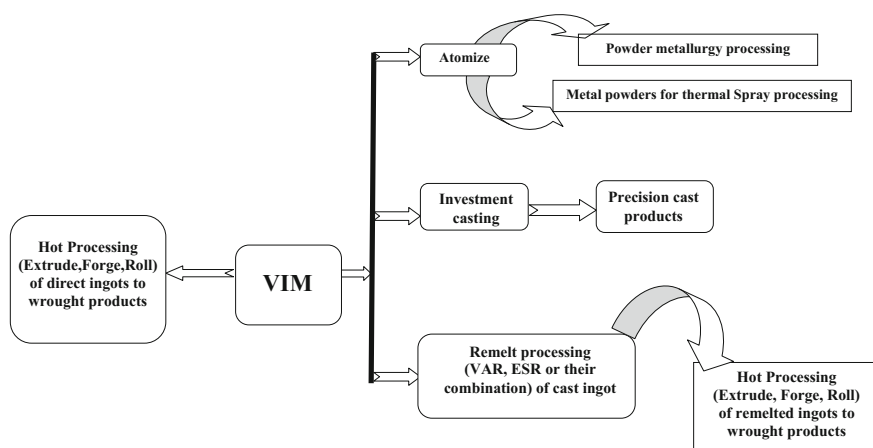


Fig. 1.6 Schematic representation of further processing routes for liquid metal produced by VIM

1.2.5 Manufacture of Nickel-Base Superalloy Investment Castings for Aerospace Gas Turbines—A Case Study

Ni-base superalloys with their FCC (γ) matrix and ordered coherent FCC (γ') precipitates have established themselves for long-term reliable performance in gas turbines. Higher operating temperatures have resulted in the use of Al + Ti-strengthened alloys with increasing additions of refractory metals, making these advanced alloys virtually unworkable. Advances in VIM and VIM-IC technologies have provided the right platform to exploit the full potential of γ' strengthening in these alloys. The manufacture of premium-quality superalloy vacuum investment castings for aircraft turbines was carried out in two stages [6].

- Stage 1 Primary melting in VIM furnace using virgin raw materials for manufacturing high-quality bar stock.
- Stage 2 Remelting and controlled solidification of small quantities of conditioned bar stock in a specially designed and dedicated VIM-IC unit for manufacturing of equiaxed or directionally solidified castings.

Stage 1 was done using a specially designed VIM furnace equipped with robust vacuum pumps and sophisticated automation for the precise monitoring and control of melt parameters. The following objectives, which are extremely important for long-term component reliability, could be successfully accomplished:

- (i) Precise chemistry control within extremely narrow desirable limits to satisfy the PHACOMP criterion indicated in the specification. This control ensured microstructural stability and prevention of topologically close-packed (TCP) phase formation.
- (ii) Precise control of extensive refining to achieve extremely low gas level (total $O_2 + N_2$ level of 5 ppm). Refining was monitored by the analysis of residual gas above the liquid metal bath using a quadrupole vacuum mass spectrometer. Dissolved oxygen in the liquid metal was estimated using solid electrolyte (calcia-stabilized zirconia) based oxygen sensors.
- (iii) An extensively clean product was obtained by controlling several factors such as (a) choice of a stable refractory lining, (b) entire melt processing under high vacuum, (c) pulse stirring to facilitate coagulation and flotation of inclusions, and (d) the use of a suitably designed high-alumina tundish fitted with dams and weirs as well as ZrO_2 filters during teeming operations.
- (iv) Effective removal of several harmful tramp elements (some of them up to a level of 0.3 ppm) by distillation.

In the second stage of melting, the stocks were further processed using a dedicated VIM-IC unit having additional mould heating and controlled mould withdrawal mechanisms to facilitate directional solidification. Ceramic shell moulds were secured over copper chill plates along with graphite susceptors. Baffled cooling units were arranged coaxially with the induction coils and were used for heating the ceramic moulds to above the alloy liquidus temperature. Suitably

conditioned bar stock of the required weight was rapidly remelted in 15 min in a presintered zirconia crucible within a 10 kg VIM furnace. The ceramic moulds were progressively preheated to around 1450 °C and soaked for 15 min before pouring the liquid metal. The liquid metal was poured into the moulds through a tundish, and the moulds were subsequently withdrawn from the heating zone at a predetermined rate, using a precision electromechanical drive. Unidirectional heat extraction and controlled solidification under a well-defined thermal gradient resulted in directional solidification of the metal to form the cast components.

1.3 Remelting Technologies

The growing demand for cleanliness and structural homogeneity can be scarcely met by conventional ladle metallurgy and VIM, since long solidification times for large-scale industrial ingots prevent controlling the solidification structure. Although these casting routes can process liquid metal of high cleanliness and chemistry control, the prolonged solidification process results in segregation-related defects causing non-uniform structures and second-phase distributions during subsequent processing.

Remelting technologies such as ESR and VAR not only bring about further refining of primary melted products, but also enable a well-defined macrostructure due to progressive melting and controlled solidification in a water-cooled copper mould. In addition, progressive melting and enhanced heat transfer conditions drastically reduce the local solidification time and consequently the extent of microsegregation in the remelted ingot.

The role of remelting technologies becomes even more prominent during the processing of highly alloyed materials such as maraging steels, tool steels, and superalloys. The so-called triple melting, i.e. VIM + ESR + VAR, is specified for aerospace superalloy gas turbine discs: this triple melting provides the very best quality products in terms of structural homogeneity and cleanliness. The following Sects. 1.3.1–1.3.3 discuss the remelting technologies with respect to melting process, refining characteristics, and solidification phenomena. Section 1.4 considers the origin of defects in remelted ingots.

1.3.1 Remelting Processes

A. Electroslag Remelting (ESR) ESR is a consumable electrode remelting–refining process wherein the material to be refined is progressively melted under a layer of highly reactive slag and subsequently solidified in a controlled manner in a water-cooled copper crucible. The slag acts primarily as the refining media and is superheated above the liquidus temperature of the metal by virtue of its high

resistivity when a high current is passed through it. Apart from liberating heat for remelting, the slag serves the following functions [7]:

- Protecting the metal droplets forming on the bottom of the consumable electrode from exposure to the atmosphere.
- Acting as a refining medium by absorbing harmful non-metallic inclusions and eliminating sulphur and oxygen from the liquid metal.
- Forming a thin layer of slag skin around the solidifying ingot, aiding directional solidification, and giving a good surface finish to the ESR ingots.

Most of the ESR slags belong to the $\text{CaF}_2\text{-Al}_2\text{O}_3\text{-CaO}$ ternary system and contain equal proportions of CaO and Al_2O_3 , corresponding to the eutectic trough in the system. This provides a range of slag compositions having a liquidus in the range 1350–1500 °C, making the slags suitable for remelting a wide variety of steels and superalloys.

B. Vacuum Arc Remelting (VAR) VAR is a secondary refining process established around 1950 for the production of high-quality and highly controlled aerospace materials. The VAR process involves continuous remelting of a consumable electrode by means of an arc under vacuum. DC power is applied to strike an arc between the electrode (cathode, $-$) and the baseplate (anode, $+$) of a copper mould contained in a water jacket. Metal droplets appear on the bottom of the electrode and quickly form a molten pool of metal. The gap between the melting electrode and metal pool (arc gap) is precisely maintained, and a controlled melt rate is established to achieve a stable melting process.

Steady-state solidification is critically dependent on establishment of a stable diffuse arc. This is facilitated by melting clean material with a constant, relatively small (6–10 mm) electrode gap in a vacuum-tight furnace, in the absence of any stray magnetic fields, such as those caused by non-coaxial power feeds. The metal droplets falling through the arc gap are exposed to vacuum and the extreme temperatures of the arc zone, resulting in refining. Towards the end of the process the power is gradually reduced to provide a controlled hot top, thereby maximizing the yield of useful product.

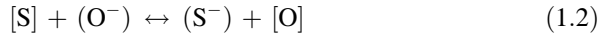
1.3.2 Refining Characteristics

A. Electroslag Remelting (ESR) The ESR process is characterized by continuous transport of liquid metal through a slag layer, wherein the slag and metal compositions change continuously according to the prevailing thermodynamic and kinetic conditions.

Reaction sites: Owing to the availability of a large surface area, active slag–metal interactions are feasible at the following sites: (i) thin films of liquid metal adhering to the electrode tip at the electrode/slag interface, (ii) droplet/slag interfaces during

the passage of metal droplets through the slag layer, and (iii) the liquid metal pool/molten slag interface.

Desulphurization reactions: The ESR process is well known for desulphurization reactions, which are favoured by high slag basicity and the reducing conditions prevalent during remelting operations [8]. The distribution coefficient of sulphur for the well-known slag-metal desulphurization reaction, namely



is given by Nafziger [9]:

$$L_1 = (\text{wt}\% S) / [\text{wt}\% S] \quad (1.3)$$

$$= K \cdot a_{(O^-)} / \left\{ [\text{wt}\% O] \cdot \gamma_{(S^-)} \right\} \quad (1.4)$$

where

L_1 Distribution coefficient,

K Equilibrium constant,

$\gamma_{(S^-)}$ Activity coefficient of S in slag and

$a_{(O^-)}$ Oxygen potential of slag.

Equation 1.4 implies that desulphurization is not only favoured by a high oxygen potential of the slag, $a_{(O^-)}$, but also influenced by low oxygen activity in the metal [wt% O]. This must be ensured by proper de-oxidation of the slag during the remelting process in order to maintain a net transfer of oxygen from metal to slag [10].

Oxidation equilibrium: The oxidation equilibrium is by far the most important reaction during remelting, since it not only controls the extent of desulphurization and cleanliness of the refined metal, but also has a decisive influence on the loss of oxidisable elements. In more detail, since the solubility of iron oxide in CaF₂-based ESR slags is very low, this leads to very high oxygen activity in the slag, even at low oxide concentrations [11]. This can easily disturb the thermodynamic equilibrium between slag and metal, resulting in uncontrolled loss of oxidisable elements during remelting. This problem is mitigated by remelting high-performance materials in inert gas electroslag remelting (IESR) furnaces. IESR prevents oxygen pickup by the ESR slag, unlike the situation when remelting is done in air. IESR shielding of the melt space has been the latest trend in recent years and offers the following advantages [12]:

- Oxidation of electrode and slag is completely avoided.
- Oxidation loss of elements such as Ti, Zr, Al and Si is almost completely avoided. This is important when remelting high Al + Ti-containing superalloys with narrow compositional ranges.
- Possibly better cleanliness of remelted ingots.
- Better retention of microadditions that have beneficial influences on material performance during subsequent processing.

B. Vacuum Arc Remelting (VAR) Refining phenomena in the VAR process are primarily governed by exposure of the molten metal in vacuo to very high arc temperatures. This causes removal of dissolved gases and vaporization of tramp elements. Gas levels are typically brought down below 20 ppm by VAR.

Chemical reactions favoured at the low pressures and high temperatures during VAR are the dissociation of less stable oxides, such as SiO_2 , and the melting of carbides. However, some of the more stable oxides and nitrides (Al_2O_3 , TiN, TiCN) present in VIM-melted primary electrodes cannot be dissociated. Instead, they are more homogeneously distributed throughout the ingot by physical disintegration, flotation, and dispersion. Since VAR is exclusively done under very high vacuum, the oxidation-induced remelting losses of potentially beneficial elements such as Ti, Al, and Si in high-performance alloys can be precisely controlled. This, together with very low gas levels, makes VAR preferable to ESR for remelting aircraft quality superalloys such as alloy 718, alloy 263, and alloy 90.

1.3.3 Solidification Phenomena

The remelting technologies discussed in the previous subsections offer highly consistent and predictable product qualities due to finely controlled solidification, which enhances the soundness and structural homogeneity. Also, directional cellular solidification, which is an important prerequisite for producing dense homogeneous ingots, can be readily achieved during remelting because of the following prevailing conditions [5, 7]:

- (i) The presence of hot superheated liquid metal at the top of the melt pool.
- (ii) Restricted lateral heat extraction from the crucible side walls, owing to a solid slag shell around solidifying ESR ingots and to vacuum in the shrinkage gap between solidifying VAR ingots and the mould wall.
- (iii) The presence of bottom chill (a water-cooled bottom plate), resulting in heat extraction predominantly from the bottom of the solidifying metal pool.

All three of the above conditions cause a very high thermal gradient ahead of the solidifying front, thereby favouring columnar dendritic structures growing in the direction of heat extraction. This growth direction is a function of molten metal pool depth and pool profile: the pool depth increases with remelting rate, and this means that the growth angle of the dendrites with respect to the ingot axis also increases. In extreme cases the directional growth of the dendrites can stop. The ingot core then solidifies non-directionally, resulting in an equiaxed dendritic structure that is invariably associated with microshrinkage and segregation-related defects.

The pool depth is largely controlled by the balance between the power input to the pool and the heat extraction rate caused by the water-cooled copper crucible. The success of remelting segregation-sensitive alloys depends on the precise control

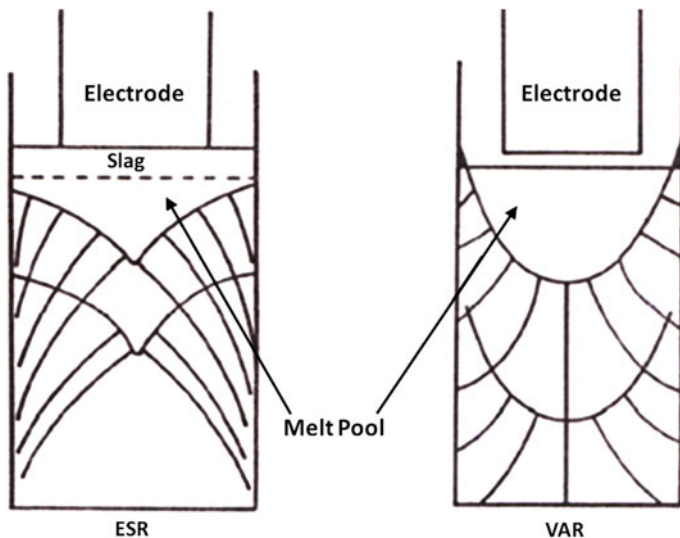


Fig. 1.7 Pool profile and grain growth directions in remelted ingots [14]

of the melt rate matched with the cooling rate through the crucible interface, so that steady-state melting is established, giving rise to an optimum shallow pool profile.

Evolution of advanced control systems incorporating pool depth estimators has greatly facilitated active control of the solidification process, thereby enabling its reproducibility [13]. Although the ESR and VAR solidification phenomena are almost similar, there are subtle differences in the magnitudes of heat extraction from the side walls and bottom of the crucible, resulting in different pool profiles (see Fig. 1.7) [14].

A well-stirred superheated slag pool on top of the ESR ingot eliminates a significant temperature gradient in the radial direction, resulting in heat extraction predominantly from the bottom of the metal pool. At the side surface of the ingot, there is thus a net heat flow vector and grain growth direction parallel (0° angle) to the ingot axis. Towards the centre of the ingot the angle approaches 45° . The combined effect of varying heat flow and grain growth directions is a well-defined V-shaped pool (see the left-hand diagram in Fig. 1.7).

In contrast, the heat input at the top of a VAR ingot is less uniformly distributed because of (i) the high energy level of the arc at the centre and (ii) simultaneous radiative heat loss from a ring of melt between the electrode and crucible side surfaces. As a result, the local axial temperature gradient is small, giving a grain growth angle close to 90° to the ingot axis at the side surface and parallel (0° angle) to the ingot axis at the centre. The combined effect gives a U-shaped pool (see the right-hand diagram in Fig. 1.7).

The following issues emerge as a result of differences in pool profile between ESR and VAR ingots:

- Since a solidification structure with dendrites parallel to the ingot axis yields optimal results for further hot working, the forgeability of VAR ingots is much inferior to that of ESR ingots.
- The ESR V-shaped pool profile extends the depth of the mushy zone and enhances the interdendritic fluid flow. On the other hand, the VAR U-shaped pool results in a shorter and relatively uniformly distributed mushy zone. Hence VAR is preferred for melting segregation-sensitive alloys in order to obtain larger diameter freckle-free ingots.
- The ESR slag cap acts as a heat reservoir. This means that columnar grains grow continuously till the end of solidification and form only a small shrinkage pipe. However, the strongly radiative heat loss from the top of a VAR ingot constitutes a large negative temperature gradient. This means that columnar grains grow from the top surface of the ingot towards the bottom of the molten pool and form a deep shrinkage cavity under the solid cap. Hence VAR melting needs a more controlled hot topping practice as compared to ESR.

1.4 Solidification Defects: Superalloys

For many years there has been a substantial effort by industry to reduce melt-related defects in specialty alloys used for aerospace applications. The major concern with these defects is that they cause chemical or microstructural discontinuities that are harder or softer than the base alloy or have an interface, all of which may act as crack-initiation sites for fatigue failure. Commercial ingot production currently utilizes a sequence of remelting processes to accomplish specific goals to produce quality ingots; but even so, these processes can be sources of defects when the process parameters are not properly designed or controlled.

In this section we discuss three classes of macrosegregation defects that are of concern in the remelting of nickel-base superalloys: one is white spots, which are local depletions in strengthening elements; the second is freckles, which are enriched in a primary strengthening element; and the third is a ring pattern of equiaxed grains which occur due to thermal fluctuations and restrict columnar grain growth. All three classes of macrosegregation defects can occur in cast alloy 718, in which the primary strengthening element associated with these defects is niobium (typically 5.5 wt%). It is generally known that freckles are more prone to form at high melt rates, while white spots are more likely to occur at low melt rates [15]. Thus melters are left with a process window that is limited by the formation of these defects.

1.4.1 White Spots

In general, white spots appear as localized light-etching areas. They are typically lean in solute elements, particularly Nb and Ti, and may have a coarser grain structure than the surrounding matrix. There are several mechanisms that could account for the formation of white spots, all involving the fall-in of particles as depicted in Fig. 1.8.

The particles may come from the following:

- Residues of unmelted dendrites that fall into the ingot from the consumable electrode.
- Pieces of the ingot crown that fall into the metal pool and are not dissolved or remelted, thereby getting embedded in the ingot.
- Pieces of the ingot shelf region transported into the solidifying interface of the ingot.

All three of the above-mentioned mechanisms, individually or combined, can be considered as possible sources for white spots. This means that white spots are uniquely associated with VAR processing. To minimize the frequency of white spot occurrence, the following conditions should be observed:

- Use the maximum acceptable remelting rate permitted by the ingot macrostructure.
- Use a short arc gap to minimize crown formation and to maximize arc stability.
- Use a homogeneous electrode substantially free of cavities and cracks or inclusions. This requirement of input electrode quality for VAR has resulted in

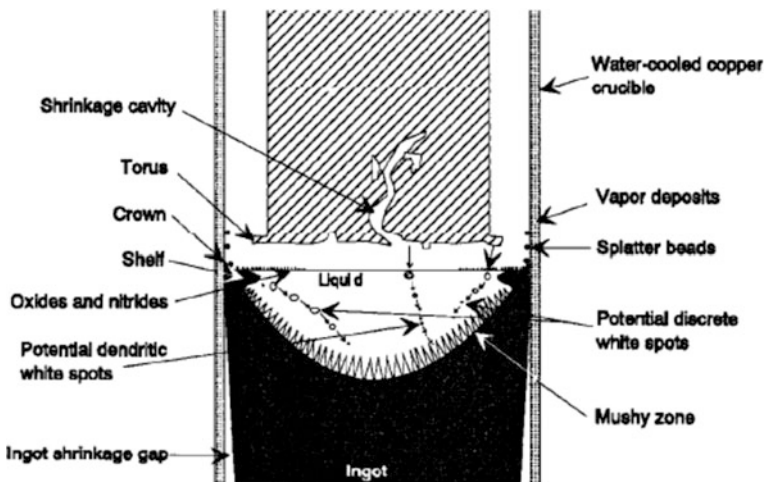


Fig. 1.8 VAR process geometry showing locations of sources for potential fall-in of discrete particles [16]

focussing on the triple melting route (VIM + ESR + VAR), since the inclusion of ESR after VIM gives a higher quality electrode for VAR.

1.4.2 Freckles

When the local solidification time (LST) is high, solidification can become sufficiently slow that the interdendritic spacing is large and the interdendritic regions combine into a continuous channel of liquid. A critical characteristic of large channels is that they become self-perpetuating. Several theories have been proposed to explain the self-perpetuating nature of freckles. They may be divided into two classes—low-density and high-density freckles:

- (i) Low-density freckles: These occur when the interdendritic liquid is less dense than the liquid in the dendritic region just above the liquidus, as occurs for alloys strengthened primarily with titanium and aluminium. Deepening of the molten pool gives rise to an extended mushy zone and encourages solute flow owing to the density differences. The freckles tend to take the form of vertical channels at slight angles to the longitudinal axis of the ingot.
- (ii) High-density freckles: These occur when the interdendritic liquid is denser than the liquid in the dendritic region, namely when the alloys are strengthened primarily with niobium. Solute flow is triggered by density differences between the two liquids. The freckles are formed radially, following the shape of the boundary between the liquid in the dendritic region and the dendrites. Alloys forming high-density interdendritic liquids also may form vertical freckles.

In general, the more highly alloyed the material, the thinner the mushy zone must be to avoid freckle formation. For a given ingot diameter, an increase in melt rate increases the mushy zone thickness and therefore favours freckle formation. Increasing ingot diameter, which decreases cooling rate, also increases the mushy zone thickness and hence the tendency for freckle formation [15].

Freckles can be avoided by optimizing the heat input to the melt pool (i) by reducing the melt rate, (ii) increasing the heat extraction through the crucible interface by inert gas cooling, and (iii) various improved melting practices. These options and possibilities are elaborated in the case study (Sect. 1.5).

1.4.3 Ring Patterns: ‘Tree Rings’

‘Tree rings’ are transverse zones of fine equiaxed grains that interrupt the continuity of a columnar grain structure. In etched transverse macrographs of VAR ingots the tree rings appear as alternating concentric dark and light rings similar in appearance

to the annular growth of rings in wood (hence their name) [17]. Although there have been no reports indicating that tree rings are detrimental to material properties, it has been observed that tree rings are associated with freckles and inclusions, since these defects are invariably associated with thermal fluctuations at the solidification front. However, it is worth noting that there is practically negligible elemental segregation across tree ring patterns.

A systematic investigation of tree rings suggests that the variation in grain growth pattern is due to a change in the pattern of heat flow at the solidification front [17]. This heat flow change is due to constricted arc stabilization as a result of higher arc power. In turn, the higher arc power results from the presence of shrinkage cavities, porosity, and heavy entrapped inclusions, which draw higher current. The higher arc power and constricted arc stabilization result in deepening of the molten metal pool and a reduction in the thermal gradient, which causes nucleation of new grains ahead of the columnar solidification front.

1.5 Case Study on Melt Processing of a Selected High-Temperature Material, Inconel 718

Alloy 718 is a nickel-base superalloy widely used for critical applications such as aerospace engine discs and blades, and oxygen storage tanks for spacecraft. Processing of this alloy is carried out via the double-vacuum melting (VIM + VAR) route, to address complex issues such as precision chemistry control, product cleanliness, and freedom from segregation-related defects. Stringent control over primary and secondary melting practices is required to produce high-quality products for the intended applications.

Alloy 718 has a wide freezing range and is prone to formation of solidification defects such as freckles after remelting. The problem is aggravated by thermal fluctuations in the liquid metal pool during solidification, resulting from improper control of remelting parameters as well as inadequate heat extraction from the crucible wall. A thorough analysis of 30 industrial VAR ingots of alloy 718 has helped in obtaining the following recommendations with respect to optimal melting practices:

- (i) The electrode for remelting should not have a secondary shrinkage cavity. This should be avoided by close control of the primary melting parameters.
- (ii) Avoid a constricted arc condition and switching to a diffused arc. This is achieved by using a drip short controller to avoid a glow condition, which occurs due to a high power arc with a longer arc gap.
- (iii) Use a suitable water-guide tube between the crucible and water jacket tube, to increase the water velocity over the crucible surface and hence the heat extraction rate.
- (iv) Use helium gas injection into the shrinkage gap to enhance the heat extraction rate.

1.6 Titanium and Its Alloys

Titanium and its alloys have found extensive application in aerospace (up to 30 % in engines and 10–20 % in *some* military airframes) by virtue of their specific strength, excellent fatigue properties and corrosion resistance, and their ability to withstand moderately high temperatures (up to nearly 600 °C for engine alloys and 350 °C for airframe alloys). The ‘workhorse’ alloy Ti-6Al-4V accounts for almost 50 % of all the titanium alloys used in aircraft [18].

Titanium melting has advanced considerably since its commercial introduction in the late 1940s. Efforts to develop effective and efficient processing techniques have included almost all of the available melting technology currently being used. Owing to their extreme reactivity, Ti alloys are processed under vacuum or inert atmosphere in a non-reactive crucible. Nowadays, the worldwide commercial processing of Ti alloys is done in consumable electrode VAR furnaces, using titanium sponge and suitable master alloys as the starting materials.

Titanium sponge and master alloys are procured against stringent material specifications to ensure extremely low levels of impurities and interstitial elements, especially nitrogen, carbon, and hydrogen. All raw materials are subjected to visual, UV light, and X-ray inspections to ensure freedom from high-density materials (W, WC, etc.) and hard TiN inclusions. Such materials represent localized stress concentrations and fatigue crack nucleation sites [19]. The titanium sponge and alloying elements are thoroughly mixed in a double-cone mixer and compacted in a press to produce briquettes. These are then plasma welded together to produce an electrode [20]. (TIG welding is not recommended for making electrodes, owing to possible contamination by high-density inclusions originating from the W welding electrodes).

Processing by VAR provides an opportunity to carry out progressive melting and solidification in a copper crucible under vacuum. The high temperature under the arc and the stirring action due to the magnetic field ensure effective dissolution of alloying elements, even those with high melting points, and also their uniform distribution in the melt pool. A steep thermal gradient ahead of the solidification front permits directional solidification, thereby helping to produce a dense, homogeneous, and segregation-free ingot.

For optimal forgeability and economic yield the VAR ingot must have a good surface, which can only be achieved with a high melting rate [21]. However, high melt rates combined with the low thermal conductivity of Ti alloys create a deep metal pool that results in equiaxed solidification in the ingot centre: this is undesirable because it is associated with macrosegregation and porosity [22]. Hence there is a restricted window for melting, governed by the conflicting requirements of higher surface quality (higher melt rate) and segregation control (lower melt rate). This restriction also places severe limitations on the maximum size of high-quality Ti alloy VAR ingots [21].

Defect-free Ti alloy ingot production is a big challenge and is one of the most important goals in research to improve remelting technologies such as VAR.

Defects may originate from foreign particles present in the raw material, such as hard alpha TiN (α -I defects) or high-density W/WC particles and segregation-related solidification defects such as α -II and β -flecks [23].

The survival of TiN particles depends on melt rate and the duration of their stay in the liquid pool. Strongly floating particles are rapidly dissolved by the arc superheat at the pool surface. Larger and higher density sinking particles are of major concern, since they rapidly settle to the pool bottom, where they may not dissolve because the alloy liquidus is below the melting temperature of TiN. This is why multiple VAR steps are followed.

The α -II and β -flecks are segregation-related defects arising during solidification. α -II defects are caused by localized α segregation, but unlike the hard α -I defects they are quite ductile and relatively harmless. In highly alloyed materials β -flecks occur due to interdendritic fluid flow (similarly to freckle defects in superalloys and steels); while in leaner alloys, the β -flecks occur from the redistribution of elements during the formation of equiaxed grains in the centre of the ingot [23]. Both the α -II and β -fleck defects are best controlled by using lower melt rates and maintaining a steeper temperature gradient at the solidification interface to facilitate directional solidification [23]. Also, during a subsequent intermediate stage of hot working some reduction in β -fleck sizes can be achieved by heating to a temperature just above the β -transus.

1.7 Secondary Metallurgical Processes

Secondary metallurgical processes are extensively used for manufacturing high-quality steels suitable for aerospace. One of the important aspects of secondary metallurgy is the use of vacuum environments, which not only help in decarburization and degassing but also prevent melt contamination from a surrounding atmosphere, and also permit precise chemistry adjustment. Addition of high-basicity synthetic slags to the liquid metal and argon purging from the melt bottom are extremely effective for controlling desulphurization, deoxidation, degassing, and inclusions in steels in a single process step. Table 1.2 summarizes the metallurgical benefits derived from different secondary metallurgical processes [24].

It is also worth noting that feedback from process modelling helps in optimizing the metallurgical reactions to produce very high-quality liquid metal with very low levels of gases, impurity, and inclusion levels.

1.8 Indian Scenario

Hindustan Aeronautics Limited (HAL) has numerous production units across India and is the major public sector aerospace metal and component manufacturer in India. Several units of this organization are also involved in production of spares

Table 1.2 Advantages of secondary metallurgical processes

Quality improvement	Secondary metallurgical processes					
	LF	VD	LF–VD	VAD	VOD	VID
H ₂ removal	–	gp	gp	gp	se	gp
N ₂ removal	–	se	se	gp	gp	gp
Deoxidation	se	gp	gp	gp	se	gp
VCD	–	gp	gp	gp	gp	gp
Desulphurisation	gp	gp	gp	gp	gp	se
Inclusion removal	se	gp	gp	gp	se	se
Extra low C	–	–	–	–	gp	gp
Temperature control	gp	se	gp	gp	se	se

gp Good possibilities; *se* Secondary effects; *LF* Ladle furnace; *VD* Vacuum degassing; *VAD* Vacuum arc degassing; *VOD* Vacuum oxygen decarburisation; *VID* Vacuum induction degassing

and accessories, as well as in aeronautical stores refurbishment. MIDHANI (Mishra Dhatu Nigam Limited), Hyderabad, is another principal special metal and alloy processing centre. This organization has been manufacturing primary and secondary aeronautical metals, alloys, and components, primarily for Indian defence and space, for the last 4–5 decades. Several other Indian industries are also involved in producing various aeronautical stores, which include several public sector units of ordinance factories; Bharat Dynamics Limited; various aluminium alloy production agencies (NALCO, BALCO, Vedanta Group, etc.); L&T (especially through NPCL–L&T joint venture); TATAs; and several small- and medium-scale industries—Star Wire, Gaziabad (speciality ESR and alloy steels); Kalyani Carpenter, Pune (special metals and alloys, forgings, and intricate aero components); IPCL, Bhavnagar (intricate investment castings); AV Alloys, Hyderabad (ESR alloys); Sandvik Materials Technology, Pune (tube, pipe, strip, wire, and metal powders); Kalva Engineers Pvt. Ltd., Hyderabad (tubes, rods, sheets, and strips); Nexgen Inc. (special metals), Secunderabad; Sanghvi Forging and Engineering Ltd., Vadodara (alloy steel forgings); Manjeera Machine Builders, Rachamalla Forging, Deccan Smith Pvt Limited, Fine Forge—units of Hyderabad, all specialized in open- and closed-die forgings.

Several new and augmented production facilities are fast emerging to cater for the ever-expanding needs of various Indian space and aeronautical programmes.

1.9 Summary

Quality and reliability have been the foremost concern during the manufacture of high-performance aerospace alloys. To meet the challenging demands the primary melting technologies have continuously evolved over the years. Introduction of furnaces with improved design, the installation of programmable controls in

combination with process computers for automation, has provided better reproducibility between melts. These improvements have been aided by various aspects of process modelling, which has not only improved the basic understanding of the metallurgical reactions, but also provided insights into the origins of defects in the products.

Acceptance standards with respect to metal cleanliness, impurity levels, and structural homogeneity have become steadily more stringent in the course of time. Such stiff demands can scarcely be met by classical melting and casting methods. Remelting technologies such as VAR or ESR, with controlled solidification in water-cooled crucibles, have largely enabled meeting the stringent requirements. However, the manufacture of larger diameter (>500 mm) defect-free remelted ingots from highly alloyed and segregation-prone materials still remains a major challenge. Evolution of advanced model-based control systems, which provide direct access to the solidification process to control pool depth and profile during remelting, is expected to mitigate the problems and ensure the reproducibility and reliability of high technology products for the aerospace industry.

Acknowledgments The authors are grateful to the reviewer and editors for their critical comments and numerous modifications. They would like to thank several sister organizations for their continued support in metal, alloy, and product development and qualification, especially the Defence Metallurgical Research Laboratory and CEMILAC, DRDO, and DGQA. They wish to also acknowledge the support and funding from the Department of Defence Production, New Delhi.

References

1. Vacuum Induction Melting Technology—A unique electrical method for production of high quality and reliable alloys needed in critical applications (1987) A publication of the Center for Metals Production—An EPRI Sponsored R&D Applications Center 3(3)
2. Hasenhündl R, Presoly P, Schützenhöfer W, Tanzer R, Hildebrand F, Reiter G (2007) Vacuum induction melting—optimisation of pressure dependent reactions. In: Lee P (ed) Proceedings of the 7th international symposium ‘Liquid metal processing and casting’. Nancy, France, pp 289–294
3. Sinha OP, Chatterjee M, Sharma VVRS, Jha SN (2005) Effect of residual elements on high performance nickel base super alloys for gas turbines and strategies for manufacture. *Bull Mater Sci* 28(4):379–382
4. Winkler O, Bakish R (1971) Vacuum metallurgy. Elsevier Publishing, New York, USA
5. Jarczyk G, Franz H (2012) Vacuum melting equipment and technologies for advanced materials. *Arch Mater Sci Eng* 56(2):82–88
6. Chatterjee M, Panikishore A, Gopalakrishna B, Narayana Rao M (2011) Performance evaluation of a Nickel base cast superalloy processed in equiaxed and directionally solidified modes for gas turbine applications. In: Mathew JMK, Williamson RL, Bellot PJ, Jardy LN (eds) Proceedings of the 9th international symposium ‘Liquid metal processing and casting’. Nancy, France, pp 275–280
7. Hoyle G (1983) Electroslag processes—principles and practice. Applied Science Publishers, London, UK

8. Bruckmann G, Choudhury A (1987) Status of remelting process under slag. *Spec Bull* 36. S11.02:5
9. Nafziger RH (1976) Thermochemistry of ESR process. *Bull US Bur Mines* 669:27
10. Choudhury A, Jaunch R, Tince F (1979) In: Bhat GK, Schlatter R (eds) *Proceedings of the 'Vacuum metallurgy: 6th international conference on special melting'*. American Vacuum Society, San Diego, USA, p 785
11. Hawkins RJ, Davies MW (1971) Thermodynamics of FeO bearing CaF₂ based slags. *J Iron Steel Inst* 226
12. Electro slag remelting (2010) A technical information brochure by ALD vacuum technologies
13. Williamson R, Beaman JJ, Atkin RM (2011) VAR control using a reduced order ingot pool depth model. In: Mathew JMK, Williamson RL, Bellot PJ, Jardy LN (eds) *Proceedings of the 9th international symposium 'Liquid metal processing and casting'*. Nancy, France, pp 33–40
14. Yu KO, Domingue JA, Flanders HD (1985) Control of Macro Segregation in ESR and VAR processed IN 718. In: Österreich E (Ed) *Proceedings of the 8th international conference 'Vacuum metallurgy-special melting/refining and metallurgical coating under vacuum or controlled atmosphere'*. Austria, p 1279
15. James A, Avyle VD, Brooks JA, Powell AC (1998) Reducing defects in remelting processes for high-performance alloys. *J Met* 50(3):22–25
16. Mitchell A (1986) White spot defects in VAR superalloy. In: Lherbier LW, Bhat GK (ed) *Proceedings of the 'Vacuum melting conference on specialty metals melting and processing'*. American Vacuum Society, Warrendale, USA, pp 55–61
17. Xu X, Ward RM, Jacobs MH, Lee PD, McLean M (2002) Tree-ring formation during vacuum arc remelting of INCONEL 718: Part I. Experimental investigation. *Metall Mater Trans A* 33 (6):1795–1804
18. Jaeger H, Mayerhofer J, Tarmann R (1984) Recycling of titanium scrap for the production of high-duty aerospace components. In: Lütjering G, Zwicker U, Bunk W (eds) *Titanium Science and Technology: Proceedings of the fifth international conference on titanium*, vol 1. Oberursel: Deutsche Gesellschaft für Metallkunde, Munich, Germany, p 257
19. Dresty JE (1984) Process of removal of high density inclusions from titanium turnings for premium quality ingots. In: Lütjering G, Zwicker U, Bunk W (eds) *Titanium science and technology: Proceedings of the fifth international conference on titanium*, vol 1. Oberursel: Deutsche Gesellschaft für Metallkunde, Munich, Germany, pp 225–232
20. Bomberger HB (1980) Segregation in titanium alloys. In: Kimura H, Izumi O (eds) *Titanium '80, science and technology: Proceedings of the fourth international conference on titanium*, vol 2. Metallurgical Society of AIME, Kyoto, Japan, p 2197
21. Mitchell A (1997) Melting casting and forging problems in titanium alloy. *J Met* 6:40–43
22. Suzuki K, Fukuda N (2007) Optimization of VAR process by applying computational simulations. In: Niinomi M, Gakkai NK (eds) *Ti-2007 science and technology: Proceedings of the 11th world conference on titanium (JIMIC5)*. Japan Institute of Metals, Kyoto, Japan, p 159
23. Mitchell A, Kawakami A, Cockcroft SL (2006) Beta flecks and segregation in titanium alloy ingots. *High Temp Mater Process* 25(5–6):337–349
24. Bruckmann G, Choudhury A, Schlebusch DW (1987) Vacuum metallurgy and its potential - a general overview of secondary metallurgy systems. *Leybold AG Spec Publ* 36.S11.01:3–15

Chapter 2

Processing of Aerospace Metals and Alloys: Part 2—Secondary Processing

S. Narahari Prasad, P. Rambabu and N. Eswara Prasad

Abstract The basics of different techniques of secondary processing of metals and alloys are presented and discussed. This chapter will also provide details of the processing of superalloys (nickel- and cobalt-based) and steels.

Keywords Secondary processing · Metal forming · Steels · Titanium alloys · Nickel superalloys

2.1 Introduction

Metallic materials are initially consolidated by a primary melting process into ingot, billet or bloom, that are subsequently shaped into various forms for commercial applications. The resultant mechanical properties are determined by the combination of alloy design and thermo-mechanical processing that involves hot deformation and heat treatment to obtain the right microstructure [1–10].

Secondary processing such as forging, hot rolling, closed-die forging, precision forging, radial forging, ring rolling, extrusion, cold rolling, and cold drawing of wires and tubes is the backbone of modern manufacturing industries, as well as being a major industry itself. In most of the secondary processing operations the shapes of the products depend on the nature of plastic deformation that the metal undergoes [1, 9]. Hence it is essential to study the influence of various plastic flow/deformation mechanisms on the processing as well as the properties of the as processed material. Also one needs to study the effects of processing conditions and the intensity (extent of) of processing on the properties.

S. Narahari Prasad (✉)
Mishra Dhatu Nigam Limited, Hyderabad, India
e-mail: narahari_prasad1965@yahoo.co.in

P. Rambabu
RCMA (Materials), CEMILAC, DRDO, Hyderabad, India

N. Eswara Prasad
DMSRDE, DRDO, Kanpur, India

The plastic flow properties are influenced by factors such as selection of tool geometry, equipment, tool and die material; and processing conditions such as workpiece, die temperatures and lubrication. Because of the complexity of deformation processes, analytic, physical or numerical models are relied on to aid in designing such processes to ensure the reproducibility of physical and mechanical properties. It is important to note that metal forming processes provide materials for further processing in order to obtain final products, either fully finished or semi-finished.

Most of the metal working process requires a combination of properties for successful forming. The three most important factors are reduction (strain), rate of reduction (strain rate), and temperature of the workpiece at any time. For heat-resistant alloys the parameters are designed to obtain better stress rupture, creep, and low-cycle fatigue life. Hence the aims are uniform grain refinement, controlled grain flow and structurally sound components.

In order to get the best properties from an alloy, the starting material has to be of the highest quality. This means the use of advanced melting techniques to obtain low gas and inclusion contents and reduced ingot segregation. This is followed by ingot breakdown, homogenization and final finishing procedures that ensure a sound and microstructurally uniform product.

One of the most important aspects of secondary processing is the workability of a metal or material, which includes forgeability, rollability, extrudability and formability. Workability of any material depends not only on the microstructure of the material, but also on the external processing parameters such as applied temperature, strain rate and strain, and more importantly the stress state in the deformation zone. In this context, the use of a processing map, which is an explicit representation of the microstructural response to the imposed process parameters, is almost essential.

A processing map involves superimposing a power dissipation map on an instability map developed from dynamic materials modelling. Such a map for metallic materials shows several safe domains for processing in terms of temperature and strain rate, and may also contain regions of flow instability and cracking that should be avoided.

2.2 Fundamentals of Metal Forming

Casting, machining, joining and deformation are the four most fundamental metal working or processing technologies. Casting makes good use of the fluidity of a metal in the liquid state to take the mould shape as it solidifies. Machining of blanks (half-products) provides the final desired shape with good accuracy and precision, but much material is removed, resulting in low yield. Joining processes can be used to fabricate complex shapes starting from simple shapes, and these processes have a wide range of applications.

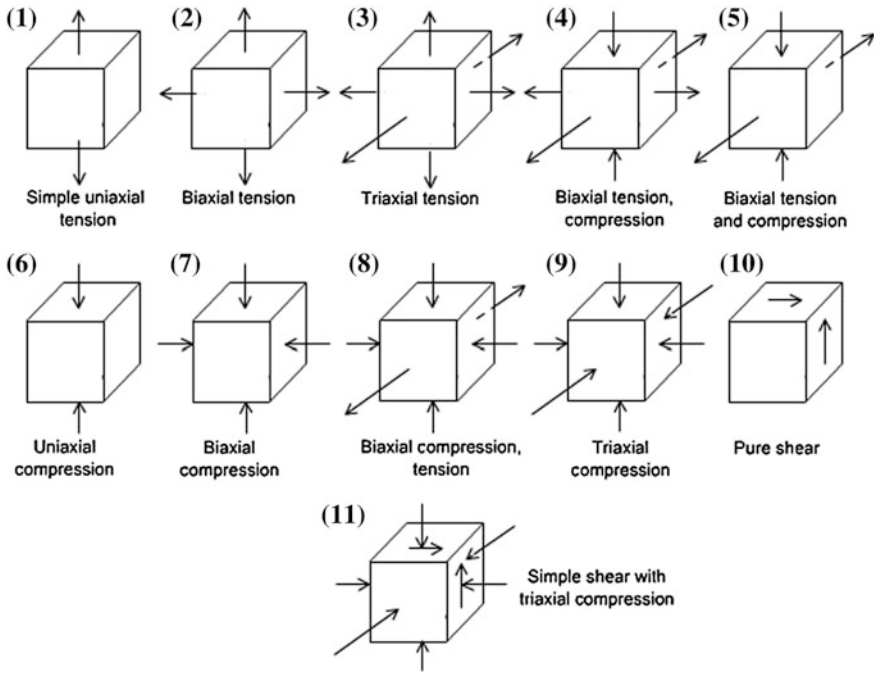


Fig. 2.1 Stress states during metal deformation and forming

As a metal is deformed into a useful shape, it experiences stresses such as tension, compression, shear, or various combinations of these. Figure 2.1 illustrates these stress states.

In order to deform the metal, one has to employ stresses that produce permanent plasticity, which occurs when one exceeds the elastic deformation conditions. Further, to deform the metal by cold working (that is when the working temperatures are less than 0.4–0.45 times the homologous temperature—the melting temperature expressed in Kelvin scale, designated as T_M), one has to use pressures that are much higher than those for hot working (working temperatures $> 0.45 T_M$). Often a combination of hot and cold working is used. When metals are cold-formed there is no grain recrystallization and no dynamic recovery from the induced deformation. As deformation proceeds, the resistance increases owing to strain hardening. In general, this refers to resistance build-up in the grains by the generation of dislocations and crystal lattice distortions.

One more metal deformation process which is carried out at temperatures intermediate to hot and cold forming is called warm forming. Advantages and disadvantages of cold, warm and hot forming processes are shown in Table 2.1.

Table 2.1 Advantages and disadvantages of cold, warm and hot forming

Forming process	Advantages	Disadvantages
Cold working	Good surface finish and dimensional control Better strength, fatigue (steels), and wear properties owing to strain hardening Directional properties may be imparted	Higher forces with heavier and more powerful equipment are required: hence higher cost Intermediate annealing may be one of the additional requirements Unacceptable levels of residual stresses may be produced
Warm working	<i>Compared to cold rolling</i> Lesser loads on tooling and equipment Greater metal ductility <i>Compared to hot forming</i> Better surface finish, closer dimensional accuracy Lesser scaling and decarburization Reduced tool and die wear	Virtually no significant disadvantages
Hot working	No strain hardening Less force required for deformation, and hence, larger components may be manufactured Lower capacity equipment sufficient (reduces equipment costs) No residual stresses in the material Reduces segregation and thus the structure becomes more homogenous	Needs external heating Poor surface finish Surfaces will often get oxidized Less accuracy and dimensional control of components Reduced life of tooling and equipment

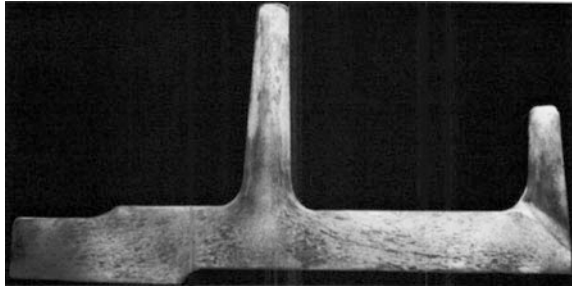
2.3 Bulk Deformation Processes

Considerable effort is required for the design and optimization of bulk metal working processes. For example, defects introduced at one stage are carried forward and amplified downstream. Therefore the optimization of processing parameters during thermo-mechanical processing is very important to produce defect-free products. Some of the important processes are discussed in the following subsections.

2.3.1 Forging

Forging is a process in which material is shaped by the application of localized compressive forces exerted manually or with power hammers, presses or special forging machines. The process may be carried out on materials in either the hot or cold state. When forging is done cold, the processes are given special names. Therefore the term ‘forging’ usually implies hot forging carried out at temperatures above the recrystallization temperature of the material.

Fig. 2.2 Directions of grain flow in a closed-die forging



Forging is an effective method of producing many useful shapes. The forged parts have good strength and toughness, and they can be used reliably for highly stressed and critical applications. This improvement in properties occurs because forging (i) breaks up the metal ingot dendritic structure and associated segregation, heals porosity, and aids homogenization; (ii) produces a fibrous grain structure that enhances mechanical properties parallel to the grain flow. The three most important categories of forging that are widely used are as follows: (i) open-die forging, (ii) closed-die forging (see Fig. 2.2 for the nature of grain flow in a closed-die forged metal piece) and (iii) press forging. Yet another important category is net shape or precision forging, and this route in general has the following benefits:

1. Greater strength to weight ratio.
2. Elimination of welding: Switching to closed-die forging from multipart welding leads to cost reduction, in addition to property improvement.
3. Reduced inspection and testing: As there are no welds, inspection is easier.
4. Replacing assemblies, fabrications: cost saving is usually achieved when forgings replace complex fabrications and assemblies.
5. There is no doubt that precision forging is more economical than fabricating metal components by extensive machining, particularly when the parts requirement is large. There are also limitations on the maximum size that can be handled through machining.
6. Quicker production, shorter delivery: less machining; faster turnaround.
7. Design optimization: Further cost reduction may be achieved by optimizing pre-forging shape/size, blocker forging design, reducing draft angle, tolerances, testing material, etc.

No other metal working process (casting, welding, machining, etc.) permits this degree of grain size and shape control and consequent property enhancement.

2.3.2 Rolling

The second most important secondary processing method is ‘rolling’. It consists of passing metal between two rollers which exert compressive stresses and reduce the metal thickness. Rolling is important because it is very versatile, capable of producing many shapes, and also it is economical. Rolled products include sheets, structural shapes and rails, as well as intermediate shapes for wire drawing or forging, circular shapes, ‘I’ beams and railway tracks. The latter two types of product are manufactured using grooved rolls.

2.3.3 Extrusion

This is a process used to create objects of a fixed cross-sectional profile. In this process a material is pushed or pulled through a die of the desired cross-section in a continuous or non-continuous manner. The two most important extrusion processes are as follows: (i) hot extrusion and (ii) cold extrusion. There are several advantages of an extrusion process. Two main advantages of extrusion over other manufacturing processes are the ability to create very complex cross-sections, and to work materials having limited ductility, since only compressive and shear stresses are involved. Extrusion also forms parts with an excellent surface finish.

The other important, but less versatile secondary processing methods are pilgering and drawing.

2.4 Secondary Processing for Specific Aerospace Materials

Aerospace specifications call for stringent quality requirements with respect to careful selection of raw materials, primary melting techniques, material processing steps, chemistry limits, low inclusion contents and microstructures.

2.4.1 Titanium Alloys

Secondary processing of titanium alloys is discussed extensively in Chap. 6 of Volume 1 of these Source Books and in Ref. [11].

2.4.2 Superalloys

Secondary processing of nickel-base superalloys is discussed to some extent in Chap. 9 of Volume 1 of these Source Books and in Refs. [12, 13]. Some additional information will be given here.

Superalloys are high-performance materials designed to provide high mechanical strength and resistance to surface degradation at high temperatures. They combine high tensile, creep rupture and fatigue strengths; good ductility and toughness; and excellent resistance to oxidation and hot corrosion. Additionally, superalloys are designed to retain these properties during long-term exposure at elevated temperatures.

Increased knowledge of the alloy system(s) has resulted in thermo-mechanical treatments that improve the properties of forgings, notably the creep resistance and high- and low-cycle fatigue crack resistance.

The material characteristics that largely influence workability are flow stress and ductility. As these alloys are designed to resist high temperatures, they are difficult to work because of their very high flow stress and limited ductility. The workability largely depends on cleanliness.

The hot working temperature is chosen such that the majority of precipitates are in solution. The high concentrations of dissolved alloying elements give rise to higher flow stresses, higher recrystallization temperatures and lower solidus temperatures. These factors limit the useful hot working temperature range. Furthermore, the alloy ductilities are influenced by the deformation temperature, strain rate, prior history of the material, composition, degree of segregation, cleanliness, and the stress state imposed by the deformation process.

Hot Working Cycles: Superalloys have low thermal conductivity and hence need to be heated to the hot working temperature at a slow rate. The forging temperature depends on the composition of the alloy and to some extent on the heat treatment and end use. High forging temperatures cause grain growth in most heat-resistant alloys; thus the forging temperature ranges are relatively narrow and temperatures must be precisely controlled. Lower hot working temperatures have positive effects on the workpiece, but will increase the forging load and erode the dies.

It is not essential to maintain a particular atmosphere for heat-resistant alloys. However, high-sulphur fuel should be avoided as it may contaminate the material. In such cases it may be better to use electrically heated furnaces, which also allow closer temperature control. For liquefied petroleum gas (LPG)-heated furnaces the atmosphere may be maintained from neutral to oxidizing. Alternatively, providing a protective atmosphere will result in cleaner surfaces.

Temperature measuring instruments should record the heating cycle so that temperature variations during loading and discharge are recorded. These measurements will also help in estimating the right time required for reheating. Forging stock needs to be continuously monitored for temperature during hot working, and when the lower limit of hot working temperature is reached, the stock has to be

recharged into the furnace. The temperature of the stock has to be raised to the hot working temperature and the stock soaked for an appropriate period. Long soaking periods are not required for reheating the stock as the material has high internal heat content.

Forging dies may be heated with gas- or kerosene-fired torches so that heat loss due to the dies is reduced.

Iron-Base Superalloys: These alloys are superaustenitic stainless steels alloyed with reactive elements such as titanium, aluminium, boron and niobium, and they respond to solution treatment and ageing. The forging practices of these alloys are in many ways similar to those for austenitic stainless steels.

These alloys are alloyed with aluminium and titanium that may form nitride and carbonitride segregations, which develop into stringers and affect the forgeability. The inclusion content also affects the hot working of the alloy, and so the melt route and processing should account for this.

Nickel-Base Alloys: All nickel-base alloys are less forgeable than the iron-base alloys, requiring more force to produce a given shape. The forging processes are highly refined to control temperatures, strain rate, strain and alloy condition. These controls are necessary to achieve uniform critical properties such as grain size and other characteristics after heat treatment. In addition, the alloys are sensitive to minor variations in composition, which can cause large variations in forgeability, grain size and final properties.

Cobalt-Base Alloys: Hot workability of cobalt-base alloys is difficult, since they contain carbon and form hard carbides. They require comparatively higher pressures than iron-base alloys. The cobalt-base alloys need to be reheated repeatedly in order to recrystallize the workpiece and lower the forging pressure.

Forging parameters such as temperature and amount of reduction have considerable effect on the grain size. Coarse grains are associated with low ductility, notch brittleness and low fatigue strength. Hence close control of the forging parameters and final heat treatment is necessary.

Cobalt-base alloys are characterized by low thermal conductivity, and they need to be heated slowly to the soaking temperature to attain temperature uniformity. The amount of forging and reduction will depend on the forging operation and component design. These alloys are prone to grain coarsening when the material is heated above 1175 °C, so the initial reduction is small to consolidate the surface, and the reductions are gradually increased with decreasing cross-section. The reheating time also becomes shorter.

Forging reductions should be such that they induce sufficient strain in the material to cause recrystallization during the reheating period. The final reduction should be close to 20 % so that after subsequent solution treatment the microstructure consists of fine grains.

2.4.3 *Special Steels*

High-Strength Low-Alloy Steels: These are readily forged into a wide variety of shapes using hot-, warm- or cold-forging processes. Despite the large number of available compositions, all of the materials in this category exhibit essentially similar forging characteristics. Carbon content of the steel has the most influence on the upper limit of forging temperatures, which decrease with increasing carbon content.

The hot forging of carbon and alloy steels into intricate shapes is rarely limited by forgeability aspects. Section thickness, shape complexity and forging size are limited primarily by the cooling that occurs when the heated workpiece comes into contact with the cold dies. For this reason, equipment that has relatively short die contact times, such as hammers, is often preferred for forging intricate shapes in steel.

Maraging Steels: These require higher forces for forging since they are highly alloyed. However, they can be forged easily into any shape.

Stainless Steels: The stainless steels, especially the martensitic and precipitation hardening (PH) grades are used as structural materials where a combination of high strength as well as corrosion resistance is required. The PH stainless steels in particular have good strength, toughness, corrosion resistance, fabricability and weldability, and comprise an important class of engineering materials for aerospace applications. They can be used in corrosive environments and at temperatures up to 350 °C.

In the case of austenitic and martensitic stainless steels the high temperature phase delta ferrite will form if the hot working temperature is not restricted. Thus all reheating and cooling operations should be optimized to ensure freedom from phases that could interfere with the product quality and mechanical properties.

Stainless steels require higher forging pressures and are considerably more difficult to forge than low-alloy steels, because of their higher elevated temperature strength and also the limitations on the maximum temperatures at which stainless steels can be forged. Forging load requirements vary very much with different types of stainless steels; the most difficult alloys to forge are those with the greatest strength at elevated temperatures.

2.5 Recent Advances in Secondary Processing

2.5.1 *Rapid Prototyping Using LENS*

Laser engineered net shaping (LENS) is a novel rapid prototyping process [14, 15]. It comprises a diverse set of techniques which involve continuous flowing of

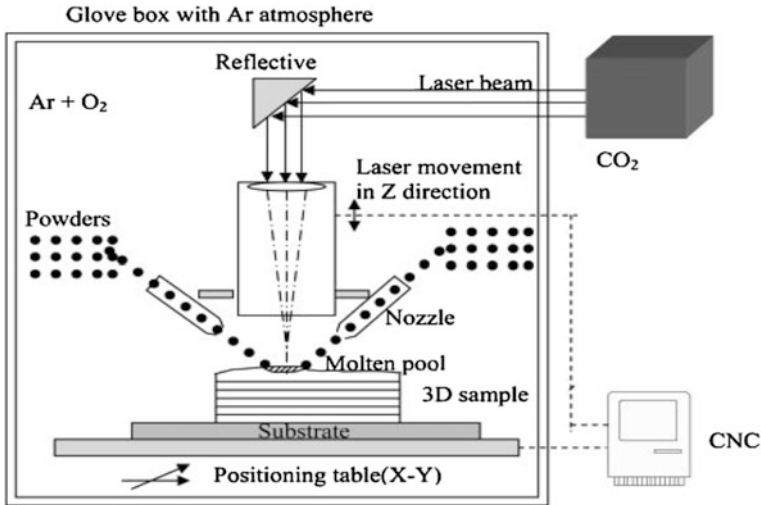


Fig. 2.3 Schematic of LENS process

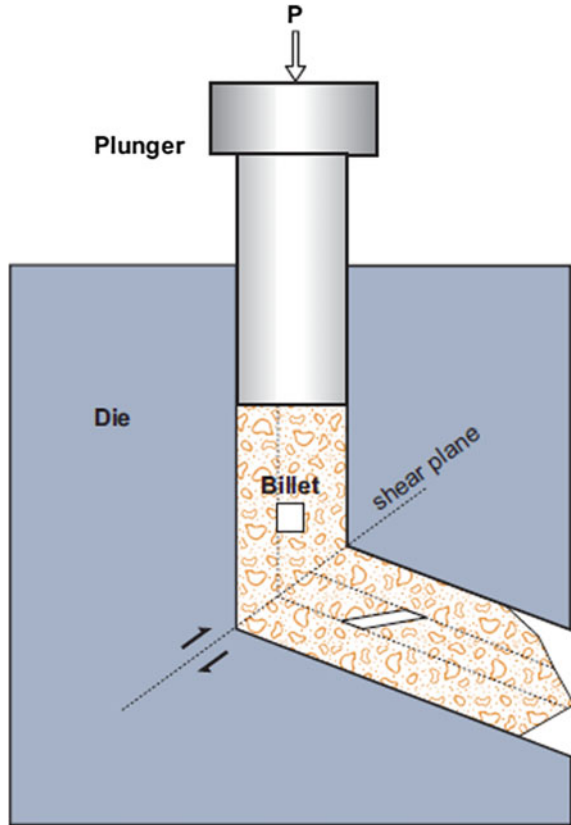
metallic powders into a melt pool that is generated on a substrate material by a focused high power laser beam as shown in Fig. 2.3.

A proper synchronization of the actions of the deposition head (consisting of powder flow mechanism and laser column), the software and the computer numerical control (CNC) platform, enables 3-D functional parts to be realized by depositing line by line, and layer by layer. An inert gas shroud is used to shield the melt pool from atmospheric oxygen for better control of properties. Parts have been fabricated by LENS processing from numerous materials including stainless steels (316, 316L, 17-4 PH), nickel-base alloys (INCO designations 718, 625, 600 and 690), tool steel (H13) and the titanium alloy Ti-6Al-4V. The resultant mechanical properties confirm the LENS process as a viable method for fabricating structural components [16].

2.5.2 Equal-Channel Angular Extrusion (ECAE)

ECAE enables deforming a billet of bulk material by shear without changing its overall dimensions. The die is formed from two channels with equal cross-section. These intersect to form a sharp corner, e.g. 90° or 120°. As the billet is pressed through the die it deforms by shear at the die corner. Since the billet dimensions are unchanged by the processing, the deformation can be repeated several times to obtain ultrahigh strain levels. A schematic is shown in Fig. 2.4.

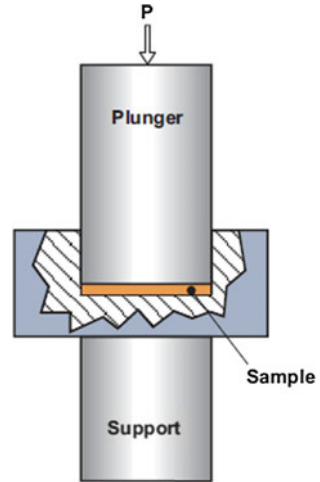
Fig. 2.4 Schematic of the ECAE process



ECAE processing can be varied by changing the die angle, and also by rotating the billet between successive passes. Billet rotation between passes requires round or square cross-sections.

Materials processed by ECAE include aluminium, magnesium and titanium alloys, copper and tungsten. The grain sizes obtained from ECAE are mostly larger than 100–150 nm, irrespective of the metal or alloy. Thus ECAE materials are not truly nanocrystalline (nc), but rather ultrafine-crystalline (ufc)—also called ultrafine-grained (ufg). The more recent research on ECAE is largely concerned with modelling and determining the processing parameters that affect and control the material homogeneity.

Fig. 2.5 Schematic of the HPT process



2.5.3 High-Pressure Torsion (HPT)

A disc-shaped sample with thickness 0.2–0.5 mm is placed between support and plunger anvils and compressed under a pressure of several GPa. The plunger anvil is rotated, and friction causes shear straining of the sample (see Fig. 2.5).

Owing to the high pressure, high strains can be imposed without fracture of the sample. HPT is convenient for investigating the influence of different parameters on the evolution of nanotechnology microstructures and their bulk properties, since it is relatively straightforward to adjust and control the cumulative strain, applied pressure and deformation speed. However, HPT is not a contender for manufacturing nanotechnology bulk metals.

2.5.4 Cryomilling

Cryomilling involves ball-milling attrition (repeated mechanically-induced fragmentation and coalescence) of elemental or alloy powders in liquid nitrogen, whereby mixtures of elemental powders undergo mechanical alloying. The starting powders are often spherical, or at least fairly regular in size. During attrition the powder particles are first flattened and then undergo concomitant fragmentation or coalescence.

The overall effect of attrition is eventually to produce powder particles with nanoscale grain sizes, which can be as small as 15–30 nm. However, the powders have to be consolidated to bulk metal, for example by vacuum degassing, hot (HIP) or cold (CIP) isostatic pressing and extrusion. Any heat treatments (e.g. HIP) during consolidation inevitably cause grain growth, such that the microstructures are ufc or even microcrystalline (mc), i.e. grain sizes in the submicrometre (100–1000 nm) to micrometre range (>1000 nm).

Cryomilling has been particularly successful—as a grain size reduction technique—for aluminium alloys. This is because the milling process results in nano-dispersions of oxides and nitrides that help to inhibit grain growth during consolidation. However, these particles are detrimental to the ductility. There are also problems in controlling material purity and obtaining full density in the consolidated product. And, of course, the entire production process, *which includes manufacturing the elemental or alloy powders to close specifications*, is much more costly than obtaining bulk materials by conventional ingot metallurgy.

2.5.5 Vacuum Plasma Spray (VPS) Forming

The VPS process first requires the synthesis of a pre-alloyed powder by inert gas atomization. The powder particle size and shape need to be closely controlled, in order to achieve optimum flow during subsequent vacuum (low pressure) plasma spraying. After spraying to the required thickness, the spray deposit is removed from the substrate. VPS deposits are characterized by a multiscale microstructure. The overall microstructure consists of splats, intersplat boundaries and porosity. As with cryomilling, the VPS process requires manufacturing metal powders to close specifications before obtaining the final product. This is a major cost disadvantage, even though consolidation is relatively straightforward.

2.5.6 Electrodeposition

This method has been used to make thin bulk samples for *model material* research, especially nickel and binary nickel alloys. Conventional electrodeposition under continuous direct current conditions can produce fine-grained nickel down to the nc range, but apparently only for sample thicknesses $\sim 20\text{--}30\ \mu\text{m}$. Thicker samples are obtainable from a patented process of pulsed direct current electrodeposition. Grain sizes can be closely controlled in the nc, ufc and mc ranges for sheets with thicknesses of $100\text{--}150\ \mu\text{m}$. It is possible to obtain thicknesses in the millimetre range, but through-thickness grain uniformity and processing-induced residual stresses become potential or actual problems.

2.6 Summary

The basics of different types of secondary processing techniques and the choice of techniques for particular types of products are discussed. The technology of manufacturing most of the advanced alloys is available in India, but there is a size (capacity) gap between the available processing facilities and the needs of the aerospace industry. Secondary processing facilities like rolling mills capable of

producing larger sheets and plates, and forging presses with higher capacity are required for indigenous processing, so that imports can be reduced or avoided.

Acknowledgments The authors would like to thank several sister organizations for their continued support in metal, alloy and product development and qualification, especially the DMRL and CEMILAC, DRDO, as well as DGAQA. They wish also to acknowledge the support and funding from the Department of Defence Production, New Delhi, and DRDO, New Delhi.

Bibliography

1. Dieter GE (1987) Mechanical metallurgy. McGraw-Hill Book Company, Singapore
2. ASM Handbook (1996) Volume 14. Forming and Forging. ASM International, USA
3. ASM Handbook (2005) Volume 14A. Metal working, bulk forming. ASM International, USA
4. ASM Handbook (2006) Volume 14B. Metal working, sheet forming. ASM International, USA
5. Bralla JG (2006) Handbook of manufacturing processes. Industrial Press Inc, New York, USA
6. Altan T, Oh S, Gegel H (1983) Metal forming, fundamentals and application's. ASM International, USA
7. Prasad YVRK, Sridhara S (1997) Hot working guide. ASM International, USA
8. Hutchinson B, Anderson M (1996) Thermomechanical processing. ASM, Sweden
9. Dieter GE, Kuhn HA, Semiatin SL (2003) Handbook of workability and process design. ASM International, USA
10. Theis HE (1999) Handbook of metal forming processes. Marcel Dekker Inc., New York, USA
11. Bridges PJ, Magnus B (2001) Manufacture of titanium alloy components for aerospace and military applications. Paper presented at RTO-AVY specialists meeting on cost effective applications of titanium alloys in military platforms. Loea, Norway, 7–11 May 2001
12. Jovanovic MT et al. Processing and some applications of nickel, cobalt and titanium-based alloys, Metallurgija. J Metall 13:91–106
13. Pollock TM, Tin S (2006) Nickel-Based superalloys for advanced turbine engines: chemistry, microstructure, and properties. J Propul Power 22(2):361–374 (March–April 2006)
14. Hofmeister W, Griffith M, Ensz, JS (2001) September, p 30
15. Pinkerton AJ, Li L (2005) Int J Adv Manuf Technol 25:471
16. Wanhill RJH (2007) Engineering properties of nanotechnology bulk metals: a preliminary survey. Technical Report NLR-TR-2006-138, National Aerospace Laboratory NLR, The Netherlands

Chapter 3

Superplastic Forming of Aerospace Materials

K.A. Padmanabhan, S. Balasivanandha Prabu and S. Madhavan

Abstract This chapter discusses the phenomenon of superplasticity, as seen in different materials such as metals/alloys, intermetallics, ceramics, bulk metallic glasses and composites. The phenomenon of low temperature/high strain rate superplasticity is also briefly discussed. The various forming operations and the recent developments in forming processes like superplastic forming-diffusion bonding, friction stir processing, roll forming, and incremental forming have also been reviewed. Finally, some applications of superplastic forming in the manufacture of aerospace components are presented.

Keywords Superplasticity · Alloys · Ceramics · Composites · Metallic glasses · Processing · Applications

3.1 Introduction

The Russian word СВЕРХПЛАСТИЧНОСТЬ (pronounced as sverkhplastichnost) was introduced by Bochvar and Sviderskaya in 1945 [1], and appeared as “superplasticity” in 1947 in English translation in Chemical Abstracts. The first application of superplasticity is traced to the Bronze Age [2].

Superplastic forming (SPF) became industrially important in the 1970s, and it exploits the near-ubiquitous phenomenon of superplasticity displayed by different classes of materials, e.g. metals and alloys, intermetallics, ceramics, composites, ultrafine/nanostructured materials, and bulk metallic glasses. This phenomenon is

K.A. Padmanabhan (✉)

Department of Mechanical Engineering, Anna University, Chennai 600 025, India
e-mail: kap@annauniv.edu; ananthaster@gmail.com

S. Balasivanandha Prabu

Department of Mechanical Engineering, College of Engineering Guindy,
Anna University, Chennai, India

S. Madhavan

Department of Mechanical Engineering, IIT Madras, Chennai, India

accompanied by an elongation of several hundred percent under the action of a small tensile stress by which the neck(s) formed is/are extremely diffuse. It was agreed quite early on that a material is superplastic if, in a tensile specimen of 1 in. (2.54 cm) gauge length, an elongation greater than 200 % is obtained [1, 2].

Superplastic forming leads to a reduction in component weight and manufacturing cost, and allows novel, monolithic designs of aircraft components. However, cavitation present during superplastic forming of some alloys could lead to inferior properties and premature failure [1, 3].

Interest in industry stems from the fact that near-net-shape components can be obtained in a single forming operation that would otherwise need several steps. SPF can also be suitable for difficult-to-form metals and alloys for which conventional forming is virtually ruled out.

There are two types of superplasticity [1]: (a) Transformation/Environmental Superplasticity in which the effect is induced by repeated thermal cycling of a material that undergoes a phase transformation, or has anisotropic thermal expansion properties, while it is subjected to a small tensile stress along the (crystallographic) direction of maximum expansion/elongation; and (b) Structural Superplasticity in which a material has a relatively stable fine grain size, usually $\sim <10 \mu\text{m}$ at a high homologous temperature of deformation, $\sim >0.5T_m$, and a strain rate of 10^{-5} to 1 s^{-1} . Type (b) is of considerable industrial importance [1, 4–8].

A detailed account of the origin of superplasticity is beyond the scope of the present chapter. Such accounts can be found in the books of Padmanabhan and Davies [1], Nieh et al. [2], Kaibyshev [9], a recent book on Al–Li alloys [10] and several other reviews and overviews.

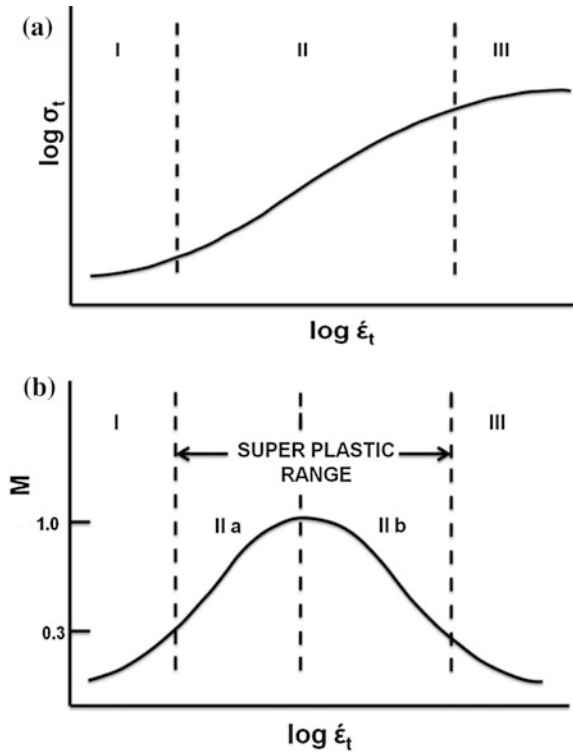
3.2 Phenomenology of Superplasticity

Many books and overviews have discussed the phenomenology of superplastic flow [1, 9–12]. The isothermal, near-constant grain size, stress–strain rate relationship in the superplastic regime can be expressed as $\sigma = K\dot{\epsilon}^m$ or as $\dot{\epsilon} = C\sigma^n$, where $C = 1/K^{1/m}$ and $n = 1/m$; here, σ is the stress at a strain rate of $\dot{\epsilon}$, ‘ m ’ is the strain rate sensitivity index of value >0.3 under uniaxial loading, and K is a material constant. Both ‘ m ’ and K are functions of strain rate, grain size and temperature [11].

From the above equations, on logarithmic co-ordinates isothermal $\log \sigma - \log \dot{\epsilon}$ would be a straight line over a small strain rate interval, the slope of which is equal to M , i.e. $M = \partial \log \sigma / \partial \log \dot{\epsilon} \big|_{d,T}$, where d is the average grain size and T is the test temperature on the absolute scale. The shape of the full stress–strain rate curve is typically sigmoidal, see Fig. 3.1a.

The isothermal M -dependence on strain rate has a dome-like shape, Fig. 3.1b, and the maximum value M_{max} corresponds to the optimal strain rate $\dot{\epsilon}_{\text{opt}}$ for superplastic deformation, for a given average grain size and deformation temperature. The boundaries of the optimum strain rate interval for superplastic flow are conventionally

Fig. 3.1 The relationship between (a) stress and strain rate and (b) strain rate sensitivity index and strain rate for superplastic deformation [1]



found from the empirical condition $M \geq 0.3$ [1, 11–13]. It is easy to show [1] that the percentage elongation is approximately proportional to (M^2) .

The deformation behaviour of the material is divided into three regions: low (I), medium (II) and high (III) strain rate ranges, see Fig. 3.1a. In region II, M is greater than or equal to 0.3 and maximum ductility is usually associated with the maximum M value. It should be noted that region II could be divided further into region IIa (left of the maximum) and IIb (right of the maximum), see Fig. 3.1b. The physical mechanisms operating in these two regions are not identical. Moreover, for an identical value of M , in region IIa an increase in strain rate *increases* the M value, while in region IIb a strain rate increase *decreases* the M value. This means that the resistance to strain localization (necking) from a strain rate increase would be different in these two regions [1].

The general conclusions based on the phenomenology of flow may be summarized as:

- The ‘ M ’ value should be around 0.4–0.7 to exhibit superplasticity of industrial relevance.
- The elongation in tension goes through a maximum with strain rate.
- Grain size is inversely related to the strain rate; and the relationship is often expressed by a power law.

- The constitutive equation of flow is often written as $\dot{\epsilon} = (C/d^a) (\sigma^n) \exp(-Q/RT)$ or $\dot{\epsilon} = (C/d^a) (\sigma - \sigma_0)^n \exp(-Q/RT)$, where $\dot{\epsilon}$ is the strain rate; σ is the corresponding stress; σ_0 is a “back” or “threshold” stress which has to be overcome before the commencement of superplastic flow; C is a material constant; ‘ a ’ is an empirical constant that usually lies between ~ 1.3 and 3 ; $n = (1/m)$, with m lying in the range 0.3 – 1.0 ; Q is the activation energy for the rate controlling process; R is the gas constant; and T is the absolute temperature of deformation [1].

3.3 A Review of Basic Research on Superplastic Flow

3.3.1 Metals and Alloys

Superplasticity is often induced in metallic materials by thermomechanical processing.

Aluminium Alloys Could be superplastic, if (i) the microstructure is fully recrystallized, or (ii) fine, cold- or warm-worked grains are present [14]. Industry finds the second condition to be more attractive, as it could lead to high strain-rate superplasticity.

The addition of 1 % lithium (Li) to aluminium offers nearly 3 % density reduction and 10 % stiffness increase, making Al–Li alloys very attractive for aerospace applications. The superplastic behavior of different classes of Al–Li alloys are described in a recent book [10].

Titanium Alloys The most widely used Ti alloy, Ti-6Al-4V (an α - β alloy), is superplastic as it comes from the mill and requires no prior treatments. However, the volume fraction of individual phases has a significant effect on its superplasticity. Results reveal that 40–50 % volume fraction of β in a two-phase α - β titanium alloy leads to the best superplastic properties. (Grain growth resistance is the maximum for this volume fraction [15–17]).

Other Alloys Superplasticity is also seen in alloys of other metals, including nickel [18], magnesium [19, 20], copper, and zinc [21, 22]. In 1981 high strain-rate superplasticity in an oxide dispersion strengthened nickel-base alloy was also reported [23]. A full list of superplastic alloys can be found in several books and reviews.

In recent times materials processed by severe plastic deformation like Equal Channel Angular Pressing (ECAP), High-Pressure Torsion (HPT), and Friction Stir Processing (FSP) have been shown to be superplastic. More discussion of the usefulness of these deformation processes is given in Sect. 3.5. In the meantime we note that Charit and Mishra [24] have reported that an elongation of ~ 525 % is obtained at a strain rate of 10^{-2} s^{-1} in FSP aluminium alloy 2024 at a relatively low

temperature of 430 °C. It is important to note that the ductility was $\sim 280\%$ even at a higher strain rate of 10^{-1} s^{-1} , i.e. the alloy could be quite rapidly subjected to large deformations.

3.3.2 *Intermetallics*

Many intermetallics, e.g. TiAl, Ti₃Al, Ni₃Al etc., in a fine-grained condition, exhibit superplasticity under certain combinations of temperature and strain rate [25–27]. Also, a decrease in grain size down to $\sim 100 \text{ nm}$ leads to a significant decrease in the homologous temperature of superplasticity [28–30]. However, superplastic forming temperatures of most intermetallics are normally higher than $0.7T_m$, as compared to $0.3\text{--}0.5T_m$ for conventional alloys [28]. On the positive side, intermetallics based on $\gamma\text{-TiAl} + \alpha_2\text{-Ti}_3\text{Al}$, Ti-25Al (Ti₃Al—superlattice DO19), and Ti-50Al alloy (TiAl—superlattice L10) demonstrate superplastic properties superior to those of many metals [26, 28–30].

Some intermetallics can exhibit superplasticity in a coarse-grained condition also, i.e. grain size $>10 \text{ }\mu\text{m}$ [31]. For example, Ti₃Al with grain size $60 \text{ }\mu\text{m}$ shows a maximum elongation of 328% at $800\text{--}900 \text{ }^\circ\text{C}$ in the strain rate range 2×10^{-4} to $4 \times 10^{-3} \text{ s}^{-1}$. But in this and other coarse-grained intermetallics that exhibit superplasticity the grain size gets refined continually and there is no steady-state flow.

3.3.3 *Ceramics*

Wakai et al. [32] reported superplasticity in a fine-grained ($0.3 \text{ }\mu\text{m}$) yttria stabilized tetragonal zirconia (YTZP), and also non-oxide ceramics [hot pressed Si₃N₄/SiC (20 wt% SiC)]. Superplasticity is also reported in other ceramic materials, e.g. ultra-fine grained alumina doped with various dopants like MgO, Y₂O₃, Ti₂O₃ and Cr₂O₃ [33].

Commercial ceramics like Al₂O₃ and SiAlON also exhibit superplasticity at high temperatures. As in metals and alloys, the tensile elongation, as well as the flow stress, strongly depends on the grain size [34]. However, severe grain growth, and in particular dynamic grain growth, is observed within the superplastic temperature regime ($1350\text{--}1500 \text{ }^\circ\text{C}$ for alumina) [35]. The addition of ZrO₂ effectively stabilizes the grain size [36, 37], and a 10 vol.% ZrO₂–Al₂O₃ ceramic mixture (with a grain size $\sim 0.5 \text{ }\mu\text{m}$) was successfully stretched severely under biaxial tension at $1400 \text{ }^\circ\text{C}$.

An equiaxed β' -SiAlON specimen containing small amounts of a transient liquid at the boundaries was biaxially stretched to a large strain with good surface finish [38] at $1600 \text{ }^\circ\text{C}$ and a strain rate of 10^{-4} s^{-1} ; and β' -SiAlON with some 15R structure and a transient liquid, was also observed to exhibit large tensile ductility

[39] (230 %) at 1550 °C. This particular facility for superplasticity is linked to the way β' -SiAlON elongates and aligns along the tensile direction. This leads to unusual strain hardening and texture, resulting in a high flow stress without premature failure.

Superplastic forming of ceramics is demanding because the SPF temperatures are very high, the grain sizes should be in the sub-micron range, and at lower temperatures the ductility is extremely low [40]. However, developments like fine powder processing have reduced the forming temperature drastically [41].

3.3.4 Composites

The methods of production of superplastic composites—based on powder metallurgical principles and/or polymer processing techniques—are different from those of most metallic materials.

High strain-rate superplasticity (HSRS) was first reported in aluminum alloy 2124/20SiC_w and a squeeze cast composite of pure aluminium reinforced with β -Si₃N₄ whiskers [12] (the suffixes “w” and “p”—see later—stand for the whisker and particulate forms of the stiffeners; the number before the stiffener gives the vol. %). HSRS was seen above or just below the solidus temperature of the matrix, and microanalysis revealed segregation of Mg or Cu at the interfaces between the aluminium alloys and reinforcements. This could decrease the melting temperature of the matrix near the interfaces and cause difficulties during processing [42].

Superplastic forming of aluminium-based metal matrix composites was also attempted [43] in alloy 7475/SiC_p; and Tong and Chan [44] successfully formed hemispherical domes of aluminium alloy 6061/20SiC_w composites at a pressure of 4 MPa and 873 K.

Most particle-reinforced metal matrix composites exhibit superplastic behaviour. The effect of the reinforcement on superplasticity is not yet defined clearly. However, Higashi et al. [45] could analyze the aluminium-based composites and arrive at a criterion to determine the strain rate up to which the accommodation mechanism is adequate to prevent cavitation. They did this by assuming that the stress relaxation on the particles occurred by diffusion.

In addition, Al-alloys are well suited to study the effect of intergranular particles because the influence of the particles is higher at lower temperatures. Recently, Mg-based composites were seen to exhibit superplasticity at even lower temperatures than Al-based composites. This led Watanabe et al. [46] to analyze the experimental data for the Mg–Zn–Zr system (ZK60 and ZK61 alloys and composites) and propose a theory of the effect of reinforcement on superplastic flow in ceramics.

It is noteworthy that Boeing already introduced fibreglass composites in aircraft in the 1950s. However, this was for secondary applications and not for primary structures.

3.3.5 Bulk Metallic Glasses

Several bulk metallic glasses (BMGs) have been rendered superplastic [47], e.g. a metallic glass of composition $Zr_{65}Al_{10}Ni_{10}Cu_{15}$, processed into a bulk form through powder metallurgy (PM), exhibited a tensile elongation of 750 % at $6.3 \times 10^{-3} \text{ s}^{-1}$ and 696 K [48].

BMGs show a drastic reduction in viscosity in the super-cooled liquid region, resulting in superplastic deformation characteristics in this temperature range, and the possibility of fabrication into near-net-shape components [49].

One notable example is the use of BMG plates, along with other high purity materials, for the solar wind collection system on the NASA Genesis spacecraft.

Owing to their unique properties, BMGs are being developed for the following military components by the US Department of Defense: fuses and sub-munition components; composite armour; lightweight casings for ordnance; MEMS casings and components; thin-walled casings and components for electronics; casings for night sights and optical devices; missile components (fins, nose cones, gimbals, and bodies); lightweight fragmentation devices; and aircraft fasteners and shielding [49–51].

3.3.6 Effect of FSP on Superplastic Forming

FSP has been employed to produce very fine-grained materials for improved superplasticity [52, 53]. FSP enhances superplasticity in several ways [54, 55]:

1. It lowers the temperature range of superplastic forming by reducing the grain size of the starting material and also causing uniform grain refinement.
2. Usually SPF is very slow, but FSP of the material reduces the forming time substantially (much finer grain size).

FSP of the magnesium alloys AM60, AZ91, AZ31, Mg–Al–Ca and Mg–Re alloys led to effective grain refinement. In the case of AZ31, experiments revealed that the starting material did not exhibit superplasticity even at increased temperatures, while the phenomenon was present in the FSP material. Thus for this material, FSP is an essential pre-treatment for facilitating SPF.

Charit and Mishra [24] have established HSRS in FSP-treated aluminium alloy 2024. This alloy and its derivatives have been and are extensively used in transport aircraft structures, notably for fuselage panels.

With the aid of FSP, new techniques like selective super (plastic) forming [56] have been tried, Fig. 3.2, because in some cases it is enough if only a selected region has a very fine grain size. This selective microstructural refinement is unique to FSP. Figures 3.2a and b show the region being “super-formed”. Figures 3.2c and d display finite element simulations of selective superplastic forming.

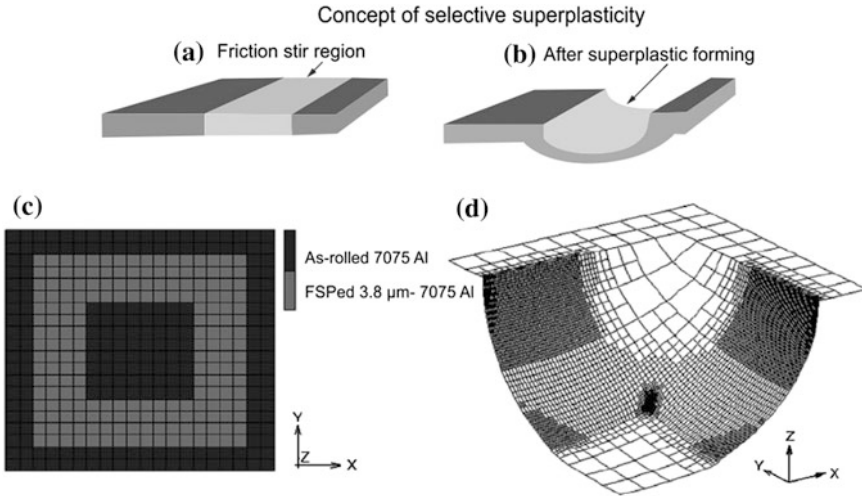


Fig. 3.2 **a** Schematic of selective superplasticity, where only the region undergoing superplastic deformation is friction stir processed (FSPed); **b** Brighter areas in commercial 7075 Al rolled sheet are selected to be FSPed to become superplastic instead of making the whole sheet superplastic; **c, d** finite element mesh after adaptive remeshing [56]

3.4 Conventional/High Temperature Superplasticity

Superplasticity usually occurs in alloys at high temperatures ($0.5\text{--}0.7T_m$). Eddahbi et al. [57] analysed the effects of dynamic recrystallization (DRX) and dynamic recovery (DRV) on the superplastic deformation mechanism and concluded that beyond an initial transient state there is steady state deformation, wherein superplastic alloys have good grain coarsening resistance and there is negligible strain hardening.

Internal cavity formation during superplastic deformation in aluminium and other alloys has been reported by Cocks and Ashby [58], Chokshi and Mukherjee [59], and Gouthama and Padmanabhan [60]. Blandin [61] suggested that cavitation in Al–Li alloys is influenced by Li depletion at high temperatures ($\sim 500\text{ }^\circ\text{C}$). Evidently, cavitation is present during superplastic deformation of high strength aluminium alloys, and it results in the development of small intergranular voids during straining.

There are conflicting suggestions that the Li depletion in Al–Li alloys could either assist or hinder grain boundary sliding (GBS), which is the dominant mechanism of superplastic flow. This means that GBS might be promoted by the creation of new cavities, or else it decreases because the cavities segregate and prevent the affected grain boundaries from further participation in the superplastic deformation process. The former point of view is vindicated in many cases.

The underlying mechanisms of deformation and cavitation under optimal and non-optimal superplastic deformation conditions are well discussed in several

books and review articles, in particular in the book of Pilling and Ridley [62]. It is also known that when a hydrostatic pressure $\geq 0.5 \sigma_y$ (σ_y is the yield stress) is applied, cavitation is completely suppressed. In superplastic sheet forming (biaxial), the hydrostatic pressure is applied on the opposite side to the forming pressure.

3.5 Low Temperature/High Strain-Rate Superplasticity

For retaining the fine grain size of superplastic alloys, low temperature superplastic forming is desirable. It is well known [7] that a decrease in grain size has a positive effect on the creep/superplastic deformation rate, similar to the positive effect of an increase in temperature. Moreover, lower SPF temperatures avoid or reduce problems with low melting point constituents, e.g. Li and Mg depletion from alloys, and cavity formation, which is detrimental to the post-forming mechanical properties [63].

Finer grain sizes, which can be retained more easily at lower temperatures, also lead to High Strain Rate (also known as Low Temperature) Superplasticity [2]. Many routes are available for producing very fine grains in materials like Al, Mg and Ti alloys, e.g. severe plastic deformation processes like High Pressure Torsion (HPT), Equal Channel Angular Pressing (ECAP), multiple forging, repeated rolling and folding, and FSP [64]. Multi-axial Alternative Forging (MAF) also proved to be successful for producing ultra-fine-grain sized (UFG) materials. The detailed procedure adopted for MAF is outlined by Noda et al. [65].

Recently Ma et al. [66] and Karthikeyan et al. [67] demonstrated that FSP is an effective technique for producing aluminium alloys with equiaxed fine grained structures and a high fraction of high-angle boundaries (HABs), both of which are beneficial to grain boundary sliding and superplasticity [68].

Preliminary work [69–72] has indicated that superplasticity in magnesium alloys occurs at low temperatures or high strain rates after grain refinement. But there are very few works [73–75] that discuss low temperature superplasticity at high strain rates.

An example of low temperature superplasticity at reasonably high strain rates was evidenced by Equal Channel Angular Extrusion (ECAE) processed Mg-10 % Li-1 % Zn Alloy [75]. Superplasticity was achieved earlier at 373 K but the strain rate was slow (10^{-4} s^{-1}) [76]. Therefore Yoshida et al. [75] ECAE-processed the material at 323 K, enabling superplasticity at 423 K (less than $T_m/2$) and a strain rate of $1 \times 10^{-3} \text{ s}^{-1}$, which is relatively high (but below the cut-off limit of 10^{-2} s^{-1}). The ECAE was in 6 passes, and resulted in grain refinement and spheroidization of α phase. The addition of Li in the β phase helped reduce the deformation temperature. As in conventional superplasticity, with an increase in strain rate the elongation and m -value decreased. At 423 K ($0.49T_m$) an elongation of 206 % was attained at a strain rate 10^{-2} s^{-1} , and the ' m ' value was 0.4.

New techniques have been developed to make SPF a quicker process. These include the availability of automatic loading/unloading systems, automatic loading

of tools in the tool holder, equipment pause reduction systems etc. Pre-treatment processes like FSP also accelerate the process by reducing grain size significantly. A commercial initiative by General Motors, in collaboration with Alcoa, has led to development of an advanced blow-forming process, which takes place at higher forming rates [77].

3.6 Forming Operations

Superplastic forming operations fall into two broad categories, namely [1]:

- (i) Those techniques which are derived from processes for forming thermoplastics, and
- (ii) Procedures which are adapted from conventional working processes for metals and alloys.

The processes may be further classified as macro-forming (bulk changes in shape) and micro-forming (local changes in shape).

3.6.1 *Bulge Forming*

Bulge forming is used to produce complex shapes from tubular blanks. Tube bulging can be done in several ways, but hydraulic bulging has the following advantages: (i) the ability to produce large circumferential expansions of the tube; and (ii) the flexibility to control the internal hydraulic pressure and the axial compression independently in order to achieve the desired bulging.

Components are formed using high internal pressure and axial loads [78]. There are two primary limitations: (i) failure due to excessive axial compressive force on the tube, which could cause buckling or collapsing of the tube; and (ii) failure of the tube owing to excessive internal pressure that causes plastic instability in tension, excessive wall thinning and eventual bursting of the tube [78].

3.6.2 *Pressure Forming*

Pressure forming, like free bulging of sheet metals (Zn-22 wt% Al eutectoid) by pressure, was first demonstrated by Backofen et al. [79]. The process involves clamping a circular diaphragm around its periphery and subjecting it to a one-sided hydrostatic pressure. Accurate control of the pressurization cycle during forming is of considerable importance.

The geometry of the bulge profile is of interest. Johnson et al. [80] experimentally demonstrated that the free surfaces have an essentially spherical shape; whereas Thomsen et al. [81] found that when the strain-rate sensitivity of the flow stress is low, forming into a circular cavity often leads to bulges that are prolate rather than spherical. In other words, strain-rate sensitivity decides the thinning characteristics of a material during forming. In the case of equi-biaxial bulging, the in-plane strains determine the shape of the bulge, whereas the thickness strain determines the thinning characteristics [82].

3.6.3 Sheet Thermoforming

In its simplest form this process is one in which a sheet (preheated as appropriate) is clamped at the edges over a female mould. The pressurized gas applied to the upper part of the sheet pushes it into the lower part of the die. The lower chamber of the die is simply left open to the atmosphere.

In some cases, a different setup is used, in which a vacuum is created in the lower chamber instead of applying pressure to the upper side of the sheet, see Fig. 3.3. If the sheets are of alloys prone to cavitation, a “back pressure” of at least $0.5\sigma_y$ is applied to obtain cavitation-free products [62].

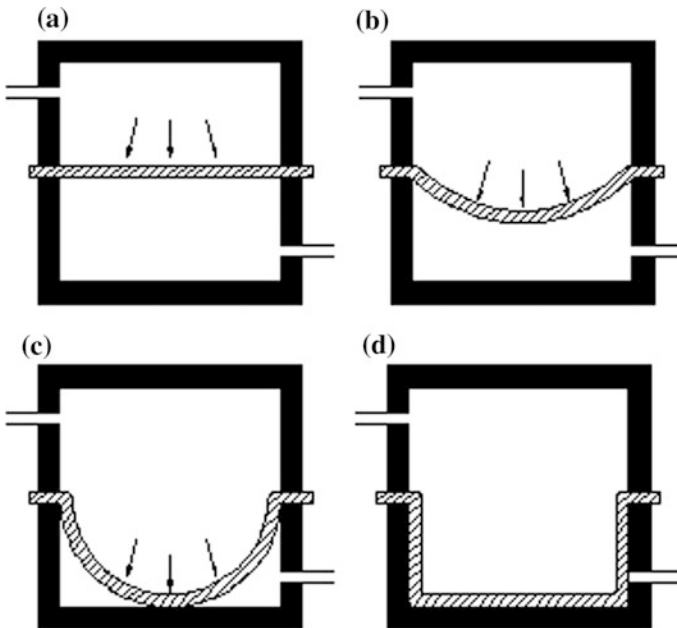


Fig. 3.3 Vacuum/pressure forming of a sheet by forcing it into a female die cavity: a four part cycle begins at the *top left* [83]

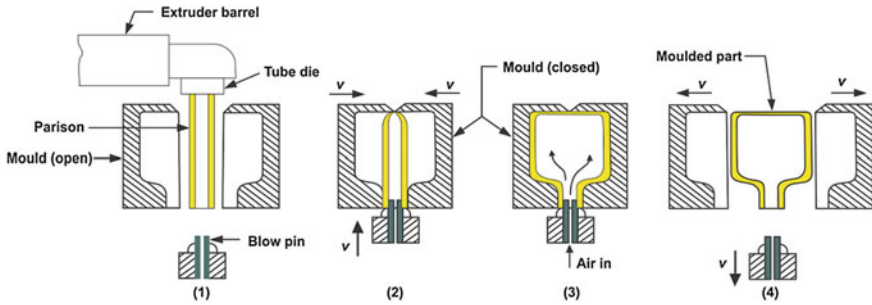


Fig. 3.4 Extrusion blow moulding [84]

3.6.4 Blow (Extrusion) Moulding

The blow-moulding technique used to produce glass and plastic bottles has been suitably developed for superplastic alloys. Firstly, an elongated preform is made (referred to as the parison) and is then expanded by internal pressure to conform to the shape of the split mould, see Fig. 3.4.

The feasibility of blow moulding for the formation of bottles from superplastic alloys has been clearly demonstrated by Petersen and Lang [84], who expanded tubes of a superplastic iron-26 % chromium-6.5 % nickel alloy using a self-contained pressurization system.

The different types of blow moulding are (i) extrusion moulding, (ii) injection moulding and (iii) stretch moulding. (The last two have not yet been used for superplastic forming.)

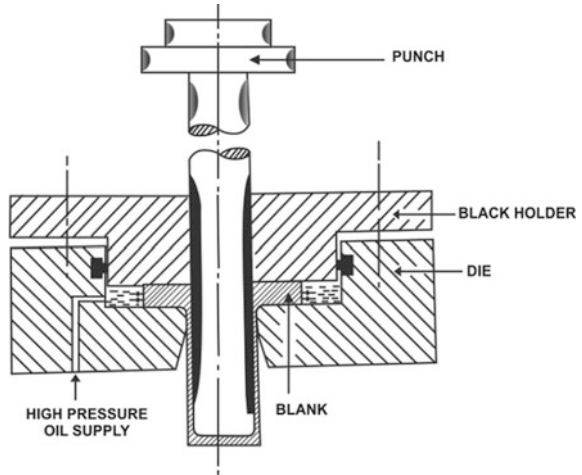
3.6.5 Deep Drawing

The failings of conventional deep drawing are overcome by using a pressure-augmented deep drawing process, Fig. 3.5. This is an effective process for producing deep cups.

3.6.6 Powder Metallurgy Processes

Near-superplasticity in pure nickel was first reported by Floreen [86]. Pratt and Whitney [87] discovered in the late 1960s that some nickel-base superalloys, which are used in aerospace gas turbines, could be superplastically deformed, and a process called Gatorizing was patented in 1970 [88].

Fig. 3.5 Equipment used for pressure augmented deep drawing [85]



This process could not eliminate macro-segregation (resulting from the ingot metallurgy (IM) primary processing) in the as-forged condition. To minimize this problem, parts such as some turbine discs are made using powder metallurgy (PM) routes, where a near-uniform grain size is obtained by atomization from the liquid state, and the powder is compacted and extruded near (but below) the recrystallization temperature of the alloy. Adiabatic heating during the extrusion initiates recrystallization, which produces the required grain size and structure for superplasticity. The alloy can then be forged at (low) superplastic strain rates to the near-finished size and shape. A subsequent high temperature annealing process is used to dissolve stabilizing precipitates and promote grain growth, thus eliminating the superplastic response, which would be undesirable in service. This is followed by an ageing treatment to develop optimal in-service properties, as done with other superalloys.

3.6.7 Incremental Forming

Incremental forming processes are characterized by successive local forming of the work-piece instead of forming in a single step. The key advantage is that specialized dies are not required: a wide range of shapes can be achieved by moving a spherical-ended indenter over a custom-designed numerically controlled tool path. Hence the process is ideally suited for small-batch-sizes or customized sheet products. Potential applications could include medical implants, architectural features, specialized laboratory equipment and parts for specialist vehicles.

In 'single-point incremental forming' or SPIF, a sheet is clamped rigidly around its edges but is unsupported underneath and formed by a single spherical-ended

indenter. Other variants referred to as ‘two-point incremental forming’ (TPIF) exist. In these the sheet is formed against full or partial dies using one or more indenters.

Further variations suggested include the use of a water jet or a combination of water jet with shots (metal balls) [89]. Although TPIF offers improved control of the deformation and better geometric accuracy through physical constraint of the sheet, it is less flexible than SPIF because specialized tooling is required.

The elimination of a die reduces the cost per piece and increases turnaround time. Several authors recognize that the formability of metallic materials under the localized deformation imposed by incremental forming is better than in conventional deep drawing. However, there is a loss of accuracy. Also, owing to the successive and local nature of incremental forming, process modelling and simulation is very complex and is at an early stage [90].

3.6.8 SPF/Diffusion Bonding of Titanium Alloys

At elevated temperatures (910–930 °C) and under high pressure, atomic diffusion between titanium alloy metal interfaces takes place, and it is possible to make a monolithic part with joint strength equal to that of the parent metal and substantial weight savings.

The optimal temperature for superplastically forming Ti-6Al-4V is 925 °C, and so SPF and diffusion bonding (DB) can be combined in a single fabrication cycle to form a highly efficient structure. Since the flow stresses of titanium alloys are low in the superplastic condition, they may be formed into a complex die cavity by the application of gas pressure, as shown in Fig. 3.6. In this process, significant SP deformation can either precede or follow the bonding process, and the degree of SP deformation can be equivalent to 300 % tensile strain [91, 92].

Another example is a high pressure spherical vessel made of titanium alloy Ti-6Al-4V/VT6, see Fig. 3.7.

Complex parts of excellent quality can be produced by SPF/DB, without the need for dissimilar joining of materials (brazing) or additional processing steps. Typical configurations include beads, sine wave, small bend radii, return flanges with joggle, compound contours, deep-formed pockets and multiple hollow parts.

Disadvantages of the DB process are that it requires a somewhat longer forming time than other joining processes; and it cannot be applied to aluminium alloys, since a tenacious surface oxide film blocks the inter-diffusion.

3.6.9 Superplastic Roll Forming

Superplastic roll forming, developed at the Institute for Metals Superplasticity Problems, Ufa, Russia, employs pairs of small opposed rollers to shape a cylindrical work-piece into a complex axi-symmetric shape by simultaneously:

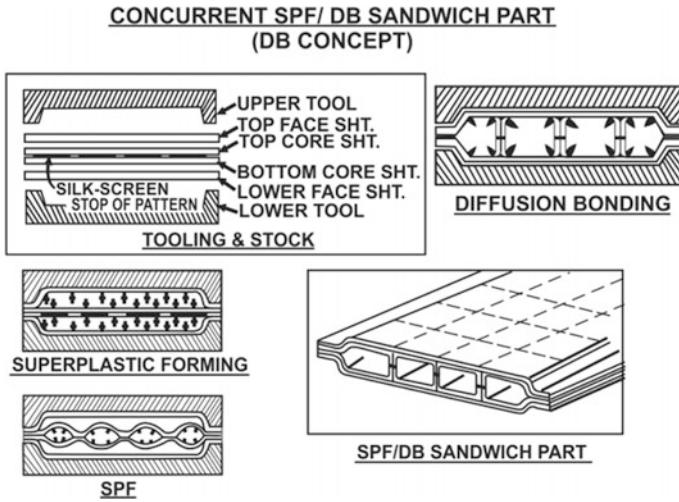
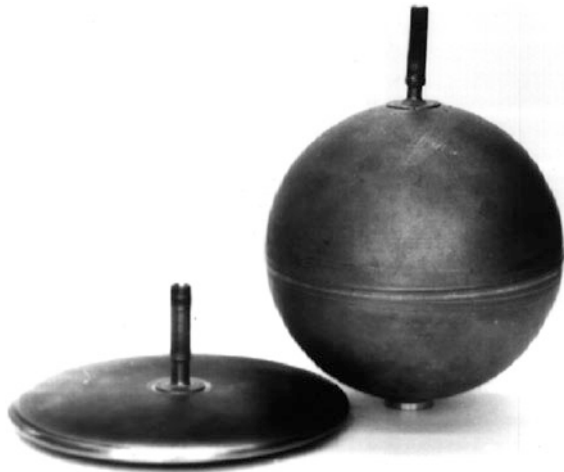


Fig. 3.6 Fabrication of a titanium alloy multilayer cellular structure from a four-sheet package by means of SPF/DB [93]

Fig. 3.7 A spherical tank with diameter 180 mm, manufactured by SPF/DB [94] and shown next to its starting blank. The Russian alloy (VT6C), equivalent to Ti-6Al-4V, was used



- adjusting the roll gap
- moving the rolls radially outward on the work-piece
- rotating the workpiece about its axis of symmetry.

Both the work-piece and the rolls are maintained at the temperatures required for SPF. Figure 3.8 shows a schematic diagram of roll forming based on the mill available at the Institute for Metals Superplasticity Problems, Ufa, Russia.

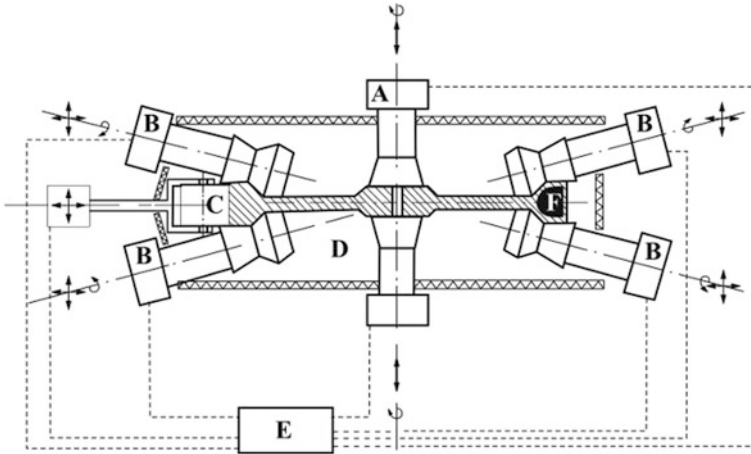


Fig. 3.8 Schematic of the roll forming mill, showing (A) the main drive shaft, (B) the axial radial work rolls, (C) the outer radial work rolls, (D) the furnace cavity, (E) the controls, and (F) the work-piece [95]

3.7 SPF Tooling

SPF of components is done using dies and tools, and inert gases to provide the necessary deformation pressure. A die is fixed in a press and the component to be formed is clamped to it. The main functions of the press are applying pressure to the tool and tool heating. Special presses are used to tolerate the required temperatures.

During the initial stages of SPF, free forming of the component occurs until it reaches the bottom of the die. The component then comes in contact with the tool (if it is located at the bottom of the die) and the material becomes locked against the tool by friction and forming pressure.

Forming using a male die requires the sheet thickness to be small, and then it leads to an accurate replication of the interior contours. The secondary contours present will not, however, be formed accurately. Also, for deep forming of sheets a conventional single die will lead to maximum thinning of the specimen and some necking. The die material should be able to withstand the thermomechanical stresses during forming. Otherwise it may fail due to fatigue cracking [96].

The tools, whether male or female, will have a single surface and these can be easily modified to the required shapes during product development [97].

Analyses to support forming operations are also available. The strain rate ($\dot{\epsilon}$) and the strain rate sensitivity (m) can be found easily using a regression analysis. Analysis of superplastic forming can be done using the LS-DYNA and ABAQUS software. These software programs can help us find the 'm' value, the flow stress, the strain rate relations, etc. Another important feature is the Pressure Control Algorithm, which predicts the pressure-time history. The software can also calculate the ratio (R) between optimum and the maximum strain rate. It could be

concluded that the forming pressure can be varied within limits in the optimal range without causing premature failure.

3.8 Techno-economic Considerations

SPF can enable forming 'hard-to-form' materials with relative ease, e.g. Ti and Mg alloys. The number of tools required for SPF will be far less compared with conventional processes. Thus when a product which would conventionally have many parts is manufactured by SPF, the tooling costs will not come into consideration, since reduction in the total number of parts leads to weight savings and compensating assembly cost reductions. However, when the total part count is small, the tool cost obviously should be minimized.

Furthermore, SPF is not suitable for small volume production of cheap parts, since it requires a substantial initial investment. On the other hand, SPF enables greater design freedom for high performance aerospace components, and is a single-step process. Also, Ti alloy components formed by the combined SPF/DB process provide higher rigidity and strength-to-weight ratio than conventional mechanically fastened assemblies [1, 98].

3.9 Aerospace Applications

Though many other industries have also profitably employed SPF, the aerospace industry has been a prime mover in some very interesting developments. Often in advanced aerospace applications, 70–90 % of the purchased material is machined away to create the complex and optimum geometries of some components.

SPF offers an alternative to conventional processing, with very limited material removal and wastage. Though SPF requires different tooling for different metals, it is of considerable demand, since it can produce complex parts in a single operation.

This greatly reduces the assembly costs. Die costs are also less, as the loads are very low and only the female die is needed. Other advantages of SPF are absence of springback and residual stresses, and highly accurate shaping.

3.9.1 Aluminium Alloys

SUPRAL 100 (Al-6 %Cu-0.4 %Zr) was the first commercial superplastic aluminium alloy used by the aircraft industry. Other aluminium alloys that have been superplastically formed are 2004, 7475, 8090 and 5083. There is an interesting overview of the applications of superplastic forming by Barnes et al. [99].

Figure 3.9 shows a 2195 Al–Li alloy SPF part produced at Boeing [100]. Other components superplastically formed from specially processed Al–Li 2090 and 2091 alloys at Superform are shown in Fig. 3.10. The final dimensions of the part in Fig. 3.10a were 175 mm (maximum) in height, 170 mm in width, and 340 mm in length. It could be established that the properties of the Al–Li alloys were equal to those of the conventionally processed alloys [101].

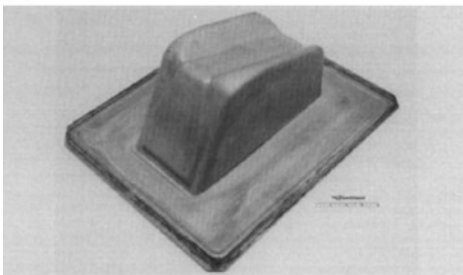
At Boeing, processes such as drop hammer forging have been replaced by superplastic forming. Owing to this, SPF has become the core process for wing tip pressings, wing flap leading edge sections, and equipment housings. The wing tip pressing shown in Fig. 3.11 was formed in 3 mm thick SPF 2004 alloy. The parts are in the T6 condition (solution heat treated and artificially aged to peak strength).

The Dassault Rafale tactical aircraft uses aluminium (and titanium) superplastically formed components that were designed at the beginning of development. There are more than 50 individual aluminium superplastic components used throughout the structure. The 7475 alloy has been used successfully to form air intake lip skins and access door assemblies. For less demanding applications 5083 alloy has found many applications for secondary features such as aerodynamic



Fig. 3.9 SPF component made from AA 2195 Al–Li alloy sheet, dimensions 560×1450 mm [100]

(a)



(b)



Fig. 3.10 Superplastically formed components made from (a) 2090Al alloy, and (b) 2091Al alloy [101]

Fig. 3.11 SPF aluminium 2004 alloy wing tip pressing used in Boeing 737 aircraft [102]



fairings and stiffeners. In the formed condition the alloy has suitable mechanical properties for internal fittings such as kicking panels and light fittings.

3.9.2 Titanium Alloys

Examples of the use of SPF titanium alloys are:

1. Engine bulkheads and heat shields for the Dassault Rafale [102].
2. Exhaust nozzle parts made from creep-resistant alloys like Ti-6Al-4V and Ti-6Al-2Sn-4Zr-2Mo, see Figs. 3.12 and 3.13.
3. The 5083-SP jet engine leading edge nacelle inlet assemblies in aircraft have been traditionally made from segments manufactured by deep-drawing, die forming, spin forming and stretch forming. However, for the Boeing 737 a



Fig. 3.12 Ti-6Al-2Sn-4Zr-2Mo alloy exhaust cone RR BR715 used for EJ-200 engines [103]



Fig. 3.13 Rear and side views of an SPF Ti-6Al-4V exhaust nozzle used for EJ-200 engines [103]

combination of SPF and Friction Stir welding (FSW) is used, saving in the assembly costs [104].

4. An early demonstration of the advantages of the combined SPF/DB technology was a helicopter firewall manufactured by Rockwell International [105]. The firewall was made from Ti-6Al-4V sheet and had dimensions of 746 mm × 1935 mm. This component had (only) 300 mechanical joints instead of the conventional firewall's 53 parts and 1074 mechanical joints, thereby providing a great reduction in the labour costs [106].
5. Figure 3.14 gives examples of SPF/DB manufactured components for the fuselage of the McDonnell Douglas F-15 tactical aircraft. This initiative resulted in a remarkable reduction of 726 part details and eliminated 10,000 fasteners [107].

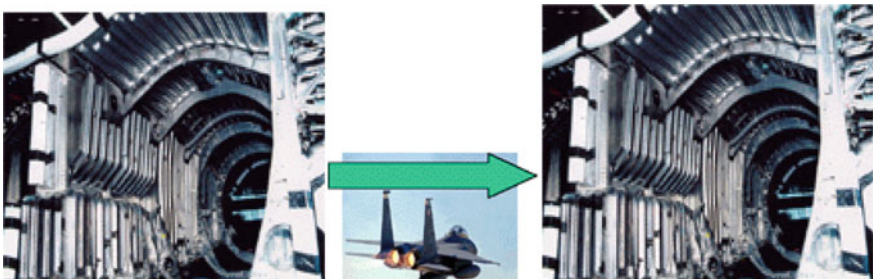


Fig. 3.14 The use of superplastic forming-diffusion bonding to reduce the fuselage part count in F-15E fuselages (blats SPF/DB) showing (a-left) before and (b-right) after SPF/DF [107]

3.10 Additional Remarks

For titanium alloys SPF initially led to an estimated cost saving of 55 % and weight savings of 33 %. The first commercial application of SPF for titanium was a Ti-6Al-4V jack housing produced by British Aircraft Corporation for the A310 Airbus aircraft in 1981. The SPF process resulted in cost savings of more than 50 %. These figures have improved with the advent of SPF/DB. Very recently, FSP has been coupled with SPF to produce extremely complicated monolithic parts, adding further to the economic advantages of SPF.

Another recent development is the new Rolls-Royce plant in Singapore, which has a fully functional SPF and SPF/DB process unit and this plant is expected to produce half of the commercial engines of Rolls-Royce in the future [108].

3.11 Conclusions

This chapter discusses basic research on superplasticity and superplastic alloys and the factors to be controlled to get the best results from superplastic forming. The different processes employed to fully exploit the potential of superplasticity in the production of components are reviewed. Innovative technologies like incremental forming and roll forming are also touched upon.

Acknowledgments The authors thank Dr. RJH Wanhill for a thorough scrutiny of the manuscript, helpful suggestions for the improvement of the text and careful editing/rewording of some of the sentences in order to remove ambiguity.

References

1. Padmanabhan KA, Davies GJ (1980) Superplasticity. Springer, Berlin, pp 1–250
2. Nieh TG, Wadsworth J, Sherby OD (1997) Superplasticity in metals and ceramics. Cambridge University Press, Cambridge, pp 1–287
3. Lee H-S, Mukherjee AK (1991) Phenomenon of intergranular cavitation and failure in superplasticity. *Eng Fract Mech* 40(4–5):843–846
4. Padmanabhan KA, Gleiter H (2004) Optimal structural superplasticity in metals and ceramics of microcrystalline and nanocrystalline-grain sizes. *Mater Sci Eng A* 381:28–38
5. Padmanabhan KA, Gleiter H (2012) A mechanism for the deformation of disordered states of matter. *Curr Opin Solid State Mater Sci* 16:243–253
6. Padmanabhan KA (2009) Grain boundary sliding controlled flow and its relevance to superplasticity in metals, alloys, ceramics and intermetallics and strain-rate dependent flow in nanostructured materials. *J Mater Sci* 44:2226–2238
7. Padmanabhan KA, Vasin RA, Enikeev FU (2001) Super plastic flow: phenomenology and mechanics. Springer, Berlin, 364 p
8. Nakatani Y, Ohnishi T, Higashi K (1984) Superplastic behavior of commercial aluminum bronze. *Jpn Inst Metals* 48:113–114

9. Kaibyshev OA (1992) Superplasticity of alloys, intermetallics and ceramics. Springer, Berlin
10. Balasivanandha Prabu S, Padmanabhan KA (2013) Superplasticity in and superplastic forming of Al-Li Alloys. In: Prasad NE, Gokhale AA, Wanhill RJH (eds) Aluminum-lithium alloys: processing, properties, and applications. Elsevier, Amsterdam, pp 221–258
11. Padmanabhan KA, Vasin RA, Enikeev FU (2001) Superplastic flow: phenomenology and mechanics. Springer, Berlin
12. Nieh TG, Henshall CA, Wadsworth J (1984) Superplasticity at high strain rates in a SiC Whisker reinforced Al alloy. *Scr Metall* 18:1405–1408
13. Vasin RA, Enikeev FU, Mazurski MI, Munirova OS (2000) Mechanical modeling of the universal superplastic curve. *J Mater Sci* 35:2455–2466
14. Wadsworth J, Palmer IG, Crooks DD (1983) Superplasticity in Al-Li based alloys. *Scr Metall* 17:347–352
15. Jain M, Chaturvedi MC, Richards NL, Goel NC (1991) Microstructural characteristics in α phase during superplastic deformation of Ti-6Al-4V. *Mater Sci Eng A* 145:205–214
16. Meier ML, Lesuer DR, Mukherjee AK (1991) α Grain size and β volume fraction aspects of the superplasticity of Ti-6Al-4V. *Mater Sci Eng A* 136:71–78
17. Inagaki H (1995) Enhanced superplasticity in high strength Ti alloys. *Z Metallkd* 86:643–650
18. Qi YH, Guo JT, Cui CY, Li GS (2002) Superplasticity of a directionally solidified NiAl-Fe (Nb) alloy at high temperature. *Mater Lett* 57:552–557
19. Yin DL, Zhang KF, Wang GF, Han WB (2005) Superplasticity and cavitation in AZ31 Mg alloy at elevated temperatures. *Mater Lett* 59:1714–1718
20. Chai F, Zhang D, Li Y, Zhang W (2013) High strain rate superplasticity of a fine-grained AZ91 magnesium alloy prepared by submerged friction stir processing. *Mater Sci Eng A* 568:40–48
21. Kawasaki M, Langdon TG (2008) The development of internal cavitation in a superplastic zinc–aluminum alloy processed by ECAP. *J Mater Sci* 43:7360–7365
22. Sheikh-Ali AD (2004) A study of deformation mechanisms of creep and superplasticity in zinc. Ph.D. thesis, McGill University, pp 1–314
23. Chen G, Zhang K, Wang G, Han W (2004) The superplastic deep drawing of a fine-grained alumina–zirconia ceramic composite and its cavitation behavior. *Ceram Int* 30:2157–2162
24. Charit I, Mishra RS (2003) High strain rate superplasticity in a commercial 2024 Al alloy via friction stir processing. *Mater Eng A* 359:290–296
25. Imayev RM, Imayev VM (1991) Mechanical behavior of the submicrocrystalline intermetallic TiAl compound at elevated temperatures. *Scr Mater* 25:2041–2046
26. Takasugi T, Rikukawa S, Hanada S (1991) Superplasticity in L1₂ Type Ni₃(Si, Ti) intermetallics. In: Hori S, Tokizane M, Furushiro N (eds) Superplasticity in advanced materials. Japan Society for Research on Superplasticity, pp 329–335
27. Maeda T, Okada M, Shida Y (1991) Superplasticity in Ti-rich TiAl. In: Hori S, Tokizane M, Furushiro N (eds) Superplasticity in advanced materials. Japan Society for Research on Superplasticity, pp 311–316
28. Takasugi T, Rikukawa S, Hanada S (1992) Superplastic deformation in Ni₃(Si,Ti) alloys. *Acta Metall* 40:1895–1906
29. Mishra RS, Lee WB, Mukherjee AK (1995) Mechanism of superplasticity in gamma TiAl alloys. In: Kim YW, Wagner RM, Yamaguchi M (eds) Gamma Titanium Aluminides. Minerals, Metals and Materials Society, pp 571–578
30. Imayev R, Shagiev M, Salishchev G, Imayev V, Valitov V (1996) Superplasticity and hot rolling of two-phase intermetallic alloy based on TiAl. *Scr Mater* 34:985–991
31. Lin D, Lin TL, Shan A, Li D (1994) Superplasticity in Fe₃Al-Ti alloy with large grains. *Scr Metall Mater* 31:1455–1460
32. Sakaguchi WS, Kato H (1986) *Yogyo-Kyokai-Shi* 94:721
33. Gruffel P, Carry C (1993) Effect of grain size on yttrium grain boundary segregation in fine-grained alumina. *J Eur Ceram Soc* 11:189–199

34. Sakka Y, Suzuki TS, Morita K, Kim BN, Hiraga K, Matsumoto T, Moriyoshi Y (2003) Low-temperature and high-strain rate superplastic zirconia. *Adv Eng Mater* 5:130–133
35. Kim BN, Hiraga K, Morita K, Sakka Y (2001) A high-strain-rate superplastic ceramic. *Nature* 413:288–291
36. Morita K, Hiraga K, Sakka Y (2002) High-strain rate superplasticity in Y_2O_3 stabilized tetragonal ZrO_2 dispersed with 30 vol.% $MgAl_2O_4$ spinel. *J Am Ceram Soc* 85:1900–1902
37. Morita K, Kim BN, Hiraga K, Sakka Y (2004) High-strain-rate superplasticity in 3 mol%- Y_2O_3 -stabilized tetragonal ZrO_2 dispersed with 30 vol.% $MgAl_2O_4$ spinel. *Mater Sci Forum* 447–448:329–335
38. Chen IW, Xue LA (1990) Development of superplastic structural ceramics. *J Am Ceram Soc* 73:2585–2609
39. Wu X, Chen I-W (1991) Exaggerated texture and grain growth in a superplastic SiAlON. *J Am Ceram Soc* 75:2733–2741
40. Wakai F, Kondo N, Shinoda Y (1999) Ceramics superplasticity. *Curr Opin Solid State Mater Sci* 4:461–465
41. Lesuer DR, Wadsworth J, Nieh TG (1996) Forming of superplastic ceramics. *Ceram Int* 22:381–388
42. Imai T, L'Esperance G, Hong BD, Kojima S (1995) High strain rate superplasticity of AlN particulate reinforced IN90 pure aluminum composite. *Scr Metall Mater* 33:1333–1338
43. Pilling J (1989) Superplasticity in aluminium base metal matrix composites. *Scr Metall* 23:1375–1380
44. Tong GQ, Chan KC (1997) High-strain-rate superplastic gas pressure forming of an Al6061/20SiCw composite. *Scr Mater* 37:1917–1922
45. Higashi K, Nieh TG, Wadsworth J (1995) Effect of temperature on the mechanical properties of mechanically-alloyed materials at high strain rates. *Acta Metall* 43:3275–3282
46. Watanabe H, Mukai T, Ishikawa K, Mohri T, Mabuchi M, Higashi K (2001) Superplasticity of a particle strengthened WE43 magnesium alloy. *Mater Trans* 42:157–162
47. Bunz J, Padmanabhan KA, Wilde G (2015) On the applicability of a mesoscopic interface sliding controlled model for understanding superplastic flow in bulk metallic glasses. *Intermetallics* submitted
48. Kim WJ, Lee JB, Jeong HG (2006) Superplastic gas pressure forming of $Zr_{65}Al_{10}Ni_{10}Cu_{15}$ metallic glass sheets fabricated by squeeze mold casting. *Mater Sci Eng A* 428:205–210
49. Wang G, Shen J, Sun JF, Lu ZP, Stachurski ZH, Zhou BD (2005) Tensile fracture characteristics and deformation behavior of a Zr-based bulk metallic glass at high temperatures. *Intermetallics* 13:642–648
50. Kawamura Y, Shibata T, Inoue A, Masumoto T (1997) Superplastic deformation of $Zr_{65}Al_{10}Ni_{10}Cu_{15}$ metallic glass. *Scr Mater* 37:431–436
51. Ramakrishna Rao B (2009) Bulk metallic glasses: materials of future. *DRDO Sci Spectr* 212–218
52. Zhilyaev AP, Langdon TG (2008) Using high-pressure torsion for metal processing: fundamentals and applications. *Prog Mater Sci* 53:893–979
53. Valiev RZ, Langdon TG (2006) Principles of equal-channel angular pressing as a processing tool for grain refinement. *Prog Mater Sci* 51:881–981
54. Mishra RS (2004) Friction stir processing for superplasticity. *Adv Mater Proc* 162:45
55. Johannes LB, Charit I, Mishra RS, Verma Ravi (2007) Enhanced superplasticity through friction stir processing in continuous cast AA5083 aluminum. *Mater Sci Eng A* 464:351–357
56. Mishra RS, Mahoney MW (eds) (2007) Friction stir welding and processing. *ASM Int OH* 312–318
57. Eddahbi M, Carreño F, Ruano OA (1998) Microstructural changes during high temperature deformation of an Al-Li(8090) alloy. *Scr Mater* 38:1717–1723
58. Cocks ACF, Ashby MF (1982) On creep fracture by void growth. *Prog Mater Sci* 27:189–244
59. Chokshi AH, Mukherjee AK (1989) The cavitation and fracture characteristics of a superplastic Al-Cu-Li-Zr alloy. *Mater Sci Eng* 110:49–60

60. Gouthama, Padmanabhan KA (2003) Transmission electron microscopic evidence for cavity nucleation during superplastic flow. *Scr Mater* 49:761–766
61. Blandin JJ (1989) Lithium effects in high temperature deformation of an Al-Li Alloy: Application to superplasticity. *Mater Sci Eng* 122:215–225
62. Pilling J, Ridley N (1989) Superplasticity in crystalline solids. The Institute of Metals London 214
63. Pu HP, Liu FC, Huang JC (1995) Characterization and analysis of low-temperature superplasticity in 8090 Al-Li alloys. *Metall Mater Trans A* 26:1153–1166
64. Padmanabhan KA, Balasivanandha Prabu S (2009) Increasing severity of deformation and decreasing forming forces for greener technology. In: Bhattacharjee D, Bhattacharyya T, Chatterjee S, Dutta M, Ghosh C (eds) *Emerging challenges for metals and materials: engineering and technology*. Allied Publishers, New Delhi, pp 163–190
65. Noda M, Hirohashi M, Funami K (2003) Low temperature superplasticity and its deformation mechanism in grain refinement of Al-Mg alloy by multi-axial alternative forging. *Mater Trans* 44:2288–2297
66. Ma ZY, Mishra RS (2005) Development of ultrafine-grained microstructure and low temperature (0.48 Tm) superplasticity in friction stir processed Al–Mg–Zr. *Scr Mater* 53:75–80
67. Karthikeyan L, Senthil Kumar VS, Padmanabhan KA (2013) Investigations on superplastic forming of friction stir-processed AA6063-T6 aluminum alloy. *Mater Manuf Processes* 28:294–298
68. Liu FC, Ma ZY, Zhang FC (2012) High strain rate superplasticity in a micro-grained Al–Mg–Sc Alloy with predominant high angle grain boundaries. *J Mater Sci Technol* 28:1025–1030
69. Mabuchi M, Asahina T, Iwasaki H, Higashi K (1997) Experimental investigation of superplastic behavior in magnesium alloys. *Mater Sci Technol* 13:825–831
70. Watanabe H, Mukai T, Kozhu M, Tanabe S, Higashi K (1999) Effect of temperature and grain size on the dominant diffusion process for superplastic flow in an az61 magnesium alloy. *Acta Mater* 47:3753–3758
71. Bussiba A, Artzy AB, Shtechman A, Sifergan KM (2001) Grain refinement of AZ31 and ZK60 Mg alloys—towards superplasticity studies. *Mater Sci Eng A* 302:56–62
72. Mohri T, Nishiwaki T, Kinoshita T, Iwasaki H, Mabuchi M, Nakamura M, Asahina T, Aizawa T, Higashi K (2000) Microstructure and tensile properties of rolled Mg-5.5 mass % Zn-0.6 mass % Zr alloy. *Mater Trans* 41:1154–1156
73. Watanabe H, Mukai T, Ishikawa K, Mabuchi M, Higashi K (2001) Realization of high-strain-rate superplasticity at low temperatures in a Mg–Zn–Zr alloy. *Mater Sci Eng A* 307:119–128
74. Watanabe H, Tsutsui H, Mukai T, Ishikawa K, Okanda Y, Kohzu M, Higashi K (2001) Grain size control of commercial wrought Mg-Al-Zn alloys utilizing dynamic recrystallization. *Mater Trans* 42:1200–1205
75. Yoshida Y, Cisar L, Kamado S, Kojima Y (2003) Effect of microstructural factors on tensile properties of an ECAE-Processed AZ31 magnesium alloy. *Mater Trans* 44:468–475
76. Segal VM (1995) Materials processing by simple shear. *Mater Sci Eng* 197:157–164
77. Kawasaki M, Langdon TG (2008) Grain boundary sliding in a superplastic zinc-aluminum alloy processed using severe plastic deformation. *Mater Trans* 49:84–89
78. Thiruvurudchelvan S, Seet GL, Ang HE (1996) Computer-monitored hydraulic bulging of tubes. *J Mater Process Technol* 57:182–188
79. Backofen WA, Turner IR, Avery DH (1964) Superplasticity in an Al-Zn alloy. *ASME Trans* 57:980–990
80. Johnson W, AL-Nam TYM, Duncan JL (1972) Superplastic forming techniques and strain distributions in a zinc-aluminum alloy. *The Japan Institute of Metals* 100:45–50
81. Thomsen TH, Holt DL, Backofen WA (1970) Forming superplastic sheet metal in bulging dies. *Met Eng Q* 10:1–3

82. Yang HS, Mukherjee AK (1992) An analysis of the superplastic forming of a circular sheet diaphragm. *Int J Mech Sci* 34:283–297
83. Carrino L, Giuliano G (1997) Modelling of superplastic blow forming. *Int J Mech Sci* 39:193–199
84. Petersen WA, Lang FH (1975) *Met Eng Q* 15:31
85. Al-Naib TYM, Duncan JL (1970) Superplastic metal forming. *Int J Mech Sci* 12:463–470
86. NASA Technical Memorandum 83623, P/M Super alloys—A Troubled Adolescent?, 1984
87. Maloney MJ (1990) DARPA/ONR program review, Pratt and Whitney Aircraft. Feb 27
88. Moore JR, Athey RL (1970) US Patent No. 3519503, July
89. Iseki H (2001) An approximate deformation analysis and FEM analysis for the incremental bulging of sheet metal using a spherical roller. *J Mater Process Technol* 111:150–154
90. Liu Z, Daniel WJT, Li Y, Liu S, Meehan PA (2014) Multi-pass deformation design for incremental sheet forming: analytical modeling finite element analysis and experimental validation. *J Mater Process Technol* 214:620–634
91. Cornfield GG, Johnson RH (1970) The forming of superplastic sheet materials. *Int J Mech Sci* 12:479–490
92. Smirnov OM (1979) Metal forming in the state of superplasticity. Mechanical Engineering Publications (In Russian), Moscow
93. Paton NE, Hamilton CH (eds) (1982) Superplastic forming of structural alloys. TMS-AIME, Warrendale, USA
94. Kruglov AA, Enikeev FU, Lutfullin Ya R (2002) Superplastic forming of a spherical shell out a welded envelope. *Mater Sci Eng A* 323:416–426
95. Bewlay BP, Gigliotti MFX, Utyashev FZ, Kaibyshev OA (2000) Superplastic roll forming of Ti alloys. *Mater Design* 21:287–295
96. Duchosal A, Deschaux-Beaume F, Lours P, Haro S, Fras G (2013) Analysis of weld-cracking and improvement of the weld-repair process of superplastic forming tools. *Mater Des* 46:731–739
97. Ceschini L, Morri A, Rotundo F (2014) Forming of metal matrix composites. *Compr Mater Process* 3:159–186
98. Bairwa ML, Date PP (2004) Effect of heat treatment on the tensile properties of Al–Li alloys. *J Mater Process Technol* 153–154:603–607
99. Barnes AJ, Raman H, Lowerson A, Edwards D (2012) Recent application of superformed 5083 aluminum Alloy in the aerospace industry. *Mater Sci Forum* 735:361–371
100. Babel HW (2005) Al–Li in Boeing products. In: 16th annual Aeromat advanced aerospace materials and processes conference and exposition, Aeromat 2005, Orlando, FL, USA
101. Yuwei X, Yiyuan Z, Wenfeng M, Jainzhong C (1997) Superplastic forming technology of aircraft structures for Al–Li alloy and high-strength Al alloy. *J Mater Process Technol* 72:183–187
102. <http://www.superform-aluminium.com/Superform>. Aluminum 2010
103. Serra D (2008) Superplastic forming applications on aero engines. a review of ITP manufacturing processes. In: 6th EUROSPF conference, Carcassonne, France, pp 1–10
104. Sanders D, Edwards P, Grant G, Ramulu M, Reynolds A (2008) Superplastically formed friction stir welded tailored aluminum and titanium blanks for aerospace applications. In: EuroSPF 2008, Carcassonne, France (hal-00338221)
105. Weisert ED (1985) The realization of SPF/DB as a commercial fabrication process. In: Agrawal SP (ed) Superplastic forming. American Society for metals, pp 84–89
106. Burroughs BA, Mocerino NJ (1979) Superplastic forming diffusion bonding of titanium helicopter airframe components. In: American Helicopter Society, Proceedings of 35th annual national forum, Washington, D.C., pp AHS79-33
107. Martin R, Evans D (2000) Reducing costs in aircraft: the metals affordability initiative consortium. *J Mater* 52:24–28
108. <http://www.ainonline.com/aviation-news/singapore-air-show/2012-02-14/rolls-royce-powers-new-singapore-site-leading-role-2>

Chapter 4

Welding Technologies in Aerospace Applications

T. Mohandas

Abstract This chapter reviews the joining of aerospace metals. The joining processes that are covered include gas tungsten arc, plasma arc and gas metal arc welding; resistance-based welding processes; flash butt welding; and high energy density processes such as electron beam welding, largely employed to weld titanium and nickel-base alloys. For enhanced strength and to weld dissimilar metals that are not weldable by fusion welding, solid-state welding processes such as friction welding and friction stir welding are employed. Brazing and diffusion bonding are largely used to join metal matrix composites and ceramics as well as ceramics to metals, and also nickel-base and titanium-base alloys. Magnetic pulse welding is a futuristic solid-phase welding process that may replace some of the current solid-state processes. The materials covered include aluminium, titanium and nickel-base alloys, steels, metal matrix composites, intermetallics and dissimilar metal combinations such as aluminium to stainless steel and maraging steel to low-alloy steel. Other aspects also discussed are online weld monitoring and fixturing during welding, and post-weld heat treatment to control distortion.

Keywords Welding technologies · Aluminium alloys · Titanium alloys · Nickel superalloys · Steels · Metal matrix composites · Intermetallics · Ceramic–metal joining

4.1 Developments in Welding Processes

The thrust in the use of materials for aerospace revolves around high specific strength and modulus for weight savings as well as high stiffness. The metallic materials used in aerospace include aluminium and titanium alloys to take advan-

T. Mohandas (✉)
Nalla Malla Reddy Engineering College, Hyderabad, India
e-mail: thondapim@rediffmail.com; thondapimohandas@gmail.com

T. Mohandas
Defence Metallurgical Research Laboratory, DRDO, Hyderabad, India

tage of their high specific strength; high-strength low-alloy steels; stainless steels; and nickel- and cobalt-base superalloys.

Advances in materials have led to the development of oxide dispersion-strengthened materials to raise the temperature capability, and metal matrix composites. The starting materials are obtained through various processing routes including casting and thermo-mechanical working.

Many components and structures made from all these materials need to be assembled from several parts. In doing so, the joint properties need to be optimised and as close as possible to those of the parent metals and alloys. To meet this requirement there is a need to employ many joining processes such as mechanical fastening, fusion welding, solid-state welding, diffusion bonding and brazing.

The fusion welding processes employed in the welding of aerospace components include gas tungsten arc welding (GTAW), plasma arc welding (PAW), gas metal arc welding (GMAW), flash butt welding, resistance welding and high energy density processes such as electron beam (EB) welding and laser welding [1, 2].

To circumvent the problems in fusion welding and mechanical fastening, solid-state welding processes such as friction welding and friction stir welding (FSW) have been introduced [3]. Friction stir welding has been under development for more than two decades, and the latest developments in friction-based welding processes (including linear friction welding) have overcome the problem of component geometry limitations in conventional friction welding [4, 5].

Diffusion bonding in combination with superplastic forming is employed for some of the applications in aerospace, notably for titanium alloys [1, 6–8]. Brazing is widely employed for heat exchangers and turbine blades [9–13].

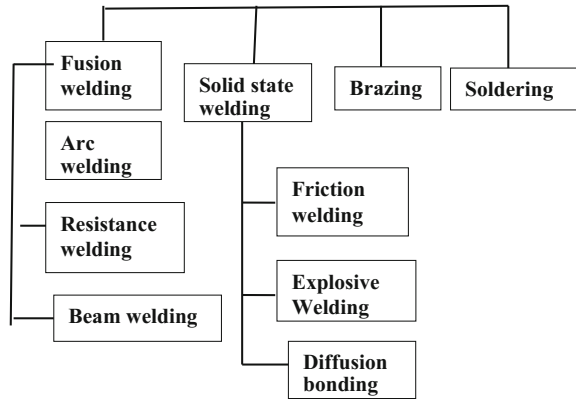
4.2 Welding of Aerospace Materials

Welding and brazing aspects of different aerospace metallic materials and the need for advanced welding processes and innovative brazing processes are discussed in the following subsections. An overview of the general welding processes employed in joining aerospace materials is given in Fig. 4.1.

4.2.1 Aluminium Alloys

Aluminium alloys are widely used for airframe structures and missile casings. High-strength aluminium alloys used in airframes are non-weldable by conventional techniques, owing to distortion and cracking problems. Fuel and oxidizer tanks in launchers and rockets made of alloys 2219 and 2014 are welded by GTAW and GMAW [1]. Thicker sections of advanced solid rocket boosters for the space shuttle were made of aluminium welded by plasma arc welding (PAW) owing to its

Fig. 4.1 Typical aerospace welding processes



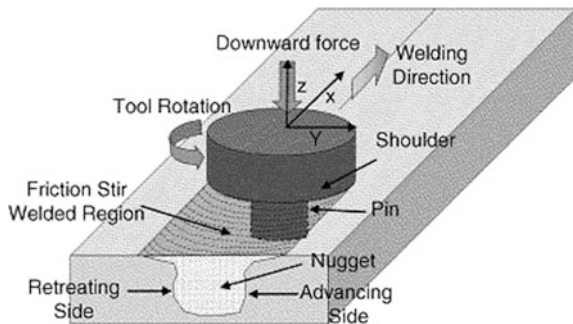
higher temperature capability [1]. The external tank of the Space Shuttle was welded by variable polarity plasma arc welding [1].

Laser Beam Welding This is gaining importance to replace some riveting, since it reduces the amount of labour and part counts [1].

Friction Stir Welding (FSW) Friction welds of aluminium alloys are free from solidification-related defects [14]. The latest process for welding aluminium alloys is friction stir welding (FSW), which is a solid-state welding process [15]. In this process, frictional heat generated between a rotating tool and the materials to be welded enables linear welds by the translatory motion of the plates to be welded, see Fig. 4.2.

FSW makes it possible to weld the high-strength 2XXX and 7XXX alloys. The strength of friction stir welds is stronger by 30–50 % than that of arc welds. It is reported that this process can replace high energy density processes such as plasma arc welding and electron beam welding. For example, the Space Shuttle Super LightWeight External Tank (SLWET) made from the aluminium–lithium alloy 2195 was GTA-welded, but work on new launchers is concentrating on FSW.

Fig. 4.2 Friction stir welding (FSW)



Flash Butt Welding This combines fusion welding with pressure application and is used for welding extruded aluminium landing gear components. The process has been reported to result in joint strengths equalling the parent metal strength.

Brazing This is widely employed in the production of compact aluminium heat exchangers (see Fig. 4.3). Aluminium clad sheets with core materials of 3XXX or 6XXX alloys and clad overlays of an Al–Si–Mg alloy are used. The Al–Si–Mg alloy has a lower melting point than the core materials and melts at the brazing temperature to enable joining the components in the heat exchanger. **N.B:** Mg in the alloy acts as a getter for oxygen, and the outer shell is generally welded by GTAW.

Brazing of heat exchangers is widely carried out in vacuum furnaces, although controlled atmosphere brazing and dip brazing in flux baths have also been reported. Fixturing is one of the salient aspects in the brazing of heat exchangers [16–18]. General brazing of aluminium is carried out with aluminium–silicon brazing alloys using fluxes. Compositions of some of the brazing alloys are provided in Table 4.1.

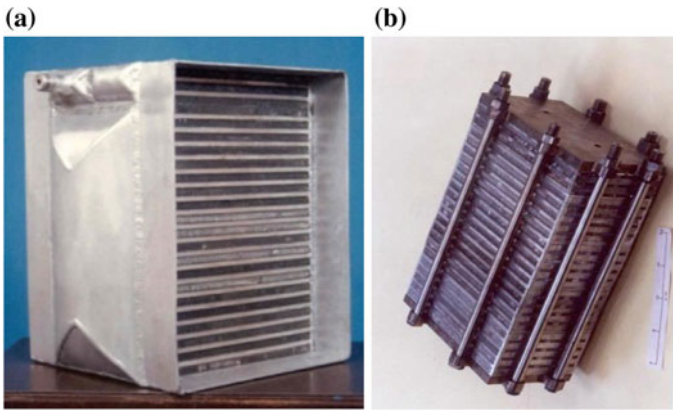


Fig. 4.3 Vacuum-brazed **a** aluminium heat exchanger and **b** fixture used for brazing

Table 4.1 Compositions of brazing fillers for aluminium alloy brazing

Composition (wt%)	Solidus (°C)	Liquidus (°C)	Remarks
Al-7.5Si	577	602	Flux brazing
Al-10Si	577	591	Flux brazing
Al-10Si-4Cu	521	585	Flux brazing
Al-12Si	577	582	Flux brazing
Al-9.75Si-1.5 Mg	554	569	Vacuum brazing
Al-9.75Si-1.5 Mg-0.1Bi	554	569	Vacuum brazing
Al-12Si-1.5 Mg	559	579	Vacuum brazing

4.2.2 Titanium Alloys

Titanium is a highly reactive metal. Hence inert gas welding processes such as gas tungsten arc welding (GTAW) are used for welding sheets, while thick section welding is done by plasma arc welding (PAW) [1, 2]. For inert gas welding of titanium there is a need to provide extra inert gas shielding in addition to primary shielding.

Welding of compressor disc assemblies made of creep-resistant titanium alloys is done by electron beam (EB) welding, see Fig. 4.4, owing to its high power density that enables welding thick sections in a single pass. The welding is done in vacuum. It is difficult to weld large components by electron beam welding, because of the need for a vacuum enclosure or chamber. However, it is reported that the Russians employed this process in welding the oxygen and fuel tanks of the Energia launcher by creating localised vacuum conditions [1].

During fusion welding, microporosity is a major problem, e.g. Fig. 4.4b, since the fatigue properties may be compromised: fatigue cracks can originate from the pores (see Fig. 4.4c). In addition, high-strength titanium alloys are cooling rate sensitive in that the microstructures obtained at high cooling rates exhibit low ductility and toughness [19–22].

To address these issues, solid-state welding processes such as friction welding are adopted. These processes have the advantage of welds being subjected to mechanical working, and this enables obtaining fine microstructures free from porosity (Fig. 4.4d). Such welds exhibit better fatigue properties and toughness. A specific example is the use of linear friction welding to obtain blisks (integral blade/disc assemblies) to replace conventional dovetailed separate blade and disc assemblies.

DB/SPF Diffusion bonding in combination with superplastic forming (DB/SPF) is employed for some titanium components [6]. The diffusion bonding between component parts is obtained by the application of pressure at high temperature in the solid state. The process can replace riveted joints to result in large cost savings, e.g. DB/SPF of titanium alloy wing access panels for the Airbus 310 and 320 resulted in cost savings of over 40 % compared to mechanically fastened aluminium alloy panels.

Other DB/SPF applications include production of wide chord hollow titanium blades for commercial engines and for joining titanium blades.

Brazing Titanium brazing is also employed in aerospace. One such application is brazing of titanium honeycomb sandwich structures using aluminium as filler metal [23]. Brazing alloys based on silver are employed for low-temperature brazing [24], while Ti–Cu–Ni type alloys are used for brazing at high temperature [25].

Brazing is an option where welding is not feasible due to the structural configuration as well as in the case of dissimilar metal combinations. Typical brazing alloys for titanium are given in Table 4.2.

Fig. 4.4 **a** Electron beam welded compressor disc, **b** porosity in EB weld, **c** fatigue originating from pores, **d** microstructure of friction weld free from pores

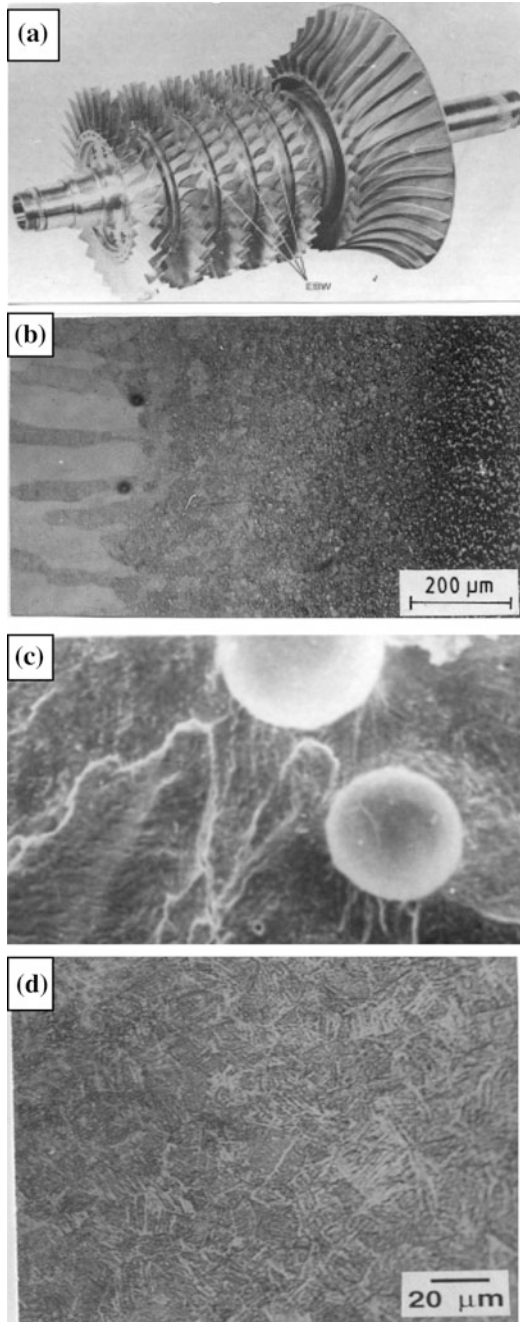


Table 4.2 Compositions of typical brazing alloys for titanium brazing in vacuum

Nominal composition (wt%)	Solidus (°C)	Liquidus (°C)
Ag-5Al	780	810
Ti-20Zr-20Cu-20Ni	842	848
Ti-15Cu-15Ni	902	932
Ag-26.7Cu-4.5Ti	830	850
Ag-9Pd-9Ga	845	880
Ag-21.3Cu-24.7Pd	900	950

It is preferable to braze titanium alloys below the beta transus to avoid grain growth. Care should be exercised in the selection of brazing alloys to overcome the problems of galvanic corrosion and the formation of brittle intermetallics. Silver-base alloys are found to meet these requirements.

Brazing of titanium is always carried out in vacuum since titanium is highly reactive and sensitive to pickup of oxygen, hydrogen and other interstitial elements.

4.2.3 Nickel-Base Alloys

Nickel-base alloys are used in applications requiring creep strength at high temperatures. These alloys are used in cast and forged form particularly in the turbine section for blades, vanes and discs.

Forged components can be welded by many fusion welding processes, including inert gas arc welding and electron beam (EB) welding, which minimises distortion and the heat-affected zone size. Flash butt welding is also used for welding these materials [1, 2]. However, some alloys are prone to liquation cracking and strain-age cracking, and these require solid-state welding processes such as friction welding (see Fig. 4.5) [26]: turbine shaft components are preferably joined by this process. Linear friction welding is reported to be employed for manufacturing and repair of blisks. For sheet metals, resistance welding is in use.

Cast nickel-base alloys with high-alloy content used in creep critical applications are not weldable by fusion welding, owing to cracking problems. These alloys are also not weldable by solid-state welding processes such as friction welding, since they do not have sufficient ductility for the reparability.

In such situations diffusion bonding is employed [6]. Diffusion bonding is feasible with special cleaning procedures, cold-working the surfaces and use of interlayers. Attempts have been made to diffusion bond IN100, by using an electroless nickel coating as an interlayer, as in Fig. 4.6 [7].

Another variant of diffusion bonding is transient liquid phase bonding (TLP). In this process, an interlayer material that melts at lower temperature than the material to be joined is employed. At the bonding temperature the interlayer material melts, and holding at this temperature causes the interdiffusion of elements.

Fig. 4.5 Friction welded Inconel 718

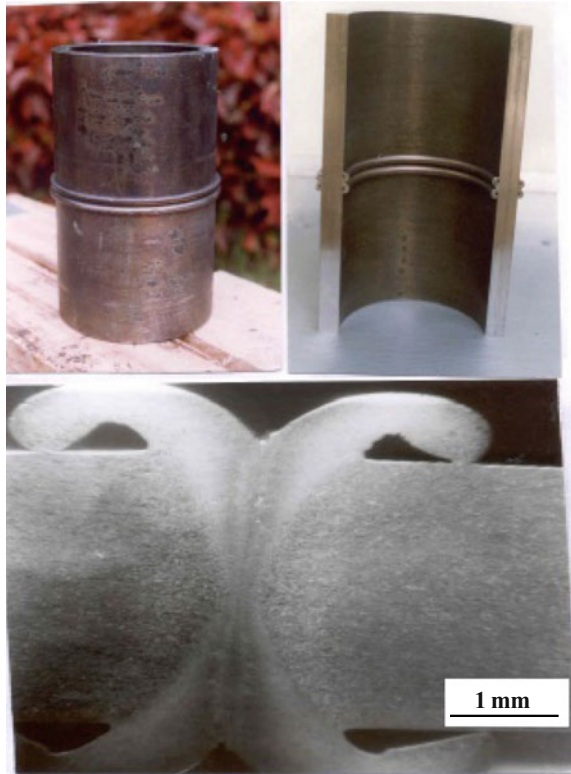
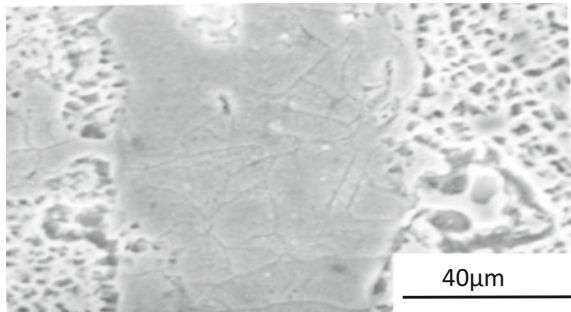


Fig. 4.6 Diffusion bonded IN 100 joint with electroless nickel interlayer



This results in a joint with high remelt temperature. This process is employed for joining and repairing of some nickel-base alloy components [27], including turbine blades and vanes.

Brazing This is widely employed for the repair of gas turbine blades and vanes [9–13, 28, 29]. Nickel-base filler metals in the form of powders, pastes and foils are used. These alloys contain B, Si, P and Au as melting point depressants. Some of these alloys and their modified versions are available in the form of foils obtained via rapid solidification.

The braze alloy selection is based on melting point, flow characteristics, the reaction with the parent metal, the permitted gaps and the remelt characteristics.

The majority of these brazing alloys exhibit high remelt characteristics that facilitate step brazing. In general, brazing is carried out either in vacuum or in a controlled atmosphere in a furnace. Special cleaning procedures are employed to remove oxidised layers to enable braze repair of used blades and vanes.

Brazing requires gap control for the flow of filler metal by capillary forces. However, in turbine blades the holes are not easily approachable, and the gaps cannot be controlled to enable capillary forces to be effective.

In such situations wide gap brazing, also known as activated diffusion brazing, is employed. In this technique the brazing alloy is mixed with parent metal alloy powder or an equivalent alloy powder to form a paste. Brazing cements are then used to apply the paste to reduce the gaps. Other approaches are the use of a solid plug of matching composition of parent metal to reduce the gaps and brazing the areas with conventional filler metals (Fig. 4.7).

In the case of plugging the holes at the bottom of a turbine blade, these holes are difficult to approach, see Fig. 4.8. To apply a brazing alloy in paste form, presintered plugs made from (i) a mixture of parent metal powder and brazing alloy or (ii) proprietary wide gap brazing filler alloys are used.

4.2.4 Steels

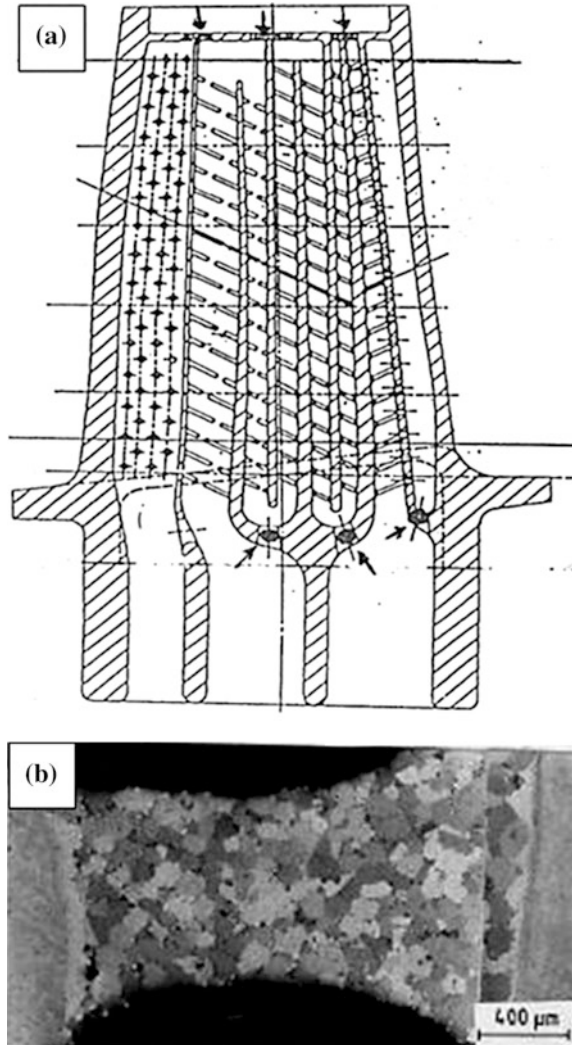
Ultrahigh-strength steels such as carbon-free maraging steels and medium carbon low-alloy steels are employed for rocket motor casings, landing gears, etc. These are mainly welded by inert gas welding processes such as GTAW, employing filler metals of similar composition, or modified versions that avoid segregation that can result in unfavourable properties [30–32]. If component sizes permit it, EB welding is another option. With the advent of friction stir welding (FSW) the possibility exists to weld rocket motor casings circumventing the fusion welding problems such as segregation and porosity, since FSW is a solid-state process.

Stainless steels are employed for tubing, cryogenic tanks, honeycomb structures, heat exchangers, etc. Vacuum brazing of honeycomb structures made of stainless steels is practiced. Nickel-base filler alloys in the form of powder, paste and transfer tape are employed for the purpose [33, 34]. The compositions of some of the brazing alloys are given in Table 4.3.

4.2.5 Dissimilar Metals

Dissimilar metal joining by fusion welding is a major problem in many instances, due to metallurgical incompatibility such as the propensity to form brittle compounds, and solubility issues and grain coarsening. For any metallurgical bonding

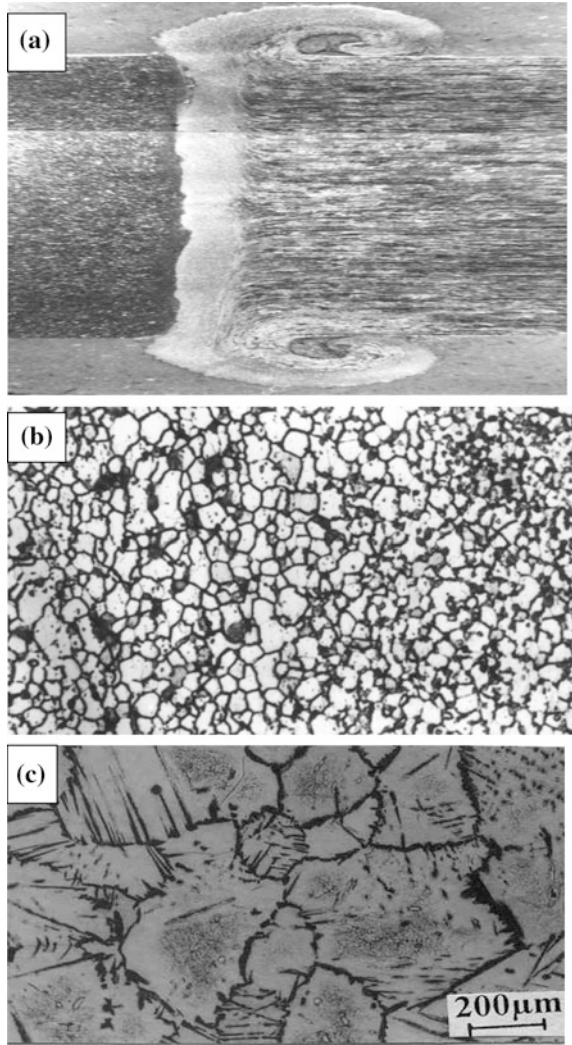
Fig. 4.7 **a** Turbine blade with holes at bottom plugged by brazing (*see arrows*); **b** microstructure in the brazed holes



the metals should exhibit mutual solubility to some degree. Some of these issues are addressed by solid-state welding processes such as friction welding [35], which is generally used to join nickel-base alloys to steels. This minimises the problem of carbon migration from steels to nickel-base alloys.

Friction welding avoids the problem of grain coarsening of ferritic stainless steel in fusion welding. For example, Fig. 4.8 shows friction welding of a ferritic stainless steel with an austenitic stainless steel. The ferritic stainless steel friction weld has a fine grain size (Fig. 4.8b) compared to the (GTAW) weld in Fig. 4.8c.

Fig. 4.8 **a** Friction weld of austenitic–ferritic stainless steel; **b** microstructure of ferritic steel side friction weld and **c** GTAW weld of ferritic stainless steel



The use of interlayers is also possible: maraging steel–low-alloy steel combinations have been successfully welded by using nickel as an interlayer to avoid carbon migration from low-alloy steel [36], and the combination of stainless steel and aluminium has been made possible by friction welding with silver as an interlayer [37].

N.B: the majority of dissimilar metal welding problems can be addressed by brazing and sometimes by diffusion bonding.

Table 4.3 Compositions of typical high-temperature brazing alloys

Alloy designation AWS/Nicrobraz	Composition (wt%)	Recommended brazing temperature (°C)	Remarks
B-Ni1/125	Ni-15.0Cr-4.0Si-3.4B-4.0Fe	1175	Vacuum brazing
BNi-2/LM	Ni-7.0Cr-4.0Si-3.15B-3.0Fe	1040	Vacuum brazing
BNi-5/30	Ni-19Cr-10.12Si	1190	Vacuum brazing (wide gap)
BNi-6/10	Ni-11.5P	980	Vacuum brazing
BNi-7/50	Ni-13Cr-9.0P	980	Vacuum brazing
BAu4/-	Ni-18.0Au	1015	

4.2.6 *Metal Matrix Composites and Oxide Dispersion-Strengthened Alloys*

In the case of metal matrix composites, fusion welding results in particle agglomeration, and in certain cases matrix–particle reactions lead to degradation in properties. For example, EB welding of AA2024 aluminium alloy reinforced with silicon carbide results in the formation of aluminium carbide, and this embrittles the composite on exposure to moisture. Solid-state welding processes, e.g. friction welding, result in particle breaking and variations in the volume fraction of particulates (see Fig. 4.9) owing to the applied pressure during the welding process [38].

Brazing and diffusion bonding are suitable processes to address these issues. These processes are also most suitable for joining oxide dispersion strengthened materials, which encounter similar problems as metal matrix composites.

Transient liquid-phase (TLP) bonding with suitable interlayers is yet another method to join MMCs: aluminium oxide MMC has been reported to have been joined by this process using an aluminium-base interlayer [39].

4.2.7 *Intermetallics*

Intermetallics of titanium such as Ti_3Al (α) and $TiAl$ (γ) that exhibit extraordinary properties at high temperature are gradually being introduced. However, owing to their low ductility at ambient temperatures they have to be fabricated with great care. Processes such as GTAW and EB welding are generally employed to fabricate components of these materials [40]. Ti_3Al has been found to be weldable by friction welding (Fig. 4.10) [41].

Fig. 4.9 AA2014 reinforced with SiC **a** fusion weld and **b** friction weld

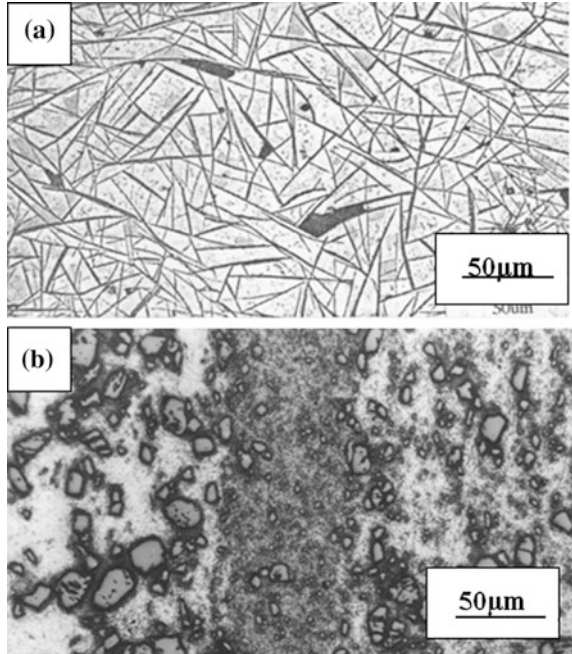
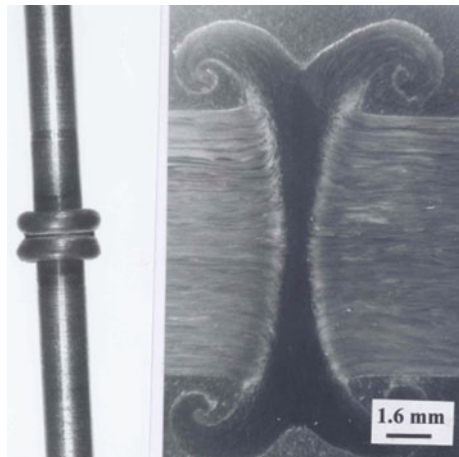


Fig. 4.10 Ti₃Al friction weld [41]



4.3 Innovative Welding Techniques

Heat input control is important in fusion welding processes to minimise distortion, control grain growth in the weld and heat-affected zone (HAZ), and limit the HAZ width. Wherever possible, low heat input high energy density processes are

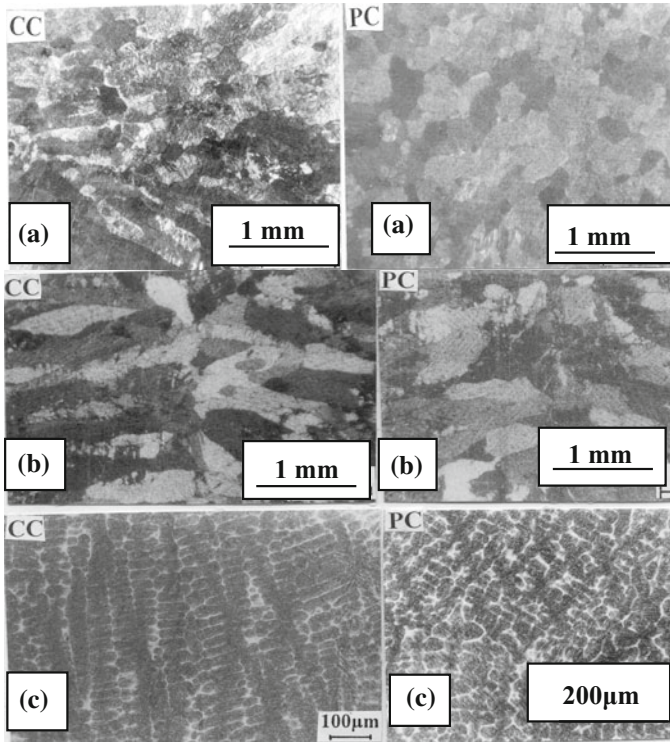


Fig. 4.11 Grain refinement and change of solidification structure in pulse current welding of **a** titanium and **b, c** steel. CC is continuous current, and PC is pulse current

employed. For example, innovative techniques such as pulse mode (PC) welding may be employed in place of continuous current welding (CC) to further reduce heat input as well as to introduce convective flow in the weld region. This achieves grain refinement in the weld region, as well as minimising grain growth in the HAZ near the weld, and also addresses the problem of segregation (Fig. 4.11).

An arc oscillation technique has also been employed to modify the solidification pattern by changing the grain growth direction, thereby reducing solidification cracking and segregation problems [31, 42–45].

4.4 Ceramic–Metal Joining

Ceramic–metal combinations need to be joined in microwave tubes, turbochargers, fuel cells for emergency power system (FCEPS), etc. The joining of metal–ceramic combinations encounters many problems due to wide variations in coefficients of thermal expansion, the inertness of ceramics and their non-conductive nature. For a

Table 4.4 Typical brazing alloys for brazing ceramics and ceramic–metal combinations

Alloy	Composition	Melting point (°C)	Remarks
Ag–Cu	Ag-28Cu	782	Flux brazing, Vacuum brazing
Ag–Cu–Ti	Ag-16Cu-1Ti	772	Vacuum brazing
Ag–Cu–Ti	Ag-26Cu-2Ti	782	Vacuum brazing
Cu–Ag–Ti	Cu-78-10Ag-4Ti	950	Vacuum brazing
Cu–Ti–Ni–B	Cu-29Ni-31Ti-2B	1145	Vacuum brazing

sound and strong bond between the ceramic and metal there should be electron exchange. However, due to their inert nature, ceramics cannot take part in such reactions.

Of the many methods available to join metal–ceramic combinations, brazing is the most versatile and widely used process. In general, ceramics are first metallized by special sintering procedures. In one such method, ceramic surfaces are metallized with an Mo–Mn coating to make them brazeable with conventional filler metals such as Ag–Cu.

Advances in this field have led to the development of active metal brazing, whereby active metals such as Ti are incorporated in the brazing alloy. The active metal reacts with the ceramic to facilitate brazing, thus avoiding the need to metallize the ceramic prior to brazing [46–50]. Compositions of some of the brazing alloys are provided in Table 4.4.

4.5 Advanced Welding Processes

As mentioned in Sect. 4.2.1, friction stir welding (FSW) has been used for welding Space Shuttle external tanks made of aluminium alloy and is reported to give stronger welds than fusion welding. FSW is likely to replace fusion welding in many aerospace applications, since there is no need to use filler metals and it is environmentally friendly. Improved mechanical properties are also important.

Potential applications of FSW include aviation fuel tanks, military and scientific rockets, external (drop) tanks for military aircraft and repair of defective fusion welds. Studies are in progress to weld high-strength steels and titanium alloys using this process. However, the major challenge in applying the process for many high-strength materials is the identification of suitable tool materials.

Another recent advance is magnetic pulse welding (electromagnetic pulse welding, EPW) to weld many similar and dissimilar metal combinations in the solid state. The weld quality is such that the welds pass helium leak detection required for high vacuum applications. EPW is likely to replace explosive welding, friction welding and diffusion bonding in some applications. In this process, forces generated by a magnetic field around a coil and eddy currents in the metal create a very

high impact energy to join the metals. This process has similarities with explosive welding [51–53].

In the future, the possibility exists for the application of friction-based processes such as friction surfacing [54, 55], which results in surface alloying to impart wear and corrosion resistance, and friction processing to grain refine cast components and produce surface composites [55].

Another area that requires careful consideration is the durability of electronic control systems. Soldering is widely employed using mainly lead–tin solders. There is a move to use lead-free solders, and these must withstand vibrations. Microsystems packaging is carried out by transient liquid-phase bonding (TLP) [56], already mentioned in Sects. 4.2.3 and 4.2.6.

4.6 Fixturing, Automation and Post-weld Heat Treatments

Fixturing is a key aspect of successful welding with minimum distortion. This is an area that is almost proprietary to a manufacturer, and is based on in-house experience. Although certain guidelines are available in the open literature, these cannot be directly translated into practice. Heat treatment atmosphere and temperature have to be given due consideration to avoid oxidation and distortion, respectively.

With respect to brazing, the fixture material should have adequate strength at the brazing and heat treatment temperatures, and the coefficient of thermal expansion should be low. For example, the brazing of ceramics to metals uses low expansion alloys such as Kovar or Invar.

Automation to a large extent addresses the problem of variation in weld quality. Weld sequencing could be simplified by deflecting the electron and laser beams in EB and LB welding such that distortion is alleviated in a welded assembly.

Online weld bead monitoring has become useful to prevent the problem of missed joints, e.g. in EB welding where the weld joint is not visible to the welder. Also, cosmetic passes at low power have been able to address undercuts that occur in EB welds

4.7 Summary

This chapter has discussed several types of processes to join similar and dissimilar metals, metal matrix composites, oxide dispersion strengthened metals and ceramic–metal combinations. The processes encompass the following:

- Fusion welding, consisting of arc welding, high energy density beam welding and resistance welding.

- Solid-state welding processes based on frictional energy, diffusion bonding and magnetic pulse welding.
- Brazing.

The selection of a joining process depends on the functional requirements such as strength, heat transfer and electrical properties. If the material characteristics and strength requirements are not met by fusion-based processes, solid-state processes can offer solutions.

Many issues may be addressed by innovative joining processes, namely pulse current and arc oscillations in fusion welding; welding with interlayers for dissimilar metal combinations and ceramic-to-metal welds; TLP bonding for metal matrix composites; and active metal brazing for ceramic-to-metal joining

Other important aspects are control of distortion during welding and post-weld heat treatments by using proper fixturing; and improved quality and consistency by using automated welding, weld sequencing, and online inspection and weld monitoring.

Acknowledgments The author wishes to thank all the former colleagues of the Metal Joining Group at the Defence Metallurgical Research Laboratory, Hyderabad, India, for their support, encouraging collaborative work and contributions that form part of the technical content of this chapter. The author is indebted to DRDO for the support and funding received to conduct some of the studies reported here.

References

1. Patricio FM, Thomas E (2001) Welding processes for aeronautics advanced materials and processes. Massachusetts Institute of Technology, Cambridge, pp 39–43
2. Kah P, Martikainen J (2012) Current trends in welding processes and materials: improve in effectiveness. *Rev Adv Mater Sci* 30:189–200
3. Broomfield RW (1986) On designing with titanium. In *Proceedings of International Conference*, The Institute of Metals, Bristol, UK, pp 69–75
4. Burford D, Widener C, Tweedy B (2006) Advances in friction stir welding and processing for aerospace applications. National Institute of Aviation Research, Wichita State University Airframer, Issue No. 4, pp 3–8
5. Mshara RS, Ma ZY (2005) Friction stir welding and processing. *Materials Science and Engineering*, pp 1–78
6. Diffusion Welding in Aeronautic Industry EWF/IAB. www.EWF.BE—INSTITUTO SUPERIOR TECNICO 2007
7. Mohandas T (Unpublished work) Diffusion bonding of IN100. Defence Metallurgical Research Laboratory, Hyderabad, India
8. Hoppin GS, Berry TF (1970) Activated diffusion bonding a new joining process produces high strength joints in difficult-to-weld superalloy. *Weld J Res Sup* 505–509
9. Demo WA, Ferrigno S, Budinger D, Huron E (2000) Improving repair quality of turbine nozzles using SA650 braze alloy. In: Pollock TM, Kissinger RD, Bowman RR, Green KA, McLean M, Olsen S, Schirra JJ (eds) *Superalloys 2000*, The Minerals, Metals & Materials Society, Warrendale, PA, USA
10. Material Product Data Sheet (2014) Amdry Wide-gap braze and filler powders. DSMB-0003.7, Oerlikon Metco, Westbury, NY, USA

11. Mohandas T, Amith Kumar S, Gopinath K (Un-published work) Wide gap brazing of cm247 LC turbine blade. Defence Metallurgical Research Laboratory, Hyderabad, India
12. Lugscheider E, Schittny Th, Halmoy E (1989) Metallurgical aspects of additive-aided wide-clearance brazing with nickel-based filler metals. *Weld Res Suppl* 19s–13s
13. Fortune D (2014) Wide-gap brazing: a practical approach to a difficult process. White Paper—Wide-Gap Brazing 2002.05, Oerlikon Metco (US) Inc., Westbury, NY, USA
14. Madhusudhan Reddy G, Mohandas T, Sobhanachalam P (2003) Metallurgical and mechanical properties of AA 8090 Al-Li alloy friction welds. In: International welding symposium on emerging trends in welding (IWS2K3), vol 22–23. Indian Welding Society, Hyderabad, India, pp 147–158
15. Madhusudhan Reddy G, Mastanaiah P, Satya P, Mohandas T (2009) Microstructure and mechanical property correlations in AA 6061 aluminium alloy friction stir welds. *Trans Ind Inst Metals* 62(1):49–58
16. Vernia P (1981) Mechanism for critical magnesium diffusion in vacuum brazing of aluminum sheet. *Weld J Res Suppl* 194s–198s
17. Engstrom, H., & Gullman, L. O. (1988). A multilayer clad aluminum material with improved brazing properties. *Weld J Res Suppl* 222s–226s
18. Mallikharjuna Rao K, Mohandas T (1989) Vacuum brazing of heat exchangers for aerospace applications. In: Proceedings of seminar on science and technology of welding in aerospace, HAL, Bangalore, pp 15–25
19. Mohandas T (1994) Mechanical property studies on electron beam and friction welds of an $\alpha+\beta$ titanium alloy. Ph.D thesis, Banaras Hindu University, Varanasi, India
20. Meshram SD, Mohandas T (2010) Comparative evaluation of friction and electron beam welds of a near- α titanium alloy. *Mater Des* 2245–2252
21. Mohandas T, Banerjee D, Kutumbarao VV (2000) Microstructure and mechanical properties of friction welds of an $\alpha+\beta$ titanium alloy. *J Mater Sci Eng A* 289:70–82
22. Mohandas T (2008) Microstructure and mechanical properties of titanium alloy welds. *Metals Mater Processes* 18(3–4):319–340
23. Elrod D, Loveland DT, Davis A (1973) Aluminium brazed titanium honeycomb sandwich structure—a new system. *Weld J Res Suppl* 426–432
24. Onzawa T, Suzumura A, Ko MW (1990) Brazing titanium with low melting point filler metal. *Weld J Res Suppl* 462–467
25. Brazing foils for titanium and titanium alloys Technical Brochure, Engineered Material Solutions, Attleboro, MA, USA
26. Neminathan PV, Mohandas T (2005) Mechanical properties of inertia friction welds of inconel 718. In: International conference 2005 AWS meet
27. Grant O, Cook III C, Sorensen D (2011) Overview of transient liquid phase bonding. *J Mater Sci* 46:5305–5323
28. Winford B (1973) Procedure development for brazing inconel 718 honeycomb sandwich structures. *Weld J Res Suppl* 433s–440s
29. Battenbough AJ, Osmanda AM, Staines AM (2011) Surface preparation for high vacuum brazing. *Nicrobraz News*, Wall Colmonoy, Madison Heights, MI, USA
30. Madhusudhan Reddy G, Mohandas T (1996) Weldability of a high strength low alloy steel. *Int J Join Mater* 8(3)
31. Mohandas T, Madhusudhan Reddy G (1997) A comparison of continuous and pulse current arc welding of ultrahigh strength steel. *J Mater Process Technol* 69:222–226
32. Mohandas T, Madhusudhan Reddy G, Rajeswara Rao SVNND (2007) Material joining R&D at DMRL. *Metals Mater Processes* 19(1–4):273–296
33. Lugscheider E, Partz KD (1983) High temperature brazing of stainless steel using nickel base fillers BNi2, BNi-5 and BNi7. *Weld J Res Suppl* 160s–164s
34. Mohandas T, Mallikharjuna Rao K (1985) Vacuum brazing of stainless steel heat exchangers. DMRL TR 8502

35. Madhusudhan Reddy G, Mohandas T, Samba Siva Rao A, Satyanarayana VV (2005) Influence of welding processes on microstructure and mechanical properties of dissimilar austenitic-ferritic stainless steel welds. *Mater Manuf Processes* 20:147–173
36. Madhusudhan Reddy G, Venkat Ramna P (2012) Role of nickel as interlayer in the dissimilar metal friction welding of maraging steel to low alloy steel. *J Mater Process Technol* 2(1):66–77
37. Madhusudhan Reddy G, Sambasiva Rao A, Mohandas T (2008) Role of electro plated interlayer in continuous drive friction welding of AA6061 to AISI304 stainless steel. *Sci Technol Weld Joining* 13(7):619–628
38. Madhusudhan Reddy G, Mohandas T, Bhanuprasad VV (2003) Friction welding studies on SiCp reinforced aluminium alloy AA2124 metal matrix composite. In: Proceedings of National welding seminar, Kolkatta, Paper No. IIB No. 3, 23–25 Jan 2003
39. Zhat Y, Nrth TH, Serrato Rodrigues J (1997) Transient liquid phase bonding of alumina and metal matrix composite base materials. *J Mater Sci* 32(6):1393–1397
40. Madhusudhan Reddy G, Mohandas T (2001) Observations in welding studies of an $\alpha_2+O+\beta$ titanium aluminide. *Sci and Technol Weld* 6(5):300–304
41. Madhusudhan Reddy G, Mohandas T (2004) Friction welding studies on $\alpha_2+O+\beta$ titanium aluminide. In: International symposium on joining of materials, SOJOM 2004, 22–23 July 2004, Tiruchirappalli, Tamil Nadu, India
42. Madhusudhan Reddy G, Mohandas T (2001) Explorative studies on grain refinement of ferritic stainless steels. *J Mater Sci Lett* 20:721–723
43. Madhusudhan Reddy G, Swati B, Mohandas T (2007) Effect of electron beam oscillation on the microstructure, residual stresses and mechanical properties of Ti-6Al-4 V welds. *Metals Mater Processes* 19(1–4):307–320
44. Mohandas T, Madhusudhan Reddy G (1996) Effect of frequency of pulsing in gas tungsten arc welding on microstructure and mechanical properties of titanium alloy welds. *J Mater Sci Lett* 15:626–628
45. Madhusudhan Reddy G, Srinivasa Murthy CV, Viswanathan N, Prasad Rao K (2007) Influence of electron beam oscillation technique on solidification behaviour and stress rupture properties of inconel 718 welds. *Sci Technol Weld Joining* 12:106–114
46. Walker CA, Hodges VC (2008) Comparing metal-ceramic brazing methods. *Weld J* 87:43–50
47. Liebherr-Aerospace & Transportation SAS (Undated) The innovative aircraft emergency power system based on fuel cell technology made by Liebherr. Toulouse, France. www.liebherr.com
48. Prakash P, Mohandas T, Rama Rao VV (2003) Studies on ceramics-metals joining through active metal brazing route. In: Proceedings of national symposium on vacuum science, technology and metallurgy IVSNS-2003, BARC, Mumbai, pp 451–457
49. Mohandas T (2007) Ceramic-metal joining. *Metals Mater Processes* 19(1–4):69–88
50. Prakash P, Mohandas T, Dharma Raju P (2005) Microstructural characterization of SiC ceramic and SiC-metal active metal brazed joints. *Scripta Materialia* 52:1169–1173
51. Shribman V (2008) Magnetic pulse welding for similar and dissimilar materials. In: 3rd international conference on high speed forming. Pulsar Ltd., Yavne
52. Shribman V, Livshitz Y, Gafri O (2007) Magnetic pulse solid-state welding. IIW/IIS Commission Florence, Italy
53. Aizawa T, Kashani M, Okagawa K (2007) Application of magnetic pulse welding for aluminum alloys and SPCC steel sheet joints. *Weld J Suppl*, May 2007 86:119s–124s
54. Madhusudhan Reddy G, Srinivasa Rao K, Mohandas T (2011) Friction surfacing: novel technique for metal-matrix composite coating on aluminum—silicon alloy. *Surf Eng* 27(2):92–98
55. Madhusudhan Reddy G, Satya Prasad K, SrivasaRao K, Mohandas T (2009) Friction surfacing of titanium alloy with aluminium metal matrix composite. *Surf Eng* 25(1):25–30
56. Welch W (2005) Transient liquid phase (TLP) bonding of microsystem packaging applications. In: 13th international conference on solid state sensors and actuators and microsystems, vol 2, pp 1350–1353

Chapter 5

Nanomanufacturing for Aerospace Applications

S. Anandan, Neha Hebalkar, B.V. Sarada and Tata N. Rao

Abstract In this chapter synthesis of nanomaterials by various nanomanufacturing (top-down and bottom-up) processes, synthesis and properties of aerogel, and advanced electrodeposited coatings and their properties, are reviewed. Further, the potential applications of nanomaterials, aerogels, and electrodeposited coatings in the aerospace industry are concisely surveyed.

Keywords Nanomanufacturing · Graphene · Aerogels · Alloys · Composites · Coatings · Propellants

5.1 Introduction

Nanomanufacturing includes all processes aimed towards building of nanoscale materials in the range of 1 to 100 nm in 1D, 2D, and 3D structures, features, devices, and systems suitable for integration across higher dimensional scales (micro, meso, and macro) to provide functional products and services. Nanomanufacturing covers the manufacturing of parts “bottom-up” from nanoscaled materials or “top-down” in small steps for high precision, used in several technologies such as laser ablation and etching. Interestingly, nanomanufacturing remains as an essential bridge between the discoveries of nanosciences and real-world nanotechnology products. Recent nanomanufacturing projects have mainly focussed on nanomaterials production or nanomaterial use in industrial processes.

The use of nanomanufacturing for the enhancement of electrical energy storage in batteries and super-capacitors is very promising. Nanotechnologies can improve the capacity and safety of lithium-ion batteries, e.g. by enabling new ceramic,

S. Anandan · N. Hebalkar · T.N. Rao (✉)
Centre for Nanomaterials, ARCI, Hyderabad, India
e-mail: tata@arci.res.in

B.V. Sarada · T.N. Rao
Centre for Solar Energy Materials, ARCI, Hyderabad, India

heat-resistant and still-flexible separators, and high-performance electrode materials.

5.2 Nanomanufacturing Processes

There is a wide variety of techniques that are capable of creating nanostructures with various degrees of quality, speed, and cost. These manufacturing approaches fall under two categories: “bottom-up” and “top-down”, as shown in Fig. 5.1.

5.2.1 Bottom-up Method

This is defined as the method which begins with atoms and molecules that react under physical or chemical circumstances to form nanostructures. Examples of the bottom-up method are as follows:

- Chemical vapour deposition (CVD)
- Atomic layer deposition (ALD)
- Crystal growth (sol-gel, hydrothermal, solvothermal, and precipitation)
- Self-assembly (building blocks, interactions, and applied forces).

The hydrothermal synthesis approach is one of the most well-known methods, and it is traditionally used for the synthesis of nanoparticles of various metal oxides.

In the subsequent paragraphs of this subsection, we briefly review the following bottom-up processes:

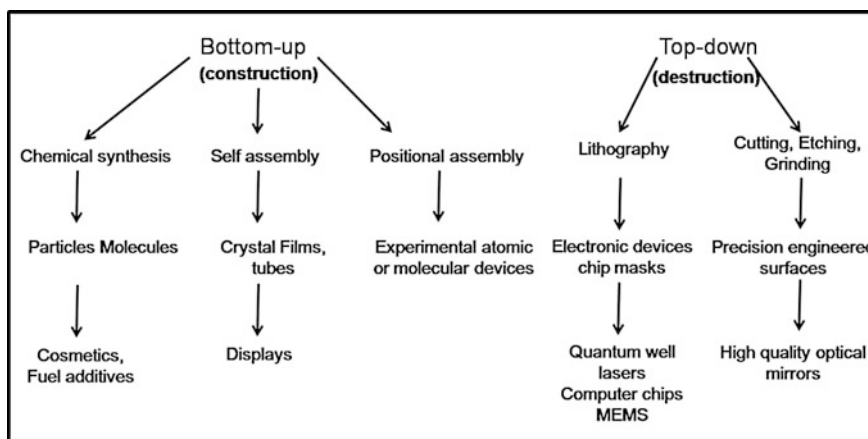


Fig. 5.1 Overview of nanomanufacturing processes

1. Hydrothermally-assisted synthesis of metal oxides.
2. Carbon-based materials synthesis.
3. Flame spray pyrolysis (FSP).

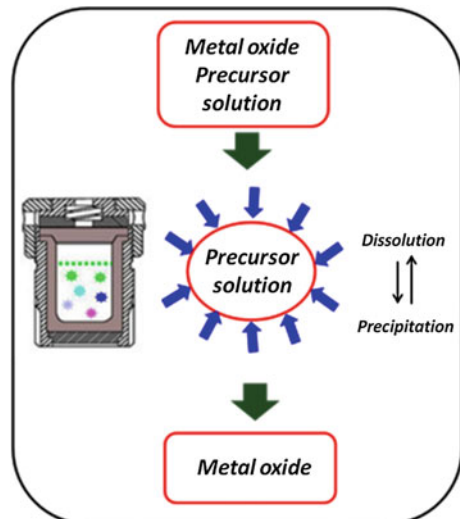
Hydrothermal Synthesis Hydrothermal synthesis is a process involving single or heterogeneous phase reactions in aqueous salt solutions, using closed-systems at elevated temperatures and pressures to crystallize nanomaterials directly from solution [1–5]. Figure 5.2 illustrates the mechanism of hydrothermally assisted synthesis of metal oxides.

The solubility of many oxides in hydrothermal solutions of salts is much higher than in pure water, and such salts are called mineralizers. Hydrothermal synthesis can be influenced both under temperatures and pressures below the critical point for a specific solvent (above which differences between liquid and vapour disappear), and under supercritical conditions.

It has been reported that the crystal orientation, size, and shape of nanocomposites synthesized by hydrothermal reactions strongly depend on the various experimental parameters, including the volume of precursor, nature of the solvent, the mineralizer, reaction time, and temperature.

Synthesis of Carbon Based Materials Carbon based materials possess excellent mechanical, electrical and thermal properties, facilitating their use as reinforcements or additives in various materials. Carbon fibre-reinforced polymer (CFRP) composites are much used in aerospace, see Chap. 14 in Volume 1 of these Source Books.

Fig. 5.2 Schematic of hydrothermal synthesis of metal oxides



Techniques have been developed to produce appreciable amounts of carbon materials in natural, incidental and controlled flame environments, and without catalysts:

1. Single wall thin and superconductive carbon nanotubes with diameters of 0.7–2 nm have been grown by carbonizing template molecules of tripropylamine.
2. Multi-walled carbon nanotubes with diameters ~ 30 nm have been synthesized using mesoporous silica as hard templates, again in the absence of metal catalysts. Here the precursor was heat treated in an inert atmosphere to pyrolyze the organic components into graphitized carbon.

In addition to carbon nanotubes, both hard- and soft-templating techniques [6, 7] have been developed for the synthesis of ordered mesoporous carbon with controlled pore size and structure, using mesoporous silica as the template and sucrose as the carbon precursor. The following steps were involved:

- Preparation of a composite of mesoporous silica impregnated with carbon, see Fig. 5.3.
- Polymerization and carbonization of the carbon at high temperature under vacuum or inert atmosphere.
- Removal of the silica template by etching with hydrofluoric acid or NaOH, resulting in regular mesoporous structures purely composed of carbon [8, 9].

As shown in Fig. 5.3, mesoporous carbon materials with various geometries can be obtained by appropriate selection of the silica template.

Flame Spray Pyrolysis (FSP) FSP is the process whereby nanoparticles are formed from conversion of a liquid precursor in a flame, followed by collision and cohesion of the reaction products in the high temperature environment, see Fig. 5.4.

Fig. 5.3 Synthesis of mesoporous carbon with the hard templating technique

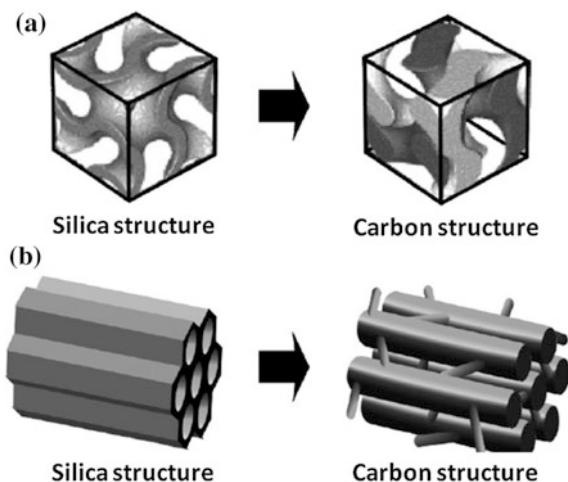
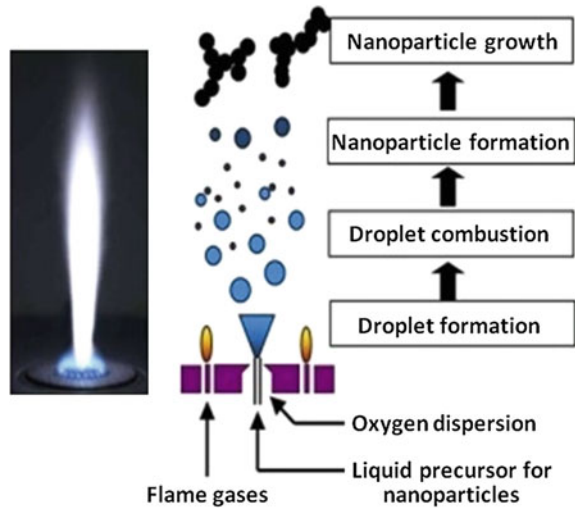


Fig. 5.4 Nanoparticle formation by flame spray pyrolysis (FSP)



FSP is a highly attractive method for large scale preparation of metal oxide nanoparticles. These are being widely applied in “high tech” industries owing to their novel electronic, chemical, catalytic, magnetic, and mechanical properties deriving from their high surface to volume ratio and quantum size effects.

There is an increasing demand for metal oxide nanoparticles from major end-user industries, including the aerospace, automotive and pharmaceutical sectors, and for electronics applications.

5.2.2 Top-Down Method

This is defined as the method which begins with bulk materials (top) that are subsequently reduced to nanostructures (down) by physical, chemical, or mechanical processes. Examples of top-down approaches are as follows:

- Mechanical (milling, extrusion, and grinding)
- Thermal (evaporation, sputtering, and ablation)
- Chemical (reactive, chemical etching)
- High energy (combustion and sonication)
- Patterning methods (optical and physical lithography, tip-based fabrication).

Two of the best-known methods are mechanical milling and use of RF-induction plasmas to synthesize various metal oxides and metal nanoparticles from bulk particles. These methods are briefly reviewed in the following paragraphs.

Mechanical Milling This method has been widely exploited for synthesizing various nanomaterials, nanograins, nanoalloys, nanocomposites, and nano- and

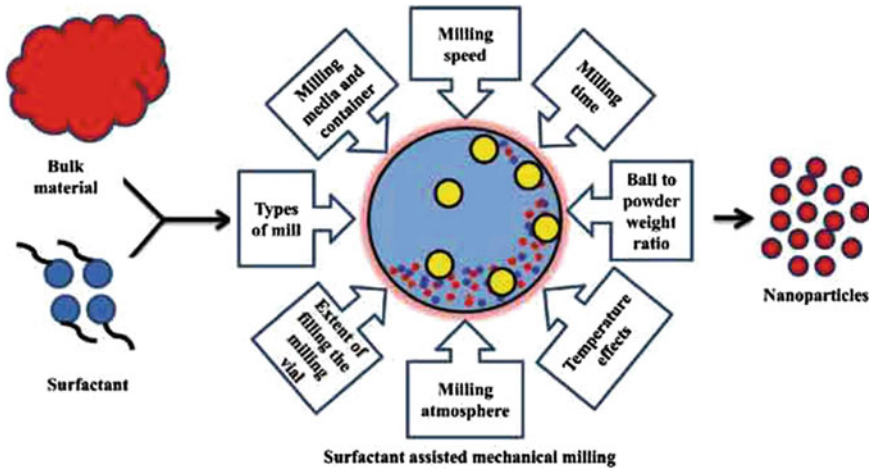


Fig. 5.5 Mechanical milling conversion of bulk material into nanoparticles

quasi-crystalline materials. Planetary and horizontal ball mills, attritors, and 1D and 3D vibrating equipment are well known and used for manufacturing powders.

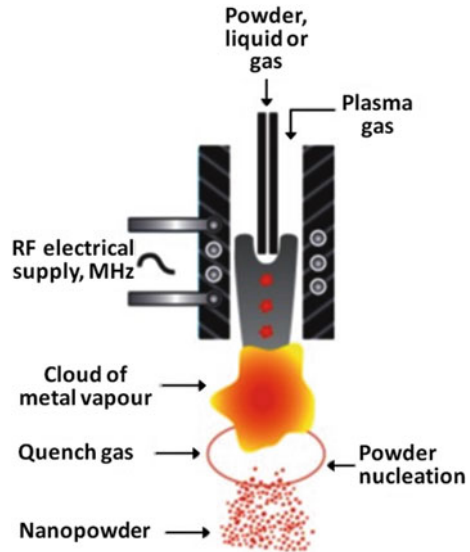
Mechanical milling or alloying is a non-equilibrium processing technique in which different elemental powders are milled in an inert atmosphere to create a single mixed powder with the same composition as the constituents. A schematic of the process is shown in Fig. 5.5. It is evident from this Figure that mechanical milling is a complex process with many parameters that determine the final product.

After milling, the powders can be added to coatings and paint systems; or else bulk materials can be made by re-consolidating the powders, e.g. by hot isostatic pressing (HIP) or cold isostatic pressing (CIP) and extrusion. These techniques have been used to produce amorphous and nanocrystalline alloys as well as metal/nonmetal nanocomposite materials.

RF-Induction Plasmas RF-induction plasmas can be used to synthesize nanometric materials starting from different precursors either in the powder, liquid, or gaseous states. High temperatures and a high heat transfer environment enable evaporating nearly any material. A controlled and rapid quench causes the formation of nanopowders in the 20–100 nm range. Figure 5.6 gives a schematic of the process (in this case producing metal powder).

The RF-induction plasma set-up is contained in a chamber enabling synthesizing a wide range of nanopowders under inert or reducing atmospheres. The chamber is typically made of stainless steel with double walls to enable water cooling the inside surface.

Fig. 5.6 RF-induction plasma set-up for producing nanopowders



5.2.3 Graphene: A Special Case

Graphene has recently emerged as the most promising nanomaterial due to its unique mechanical properties (Young's modulus ~ 1 TPa; tensile strength ~ 130 GPa), good electrical conductivity, and excellent thermal properties (thermal conductivity $\kappa \sim 5000 \text{ W m}^{-1} \text{ K}^{-1}$).

The quality of the graphene plays a crucial role in improving the structural, physical, and chemical properties. Despite intensive R&D over the last decade, the reproducible production of high-quality graphene on a regular and reproducible basis has not yet been achieved.

Graphene can be manufactured both by bottom-up processes, e.g. CVD, epitaxial growth on SiC, arc discharge, and chemical synthesis; and top-down methods, e.g. chemical and electrochemical exfoliation processes.

Figure 5.7 shows a complex schematic illustrating the different production methods for graphene and a survey of its potential applications.

5.2.4 Challenges

The challenge facing integrated system nanomanufacturing is the control of nanoscale multidisciplinary phenomena, i.e. involving physics, chemistry, biology, material sciences, engineering, and information technology.

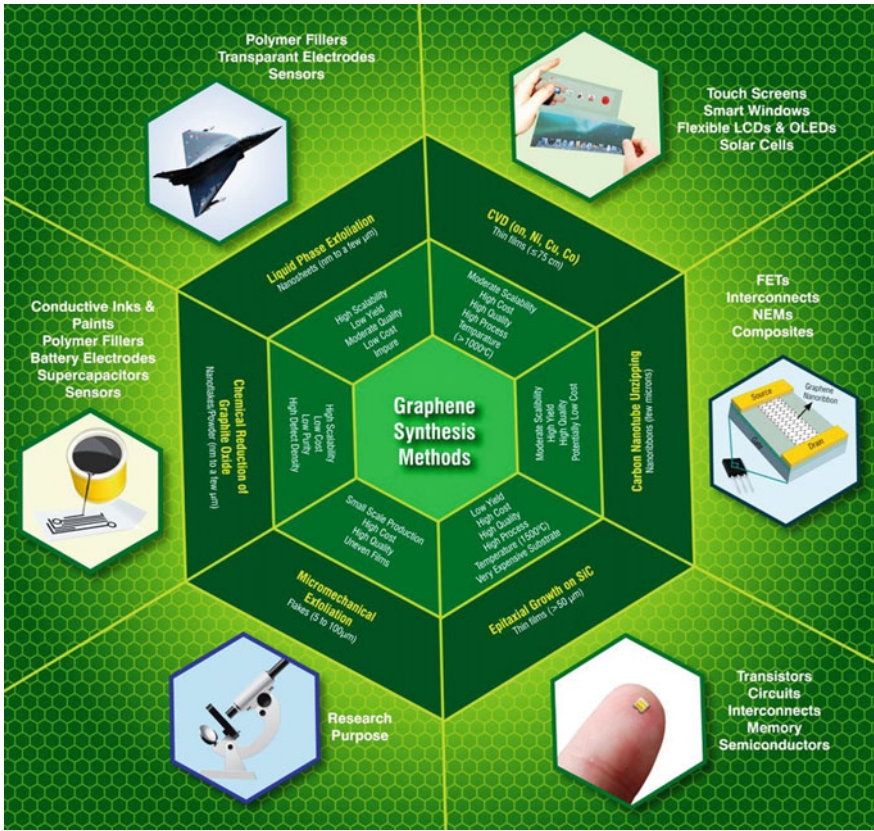


Fig. 5.7 |Schematic of production methods for graphene and a survey of its potential applications

The collective knowledge of these disciplines will redefine the relationships between materials, processes, and property phenomena, allowing for the development of novel nanomanufacturing techniques.

Novel techniques will help to bridge the manufacturing gap between R&D innovations and the commercial viability of nanotechnology. The critical challenges for systems nanomanufacturing are the need to (i) control assembly of three-dimensional heterogeneous systems, (ii) process nanoscale structures in high-rate/high-volume applications without compromising their inherent properties, and (iii) ensure the long-term reliability of nanostructures.

These challenges reflect the need for research in the characterization of nano-materials in terms of the building blocks of nanostructures, in both top-down and bottom-up processes. Further, they require advanced instrumentation to measure and characterize nanostructures in order to (i) provide predictive simulation of nanostructural behaviour and (ii) contribute to the design and integration of nano-devices and systems. Finally, knowledge sharing and outreach is a challenge to be

overcome to enable technology transfer and contribute to public awareness of nanotechnologies.

5.3 Nanoporous Aerogels

Highly porous aerogels with nanopores are superior thermal insulators and extremely lightweight. Aerogels consist of 99 % air and 1 % solid. Consequently they weigh almost nothing. They can be made from various materials, including silica, alumina, titanium oxide, mixed oxides, a variety of polymers, carbon, and composites with other nanomaterials. In particular, silica aerogel possesses extraordinary properties such as ultra-low density, excellent thermal insulation, lower refractive index, and lower dielectric constant than any solid.

Despite several efforts, the commercial use of aerogels has not been realised. NASA has used aerogels for some space missions, including capturing comet and interstellar dust (the Stardust Mission) and for thermal insulation in the Mars Pathfinder and Mars Exploration Rovers [10]. Potential applications in aircraft are as thermal and acoustic insulation [10, 11], but aerogels are expensive materials and current materials perform these tasks adequately.

5.3.1 Preparation of Aerogels

Aerogels are synthesized by the sol-gel process, illustrated schematically in Fig. 5.8. The silicon alkoxide is Tetraethoxyorthosilicate (TEOS). This forms a 3D silica network when hydrolyzed. A special drying process, supercritical drying

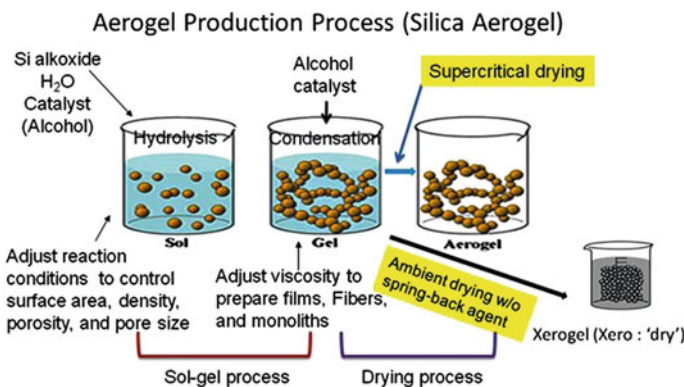


Fig. 5.8 Schematic of the sol-gel production process for silica gel. Courtesy of Dr. Pamela Norris, Aerogel Research Laboratory, Department of Mechanical and Aerospace Engineering, University of Virginia, Charlottesville, VA 22904-4242, USA

Table 5.1 Typical properties of silica aerogels

Property	Value	Comment
Porosity	>90 %	Highly porous synthetic material
Density	0.003–0.5 g/cm ³	Most common value ~0.1 g/cm ³
Surface area	>1000 m ² /gm	Determined by nitrogen adsorption
Refractive index	1.05–1.1	Very low for a solid material
Thermal tolerance	800 °C	Weight loss starts slowly above 800 °C
Thermal conductivity	~0.003 W/mK	Lower than values for most common insulators
Electrical resistance	~GΩ	Similar to dense silica
Dielectric constant	~1.1	For density 0.1 g/cm ³ : very low for a solid material
Young's modulus	10 ⁴ –10 ⁷ N/m ²	Very low compared to dense silica
Speed of sound	20 m/s	For density 0.005 g/cm ³

(SCD) [12], is used to remove liquid from the wet gel. SCD entails drying above the critical point of the liquid in the gel, thereby avoiding surface tension and capillary pressure that would alter the pore structure and network shape.

5.3.2 Properties of Aerogels

Aerogels possess many interesting properties because of their highly porous structure. Some typical properties of silica aerogels are listed in Table 5.1:

1. **Porosity.** This varies from 500–1500 m²/gm for different density aerogels [13].
2. **Thermal conductivity.** This is explained by Lu et al. [14]. In porous materials like aerogels, the total thermal conductivity (λ_t) is the summation of all three modes of thermal conduction: viz. gaseous (λ_g), radiative (λ_r), and solid (λ_s).

$$\lambda_t = \lambda_g + \lambda_r + \lambda_s.$$
3. **Mechanical properties.** Aerogels become more brittle as the density decreases. Various strategies have been used to incorporate aerogels into fibre matrices [15]. Another approach is to make aerogels in granular form and sandwich the granules between plates, fabrics, and plastic sheets to make insulating panels or sheets. Figure 5.9 illustrates such sheets prepared in the authors' laboratory and their insulating properties.

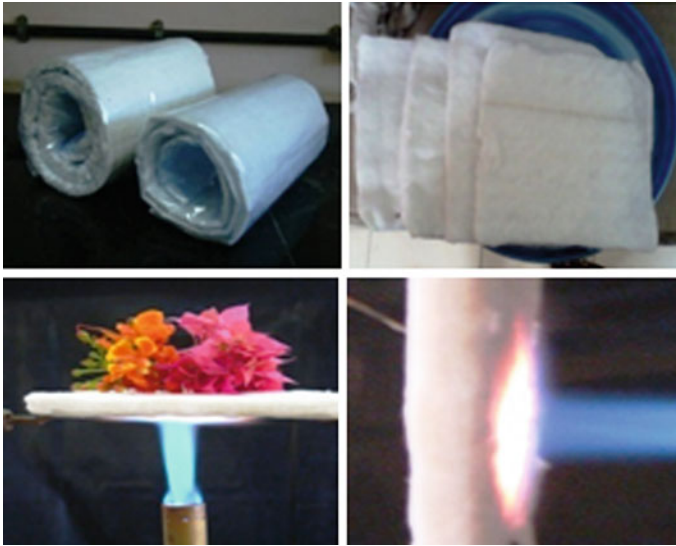


Fig. 5.9 Silica aerogel flexible rolls and sheets and their excellent thermal insulation and fire resistance: authors' laboratory (ARCI)

5.4 Electrodeposited Nanostructured Coatings

The aerospace sector has been a major promoter of the development and application of advanced engineering materials [16]. There is a need for advanced coatings in the aerospace industry [17]. Coatings consisting of nanograins, nanostructures and nanophases, known as nanocoatings, have gained much importance in recent years owing to their much improved properties compared to conventional ones. Nanocoatings are expected to have the potential to replace conventional coatings owing to the unique mechanical, electrical, thermal, and anticorrosive properties that they offer [18, 19].

Although there are other techniques used for producing nanocoatings, including both vacuum and non-vacuum thermal spray and sputtering deposition methods, the most widely used industrial coating techniques involve electrodeposition and electroless deposition. These approaches are widely used since they are comparatively simple and economical, and may be used for a wide variety of coatings.

Electroplating or electrodeposition is one of the oldest and most widely used coating techniques in several fields of technology to protect materials against corrosion, improve the surface properties, and achieve optimum decorative effects [20]. Since electrodeposition is an atomistic deposition process, it can be used to produce nanocoatings.

The obvious advantages of electrodeposition are its rapidity, low cost, freedom from pores, high purity, ability to produce coatings on widely differing substrates,

and potential to overcome shape limitations, i.e. allowing the production of free-standing parts with complex shapes.

Owing to these advantages, electrodeposition technology with novel pulsed processes has progressed into nanotechnology to produce several metal and metal-ceramic nanocoatings [21]. Pulsed electrodeposition (PRED) can be done by the application of voltages or currents in the form of forward and reverse pulses in millisecond frequencies. The alternate forward and reverse pulses separated by zero voltage/current facilitate better control over the deposition process [22].

5.5 Potential Aerospace Applications: A Concise Survey

Nanotechnology is being proposed for many applications, mainly for engines, in the automotive and aerospace industries. However, the commercial introduction of nanostructured materials in the aerospace industry is unlikely in the near future, even for the most promising developments. Thus for this Source Book chapter, a concise survey will be given here.

5.5.1 Nanostructured Alloys

A major reason for developing nanotechnology alloys is the potential for ultrahigh yield and tensile strengths. Equal Channel Angular Extrusion (ECAE) is the most widely used method to obtain nanotechnology bulk metals and alloys: see Sect. 2.5.2. in Chapter 2 of this Volume.

There are at least three major problems concerning the use of nanostructured alloys in aerospace components: (i) processing to achieve the necessary ultrafine grain sizes is poorly reproducible, (ii) important mechanical properties like ductility and fatigue and fracture are inferior to those of conventional structural alloys, and (iii) the higher manufacturing costs [23].

5.5.2 Carbon Nanocomposites

Excellent mechanical, thermal and electrical properties, along with their ultrahigh surface area make carbon nanotubes and graphene promising nanoscale fillers for metal, ceramic, and polymer composites.

For nonstructural applications these materials could act as matrix modifiers in controlling the electrical and thermal conductivity. Electrical conductivity applications include improved resistance of CFRP components to lightning strikes and for EM shielding. For structural applications carbon nanotubes and mesoporous carbon have the potential to improve the compression strength, stiffness, and damage resistance of CFRPs.

5.5.3 *Aluminium-Based Propellant Materials*

Metallic nanoparticles have unique combustion properties, such as very rapid ignition and short combustion times. Since aluminium is an important ingredient in propellants, aluminium nanoparticles could be used to improve the ballistic performance of propulsive systems [24].

For example, nanoparticles could favour the use of cryogenic solids and water slurries in chemical rocket propulsion. This is because the rate-limiting step for combustion is the mixing and reacting of the pyrolyzing fuel grain with the liquid oxidizer flowing through the centre port of the solid–fuel grain [25].

Nanosized aluminium particles can be coated with a protective oxide layer to avoid the disadvantages of aggregation, agglomeration, and inadvertent ignition.

N.B: The ARCI (Hyderabad) has the capability to produce passivated nanosized Al powder in kilogram quantities with active aluminium contents of 85–90 wt%.

5.5.4 *Aerogel Thermal Insulation*

As mentioned at the beginning of Sect. 5.3, the commercial use of aerogels (which includes suggested aircraft applications) has not been realised. However, NASA has used aerogels for some space missions. Also, the use of aerogel insulation for space vehicle cryogenic tanks has been investigated [26–28].

5.5.5 *Electrodeposited Coatings*

Nanocoatings represent the most likely near-term incursions of nanotechnology into aerospace usage. A shortlist of the potential applications is given in the following paragraphs.

Hard Chromium Replacement Hard chromium electroplating has been—and still is—widely used for corrosion and wear protection in aerospace applications. However, the plating process uses an electrolytic bath containing hexavalent chromium, which is a carcinogen.

Most of the conventional electroplating alternatives have been based on nickel alloys [29], but these are also undesirable from an environmental standpoint. Since electroplating should be an environmentally friendly process, the foregoing problems have stimulated the search for better protective coatings [30, 31].

Environmentally compatible electrodeposited nanoscale coating alternatives for hard chromium have been widely investigated [32–35]. Nanocrystalline coatings of Co-based alloys (Co–P, Co–W, Co–Ni–Fe, Co–W–Fe) or Co-based

nanocomposites (Co–P–SiC, Co–Ni–YZA, Co–W–Al₂O₃) coatings have shown superior mechanical and corrosion properties for aerospace use [32–34].

Cadmium Replacement Cadmium plating has several highly attractive properties: excellent corrosion resistance, sacrificial protection for steels, galvanic compatibility with aluminium, inherent lubricating ability (essential for plated steel bolts), and good electrical conductivity, making cadmium plating well-suited to electronic equipment.

Unfortunately, cadmium plating also uses carcinogenic electrolytes. Electrolytic nanocoatings with zinc-based alloys and composites have been developed for this purpose. Some of them (Zn–Ni, Zn–Sn, Zn–Fe, Zn–Ni–TiO₂, Zn–Ni–SiO₂, and Zn–Ni–Al₂O₃) have corrosion resistance and protective properties comparable to cadmium and may even be somewhat better [35–37].

De-icing and Hydrophobicity Ice build-up on aircraft, particularly the wing leading edges, is a major concern. Considerable efforts have been made to develop hydrophobic and superhydrophobic surfaces and coatings: see also Chap. 25 in Volume 1 of these Source Books.

Superhydrophobic coatings are expected to lower the heating power required to keep leading edges ice-free, reduce any runback ice, and lower water adhesion. Kim et al. [38] have shown that nanoscale liquid-infused nanoscale porous surfaces on aluminium (i) significantly reduce ice accumulation by allowing water droplets to slide off before they freeze and (ii) enable easy removal of the accumulated ice and melted water by gravity at low tilt angles.

5.6 Indian Scenario

Nanomanufacturing research activities are progressing in India through various academic (IIT, NIT, IISc) and R&D (CSIR, DST, DRDO) institutes and industries. However, it remains a big challenge to scale-up the nanomanufacturing process for mass production and industrial applications. There is an urgent need for up-scaling to make nano-based technology commercially viable in India.

At the International Advanced Research Centre for Powder Metallurgy and New Materials (ARCI) we are taking up this challenge by establishing suitable pilot scale and testing facilities for potential applications that will cater to either a large Indian market or a market unique to India. Some of these activities are listed below:

1. Large scale synthesis of nanosized aluminium powder for increased performance of solid rocket propellants has been carried out at the ARCI using the RF-induction plasma method.
2. Aerogel research is done in several R&D laboratories. The basic research on silica aerogels, their functionalities, and thermal insulation properties has been done by Shivaji University and the University of Pune. Various organic,

carbon-based aerogel applications in the energy sector, such as fuel cells and supercapacitors, are being studied in the Centre for Electrochemical Research Institute and the Centre for Materials for Electronics Technology.

ARCI has made substantial efforts to develop aerogel-based thermal insulation technology and also has demonstrated its use for aerospace application.

3. ARCI has been working on layered and graded nickel coatings and nanocoatings of Ni–W obtained from pulse electrodeposition. These coatings show great improvements in corrosion and tribological properties with respect to their monolithic counterparts [39].
4. Pulsed electrodeposition (PRED) has been used to make graphene-reinforced copper (Cu–Gr) composite foils in order to enhance the mechanical properties of copper while maintaining the electrical properties for their use in electronics [40].
5. Research groups at the National Aerospace Laboratories (NAL) have developed Ni–Co and Ni–Co–ZrO₂ coatings by electrodeposition and heat treatment. The tribological properties and corrosion resistance of the Ni–Co–ZrO₂ coating were found to be better compared to hard chromium plating.
6. Ullal and Hegde [41] have shown that multilayer nanocoatings of Zn–Ni–SiO₂ are enormously more resistant to corrosion than similar monolayer Zn–Ni–SiO₂ coatings, which are themselves about 1.5 times more resistant than monolayer Zn–Ni alloy coatings.
7. The research group at Alagappa University has recently shown that the corrosion properties of Ni–Si₃N₄ nanocomposite coatings are superior to those of pure Ni coatings deposited under similar PRED conditions [42].

5.7 Summary and Conclusions

The first section of this chapter has discussed some bottom-up and top-down nanomanufacturing processes: in particular, hydrothermal synthesis, synthesis of carbon-based materials, and flame spray pyrolysis (bottom-up); and mechanical milling and RF-induction plasma synthesis (top-down).

The following section describes the general process of aerogel production and summarizes the extraordinary properties of aerogels, in particular silica aerogels. The next section discusses advanced coatings for improved resistance to corrosion, friction, and wear. The final sections are concise surveys of (i) potential applications of nanomaterials, aerogels, and electrodeposited coatings in the aerospace industry and (ii) the nanomanufacturing R&D activities in India.

Acknowledgments The authors thank the editors for many useful corrections and they are particularly grateful to Dr. RJH Wanhill for a number of critical review comments.

References

1. Byrappa K (ed) (1992) Hydrothermal growth of crystals. Pergamon Press, Oxford
2. Yoshimura M, Suda H (1994) Hydrothermal processing of hydroxyapatite: past, present, and future. In Brown PW, Constanz B (eds) Hydroxyapatite and related materials. CRC Press Inc., Boca Raton, pp 45–72
3. Boyer R, Welsch G, Collings EW (eds) (1994) Materials properties handbook: titanium alloys. ASM International, Materials Park
4. Jeng SM, Yang J-M (1993) Creep behavior and damage mechanisms of SiC fiber-reinforced titanium matrix composites. *Mater Sci Eng A* 171:65–75
5. Leyens C, Hausmann J, Kumpfert J (2003) Continuous fiber reinforced titanium matrix composites. Fabrication, properties and application. *Adv Eng Mater* 5:399–410
6. Wan Y, Shi YF, Zhao DY (2008) Supramolecular aggregates as templates: ordered mesoporous polymers and carbons. *Chem Mater* 20(3):932–945
7. Zakhidov AA, Baughman RH, Iqbal Z, Cui CX, Khayrullin I, Dantas SO, Marti J, Ralchenko V (1998) Carbon structures with three dimensional periodicity at optical wavelengths. *Science* 282:897–901
8. Ryoo R, Joo SH, Jun S (1999) Synthesis of highly ordered carbon molecular sieves via template-mediated structural transformation. *J Phys Chem B* 103(37):7743–7746
9. Kleitz F, Choi SH, Ryoo R (2003) Cubic Ia3d large mesoporous silica: synthesis and replication to platinum nanowires, carbon nanorods and carbon nanotubes. *Chem Commun* 17:2136–2137
10. Bheekhun N, Abu Talib AR, Hassan MR (2013) Aerogels in aerospace: an overview. *Adv Mater Sci Eng* 1–18 (Article ID 406065)
11. Laurenzi S, Circi C, Marchetti M (2012) Aerogel for aerospace applications. *Recent Patents Space Technol* 2(2):102–107
12. Kistler SS (1931) Coherent expanded aerogels and jellies. *Nature* 127:741
13. Lenhard W, Emmerling A, Fricke J (1994) Investigation of isothermal sintering of silica aerogels. In: Attia YA (ed) Sol gel processing and applications. Plenum Press, New York and London, pp 257–266
14. Lu X, Caps R, Fricke J, Alviso CT, Pekala RW (1995) Co-relation between structure and thermal conductivity of organic aerogels. *J Non-Cryst Solids* 188:226–234
15. Hajar M, Luisa D, António P (2014) An overview on silica aerogels synthesis and different mechanical reinforcing strategies. *J Non-Cryst Solids* 385: 55–77
16. Mouritz AP (2012) Introduction to aerospace materials, 1st edn. Woodhead Publishing Limited, Sawston
17. Larson C, Smith JR, Armstrong GJ (2013) Current research on surface finishing and coatings for aerospace bodies and structures—a review. *Trans Inst Metal Finish* 91:120–132.
18. Makhlof ASM, Tiginyanu I (eds) (2011) Nanocoatings and ultra-thin films technologies and applications. Woodhead Publishing Limited, Sawston
19. Narendra BD, Nayak S (2005) Nanocoatings for engine application. *Surf Coat Technol* 194 (1):58–67
20. Gamburg YG, Zangari G (2011) Theory and practice of metal electro deposition. Springer, New York
21. Gurrappa, I., & Binder, L. (2008). Electrodeposition of nanostructured coatings and their characterization—a review. *Sci Technol Adv Mater* 9(4):43001–43011
22. Chandrasekar MS, Pushpavanam M (2008) Pulse and pulse reverse plating—Conceptual, advantages and applications. *Electrochim Acta* 53(8):3313–3322
23. Wanhill RJH (2007) Engineering properties of nanotechnology bulk metals: a preliminary survey. NLR Technical Report NLR-TR-2006-138, National Aerospace Laboratory NLR, Amsterdam, The Netherlands

24. De Luca LT, Galfetti L, Severini F, Meda L, Marra G, Vorozhtsov AB, Sedoi VS, Babuk VA (2005) Burning of nano-aluminized composite rocket propellants. *Combust Explosion Shock Waves* 41(6):680–692
25. Strand LD, Jones MD, Ray RL, Cohen NS (1994) Characterization of hybrid rocket internal heat flux and HTPB fuel pyrolysis. In: *Proceedings of the 30th joint propulsion conference and exhibit*, Indianapolis, IN, USA, 27–29 June 1994 (AIAA Paper No. 94-2876)
26. Fesmire JE (2006) Aerogel insulation systems for space launch applications. *Cryogenics* 46:111–117
27. Fesmire JE, Sass JP (2008) Aerogel insulation applications for liquid hydrogen launch vehicle tanks. *Cryogenics* 48(5–6):223–231
28. Coffman BE, Fesmire JE, White S, Gould G, Augustynowicz S (2010) Aerogel blanket insulation materials for cryogenic applications. In: *Advances in cryogenic engineering: AIP conference proceedings*, vol 1218(1). American Institute of Physics, Melville, pp 913–920
29. Pouladi S, Shariat MH, Bahrololoom ME (2012) Electrodeposition and characterization of Ni–Zn–P and Ni–Zn–P/nano-SiC coatings. *Surf Coat Technol* 213:33–40
30. Vernhes L, Azzi M, Klemberg-Sapieha JE (2013) Alternatives for hard chromium plating: nanostructured coatings for severe- service valves. *Mater Chem Phys* 140(2–3):522–528
31. Weston DP, Shipway PH, Harris SJ, Cheng MK (2009) Friction and sliding wear behaviour of electrodeposited cobalt and cobalt–tungsten alloy coatings for replacement of electrodeposited chromium. *Wear* 267(5–8):934–943
32. Shin JH, Lee JW, Park HS, Suh SJ (2014) Corrosion resistance of ultrasonic electrodeposited Ni–Co–Fe ternary alloy films according to current density. *J Nanosci Nanotechnol* 14(12):9579–9583
33. Prado RA, Facchini D, Mahalanobis N, Gonzalez F, Palumbo G (2009) Electrodeposition of nanocrystalline cobalt alloy coatings as a hard chrome alternative. NAVAIR Public Release 09-776, U.S. Navy Naval Air Systems Command, Patuxent River, MD 20670, USA
34. Amadeh A, Ebadpour R (2013) Effect of cobalt content on wear and corrosion behaviors of electrodeposited Ni-Co/WC nano-composite coatings. *J Nanosci Technol* 13(2):1360–1363
35. Zeng L, Brown CJ, Smith MW, Haylock L, Gurrola RH, Monserratt E, Youngblood D (2006) Evaluation of alternatives to electrodeposited cadmium for threaded fastener applications. Lockheed Martin Corporation 1–13 (Article ID2009/01/3228)
36. Baldwin KR, Smith CJE (1996) Advances in replacements for cadmium plating in aerospace applications. *Trans Inst Metal Finish* 74(6):202–209
37. Praveen BM, Venkatesha TV (2011) Electrodeposition and corrosion resistance properties of Zn-Ni/TiO₂ nano composite coatings. *Int J Electrochem* 1–4 (Article ID 261407)
38. Kim P, Wong TS, Alvarenga J, Kreder MJ, Adomo-Martinez WE, Aizenberg J (2012) Liquid-infused nanostructured surfaces with extreme anti-ice and anti-frost performance. *ACS Nano* 6(8):6569–6577
39. Wasekar NP, Haridoss P, Seshadri SK, Sundararajan, G (2012) Sliding wear behavior of nanocrystalline Ni coatings: influence of grain size. *Wear* 296(1–2):536–546
40. Pavithra ChLP, Sarada BV, Rajulapati KV, Rao TN, Sundararajan G (2014) A new electrochemical approach for the synthesis of copper-graphene nanocomposite foils with high hardness. *Sci Rep* 4:1–7 (Article ID 4049)
41. Ullal Y, Hegde AC (2013) Corrosion protection of electrodeposited multilayer nanocomposite Zn–Ni–SiO₂ coatings. *Surf Eng Appl Electrochem* 49(2):161–167
42. Kastirbai S, Kalaiganan GP (2014) Pulse electrodeposition and corrosion properties of Ni–Si₃N₄ nanocomposite coatings. *Bull Mater Sci* 37(3):721–728

Part II
Characterisation and Testing

Chapter 6

Microstructure: An Introduction

C. Suryanarayana

Abstract This chapter gives a brief account of the different microscopic techniques to observe and interpret the microstructures of metals and alloys. The whole range of techniques from optical, scanning electron and transmission electron to field ion microscopy techniques is covered. The basic principles of the different microscopes, the advantages and limitations of the variety of techniques, and interpretation of microstructural features are described. Since it would be difficult to include the details of all the techniques, the list of references contains important resources for additional details of all of the techniques described in this chapter.

Keywords Microstructures • Optical microscopy • Electron microscopy • High-temperature microscopy • Field ion microscopy • Atom probe microscopy • Aerospace alloys

6.1 Introduction

Microstructures determine the mechanical, physical, and chemical properties of materials. For example, the strength and hardness of materials are determined by the number of phases and their grain sizes. The electrical and magnetic properties and also the chemical behaviour (corrosion) are determined by the grain size and defects (vacancies, dislocations, grain boundaries, etc.) present in the material.

A complete description of microstructures involves describing the size, shape, and distribution of grains and second-phase particles and their composition; and also the defect structures, although these are often omitted. Hornbogen has provided a systematic treatment of microstructures [1–3], and Gleiter [4] has described in some detail how microstructures develop under different processing conditions. These are useful reference sources, but they are more detailed than required for a general Source Book.

C. Suryanarayana (✉)

Department of Mechanical and Aerospace Engineering,
University of Central Florida, Orlando, FL 32816-2450, USA
e-mail: Surya@ucf.edu

Thus in the present chapter the approach is the conventional one of describing the observation and interpretation of microstructures with increasing levels of fineness, using optical, scanning electron, transmission electron, and field ion microscopes.

6.2 Microstructures: General Remarks

The microstructure of a metal or alloy is not unique. It can be modified by different methods, e.g. by:

1. Alloying additions, when a new phase may appear.
2. Deformation processing, when the grains may be elongated in the direction of working.
3. Phase transformations, when a completely new microstructure may develop. Two common examples are the transformation of austenite to (i) martensite when quenching a steel or (ii) pearlite when the steel is slowly cooled and annealed.

Microstructural features of interest are the size, shape, and distribution of grains in the case of a single-phase material. In a two-phase or multi-phase material the size, shape, and distribution of the secondary phases are important in addition to the microstructural parameters of the matrix (the major component).

The majority of the microstructural features and parameters of interest in engineering alloys are on a scale of a few tens of micrometres ($1\ \mu\text{m} = 10^{-6}\ \text{m}$) or less. Also, in recent times there has been much interest in characterizing nanocrystalline materials with nanoscale grain sizes of $\leq 100\ \text{nm}$ ($1\ \text{nm} = 10^{-9}\ \text{m}$). To observe these small and very small details it is necessary to use several types of microscopes, covering a wide range of magnifications and resolutions.

Microstructural features in the size range of a few tens of micrometres, i.e. submillimetre scale, may be observed using optical microscopy and also scanning electron microscopy, which, however, can be used up to much higher magnifications. Transmission electron microscopy is especially useful at very high magnifications, allowing observations on the nanoscale.

Resolutions on an atomic scale are provided by field ion microscopy, scanning tunnelling microscopy, and atomic force microscopy. The latter two techniques have become very popular because they can provide additional information, namely mapping magnetic and electrostatic forces (scanning tunnelling microscopy) and chemical interactions at surfaces (atomic force microscopy).

Microstructural information may be viewed directly, recorded using photographic methods, stored digitally, or received by a television camera for input into an analysis system.

6.3 Optical Microscopy

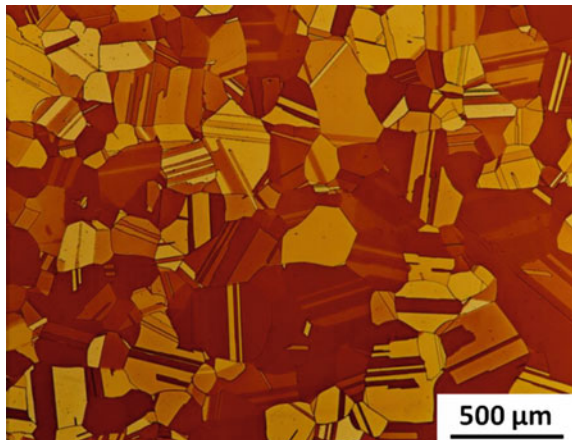
In an optical microscope the light is incident on the sample and a magnified image is produced by the combined action of objective and eyepiece lenses. Typical maximum magnifications achieved in this type of microscope are in the range of 1000–2000 \times . Most features of common interest can be observed and quantified using quantitative microscopy methods. These include observation and determination of grain sizes and also shapes, sizes, and amounts of the different phases in multi-phase systems. Figure 6.1 shows an example optical micrograph showing the grain structure and annealing twins in a polished and etched sample of alpha brass.

By observing the microstructure, one will also be able to decide (or at least estimate) whether the sample indicates that the material is in the cast, annealed, or cold-worked condition. The way the microstructure is normally observed is referred to as the bright-field mode, where the features of interest appear dark on a bright background. However, there are several other observation modes that can be used to derive useful information about the sample. These include dark-field microscopy (where the features of interest appear bright on a dark background); polarized light (when the presence of optically anisotropic phases can be determined); interference microscopy (to obtain information about specimen relief or surface topography); and phase contrast microscopy (to differentiate between phases at (slightly) different surface levels).

The reader is referred to standard books on microscopy [5–11] for details of the different optical microscopic techniques and books on quantitative microscopy [12] for details of quantification of microstructural features.

Resolution One of the most important features of any microscope is its resolving power, d (also referred to as the limit of resolution or simply the resolution). The resolution is defined as the least separation between two points at which they may be distinguished as separate, and is given by:

Fig. 6.1 Optical micrograph of alpha brass (Cu-30 % Zn alloy) showing polyhedral grains and the presence of annealing twins in most of the grains. The sample has been polished and etched



$$d = \frac{0.61 \lambda}{\mu \sin \alpha} \quad (6.1)$$

where λ is the wavelength of the light, μ is the refractive index of the medium between the sample and the objective lens, and α is one-half the maximum angle of the light beam that is able to be collected by the objective lens.

From Eq. 6.1, it follows that the resolving power is limited by the wavelength of the light: in fact, the maximum resolution (minimum d) is typically about one-half of the wavelength. However, μ can be increased by changing the medium to oil immersion, which also increases α .

The limit of resolution for an optical microscope which uses visible radiation ($\lambda = 300\text{--}700$ nm) is about 200 nm. However, many microstructural features (e.g. fine second-phase precipitate particles, dispersoids, and Guinier-Preston zones in precipitation hardening alloys) have smaller dimensions, and their observation therefore requires the use of more powerful microscopes.

6.4 Scanning Electron Microscopy

In a scanning electron microscope (SEM), an electron beam is generated by heating a tungsten filament, a lanthanum hexaboride (LaB_6) crystal, or a field-emission source, and this beam is focussed by electromagnetic lenses to form the image. The wavelength of the electron beam, λ , is determined by the operating excitation voltage and is given by the equation:

$$\lambda = \frac{h}{\sqrt{2m_0eV}} \quad (6.2)$$

where h is Planck's constant, m_0 is the electron mass at rest, e is the charge on the electron, and V is the excitation voltage. From Eq. 6.2 it follows that the wavelength will be shorter for higher excitation voltages.

The electron beam interacts with the specimen and generates a variety of signals, including secondary electrons, backscattered electrons, characteristic X-rays, elastically scattered electrons, Auger electrons, and cathodoluminescence. These signals can be used to obtain information about the microstructure of the sample:

1. Secondary electrons. These are formed due to interaction between the primary electrons in the electron beam and the loosely bound electrons in the atoms of the sample. The secondary electrons have energies in the range of 10–50 eV and are generated from near the sample surface. Secondary electron imaging is the

most generally used technique for examining microstructures, usually in combination with chemical analysis using X-ray signals (see point (3) below).

The yield of secondary electrons depends on the angle between the incident beam and the sample surface. This important characteristic enables imaging the surface topography of the sample and is essential for viewing and interpreting fracture surfaces, discussed in Sect. 6.4.1.

2. **Backscattered electrons.** These are produced by single large-angle or multiple small-angle scattering events, and their proportion depends mainly on the atomic numbers of the elements in the constituents of the microstructure. The backscattered electrons originate in a surface layer, usually 0.1–1 μm , with the depth increasing with increasing excitation voltage and decreasing atomic number.

Phases and particles with a higher average atomic number image as “bright” because many primary electrons are backscattered. Thus backscattered electron imaging can be used to differentiate between phases and particles with different average atomic numbers.

3. **Characteristic X-rays.** These are produced when the primary electron beam has sufficient energy to knock out electrons from atoms. The X-rays generated from the sample may be utilized to (i) determine the chemistry of the sample using either energy dispersive spectroscopy (EDS) or wavelength dispersive spectroscopy (WDS), which is more accurate than EDS; (ii) create an X-ray dot image or elemental map showing the distribution of different elements in the sample; or (iii) generate line scans across the sample to determine elemental variations, e.g. across phase boundaries and interfaces.

Figure 6.2 is a simplified schematic of an SEM showing the positions of secondary and backscattered electron detectors and an EDS detector.

Electron Backscatter Diffraction In the last two decades a powerful and versatile technique called electron backscatter diffraction (EBSD) has been increasingly used for crystallographic (texture) and microstructural characterization. Among other applications, EBSD is very useful for studying the processing of engineering alloys.

An example is given in Fig. 6.3. This shows EBSD orientation imaging microscopy (EBSD-OIM) maps for an undeformed (homogenized) and slow-strain-rate hot-deformed aluminium–lithium (Al–Li) alloy [13]. The hot deformation took place at 575 °C at a strain rate of 3×10^{-4} /s, resulting in dynamic recrystallization and a random texture.

More details about SEM microscopy and its capabilities are given in the excellent and comprehensive book by Goldstein et al. [14].

6.4.1 SEM and Failure Analysis

The image magnifications that can be obtained in an SEM are typically about 10,000–50,000 \times , though higher magnifications are possible with advanced

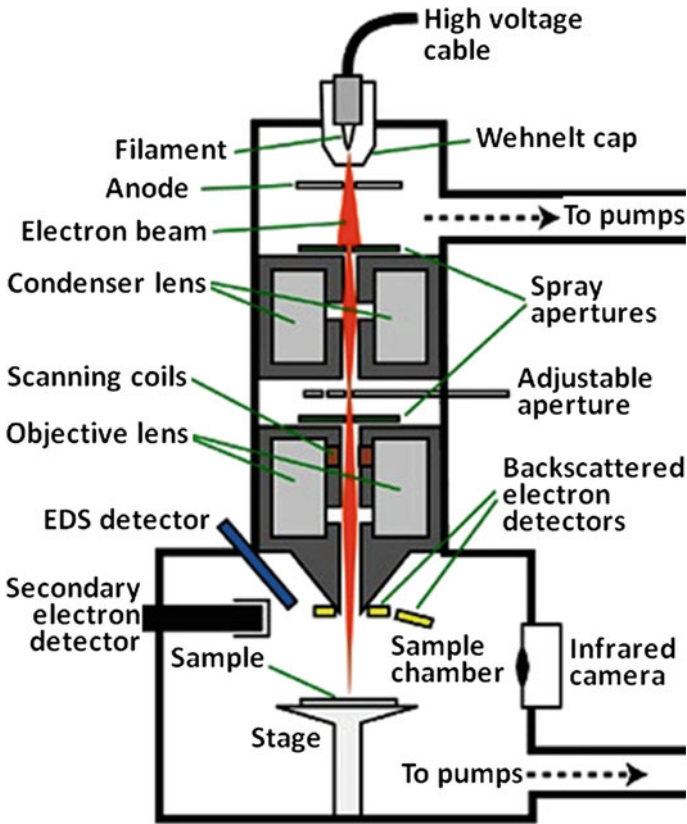


Fig. 6.2 Schematic of an SEM with some of the possible detectors

field-emission (FE) SEMs. The resolution that can be achieved is normally about 10 nm but can be brought down to much lower values (~ 1 nm).

Owing to the large depth of focus, SEM imaging is much used in failure analysis (see Chap. 23 in this Volume of the Source Books), notably for the examination of fracture surfaces. The large depth of focus provides a three-dimensional (3D) appearance of the fracture surfaces, and the fracture characteristics and topographies provide essential information about the modes or causes of failures. In particular, stereo pairs of fractographs, giving a full 3D effect, can be very useful for detailed fractographic analyses.

Examples of fractographs are shown in Fig. 6.4. These are secondary electron (SE) images of (a) a ductile transgranular fracture and (b) a brittle (or low ductility) intergranular fracture.

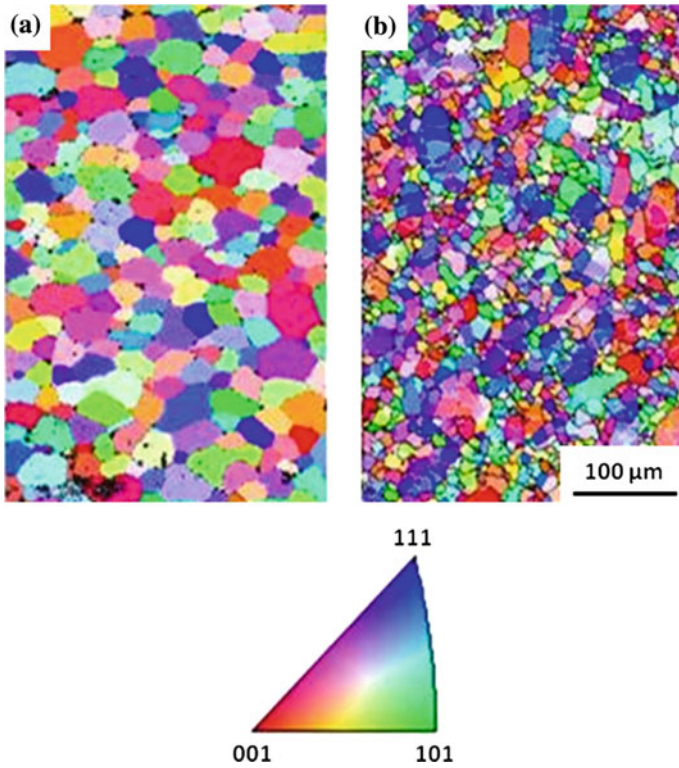


Fig. 6.3 EBSD-OIM maps for **a** an undeformed (homogenized) and **b** hot-deformed and dynamically recrystallized aluminium–lithium (Al–Li) alloy [13]. The stereographic triangle globally indicates the grain orientations

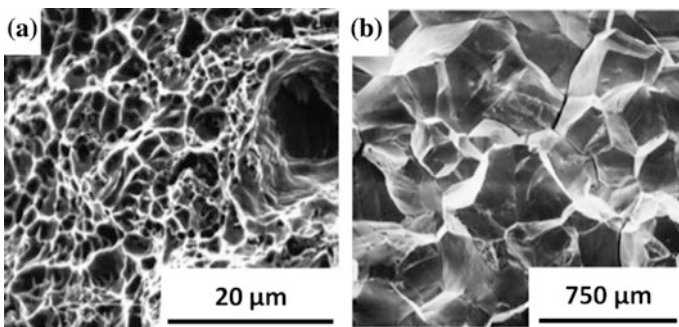


Fig. 6.4 SEM SE images of **a** ductile transgranular fracture by microvoid coalescence and **b** brittle (or low ductility) intergranular fracture

6.5 Transmission Electron Microscopy

The transmission electron microscope (TEM) is a powerful tool to fully characterize the microstructure, crystal structure, and chemistry of the different phases present in materials. In fact, this is one of the most common techniques used to characterize materials at an advanced level. Consequently, there have been several developments in this area in recent years [15].

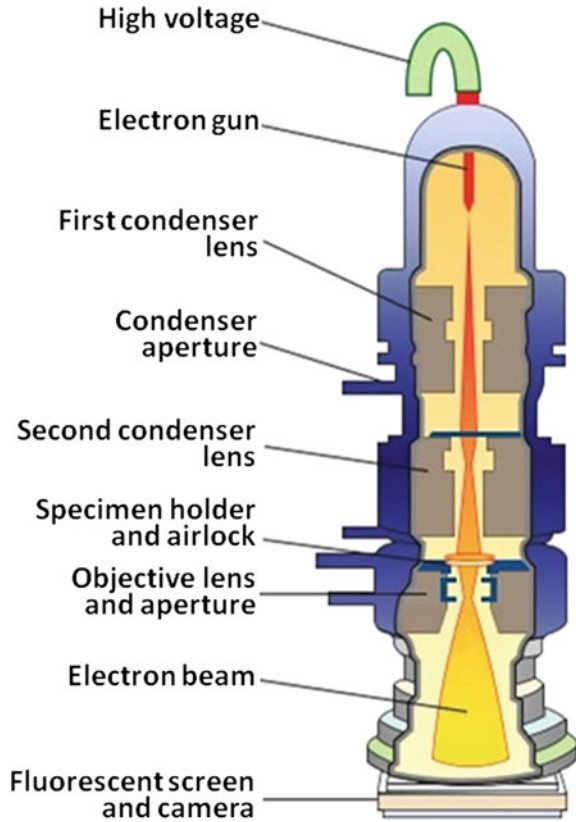
TEM is done with very thin foil specimens (typically ≤ 100 nm in thickness). These are obtained by either conventional electropolishing techniques, ion milling, or focussed ion beam methods. A high-energy electron beam (accelerated to a high potential) passes through a specimen to produce (i) a transmitted beam, the intensity of which depends on the original intensity of the beam and the specimen mass absorption coefficient and thickness, and (ii) numerous diffracted beams. Both types of beams may be used to obtain crystallographic and microstructural information, as will be briefly discussed in Sects. 6.5.1–6.5.4.

6.5.1 Transmitted and Diffracted Beam Imaging

This is a common way of characterizing the microstructure and will be described with the aid of Fig. 6.5, which is a generic schematic of a TEM microscope in operation. A thin foil specimen is inserted into the TEM specimen holder, which in turn is placed inside the microscope column. This is then pumped down to vacuum. An electron beam from the gun at the top of the column then travels down through condenser lenses and the specimen, generating a transmitted beam and an array of diffracted beams. After these beams pass through the objective lens, one beam may be selected for viewing on the fluorescent screen. This is done by using an aperture to filter out the other beams:

1. The objective aperture enables selecting either the transmitted beam or one of the diffracted beams for focussing on the fluorescent screen. If the transmitted beam is selected, this forms a **bright-field** image on the screen. If one of the diffracted beams is selected, this is focussed to form a **dark-field** image on the screen.
2. A selected area diffraction (SAD) aperture (not indicated in Fig. 6.5) that lies below the objective aperture filters out all diffracted beams except those from a particular area of the specimen. The purpose is to obtain diffracted beams from this area and focus them onto the screen to form a **diffraction pattern**. This pattern can be analysed to determine the crystal structure and examine crystal defects.

Fig. 6.5 Schematic of a TEM in operation

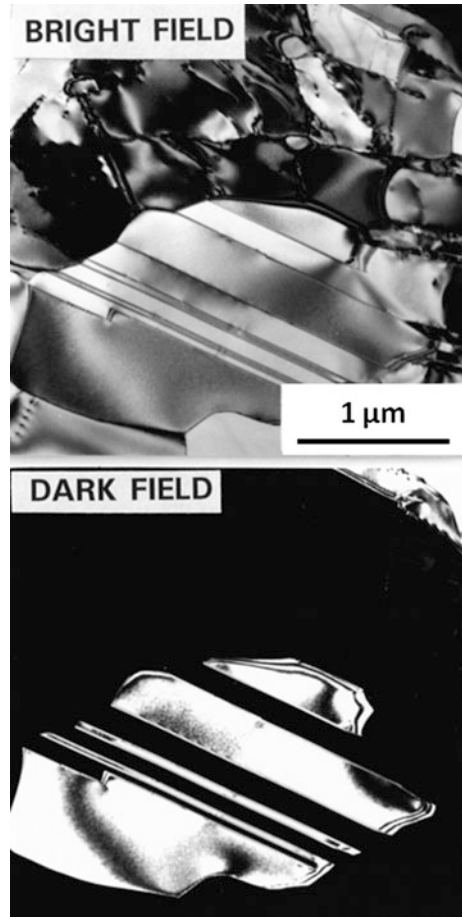


6.5.2 *Bright-Field and Dark-Field Images*

Figure 6.6 shows an example of bright-field and dark-field images from the same area of a specimen. These two images are complementary in contrast: for example, the annealing twins in the large grain appear light in the bright-field image and dark in the dark-field image.

An important advantage of dark-field images is that second-phase particles, even if they are relatively small, can be easily identified and their amount evaluated using quantitative microscopy methods. A slightly modified technique is weak-beam imaging, for which the diffraction conditions are set up so that the dark-field image is recorded from a slightly off-diffracted beam. This technique has been used very effectively to study dislocation structures in materials.

Fig. 6.6 Bright-field and dark-field TEM images of a polycrystalline area in a thin foil γ -titanium aluminide specimen

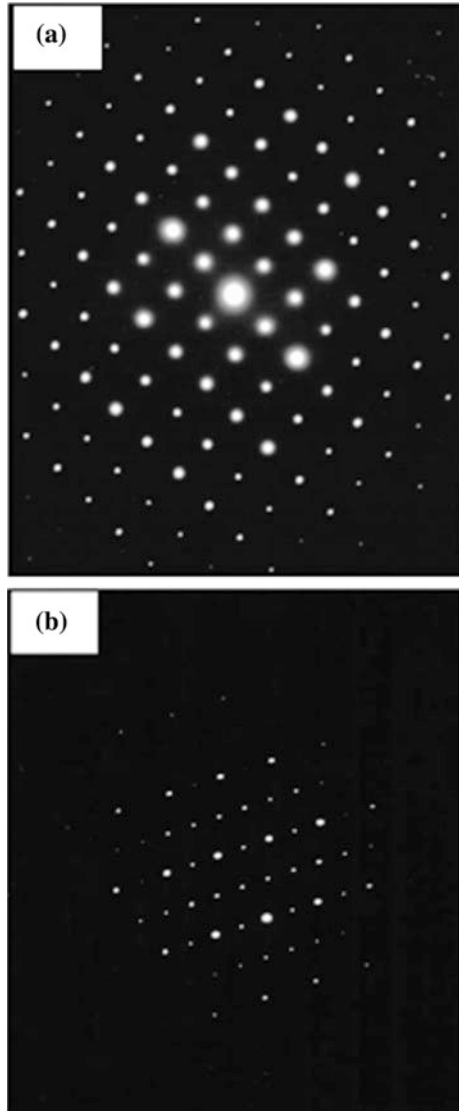


6.5.3 Diffraction Patterns

There are two basic kinds of diffraction patterns: either a ring pattern from a polycrystalline area, or a spot pattern from a single-crystal area. Analysis of a ring pattern gives the crystal structure and lattice parameter(s) of the phase responsible. A spot pattern enables determining the orientation of the crystal as well as the crystal structure and lattice parameter(s). Furthermore, a superimposed spot pattern from two coexisting phases will allow determining the orientation relationship between the two phases.

Diffraction patterns can also provide information about lattice ordering (indicated by weak diffraction spots between the main diffraction spots), the shapes of precipitates (suggested by streaking in the diffraction pattern), and other fine

Fig. 6.7 Diffraction patterns from **a** a disordered lattice and **b** an ordered lattice. The ordering in **(b)** is shown by weak diffraction spots midway between the main diffraction spots



microstructural details. For example, Fig. 6.7 shows two single-crystal (spot) diffraction patterns from (a) a *disordered* crystal lattice and (b) an *ordered* lattice. These terms require some explanation: in a disordered lattice the atoms are arranged randomly on the lattice sites, while in an ordered lattice atoms of different elements occupy particular lattice sites.

6.5.4 Characterization of Defects

It is well known that crystal defects and material discontinuities influence the deformation behaviour and some of the physical and chemical properties of metals and alloys. Thus it is important to determine the nature and quantity of defects present in a material.

TEM is eminently suited to characterize crystal defects. These could be point defects (vacancies and interstitials), line defects (dislocations), surface defects (grain boundaries, stacking faults, and other types of interphase interfaces), or volume defects or discontinuities (pores, second-phase particles, and constituent particles):

1. Vacancies. Although individual vacancies cannot be seen in the TEM, their aggregation into voids, resulting in the formation of dislocation loops in quenched metals, helps in estimating the vacancy concentration. By characterizing the dislocation loops, it is also possible to determine whether they are formed from vacancy condensation or interstitial atoms.
2. Dislocations. Determination of the types of dislocations (whether they are edge, screw, or mixed edge and screw) and the Burgers vector, \mathbf{b} , is conveniently done using the extinction (invisibility) criterion $\mathbf{g}\cdot\mathbf{b} = 0$, where \mathbf{g} is the reciprocal lattice vector. By properly orientating the specimen, a dislocation will become invisible, and this can occur at more than one \mathbf{g} value. Simply put, the determination of two (or more) of these \mathbf{g} values enables calculating \mathbf{b} .
3. Other features. TEM enables determination of the misorientation between grains (for both low-angle and high-angle grain boundaries); the fault vector in stacking faults; the extent of coherency or incoherency between two phases; the sizes and volume fractions of precipitates; and many other features [15].

6.6 High-Temperature Microscopy

Observation of microstructures at high temperatures is sometimes necessary and useful. For example, some phases may be stable only at high temperatures and transform on cooling or quenching the alloy to room temperature.

The classic examples already mentioned at the beginning of Sect. 6.2 are the transformation of austenite to (i) martensite when quenching a steel or (ii) pearlite when the steel is slowly cooled and annealed. Thus if one is interested in studying the microstructural changes in austenite, then high-temperature microscopy must be used.

It is also possible to investigate the in situ transformation behaviour of metastable phases, e.g. metallic glasses, to follow the crystallization (structural change) that occurs as a function of temperature. High-temperature microscopy may also be employed to study processes such as grain growth, martensitic transformations where surface relief effects are observed, or melting and solidification.

High-temperature stages are available for optical microscopes, SEMs, and also TEMs. The details of construction, the temperature capabilities, and other details may differ for different microscopes. One common problem is that when specimens are heated under vacuum, vaporization occurs and must be taken into consideration. In an optical microscope protective glasses must be provided to prevent coating of the observation window by the evaporants. Long-distance working objectives are also desirable to prevent damage to the objective lenses. Consequently, the typical magnifications for optical microscopes are low.

For SEMs and TEMs, the evaporation from sample or specimen surfaces results in lower vacuum levels than in normal use. The pumping system should be able to cope with this.

An example of the use of high-temperature TEM microscopy is given in Fig. 6.8. This presents a sequence of micrographs showing the precipitation of

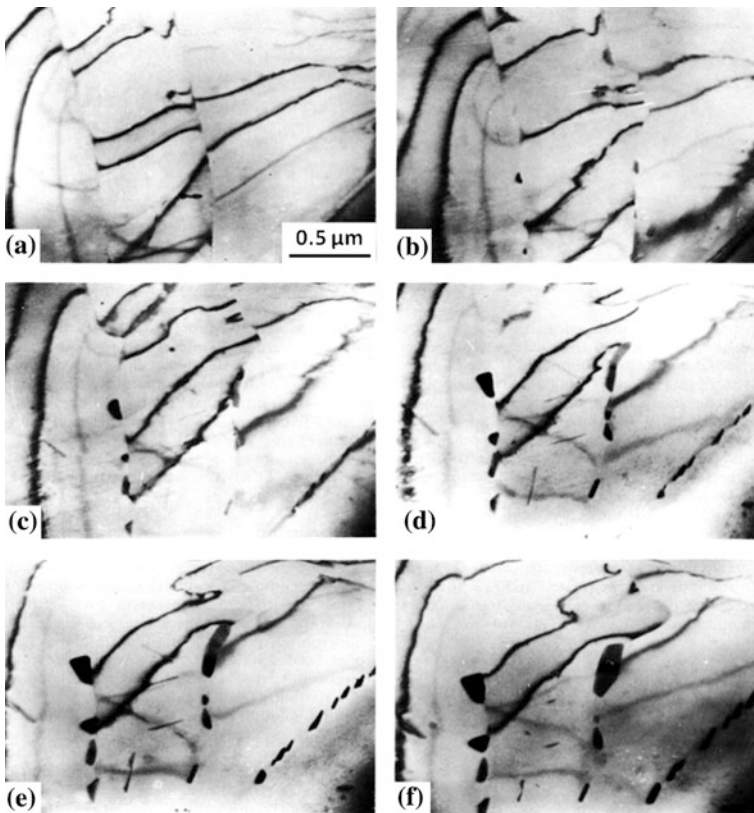


Fig. 6.8 Sequence of micrographs taken during continuous heating of a melt-quenched Al-Rh alloy from room temperature up to about 555 °C in a TEM hot stage [16]: **a** supersaturated solid solution in the as-quenched condition, stable up to ~275 °C. **b** Matrix and grain boundary precipitate nucleation on heating to ~370 °C. **c-f** The precipitates begin to coarsen on further heating to (c) 424 °C and (d-f) higher temperatures

matrix and grain boundary second-phase particles from a supersaturated solid solution of an aluminium–rhodium (Al–Rh) alloy [16]. The matrix particles appear needle-like (especially visible in Figs. 6.8d and e), while the grain boundary particles are irregular and larger. All the precipitates coarsened with increasing temperature, as would also occur with increasing time at a given temperature.

6.7 Field Ion Microscopy

The field ion microscope (FIM) has atomic resolution and the ability to conduct chemical analysis of individual atoms, resulting in many applications [17]. The development of 3D atom probe microscopy (3DAP) [18, 19] has further enhanced the utility of this type of instrument.

In an FIM a specimen tip with an end radius of about 50–100 nm is prepared by electropolishing or other methods and held at a high positive potential in a vacuum chamber at cryogenic temperatures. A small amount of a noble gas, usually helium or neon, is leaked into the chamber. When the potential on the specimen is increased the noble gas atoms near the specimen tip become ionized by the quantum mechanical tunnelling process of field ionization, and the electrons are drawn into the specimen. The positively charged gas ions are repelled from the sample towards a phosphor screen about 50 mm from the specimen tip, where they generate a much magnified image of the tip.

To a first approximation, the magnification of the image is given by the ratio of the distance between the tip and the screen and the specimen tip radius: this ratio is typically 10^6 (one million). The intensity of the image can be enhanced by a microchannel plate electron multiplier. Also, the specimen tip surface atoms can be field-evaporated by applying a voltage pulse, and so the layer below the previous observed layer can be examined. Hence it is possible to make a 3D examination of the specimen tip.

In an atom probe a mass spectrometer is attached to a basic FIM. The spectrometer enables analysing the mass-to-charge ratio of the field-evaporated ions, and therefore these can be chemically identified.

6.7.1 FIM Image Interpretation

FIM images are interpreted by identifying the major crystallographic planes. This procedure is aided by computer simulations. Figure 6.9 shows a typical FIM image with indexing of the different crystallographic planes. Atomic resolution is easily achieved, and the resolution is better for higher index planes, e.g. the {022} and higher-order planes in Fig. 6.9.

Fig. 6.9 Typical FIM image with indexing of the different crystallographic planes

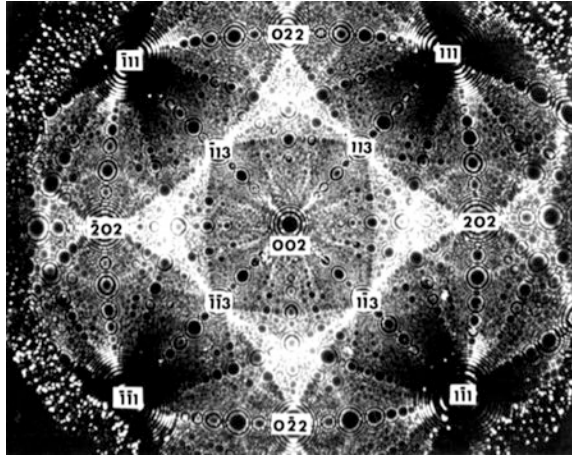
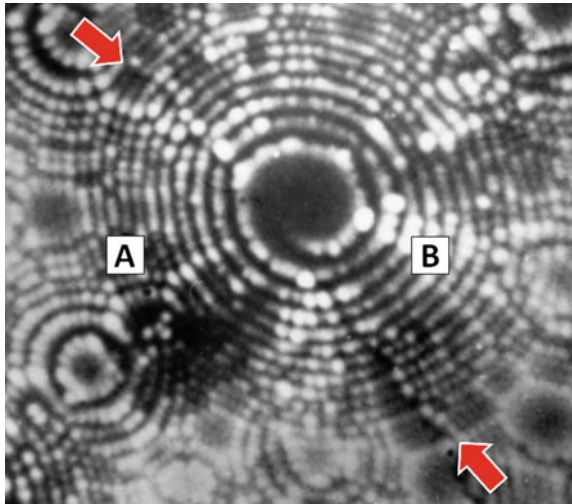


Fig. 6.10 An FIM image showing (i) two grains, *A* and *B*, with the grain boundary indicated by arrows, and (ii) a dislocation-induced spiral at the centre of the image. Courtesy of S. Ranganathan, Indian Institute of Science, Bangalore, India



Atomic resolution in the FIM greatly benefits defect characterization. For example, the absence of a bright spot (indicating an atomic position) in a continuous ring of spots suggests that a vacancy exists there. Grain boundary structures can also be studied, and the presence of dislocations can be inferred from the observation of helical spirals, for example the image in Fig. 6.10.

FIM can also be used to investigate phase transformations on an atomic scale. However, the volume of material investigated is very small, and this could present problems in quantifying the results.

6.7.1.1 3D Atom Probe Microscopy (3DAP)

The 3DAP method has been used frequently in recent times to investigate compositional variations on a very fine scale [20, 21]. Such analyses are difficult or impossible using other techniques. For example, Uma Maheswara Rao et al. [20] investigated 304 stainless steel + 10 wt% Al coatings deposited on a 304 stainless steel substrate. A cubic phase with very fine structural features was detected in the coatings, but X-ray diffraction and TEM were unable to determine whether the cubic phase was NiAl, FeAl, or (Fe, Ni) Al. An additional complication was that the fine cubic phase coexisted with the α -ferrite phase, which also has a cubic structure, and similar lattice parameter.

For further analysis, recourse was made to 3DAP. Figure 6.11 shows the mass spectrum from a 3DAP needle sample of the coating. The spectrum showed that the needle sample contained predominantly Fe, Cr, Ni, and Al, together with small quantities of Mn, C, Ga, and H.

An area away from the sample tip and containing Ga was chosen for further analysis. Figure 6.12 shows the area selected and two 3DAP reconstruction maps for Al in progressively greater detail. Careful observation suggested that a banded (layered) structure existed in the sample.

The reconstructed 3DAP maps of selected elements (Al and Ni and Al and Cr) from another smaller volume of $24 \text{ nm} \times 6 \text{ nm} \times 10 \text{ nm}$ are shown in Fig. 6.13. The distributions of Ni and Cr relative to the Al-banded structure suggest there was more affinity between Al and Ni than between Al and Cr. This result could not have been obtained from other analysis techniques.

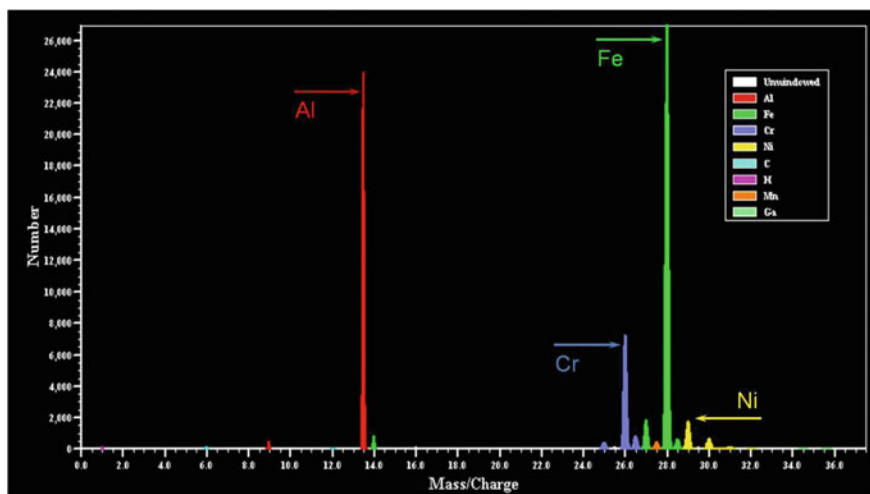


Fig. 6.11 Mass spectrum obtained from a 3DAP needle sample of a 304 stainless steel + 10 wt% Al coating [20]

Fig. 6.12 Reconstructed 3D maps for Al atoms: **a** needle overview, **b** evidence of a layered structure in a volume of $64 \text{ nm} \times 12 \text{ nm} \times 10 \text{ nm}$ of the needle, and **c** further analysis from a smaller volume of $24 \text{ nm} \times 6 \text{ nm} \times 10 \text{ nm}$ [20]

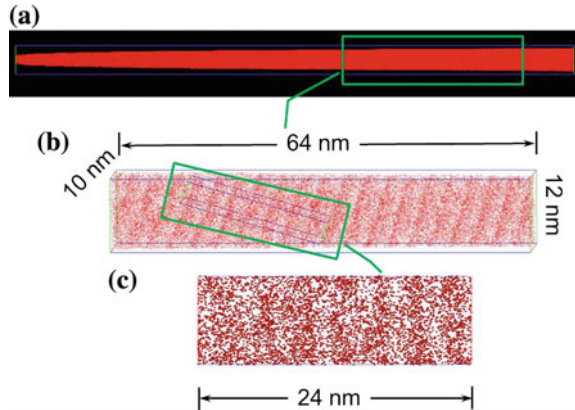
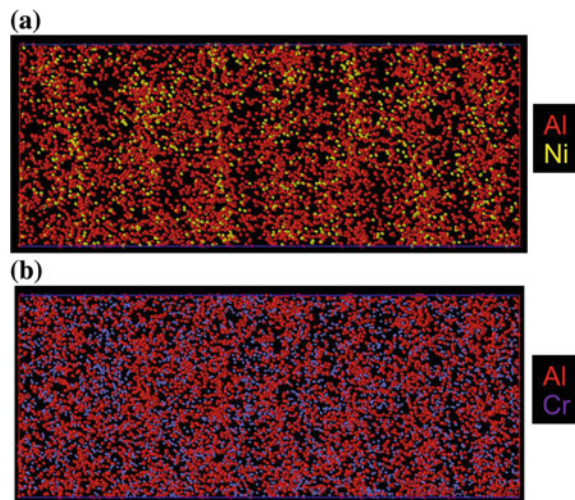


Fig. 6.13 Reconstructed 3DAP map of selected elements: distributions of **a** Al and Ni atoms and **b** Al and Cr atoms [20]



6.8 Microstructural Studies in Aerospace Alloys: An Overview

Several chapters in the two Source Book Volumes discuss the influences of microstructural parameters on the design, development, and properties of aerospace alloys. Table 6.1 summarizes these influences and their chapter, section, and volume locations. The reader is advised to consult these locations for details about the microstructural techniques and evaluations, and how they aid in the development of aerospace materials.

Table 6.1 Studies in the present Source Book Volumes that discuss the microstructural influences on the design, development, and properties of aerospace alloys

Materials	Microstructural parameter(s)	Influenced feature of the material	Source Book sections and additional references
Mg-10.7 wt% Li	Grain structure	Stress corrosion resistance	1.4.4/Vol. 1
Al-Li alloys	Phases, their crystal structures, morphologies, and other characteristics	Most mechanical properties	3.3/Vol. 1; Refs. [22–24]
Ti alloys	Phase amounts and grain structure	Phase transformation effects on the microstructure	5.2.6, 6.2.3.1, 6.2.4/Vol. 1
Ni-base superalloys	Phase contents and grain structure	Most mechanical properties	9.3.2, 9.3.3/Vol. 1
Molybdenum disilicide	Grain boundary and interface structures	Strength/hardness and toughness combinations	10.4.3/Vol. 1
C/SiC composites	Interface characteristics	Fracture mechanisms and toughening behaviour	15.7, 15.9/Vol. 1
Nanomaterials	Structure	Mechanical properties	19.5/Vol. 1
Shape memory alloys	Phase contents and grain structure	Most mechanical properties	21.2/Vol. 1
Cr ₃ C ₂ -NiCr coatings	Microstructure	Wear resistance	22.4/Vol. 2
Ti alloy friction welds, GTAW of steels, and Al alloy fusion welds	Weld structures	Fatigue and fracture toughness	4.2/Vol. 2

6.9 Concluding Remarks

Microstructural analysis provides much essential and useful information for the understanding and development of metals and alloys and also their properties. This information includes the grain sizes and morphologies; the numbers, amounts, and distributions of phases; the structures of interfaces between different phases; and the defect structures and discontinuities that may (or will) be present in the materials. A wide variety of techniques is available for microstructural characterization at different levels of resolution down to the atomic scale. The choice of technique(s) depends on the type of information required, and the most advanced techniques are not necessarily the most suitable ones.

Acknowledgments The author is grateful to Dr. R.J.H. Wanhill for a critical reading of the manuscript and suggesting useful modifications to improve its readability.

References

1. Hornbogen E (1984) On the microstructure of alloys. *Acta Metall* 32:615–627
2. Hornbogen E (1986) A systematic description of microstructure. *J Mater Sci* 21:3737–3747
3. Hornbogen E (2008) “Evolution” of microstructure in materials. *Int J Mater Res* 99:1066–1070
4. Gleiter H (1996) Microstructure. In: Cahn RW, Haasen P (eds) *Physical metallurgy*, 4th edn, vol I. North-Holland, Amsterdam, The Netherlands, pp 843–942
5. Modin H, Modin S (1973) *Metallurgical microscopy*. Butterworth-Heinemann, London
6. Vander Voort GF (1984) *Metallography principles and practice*. McGraw-Hill, New York, USA
7. Brandon DG, Kaplan WD (1999) *Microstructural characterization of materials*. Wiley, Chichester, UK
8. Clarke AR, Eberhardt CN (2002) *Microscopy techniques for material science*. CRC Press, Boca Raton, USA
9. Vander Voort GF (ed) (2004) *Metallography and microstructures*. In: *ASM Handbook*, vol 9. ASM International, Materials Park, USA
10. Zhang S, Li L, Kumar A (2009) *Materials characterization techniques*. CRC Press, Boca Raton
11. Suryanarayana C (2011) *Experimental techniques in materials and mechanics*. CRC Press, Boca Raton, USA
12. Russ JC (1995) *The image processing handbook*. CRC Press, Boca Raton, USA
13. Reddy GJ, Wanhill RJH, Gokhale AA (2013) Mechanical working of aluminum–lithium alloys, Chapter 7. In: Prasad NE, Gokhale AA, Wanhill RJH (eds) *Aluminum-Lithium alloys, processing properties and applications*. Butterworth-Heinemann, Elsevier Inc., Oxford, UK, pp 187–219
14. Goldstein JI, Newbury DE, Joy DC, Lyman CE, Echlin P, Lifshin E et al (2003) *Scanning electron microscopy and X-ray microanalysis*, 3rd edn. Springer Science + Business Media LLC, New York, USA
15. Williams DB, Carter CB (1996) *Transmission electron microscopy: a textbook for materials science*, vol 4. Springer Science + Business Media LLC, New York, USA
16. Chaudhury ZA, Suryanarayana C (1983) Electron microscopic investigations on a melt-quenched Al-Rh alloy. *J Mater Sci* 18:3011–3022
17. Müller EW, Tsong TT (1969) *Field ion microscopy: principles and applications*. American Elsevier Publishing Company, Inc., New York, USA
18. Miller MK, Smith GDW (1989) *Atom probe microanalysis: Principles and applications to materials problems*. Materials Research Society, Pittsburgh, USA
19. Miller MK, Cerezo A, Hetherington MG, Smith GDW (1996) *Atom probe field ion microscopy*. Oxford Science Publications, Oxford, UK
20. Uma Maheswara Rao S, Suryanarayana C, Heinrich H, Ohkubo T, Cheruvu NS (2012) Structural characterization of sputter-deposited 304 stainless steel + 10 wt pct Al coatings. *Metall Mater Trans A* 43A:2945–2954
21. Chen YZ, Herz A, Li YJ, Borchers C, Choi P, Raabe D, Kirchheim R (2013) Nanocrystalline Fe-C alloys produced by ball milling of iron and graphite. *Acta Mater* 61:3172–3185
22. Eswara Prasad N, Gokhale AA, Wanhill RJH (eds) (2014) *Aluminum-Lithium alloys: processing properties and applications*. Elsevier Inc., Oxford, UK
23. Sanders TH Jr, Starke EA Jr (1982) The effect of slip distribution on the monotonic and cyclic ductility of Al-Li binary alloys. *Acta Metall* 30:927–939
24. Rioja RJ, Liu J (2012) The evolution of Al-Li base products for aerospace and space applications. *Metall Mater Trans A* 43A:3325–3337

Chapter 7

Texture Effects in Important Aerospace Materials

R.J.H. Wanhill

Abstract This chapter summarizes the effects of processing-induced crystallographic texture on the properties of three important classes of aerospace metallic materials, namely aluminium alloys, titanium alloys and nickel-base superalloys.

Keywords Texture · Aluminium alloys · Titanium alloys · Nickel superalloys

7.1 Introduction

Three important classes of aerospace metallic materials are (i) aluminium alloys, (ii) titanium alloys, and (iii) nickel-base superalloys. These materials require careful control of texture during processing, in order to obtain optimum properties for design and service use.

Most aerospace alloys are used in wrought forms. Notable exceptions are cast nickel-base superalloys for gas turbine blades and vanes, and cast titanium aluminium turbine blades (see Chaps. 9 and 10 in Volume 1 of these Source Books).

One of the primary concerns for wrought products is processing-induced crystallographic texture. This can result in anisotropic mechanical properties, thereby affecting the design allowables and a material's suitability for use. Here another notable example must be mentioned, namely aluminium–lithium (Al–Li) alloys, which are the subject of a recent book [1] and also Chap. 3 in Volume 1 of these Source Books.

Texture formation is inevitable for any kind of processing. For example, casting processes lead to solidification textures, and processes such as rolling, forging, extrusion, or drawing cause deformation textures. Also, heat treatments result in annealing textures or transformation textures, depending on whether annealing

R.J.H. Wanhill (✉)
NLR, Emmeloord, The Netherlands
e-mail: rjhwanhill@gmail.com

involves recrystallization and grain growth, or crystallographic phase transformations as in many titanium alloys (see Chap. 6 in Volume 1 of these Source Books).

7.1.1 Texture Definition and Representations

Crystallographic texture is also known as preferred orientation. When most of the crystals in a polycrystalline material have a preference for certain orientations with respect to the sample or product axes, e.g. the rolling direction and tensile axis, the material is said to be textured. Figure 7.1 shows a schematic example of texture-free and textured sheet or plate materials.

Pole Figures Textures are most often described by one or a series of pole figures [2, 3], which are determined from specimens/samples by X-ray diffraction methods. A pole figure is a two-dimensional stereographic projection that shows the variation of pole density with pole orientation for a selected set of crystal planes. The poles represent the disposition of plane normals.

For *cubic* crystal structures, the crystal planes are assigned the Miller indices $\{hkl\}$. For *hexagonal* crystal structures (e.g. the α phase in titanium alloys), either Miller indices may be used, or more commonly the Miller–Bravais indices $\{hkil\}$.

An example pole figure for the commercial aluminium alloy AA6063 is shown in Fig. 7.2.

From pole figure data, it is possible to describe a well-developed texture by relating the positions and intensities of specific orientations with those of the specimen geometry. For example, textures in rolled sheet and plate metals are represented as being of the type $\{hkl\} \langle uvw \rangle$, which means that (i) the orientations of the grains in the sheet are such that their $\{hkl\}$ planes lie parallel to the plane of the sheet and (ii) their Miller index $\langle uvw \rangle$ directions lie parallel to the rolling direction (RD).

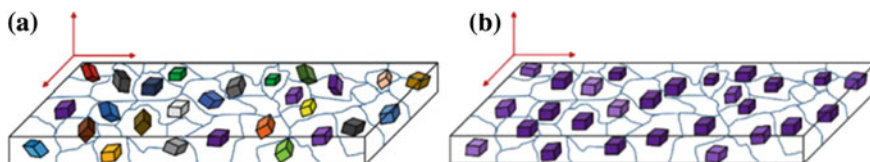
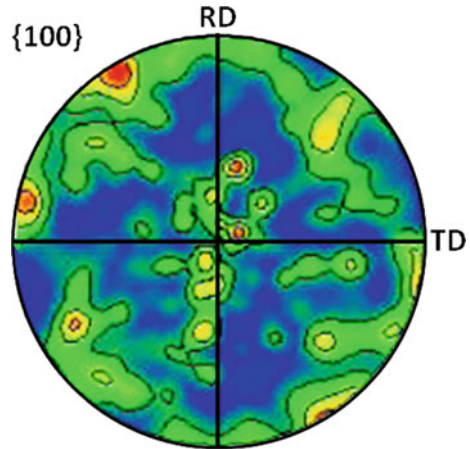


Fig. 7.1 Schematic representation of crystal or grain orientations in a sheet or plate: **a** random orientation and **b** preferred orientation. After [2]

Fig. 7.2 $\{100\}$ pole figure for aluminium alloy AA6063 sheet bent and subsequently annealed at 243 °C [4]: *RD* rolling direction; *TD* transverse direction



For extrusions and drawn products only one set of Miller indices $[uvw]$ is required, where $[uvw]$ represents the crystallographic direction of the unit cell parallel to the extrusion/drawing direction. Forging textures are represented by $\{hkl\}$ alone, where $\{hkl\}$ are the planes parallel to the forging plane.

Orientation Distribution Functions Although pole figures provide a useful description of the texture present in a material and are usually sufficient for engineering purposes, the information is incomplete and at best semi-quantitative.

This difficulty can be removed by the use of the crystallite orientation distribution function (ODF), which describes the frequency of occurrence of particular orientations in a three-dimensional orientation space (Euler space). This space is defined by three Euler angles which constitute a set of three consecutive rotations that must be given to each crystallite in order to bring its crystallographic axes into coincidence with the specimen axes. The complete ODF consists of the sets of rotations pertaining to all the crystallites in the specimen. A very useful summary is given in Ref. [2], and more details are given in Refs. [3, 5].

7.1.2 Methods of Measuring Texture

Many methods have been used to determine preferred orientation or texture. Almost all the methods are based on X-ray diffraction, with the exception of an ultrasonic method. The measurement of pole figures by X-ray diffraction using a goniometer is the most widely used technique. However, neutron diffraction offers some distinct advantages, particularly for bulk samples.

Electron diffraction using the transmission electron microscope (TEM) provides an accurate method for determination of local orientation, but the overall texture cannot be estimated by this method. Electron backscatter diffraction (EBSD) in a

scanning electron microscope (SEM) is the other method involving electron diffraction, and is currently the most popular method, because it permits correlating textures with microstructures. It is possible to determine the bulk texture of a material using EBSD if the scan is recorded from a large area (see for example Fig. 7.2), but there are some limitations [3].

A comprehensive description of all the foregoing methods is given in Ref. [3].

7.2 Aluminium Alloys

Aluminium alloys have been widely used for aerospace structures since the 1930s. These alloys constitute the majority of airframe components and structures in most civil aircraft and are still used in significant amounts in military aircraft. The products are mostly in the form of sheets, plates, forgings, and extrusions. More details are given in Chaps. 2 and 3 of Volume 1 of these Source Books.

7.2.1 Processing of Aerospace Aluminium Alloys

The three main classes of aerospace aluminium alloys are the conventional AA2XXX and AA7XXX series and the third-generation AA2XXX Al–Li alloys. These alloys are processed by hot deformation, followed by annealing, solution treatment, and ageing.

The processing of rolled products of these alloys (plates and sheets) is the most informative with respect to texture development and its effects on subsequent properties. Therefore the following discussion will concentrate on these materials.

Figure 7.3 shows generic processing maps for plates of (a) conventional alloys and (b) third-generation Al–Li alloys. There is a major difference between the maps, namely the inclusion in Fig. 7.3b of recrystallization annealing between breakdown and finish rolling for the Al–Li alloys. As will be discussed, this is an essential step for reducing texture-induced anisotropy in the finished products.

The processing includes several implicit features and mechanisms such as strain hardening, dynamic recovery, dynamic recrystallization, partial or full recrystallization, residual stress relief (ambient temperature stretching), and precipitation hardening during ageing. These all signify that processing must be carefully controlled. With respect to texture development and control, the primary influences are hot deformation (in these examples hot rolling) and recrystallization.

Hot Rolling and Recrystallization Textures The main hot rolling deformation and recrystallization texture components for aluminium alloys, which have a face-centred-cubic (FCC) crystal structure, are listed in Table 7.1.

The locations of the deformation and Goss texture components in the Euler orientation space are shown in Fig. 7.4. Sometimes the FCC textures are also

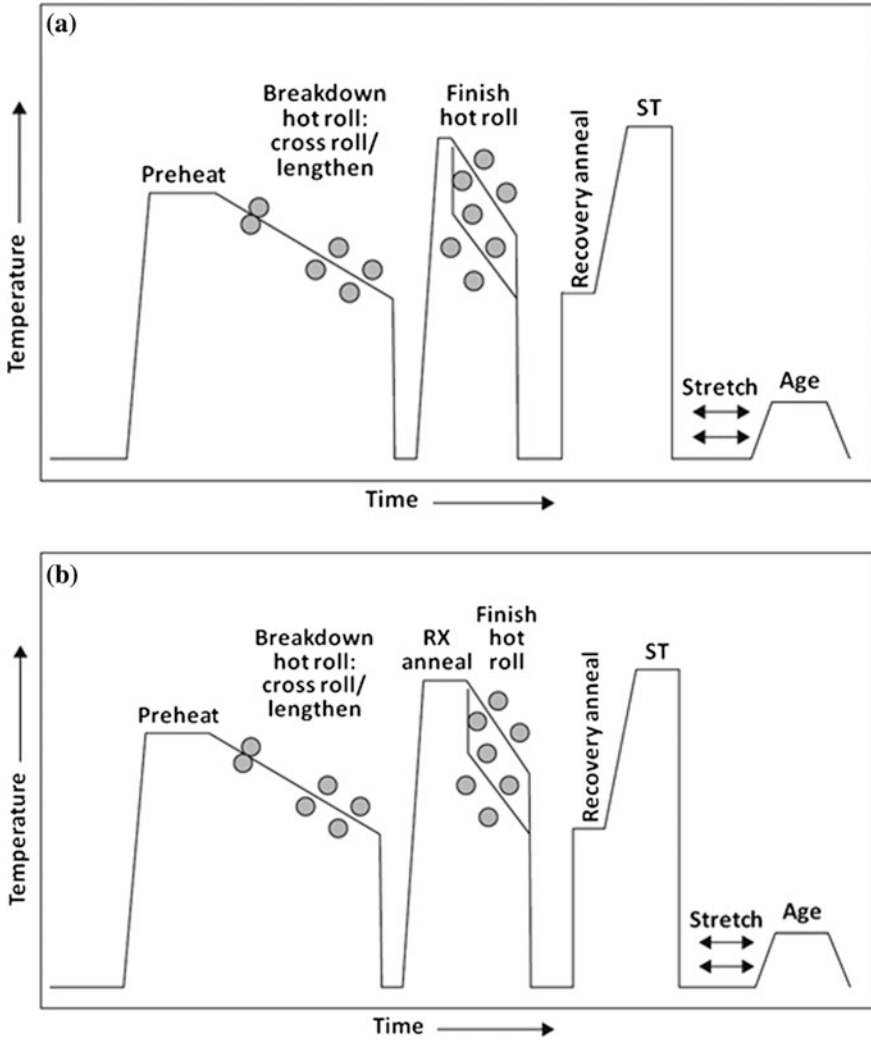


Fig. 7.3 Generic processing maps for plate products of **a** conventional AA2XXX and AA7XXX alloys and **b** third-generation Al-Li alloys: *RX* recrystallization anneal; *ST* solution treatment. Figure 7.3b is originally from Ref. [6]

represented by α , β , and τ fibres, which are the skeleton lines that connect the above-mentioned orientations in the three-dimensional orientation space. These lines are also depicted in Fig. 7.4.

Aerospace aluminium alloys typically show strings of texture orientations, as may be visualized from Fig. 7.4. These associations include links between deformation and recrystallization textures. For example, the Goss texture is associated

Table 7.1 Main hot rolling and recrystallization texture components in aluminium alloys

Name	Miller indices
Rolling deformation texture components	
Bs (Brass)	{011} <211>
Cu	{112} <111>
S	{123} <634>
Recrystallization texture components	
Cube	{001} <100>
Goss	{011} <100>
R	{124} <211>

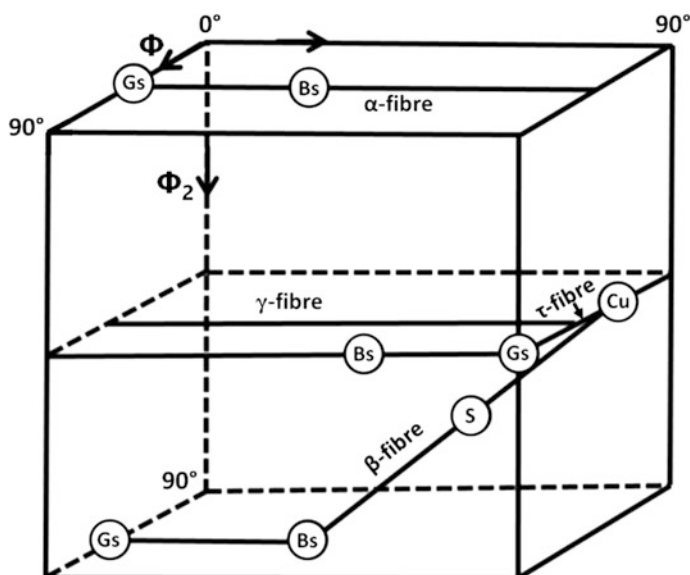


Fig. 7.4 Important texture components and fibres in FCC materials [4]

with the Bs deformation texture, and the Cube texture is associated with the Cu and S deformation textures [7].

Most importantly, hot-rolled or hot-extruded alloys can develop a strong Bs texture component [6, 8]. This results in anisotropic properties and must be reduced by further processing. For conventional alloys control of the finish rolling and the remaining steps, resulting in a 'balanced' mixture of the retained rolling and recrystallization textures, is apparently sufficient. However, third-generation Al–Li alloys have required several processing and alloy chemistry modifications [6, 8], including an intermediate recrystallization anneal, as shown in Fig. 7.3b. This annealing treatment has a necessary moderating effect on the Bs texture of the final product [6, 8].

N.B: Development and retention of a strong Bs texture and the resulting severe anisotropy of various mechanical properties are one of the main reasons why the earlier first- and second-generation Al–Li alloys were not a commercial success [1].

7.2.2 *Texture Effects on Aerospace Aluminium Alloy Properties*

Yield Strength The influence of texture on yield strength is a prime consideration for commercial products. Yield strength anisotropy in aluminium alloys must normally be minimized, and a further general consideration is the optimization of yield strength and fracture toughness [8, 9] (see next page).

Strong deformation textures (mainly Bs) result in significantly lower yield strengths at 45° to the rolling direction [6–8, 10], and this effect needs to be avoided in the final product. Conventional aluminium alloys are readily processed to avoid strong textures and yield strength anisotropy in the final product. However, as should be clear from Sect. 7.2.1, the avoidance of anisotropy in Al–Li alloys is more difficult. Moreover, this is true for both unrecrystallized and recrystallized flat-rolled products [6].

Another complication for Al–Li alloys is that anisotropy is due to both texture and precipitate–dislocation interactions [6, 8]. This means that the final steps of stretching (which influences the precipitation) and degree of ageing (which influences the slip homogeneity) are very important as well as texture control.

The overall result for achieving optimum combinations of strength and fracture toughness in Al–Li alloys is somewhat counter-intuitive, namely that finished products should be *unrecrystallized*, but with a moderate texture, and sheets should be recrystallized [6]. However, the final ageing is consistently to near-peak strength, which reduces slip planarity and hence the microstructurally-induced anisotropy.

Fatigue Texture does not appear to influence the basic fatigue properties of aerospace aluminium alloys, nor does it much affect the fatigue crack growth (FCG) behaviour of conventional recrystallized aluminium alloys. However, strong Bs textures do affect the FCG behaviour of unrecrystallized conventional AA2XXX alloys [9] and have also been found to greatly affect the fatigue crack growth behaviour of first- and second-generation Al–Li alloys, e.g. Ref. [11]. The third-generation Al–Li alloys do not have this problem [11], owing most probably to the processing and alloy chemistry modifications mentioned in Sect. 7.2.1 and discussed in Refs. [6, 8].

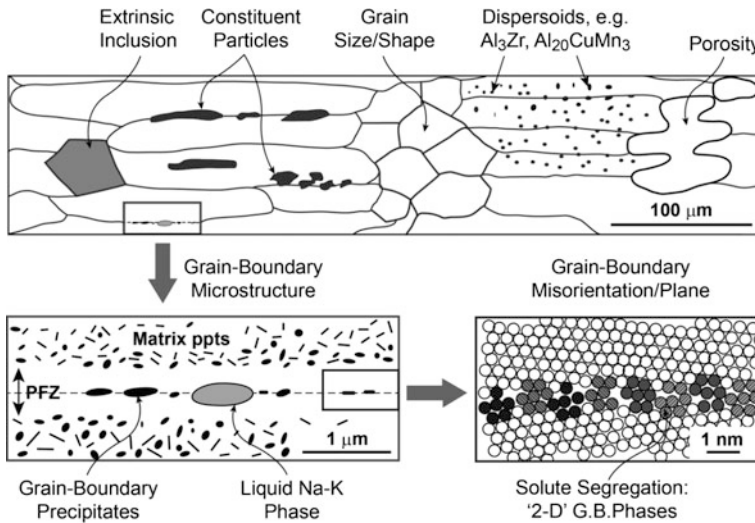


Fig. 7.5 Schematic diagram showing the principal microstructural features that can affect fracture toughness (and other properties) in high-strength aluminium alloys [12]

Fracture Toughness The fracture toughness of aerospace aluminium alloys does not appear to be much influenced by texture, but there are numerous microstructural features that *do* have an influence [12] (see Fig. 7.5).

Yield Strength—Fracture Toughness Figure 7.5 is useful in showing that high-strength aluminium alloys are complex materials, from which it may be inferred that texture need not always be significant for determining the properties of the final products.

On the other hand, research by the ALCOA company has shown the following [9]:

1. A Goss texture component improves the strength/toughness relationship for conventional AA2XXX recrystallized sheet in naturally aged (T3) tempers.
2. Control of the Goss texture is needed for improved strength/toughness combinations in Al–Li AA2199 recrystallized sheet in artificially aged T8 tempers.

7.3 Titanium Alloys

Titanium alloys are essential to both civil and military aircraft and in space applications. Major applications include aeroengine fan and compressor discs, blades, vanes, and nacelles; heavily loaded airframe and landing gear parts; sheet structures in engine vicinities; and propellant tanks and other pressure vessels for

space vehicles. More details are given in Chap. 6 of Volume 1 of these Source Books and in Refs. [13, 14].

7.3.1 *Types of Commercial Titanium Alloys*

The primary alloy phases in titanium alloys are α , which has a hexagonal-close-packed (HCP) crystal structure, and β , which is body-centred-cubic (BCC). Titanium alloys are classified as α alloys, near- α alloys, $\alpha + \beta$ alloys, and β alloys. Many have been developed for aerospace applications, but the most widely used is the two-phase $\alpha + \beta$ alloy Ti-6Al-4V. This is also the alloy for which most texture studies have been done and therefore suitable as the guideline for further discussion in this section.

7.3.2 $\alpha + \beta$ Titanium Alloy Processing

Processing can be varied to obtain three distinct types of microstructures for $\alpha + \beta$ alloys: fully lamellar, bimodal, and fully equiaxed. A less defined microstructural type is the so-called mill-annealed condition, which is a general purpose treatment for all products. These microstructural types are discussed in Chap. 6 in Volume 1 and in more detail in Ref. [14]. Schematic processing maps for obtaining all these microstructural types are shown in Figs. 7.6 and 7.7.

7.3.3 *Processing Effects on Texture*

Deformation processing of Ti-6Al-4V, other $\alpha + \beta$ alloys, and near- α alloys involves phase transformations and hence microstructural changes, as well as texture changes. Recrystallization annealing also changes the microstructure and texture, especially at higher temperatures. Thus the processing and heat treatment of these alloys is complex, as may be ascertained from Chap. 6 in Volume 1 and Refs. [13, 14].

Nevertheless, some general statements may be made about the deformation and annealing textures obtained from processing $\alpha + \beta$ alloys, as follows:

Deformation Textures These can be generally described as basal (B) and transverse (T), as shown schematically in Fig. 7.8. These textures represent the orientations of the hexagonal α phase (0002) planes with respect to the plane of deformation and the direction of deformation. In this idealized schematic the (0002) planes are either parallel or normal to the plane of deformation.

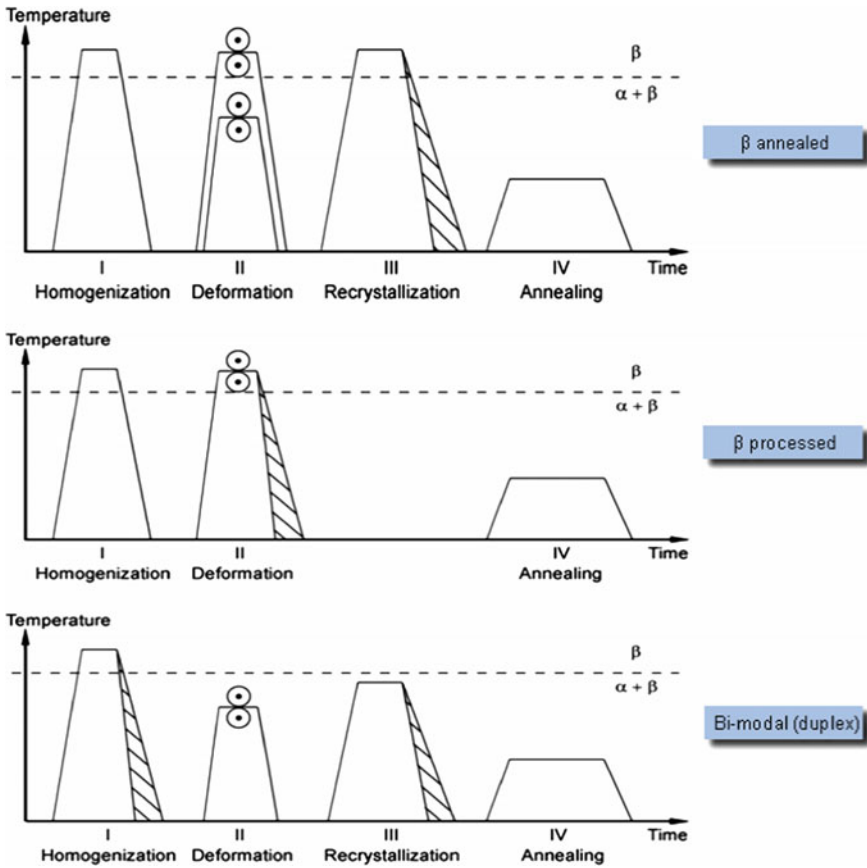


Fig. 7.6 Processing maps for fully lamellar (β annealed and β processed) and bimodal microstructures [14]

In more detail, Fig. 7.9 shows a schematic of the different textures obtainable from an $\alpha + \beta$ alloy as functions of the deformation temperature and mode of deformation, namely unidirectional rolling or radial deformation, e.g. upset forging, which is required for titanium alloy aeroengine fan and compressor discs, and also other components.

For Ti-6Al-4V there are four deformation temperature regimes corresponding to the four columns of pole figure schematics in Fig. 7.9. These deformation temperature regimes are discussed in the following points (1)–(4).

- (1) Below about 900 °C there is a high volume fraction of α phase: unidirectional rolling results in an α -deformation basal/transverse (B/T) texture, while radial deformation develops a basal (B) texture.
- (2) Between about 900 and 930 °C a fairly weak texture from the α phase can be obtained. This is partly because the α -deformation B/T texture intensity

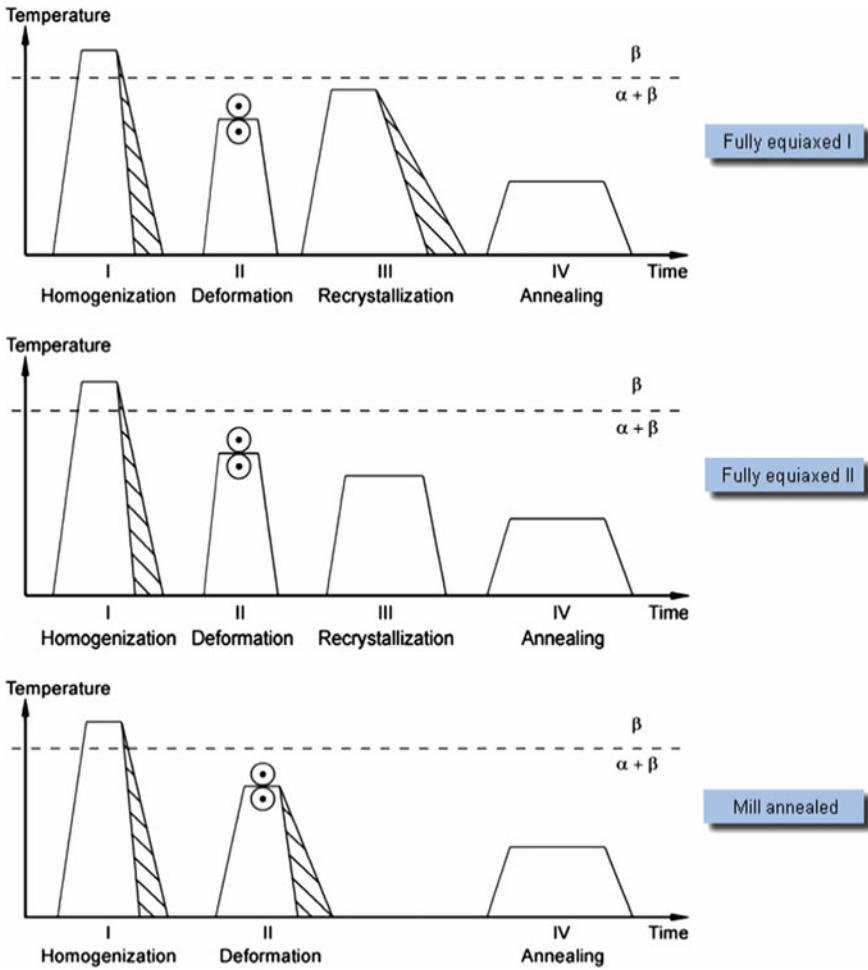


Fig. 7.7 Processing maps for fully equiaxed and mill annealed microstructures [14]

decreases with increasing temperature. However, an additional cause is a weak *transformation* texture owing to a low volume fraction of β phase being present during the deformation [see point (3)].

- (3) At temperatures approaching the β *transus*, i.e. the $(\alpha + \beta) \rightarrow \beta$ phase boundary, a high volume fraction of β phase is present during deformation, and a β -deformation texture develops. During subsequent cooling, α phase forms with preferential orientations in the textured β phase, resulting in a transverse (T) type of transformation texture.

(Note that the (0002) pole figure deriving from this transformation texture appears ring-shaped when the prior deformation is radial.)

Fig. 7.8 Schematic basal (B) and transverse (T) (0002) pole figure textures for titanium alloys [15]

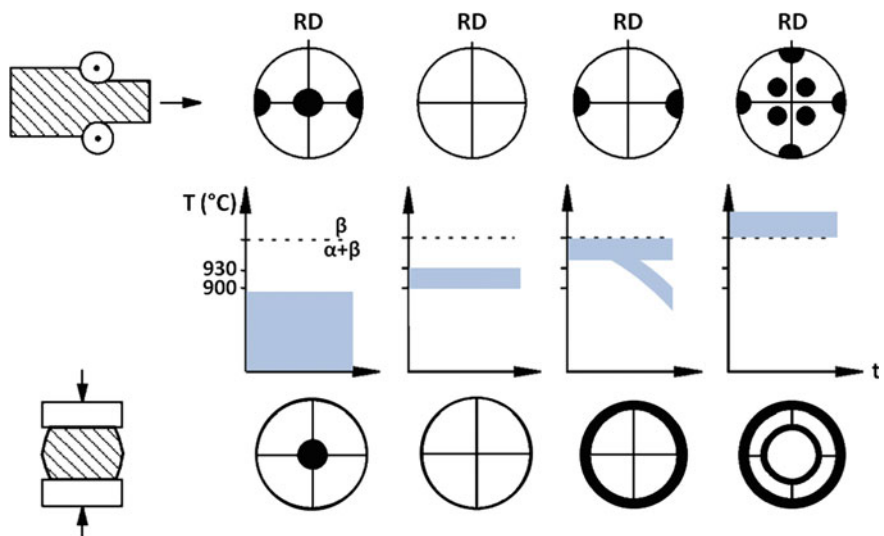
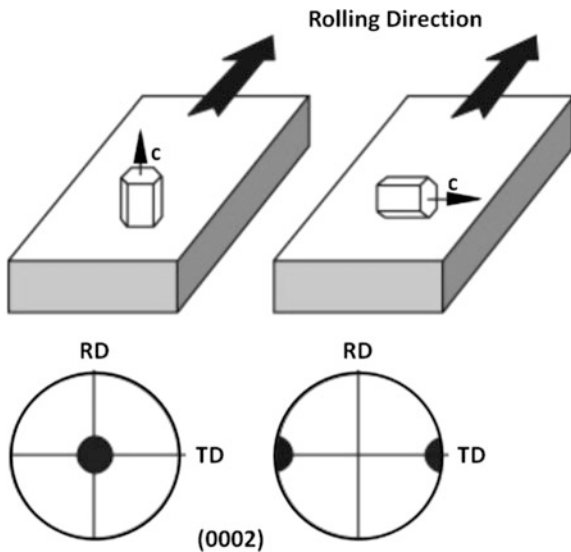


Fig. 7.9 Schematic (0002) pole figure textures in $\alpha + \beta$ titanium alloys as functions of deformation temperature and mode (unidirectional rolling or radial deformation) [15]

- (4) Above the β transus only the BCC β phase is present, and deformation results in a classic Cube texture [15]. This texture is inherited as a transformation texture on subsequent cooling [16].

Annealing Textures Texture changes during ($\alpha + \beta$) annealing are relatively unimportant compared to microstructural changes. This is true even for high annealing temperatures, used as part of the processing for bimodal and fully equiaxed I microstructures (see Figs. 7.6 and 7.7).

In other words, the deformation textures are largely retained, although high annealing temperatures close to the β transus tend to randomize the texture by introducing additional texture components [17].

N.B: Annealing above the β transus (β annealing) results in complete loss of the original texture [17].

7.3.4 Texture Effects on Aerospace Titanium Alloy Properties

Studies going back to the 1960s have shown that strong textures affect the strength, elastic modulus, fatigue, and fracture toughness properties of titanium alloys. In particular, there have been detailed investigations of the effects of strong basal (B) and transverse (T) textural influences on the mechanical properties. A summary of some results is given in this subsection. More information may be obtained from the following Reference Book:

- Boyer, R., Collings, E.W., and Welsch, G. (Eds.), 1994, 'Materials Properties Handbook: Titanium Alloys', ASM International, Materials Park, OH 44073-0002, USA.

Table 7.2 shows mechanical property and fracture toughness data for a T-textured high-strength $\alpha + \beta$ alloy, Ti-6Al-2Sn-4Zr-6Mo. The strengths and fracture toughness were much higher when loading was in the transverse (TD) direction, i.e. parallel to the HCP c-axis and normal to the (0002) planes.

Similar results for the elastic modulus of textured Ti-6Al-4V are shown in Fig. 7.10: both the T and B/T textures gave much higher elastic moduli in the transverse (TD) direction, with the 45° direction giving values intermediate between the longitudinal (RD) and transverse (TD) directions.

Table 7.2 Effect of texture on the properties of a highly T-textured Ti-6Al-2Sn-4Zr-6Mo plate [18]

Loading direction	UTS (MPa)	YS (MPa)	$\Delta L/L_0$ (%)	E (GPa)	K_{Ic} (MPa \sqrt{m})
RD	1027	952	11.5	107	75 (L-T)
TD	1358	1200	11.3	134	91 (T-L)

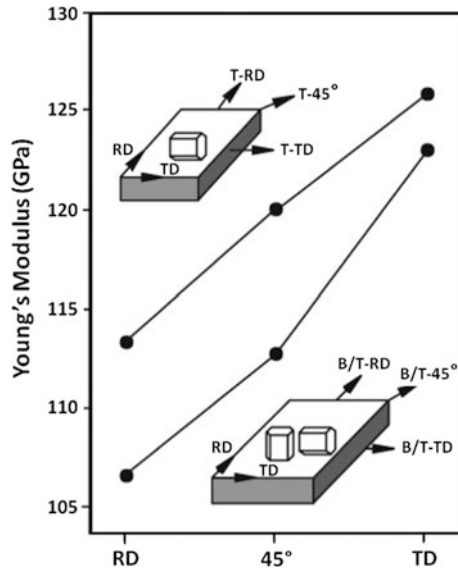


Fig. 7.10 Influence of texture on the elastic modulus of Ti-6Al-4V plate [15]

Microstructure, texture and loading directions	Fatigue strength	Fatigue crack growth
Equiaxed	-	-
Bi-modal (Duplex)	+	-

Fig. 7.11 Texture effects on fatigue strength and fatigue crack growth for highly textured Ti-6Al-4V plates [19]: + beneficial; - detrimental

Fatigue Properties Figure 7.11 qualitatively summarizes fatigue results for strongly textured Ti-6Al-4V plates from various sources [19]:

1. *Fatigue strength* Full explanation of the results is complicated [19, 20], since both texture and microstructural effects are involved. However, the difference in *unnotched* fatigue strength between ‘+’ and ‘-’ for the equiaxed alloy was only about 6%. This would be even less for *notched* fatigue, which is more appropriate for aerospace components and structures.

2. *Fatigue crack growth* Highly textured equiaxed microstructures tend to provide easier paths for early FCG, especially if the (0002) planes are normal to the principal loading direction [19].

Summary From the foregoing survey, it is reasonable to conclude that strong textures have large effects on the basic mechanical properties and fracture toughness of titanium alloys. However, the effects on fatigue strength are negligible and can be detrimental for fatigue crack growth. Furthermore, anisotropy is generally undesirable in aircraft structural alloys, e.g. the first- and second-generation Al–Li alloys mentioned in Sect. 7.2.

Thus, there seems little incentive to exploit texture-induced anisotropy for titanium alloy aircraft structures. In fact, the modern trend is just the opposite. For example, β -annealed Ti-6Al-4V plate with an *effectively* random texture and uniformly high strength is being used for highly loaded and fatigue critical components in the Lockheed Martin F-35 tactical aircraft [21].

One final point is that texture strengthening of titanium alloys for spacecraft pressure vessels (tanks) has also been considered since the 1960s [22]. However, the advent of modern β alloys that can be cold- or superplastically-formed into half shells before assembly by welding offers a more cost-effective solution with very good mechanical properties [23].

7.4 Nickel-Base Superalloys

Developments over the last 50 years have led to the replacement of wrought superalloy turbine blades and vanes by cast components. Initially, the cast components had polycrystalline equiaxed microstructures. In the 1960s, directionally solidified (DS) castings were developed, followed in the 1980s by the first generation of single crystal (SX) castings [24]. Since then, the technology has steadily evolved, resulting in the current sixth generation of SX alloys (see Chap. 9 in Volume 1 of these Source Books). Figure 7.12 shows examples of the different microstructures for cast superalloy blades [25].

The DS and SX microstructures are superior to conventionally cast equiaxed microstructures for two main reasons [26]:

1. Alignment or elimination of grain boundaries normal to the spanwise stress axis enhances the high-temperature ductility by preventing failure initiation at such boundaries.
2. Nickel-base superalloys have an FCC crystal structure, and the directional casting process for DS and SX blades (and vanes) is designed to provide a spanwise preferred low-modulus $\langle 001 \rangle$ direction. This results in improved thermal fatigue resistance, which is an important life-limiting property for both blades and vanes.

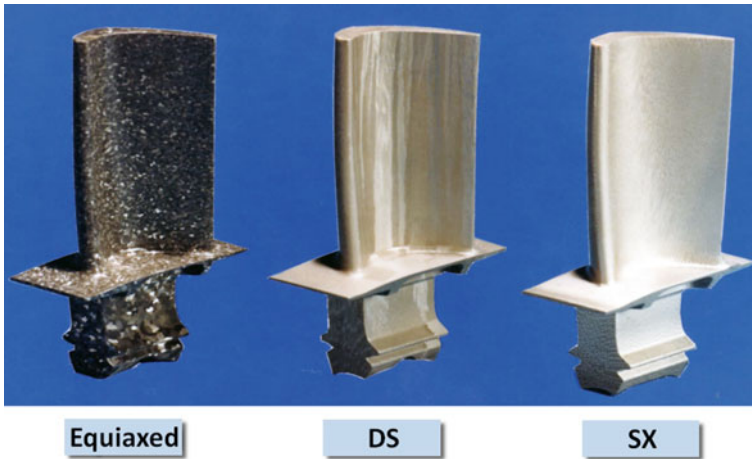


Fig. 7.12 Examples of cast nickel-base superalloy turbine blades [25]: *DS* directionally solidified; *SX* single crystal

As stated in Chap. 9 in Volume 1, the above two factors can result in much improved ($3\text{--}5\times$) creep rupture lives.

The development of DS and SX superalloy turbine components is an outstanding example of property improvements via microstructural and crystallographic texture changes. With respect to texture this technology may be regarded as mature. Improvements since the first generation of SX alloys have been principally due to modifications in alloy chemistry.

7.5 Summary

In this chapter, the effects of processing-induced crystallographic textures on the engineering properties of aerospace aluminium alloys, titanium alloys, and nickel-base superalloys are discussed and referred to.

In general, texture effects on the properties of aluminium alloys and titanium alloys are undesirable and to be avoided. However, texture effects are actively exploited for nickel-base superalloy turbine blades and vanes.

References

1. Eswara Prasad N, Gokhale AA, Wanhill RJH (eds) (2014) Aluminum—lithium alloys: processing, properties and applications. Elsevier Inc., Oxford, UK
2. Rout M, Pal SK, Singh SB (2015) Cross rolling: a metal forming process. In: Davim JP (ed) Chapter 2 in ‘Modern manufacturing engineering’. Springer International Publishing AG, CH-6330 Cham, Switzerland, pp 41–64

3. Suwas S, Ray RK (2014) Crystallographic texture of materials. Springer, London
4. Anon (2014) Microstructure analysis of a bent aluminium alloy using in-situ EBSD. <http://www.azom.com/article.aspx?ArticleID=10824>
5. Bunge H-J (1982) Texture analysis in materials science: mathematical methods, digital edn. 2015. Helga and Hans-Peter Bunge, Wolfratshausen, Germany
6. Rioja RJ, Liu J (2012) The evolution of Al-Li base products for aerospace and space applications. *Metall Mater Trans A* 43A:3325–3337
7. Bowen AW (1990) Texture development in high strength aluminium alloys. *Mater Sci Technol* 6(11):1058–1071
8. Jata KV, Singh AK (2014) Texture and its effects on properties in aluminum–lithium alloys. In: Eswara Prasad N, Gokhale AA, Wanhill RJH (eds) Chapter 5 in ‘Aluminum–lithium alloys: processing, properties and applications’. Elsevier Inc., Oxford, UK, pp 139–163
9. Rioja RJ, Giummarra C, Cheong S (2008) The role of crystallographic texture on the performance of flat rolled aluminum products for aerospace applications. In: DeYoung DH (ed) *Light metals 2008*. TMS, The Minerals, Metals & Materials Society, Warrendale, PA 15086-7514, USA, pp 1065–1069
10. Mondal C, Singh AK, Mukhopadhyay AK, Chattopadhyay K (2012) Mechanical property anisotropy of 7010 aluminum alloys sheet having single rotated-brass texture. *Mater Sci Forum* 702–703:303–306
11. Wanhill RJH, Bray GH (2014) Fatigue crack growth behavior of aluminum–lithium alloys. In: Eswara Prasad N, Gokhale AA, Wanhill RJH (eds) Chapter 12 in ‘Aluminum–lithium alloys: processing, properties and applications’. Elsevier Inc., Oxford, UK, pp 381–413
12. Lynch SP, Wanhill RJH, Byrnes RT, Bray GH (2014) Fracture toughness and fracture modes of aerospace aluminum–lithium alloys. In: Eswara Prasad N, Gokhale AA, Wanhill RJH (eds) Chapter 13 in ‘Aluminum–lithium alloys: processing, properties and applications’. Elsevier Inc., Oxford, UK, pp 415–455
13. Leyens C, Peters M (eds) (2003) *Titanium and titanium alloys: fundamentals and applications*. Wiley-VCH Verlag GmbH & Co, KGaA, Weinheim, Germany
14. Lütjering G, Williams JC (2007) *Titanium*, 2nd edn. Springer, Berlin, Germany
15. Peters M, Hemptenmacher J, Kumpfert J, Leyens C (2003) Structure and properties of titanium and titanium alloys. In: Leyens C, Peters M (eds) Chapter 1 in ‘Titanium and titanium alloys: fundamentals and applications’. Wiley-VCH Verlag GmbH & Co, KGaA, Weinheim, Germany, pp 1–36
16. Zarkades A, Larson FR (1971) A review of textures found in commercial titanium sheet. AMMRC Technical Report TR 71-60, Army Materials and Mechanics Research Center, Watertown, MA 02172, USA
17. Bowen AW (1977) Texture stability in heat treated Ti-6Al-4V. *Mater Sci Eng* 29(1):19–28
18. Donachie MJ Jr (2000) *Titanium: a technical guide*, 2nd edn. ASM International, Materials Park, OH 44073-0002, USA, p 101
19. Wanhill RJH (1999) Material-based failure analysis of the Lynx-282 rotor hub. NLR Contract Report NLR-CR-99189, National Aerospace Laboratory NLR, Amsterdam, The Netherlands
20. Peters M, Gysler A, Lütjering G (1984) Influence of texture on fatigue properties of Ti-6Al-4V. *Metall Trans A* 15A:1597–1605
21. Wanhill RJH, Barter SA (2012) *Fatigue of beta processed and beta heat-treated titanium alloys*. Springer Briefs in Applied Sciences and Technology, Springer, Dordrecht, The Netherlands
22. Sullivan TL (1968) Texture strengthening and fracture toughness of titanium alloy sheet at room and cryogenic temperatures. NASA Technical Note NASA TN D-4444, National Aeronautics and Space Administration, Washington, DC, USA
23. Peters M, Kumpfert J, Ward CH, Leyens C (2003) Titanium alloys for aerospace applications. In: Leyens C, Peters M (eds) Chapter 13 in ‘Titanium and titanium alloys: fundamentals and applications’. Wiley-VCH Verlag GmbH & Co, KGaA, Weinheim, Germany, pp 333–350

24. Dilmetiz SF, Zhang S (2013) Superalloys for super jobs. In: Zhang S, Zhao D (eds) Chapter 1 in 'Aerospace materials handbook'. CRC Press, Taylor & Francis Group, Boca Raton, FL 33487-2742, USA, pp 1–75
25. Clarke DR (2015) Thermal barrier coatings for gas turbines. Presentation for the Hong Kong Institute of Engineers, January 2015, Hong Kong University of Science and Technology, Clear Water Bay, New Territories, Hong Kong
26. Davis JR (ed) (1997) Directionally solidified and single-crystal superalloys. In: ASM specialty handbook, heat-resistant materials. ASM International, Materials Park, OH 44073-0002, USA, pp 255–271

Chapter 8

Physical Property Significances for Aerospace Structural Materials

R.J.H. Wanhill

Abstract This chapter summarises the significances of material density, elastic modulus, thermal expansion coefficient and thermal conductivity for the selection and use of some aerospace structural materials. The summary focusses on airframe materials, but thermal barrier coatings (TBCs) are also considered.

Keywords Physical properties · Aerospace alloys · Density · Stiffness · Thermal properties · Thermal barrier coatings

8.1 Introduction

Development of aerospace components is a multistage *iterative* process. The key issues are (i) knowledge of design and property requirements, (ii) identification and selection of materials likely to possess these properties, (iii) optimisation of composition and processing methods to achieve the desired and reproducible combinations of properties in the required types of products and components and (iv) the economic viability and service durability of the finished components.

The foregoing issues are discussed to some extent for specific materials in other chapters of these Source Book Volumes. However, a generalised systematic treatment, as in a recent NASA report [1], is not included. Some of this report is appropriate to the present chapter, which considers basic physical properties of aerospace structural materials and the significance of these properties for material selection and use.

The physical properties particularly relevant to aerospace materials are specific gravity (density), the coefficient of thermal expansion, and thermal conductivity. The elastic modulus (Young's modulus) is added to this list, since although it is usually classed as a mechanical property, it is linked to material density when considering and evaluating structural applications.

R.J.H. Wanhill (✉)
NLR, Emmeloord, The Netherlands
e-mail: rjhwanhill@gmail.com

8.2 Aerospace Structural Components

Aerospace structural components may be considered in a general way with respect to their shapes, types of loading, property requirements and constraints [1]. In this context constraints are taken to mean essential design requirements. A modified summary of this generalised approach for important structural and component types is given in Table 8.1. Density and elastic modulus are always primary factors, but thermal properties may not be.

Table 8.1 Aerospace structural components loads and design constraints: modified from Ref. [1]

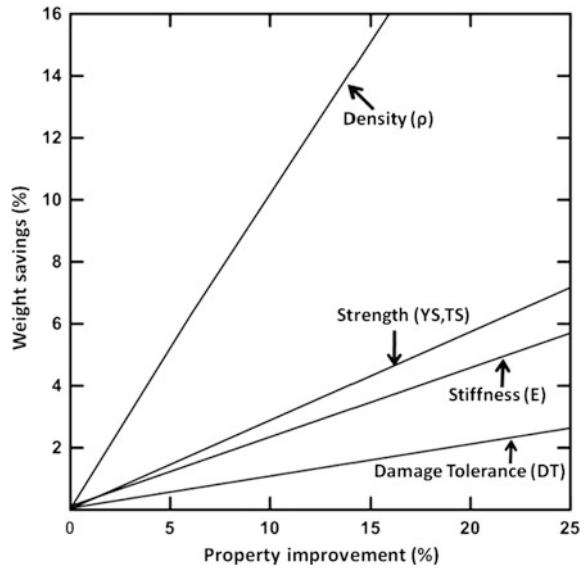
Structures/components	Idealised forms	Loading types	Constraints
Fuselages	Cylinders	<ul style="list-style-type: none"> • Compression • Tension • Bending • <i>Fatigue</i> 	<ul style="list-style-type: none"> • Buckling • Strength • Deflection • <i>Damage tolerance (DT)^a</i>
Wings	Plates	<ul style="list-style-type: none"> • Bending • Tension • Twist • Vibration • Fatigue 	<ul style="list-style-type: none"> • Buckling • Strength • Deflection • Vibration • <i>Damage tolerance (DT)^a</i>
<i>Landing gears</i>	<i>Cylinders</i>	<ul style="list-style-type: none"> • <i>Compression</i> • <i>Tension</i> • <i>Bending</i> • <i>Fatigue</i> 	<ul style="list-style-type: none"> • <i>Buckling</i> • <i>Strength</i> • <i>Deflection</i> • <i>Safe-life fatigue</i>
Engine discs	Discs	<ul style="list-style-type: none"> • Rotation • Thermomechanical fatigue 	<ul style="list-style-type: none"> • Strength, ductility • <i>Low-cycle fatigue</i>
Engine blades: fan, compressor, turbine	Tie beams	<ul style="list-style-type: none"> • Bending • Tension • Creep: <i>compressor, turbine</i> • <i>Thermal fatigue: turbine</i> • Fatigue: <i>fan, compressor</i> 	<ul style="list-style-type: none"> • Deflection • Strength • Vibration • Temperature • <i>Microstructure^b</i>
Combustion chambers	Cylinders	<ul style="list-style-type: none"> • Pressure, noise 	<ul style="list-style-type: none"> • Thermal, oxidation
<i>Cryogenic pressure vessels (spacecraft)</i>	Spherical and cylindrical shells	<ul style="list-style-type: none"> • Internal pressure • Thermal 	<ul style="list-style-type: none"> • Strength, <i>fracture toughness</i> • Yield/leak before break

Significant modifications are indicated by italic texts

^aDamage tolerance (DT) is essential for airframes (fuselage, wings, empennage) (see Chaps. 13 and 14 in Volume 1 and Chaps. 16 and 18 in Volume 2 of these Source Books) and is increasingly required for aerospace gas turbines

^bTurbine blade capabilities depend largely on whether they have equiaxed polycrystalline, directionally solidified (DS) polycrystalline, or single crystal (SX) microstructures: see Chap. 9 in Volume 1 and Chap. 7 in Volume 2 of these Source Books

Fig. 8.1 Effects of property improvements on potential weight savings [2]



8.3 Density and Stiffness

Material density is a prime consideration, together with the elastic modulus, for the structural efficiency of aircraft and spacecraft. In fact, the weight savings due to lower density outrank all other property improvements (see Fig. 8.1).

For design purposes, the density is always associated with the elastic modulus to derive two parameters:

1. Specific stiffness E/ρ : This is important for wing lower surfaces, spars, ribs and frames, engine discs and blades, and some landing gear components.
2. Specific buckling resistance $E^{1/3}/\rho$: This is important for wing upper surfaces, the fuselage, and landing gear main cylinders.

8.3.1 Aerospace Alloy Density and Stiffness Data

Table 8.2 presents some aerospace structural alloy density and stiffness data, and these have been used to derive Fig. 8.2. Two (very) general trends may be observed from this figure:

Table 8.2 Aerospace structural alloy densities and specific stiffness: data from various sources

Alloys	Density (g/cm ³)	Elastic modulus (GPa)	E/ρ		E ^{1/3} /ρ	
			Range	Average	Range	Average
Magnesium (wrought)	1.77–1.81	45	24.9–25.6	25.3	1.96–2.02	1.99
AA2XXX ^a	2.77–2.80	70–73	26.1–27.1	26.6	1.48–1.52	1.50
Aluminium: AA7XXX ^a	2.80–2.85	69–83	25.9–26.4	26.2	1.46–1.50	1.48
Al–Li ^b	2.63–2.72	75–82	28.9–31.2	30.1	1.58–1.65	1.62
TiAl	3.7–3.9	160–176	41.0–47.6	44.3	1.39–1.51	1.45
Ti ₃ Al	4.1–4.7	100–145	21.3–35.4	28.4	0.99–1.28	1.14
Titanium (α + β)	4.37–4.82	100–124	20.7–28.3	24.5	0.96–1.14	1.05
High-strength low-alloy steels	7.75–8.00	203–230	25.8–29.6	27.7	0.74–0.79	0.77
austenitic	7.72–8.03	193–200	24.0–25.9	25.0	0.72–0.76	0.74
Stainless steels: martensitic	7.74–7.78	193–221	24.8–28.5	26.7	0.74–0.78	0.76
PH ^c	7.74–7.92	197–221	24.9–28.6	26.8	0.73–0.78	0.76
Nickel-base superalloys	7.75–8.50	200–220	23.4–28.4	25.9	0.69–0.78	0.74

^aAA Aluminium association

^bThird-generation alloys

^cPH Precipitation hardening alloys

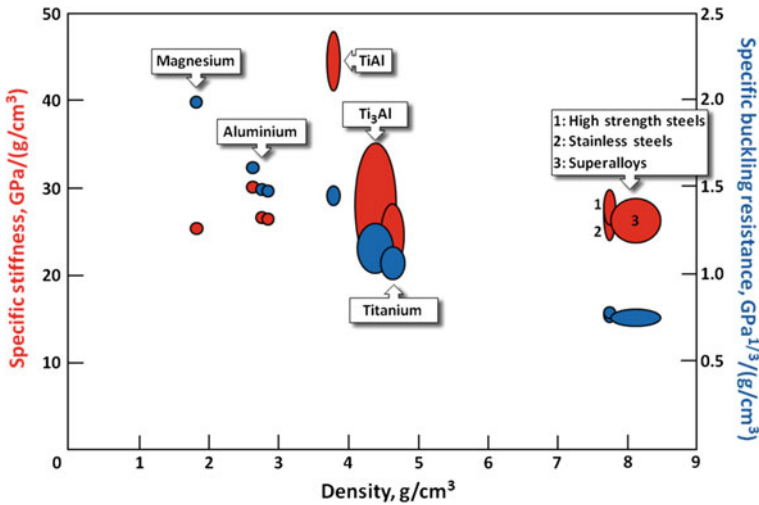


Fig. 8.2 Specific stiffnesses and buckling resistances for wrought magnesium, aluminium, titanium (α + β) and steel alloys, and nickel-base superalloys and wrought/cast titanium aluminides: data from Table 8.2

1. Most of the alloys have specific stiffness in the range 20–30 GPa/(g/cm³), the exceptions being the titanium aluminides, especially TiAl, and some Al–Li alloys (see Table 8.2 also).
2. The specific buckling resistance decreases with increasing density.

Neither of these general trends is useful for alloy selection, but the exceptions are. The reasons for these statements will be given in the following Sect. 8.3.2 on applications for the various alloy classes.

8.3.2 Alloy Classes and Applications

Applications of the alloys in Table 8.2 and Fig. 8.2 are summarised in Table 8.3 together with some characteristic properties and footnotes. It is evident that alloy selections must consider many aspects and that specific property maps like Fig. 8.2 are generally too ‘broad-brush’. However, as mentioned in Sect. 8.3.1, there can be exceptions:

Table 8.3 Aerospace structural alloy classes and applications: for more information see Chaps. 1–3, 6, 9 and 10 from Volume 1 and Chaps. 16, 18 and 19 from Volume 2 of these Source Books

Alloys	Typical applications	Characteristic properties	
		Pros	Cons
Magnesium	<ul style="list-style-type: none"> • Thick-section light components: helicopter gear boxes, landing gear wheels 	<ul style="list-style-type: none"> • Specific stiffness 	<ul style="list-style-type: none"> • Low strength, ductility • Low load density • Galvanic corrosion
Aluminium	<ul style="list-style-type: none"> • Airframes: fuselages, wings, empennage 	<ul style="list-style-type: none"> • Specific stiffness • High DT 	<ul style="list-style-type: none"> • Moderate load density • Temperature limit ~ 130 °C
Titanium aluminides	<ul style="list-style-type: none"> • Low-pressure (LP) turbine blades 	<ul style="list-style-type: none"> • High specific stiffness • Temperatures up to ~ 750 °C 	<ul style="list-style-type: none"> • Low temperature brittleness • Impact resistance
Titanium	<ul style="list-style-type: none"> • Aeroengine fan and compressor sections, nacelles and surrounding airframe • High-strength and high load density components: engine pylons, landing gear • Cryogenic pressure vessels 	<ul style="list-style-type: none"> • Specific strength • Creep and oxidation resistance up to ~ 650 °C • High load density • Fracture toughness • Corrosion resistance 	<ul style="list-style-type: none"> • Moderate specific stiffness • High material and manufacturing costs

(continued)

Table 8.3 (continued)

Alloys	Typical applications	Characteristic properties	
		Pros	Cons
High-strength low-alloy steels	<ul style="list-style-type: none"> • Landing gears • High-strength and load density airframe components 	<ul style="list-style-type: none"> • Specific strength • Very high load density^a • Fatigue strength 	<ul style="list-style-type: none"> • Low DT • Low corrosion resistance
Stainless steels	<ul style="list-style-type: none"> • Fuel, hydraulic and plumbing lines • High-strength (PH) airframe and landing gear components 	<ul style="list-style-type: none"> • Corrosion resistance^b • Some heat-resistant alloys usable up to ~ 650 °C^c 	<ul style="list-style-type: none"> • Moderate strength (except PH) • Stress corrosion susceptibility^b
Nickel-base superalloys	<ul style="list-style-type: none"> • Aeroengine turbine sections: discs, blades, vanes and other components 	<ul style="list-style-type: none"> • High temperature strength and creep resistance • Low temperature ductility 	<ul style="list-style-type: none"> • High density • High costs, especially DS and SX blades

^aLanding gears require very high load densities because they must be compact, i.e. taking up minimum space when retracted

^bStainless steels are not necessarily immune to corrosion and stress corrosion

^cRef. [3]

1. Titanium aluminides: Table 8.2 and Fig. 8.2 indicate that these materials have, or can have, much higher specific stiffness than titanium alloys and nickel-base superalloys. With the additional knowledge that titanium aluminides have temperature capabilities up to about 750 °C (Table 8.3), it is clear why there is much interest in using them to save weight in aeroengines. More information is given in Chap. 10 of Volume 1 of these Source Books.
2. Al–Li alloys: High-strength aluminium alloys are undergoing increasing competition from carbon fibre reinforced plastic (CFRP) composites. This means it is useful to take a more detailed look at the specific stiffnesses and buckling resistances of aluminium alloys, particularly the higher values obtainable from Al–Li alloys, to compare with those of CFRPs.

The comparisons are given in Fig. 8.3, using examples of high-fibre-density CFRPs. It is seen that the conventional aluminium alloys can match the specific stiffness of the 25 % aligned fibre composites (this is a realistic value for major components subjected to multiaxial loading), while Al–Li alloys have a clear advantage.

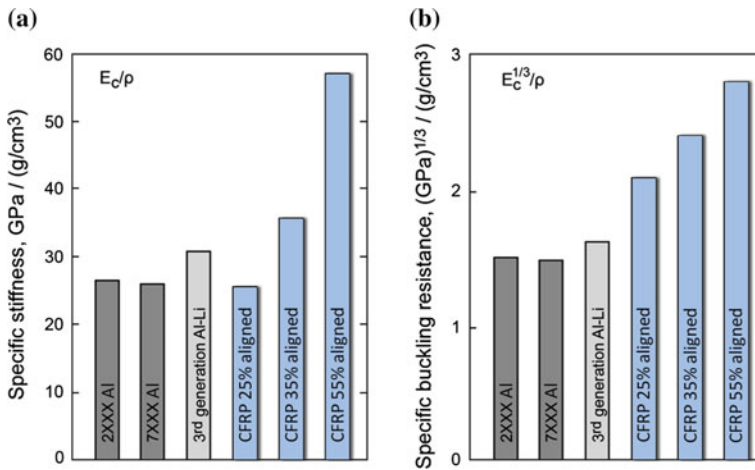


Fig. 8.3 Specific stiffnesses (average values) for high-fibre-density (60 % volume) CFRP composites tested in the aligned fibre direction, conventional aerospace aluminium alloys and third-generation Al–Li alloys: see Chap. 14 in Volume 1 of these Source Books

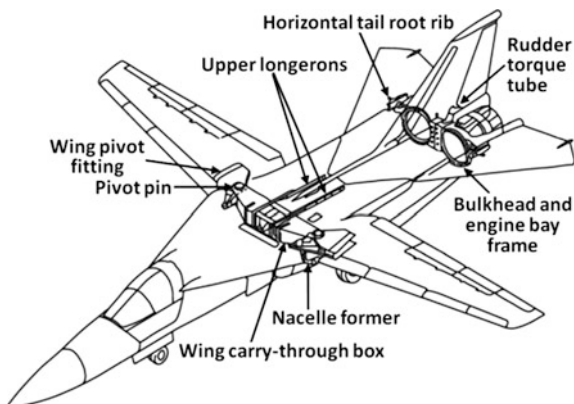
On the other hand, the aluminium alloys cannot compete in terms of specific buckling resistance. Thus, *in the absence of other considerations*, the CFRPs always have a large advantage for compressive loaded structures, such as lower fuselage sections and upper wing skins.

However, the ‘other considerations’ are important. Firstly, the property variabilities of CFRPs require reduction factors to be imposed, which signify weight penalties. Secondly, ensuring an acceptable DT level can incur further weight penalties. More information on this complex topic is given in Chap. 14 of Volume 1 of these Source Books.

8.3.3 Inadvisable Alloy Selection: A Case History

An important case history is discussed briefly here as an illustration of misapplying (*this is hindsight*) the structural efficiency properties. It is shown in Table 8.2 and Fig. 8.2 that high-strength low-alloy steels have specific stiffnesses comparable to those of aluminium alloys. Broadly speaking, this equivalence, a high specific strength, and especially a high load density capability led to the use of D6ac steel for major parts of the General Dynamics F-111 airframe [4] (see Fig. 8.4).

Fig. 8.4 D6ac steel parts in the General Dynamics F-111 airframe



This innovative use turned out to give fatigue and fracture problems during the airframe test programmes [4], leading to concerns about the overall structural integrity. These concerns and a notorious crash in 1969 [5] resulted in a very expensive fracture control programme. This programme required periodically removing aircraft from service and proof-testing the wing pivot and carry-through assembly at $-40\text{ }^{\circ}\text{C}$ [4]. This meant that the entire aircraft had to be cooled to $-40\text{ }^{\circ}\text{C}$.

On the positive side, the 1969 crash, the test programme problems, and also early cracking in Lockheed C-5A aluminium alloy wing boxes [5] resulted in the United States Air Force (USAF) deciding to implement DT for all types of military aircraft. This was a very important development.

DT is now the norm for both civil aircraft and military aircraft: see the first footnote for Table 8.1, Chaps. 13 and 14 in Volume 1 and Chaps. 16 and 18 in Volume 2 of these Source Books.

8.4 Thermal Properties

Thermal properties and their effects on aerospace structures have a long history. They are obviously important for cryogenic systems [6] and engines (see Table 8.1). In this section the focus is on airframe material issues, particularly those due to thermal expansion mismatch. However, mention will also be made of thermal barrier coatings (TBCs), which are included briefly in Chap. 22 of Volume 1 of these Source Books.

The effects of thermal stresses on airframes became important in the mid-1950s–1960s, with the designing of the Aérospatiale/BAC Concorde, the BAC TSR-2 and the Lockheed SR-71. The latter two aircraft are shown in Fig. 8.5.

Fig. 8.5 BAC TSR-2 (*top*)
and Lockheed SR-71 (*bottom*)



It must immediately be said that the three aircraft represent two very different technologies:

1. Concorde and the TSR-2 were designed to cruise just above Mach 2. The airframes were mainly aluminium alloys. In AA equivalents, these were 2618 for Concorde [7]; and 2020 skins, 2014 frames and panels, and 2618 near the engines for the TSR-2 [8]. Both aircraft had very powerful but conventional turbojets.
2. The SR-71 was designed to cruise at about Mach 3. Aerodynamic heating and structural efficiency required the airframe to consist primarily of titanium alloys. The skin was the β alloy Ti-13V-11Cr-3Al, and there was additional use of Ti-5Al-2.5Sn and Ti-6Al-4V [9]. The engines were special turbojets with provision for continuous afterburner operation at the very high cruising speed.

There were also some differences in how the thermal stresses from aerodynamic heating were alleviated. Concorde and the TSR-2 were subjected to relatively mild heating, such that thermal expansion could be accounted for by structural features like corrugated webs, expansion joints, slotted lug attachments and leading edge slits.

Analogous features were used for the SR-71, but additional and more extensive measures were needed. These included structural design for load alleviation; using the fuel as a heat sink; chordwise-corrugated wing ribs; and skin panels corrugated

on the inside surfaces and assembled to allow thermal expansion relative to cooler spar caps [9]. Also, an obvious feature is the black paint scheme, which promoted heat radiation to the environment.

8.4.1 Thermal Expansion Mismatch: Airframes

Over the last 30 years, thermal expansion mismatch has become increasingly relevant for both civil and military aircraft owing to hybrid airframes, e.g. the Airbus A380, Fig. 8.6, and composite repairs of structures and components.

Hybrid Airframes Since the design and development of the A380, Airbus and Boeing have greatly increased the amounts of CFRP used in transport aircraft airframes, for example the A350XWB, A400M and Boeing 787. Composites are also much used in high-performance military aircraft. Hence the technology of integrating composite structures and components in hybrid airframes may be regarded as mature. Details are not available in the open literature and are most probably proprietary, but some general guidelines are available [10, 11].

Patch Repairs Using Dissimilar Materials Patch repairs may be bolted-on or adhesively bonded, with the latter being favoured if the underlying structure is relatively lightly loaded and thin, e.g. fuselage skins. Most of the interest has been about adhesively bonded composite patches [12–15], which can be applied to both metallic and composite components. Discussions of the *pros* and *cons* of mechanically fastened repairs and bonded repairs are also given in Refs. [12–15].



Fig. 8.6 GLARE (GLASS REinforced aluminium laminates) and CFRP components in the Airbus A380: see Chaps. 13 and 14 in Volume 1 of these Source Books

Table 8.4 Properties of materials involved in bonded repairs example [14]

Property	2024-T3	GLARE 2- 3/2-0.2	Boron-epoxy
E_L (GPa)	72.4	69	207
E_{LT} (GPa)	72.4	54	19
CTE_L ($10^{-6}/^{\circ}C$)	22.5	16.3	4.5
CTE_{LT} ($10^{-6}/^{\circ}C$)	22.5	24.5	20
YS_L (MPa)	310	383	n/a
YS_{LT} (MPa)	310	242	n/a
UTS_L (MPa)	427	1187.5	1585
UTS_{LT} (MPa)	427	313.4	62.7

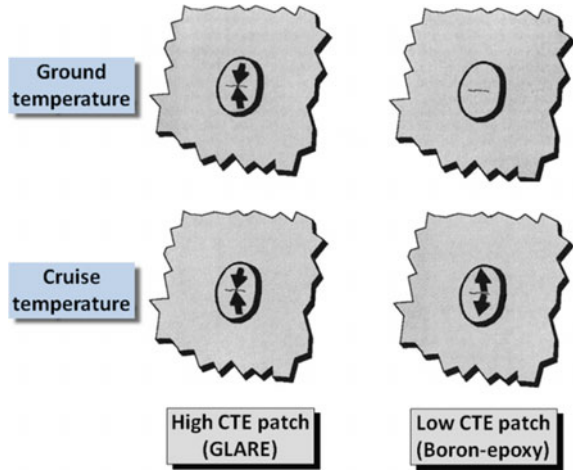
Durable bonded patches require adhesives that are cured at elevated temperatures, which should be as low as possible to minimise thermal residual stresses [14], and preferably no more than about 125 °C if repairing aluminium alloy structures, to avoid affecting the alloy properties.

An instructive example is given by Vlot et al. [14], comparing patch repairs of cracked AA2024 aluminium alloy using GLARE and boron–epoxy composite, which has a long history of successful patching use [16]. The relevant properties of these materials are given in Table 8.4, and the coefficients of thermal expansion, CTE, are highlighted. This shows that the longitudinal CTE of boron–epoxy is much lower than those of GLARE and AA2024-T3.

There are two basic crack-patching scenarios to consider, and a possible third one:

1. No constraint: Unconstrained AA2024-T3 will contract more than the patches after elevated temperature curing. Thus both boron–epoxy and GLARE patches will result in thermally induced residual tensile stresses in the aluminium substrate. However, the GLARE-induced residual tensile stresses will be less.
2. Constrained substrate: An in situ patch repair (e.g. on an AA2024-T3 fuselage skin) has supporting structure that partially prevents the skin from expanding during curing, thereby significantly reducing its *effective* CTE. Hence after cooling to room temperature the thermally induced residual stresses in the skin are close to zero under a boron–epoxy patch and compressive under a GLARE patch [14].
3. Service conditions: Scenario (2) obviously favours patching with GLARE. It also leads to the following considerations for transport aircraft. During high-altitude cruise a patched pressure cabin skin and its supporting structure will cool down as if unconstrained [14]. The patch therefore always contracts less than the skin, causing additional tensile stresses in the skin. These stresses result in the cumulative thermally induced stresses becoming tensile in a boron-patched skin but remaining compressive in a GLARE-patched skin.

Fig. 8.7 Schematic patch CTE influences on stresses in crack-patched pressure cabin skin areas [14]

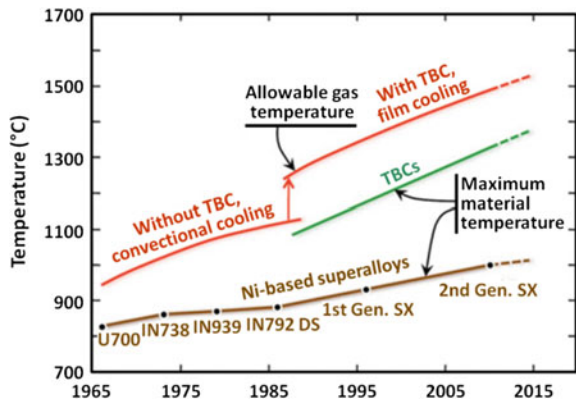


This can lead to a situation like that shown in Fig. 8.7, namely that even under cabin pressurisation, which causes tensile stresses, the overall skin stresses under a GLARE patch can remain compressive [14].

8.4.2 Thermal Barrier Coatings (TBCs)

The origins of TBCs date back to the 1940s [17]. However, their use on gas turbine blades and vanes began only in the mid-1980s (see Fig. 8.8): the red lines indicate the maximum allowable gas temperatures and the large increase ($\approx 150\text{ }^{\circ}\text{C}$) due to coating nickel-base superalloys with TBCs. This illustrates their importance, which is reflected by extensive literature, including a recent book [19].

Fig. 8.8 Temperature capabilities of nickel-base superalloys and TBCs over the last 35–50 years [18]



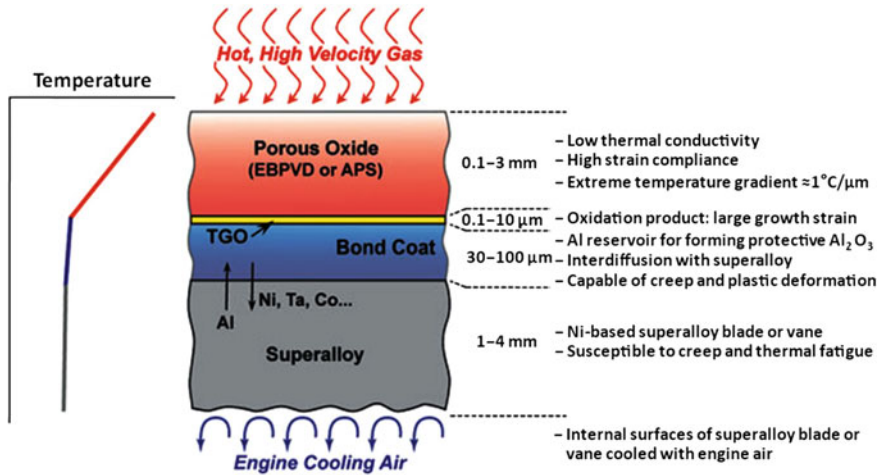


Fig. 8.9 Schematic of a TBC system deposited on a superalloy substrate [18]. The ceramic (porous oxide) topcoat is deposited by electron beam physical vapour deposition (EBPVD) or air plasma spraying (APS). Some of the properties of the various layers are indicated, and also the large temperature decrease owing to the topcoat's thermal barrier function

A TBC consists initially of a metallic bond coat and ceramic topcoat. A thermally grown oxide (TGO) intermediate layer forms during service. All three layers are important. They are shown schematically in Fig. 8.9 together with a superalloy substrate and some of their properties.

The performance of these TBC multilayer systems depends on their mechanical and thermophysical properties. These are influenced by the microstructures, which in turn depend on the coating deposition parameters, and can also change significantly during service [18].

The most important a priori property of TBCs is low thermal conductivity, which is responsible for the thermal barrier effect. However, they are also multifunctional and must (i) provide thermal insulation for the underlying superalloy blades or vanes, (ii) reflect radiant heat from the hot gas, (iii) be strain-compliant to minimise CTE mismatch stresses between the topcoat, bond coat and superalloy, and (iv) maintain thermal protection for prolonged service (several thousands of hours) with (v) frequent thermal cycling (engine start–stop cycles and intermediate power adjustments).

The multilayer and multifunctional nature of TBC systems inevitably results in compromises and complex optimisation processes. Table 8.5 lists some of the properties and considerations as an admittedly simplified illustration of the difficulties involved. There are also several excellent and concise reviews in the open literature [18, 20–22] as well as the above-mentioned book [19].

Table 8.5 Properties and considerations for TBC systems: information mainly from Refs. [18, 20–22]

Layers	Specific property requirements and considerations
Topcoat	<ul style="list-style-type: none"> • Low thermal conductivity • High melting point • Compliant (strain-tolerant) to accommodate CTE mismatch with the bond coat • Toughness • Spalling resistance: this actually depends on all three layers • Erosion resistance • Resistance to degradation by calcium–magnesium–aluminosilicate (CMAS) owing to engine ingestion of siliceous mineral debris • Phase and pore stability • Resistance to sintering: reduces insulating and compliance capabilities • Thermodynamic compatibility with Al_2O_3 (the TGO)
TGO	<ul style="list-style-type: none"> • Low CTE • Low growth rate • Adhesion to topcoat and bond coat for chemical and mechanical compatibility of entire system
Bond coat	<ul style="list-style-type: none"> • Oxidation resistance • Low CTE (if possible) to minimise mismatch with the TGO and topcoat • Creep resistance • Phase stability • Sulphur content • Chemistry allowing controlled interdiffusion and an optimum TGO

8.5 Concluding Remarks

This chapter provides examples of the significances of material density, elastic modulus, thermal expansion coefficient and thermal conductivity for some aerospace structural materials and applications. The emphasis is on airframe materials, but thermal barrier coatings (TBCs) are included as outstanding examples of the complex issues often faced by aerospace materials technologists.

References

1. Arnold SM, Cebon D, Ashby M (2012) Materials selection for aerospace systems. NASA Technical Memorandum NASA/TM-2012-217411, National Aeronautics and Space Administration Center for Aerospace Information, Hanover, MD 21076-1320, USA
2. Ekvall JC, Rhodes JE, Wald GG (1982) Methodology for evaluating weight savings from basic material properties. In: Design of fatigue and fracture resistant structures, ASTM STP 761. American Society for Testing and Materials, Philadelphia, PA 19104, USA, pp 328–341
3. Davis JR (ed) (1997) ASM specialty handbook, heat-resistant materials. ASM International, Materials Park, OH 44073-0002, USA, pp 124–145
4. Buntin WD (1977) Application of fracture mechanics to the F-111 airplane. In: AGARD conference proceedings no. 221 on fracture mechanics design methodology. Advisory Group for Aerospace Research and Development, Neuilly-sur-Seine, France, pp. 3-1–3-12

5. Mar JW (1991) Structural integrity of aging airplanes: a perspective. In: Atluri SN, Sampath SG, Tong P (eds) *Structural integrity of aging airplanes*. Springer, Berlin, Germany, pp 241–262
6. Johnson TF, Natividad R, Rivers HK, Smith RW (2005) Thermal structures technology development for reusable launch vehicle cryogenic propellant tanks. NASA Technical Memorandum NASA/TM-2005-213913. National Aeronautics and Space Administration Center for Aerospace Information, Hanover, MD 21076-1320, USA
7. Doyle WM (1969) The development of Hiduminium-RR.58 aluminium alloy: the background to the choice of the main structural material for concorde. *Aircr Eng Aerosp Technol* 41 (11):11–14
8. Hastings D (2013) *Structure and systems. Target lock: British Aircraft Corporation TSR.2*. www.targetlock.org.uk
9. Merlin PW (2009) Design and development of the Blackbird: challenges and lessons learned. AIAA paper 2009-1522, 47th AIAA Aerospace Sciences Meeting Including the New Horizons Forum and Aerospace Exposition, 5–8 January 2009, Orlando, FL 32801, USA
10. Department of Defense Handbook, *Composite Materials Handbook (2002) Volume 3. Polymer matrix composites materials usage, design, and analysis*, MIL-HDBK-17-3F. Document Automation and Production Service (DAPS), Philadelphia, PA 19111-5094, USA
11. Camanho P, Tong L (eds) (2011) *Composite joints and connections: principles, modelling and testing*. Woodhead Publishing Limited, Sawston, Cambridge, UK
12. Baker AA, Dutton S, Kelly D (2004) Chapter 10 in ‘*Composite materials for aerospace structures*’, 2nd edn. American Institute of Aeronautics and Astronautics, Inc., Reston, VA 20191-4344, USA, pp 369–402
13. Advisory Group for Aerospace Research and Development (1995) *Composite repair of military aircraft structures*. In: Conference proceedings AGARD-CP- 550. Neuilly-sur-Seine, France
14. Vlot A, Verhoeven S, Nijssen PJM (1998) *Bonded repairs for aircraft fuselages*. Delft University Press, Delft, The Netherlands
15. Günther G, Maier A (2010) *Composite repair for metallic aircraft structures: development and qualification aspects*. ICAS paper 2010-8.4.1, ICAS 2010, 27th congress of the international council of the aeronautical sciences, CD-ROM proceedings, 19–24 September 2010. Nice, France
16. Baker AA (1995) *Bonded composite repair of metallic aircraft components—overview of Australian activities*. In: ‘*Composite repair of military aircraft structures*’, AGARD conference proceedings AGARD-CP-550. Advisory Group for Aerospace Research and Development, Neuilly-sur-Seine, France, pp 1-1–1-14
17. Miller RA (2009) History of thermal barrier coatings for gas turbine engines: emphasizing NASA’s role from 1942 to 1990. NASA Technical Memorandum NASA/TM-2009-215459. National Aeronautics and Space Administration Center for Aerospace Information, Hanover, MD 21076-1320, USA
18. Clarke DR, Oechsner M, Pature NP (2012) Thermal-barrier coatings for more efficient gas-turbine engines. *MRS Bull* 37(10):891–898
19. Xu H, Guo H (eds) (2011) *Thermal barrier coatings*. Woodhead Publishing Limited, Sawston, Cambridge, UK
20. Pature NP, Gell M, Jordan EH (2002) Thermal barrier coatings for gas-turbine engine applications. *Science* 296(5566):280–284. 12 April 2002
21. Bacos M-P, Dorvaux J-M, Landais S, Lavigne O, Mévrel R, Poulain M, Rio C, Vidal-Sétif M-H (2011) 10 years-activities at Onera on advanced thermal barrier coatings. Paper AL03-04, *Journal Aerospace Lab*, Issue 3, November 2011. www.aerospacelab-journal.org
22. Martin P (2012) Thermal barrier coatings. *Society of Vacuum Coaters SVC Bulletin*, Summer 2012, pp 28–33, 36–38

Chapter 9

Structural Alloy Testing: Part 1—Ambient Temperature Properties

R.J.H. Wanhill

Abstract Standard data on ambient temperature mechanical and environmental properties, including yield and tensile strengths, fatigue and fatigue crack growth, fracture toughness, corrosion and stress corrosion, are essential—indeed mandatory—for the qualification and certification of aerospace structural materials and the design of actual structures and components. This chapter discusses the determination of important ambient temperature mechanical and environmental properties of aerospace alloys at the basic level of specimen and coupon testing.

Keywords Ambient temperature testing · Mechanical properties · Fatigue · Fracture · Corrosion

9.1 Introduction

Ambient (room temperature) aeromaterials testing is usually taken to mean the determination of various mechanical and environmental properties. This is an essential (mandatory) part of qualification and certification programmes, which are discussed in Chap. 24 of this Volume of the Source Books and also in Ref. [1].

The present chapter concentrates on the mechanical and environmental properties of aerospace structural alloys, but it should be remembered that qualification also involves manufacturing and process technologies. For example, an overview of an ambient temperature qualification programme for an aluminium alloy is given in Table 9.1.

R.J.H. Wanhill (✉)
NLR, Emmeloord, The Netherlands
e-mail: rjhwanhill@gmail.com

Table 9.1 Example of a qualification programme (Al–Li sheet/plate alloy) [2]

Properties	Property details	Special considerations
Mechanical	<ul style="list-style-type: none"> • TYS, CYS, TS, E, ductility • Shear and bearing strengths 	<ul style="list-style-type: none"> • Multi-angle (texture and anisotropy effects) • Temperature: 225–424 K; cryogenic (space)
Fatigue strength	<ul style="list-style-type: none"> • HCF^a of notched coupons and structural joints • CA^a and VA^a load histories 	<ul style="list-style-type: none"> • Texture and anisotropy effects • Environmental effects • Corrosion protection (coatings and primers)
Fatigue crack growth	<ul style="list-style-type: none"> • Long and short cracks • CA and VA load histories 	<ul style="list-style-type: none"> • Texture and anisotropy effects • Environmental effects • Modelling and prediction of crack growth
Fracture	<ul style="list-style-type: none"> • Plane-strain/plane-stress fracture toughness • K_R curves • Residual strength of stiffened panels 	<ul style="list-style-type: none"> • Texture and anisotropy effects • Temperature: 225–295 K; cryogenic (space) • Thermal stability during service • Possible dynamic effects on toughness
Corrosion	<ul style="list-style-type: none"> • Pitting and exfoliation • Stress corrosion cracking (SCC) • Accelerated and natural environments 	<ul style="list-style-type: none"> • Intergranular attack • Microbiological attack in fuel tanks • Structural joints • SCC resistance in thicker sections
Manufacturing and process technologies	<ul style="list-style-type: none"> • Forming: stretch and spin forming • Machining, cutting, hole drilling • Mechanical fastening: rivets and bolts • Welding: FSW^a and LBW^a • Surface treatments: chemical milling, etching, anodizing, priming, adhesive bonding 	<ul style="list-style-type: none"> • Texture and anisotropy • Superplastic forming • Combinations of forming and heat treatment • Automated 3-D welding; post-weld heat-treatments and stress relief

^aTYS Tensile yield strength; CYS Compressive yield strength; TS Tensile strength; E Young's modulus; HCF High cycle fatigue; CA Constant amplitude; VA Variable amplitude; FSW Friction stir welding; LBW Laser beam welding

Furthermore, the testing discussed in this chapter is restricted to coupon and specimen tests, which represent the lowest level of a building block (BB) test approach for materials and components airworthiness certification. The BB approach is shown schematically in Fig. 9.1.

The reader should consult Chaps. 16–18 of this Volume of the Source Books for information about structural alloy fatigue and residual strength tests at higher levels in the BB approach.

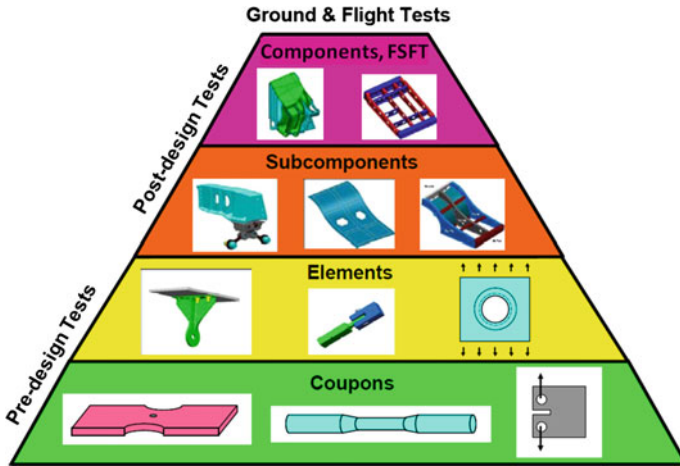


Fig. 9.1 ‘Building Block’ test approach for materials, components and structures: after Ref. [3]

9.2 Mechanical Properties

The mechanical properties include tensile and compressive yield strengths, tensile strengths and elastic modulus (Young’s modulus); tensile ductility (measured in terms of percent elongation or percent reduction of area); shear and bearing strengths; and hardness, which is particularly important for steels.

The basic properties of tensile strengths, ductility, Young’s modulus and hardness are of interest to both alloy manufacturers and users. Compression, shear and bearing strengths are mainly of interest for engineering design.

The following subsections summarise these tests in the context of the requirements in the American Society for Testing and Materials **ASTM International Book of Standards**. *N.B:* These Standards are updated from time to time.

9.2.1 Tension Testing

The ASTM Standard for tension testing of metallic materials is ASTM E8/E8M-15a. The test methods cover tension testing at room temperature to determine the yield strength, yield point elongation, tensile strength, and elongation and reduction of area. Exceptions may need to be made for particular materials. Examples are the test methods in ASTM A370-15 (steels) and ASTM B557-15 and ASTM B557M-15 (wrought and cast aluminium and magnesium alloys).

Besides these Standards, the American Society of Metals (ASM International) has published a book devoted to tensile testing [4]. This also includes testing at both elevated and low temperatures. Note that Table 9.1 includes cryogenic testing, which is required for space applications.

9.2.2 Compression Testing

The ASTM Standard for compression testing of metallic materials is ASTM E9-09. The data include the yield strength, yield point, Young's modulus and the compressive strength. This type of information is needed for structural analyses that include compressive and bending loads.

Note that Young's modulus may be obtained from compression tests. This differs formally from tension tests, which can also be used to *estimate* this modulus, but the values are not recognised as definitive.

9.2.3 Stress–Strain Curve Moduli

The ASTM Standard for determination of stress–strain curve moduli is ASTM E111-04(2010). This Standard covers Young's modulus, and also the tangent and chord moduli, which are useful for materials that show nonlinear elastic stress–strain behaviour:

- The tangent modulus is the slope of the stress–strain curve at any specified point and is equivalent to Young's modulus below the elastic limit.
- The chord modulus is the slope of the chord between any two specified points on the stress–strain curve.

N.B: There is another Standard, ASTM E1876-09, which includes determination of Young's modulus dynamically. This is useful for viscoelastic materials and also for research purposes, but it is not required as part of the qualification and certification of structural metals and alloys.

9.2.4 Shear and Bearing Strengths

There is an ASTM Standard for measuring the shear strength of wrought and cast aluminium alloys, ASTM B769-11. The data for wrought alloys are relevant particularly to aircraft primary structures. A highly specific Standard is ASTM B565-04(2015), which is only for shear testing of aluminium alloy rivets and cold-heading wire and rods. These Standards are not interchangeable, i.e. the measured shear strengths are not equivalent.

Another important engineering Standard is ASTM E238-12, which concerns basic data for the bearing strengths of cylindrical pin- and bolt-loaded holes. The data may be used in the design of lugs and bolted joints.

9.2.5 Hardness

There are several ASTM Standards for hardness testing:

- Rockwell hardness: ASTM E18-15.
- Brinell hardness: ASTM E10-15a.
- Knoop and Vickers hardness: ASTM E384-11e1. This includes microhardness testing also.

In addition, ASM International has published two books on hardness testing [5, 6].

Hardness data are very useful for quality control of structural alloys, especially steels but also aluminium and other alloys. Hardness measurements, including microhardness, may also be very useful in failure analyses, e.g. checking that materials, plating or case-hardening for steels conform to the specifications.

It is also important to note that conversion tables are available for comparing and correlating the results from different types of tests.

9.3 Fatigue

There is a vast amount of information on the fatigue of aerospace structural alloys at all levels of testing. As stated in Sect. 9.1, the present chapter is confined to the coupon and specimen level. The following book is recommended:

- Schijve, J., 2009, ‘Fatigue of Structures and Materials’, Second Edition, Springer Netherlands, Dordrecht, the Netherlands.

9.3.1 Some Important Remarks About the Commencement of Fatigue Cracking

Before considering the coupon and specimen fatigue testing methods, an important and long-standing issue needs to be mentioned. This is the concept of fatigue crack ‘initiation’. This concept has often been taken to mean that a specimen or component is crack-free up to a certain estimable fatigue lifetime. This assumption—which is all it is—has been a spurious cornerstone of aircraft fatigue design and analysis for over half a century. However, this situation has been gradually changing over the last 20–30 years.

It is now recognised that aerospace engineering materials, components and structures contain various types of discontinuities that can and do act as nucleation sites for fatigue cracks, e.g. Refs. [7–9]. Furthermore, for high performance aircraft

the first fatigue cracks (so-called *lead cracks*) begin to grow very early in the service life, such that there is virtually no crack-free life [8].

The foregoing remarks illustrate that the concept of fatigue crack ‘initiation’, implying a more or less determinable crack-free life, is phenomenologically incorrect and should actually be abandoned for fatigue design of aircraft structures.

Notwithstanding these caveats, conventional fatigue testing is useful for material qualification programmes, and it is still used for some airframe lifting methods and analyses. More information on these latter topics is given in Sect. 9.3.2 and especially in Sects. 16.3 and 16.4 of Chap. 16 of this Volume.

9.3.2 Fatigue Test Approaches

There are two basic fatigue life approaches that determine the type of testing:

1. **Stress–life:** This is the traditional controlled-force stress versus number of cycles (S–N) type of testing, much used for material comparisons and qualification programmes, and also for preliminary design analyses. The emphasis in this type of testing is on determination of the high cycle *fatigue limit*, also called the *fatigue strength*.
2. **Strain–life:** This is controlled-strain versus number of cycles (ϵ –N) testing, typically used for evaluating the low cycle fatigue properties of gas turbine discs and also for analysing fatigue damage in aircraft fleets.

Stress–Life (S–N) The most relevant ASTM Standard is ASTM E466-15. This covers axial fatigue of unnotched or notched specimens tested under constant amplitude loading in air at room temperature.

The Standard states that such tests may be used to determine the effects of material variations, surface conditions, and geometry; and that it is important to maintain consistency of as many variables as possible.

The main limitations are that variable amplitude loading is not included, nor are environmental effects. These types of tests may be required in a qualification programme, see Table 9.1, and one then has to ‘go outside the box’.

The basic result of stress–life tests is an S–N (Wöhler) diagram, illustrated schematically in Fig. 9.2.

Strain–Life (ϵ –N) The ASTM Standard for strain-controlled fatigue testing is ASTM E606/E606M-12. This Standard concerns uniaxial fatigue of *unnotched* specimens and is intended as a guide for R&D, materials qualification, design and failure analysis. It does not cover testing of full-scale components or structures.

Strain–life testing and analysis is more complicated than stress–life testing. Not only does it require the basic fatigue data, but also experimental determination of the S– ϵ cyclic stress–strain curve.

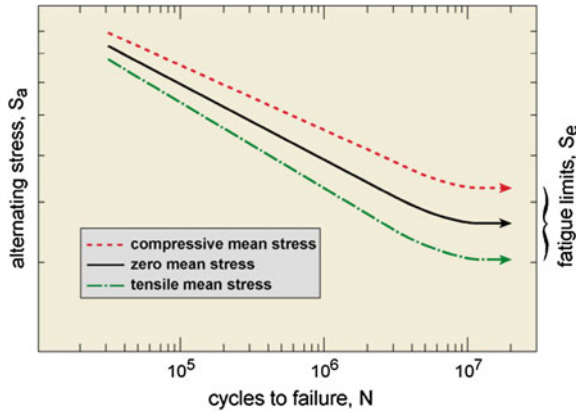


Fig. 9.2 Schematic S–N fatigue diagram showing the effect of mean stress and the corresponding fatigue limits: the stress axis may be either linear or logarithmic, as in this case

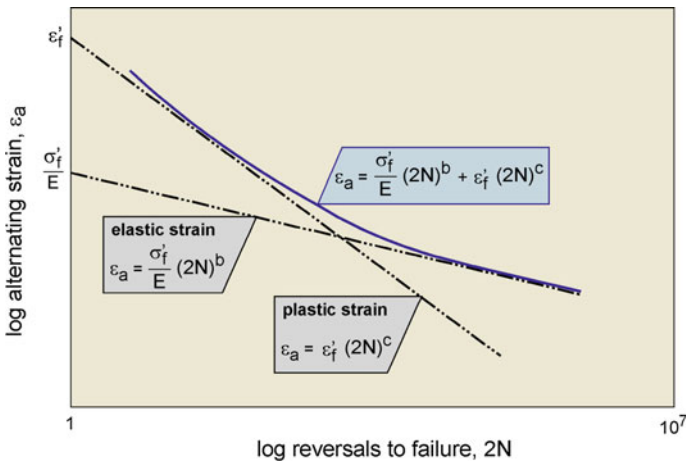


Fig. 9.3 Schematic ϵ – $2N$ fatigue diagram showing the plastic, elastic and combined equations: the strain axis has to be logarithmic. The fatigue symbol definitions are as follows: σ'_f = fatigue strength coefficient; b = fatigue strength exponent (Basquin). ϵ'_f = fatigue ductility coefficient; c = fatigue ductility exponent (Coffin–Manson)

The basic result of the fatigue tests is an ϵ – $2N$ (2 reversals = 1 cycle) diagram for fully reversed strain-controlled constant amplitude loading. A schematic example is given in Fig. 9.3, together with the strain–life equations obtained from the data:

1. The plastic strain equation is especially relevant to the low cycle fatigue regime, typically for lives less than 10^5 cycles.

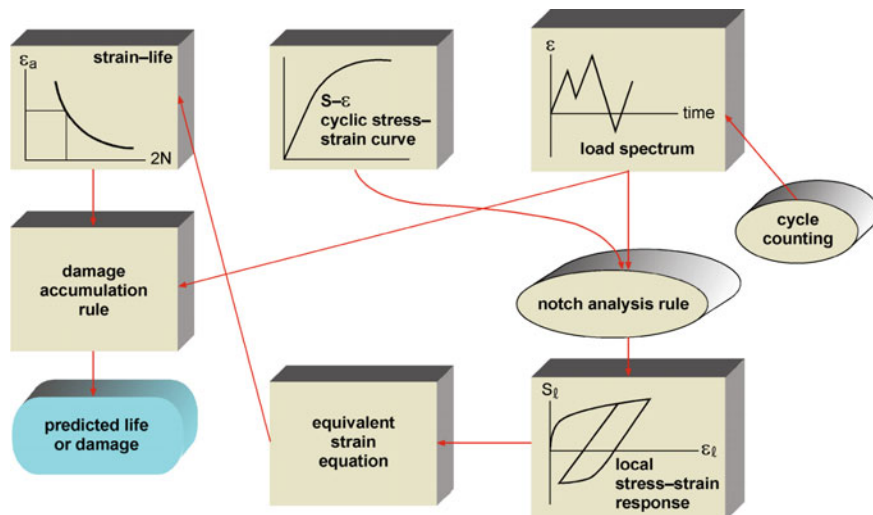


Fig. 9.4 Generic flowchart for calculating fatigue lives under variable amplitude (spectrum) loading from basic strain-controlled fatigue test data obtained from unnotched specimens [10]

2. The elastic strain equation is relevant to the high cycle fatigue regime, where the fatigue behaviour would be expected to be the same as in stress-controlled testing.
3. The combined strain–life equation (**blue curve**) is used for fatigue life estimations.

As stated previously, lifing methods and analyses are discussed in more detail in Sects. 16.3 and 16.4 of Chap. 16 of this Volume. However, at this point Fig. 9.4 may be helpful in showing how this is done using the strain-controlled test data. In the flowchart the testing inputs are the fatigue ($\epsilon-2N$) and cyclic stress–strain curve ($S-\epsilon$) data.

9.4 Fatigue Crack Growth: Part I–Constant Amplitude Testing

9.4.1 Long/Large Cracks

There is much information on fatigue crack growth (FCG) in aerospace structural alloys. Most of the data concern so-called long/large crack growth under constant amplitude (CA) loading or constant stress ratio (CR) load-shedding of pre-cracked or notched specimens. These effectively equivalent data are used for material comparisons and qualification programmes, and also design analyses, which are briefly discussed in Sect. 16.4.2 of Chap. 16 of this Volume.

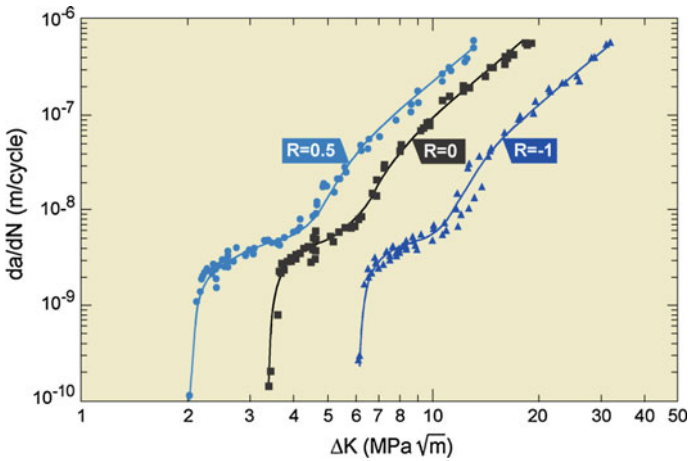


Fig. 9.5 Long/large CA and CR fatigue crack growth rates in aluminium alloy AA2024-T3 sheet [13]

The current ASTM Standard for long/large FCG testing is ASTM E647-15. This covers linear elastic fracture mechanics (LEFM) FCG over a range of growth rates from near the crack growth threshold to final instability (fast fracture). This Standard applies mostly to testing in ambient air, but also includes testing in aqueous environments. *However, see Sect. 9.5.1 about environmental FCG testing of aircraft structural alloys.*

Data Presentation The long/large fatigue crack growth rates obtained from CA and CR loading are customarily plotted against the LEFM stress intensity factor range, ΔK , on double-logarithmic (log–log) coordinates. Figure 9.5 gives an example for the aerospace industry legacy damage tolerant aluminium alloy AA2024-T3. This example illustrates the following points:

1. The FCG curves have consistently complex shapes.
2. The crack growth rates depend on the stress ratio, $R = S_{\min}/S_{\max}$.
3. The trend towards FCG thresholds at crack growth rates less than 10^{-9} m/cycle.

9.4.2 Short/Small Cracks

The need to study and account for the early FCG regime is mentioned in Sect. 16.4.2. of Chap. 16 of this Volume. In this early FCG regime the fatigue cracks are short/small, and their growth represents much of the total crack growth life, hence their importance. It is also important to recognise and define the types of short/small cracks [11, 12]:

1. Microstructurally short or small cracks: These are cracks with one or more dimensions smaller than a characteristic microstructural dimension, usually based on the grain size. For titanium alloys, this could be the primary α grain size in conventionally ($\alpha + \beta$) processed and heat-treated alloys, and the prior β grain size or colony size in β processed and β heat-treated alloys.
2. Mechanically short or small cracks: These are cracks with one or more dimensions smaller than characteristic mechanical dimensions. These dimensions typically define regions of plastic deformation, e.g. crack tip plastic zones or local plasticity at notch roots or other stress concentrations.
3. Physically/chemically short or small cracks: These have one or more dimensions larger than characteristic microstructural and/or mechanical dimensions, but nevertheless can grow significantly faster than large cracks at comparable ΔK values.

Size Criteria Table 9.2 gives suggestions for classifying small and large crack sizes according to microstructural and mechanical criteria [12]:

- Cracks are generally considered to be microstructurally small when (a) their size is less than 5–10 times the microstructural unit size, M , or (b) the crack tip plastic zone size is less than or equal to M .
- Cracks often behave in a mechanically small manner when the ratio of crack size to crack tip plastic zone size is less than 4–20.

ASTM E647-15 Applicability Although this Standard does not apply directly to short/small cracks, it provides extensive guidelines in Appendix X3 about specimen types and measuring the CA FCG rates.

Data Presentation The CA short/small fatigue crack growth rates may also be plotted against ΔK on log–log coordinates. It will then usually be observed that (i) there is no indication of a possible threshold FCG, and (ii) the data show high scatter, e.g. Figure 9.6 [14]. Possible/probable reasons for both characteristics are discussed in Appendix X3 of ASTM E647-15 and also in Ref. [15].

Table 9.2 Size criteria for small cracks [12]

Microstructural size	Mechanical size	
	Large: $a/r_p > 4-20$ (SSY)	Small: $a/r_p < 4-20$ (ISY and LSY)
Large: $a/M > 5-10$ and $r_p/M \gg 1$	Mechanically and microstructurally large (LEFM valid)	Mechanically small but microstructurally large (may need EPFM)
Small: $a/M < 5-10$ and $r_p/M \sim 1$	Mechanically large but microstructurally small	Mechanically and microstructurally small

a Crack size; r_p Crack tip plastic zone size; M Microstructural unit size; SSY Small scale yielding; ISY Intermediate scale yielding; LSY Large scale yielding; LEFM Linear elastic fracture mechanics; EPFM Elastic–plastic fracture mechanics

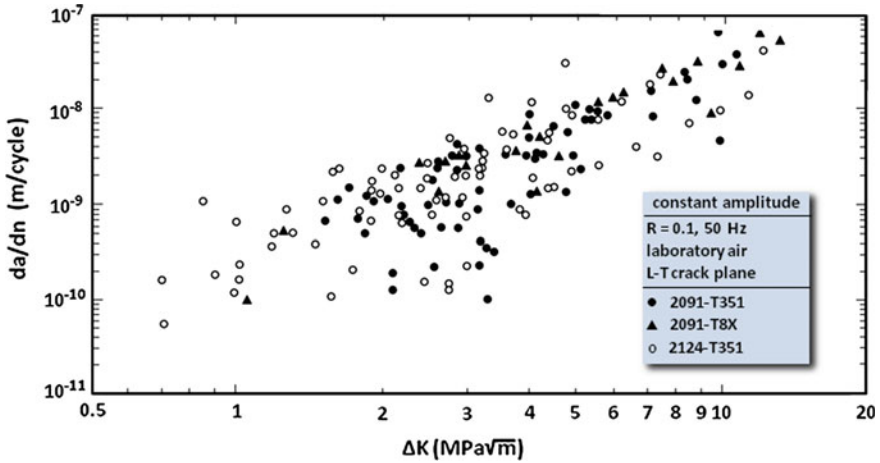


Fig. 9.6 Short/small CA fatigue crack growth rates in three aerospace aluminium alloys: after [14]

9.5 Fatigue Crack Growth: Part II—Variable Amplitude Testing

9.5.1 Introduction

Variable amplitude (VA) fatigue and FCG testing of aircraft materials and structures has a long history, reviewed by Schütz [16] and more specifically by Schijve in his book (*q.v.*). Nevertheless, there are no Standards for VA FCG testing, but there are *reference* load spectra for transport and tactical aircraft [17–19]: these may be obtained from the NLR ready for use on the control computers of electrohydraulic testing machines. These reference spectra are suitable for long/large crack growth studies, but less so for short/small FCG, as will be discussed in Sect. 9.5.3.

Another significant aspect is the question of testing environment. Until recently, it was not possible to state much more than that the environment should be representative, and that testing in aqueous environments is debatable [20]. However, teardown analyses of a variety of service aircraft structures have shown that the FCG process is nominally unaffected by corrosion [21, 22], although—as is well known—the nucleation of fatigue cracking can be. Hence, one may reasonably conclude that FCG tests in ambient air will often be sufficient for aircraft structural alloys. *N.B:* this is also relevant to CA and CR testing, see Sect. 9.4.1.

9.5.2 Long/Large Cracks

There are many data for flight simulation (VA) FCG of long/large cracks, including property comparisons for several aluminium alloy types and products [23]. These data can be useful for material qualification programmes, especially if they show that material rankings are different or accentuated as compared to CA and CR results [20, 23, 24].

The most notable example is a reversed FCG ranking of the second-generation aluminium–lithium (Al–Li) alloys with respect to legacy conventional alloys. Under CA and CR loading the Al–Li alloys were superior, but gust spectrum loading reversed this result: see Ref. [24] for the data and the most recent explanation.

Testing Guidelines These are based on the experience documented in Ref. [23] and are specified in Ref. [20]. The topics include specimen geometries; types of load spectra and spectrum variations; and choice of stress levels, cycle frequencies and environments (usually ambient air).

Data Presentation Double-linear coordinates are generally used for plots of crack length versus number of simulated flights; and log-linear coordinates for plots of crack growth rates versus crack length. Illustrative examples are given in Refs. [20, 23] with interpretations of the effects of particularly severe simulated flights.

9.5.3 Short/Small Cracks

Over the last 30 years it has become increasingly evident that it is *essential* to study the behaviour of short/small fatigue cracks under VA loading, particularly short/small cracks occurring in service aircraft and during full-scale fatigue tests (FSFT); see Chap. 16 in this Volume for an historical overview, and example Refs. [8, 21, 22].

Some of the earliest VA tests on short/small cracks are reported in Ref. [25]. At that time (the late 1980s), the short/small crack growth was observed from surface measurements, which have limitations owing to the three-dimensional nature of the cracks. On the other hand, the reference spectra load histories had not been developed with crack front marker loads, and these load histories were found to be unsuitable for fracture surface measurements of FCG.

A Macchi MB326H crash in 1990, and major cracking problems in the fleet, have resulted in significant advances in quantitative fractography (QF) by the Defence Science and Technology Group (DSTG) in Melbourne, Australia. These advances have led to (i) QF implementation as a standard technique for fatigue-related service failures and FSFT, and (ii) development of representative spectrum load histories with marker loads suitable for both FSFT and coupon and specimen tests [26].

Testing Guidelines Appendix X3 of ASTM E647-15 gives extensive guidelines applicable to both VA and CA loading. However, the following additional points are relevant and important for VA loading and QF:

- Some suitable specimen geometries are given in Refs. [25, 27, 28] with details about surface finishes and crack starters. N.B: specimens must be thick enough to withstand buckling under (any) spectrum compression loads.
- Reference [26] should be consulted about incorporating marker loads into VA load histories.
- QF requires much skill and patience. Scanning electron microscope images may be difficult to interpret despite the application of marker loads. The DSTG has found that QF can often be assisted by deep focus light microscopy [29], even to the extent of preferring this technique.

Data Presentation Many QF investigations by the DSTG of service, FSFT and coupon tests have shown the most informative presentations are in log-linear coordinates for plots of crack length versus number of flight hours, simulated flights or flight blocks.

Figure 9.7 is especially illustrative. These data indicate approximately exponential FCG, as do many other VA short/small FCG data [8, 30]. This exponential trend is relatively easy to use in FCG life analyses [8, 30]. Another important point is that this method of data presentation allows showing that the major source of scatter is the initial discontinuity/crack size.

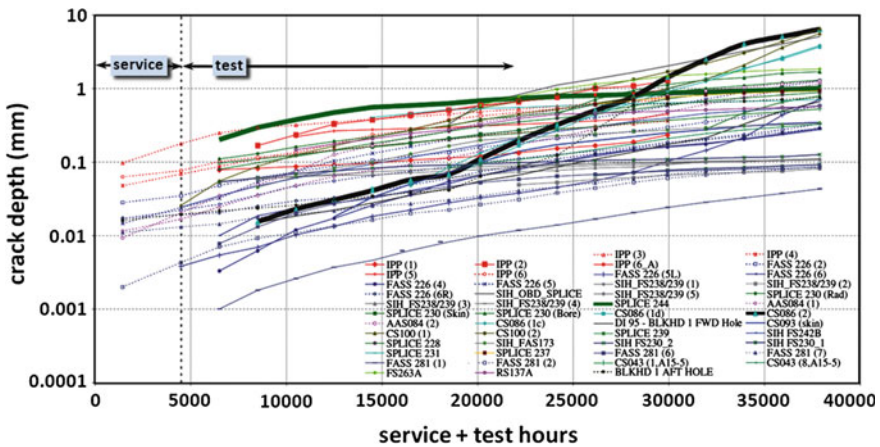


Fig. 9.7 Sample QF-obtained FCG data from different locations in the aluminium alloy AA2024-T851 lower wing skin of a General Dynamics F-111 removed from service [8, 30]

9.6 Fracture Toughness Testing

9.6.1 Introduction

Table 9.1 shows that fracture toughness testing may be separated into three topics, namely:

- Plane-strain/plane-stress fracture toughness.
- K_{R} curves.
- Residual strength of stiffened panels.

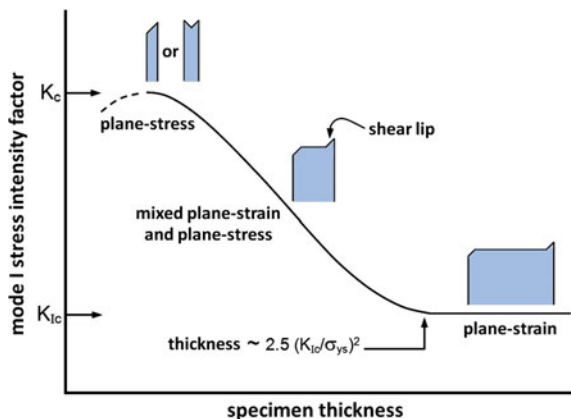
This section considers the first two topics only. Residual strength is a specialist subject: tests are done on subcomponents and full-scale components at higher building block (BB) levels than specimen tests; see Chap. 18 of this Volume also.

9.6.2 Plane-Strain/Plane-Stress Fracture Toughness

Fracture toughness data are primarily of interest for material qualification programmes and alloy development, although they may sometimes be useful or required for design. The relevant data and testing Standards for aerospace components and structures apply to mode I loading, whereby the applied loads and stresses are normal to the plane of cracking.

Figure 9.8 shows schematically the general relation between mode I plane-strain and plane-stress fracture toughness, illustrating the trend in decreasing fracture toughness with increasing specimen thickness. This figure also includes (i) sketches of the fracture surface profiles, which are slant or double-slant in plane-stress, transitioning to almost flat fracture in plane-strain; and (ii) the critical thickness at which full plane-strain is achieved. At this thickness, and for greater thicknesses, the fracture toughness is deemed to have a constant value, the plane-strain fracture toughness K_{Ic} .

Fig. 9.8 Schematic of the effects of specimen thickness on fracture toughness and fracture surface profiles



Note that the critical thickness depends on the material yield stress, σ_{ys} : plane-strain conditions are reached at lesser thicknesses in higher strength materials. Also, for all structural alloy classes there is a general trend of decreasing fracture toughness with increasing yield strength: see, for example, Ref. [31].

Plane-Strain Fracture Toughness There are two ASTM Standards for plane-strain fracture toughness testing:

1. ASTM E399-12e3: This Standard is the most usual one and covers LEFM determination of plane-strain fracture toughness using several types of fatigue pre-cracked specimens. Compact tension (CT) specimens are most commonly used.
2. ASTM E1304-97(2014): This Standard is for plane-strain fracture toughness using ‘short bar’ and ‘short rod’ chevron-notched specimens. These specimens are smaller and therefore sometimes convenient to use. However, although the fracture toughness is generally within $\pm 10\%$ of the values obtained from CT specimens [32], they are not regarded as valid K_{Ic} values.

Plane-Stress (and Mixed Plane-Stress/Plane-Strain) Fracture Toughness Tests in this regime are usually done using middle-cracked tension (MT) specimens, which are flat panels of sheet or thin plate containing a central crack starter notch or pre-crack.

There is no Standard for this regime, since the fracture toughness depends on the specimen and starter notch widths as well as the material thickness. Also, the fracture toughness values are commonly determined in one of two ways:

1. The toughness K_c (or K_{Rc}) is calculated from the maximum load and the effective crack length (physical crack length + plastic zone size) and is the crack tip stress intensity factor corresponding to rapid unstable fracture. This measurement includes stable crack growth in the calculation.
2. The toughness designated as K_{app} (or K_{co}) is the apparent stress intensity factor at maximum load using the pre-crack length, a_0 , and takes no account of stable crack growth.

These fracture toughnesses are different, and they are also not simply related. More information is given in ASTM Standard E561-15a (see Sect. 9.6.3) even though the tests are not standardized.

9.6.3 K_R Curves

K_R curves are also useful for qualification programmes and alloy development. In addition they are required as inputs to residual strength design, as mentioned in Sect. 18.4.1 of Chap. 18 in this Volume.

The current ASTM Standard for K_R curve determination is ASTM E561-15a. A K_R curve is a record of the mode I resistance to crack extension in terms of K_R plotted against crack extension in a specimen as the crack driving force is increased. The Standard covers MT and CT specimens only, and MT specimens are usually used.

9.6.4 Examples of K_{Ic} and K_R Curve Use

K_{Ic} versus Yield Strength The general trend in decreasing fracture toughness with increasing yield strength is a continuing challenge for aerospace alloy producers, especially during the recent development of the third-generation Al–Li alloys [33].

Figure 9.9 compares K_{Ic} – σ_{ys} combinations for two third-generation Al–Li plate alloys and the legacy alloy AA7050-T7451. Bearing in mind that the fracture toughness anisotropy of aluminium alloy plate alloys results in orientation-dependent K_{Ic} values, the data envelopes show that the Al–Li alloys achieve comparable fracture toughnesses at higher yield strength levels. In addition, the Al–Li alloys have a density advantage that could enable significant weight savings in actual components.

K_R Curves Figure 9.10 compares K_R curves for several through-cracked GLARE (GLASS REINFORCED aluminium laminates), the legacy damage tolerant alloy AA2024-T3 and the improved modern alloy AA2524-T351. All the GLARE types

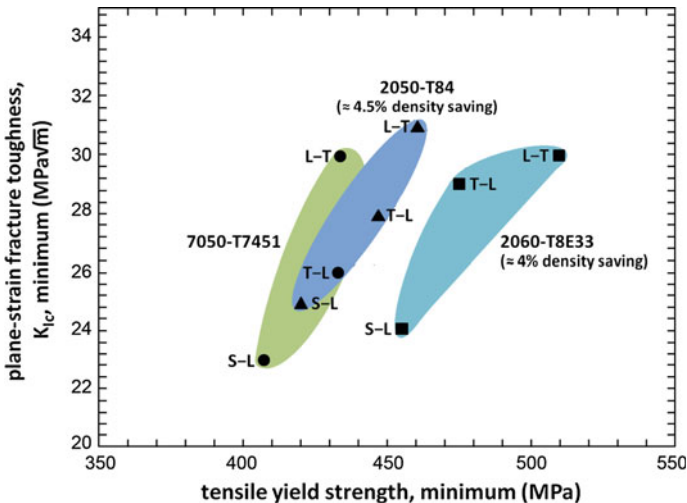


Fig. 9.9 Combinations of K_{Ic} values (L–T, T–L and S–L crack plane orientations) and tensile yield strengths for the medium-to-high strength Al–Li plate alloys AA2050-T84 and AA2060-T8E33, and the legacy alloy AA7050-T7451: after [33]

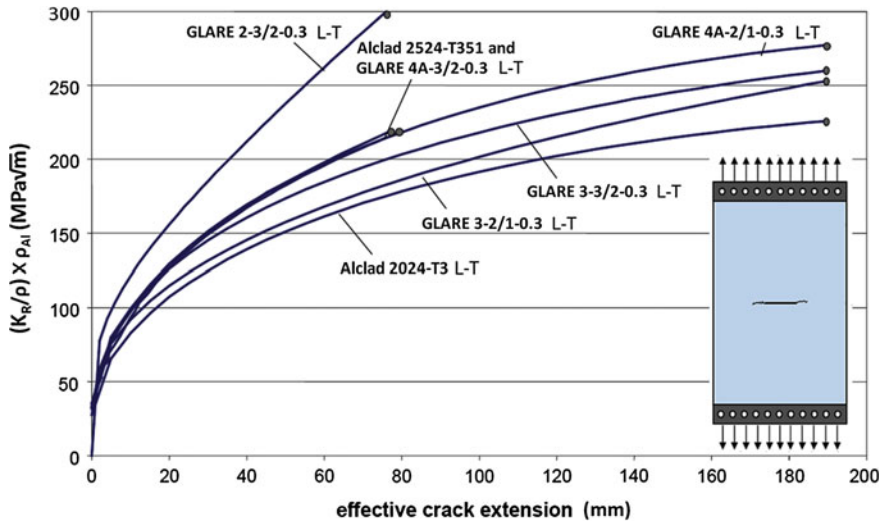


Fig. 9.10 Comparison of MT specimen K_R curves for through-thickness cracked GLARE laminates and the AA2024-T3 and AA 2524-T351 damage tolerant aluminium alloys [34]. The results have been adjusted to account for the different densities (ρ) and hence specific weights of the materials

showed better crack growth resistance than AA2024-T3. However, it is clear that crack growth resistance equivalent to or better than that of AA2524-T351 depends on the type of GLARE. A better crack growth resistance is certainly achievable with GLARE; and as discussed in Chap. 13 of Volume 1 of these Source Books, the excellent crack resistance of GLARE has contributed to its use in upper fuselage panels of the Airbus A380.

9.7 Corrosion and Stress Corrosion Cracking (SCC)

9.7.1 Introduction

Corrosion and stress corrosion cracking (SCC) are very important considerations for aerospace structural alloys. Table 9.1 lists the following topics:

- Pitting and exfoliation.
- Stress corrosion cracking (SCC).
- Accelerated and natural environments.

This Section treats corrosion and SCC as separate phenomena, though the distinction is sometimes open to question. Also it is important to note that a high corrosion resistance does not necessarily imply a high SCC resistance, as will be mentioned in Sect. 9.7.4.

Further, the reader may wish to consult Chap. 19 of this Volume, which is devoted predominantly to SCC in aircraft structures, but also mentions corrosion and corrosion susceptibilities.

9.7.2 Corrosion

Corrosion of aerospace structural alloys is primarily an issue for low alloy steels, aluminium alloys and, perhaps surprisingly, stainless steels. Magnesium alloys *could* be added to this list, but their use is limited, e.g. to helicopter gear boxes and the flying controls and wheels of some (older) aircraft. Also, service failures of corrosion-protected magnesium alloy components are rare, see Chap. 19.

The corrosion resistance of high-strength low alloy steels used in aerospace components is generally so poor that corrosion tests are not strictly necessary. Components made from these materials rely on high-quality cadmium, chromium and nickel plating, sometimes in combination, and additional protection is provided by paint systems.

ASTM has many standards relating to the corrosion of metals. The following are the most relevant for aerospace structural alloys:

1. ASTM B117-11: This Standard covers the equipment, procedure and conditions for generating a 5 % NaCl salt spray environment, but is non-specific about specimens or exposure periods. See ASTM G85-11 for more information.
2. ASTM G31-12a: This is a *standard guide* for immersion corrosion testing. The guide covers many factors that influence immersion corrosion tests and is a reference for setting up a satisfactory test procedure. However, it is not intended for specific evaluations.
3. ASTM G34-01(2013): This Standard is an accelerated exfoliation corrosion test (EXCO test) for AA7XXX and conventional AA2XXX aluminium alloys. The method is useful in predicting outdoor and in-service exfoliation behaviour and may be used as part of a material qualification programme.
N.B: this test method is unsuitable for Al-Li alloys, since it does not rank them according to their outdoor and service behaviour [35]. See ASTM G85-11 for more information.
4. ASTM G44-99(2013): This Standard describes a general procedure for alternate immersion corrosion testing in a neutral 3.5 % NaCl solution. The test method is primarily for aluminium alloys and ferrous alloys, and for alloy development and quality assurance.
5. ASTM G48-11(2015): This Standard is specifically for ranking the pitting and crevice corrosion resistance of stainless steels and nickel- and chromium-based alloys, using aqueous ferric chloride solutions.

There are six specific methods. These cover pitting and crevice corrosion, and critical pitting and crevice temperatures.

6. ASTM G85-11: This Standard is related to ASTM B117 (see above). ASTM G85-11 covers five modifications of salt spray testing, but does not specify which modification, specimen type or exposure periods should be used for specific alloys and products.

However, one variant, the modified ASTM acetic acid salt intermittent spray (MASTMAASIS) test, is strongly recommended [35] for exfoliation corrosion testing of Al–Li alloys instead of using the EXCO test.

Finally, corrosion owing to microbiological attack of aluminium alloys in fuel tanks (see Table 9.1) is a well-known problem [36–38]. Tests on aerospace alloys have been reported [39, 40], but these are not standardized. However, there are several ASTM Standards for sampling and testing fuel and fuel-associated water for microbial contamination [38].

9.7.3 *Stress Corrosion Cracking (SCC)*

Many aerospace alloys are susceptible to SCC [41], and many examples for aircraft structures are discussed in Chap. 19. SCC failures can have serious consequences, resulting even to loss of an aircraft or spacecraft. Hence some form of screening for SCC susceptibility is always included in aerospace alloy development and qualification programmes.

There are a number of ASTM Standards for SCC testing of aerospace alloys. The Space Agencies ESA and NASA also have their own Standards and guidelines [42, 43], which are particularly stringent owing to past experience [41].

Table 9.3 gives a summary of the Standards and guidelines for aerospace alloys. This summary is not entirely clear-cut, since the ASTM Standards frequently cross-reference with other Standards, and some are non-specific about the alloys to be tested and the selection of test environments.

However, where the Standards are non-specific about the test environments, they refer to one or more of the following ASTM Standards:

- D1141: preparation of substitute ocean water.
- G44: neutral 3.5 % NaCl.
- G50: atmospheric (outdoor) corrosion testing.
- G85: modified salt spray.

Furthermore, ESA and NASA base their SCC screening on NaCl solutions and salt spray, as indicated in Table 9.3. Thus any general programme of SCC evaluation of aerospace alloys, whether during alloy development or qualification for service, will select some form of salt water accelerated testing. This is entirely reasonable for aircraft structures, see Chap. 19; and also for spacecraft except in propellant systems, which include very reactive chemicals such as hydrazines and nitrogen tetroxide.

Table 9.3 Stress corrosion cracking (SCC) standards and guidelines for aerospace alloy evaluations

	Source	Standards/guidelines	Alloys	Specimens/loading	Environments	Remarks/references	
Smooth	ASTM	G30-97(2015)	n.s.	U-bend: constant strain	n.s.	Severe screening test	
		G38-01(2013)	n.s.	C-ring: constant strain	n.s.	Quantitative comparisons	
Cracked	ASTM	G39-99(2011)	n.s.	Bent-beam: elastic stresses	n.s.	Quantitative comparisons	
		G47-98(2011)	2XXX, 7XXX	Direct tension	3.5 % NaCl: A.I.	Particularly ST loading	
		G49-85(2011)	n.s.	Direct tension	n.s.	Quantitative, widely used	
		G58-85(2015)	n.s.	n.s.: static loading	n.s.	Weldment evaluations	
		G64-99(2013)	2XXX, 6XXX, 7XXX	n.s.: static loading	n.s.	SCC classification only	
		G103-97(2011)	low-Cu 7XXX	n.s.: static loading	boiling 6 % NaCl	Rapid screening test	
		G129-00(2013)	n.s.	Direct tension: SSR	n.s.	Severe screening test	
		ESA [41]	ECSS-Q-ST-70-37C	n.s.	• Direct tension, 75 % Y. • Various types for ST tests	3.5 % NaCl: A.I.	Severe screening test: alloys and weldments
		NASA [42]	MSFC-STD-3029A	Engineering alloys: Al, Fe, Ni, Cu, Ti	• Various types • Static loading; SSR	-3.5 % NaCl: A.I. -5 % NaCl salt spray	Comprehensive guidelines; alloys and weldments; ST loading when appropriate
		ASTM	G129-00(2013) E1681-03(2013)	n.s. n.s.	Direct tension: SSR CT, SEB: constant force; and CT: constant displacement	n.s. Aggressive	Severe screening test Threshold stress intensity, K_{IEAC} for crack growth

A.I. Alternate immersion; CT Compact tension specimen; n.s. Non-specific; SEB Single edge (cracked) beam specimen; SSR Slow strain rate; ST Short transverse; Y.S. 0.2 % proof stress

9.7.4 Some SCC and Corrosion Issues

Screening Criteria ESA and NASA classify alloys into high, moderate and low SCC resistance [42–44]. The classification system is currently based on the ratio of the absolute SCC threshold stress and the yield strength (0.2 % offset), σ_{SCCth}/σ_y .

This system has recently been criticised by Niedzinski et al. [45], who showed that use of this ratio can favour established (legacy) alloys to the detriment of new materials, specifically the third-generation Al–Li alloys. They propose that *absolute* SCC threshold stresses should be the basis for alloy classification; and that σ_{SCCth}/σ_y values should be an additional aid to alloy selection.

The importance of optimising the SCC classification of third-generation Al–Li alloys, which have great promise for aerospace vehicles [1], is emphasized by Table 9.4. This shows that there are several Al–Li candidate alloys for spacecraft applications that have significantly higher specific stiffnesses than the legacy alloy AA2219.

Corrosion and SCC Rankings Recent ESA work showed that a martensitic stainless steel, Cronidur 30, has outstanding corrosion resistance but low SCC resistance [46]. Thus improving the corrosion resistance of a stainless steel does not necessarily improve the SCC resistance.

The issue of corrosion and SCC rankings is reinforced by the reverse situation for 21-6-9 stainless steel. This alloy is popular for spacecraft fluid systems and is classified by ESA as having high SCC resistance [42]. However, helicopter service experience has shown that 21-6-9 is susceptible to crevice corrosion followed by SCC, see Sect. 19.3.2.3 in Chap. 19.

Another important example is provided by third-generation Al–Li alloys. These have generally good-to-excellent corrosion resistance in commercial temps. Nevertheless, there are concerns about elongated intergranular corrosion pits that can develop in sheet and plate materials undergoing SCC testing [46, 47].

Finally, it is worth mentioning that titanium alloys are essentially immune to corrosion in aqueous environments, but some are highly susceptible to SCC when a

Table 9.4 Actual/proposed uses of Al–Li alloys to replace legacy alloys in spacecraft [2]

Alloys	Current or proposed uses	Density ρ (g/cm ³)	Compression modulus (GPa)	Specific stiffness GPa/(g/cm ³)
2219-T851	Legacy alloy: Ariane V, SLS	2.85	74.5	26.1
2050-T84	Orion, SLS	2.70	77.9	28.85
2098-T82	Falcon 9	2.70	79.0	29.3
2195-T82	SLS	2.71	78.6	29.0
2297-T87	SLS	2.65	77.2	29.1
2055-T8X	–	2.70	78.5	29.1
2099-T86	–	2.63	79.3	30.15

specimen is cracked (e.g. by fatigue) while immersed in an aqueous environment. Titanium alloys are also susceptible to SCC in some organic and spacecraft propellant environments. All these problems are known since the 1960s, e.g. Refs. [48–50].

9.8 Summary

This chapter discusses ambient temperature engineering properties of aerospace structural alloys at the coupon and specimen level of testing. This is the foundation of the building block (BB) test approach for materials and components airworthiness certification.

The properties discussed are yield and tensile strengths; compressive strengths; stress–strain curve moduli; shear and bearing strengths; hardness; fatigue and fatigue crack growth; fracture toughness and crack growth resistance (K_R curves); and corrosion and stress corrosion. Reference is made to standard test methods, where available, and recent developments are highlighted.

Reference is also made to other chapters in these Source Volumes, particularly to Chaps. 16–19 of this Volume. Chaps. 16–18 provide information about fatigue and residual strength tests at higher levels in the BB approach, and Chap. 19 presents many examples of stress corrosion cracking (SCC) and corrosion problems for aircraft structures.

References

1. Eswara Prasad N, Gokhale AA, Wanhill RJH (eds) (2014) Aluminum–lithium alloys: processing, properties and applications. Butterworth-Heinemann, Elsevier Inc, Oxford, UK
2. Wanhill RJH (2014) Aerospace applications of aluminum–lithium alloys. In: Eswara Prasad N, Gokhale AA, Wanhill RJH (eds) Aluminum–lithium alloys: processing, properties and applications. Butterworth-Heinemann, Elsevier, Inc., Oxford, UK, pp 503–535
3. Ball DL, Norwood DS, TerMaath SC (2006) Joint strike fighter airframe durability and damage tolerance certification. AIAA paper 2006-1867, 47th AIAA/ASME/ASCE/AHS/ASC Structures, Structural Dynamics, and Materials Conference, 1–4 May 2006, Newport, Rhode Island
4. Davis JR (ed) (2004) Tensile testing, 2nd edn. ASM International, Materials Park, OH 44073-0002, USA, pp 239–250
5. Chandler H (ed) (1999) Hardness testing, 2nd edn. ASM International, Materials Park, OH 44073-0002, USA
6. Herrmann K (ed) (2011) Hardness testing: principles and applications. ASM International, Materials Park, OH 44073-0002, USA
7. Barter SA, Molent L, Wanhill RJH (2012) Typical fatigue-initiating discontinuities in metallic aircraft structures. *Int J Fatigue* 41(1):11–22
8. Barter SA, Molent L, Wanhill RJH (2010) Fatigue life assessment for high performance metallic airframe structures—an innovative practical approach. In: Ho S-Y (ed) Structural failure analysis and prediction methods for aerospace vehicles and structures. Bentham E-Books, Bentham Science Publishers, Sharjah, UAR, pp 1–17

9. Clark PN, Bellinger NC, Hoepfner DW (2015) Is the world ready for HOLSIP? In: Siljander A (ed) ICAF 2015 structural integrity: embracing the future—respecting the past; supporting aging fleets with new technologies. E-Book, VTT Technical Research Centre of Finland Ltd, Espoo, Finland, pp 34–46
10. Hu W, Tong YC, Walker KF, Mongru D, Amaratunga R, Jackson P (2006) A review and assessment of current lifing methodologies and tools in air vehicles division. DSTO Research Report DSTO-RR-0321, Defence Science and Technology Organisation, Melbourne, Australia
11. Ritchie RO, Suresh S (1983) Mechanics and physics of the growth of small cracks. In: Behaviour of short cracks in aircraft components, AGARD conference proceedings No. 328. Advisory Group for Aerospace Research and Development, Neuilly-sur-Seine, France, pp 1-1–1-14
12. McClung RC, Chan KS, Hudak SJ Jr, Davidson DL (1996) Behavior of small fatigue cracks. In: Lampman SR et al (eds) ASM handbook volume 19 fatigue and fracture. ASM International, Materials Park, OH 44073-0002, USA, pp 153–158
13. Wanhill RJH (1988) Low stress intensity fatigue crack growth in 2024-T3 and T351. Eng Fract Mech 30:223–260
14. Venkateswara Rao KT, Ritchie RO (1989) Mechanical properties of Al–Li alloys: part 2. Fatigue crack propagation. Mater Sci Technol 5:896–907
15. Suresh S, Ritchie RO (1984) Propagation of short fatigue cracks. Int Met Rev 29(6):445–476
16. Schütz W (1996) A history of fatigue. Eng Fract Mech 54(2):263–300
17. De Jonge JB, Schütz D, Lowak H, Schijve J (1973) A standardized load sequence for flight simulation tests on transport aircraft wing structures. NLR Technical Report TR 73029U, National Aerospace Laboratory NLR, Amsterdam, The Netherlands
18. Lowak H, De Jonge JB, Franz J, Schütz D (1979) MINITWIST: a shortened version of TWIST. NLR Miscellaneous Publication MP 79018U, National Aerospace Laboratory NLR, Amsterdam, The Netherlands
19. Anon (1976) Description of a Fighter Aircraft Loading STANDARD For Fatigue evaluation. Combined report of the F+W, LBF, NLR and IABG: available from the National Aerospace Laboratory NLR, Amsterdam, The Netherlands
20. Wanhill RJH (1994) Flight simulation fatigue crack growth testing of aluminium alloys: specific issues and guidelines. Int J Fatigue 16(2):99–110
21. Wanhill RJH, Koolloos MFJ (2001) Fatigue and corrosion in aircraft pressure cabin lap splices. Int J Fatigue 23:S337–S347
22. Molent L, Barter S, Wanhill R (2015) The decoupling of corrosion and fatigue for aircraft service life management. In: Siljander A (ed) ICAF 2015 structural integrity: embracing the future—respecting the past, supporting aging fleets with new technologies. E-Book, VTT Technical Research Centre of Finland Ltd, Espoo, Finland, pp 1062–1073
23. Wanhill RJH (1994) Damage tolerance engineering property evaluations of aerospace aluminium alloys. NLR Technical Publication TP 94177 U, National Aerospace Laboratory NLR, Amsterdam, The Netherlands
24. Wanhill RJH, Bray GH (2014) Fatigue crack growth behavior of aluminum–lithium alloys. In: Eswara Prasad N, Gokhale AA, Wanhill RJH (eds) Aluminum–lithium alloys: processing, properties and applications. Butterworth-Heinemann, Elsevier, Inc., Oxford, UK, pp 381–413
25. Edwards PR, Newman JC Jr (eds) (1990) Short-crack growth behaviour in various aircraft materials. AGARD Report No. 767, Advisory Group for Aerospace Research and Development, Neuilly-sur-Seine, France
26. Barter SA, Molent L, Wanhill RJH (2009) Marker loads for quantitative fractography of fatigue cracks in aerospace alloys. In: Bos MJ (ed) Bridging the gap between theory and operational practice. Springer Netherlands, Dordrecht, The Netherlands, pp 15–54
27. Huynh J, Molent L, Barter S (2008) Experimentally derived crack growth models for different stress concentration factors. Int J Fatigue 30:1766–1786
28. Molent L (2014) A review of equivalent pre-crack sizes in aluminium alloy 7050-T7451. Fatigue Fract Eng Mater Struct 37:1055–1074

29. Goldsmith NT (2000) Deep focus: a digital image processing technique to produce improved focal depth in light microscopy. *Image Anal Stereol* 19:163–167
30. Molent L, Barter SA, Wanhill RJH (2011) The lead crack fatigue lifing framework. *Int J Fatigue* 33:323–331
31. Janssen M, Zuidema J, Wanhill RJH (2002) *Fracture mechanics*, 2nd edn. Delft University Press, Delft, The Netherlands, pp 330–334
32. Brown KR (1984) The use of the chevron-notched short-bar specimen for plane-strain toughness determination in aluminum alloys. In: Underwood JH, Freiman SW, Baratta FI (eds) *Chevron-notched specimens: testing and stress analysis*, ASTM STP 855. ASTM International, West Conshohocken, PA 19428, USA, pp 237–254
33. Lynch SP, Wanhill RJH, Byrnes RT, Bray GH (2014) Fracture toughness and fracture modes of aerospace aluminum–lithium alloys. In: Eswara Prasad N, Gokhale AA, Wanhill RJH (eds) *Aluminum–lithium alloys: processing, properties and applications*. Butterworth-Heinemann, Elsevier, Inc., Oxford, UK, pp 415–455
34. De Vries TJ (2001) Residual strength. In: Vlot A, Gunnink JW (eds) *Fibre metal laminates: an introduction*. Kluwer Academic Publishers, Dordrecht, the Netherlands, pp 197–217
35. Holroyd NJH, Scamans GM, Newman RC, Vasudevan AK (2014) Corrosion and stress corrosion in aluminum–lithium alloys. In: Eswara Prasad N, Gokhale AA, Wanhill RJH (eds) *Aluminum–lithium alloys: processing, properties and applications*. Butterworth-Heinemann, Elsevier, Inc., Oxford, UK, pp 457–500
36. Iverson WP (1987) Microbial corrosion of metals. In: Laskin AL (ed) *Advances in applied microbiology*, vol 32. Academic Press Inc., Harcourt Brace Jovanovich, Orlando, FL 32887, USA, pp 1–36
37. Videla HA, Herrera LK (2005) Microbiologically influenced corrosion: looking to the future. *Int Microbiol* 8:169–180
38. Passman FJ (2013) Microbial contamination and its control in fuels and fuel systems since 1980—a review. *Int Biodeterior Biodegradation* 81:88–104
39. Yang SS, Lin JY, Lin YT (1998) Microbiologically induced corrosion of aluminum alloys in fuel-oil/aqueous system. *J Microbiol Immunol Infect* 31(3):151–164
40. Rajasekar A, Ting Y-P (2010) Microbial corrosion of Aluminum 2024 aeronautical alloy by hydrocarbon degrading bacteria *Bacillus cereus* ACE4 and *Serratia marcescens* ACE2. *Ind Eng Chem Res* 49(13):6054–6061
41. Korb LJ (1987) Corrosion in the aerospace industry. In: *Metals handbook ninth edition*, vol 13 corrosion. ASM International, Metals Park, OH 44073-0002, USA, pp 1058–1100
42. European Cooperation for Space Standardization (2009) Determination of the susceptibility of metals to stress-corrosion cracking. European Space Agency ECSS-Q-ST-70-37C, ESA Requirements and Standards Division, Noordwijk, The Netherlands
43. National Aeronautics and Space Administration (2005) Guidelines for the selection of metallic materials for stress corrosion cracking resistance in sodium chloride environments. NASA EM30, MSFC-STD-3029, Revision A, George C. Marshall Space Flight Center, Huntsville, AL 35812, USA
44. European Cooperation for Space Standardization (2008) Material selection for controlling stress-corrosion cracking. European Space Agency ECSS-Q-ST-70-37C, ESA Requirements and Standards Division, Noordwijk, The Netherlands
45. Niedzinski M, Ebersolt D, Schulz P (2013) Review of airware alloys currently used for space launchers. In: Workshop: technical interchange meeting (TIM) on fracture control of spacecraft, launchers and their payloads and experiments, 20–21 March 2013, ESA/ESTEC, Noordwijk, The Netherlands
46. Tesch A (2013) Stress corrosion tests at ESA—recent highlights. In: Workshop: technical interchange meeting (TIM) on fracture control of spacecraft, launchers and their payloads and experiments, 20–21 March 2013, ESA/ESTEC, Noordwijk, The Netherlands
47. Warner-Locke J, Moran J, Hull B, Reilly L (2013) The effect of corrosion pit morphology on SCC and fatigue of 2x99 alloys compared to 7xxx Alloys. *CORROSION 2013*, NACE International, 17–21 March 2013, Orlando, FL 32819, USA

48. Brown BF (1966) A new stress-corrosion cracking test for high-strength alloys. *Mater Res Stan* 6(3):129–133
49. Defense Metals Information Center (1967) Accelerated crack propagation of titanium by methanol, halogenated hydrocarbons, and other solutions. DMIC Memorandum 228, Battelle Memorial Institute, Columbus, OH 43201, USA
50. Lisagor WB, Manning CR Jr, Bales TT (1968) Stress-corrosion cracking of Ti-6Al-4V titanium alloy in nitrogen tetroxide. NASA Technical Note NASA TN D-4289, National Aeronautics and Space Administration, Washington, DC, USA

Chapter 10

Structural Alloy Testing: Part 2—Creep Deformation and Other High-Temperature Properties

R.J.H. Wanhill, D.V.V. Satyanarayana and N. Eswara Prasad

Abstract Information on mechanical properties such as yield strength, tensile strength, fracture toughness and fatigue strength of materials is important in designing structures and components used at ambient temperatures (see Chap. 9 in this Volume of the Source Books). However, for high-temperature applications such as in power plants, petrochemical industries and aeroengines, data on the mechanical behaviour of materials at elevated temperatures are required. This chapter discusses creep deformation and fracture mechanisms of alloys, experimental determination of creep and stress rupture properties and various methods for the prediction of these properties. In addition, other aspects of high-temperature mechanical behaviour are briefly considered, namely creep–fatigue interactions; thermal and thermomechanical fatigue; dwell cracking; and creep crack growth.

Keywords High temperature testing · Creep · Creep–fatigue · Thermal fatigue · Thermomechanical fatigue · Dwell cracking

10.1 Introduction: Creep

With increasing temperature the strengths of metals and alloys decrease and deformation becomes time-dependent. Metals and alloys subjected to a constant load at elevated temperatures will undergo a time-dependent length increase known as ‘creep’. At homologous temperatures $T/T_m > 0.4$, where T is the test temperature and T_m is the melting point on the absolute temperature scale, creep is of

R.J.H. Wanhill (✉)
NLR, Emmeloord, The Netherlands
e-mail: rjhwanhill@gmail.com

D.V.V. Satyanarayana
DMRL, DRDO, Hyderabad, India

N. Eswara Prasad
DMSRDE, DRDO, Kanpur, India
e-mail: nep@cemilac.drdo.in

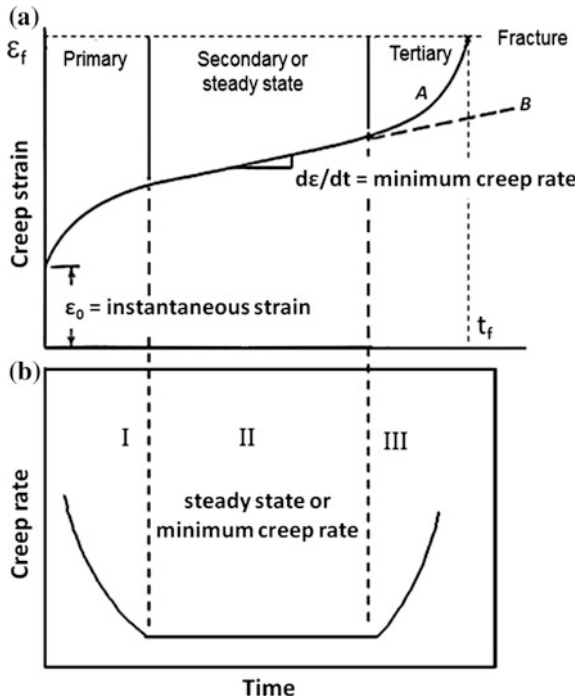
engineering significance. Materials intended for high-temperature structural applications, such as components in power plants, petrochemical industries and aero-engines, need better resistance to creep deformation and fracture (stress rupture) and hence must be evaluated for their creep performance.

Time-dependent deformation of metallic materials is characterized by a ‘creep curve’, which describes the evolution of strain with time (see the schematic in Fig. 10.1a). Such a curve usually shows three distinct stages after load application: (i) primary or transient creep, where the creep rate usually decreases with time; (ii) secondary or steady-state creep, where the creep rate reaches a minimum and remains constant (see Fig. 10.1b); and (iii) tertiary creep, where the creep rate increases continuously with time until fracture occurs.

The steady-state part of the creep curve constitutes most of the creep life and has therefore attracted the most attention with respect to the mechanisms involved. Tertiary creep begins usually because of microvoid and grain boundary cavity nucleation, and fracture can then occur quickly: *hence engineering design is directed to avoiding tertiary creep*. Note that the tertiary creep curve shown in Fig. 10.1a is separated into curves **A** and **B**. This is because the tertiary creep behaviour depends on the loading conditions: under *constant strain* curve **A** is followed, while under *constant stress* curve **B** is followed, since material extension relaxes the strain.

The creep behaviour is influenced by other factors besides the loading conditions. In particular, environmental interactions can be deleterious. Thus it is important that design engineers have a clear understanding of creep phenomena in

Fig. 10.1 **a** Schematic constant temperature creep curve showing the three stages such as primary, secondary and tertiary creep and **b** the creep rate versus time plot, showing the creep rate first decreasing, then constant, and finally increasing



both hostile and innocuous or inert environments, so that critical components are designed to work within well-defined safety limits (which are intended to include avoiding tertiary creep, as mentioned above). This is especially important for critical technologies such as aeroengines and nuclear power plants.

Many systematic studies have been conducted to understand the creep deformation and fracture behaviour of metals and alloys, notably single-phase and precipitation-hardened alloys. Two useful reference publications are the following books [1, 2]:

- Kassner, M.E., 2015, ‘Fundamentals of Creep in Metals and Alloys’, Third Edition, Butterworth Heinemann, Elsevier, Oxford, UK.
- Davis, J.R. (Ed.), 1997, ‘ASM Specialty Handbook, Heat-Resistant Materials’, ASM International, Materials Park, OH 44073-0002, USA.

Of particular relevance in this chapter is the creep behaviour of aerospace alloys, notably nickel-base superalloys for aeroengine/turbine components. These alloys are discussed in Chap. 9 in Volume 1 of these Source Books. They owe their outstanding creep properties to precipitation hardening or dispersion hardening, and their creep behaviour is mainly controlled by dislocation creep mechanisms (see e.g. Kassner’s book and Refs. [3–5]). This topic is discussed briefly in Sect. 10.2.

10.2 Secondary (Steady-State) Creep

Much attention has been paid to this creep regime, particularly with respect to modelling creep deformation using power law equations. The most general form of power law equation is as follows:

$$\dot{\epsilon}_{ss} = A\sigma^n \exp(-Q/RT) \quad (10.1)$$

where $\dot{\epsilon}_{ss}$ = steady-state creep rate; Q = activation energy; n = stress exponent; and A = constant. The activation energy Q and stress exponent n can be determined experimentally, by plotting the natural log of the creep rate $\dot{\epsilon}_{ss}$ against (i) the reciprocal of the absolute temperature ($1/T$) and (ii) the natural log of the stress, see Fig. 10.2.

For many pure metals and low stress levels the stress exponent, n , has a value in the range 3–5, and the value of Q is only slightly larger than that for lattice self-diffusion, Q_D [6]. On the other hand, for many engineering alloys the values of n and Q are much larger. This is especially true of precipitation-hardened and dispersion-hardened alloys, whose creep resistances are much higher than those of pure metals and single-phase alloys. These improvements are due to second-phase particles in the form of fine coherent precipitates (precipitation-hardened alloys) or fine incoherent non-shearable particles (dispersion-hardened alloys).

For both types of particle-strengthened alloys the stress dependence of the steady-state creep rate, as described by n in Eq. 10.1, is anomalously high. For example, the stress exponent for superalloys takes values of $n = 8$ or above [5].

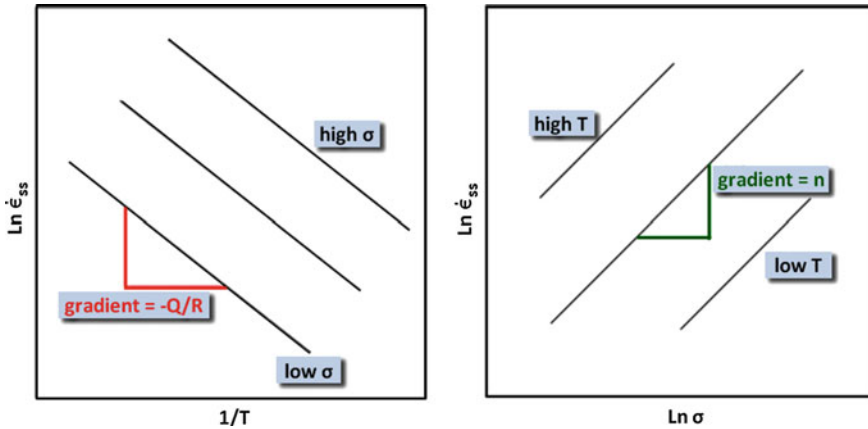


Fig. 10.2 Schematics of determining the steady-state creep rate activation energy, Q , and stress exponent, n , from test data. N.B: These methods assume that the creep mechanism does not change within the chosen stress and temperature ranges

Despite intensive modelling efforts, see Sect. 10.2.1, this has not (yet) been satisfactorily explained.

10.2.1 Modelling Steady-State Creep for Particle-Strengthened Alloys: A Summary

Cadek [7] has discussed in detail the modelling of steady-state creep in particle-strengthened alloys. In particular, Cadek referred to a model developed by Ansell and Weertman [8] for predicting the steady-state creep rate of particle-strengthened materials. However, the model did not explain the observed high values of stress exponent and activation energy. Many researchers suggested that these high values could be rationalized in terms of a threshold or resisting stress [7]. The threshold stress, σ_0 , is defined as the stress below which no appreciable creep deformation takes place. In this situation, creep in the matrix will occur only under the effective stress ($\sigma - \sigma_0$) but not under the entire applied stress. The creep rate can then be described by the phenomenological equation:

$$\dot{\epsilon}_{ss} = A(D_L G b / kT) ((\sigma - \sigma_0) / G)^n \quad (10.2)$$

where $\dot{\epsilon}_{ss}$, n , A and T have the same meanings as for Eq. 10.1; D_L = lattice diffusivity; G = shear modulus; b = Burgers vector; and k = Boltzmann's constant.

The origin of the threshold stress has usually been related to one or more of the following dislocation-based mechanisms: Orowan bowing between particles, particle bypassing by general or local climb, and particle cutting (shearing) [7].

Despite the introduction of the threshold stress concept, Cadek's detailed discussion [5] demonstrates that physically based predictions of steady-state creep rate are problematical owing to the number and complexity of the actual and possible mechanisms involved. However, research on this topic has continued, e.g. Refs. [5, 6, 9, 10], making use of experimentally determined parameters.

Even so, the primary goal of developing creep rate equations is to generate *necessarily empirical* design curves that enable predictions of creep life as a function of stress and temperature. This very important topic is discussed in Sect. 10.5.

10.3 Creep Fractures

The most general characteristics of creep fractures are intergranular failures. Figure 10.3 illustrates schematically the beginnings of the two basic types of intergranular creep fracture [2]:

1. At intermediate temperatures and relatively high strain rates grain boundary sliding causes the formation and linking-up of wedge cracks at triple points. Cracks can also nucleate *in* grain boundaries when slip interacts with sliding boundaries.
2. At high-temperatures and low strain rates, grain boundary sliding favours cavities, which nucleate at discontinuities such as grain boundary particles and inclusions and then grow mainly by vacancy diffusion. Eventually, the cavities link up to form cracks.

At lower temperature and for high strain rates there is a general trend towards transgranular creep fractures [2]. For example, Fig. 10.4 shows schematically how

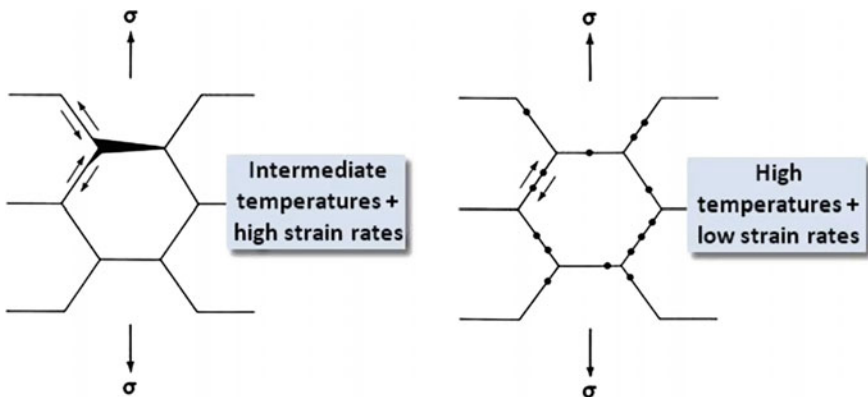
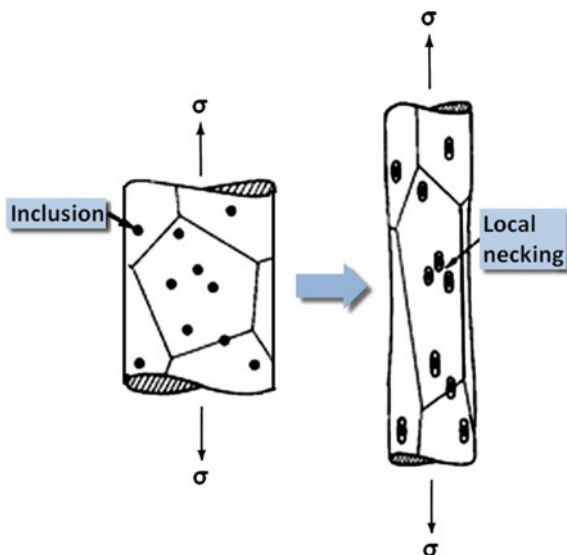


Fig. 10.3 General characteristics of intergranular creep fracture initiation: The *small arrows* indicate grain boundary sliding [2]

Fig. 10.4 Transgranular creep fracture initiation [11]



transgranular microvoids nucleate at inclusions in stainless steels [11]. The microvoids grow and coalesce by strain-controlled local necking, leading to transgranular fracture. This process is similar to low-temperature tensile fracture.

Figure 10.5 shows some examples of creep fractures in superalloys. These are scanning electron microscope (SEM) fractographs. The first two fractographs show intergranular fracture owing to wedge cracking [2]. The third shows intergranular fracture due to the linking-up and coalescence of grain boundary cavities.

It should also be noted that all three fracture surfaces shown in Fig. 10.5 have been oxidized owing to high-temperature exposure to air. The central fractograph shows evident formation and spalling of an oxide layer. While oxidation does not necessarily affect the early creep behaviour, it is known that creep crack growth in

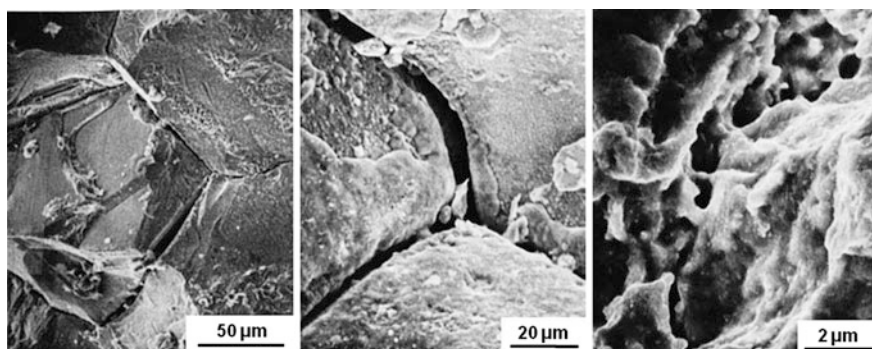


Fig. 10.5 SEM fractographs of creep fractures in superalloys: the first two are from Ref. [2] and the third is from S.P. Lynch, DSTG, Melbourne, Australia

nickel-base superalloys can be accelerated greatly by oxidation. This environmental influence is sometimes referred to as the stress-assisted grain boundary oxidation (SAGBO) mechanism [12].

10.4 Experimental Determination of Creep Properties

Creep tests are conducted under constant load or constant stress. Engineering service conditions usually mean that components are subjected to constant load conditions, and so most creep tests are done at constant load. However, for research purposes (e.g. investigating the effects of stress) much useful information is obtained from constant stress tests. In constant stress tests the creep rig is designed to reduce the load on the specimen in proportion to its extension. This keeps the load constant, provided the strain is homogeneously distributed along the specimen.

A material's creep resistance can be determined by conducting either *creep tests* or *stress rupture tests*, or both types of test:

1. **Creep tests** measure dimensional changes accurately under constant high-temperature and constant load or stress conditions. The creep strain is usually measured using an extensometer and a sensitive strain measuring device such as a linear variable differential transducer (LVDT) or dial gauge assembly (see Fig. 10.6).

The measured creep strains are plotted against time to give a creep curve. This curve usually shows the three stages of primary, secondary and tertiary creep that are illustrated schematically in Fig. 10.1.

2. **Stress rupture tests** measure the time to failure (t_f) for specified combinations of stress and temperature. The creep strains are generally not measured very accurately.

The creep and stress rupture data are reported in the form of $\log(\sigma)$ versus $\log(\dot{\epsilon}_{ss})$ plots and $\log(\sigma)$ versus $\log(t_f)$ plots at various temperatures. These plots may or may not yield linear relationships between the variables (see e.g. the schematic diagram in Fig. 10.2b) (which, however, has natural log axes rather than the commonly used base 10 log axes).

Several creep design parameters can be derived from the creep and stress rupture tests:

Creep strength: the stress to produce a nominal strain (normally 1.0 %) in a given time.

Creep life: the time to reach a nominal 1 or 2 % strain at a given stress and temperature.

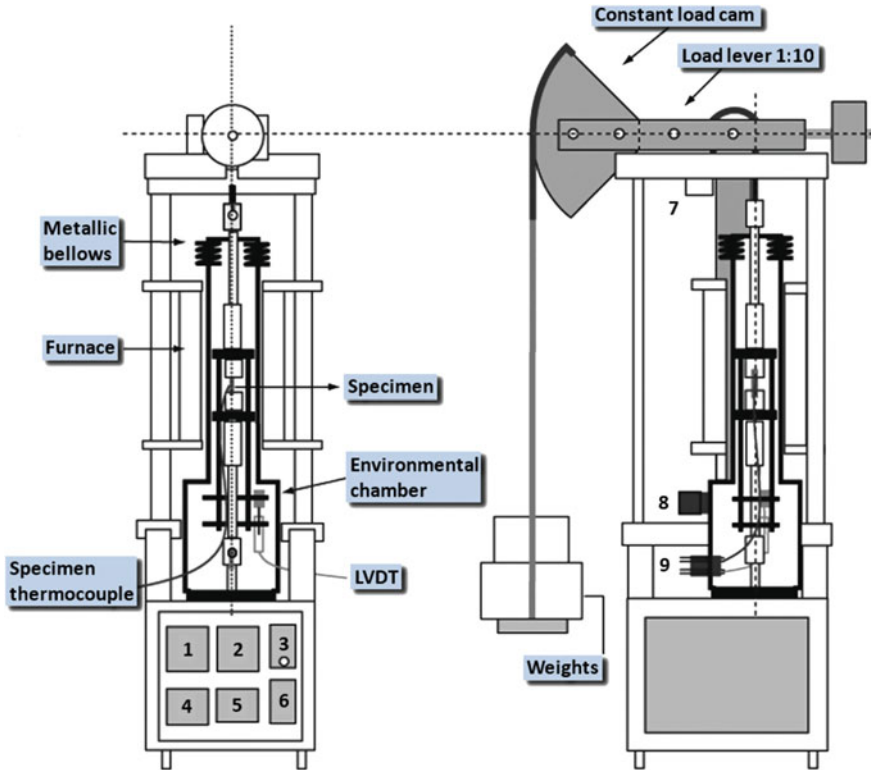


Fig. 10.6 Schematic of a creep test rig: 1 temperature controller, 2 temperature indicator, 3 LVDT power unit, 4 digital clock, 5 ammeter, 6 On/off switch, 7 range limiting switch, 8 environment (vacuum) measurement unit and 9 thermocouple and LVDT outputs [13]

Minimum creep rate: $\dot{\epsilon}_{ss}$ is measured as a function of stress and temperature. The tests are expensive, focussing on obtaining accurate values for the minimum creep rates, and it is necessary to maintain constant stress and temperature over very long periods of time. Some tests can last up to 100,000 h, though this is exceptional.

Stress rupture life: the time to failure (fracture) at a particular stress and temperature. Use of the word ‘rupture’ implies tests done at high stress. These are often accelerated tests, whose data are inputs for parametric modelling (see Sect. 10.5).

More information about creep testing is obtainable from the following source:

- American Society for Testing and Materials ‘ASTM E139 - 11, Standard Test Methods for Conducting Creep, Creep-Rupture, and Stress-Rupture Tests of Metallic Materials’, ASTM International, West Conshohocken, PA 19428-2959, USA.

N.B: There are two important rules of thumb for all types of test: (i) the test time must be at least 10 % of the design time and (ii) the creep and/or failure

mechanisms must not change with time, temperature or stress (see e.g. Fig. 10.3). If the mechanisms change, then the usefulness of the data is compromised, since serious errors could occur when extrapolating the data to longer lives (see also Sect. 10.5.1).

Ideally, the test durations and the ranges covered by the creep and stress rupture plots should be comparable to the design service lives. However, this is often not possible, since it is impractical or inopportune to sequester expensive equipment from being used for other tests for more than, say, 1–2 years. It follows that some means of extrapolating the test data to longer lives is required, as discussed in Sect. 10.5.

10.5 Creep Life Prediction Methods

The goal of creep and stress rupture testing is to provide data for predicting the long-term high-temperature mechanical behaviour and hence establishing design service lives. For these purposes the test data are presented in two basic forms: (i) stress versus rupture time for different temperatures and (ii) minimum strain rate versus time to failure for different temperatures.

In addition, and most importantly, *accelerated* test data are used to establish correlations between temperature, time to failure and stress. There are several correlation methods, and these are concisely discussed in the first part of Sect. 10.5.1.

10.5.1 Data Correlations Using ‘Classical’ Methods

Time–Temperature Parameters Creep test results are frequently displayed as plots of time or stress to cause a specified strain, or to cause creep fracture in a given time, plotted against temperature. These plots are constructed from creep curves, often using statistical methods to obtain best fits to the data and always using one of several alternative extrapolation procedures.

These statistical methods and extrapolation procedures plot failure stresses against a time–temperature parameter, P , which collapses the data for different temperatures onto a master curve. Two of the most generally used parameters are the Larson–Miller parameter [14] and the Orr–Sherby–Dorn parameter [15]; but there are others, such as the Manson–Haferd [16] and Manson–Succop [17] parameters. All these parameters have been recently reviewed [18, 19].

Table 10.1 gives essential information on the above parameters, and Fig. 10.7 shows schematics of deriving the two most popular ones, the Larson–Miller and Orr–Sherby–Dorn parameters. An actual Larson–Miller master curve for a nickel-base superalloy is shown in Fig. 10.8.

Table 10.1 Some ‘classical’ parametric equations for correlating stress rupture data: see Fig. 10.7 also

Parametric equations	Data plot axes	Data assumptions
Larson–Miller [14]: $P_{LM} = T(\log t_f + C)$	$\log t_f$ versus $1/T$	• Convergence of isostress lines to a point on the $\log t_f$ axis having the value $-C$
Orr–Sherby–Dorn [15]: $P_{OSD} = \log t_f - A/T$	$\log t_f$ versus $1/T$	• Parallel isostress lines with slope = A
Manson–Haferd [16]: $P_{MH} = (T - T_a)/(\log t_f - \log t_a)$	$\log t_f$ versus T	• Convergence of isostress lines to a point with coordinates $[\log t_a; T_a]$ above the data region
Manson–Succop [17]: $P_{MS} = \log t_f + B/T$	$\log t_f$ versus T	• Parallel isostress lines with slope = B

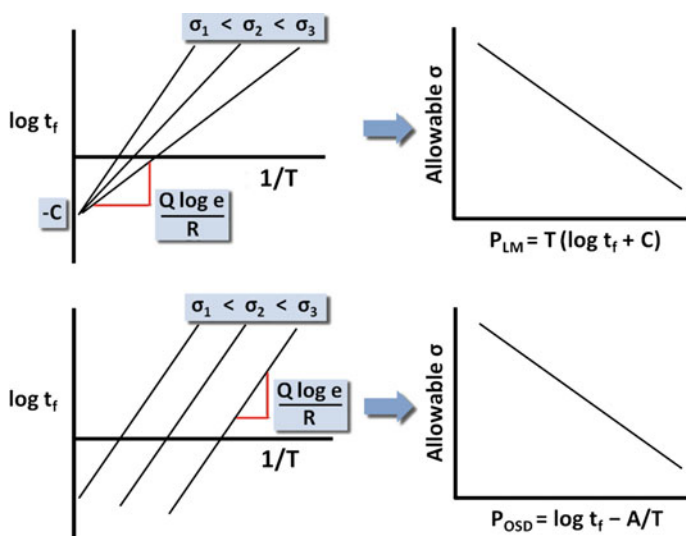


Fig. 10.7 Schematic derivations of the Larson–Miller and Orr–Sherby–Dorn parameters: $A = (Q \log e)/R$

These ‘classical’ time–temperature parametric methods are widely used for creep life predictions, sometimes for interpolation, but notably for extrapolation to (much) longer lives, *which are primarily of interest to the power generation industry, not aerospace gas turbines* (see Sect. 10.5.2).

The extrapolation reliabilities are subject to the condition that the creep mechanisms did not change during the tests that provided the original data. Any changes in mechanisms could lead to serious extrapolation errors, as was already mentioned in Sect. 10.4.

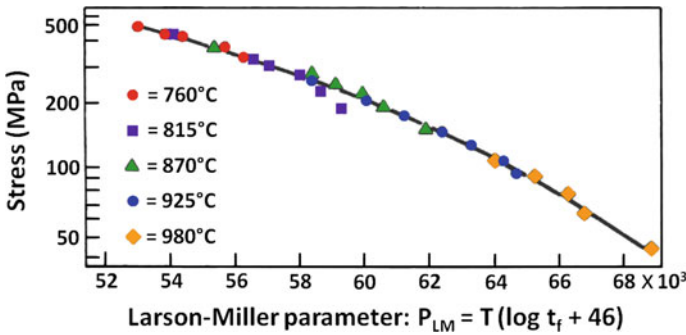


Fig. 10.8 Larson–Miller parameter plot for a nickel-base superalloy (Astroloy): after Ref. [20]

Monkman–Grant (MG) Relationship This empirical relationship correlates the steady-state minimum creep rate and stress rupture life:

$$\dot{\epsilon}_{ss}^m \cdot t_f = C_{MG} \quad (10.3)$$

where m and C_{MG} are constants. For the metals and alloys originally evaluated by Monkman and Grant [21] the exponent m ranged from 0.8 to 0.95, while C_{MG} varied between 3 and 20 (with $\dot{\epsilon}_{ss}$ and t_f in units of pct/hour and hours, respectively).

A better fit for many materials can be obtained from the modified Monkman–Grant (MMG) relationship [22]:

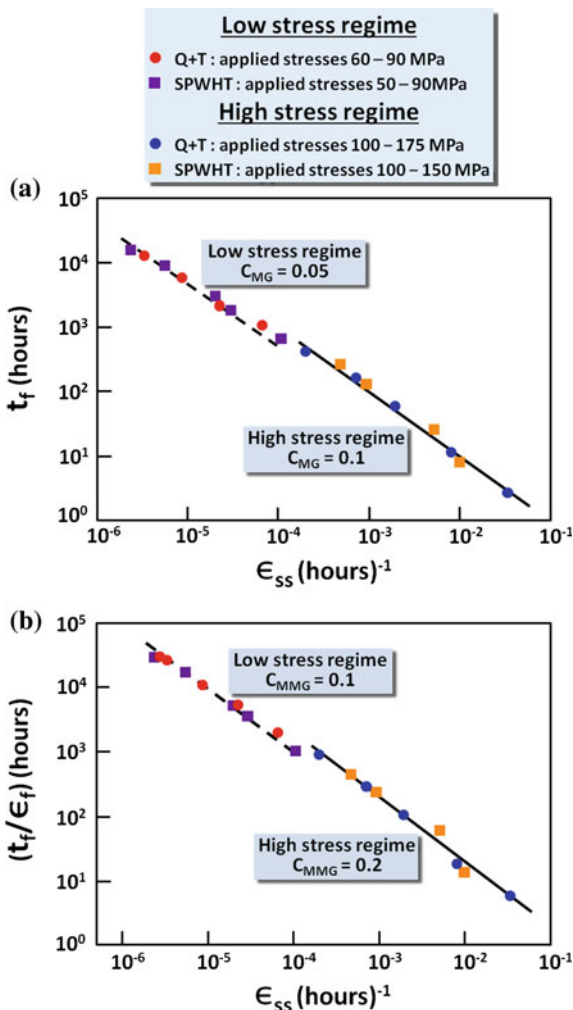
$$(\dot{\epsilon}_{ss}^{m'} \cdot t_f) / \epsilon_f = C_{MMG} \quad (10.4)$$

where m' is close to unity; ϵ_f is the strain to failure; and C_{MMG} is a temperature-independent constant [22].

Figure 10.9 gives examples comparing MG and MMG correlations for a high-temperature ferritic steel [23]. For these examples there is little to choose between the MG and MMG correlations. Both worked well in correlating data for two metallurgical conditions ($Q + T$ and SPWHT), but it is noteworthy that the correlations depended—albeit slightly—on the stress regimes. This reinforces the previous cautionary remarks about extrapolations.

Like the ‘classical’ time–temperature parametric methods, MG and MMG correlations can (or could) be used for long-term creep life predictions [24]. However, similar caveats about extrapolations apply, i.e. there should be no change in creep mechanisms. Also, it may not be advisable to assume that C_{MMG} is a temperature-independent constant unless this is validated by tests at several different temperatures.

Fig. 10.9 MG and MMG correlations of steady-state creep rate and stress rupture lives for a 9Cr-1Mo steel tested at 600 °C [23]: *Q + T* = quenched and tempered; *SPWHT* = simulated post-weld heat-treatment



10.5.2 Developments in Correlation Methods

The ‘classical’ correlation methods have been intensively investigated over the last 50-odd years, and a general evaluation of the parametric techniques was already made by 1979 [25]. None of the methods have a consistent physical basis, and their success is circumstantial [26], i.e. it cannot be assumed that they will generally provide satisfactory correlations. For example, the Larson–Miller and Orr–Sherby–Dorn parameters work best at lower temperatures, while the Manson–Haferd and Manson–Succop parameters are more reliable at intermediate temperatures [19, 26].

More recent prediction methods include the θ projection method [27]; the hyperbolic tangent [19] and Wilshire equations [28–30]; and the uniaxial creep

lifing (UCL) approach [31]. These have recently been reviewed by Abdallah et al. [19] and are summarized in Table 10.2. It is obvious that these modern methods are largely empirical and more complicated than the ‘classical’ methods discussed in Sect. 10.5.1. This means that more extensive data sets are required.

On the other hand, the modern methods give more reliable creep lifing predictions, and they also enable good predictions for complete creep curves [19]. More specifically, Abdallah et al. [19] came to the following conclusions:

1. **Creep lifing:** Both the hyperbolic tangent and Wilshire §1 equations provided good fits to the data with only two fitting parameters. They are therefore improvements on the ‘classical’ methods.
2. **Full creep curves:** All three techniques gave good results, but the UCL approach was inaccurate for primary creep. Overall, the Wilshire §2 equation was the most accurate.

Table 10.2 Modern creep life prediction methods [19]

Creep lifing (long-term): Power generation industry	
Hyperbolic tangent: $\sigma = \sigma_{TS}/2\{1 - \tan h[k \cdot \log(t/t_1)]\}$	
Wilshire §1: $\sigma/\sigma_{TS} = \exp(-k_1[t_f \cdot \exp(-Q_c^*/RT)]^u)$	
Creep strain predictions and full creep curves: aerospace industry	
θ projection: $\varepsilon = \theta_1[1 - \exp(-\theta_2 \cdot t)] - \theta_3[1 - \exp(\theta_4 \cdot t)] + \theta_5[1 - \exp(-\theta_6 \cdot t)]$	
Uniaxial creep lifing (UCL): $\varepsilon = \varepsilon_0 + \varepsilon_p[1 - \exp(-t/t_{tr})] + 1/M [\exp(M \cdot k_{ss} \cdot t) - 1]$	
Wilshire §2: $\sigma/\sigma_{TS} = \exp(-k_3[t_\varepsilon \cdot \exp(-Q_c^*/RT)]^w)$	
With $w = f_1(\varepsilon)$ and $k_3 = f_2(\varepsilon)$ this gives:	
$\sigma/\sigma_{TS} = \exp(-f_2(\varepsilon) \cdot [t_\varepsilon \cdot \exp(-Q_c^*/RT)]^{f_1(\varepsilon)})$	
Rearranging gives: $\varepsilon = f(t, \sigma, T)$	
Nomenclature (see Fig. 10.1 also)	
σ_{TS}	Tensile strength
k, t_1, k_1, u	Fitting parameters
t_f	Time to failure (stress rupture)
Q_c^*	Activation energy from minimum creep rate and/or t_f at constant σ/σ_{TS}
θ_1, θ_3	‘Scaling’ parameters defining strain extents of primary and tertiary creep
θ_2, θ_4	‘Rate’ parameters characterizing curvature of primary and tertiary creep curves
θ_5, θ_6	Parameters describing early primary creep behaviour
ε_0	Instantaneous strain
ε_p	Primary strain from linear projection of steady-state creep curve to $t = 0$
t_{tr}	Time at transition point from primary to secondary/steady-state creep
M	Factor obtained from gradient of \log [total strain rate] versus t
k_{ss}	Gradient corresponding to minimum creep rate
k_3, w	Constants
t_ε	Time to a predefined strain level

10.6 Other Important High-Temperature Properties: A Brief Survey

10.6.1 Creep–Fatigue Interactions (CFI)

Background A comprehensive review of creep–fatigue interactions (CFI), including a survey of life prediction models, is given by Halford [32]. CFI can be important for high-temperature engineering components when (i) the sustained loads at temperature are sufficiently long and the cycle frequency is low, or (ii) the cyclic stress and strain amplitudes are small compared to the sustained loads. These conditions pertain primarily to power generating components, as is evident from a recent specialist book [33] and other publications.

However, there is also interest in CFI for aerospace gas turbine nickel-base superalloys, notably single-crystal alloys used in turbine blades [33–35]. This interest arises from (i) long missions at high-temperatures and engine throttle changes causing fatigue cycling of the blades and (ii) the fact that airworthiness authorities, e.g. the Federal Aviation Administration (FAA) [36] and the US Department of Defense (DoD) [37], encourage damage tolerance assessments for the design and operation of aircraft engines.

Test Methods As stated in ASTM Standard E2714-13 [38], creep–fatigue testing involves the sequential or simultaneous application of the loading conditions necessary to generate cyclic deformation/damage enhanced by creep deformation/damage or vice versa.

ASTM E2714-13 gives guidelines for the types of tests needed. However, it points out that there is no single standard procedure for creep–fatigue testing and also that an oxidizing environment can greatly affect the damage accumulation. Specific information about creep–fatigue testing of nickel-base superalloys is given in Refs. [34, 35, 39], and a representative test set-up is shown in Fig. 10.10.

10.6.2 Thermal Fatigue (TF)

Background Thermal fatigue (TF) is the accumulation of damage in materials under thermal cycling without external loading. The damage process is due to cyclic thermal stresses originating primarily from steep temperature gradients within the materials:

1. During heating, the surface and near-surface regions heat up more rapidly and are constrained by the cooler underlying regions. This constraint causes tensile stresses in the outer regions and compressive stresses in the underlying regions.

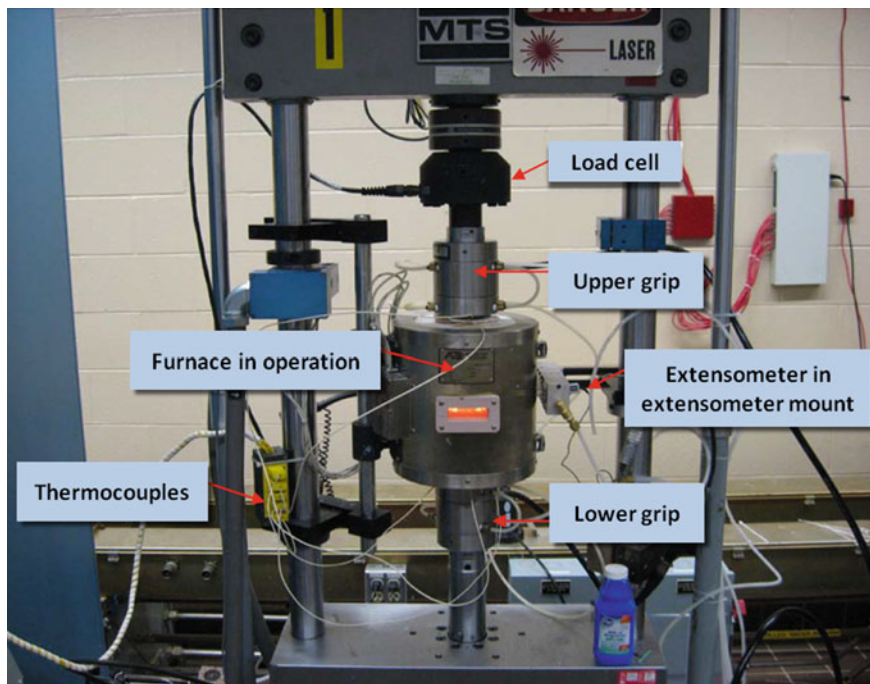


Fig. 10.10 Creep-fatigue testing of a single-crystal nickel-base superalloy: more details are given in Ref. [39]

2. During cooling, the surface and near-surface regions cool more rapidly and are constrained by the hotter underlying regions, thereby reversing the previous stress distributions.

The overall result is that the surface and near-surface regions undergo TF damage.

The significance of TF for aerospace components lies mainly in the evaluation of superalloys, usually with their protective coatings: nickel-base alloys for turbine blades and vanes, and cobalt-base alloys for vanes and combustion chambers.

Test Methods There are several test methods [2], with burner rig testing becoming increasingly popular, especially for evaluating thermal barrier coatings (TBCs) [40]. This is because such rigs are capable of closely simulating the conditions in the hot sections of gas turbines.

Figure 10.11 is a schematic of a burner rig with the following capabilities: high-velocity hot and cold gas flows; inclusion of pollutants and erodents in the hot gas stream (if required); and fully computer-controlled testing with rotation and movement of specimens between the hot and cold gas streams to simulate flight-by-flight turbine entry temperatures.

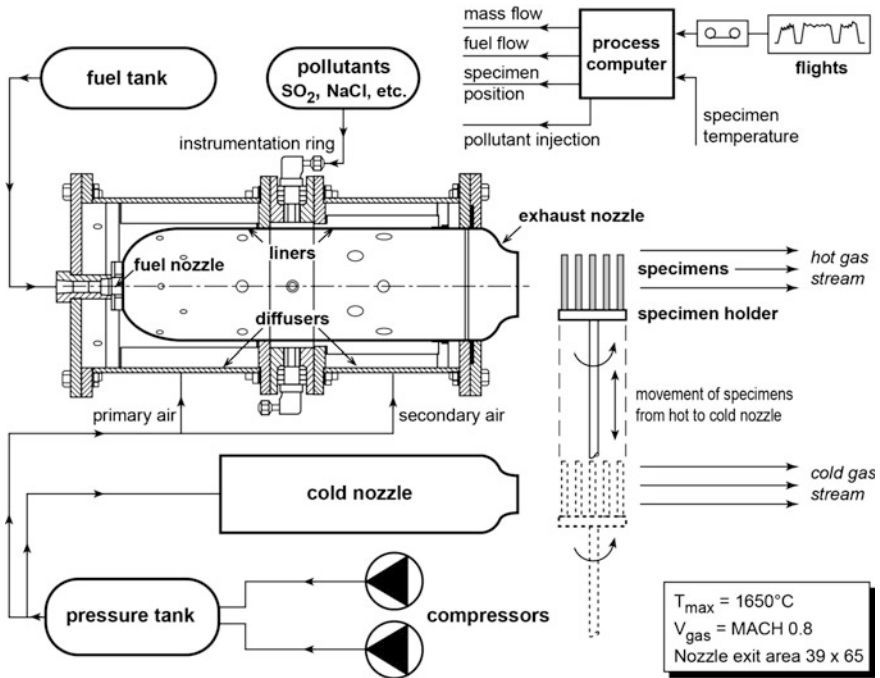


Fig. 10.11 Schematic of a burner rig used for thermal fatigue (TF) testing [41]

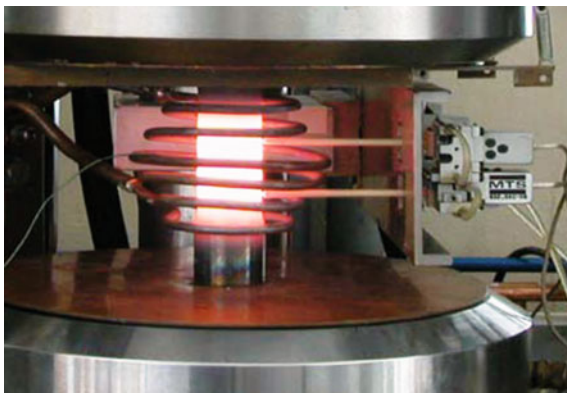
10.6.3 Thermomechanical Fatigue (TMF)

Background Reviews of thermomechanical fatigue (TMF), including life prediction models, are given in Refs. [2, 42, 43]. TMF is fatigue under simultaneous variations in temperature and mechanical strain, which occurs because of external loading or external constraints. Constraint by other structural parts induces ‘external’ compressive mechanical strains.

TMF occurs in structural components in some industrial sectors, including the power generation and aerospace industries, where it is important for turbine blades and discs. The TMF behaviour cannot be predicted from isothermal fatigue (IF) properties because it includes creep and oxidation, whose damage contributions differ for different strain–temperature histories [2] and are generally material specific. For example, the TMF behaviour of nickel-base superalloys is particularly complex [44]. In short, the prediction of TMF behaviour is a challenging problem.

Test Methods There is an ASTM Standard, E2368-10 [45], for TMF testing under uniaxial strain-controlled conditions. Many research facilities develop their own systems, but commercial test rigs are also available.

Fig. 10.12 Induction-heated TMF specimen and two extensometers in a test frame



TMF testing requires rapid heating, either by electrical resistance or induction, or by quartz lamps. Induction heating is preferred [2]. Fig. 10.12 shows a specimen heated by an induction coil, with two extensometers inserted between the coil turns and mounted on the specimen. Generic details of such test set-ups are given in Ref. [2].

TMF tests are complex low-cycle fatigue (LCF) tests, usually not going much beyond 10,000 cycles [2]. The most common tests are in-phase (IP) and out-of-phase (OP), illustrated schematically in Fig. 10.13:

- For in-phase (IP) tests the maximum mechanical strain, ϵ_{\max} , coincides with the maximum temperature, T_{\max} .
- For out-of-phase (OP) tests the minimum mechanical strain, ϵ_{\min} , coincides with T_{\max} .

Figure 10.13 also shows the differences between IP and TMF tests and the very different stress–strain responses (hysteresis loops) of IP and OP tests. This is a generic illustration of the complexity of TMF.

10.6.4 Dwell Cracking

Background Dwell cracking can occur when hold times are included in isothermal fatigue (IF). Cold dwell fatigue cracking of titanium alloys is well known and is a major concern for aeroengine discs [46, 47]. It was first encountered in 1972 with two *in-service* fan disc failures [48]. Although not fully understood, the cracking involves time-dependent plastic strain accumulation [47], i.e. creep.

Dwell fatigue cracking is a potential problem for superalloy turbine discs [49]. Crack acceleration due to dwell has been demonstrated for several widely used nickel-base superalloys [44, 49–52]. However, there is a caveat, at least for military aircraft: dwell cracking can be suppressed by peak loads [44, 50], which in tactical aircraft turbine discs are always above the dwell loads [53].

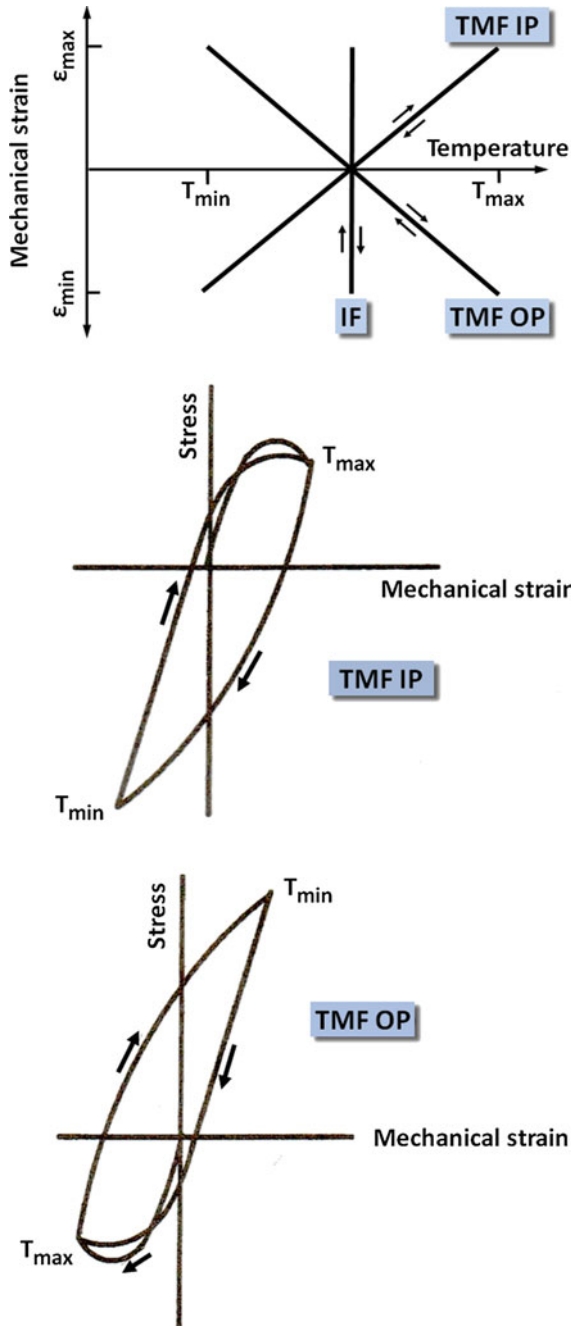


Fig. 10.13 Top mechanical strain variations in IP, OP and IF tests. Middle and bottom IP and OP stress-strain responses. After Ref. [2]

Another caveat, this time with respect to the mechanism of dwell cracking in superalloys, is that the environment has a strong, sometimes controlling influence [44, 50, 54–56], as already mentioned in Sect. 10.3. In other words, the dwell cracking should not be wholly attributed to creep.

Simple linear superposition models have been used to predict the total (fatigue + dwell) crack growth with reasonable success [51]. However, the models are too simple to be relied upon for interpolations and extrapolations of the data between and beyond the original test conditions [51].

Test Methods There are no standard procedures for investigating dwell cracking, notably under simulated flight-by-flight loading [50]. However, ASTM Standard E647 - 15 [57] provides useful guidelines for constant amplitude IF testing.

10.6.5 Creep Crack Growth

Background A review of creep crack growth, including life prediction models, is given in Ref. [2]. This review immediately distinguishes between creep-ductile and creep-brittle materials:

1. **Creep-ductile materials:** These undergo creep cracking with significant amounts of creep deformation at the crack tip. Examples are Cr-Mo and Cr-Mo-V steels and stainless steels, which are extensively used in the power generation industry.
2. **Creep-brittle materials:** These undergo creep cracking with only small-scale creep deformation. Examples include typical high-temperature aerospace engine alloys, i.e. creep-resistant titanium alloys and superalloys.

For aerospace engine materials further distinctions can be made based on design and operating conditions. In aeroengines any time-dependent deformation and/or crack growth is necessarily limited, since (i) designers use materials in the elastic region with only small excursions into elastic–plastic conditions [49]; (ii) dimensional tolerances are tight; and (iii) despite the modern trend of encouraging damage tolerance design [36, 37], the amount of cracking damage that highly stressed components such as discs and blades can sustain is severely limited.

The foregoing considerations imply that creep crack growth is not of general interest for aerospace engine components. However, it is important for the power generation industry.

Test Methods There is an ASTM Standard, E1457-15 [58], and also a European Code of Practice [59] for creep crack growth testing. Both documents emphasize the importance of the test environment and that aggressive environments can significantly affect the creep crack growth behaviour.

10.7 Summary

This chapter discusses engineering high-temperature properties for aerospace gas turbine materials, especially superalloys, concentrating on creep. Particular attention is paid to creep life prediction methods, which have evolved well beyond the ‘classical’ methods of the 1950s. A brief survey of creep–fatigue interactions, thermal fatigue, thermomechanical fatigue, dwell cracking and creep crack growth is also given.

Reference is made to standard test methods, where available, and illustrations of testing equipment and test set-ups are included.

References

1. Kassner ME (2015) *Fundamentals of creep in metals and alloys*, 3rd edn. Butterworth Heinemann, UK
2. Davis JR (ed) (1997) *ASM specialty handbook, heat-resistant materials*. ASM International, Materials Park, OH 44073-0002, USA.
3. Epishin A, Link T (2004) Mechanisms of high temperature creep of nickel-base superalloys under low applied stress. In: Green KA, Pollock TM, Harada H, Howson TE, Reed RC, Schirra JJ, Walston S (eds) ‘Superalloys 2004’ (The Minerals, Metals & Materials Society, Warrendale, PA 15086, USA), pp 137–143.
4. Zhang JX, Murakumo T, Harada H, Koizumi Y, Kobayashi T (2004) Creep deformation mechanisms in some modern single-crystal superalloys. In: Green KA, Pollock TM, Harada H, Howson TE, Reed RC, Schirra JJ, Walston S (eds) ‘Superalloys 2004’ (The Minerals, Metals & Materials Society, Warrendale, PA 15086, USA). pp 189–195.
5. Basoalto H, Sondhi SK, Dyson BF, McLean M (2004) A generic microstructure-explicit model of creep in nickel-base superalloys. In: Green KA, Pollock TM, Harada H, Howson TE, Reed RC, Schirra JJ, Walston S (eds) ‘Superalloys 2004’ (The Minerals, Metals & Materials Society, Warrendale, PA 15086, USA), pp 897–906
6. Tamura M, Esaka H, Shinozuka K (2003) Applicability of an exponential law in creep of metals. *Mat Trans* 44(1):118–126
7. Cadek J (1988) *Creep in metallic materials*. Elsevier Science Publishers, Amsterdam, Chapter 11: pp 176–204
8. Ansell GS, Weertman J (1959) Creep of a dispersion-hardened aluminium alloy. *Trans AIME* 215:838–843
9. Chaturvedi MC, Han Y (1989) Creep deformation of alloy 718. In: Loria EA (ed) *Superalloy 718—metallurgy and applications* (The Minerals, Metals & Materials Society, Warrendale, PA 15086, USA), pp 489–498.
10. Wright JK, Wright RN (2013) Creep rupture of pressurized alloy 617 tubes, Idaho National Laboratory report INL/EXT-13-30251, Idaho Falls, ID 83415, USA.
11. Miller DA, Langdon TG (1979) Creep fracture maps for 316 stainless steel. *Metall Trans A* 10A:1635–1641
12. Carpenter W, Kang BS-J, Chang KM (1997) SAGBO mechanism on high temperature cracking of Ni-base superalloys. In: Loria EA (ed) ‘Superalloys 718, 625, 706 and various derivatives’, (The Minerals, Metals & Materials Society, Warrendale, PA 15086, USA), pp 679–688.
13. Bueno LO, Sordi VL, Marino L (2005) Constant load creep data in air and vacuum on 2.25Cr-1Mo steel from 600 to 700°C. *Mat Res* 8(4):401–408

14. Larson FR, Miller J (1952) A time–temperature relationship for rupture and creep stresses. *Trans ASME* 74(5):765–775
15. Orr RL, Sherby OD, Dorn JE (1954) Correlation of rupture data for metals at elevated temperatures. *Trans ASM* 46:113–128
16. Manson SS, Haferd AM (1953) A linear time–temperature relation for extrapolation of creep and stress rupture data. National Advisory Committee for Aeronautics Technical Note NACA-TN-2890
17. Manson SS, Succop G (1956) Stress-rupture properties of Inconel 700 and correlation on the basis of several time–temperature parameters. In: ‘Symposium on metallic materials for service at temperatures above 1600 F’, ASTM Special Technical Publication STP 174 (American Society for Testing Materials, PA, USA), Philadelphia, pp 40–46
18. Sobrinho JFR, Bueno LO (2005) Correlation between creep and hot tensile behaviour for 2.25Cr-1Mo steel from 500 to 700 °C. Part 2: an assessment according to different parameterization methodologies. *Revista Matéria* 10(3):463–471
19. Abdallah Z, Gray V, Whittaker M, Perkins K (2014) A critical analysis of the conventionally employed creep lifing methods. *Materials* 2014 7:3371–3398
20. Dieter GE (1986) *Mechanical metallurgy*, 3rd/SI metric edition. McGraw-Hill, Inc., New York, p 464
21. Monkman FC, Grant NJ (1956) An empirical relationship between rupture life and minimum creep rate in creep-rupture tests. *Proc ASTM* 56:593–620
22. Dobes F, Milicka K (1976) The relation between minimum creep rate and time to fracture. *Metal Sci J* 10:382–384
23. Choudhary BK, Phaniraj C, Raj B (2010) Interesting relationships for creep deformation and damage and their applicability for 9Cr-1Mo ferritic steel. *Trans Indian Institute Metals* 63(2–3):675–680
24. Phaniraj C, Choudhary BK, Bhanu Sankara Rao K, Raj B (2003) Relationship between time to reach Monkman-Grant ductility and rupture life. *Scripta Materialia* 48:1313–1318
25. Manson SS, Ensign CR (1979) A quarter-century of progress in the development of correlation and extrapolation methods for creep rupture data. *J Eng Mat Technol* 101:317–325
26. Pink E (1994) Physical significance and reliability of Larson-Miller and Manson-Haferd parameters. *Mat Sci Technol* 10(4):340–344
27. Evans RW, Parker JD, Wilshire B (1982) An extrapolation procedure for long-term creep strain and creep life prediction with special reference to 0.5Cr0.5Mo0.25V ferritic steels. In: Wilshire B, Owen DRJ (eds) *Proceedings of recent advances in creep and fracture of engineering materials and structures*. Pineridge Press, Swansea, pp 135–184
28. Wilshire B, Battenbough AJ (2007) Creep and creep fracture of polycrystalline copper. *Mat Sci Eng A* 443:156–166
29. Harrison W, Whittaker M, Williams S (2013) Recent advances in creep modelling of the nickel base superalloy, alloy 720Li. *Materials* 2013 6:1118–1137
30. Harrison W, Abdallah Z, Whittaker M (2014) A model for creep and creep damage in the γ -titanium aluminide Ti-45Al-2Mn-2Nb. *Materials* 2014 7:2194–2209
31. Wu X (2010) Uniaxial creep lifing: methodology-II: creep modeling for Waspaloy and Udimet 720Li, Report LTR-SMPL-2010-0156, National Research Council (NRC) Rolls-Royce, Montreal, QC, Canada: quoted in Ref. [19].
32. Halford GR (1997) Creep-fatigue interaction. In: Davis JR (ed) ‘ASM specialty handbook, heat-resistant materials’, (ASM International, Materials Park, OH 44073-0002, USA), pp 499–517
33. Saxena S, Dogan B (eds) (2011) *Creep-fatigue interactions: test methods and models*, American Society for Testing and Materials Special Technical Publication STP 1539, ASTM International, West Conshohocken, PA 19428-2959, USA
34. Wright PK, Jain M, Cameron C (2004) High cycle fatigue in a single crystal superalloy: time dependence at elevated temperature. In: Green KA, Pollock TM, Harada H, Howson TE,

- Reed RC, Schirra JJ, Walston S (eds) 'Superalloys 2004', (The Minerals, Metals & Materials Society, Warrendale, PA 15086, USA), pp 657–666
35. Pierce CJ, Palazotto AN, Rosenberger AH (2010) Creep and fatigue interaction in the PWA1484 single crystal nickel-base alloy. *Mat Sci Eng A* 527:7484–7489
 36. Federal Aviation Administration (2009) Guidance material for aircraft engine life-limited parts requirements. Advisory Circular FAA AC 33.70-1, U.S. Department of Transportation, Washington, DC
 37. Department of Defense Handbook, Engine Structural Integrity Program (ENSIP) (2004) MIL-HDBK-1783B, ASC/ENOI, 2530 Loop Road West, Wright-Patterson AFB, OH 45433-7101, USA
 38. American Society for Testing and Materials, ASTM E2174 - 13, Standard test method for creep-fatigue testing. ASTM International, West Conshohocken, PA 19428-2959, USA
 39. Pierce CJ (2009) Creep and fatigue interaction characteristics of PWA1484. Air Force Institute of Technology report AFIT/GMS/ENY/09-M02, 2950 Hobson Way, Building 640, Wright-Patterson Air Force Base, OH 45433-8865
 40. Cernuschi C, Vassen R (2015) High temperature oxidation and burner rig testing of different TBCs in the frame of the European Project TOPCOAT: a summary of results. In: Schulz U, Maloney M, Darolia R (eds) Thermal barrier coatings IV (ECI Symposium Series http://dc.engconfintl.org/thermal_barrier_iv/21)
 41. Wanhill RJH, Mom AJA, Hersbach HJC, Kool GA, Boogers JAM (1989) NLR experience with high velocity burner rig testing 1979–1989. *High Temp Technol* 7:202–211
 42. Sehitoğlu H (1996) Thermal and thermo-mechanical fatigue of structural alloys. In: Lampman SR et al (ed) ASM handbook volume 19, 'Fatigue and fracture', (ASM International, Materials Park, OH 44073-0002), Section 4, pp 527–556
 43. Antolovich SD, Saxena A (2002) Thermomechanical fatigue: mechanisms and practical life analysis. In: Becker WT, Shipley RJ et al (eds) ASM handbook volume 11, 'Failure analysis and prevention', (ASM International, Materials Park, OH 44073-0002), pp 738–745
 44. Pineau A, Antolovich SD (2009) High temperature fatigue of nickel-base superalloys—a review with special emphasis on deformation modes and oxidation. *Eng Fail Anal* 16:2668–2697
 45. American Society for Testing and Materials, ASTM E2368 - 10, Standard practice for strain controlled thermomechanical fatigue testing. ASTM International, West Conshohocken, PA 19428-2959, USA
 46. Bache MR (2003) A review of dwell sensitive fatigue in titanium alloys: the role of microstructure, texture and operating conditions. *Int J Fatigue* 25(9–11):1079–1087
 47. Whittaker MT, Evans WJ, Harrison W (2009/2010) Time dependent fatigue fractures of titanium alloys. In: 12th International conference on fracture 2009 (ICF-12), (Curran Associates, Inc., Red Hook, NY 12571, USA), vol 3, pp 2023–2031
 48. Jeal RH (1982) Defects and their effect on the behaviour of gas turbine discs. In: Maintenance in service of high temperature parts. AGARD conference proceedings no. 317, Advisory Group for Aerospace Research and Development, Neuilly sur Seine, France, pp 6-1–6.15
 49. Harrison GF, Tranter PH, Grabowski L (1993) Defects and their effects on the integrity of nickel based aeroengine discs. In: Impact of materials defects on engine structures integrity. AGARD report 790, Advisory Group for Aerospace Research and Development, Neuilly sur Seine, France, pp 9-1–9-16
 50. Wanhill RJH (2002) Significance of dwell cracking for IN718 turbine discs. *Int J Fatigue* 24 (5):545–555
 51. Hörnqvist M, Månsson T, Gustafsson D (2011) High temperature fatigue crack growth in Alloy 718—Effect of tensile hold times. *Procedia Eng* 10:147–152
 52. Yang H, Bao R, Zhang J (2013/2014) Creep-fatigue interaction model for crack growth of nickel-based superalloys with high temperature dwell time. In: 13th International conference

- on fracture 2013 (ICF-13), (Curran Associates, Inc., Red Hook, NY 12571, USA), vol 3, pp 1842–1849
53. Bergmann JW, Schütz W (1990) Standardised load sequence for turbine and hot compressor discs of combat aircraft engines. Industrieanlagen-Betriebsgesellschaft (IABG) report TF-2809, Ottobrunn, Germany (in German)
 54. Andrieu E, Ghonem H, Pineau A (1990) Two-stage crack tip oxidation mechanism in alloy 718. In: Elevated temperature crack growth (The American Society of Mechanical Engineers, New York, NY 10016-5990, USA), MD-Vol. 18, pp 25–29
 55. Ghonem H, Nicholas T, Pineau A (1991) Analysis of elevated temperature fatigue crack growth mechanisms in alloy 718. In: Creep-fatigue interaction at high temperature (The American Society of Mechanical Engineers, New York, NY 10016-5990, USA), AD-Vol. 21, pp 1–18
 56. Gao M, Chen S-F, Chen GS, Wei RP (1997) Environmentally enhanced crack growth in nickel-based alloys at elevated temperatures. In: Elevated temperature effects on fatigue and fracture. ASTM Special Technical Publication STP 1297 (American Society for Testing and Materials, West Conshohocken, USA), pp 74–84
 57. American Society for Testing and Materials, ASTM E647 - 15, Standard test method for measurement of fatigue crack growth rates. ASTM International, West Conshohocken, PA 19428-2959, USA
 58. American Society for Testing and Materials, ASTM E1457 - 15, Standard test method for measurement of creep crack growth times in metals. ASTM International, West Conshohocken, PA 19428-2959, USA
 59. Dogan B, Nikbin K, Petrovski B, Dean D (2005/2010) Code of practice for creep crack growth testing of industrial specimens, In: '11th international conference on fracture 2005 (ICF11)', (Curran Associates, Inc., Red Hook, NY 12571, USA), vol 4, pp 3073–3078

Bibliography

1. Kassner, M.E., 2015, 'Fundamentals of Creep in Metals and Alloys', Third Edition, Butterworth Heinemann, Elsevier, Oxford, UK.
2. Davis, J.R. (Ed.), 1997, 'ASM Specialty Handbook, Heat-Resistant Materials', ASM International, Materials Park, OH 44073–0002, USA.
3. American Society for Testing and Materials 'ASTM E139 - 11, Standard Test Methods for Conducting Creep, Creep-Rupture, and Stress-Rupture Tests of Metallic Materials', ASTM International, West Conshohocken, PA 19428–2959, USA.

Chapter 11

Non-destructive Testing and Damage Detection

B. Purna Chandra Rao

Abstract This chapter briefly describes various techniques used for non-destructive inspection (NDT) of aerospace components for detecting defects, cracks, corrosion, and other degradation features, as part of quality assurance and in-service inspection. The capabilities and applications of widely used NDT techniques for examining metallic as well as composite aerospace structures are discussed. Recent advances in NDT techniques for automated, fast and cost-effective in-service and in situ monitoring of aircraft are highlighted, as well as future directions.

Keywords Non-destructive testing · Optical · Penetrant · Magnetic particle · Eddy current · Ultrasonic · X-ray · Isotope radiography

11.1 Introduction: The Role of NDT

Both the safe-life and the fail-safe philosophies applicable to aircraft structures require non-destructive testing (NDT). NDT techniques play a vital role in quality assurance, structural integrity assessment, condition monitoring, structural health monitoring, and life extension programmes [1].

The aerospace industry employs NDT techniques for producing components without any defects and also for assessing the structural integrity of installed components through periodic scheduled inspections. These inspections are necessary because of the likely deterioration due to fatigue and corrosion in metallic structures [2]; and disbonding, internal delamination and cracking in composite structures owing to their susceptibility to impact damage, especially barely visible impact damage (BVID), see Chap. 14 in Volume 1 of these Source Books.

Since the modes of failure of metallic and composite structures are very different, they require different NDT techniques. An overview is given in Table 11.1.

B. Purna Chandra Rao (✉)
IGCAR, Kalpakkam, India
e-mail: bpcrao@igcar.gov.in

Table 11.1 NDT techniques for detecting damage in aerospace structures

Damage	Suitable NDT techniques
Surface cracks	Visual and optical Liquid penetrant Magnetic particle (ferromagnetic materials) Eddy current
Fatigue cracks under fasteners	Magnetic particle (ferromagnetic materials) Eddy current arrays Pulse thermography Phased array ultrasonics
Subsurface corrosion	Pulsed eddy current Multi-frequency eddy current Active thermography Micro-focal radiography Neutron radiography
Cracks or corrosion in multi-layer structures	Pulsed eddy current Multi-frequency eddy current Active thermography Real-time radiography
Composite structures	Shearography Active thermography Phased array ultrasonics Acoustic, resonance, and mechanical impedance

Improvements and developments in NDT since World War II have led to its widespread use in aerospace manufacturing, quality control, in-service inspection of aircraft, and the development of maintenance procedures [3]. Besides crack and corrosion detection in metallic structures, and disbonding, delamination, and cracking in composites, NDT is used to detect leaks, map the extent of damage in susceptible locations, and measure thickness reductions due to corrosion.

Thus NDT is an essential tool for guaranteeing the safety of aerospace components and structures. NDT is also used during forensic engineering investigations to assist in finding the basic physical causes of failure and to help in suggesting remedial measures [4].

11.2 Generic NDT Systems

More than 50 NDT techniques based on physical principals are available today. Nearly all involve subjecting the material to be examined to some form of external energy and analysing the detected response. Likewise, nearly every property of the materials to be inspected has become the basis for some NDT technique [5]. The essential steps involved in a generic NDT system are as follows:

- Application of a testing or inspection medium.
- Modification of the testing or inspection medium by flaws, cracks, or variations in material properties or microstructure.
- Detection of this modification by a suitable detector or receiver.
- Conversion of this change into suitable data or signal or image.
- Interpretation of the information obtained.

NDT results are indirect measurements. Hence NDT techniques always require the use of reference standard specimens with flaws or discontinuities of known dimensions for calibrating the NDT instruments, and for sizing the actual flaws, cracks, and other discontinuities.

NDT techniques can be classified into surface techniques and volumetric techniques, depending on whether the flaws or discontinuities are surface connected or internal. The most popularly used surface NDT techniques include visual, liquid penetrant, magnetic particle, eddy current, and infrared thermography; volumetric inspection includes ultrasonics, radiography and acoustic emission [4, 5]. The capabilities and applications of surface and volumetric techniques are discussed in Sects. 11.3 and 11.4.

11.3 Surface Techniques

11.3.1 Visual Evaluation

Visual inspection is probably the most widely used technique for aircraft structures. It provides the first and quickest means to assess the condition of an aircraft and its components. Optical aids include magnifying lenses, and mirrors and periscopes for locations not directly accessible to viewing [5].

Boroscopes, endoscopes, and microscopes with built-in illumination and zoom possibility are also used for in situ inspections as well as on component assemblies removed from aircraft. Boroscopes and endoscopes enable inspections of landing gear cylinders and engine parts, including turbine discs, blades, vanes, and burner cans. Flexible fibrescopes and video image scopes permit remote inspection of inaccessible locations. Use of charge-coupled devices and computer-assisted viewing systems with data storage and image processing possibilities is also common.

11.3.2 Optical Testing Techniques

Two popular surface NDT techniques are laser speckle interferometry and shearography.

Laser Speckle Interferometry This is a non-contact technique that makes use of the intensity distribution pattern formed from space interference, generated by coherent light illumination of an object surface [1, 4]. This technique can be used for inspection of metal, ceramic, glass, rubber and composite materials. Furthermore, electronic speckle pattern interferometry and digital image correlation techniques are used for online quality control and for tracking damage paths and extents.

Shearography Shearography is a whole-field real-time imaging technique that reveals out-of-plane deformation derivatives in response to applied stress. This technique is suitable for composites, since it can detect subsurface flaws such as disbonds, delaminations, core defects, and impact damage. Other advantages are rapid and cost-effective inspection especially during manufacturing and quality assurance [1, 7], and also the equipment can be made portable.

11.3.3 Liquid Penetrant Technique

Liquid penetrant inspection (LPI) is useful for detection of surface-connected cracks and flaws in metallic and composite structures and components, and is simple, fast, and inexpensive. In this technique a component is coated with a dye penetrant for a certain time called 'dwell time', after which excess penetrant is carefully removed from the surface and a developer (white powder) *may be* applied to draw penetrant out of any cracks. The surface is then examined for penetrant retained in or issuing from the cracks. Three different LPI systems based on removal of excess penetrant are water-washable, solvent-removable, and post-emulsifier [4].

It is essential to increase the visible contrast between a crack and the surrounding surface. For normal visual inspection the penetrant is therefore usually coloured bright red. Fluorescent penetrants are also used, and these are combined with inspection under ultraviolet light.

The equipment can be portable (spray cans), stationary, or automated, depending on the accessibility and the required level of sensitivity. It is essential to ensure that (i) inspected regions are cleaned before and after testing, and (ii) the penetrant and developer are free of halogens and sulphur. Specially prepared cracked panels can be made in order to check the performance of the penetrant systems [4–7].

11.3.4 Magnetic Particle Technique

Magnetic particle inspection (MPI) is principally used for detection of surface flaws in ferromagnetic materials [4, 8], although it can provide limited detection of subsurface flaws. MPI is routinely applied to low-alloy steel components in

engines, landing gear, and gearboxes, and also to fasteners (bolts). It is also possible to use MPI on ferritic and martensitic stainless steels.

In this technique, fine magnetic particles are applied to a magnetized component surface that may have a flaw. Magnetic flux emanating from any flaws causes the particles to cling to the flaw regions, thus enabling their detection. However, it is important to note that flaws are best detected when they are perpendicular to the magnetization direction. Therefore, complete examination of a component requires magnetizing it in two directions, i.e. longitudinal and transverse (or circumferential).

Various magnetization methods are used [4]. Also, depending on the sensitivity required and the geometry of the part, AC, DC, half-, and full-wave rectified DC and permanent magnet methods are employed. AC magnetization is ideal for detection of shallow surface flaws, while DC or half-wave rectified DC (HWDC) magnetization is preferred for detection of near-surface flaws. It should be noted that not only cracks, but material variations, stresses, and surface roughness influence the magnetic leakage flux. In other words, careful interpretation of MPI results is essential.

After any inspection the component has to be demagnetized, especially for *subsequent* detection of near-surface flaws, and this has to be ensured to less than 3 Gauss using field meters.

Magnetic particle testing can be performed dry or wet. In both cases the particle size has to be small (dry < 150 μm ; wet < 25 μm) to enable easy migration and local accumulation of the particles such that small cracks are detected. Fluorescent particles and inspection under ultraviolet light are used for high sensitivity crack detection.

Magnetic Rubber For examination of visually inaccessible regions, e.g. bolt holes and internal threads, the magnetic rubber inspection technique [5] is employed.

Magnetic Flux Leakage Technique Sensor-based detection of magnetic leakage flux transforms the MPI technique to the magnetic flux leakage technique. Use of a sensor enables automatic inspection of components, especially during manufacturing, and sizing of the flaws without human inspectors [9]. The sensors include inductive coils, Hall elements, magnetometers, magnetodiodes, and giant-magneto-resistive (GMR) sensors.

11.3.5 *Eddy Current Technique*

Eddy current inspection involves measurement of the change in coil impedance (or induced voltage in a receiver coil) that occurs due to distortion of eddy currents by flaws or variations in electrical conductivity and magnetic permeability [10]. Discontinuities that cause maximum perturbation to eddy currents produce large impedance changes, and hence are detected with high sensitivity.

Eddy current inspection uses probe coils, usually excited with AC in the frequency range of 1 kHz to 1 MHz, and these possess directional properties, i.e. regions of high sensitivity and low sensitivity. The types of probes depend on the geometry of the components to be inspected. Commonly used probes include pancake probes, bolt hole probes, and sliding probes operating in absolute, differential, and transmit–receive modes [11]. Ferrite cores and shields are used to focus and shape the eddy currents and to increase the crack detection sensitivity. Flexible eddy current coils that wrap around corners and follow complex shapes are also used.

The locus of impedance change during the movement of a probe coil over the component surface is called the signal. The amplitude of the signal depends on the flaw size, while the signal phase angle provides information about the flaw depth. During inspection, any region that produces signals with peak-to-peak amplitude or phase angle greater than the threshold signal parameters is recorded and is considered defective.

Use of proper probes, optimum inspection frequencies, and accurate reference calibration standards is essential. The excitation frequency and instrument gain are optimized to detect all the specified reference flaws. Lower frequencies are used for detection of subsurface flaws and corrosion damage in underlying layers of a built-up structure or laminate. For such applications, *multi-frequency* techniques are employed: these involve signal mixings to eliminate the contribution of disturbing variables.

The eddy current technique is very versatile, and its excellent sensitivity to surface and subsurface flaws makes it an ideal candidate for inspecting critical regions in aircraft structures for cracks, corrosion damage, and coating thickness measurements [7]. Eddy current inspection is routinely used for aircraft wheel hubs, fastener holes and bolt holes; and for detection of damage and cracking in countersunk rivet holes in built-up structures [12]. In particular, automated inspection of long rows of fasteners, e.g. in fuselage lap joints, can be done at speeds as high as 5 m/s.

Example 1, Riveted Panel Figure 11.1 shows an example of the detection equipment and a sample being used for eddy current testing countersunk rivet holes in an air intake panel. This sample was a 2-layer panel with machined notches in rivets, some of which were filled with simulated corrosion products. Inspection was done with a ring reflection probe.

The ‘lift-off’ signal was used to distinguish the ‘defective’ rivets (G) and ‘defective’ rivets with simulated corrosion products (GA) from the defect-free rivets, see Fig. 11.2. In fact, it was found that the eddy current technique was able to reliably detect 0.25 mm deep ‘defects’ in 4.0 mm diameter rivets and 0.75 mm deep ‘defects’ in 5.0 mm diameter rivets. It was also possible to detect fatigue cracks and corrosion in second and third layers even without removing the surface paint system.

Example 2, Compressor Disc Crack The complex geometry of the dovetail regions of aeroengine compressor and turbine discs produces large amplitude

Fig. 11.1 Eddy current testing of countersunk rivet holes in an air intake panel

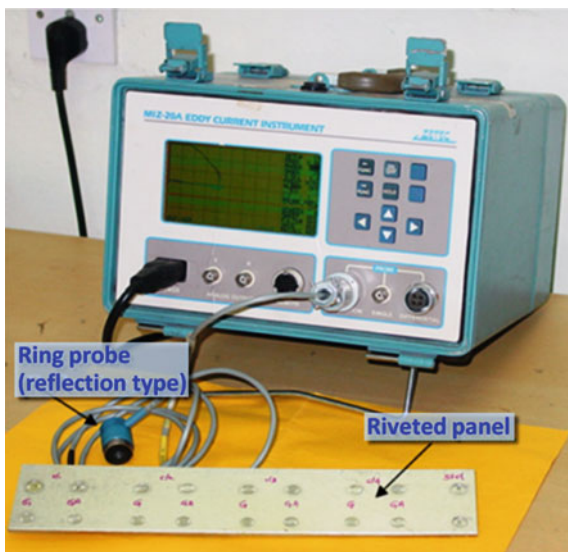
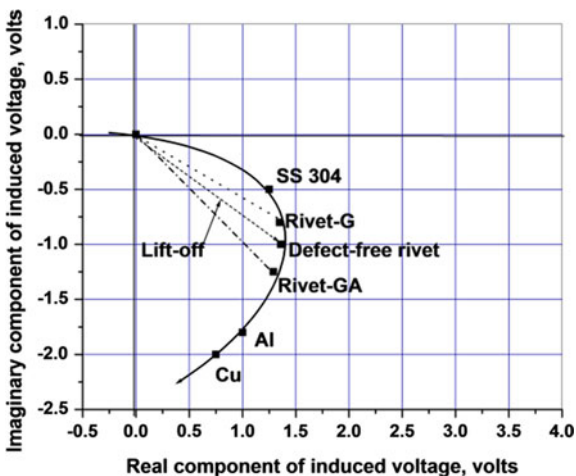


Fig. 11.2 Impedance plane diagram showing the lift-off response for different electrically conducting materials



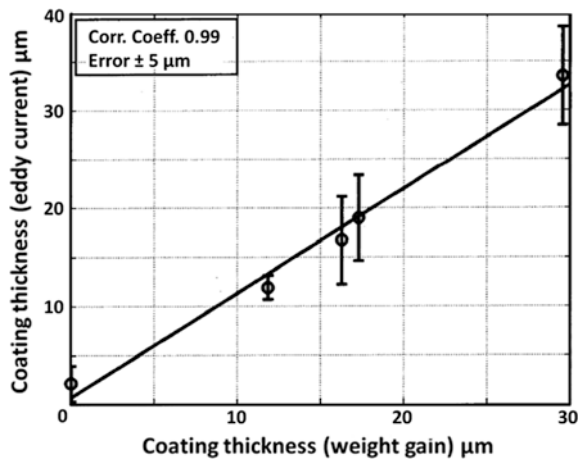
signals, masking any cracks that might be present at the dovetail roots, which are regions with high stress concentrations (even though very carefully machined and finished).

Figure 11.3 shows the location of an actual crack, which was detected using the dual-frequency eddy current technique. This technique can suppress the disturbing signals due to edge effects and probe tilt, and is able to reliably detect fatigue cracks as small as 2 mm long.

Fig. 11.3 Compressor disc with a 4.0 mm long crack in a blade dovetail (circled region under arrow)



Fig. 11.4 Eddy current measurement of SiC coating thickness on a Carbon–Carbon composite



Example 3, SiC Coating Thickness Silicon carbide coatings are used to protect re-entry vehicle Carbon–Carbon composite nose caps and leading edges from oxidation. The coating thickness is critical and must be very accurately measured and assessed.

The eddy current technique is well-suited to these measurements. A calibration graph has to be established between signal amplitude and coating thickness (by weight gain) to evaluate the accuracy. Figure 11.4 is an example of such a calibration, showing an excellent correlation. The coating thickness can be measured by eddy current to within an error of $\pm 5 \mu\text{m}$ [13].

Furthermore, by raster scan imaging it is possible to assess the uniformity of the coating thickness and identify thinly coated regions, which in this application signifies coating thicknesses $< 20 \mu\text{m}$.

11.3.5.1 Other Types of Eddy Current Testing

Pulsed Eddy Current Besides single- and multi-frequency eddy current testing, the pulsed eddy current technique is gaining importance for inspection of aircraft structures [14]. A pulse contains a continuum of frequencies, and this means that it is possible to interrogate different depths, with the response received by highly sensitive Hall sensors and giant-magneto-resistive (GMR) sensors, (already mentioned in subsection 11.3.4, with respect to the magnetic particle technique).

Pulsed eddy current images of flaws in second and third layers can be obtained from line scans by array sensors or raster scans by matrix array sensors [15].

Eddy Current C-scan Imaging and Magneto-Optic Imaging (MOI) These are useful for detection and sizing of cracks as small as 0.5 mm, and detecting corrosion damage in aluminium alloy aircraft structures.

The MOI technique uses a film sensor, and an optical polarization effect that occurs as a result of the electromagnetic field, to detect and view eddy currents [16]. MOI detects cracks around aircraft rivets and flaws under painted or coated surfaces several times faster than the eddy current technique.

MOI also does not require calibration and it can rapidly inspect large fuselage areas for cracks and corroded areas. High-frequency heads operating in the 20–200 kHz range and low-frequency heads operating in the 1.5–50 kHz range are used for imaging and viewing surface and subsurface cracks, respectively.

Small Coil and Smart Sensor Arrays These enable efficient imaging of cracks near fasteners, irrespective of their orientation, thereby improving and replacing the MOI technique, which is prone to lift-off variations and associated false indications.

11.3.5.2 Summary

The usefulness and acceptability of eddy current techniques for the aerospace industry have been enhanced by developments in automated inspections of large areas, elimination of operator fatigue and uncertainties, inspection of inaccessible as well remote areas, and online inspection ensuring a high probability of detection and accurate sizing [1, 16].

11.3.6 Infrared Thermography Technique

Infrared thermography enables measuring and displaying the changes in temperature on a component. This technique is non-contact, non-invasive, dry, safe, and fast; and it displays the inspection results in a convenient visual image format. Differences in temperature on the surface facing the infrared camera are measured and related to flaws or other abnormalities.

Infrared thermography can be passive or active. In passive thermography the natural heat distribution over the surface of a warm/hot component is measured for assessing its integrity or for condition monitoring [4].

In active thermography, the component is heated or cooled and the redistribution of temperature across the component surface is measured. The heat flow on the component can be induced either by applying energy in a pulsed form (pulsed or transient thermography) or in a harmonic-modulated way (lock-in thermography). In pulsed thermography a single heat pulse is used for external heating, while in lock-in thermography a sinusoidal heat wave of fixed frequency is used [17].

Pulsed thermography is gaining increased use for detection of surface as well as subsurface damage in aerospace structures. Propagation of the heat flow inside the component directly affects the surface temperature changes, which are recorded with a high-speed infrared camera and displayed and analysed. The presence of a flaw reduces heat diffusion, and the flaw region therefore shows a different temperature compared to its surroundings. Since the thermal front propagates by diffusion, a deeper flaw will be observed later, although with reduced contrast.

Active thermography can detect different defects in carbon fibre reinforced plastic (CFRP) composites, and its attractive features include rapid inspection, easy operability, inspection without extensive disassembly, and easy interpretation of the inspection results.

Thermography has proven to be a valuable technique for detection of impact damage, disbonds, stringer ruptures, cracks, foreign objects, or voids in composites; and it can also detect contamination or liquid ingress into aircraft honeycomb panels [18]. For rapid inspection of large composite areas, active thermography appears to be better than the phased array ultrasonic testing and radiography techniques [1, 19].

11.4 Volumetric Techniques

Volumetric NDT techniques can detect and size flaws or damage within a component. Four of the most commonly used techniques are acoustic testing, acoustic emission testing, ultrasonic testing, and radiography testing.

11.4.1 *Acoustic Testing Techniques*

NDT of adhesive bonding in laminates and honeycomb structures is carried out using acoustic techniques. The simplest is the tap test using a tap hammer or coin, and qualified personnel can detect the presence of damage (which may be cracks, corrosion, impact damage, or disbonding). Usually a well-bonded area produces an even pitch sound, as compared to a dead or dull sound produced by a disbonded area [1]. However, the judgment is based on comparing the acoustic response from the entire component and it cannot detect disbonds or voids in discrete layers.

Other popular acoustic techniques are sonic testing, resonance testing, vibration testing, and mechanical impedance testing. These depend on exciting vibrations in a component by a local (light) impact and measuring some properties of the vibrations such as resonant frequency and decay time to assess the structural integrity [1].

Sonic And Resonance Testing These operate at audio or near-audio frequencies and are used for detecting separations between layers of laminated structures, disbonds in adhesive-bonded honeycomb structures, impact damage, and exfoliation corrosion.

Process-compensated resonance testing is a possible technique for detecting hidden flaws in widely different components such as turbine blades, aircraft wheels, and fasteners.

Mechanical Impedance Testing The basic principle for mechanical impedance analysis is measurement of the impedance (stiffness) of a structure. Since no couplant is required, it offers advantages over ultrasonic testing (see subsection 11.4.3.).

In addition, it should be noted that a combined eddy current/sonic technique called ***eddy sonic harmonic testing*** can be used for detection of both near-side and far-side disbonds in composites, while mechanical impedance is useful for detection of subsurface defects in composite structures [1].

11.4.2 *Acoustic Emission Technique*

Acoustic emission testing is a ‘global’ technique that detects growing cracks or leaks in a component subjected to an external stress. By placing several piezoelectric sensors at various locations on a structure and applying appropriate loads, it is possible to detect and locate growing flaws/damage and assess the structural integrity [4]. This technique offers potential for structural health monitoring of composite aerospace structures, since the sensors can be mounted at damage-prone locations [20].

11.4.3 Ultrasonic Testing Technique

Ultrasonic testing uses pulsed sound waves with frequencies in the range 200 kHz to 800 MHz. The sound waves are emitted by a transducer, and reflected waves (echoes) are detected by a receiver. When a sound wave undergoes reflection owing to internal discontinuities, the total echo or through-transmitted sound loses energy, changing the pulse amplitude and its appearance on a visualizing screen.

In the *pulse echo* method, the reflected energy is detected by the same transducer. In the *through-transmission* and *pitch-catch* methods the energy is detected by a separate receiver. The received energy is converted into an electrical signal, which is displayed as (i) an A-scan signal on an oscilloscope or computer screen; (ii) a B-scan line image obtained by scanning the transducer along a line; or (iii) a C-scan image by raster scanning the transducer [4].

Each display mode enables a different way of looking at the data and evaluating the inspected region. In order to correct inaccuracies due to ultrasonic beam spreading, correction methods such as distance amplitude corrections (DAC) are employed. This is done by introducing a series of side-drilled holes, flat-bottom holes, and machined notches at different depths in the component to be inspected.

In order to detect flaws efficiently, it is necessary for the wavelength to be comparable to the expected flaw dimensions. Hence for detection of smaller flaws and enhanced resolution it is necessary to use higher frequencies. However, increased frequencies also result in increased ultrasonic wave attenuation and noise owing to scattering by the material microstructure [21].

This technique can detect surface as well as subsurface flaws that are orientated both parallel and normal to the component surface by using normal beam or angle beam transducers. It is also essential to properly address the dead zone caused by finite pulse length. Use of couplants such as grease, gel, or water is essential to efficiently couple the acoustic energy to the component surface.

Applications Ultrasonic testing is specified for examination of welds, forgings, castings, bolts, and other products. During aircraft maintenance, critical areas such as structural fittings of landing gear legs, engine attachments, and pylons are inspected by ultrasonic testing.

The through-transmission method is used for inspection of multi-layered and composite materials for assessing the bond quality and detection of flaws and other discontinuities. Dry testing with couplant as well as water immersion techniques are employed, depending on the acceptability of immersion. Immersion scanners and robotic arms enable automated ultrasonic inspection. When immersion in water is undesirable due to moisture absorption or ingress, 'squirters' or 'bubblers' are used as acoustic couplers [1].

Wave Variations Besides longitudinal (compression) waves and transverse (shear) waves, Rayleigh and Lamb waves are used for damage detection. This technique may be used for detection and sizing of cracks, voids and delaminations; and also

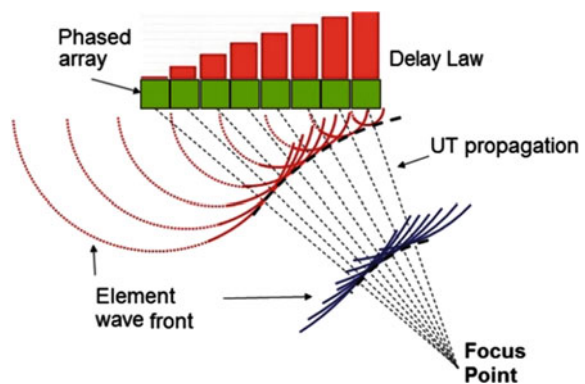
for thickness reductions or corrosion damage in a variety of materials, both metallic and non-metallic [1].

11.4.3.1 Advanced Ultrasonics

Advanced technologies are enhancing the accuracy, speed, and cost-effectiveness of ultrasonic inspection:

1. *Time-of-flight diffraction*. This technique is used for accurate location and sizing of surface, subsurface, and internal cracks, which is possible because it is based on the arrival times of the diffracted pulses, not on signal amplitude.
2. *Synthetic aperture focussing*. This technique is useful for enhancing the signal-to-noise ratio. This is achieved by orbital measurement of the complete sound field scattered by a crack and reconstruction to back-calculate the region where the scattering occurred, making use of well-known wave propagation formulae.
3. *Fourier transform/wavelet transform method*. These signal and image processing methods are also being explored for reduction of noise and enhancement of flaw information.
4. *Phased array ultrasonic technique*. This is gaining popularity for inspection of aerospace components [1]. This technique uses a number of array elements that can function separately as transmitter and/or receiver. The ultrasonic beam is selectively steered and focussed by using a number of array elements excited with different time delays following the delay laws. As shown schematically in Fig. 11.5, the delay law is computed such that the arrival of each element contribution is in phase at the focus point. The test data are presented as A-, B-, or C-scans, as well as 3-D displays for enhanced interpretation and decision making.

Fig. 11.5 Focussing of an ultrasonic beam in phased array testing



Phased array systems are portable and have advantages for automated inspection of aircraft fastener holes, with digital alarms and imaging possibilities. The ability to electronically control the beam characteristics is attractive for automated systems that use a large number of different probe angles for reliable inspection [22].

Other advantages of the phased array technique are (i) inspection of large areas in one scan, (ii) inspection at several angles by sweeping to produce an S-scan, (iii) collection of higher resolution data with fully encoded C-scan imaging systems for detection and sizing of cracks and wall thickness loss due to corrosion, abrasion and erosion, and (iv) detection of accumulated damage prior to crack nucleation as well as detecting just-formed tiny cracks by measuring the acoustic nonlinearity and interpreting the resulting images.

5. *Guided wave ultrasonics*. This technique is useful for long-range ultrasonic detection of corrosion damage and cracks in remote and inaccessible regions. Guided or Lamb wave-based acousto-ultrasonic techniques have shown potential for detection of visually unnoticeable lightning and fire damage in composites.
6. *Air-coupled ultrasonic and laser-generated ultrasonics*. These techniques show promise for non-contact inspection of adhesively bonded multi-layer structures.

11.4.4 X-Radiography Technique

X-radiography is one of the widely used NDT techniques for detecting cracks and corrosion in aircraft components. The variation in image darkness/contrast is used to detect flaws in the material and to determine the thickness (or loss of thickness). Figure 11.6 shows a typical real-time radioscopic image of a honeycomb mid-section and the adhesive-bonded nose section of a tail rotor blade.

Fig. 11.6 Real-time X-radiography image of the honeycomb mid-section and adhesive-bonded nose section of a tail rotor blade



Successive developments have upgraded conventional X-radiography systems, and digital radiography systems are available now for efficient and cost-effective volumetric inspections [23]. The main benefits of digital radiography are high-quality imaging, no film processing chemicals, lower levels of radiation with reduced risk of overexposure, and efficient storage and retrieval of radiographs.

A variety of digital image processing techniques are applied to the digital as well as digitized radiographs to enhance the contrast in the radiographs and for reliable detection as well as accurate sizing of flaws. Even so, this technique requires a high level of skill and experience for setting up the equipment for testing, and a similar skill is needed for image interpretation. For example, tight or narrow cracks are difficult to detect, especially if they are not orientated nearly parallel to the X-ray beam.

Difficulties in interpreting X-radiography images of composite structures are the reasons that this technique is commonly combined with ultrasonics [1].

11.4.5 Isotope Radiography Technique

Isotope gamma radiography using Iridium-192 and Cobalt-60 is a less expensive technique than X-radiography, and is also portable and does not require an external electrical source [4]. It is particularly attractive for detection of subsurface flaws in thick engine components, since these require higher energy levels than those obtainable from X-radiography. Non-metallic parts can also be inspected using gamma radiography.

N.B: Both X-radiography and isotope radiography entail a radiation hazard. This means that the use of these techniques is subject to restrictions.

11.4.6 Neutron Radiography

Neutron radiography is complementary to the X-radiography and isotope gamma radiography techniques. Neutron radiography is well suited for detection of corrosion and moisture entrapment (hydrogen absorbs and scatters neutrons well) in aircraft structures [24]. It is useful to identify moisture ingress, honeycomb cell corrosion, and adhesive/composite hydration.

However, this technique requires access to an intense source of low energy neutrons [24]. The currently most feasible source is a non-commercial nuclear reactor. This is an obvious severe limitation even for special investigations, let alone aircraft component NDT.

11.5 Certification of NDT Personnel

The inspection of aerospace components has to be performed by certified personnel as per the approved procedures prepared by qualified experts. The interpretation of NDT results must also be done by experienced certified personnel, since this determines the success or failure of the inspection.

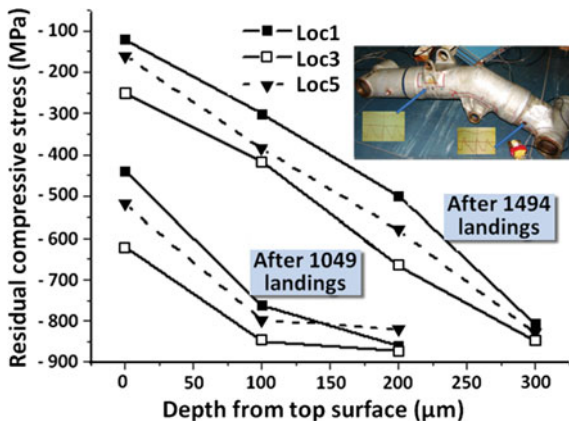
It follows that training and certification of NDT personnel is very important. Professional bodies certify Level-I (operator), Level-II (Engineer), and Level-III (Manager) personnel [25]. A Level-III NDT expert is expected to have the necessary skills and knowledge to select the most appropriate NDT techniques for the problems in hand, train other personnel, prepare and approve the procedure documents, and interpret the applicable codes and standards.

11.6 Recent Advances and Future Trends

There are a number of recent advances in NDE for inspection of aircraft structures. These include the following:

1. Multi-sensor fusion, embedded sensors, and wireless sensor networks [1].
2. Numerical modelling of NDT techniques for optimizing sensors and sensor configurations, as well as for prediction of signals and images from a variety of flaws. 3-D models can now simulate complex geometries such as rivet holes, countersunk rivets heads, layered aluminium structures, and accurately predict responses from flaws orientated and located in unfavourable locations. The models also provide inputs for generating probability of detection (POD) curves and the signals/images for inversion studies. These are aids to minimizing expensive experimental measurements [1].
3. Multi-modality NDE, using multiple sensors, has several advantages over single-modality NDE, including reduction in inspection time, increased reliability, improved defect visualization, and information redundancy. A notable example is improved quantification of corrosion damage using visual, ultrasonic, and thermographic inspections. Eddy current, guided wave ultrasonics, and the 'edge-of-light' technique have been combined to provide comprehensive external surface inspections of pressure cabin skins [26].
4. Service loadings can reduce fatigue-beneficial surface and near-surface compressive stresses in landing gear components. X-ray diffraction (XRD) is useful for measurement of the residual stresses and their reduction, see Fig. 11.7; and also for qualifying shot peening rejuvenation, which restores the compressive stresses to their original levels.

Fig. 11.7 XRD-determined residual stresses in a landing gear component [27]



Future Trends Multi-NDT and multi-sensor techniques hold promise for fast and comprehensive inspection of aerospace components. They are expected to employ image fusion, data fusion, and artificial intelligence techniques for combining the information from different sources for (i) generating a comprehensive image of the inspected regions and (ii) more effective decisions on repair or replacement of components.

Structural health monitoring is gaining importance: see Chap. 22 in this Volume of the Source Books and also Refs. [1, 20]. Sensors such as strain gauges, Fibre Bragg Gratings, piezoelectric sensors, and microwave sensors may be attached or embedded in aircraft structures to provide real-time monitoring of the stress-strain states and detect damage. The data would then be used to continuously update the life assessments and determine whether maintenance intervals should be rescheduled. However, the major challenge is to make the embedded sensors or sensor networks fail-safe.

11.7 An Overview of NDT Techniques

The United States Federal Aviation Administration (FAA) provides an authoritative overview of various NDT techniques and their suitability for aircraft [28]. This overview is given in Table 11.2. Infrared thermography and acoustic emission are not included because the FAA document (an Advisory Circular) is concerned with well-established and proven techniques. However, the Advisory Circular is very useful since it represents mainstream expertise and opinion.

Table 11.2 FAA overview of NDT (NDI) techniques and their advantages and disadvantages [28]

NDI methods	Advantages	Disadvantages
Visual	Inexpensive Highly portable Immediate results Minimum training Minimum part preparation	Surface discontinuities only Generally only large discontinuities Misinterpretation of scratches
Dye penetrant	Portable Inexpensive Sensitive to very small discontinuities 30 min. or less to accomplish Minimum skill required	Locate surface defects only Rough or porous surfaces interfere with test Part preparation required (removal of finishes and sealant, etc.) High degree of cleanliness required Direct visual detection of results required
Magnetic particle	Can be portable Inexpensive Sensitive to small discontinuities Immediate results Moderate skill required Detects surface and subsurface discontinuities Relatively fast	Surface must be accessible Rough surfaces interfere with test Part preparation required (removal of finishes and sealant, etc.) Semi-directional requiring general orientation of field to discontinuity Ferro-magnetic materials only Part must be demagnetized after test
Eddy current	Portable Detects surface and subsurface discontinuities Moderate speed Immediate results Sensitive to small discontinuities Thickness sensitive Can detect many variables	Surface must be accessible to probe Rough surfaces interfere with test Electrically conductive materials Skill and training required Time consuming for large areas
Ultrasonic	Portable Inexpensive Sensitive to very small discontinuities Immediate results Little part preparation Wide range of materials and thickness can be inspected	Surface must be accessible to probe Rough surfaces interfere with test Highly sensitive to sound beam—discontinuity orientation High degree of skill required to set up and interpret Couplant usually required
X-ray radiography	Detects surface and internal flaws Can inspect hidden areas Permanent test record obtained Minimum part preparation	Safety hazard Very expensive (slow process) Highly directional, sensitive to flaw orientation High degree of skill and experience required for exposure and interpretation Depth of discontinuity not indicated
Isotope radiography	Portable Less expensive than X-ray Detects surface and internal flaws Can inspect hidden areas Permanent test record obtained Minimum part preparation	Safety hazard Must conform to Federal and State regulations for handling and use Highly directional, sensitive to flaw orientation High degree of skill and experience required for exposure and interpretation Depth of discontinuity not indicated

11.8 Summary

Non-destructive testing is essential in the aerospace industry, since it plays a safety-critical role deriving from the production process and especially during the service life. A variety of NDT techniques, including visual, penetrant, magnetic particle, eddy current, infrared thermography, acoustic emission, ultrasonics, and radiography, are available, as shown in Tables 11.1 and 11.2.

Looking to the future, eddy current array imaging and phased array ultrasonics will be valuable for reliable detection and sizing of surface as well as subsurface flaws. Multi-modal and multi-sensor approaches with data and image fusion are also showing promise, and the use of structural health monitoring is likely to increase greatly.

The use of composite aircraft structures is also increasing. The most easily used NDT techniques for these materials are shearography and infrared thermography, since they are contactless, relatively fast, and do not require complex sensing systems. Even so, the development of new composite materials will require new ways to inspect them during manufacturing and service.

New and sophisticated NDT technologies will make further demands on the development of inspection procedures and operator training. The primary goals will remain the achievement of high probabilities of detection, faster inspections, and lower inspection costs.

Acknowledgments Special thanks are due to Dr. Baldev Raj, Dr. T. Jayakumar, Dr. R.J.H. Wanhill, and several colleagues from the Nondestructive Evaluation Division, Indra Gandhi Centre for Atomic Research, Kalpakkam, for their valuable suggestions that enabled preparation of this chapter.

References

1. Fahr A (2014) *Aeronautical applications of non-destructive testing*. DEStech Publications Inc., Lancaster, PA 17602-4967, USA
2. Wilson DS, Hagemaijer DJ (1999) ABCs of NDT development and adoption for aging aircraft. *Mater Eval* 57(3):336–346
3. Raj B (2001) Nondestructive testing and evaluation: overview. In: Buschow KH et al (eds) *Encyclopedia of materials: Science & technology*. Elsevier Science Publishers, Amsterdam, The Netherlands, pp 6177–6185
4. Raj B, Thavasimuthu M, Jayakumar T (2014) *Practical non-destructive testing*, 3rd edn. Narosa Publishing House, New Delhi, India
5. Baldev Raj T, Jayakumar T, Rao BPC (1995) Review of NDT techniques for structural integrity. *Sadhana Ind Acad Proc Eng Sci* 20:5–38
6. Matzkanin GA (2006) Selecting a nondestructive testing method: Visual inspection. *AMMTIAC Q* 1(3):7–10 (Advanced Materials, Manufacturing, and Testing Information Analysis Center)
7. Hull B, John V (1988) *Non-destructive testing*. Macmillan Education Ltd., London, UK
8. Bray DE, McBride D (1992) *Nondestructive testing techniques*. In: *Ultrasonic testing of aerospace materials*. John Wiley & Sons, Inc., Hoboken, NJ 07030-5774, USA

9. Rao BPC (2012) Magnetic flux leakage technique: basics. *J Non Destr Test Eval* 11(3):7–17
10. Rao BPC (2009) Practical eddy current testing. Narosa Publishing House, New Delhi, India
11. Smith RA (1995) Non-destructive evaluation for corrosion in aging aircraft. 1: introduction, ultrasonic and eddy current methods. *Insight Non-Destr Test Cond Monit* 37(10):798–807
12. Sasi B, Rao BPC, Jayakumar T, Raj Baldev (2009) Development of eddy current test procedure for non-destructive detection of fatigue cracks and corrosion in rivets of air-intake structures. *Defence Sci J* 59(2):106–112
13. Thirunavukkarasu S, Rao BPC, Jayakumar T, Narayanankutty N, Prabhakaran PV (2011) Eddy current methodology for nondestructive assessment of thickness of silicon carbide coating on carbon-carbon composites. *J Aerosp Sci Technol* 63(3):223–229
14. Lepine BA, Wallace BP, Forsyth DS, Wyglinski A (1999) Pulsed eddy current method developments for hidden corrosion detection in aircraft structures. *NDT.net* 4(1)
15. Brassard M, Chahbaz A, Pelletier, A, Forsyth DS (2000) Combined NDT inspection techniques for corrosion detection of aircraft structures. In: Proceedings of the 15th world conference on nondestructive testing, Rome, 15–21 Oct 2000. <http://www.ndt.net/article/wcndt00/papers/idn534/idn534.htm>
16. Thome DK, Fitzpatrick GL, Skaugset RL (1996) Aircraft corrosion and crack inspection using advanced MOI technology. In: Non-destructive evaluation of aging aircraft, airports, and aerospace hardware, SPIE Proceedings, vol 2945, pp 365–373
17. Ibarra-Castanedo C, Genest M, Servais P, Maldague XPV, Bendada A (2007) Qualitative and quantitative assessment of aerospace structures by pulsed thermography. *Non-destr Test Eval* 22:199–215
18. Heida JH, Platenkamp DJ (2011) Evaluation of non-destructive inspection methods for composite aerospace structures. In: 6th NDT in progress 2011, international workshop of NDT experts, Prague, 10–12 Oct 2011
19. Fahr A, Genest M, Brothers M, Rutledge R (2009) A comparison of pulsed thermography and ultrasonic C-scanning for inspection of aircraft composite structures. NRC Report CPR-SMPL-2009-0003, National Research Council, Ottawa, Ontario, Canada
20. Chang F-K (ed) (2013) Structural health monitoring 2013: a roadmap to intelligent structures. DEStech Publications Inc., Lancaster, PA 17602-4967, USA
21. Green RE (1991) Ultrasonic testing, Sect. 3, Part 5. In: Birks AS, Green Jr. RE, McIntire P (eds) *Nondestructive Testing Handbook*, 2nd ed, vol 7. American Society for Nondestructive Testing, Columbus, OH 43228, USA
22. Brotherhood CJ, Drinkwater BW, Freemantle RJ (2003) An ultrasonic wheel-array sensor and its application to aerospace structures. *Insight Non-Destr Test Cond Monit* 45(11):729–734
23. Chapman CE, Marincak A (1996) Corrosion detection and thickness mapping of aging aircraft lap joint specimens using conventional radiographic techniques and digital imaging. NRC Report LTR-SMPL-1996-0067, National Research Council, Ottawa, Ontario, Canada
24. Lewis WJ, Bennett LGI (1999) The use of neutron radiography in the inspection of aircraft composite flight control surfaces. *NDT.net* 4(1)
25. American Society for Nondestructive Testing (1988) Recommended practice No. SNT-TC-1A, personnel qualification and certification in nondestructive testing. American Society for Nondestructive Testing, Columbus, OH 43228, USA
26. Forsyth DS, Komorowski JP (2000) The role of data fusion in NDE for aging aircraft. In: *Non-destructive evaluation of aging aircraft, airports, and aerospace hardware IV*, SPIE Proceedings, vol 3994, pp 47–58
27. Raj Baldev, Jayakumar T, Mahadevan S, Rai SK (2009) X-ray diffraction based residual stress measurements for assessment of fatigue damage and rejuvenation process for undercarriages of aircrafts. *J Nondestr Eval* 28:157–162
28. Federal Aviation Administration (1998) Acceptable methods, techniques, and practices—Aircraft inspection and repair. Advisory Circular FAA AC 43.13-1B, U.S. Department of Transportation, Washington, DC, USA

Part III
Structural Design

Chapter 12

Design of Aircraft Structures: An Overview

S. Kamle, R. Kitey, P.M. Mohite, C.S. Upadhyay, C. Venkatesan
and D. Yadav

Abstract This chapter presents some of the important aspects in the design and analysis of aircraft structures. These important aspects are related to material selection, structural configuration, loads evaluation, static strength and deflection estimation, static stability evaluation, fatigue and fracture effects, aeroelastic considerations, and influence of dynamic loadings. The key aspects in specific areas are combined to provide an overall perspective of aircraft structural design and analysis. It must be noted that manufacturing and ground and flight testing are integral parts of the whole process of design, but these aspects are not addressed here.

Keywords Aircraft structures · Material properties · Stiffened shells · Buckling · Landing gear

12.1 Introduction

For the design of aircraft structures, expertise is required in four broad areas, namely structural analysis, design including configuration and material selection, manufacturing (including assembly and testing), and flight testing. For the success of a vehicle additional aspects such as cost, operational and maintenance issues, environmental impact, safety, and comfort will need to be included. In this chapter, we set forth a broad perspective of aircraft structural design, based on the authors' individual expertise and knowledge.

In general, aircraft structural design is driven by two design philosophies, namely fail-safe design and safe-life design. Fail-safe design (denoted also as damage tolerant design) ensures that between two consecutive inspection intervals the overall structural integrity and function are not affected by failure or damage in some part of the structure. When failure or damage is detected, the aircraft is repaired and validated for continued service.

S. Kamle · R. Kitey · P.M. Mohite · C.S. Upadhyay · C. Venkatesan (✉) · D. Yadav
Department of Aerospace Engineering, Indian Institute of Technology, Kanpur, India
e-mail: cven@iitk.ac.in

Safe-life design implies that the structure and its components will function without any failure during the prescribed lifetimes for the components. Upon reaching the prescribed lifetime, it is the intention that a component or components is/are replaced or that the aircraft is retired from service. In practice, it may be feasible to justify extension of the service life, and this is sometimes done.

In the following, some important aspects of aircraft structural design and analysis are presented.

12.2 Major Structural Components of an Aircraft

The typical functions of a structural component are primarily to resist and transmit the forces that it experiences. However, in aerospace applications the structure as a whole also has to provide aerodynamic shape and enclose, as well as protect, the passengers and payloads. Furthermore, it is essential that the overall structure is lightweight. The most efficient structure that satisfies these functional requirements will have the material weight located towards the outer surface of the vehicle. Thus the resulting structures consist mainly of thin plates and shells with the ability to maintain their cross-sectional shape. Shell structures without stiffening members are known as *monocoque*. However, thin monocoque shells can be only lightly loaded. More efficient, high-load-bearing structures need the addition of stiffening members: these structures are known as *semi-monocoque*.

In general, aerospace vehicle structural components are subjected to bending, compression, shear and torsion loadings. A monocoque may have to resist all these loads. Therefore it must have relatively high thickness. In this regard, a semi-monocoque structure is more efficient since some of the loads are carried by the stiffening members. In such structures a relatively thin covering shell or skin with stiffening members is used. Further, the stiffening members also carry the concentrated loads that may be applied to the structure via major joints, struts, engine mounts, stores, etc.

12.2.1 *Semi-monocoque Structures*

Typical semi-monocoque structures are shown in Fig. 12.1. For body (fuselage) structures the longitudinal stringers (stiffeners) stiffen the structures, while the transverse frames are the elements that maintain the cross-sectional shapes. If frames cover all or most of the cross-sectional area, then they are called bulkheads.

For aerodynamic or control surface structures, i.e. the wings, empennage (the tailplane elements), and canards (control surfaces forward of the wings), the spars are the main longitudinal members. Spars generally have an I-shaped cross-section and are attached rigidly to the body structure. There can be one or more spars,

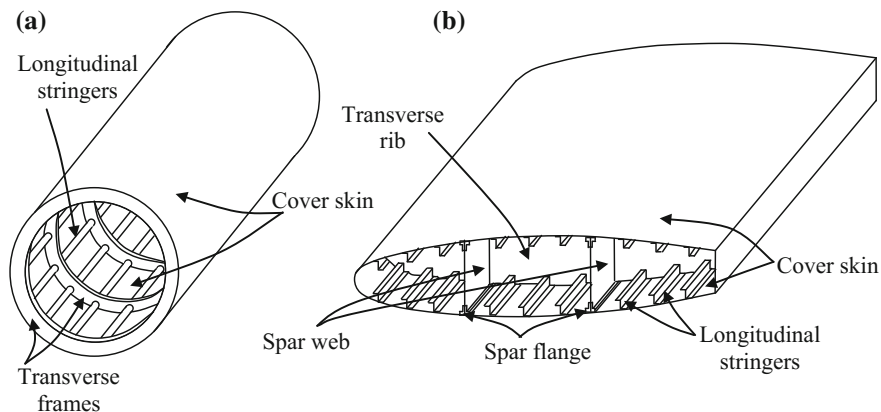


Fig. 12.1 Typical semi-monocoque structures: **a** body (fuselage) structure and **b** aerodynamic surface (wing and empennage) structures

depending upon the size and type of the vehicle, the lifting forces to be generated, and the design philosophy: more than one spar is a fail-safe necessity.

The spars are joined to the cover skins by spar caps, and they are also attached to transverse members called ribs (not shown in Fig. 12.1). Additional stiffening of the cover skins is provided by longitudinal stringers.

12.2.2 *Functions of Semi-monocoque Structural Components*

In semi-monocoque structures the skin or cover transmits the aerodynamic loads to longitudinal and transverse members, and it resists torsional moments by developing shear stresses. Together with longitudinal stiffeners the skin resists bending and axial loads; and with transverse members the fuselage skin takes the hoop stress.

The longitudinal stiffeners also increase the skin's resistance to buckling and failure stresses, by dividing it into small panels. The transverse members maintain the cross-sectional shape. They increase the buckling resistance of the longitudinal stiffeners and the skins by providing lengthwise constraint (stiffeners) and edge restraint (skins). More details are given in Refs. [1–3].

The demand for lightweight structures constrains the allowable factors of safety, particularly for high-performance aircraft. Besides strength and general damage tolerance, aircraft structures must also be resistant to degradation from fatigue, corrosion, and stress corrosion; and for elevated temperature applications the materials must be resistant to creep and thermal instability. All these requirements necessitate the careful selection of materials. In the following Section, we look at the issue of materials selection for contemporary aircraft.

12.3 Materials for Aircraft Applications

Current developments in aircraft technology are geared towards two distinct goals. Military aircraft are designed with emphasis on performance (manoeuvrability, endurance, speed, altitude, payload, landing/take-off distance), while civil transport aircraft are designed for high safety, fuel economy at cruise altitudes, compliance with environmental regulations, and other concerns. However, both categories of aircraft need materials which minimize structural weight without compromising on strength and damage tolerance properties.

Aluminium alloys have established their use in civilian and military airframes since their introduction in the early part of the twentieth century. In the 1950s titanium alloys came into use for some airframe applications in high-performance aircraft and later for civil aircraft. Since the 1970s significant developments in composite material fabrication, mainly carbon fibre-reinforced plastic (CFRP), and the understanding of composite structures have enabled their increasing use as structural materials.

Other materials for more specific applications, as in landing gear and fluid systems, include high-strength low-alloy steels and stainless steels. Engine materials form a separate category: they include titanium alloys, specialist steels, and nickel-base superalloys.

The single most important criterion in material selection is weight. Ensuring structural integrity and meeting functional requirements also require consideration of factors such as strength, stiffness, fatigue, corrosion resistance, impact resistance and fracture toughness, and elevated temperature performance.

Strength and Stiffness The typical semi-monocoque airframe construction requires materials with high *specific* strength and stiffness, i.e. strength and stiffness factored for the material density. *Unidirectional* CFRP composites achieve much higher specific strengths and stiffnesses than metallic alloys, but the need for multiaxially aligned fibres to carry loads in more than one direction can reduce the CFRP efficiencies by more than 50 % for the specific stiffness and up to 30 % for the buckling resistance: see Sect. 14.4.1 in Chap. 14 of Volume 1 of these Source Books.

All-composite joints subjected to multiaxial stresses also tend to fail at unpredictably low static loads, as occurred during a full-scale test of the Boeing 787 all-CFRP wing box.

Fatigue and Fracture Toughness Aircraft components undergoing cyclic loading are subject to failure by fatigue. In general, the alloys used are in heat treatment conditions that optimize the fatigue resistance and fracture toughness in order to achieve damage tolerance. There are exceptions, notably high-strength steels in landing gears.

CFRP composites offer potentially high fatigue strengths, but they are susceptible to impacts and subsequent associated fatigue damage that is difficult to detect and repair. These issues are also discussed in Chap. 14 of Volume 1.

Corrosion Resistance Corrosion and stress corrosion resistance are particularly important for aluminium alloys and high-strength steels. In modern aircraft aluminium alloys are usually used in heat treatment (temper) conditions that trade strength for better stress corrosion properties. This is also true for precipitation hardening stainless steels. All high-strength low-alloy steels are highly susceptible to corrosion and stress corrosion and require protection by plating and coating with robust paint systems.

Elevated Temperatures Aluminium airframe alloys may be used up to a surface temperature of about 130 °C. Further increase in temperature rapidly decreases the alloys' creep resistance. High-strength low-alloy steels are not suitable for elevated temperature applications. However, titanium alloys may be used as airframe materials up to 500 °C, although the most commonly used alloy, Ti-6Al-4V, loses creep resistance above 300 °C. Specialist steels in aircraft engines can be used up to 400–450 °C, and creep-resistant titanium alloys can be used up to about 650 °C. Higher temperatures are the province of nickel- and cobalt-base superalloys.

Other Considerations

1. **Production costs.** Although material costs differ greatly, the total costs depend on the production and assembly of components. Metallic airframe components have the advantages that the manufacturing equipment is already available and that their fabrication is well understood. CFRP and other composites present several manufacturing challenges, although with sufficient investment and experience the production costs should become competitive. *It must be noted here that there is no 'either-or' problem.* Both metallic materials and composites are now established in military and civil aviation, and there is an increasing tendency to design and build hybrid structures.
2. **Computational fluid dynamics influences.** For civil aircraft the developments in computational fluid dynamics (CFD) techniques have led to design of better airfoils and the possibilities of improved fuel efficiency by maintaining close dimensional tolerances. This impacts on the selection of external coatings and surface finish.

For military aircraft, the CFD developments relate to the application of radar absorbent coatings (a key element in stealth warfare) and selection of structures and coatings providing good thermal protection. In this latter case CFD is combined with the thermal properties in an iterative process for optimum material selections.

12.3.1 Experimental Methods for Material Characterization

Testing is imperative for determining the relevant properties of materials for design purposes. Coupon and component-level tests have to be designed and implemented

to determine stiffness, strength, fracture, and damage characteristics of materials—possibly subjected to different ambient environmental conditions. The anisotropic nature of most of the non-conventional materials such as composites and multi-functional smart materials has significantly increased the material parameters which are required to model the mechanical behaviour of materials. For example, the elastic response of an orthotropic laminate cannot be completely described unless nine elastic constants are known, whereas the mechanical behaviour of an isotropic material can be modelled by defining just two elastic constants. Here we discuss some of the test methodologies used to measure the mechanical properties of aerospace materials.

Uniaxial tension and compression tests provide strength, stiffness, and yielding parameters of metallic materials [4, 5], polymers [6, 7], and polymer composites [8, 9]. Additionally, Poisson's ratio can be obtained by measuring strains perpendicular to the loading direction on the test specimens. Usually, universal testing machines (UTMs) are employed to record the synchronized load and deformation data with or without external strain measuring devices. The test standards are also well defined to study the flexural [10, 11] response of metallic and polymeric materials. However, the choice of test methodology for obtaining shear properties [12–15] depends upon the material's degree of non-homogeneity and anisotropy, geometry, and its service application.

Classical Failure Theories The strength parameters obtained from experimental measurements are used in classical failure theories. Predictions in regard to yielding (in ductile materials) or fracture (in brittle materials) are made by employing stress-based failure criteria. For isotropic materials the maximum normal stress (Rankine) theory, maximum shear stress (Tresca) theory, and distortion energy (von Mises) theory are commonly used. Several criteria have been proposed to predict failure in fibre-reinforced composites as well; most of them are modified classical failure theories and are based on the stresses along a laminate's material axes. The Tsai–Hill [16] and Tsai–Wu [17] failure criteria are among the ones that are used often in the design process for composites.

The classical failure theories for metals predict failure to a reasonable accuracy when the stress field is relatively uniform. Even for cases when the stress gradients are moderately higher, such as around a smooth cut-out or near a smooth corner, they can be adopted following stress analysis by the theory of elasticity approach.

However, the classical theories fail to provide a realistic solution around the zones of extreme stress gradient typically developed due to sharp discontinuities, cracks, microvoids or processing defects. For these situations recourse must be made to *fracture mechanics*. Other limitations of most classical theories are that they do not take into account the factors such as strain rate and temperature.

Fracture Mechanics In general, linear elastic fracture mechanics (LEFM) is sufficient for analysing high-strength metallic aerospace structures that may or do contain cracks or flaws. The well-known stress intensity factor (K) approach is

generally used for both static and dynamic (fatigue) loading conditions. Critical values of K for quasi-static fracture are referred to as fracture toughness values.

The test methods to characterize the fracture toughness of *macroscopically* brittle (limited ductility) materials subjected to quasi-static loading is described in ASTM Standard E399 for plane-strain (thick section) conditions and in ASTM Standard E561-05 for mixed plane-strain/plane-stress and full plane-stress conditions. Similarly, ASTM Standard E647 has been developed for fatigue crack growth testing under nominal LEFM conditions. The geometric effects on stress intensity factors have been compiled in several handbooks [18–20].

Following the description of materials and tests (and theories) required to characterize the materials, the discussion will now shift back to aircraft structures. Engineering analysis uses appropriate idealizations of structures, in order to make the analysis simple. Aircraft structures, being thin, are amenable to such idealizations, which greatly simplify the analyses without much penalty on the accuracy of the predictions. The standard idealizations used in a first (preliminary) analysis of the structure are described below.

12.4 Idealization of Thin Stiffened Shell Aerospace Structures

12.4.1 Idealization of Structures

The analysis of structures like those shown in Fig. 12.1 is quite involved and tedious. Hence to make analysis manageable some simplifying assumptions must be made. However, the number and nature of assumptions affect the accuracy as well as the complexity of the analysis. For the preliminary design procedure the speed and simplicity are of greater concern than the accuracy, and for the final solution the accuracy must approximate to that of the actual structure.

The model which results after making simplifying assumptions is idealized as a ‘mechanical model’. It is possible that one can have different idealized models to simulate actual behaviour under different loading systems. Thus in making these simplifying assumptions there is a loss of detail of the structure as well as the stress distributions in it. In general, when idealizing a structure the elastic characteristics such as area, moment of inertia, and shear centre of the idealized structure must be the same as for the original structure. The other criteria having equivalence in actual and idealized structures can be force and compatibility criteria.

The simplifying assumptions are based on the facts observed for the actual structure. The stringer and spar flanges carry most of the direct stress, whereas the skin and spar webs are effective in resisting shear. Further, stringer and spar flanges have small cross-sectional areas as compared to the overall area of the structure. Therefore the variation of direct stress over the flanges can be considered constant.

And lastly, the skin and spar webs can be considered to carry only shear stresses, which are assumed to be uniform since these components are thin.

Figure 12.2 shows the idealization of a skin panel and a spar. For the skin panel (Fig. 12.2a), the conservation of area and moment of inertia about the neutral axis (NA) has been achieved in the idealized structure. It also shows the position of the effective longitudinals (O), which resist the direct stress only, to maintain the moment of inertia. In this idealized structure the skin is also effective in resisting the shear. One can idealize the skin to have more effective longitudinals for better accuracy. However, their positions to conserve the moment of inertia will need to be different from the positions as shown in the example.

Figure 12.2b shows the idealization of a spar section. The effective longitudinals are positioned at the respective neutral axes of the top and bottom web flanges of the individual structure. The position of the neutral axis of the effective structure is maintained the same as that of the actual structure. However, the effective areas of these longitudinals are different than the areas of actual structure: therefore the neutral axis loses its physical meaning. Further, the analysis of the idealized structure gives only the average shear flow in the effective web. The parabolic variation of the actual shear flow is lost in this idealization process.

In idealized structures the stiffeners are represented by circles called *booms*, which have a concentrated mass in the plane of the skin. Since the difference between the distances of the centroids of the stringer and the adjacent skin from the wing axis is very small, the stringers and spar flanges are replaced by booms located at the mid-line of the adjacent skin. The direct stresses are calculated at the centroids of these booms. Further, the direct stress carrying capability of the skin is represented as an addition to existing booms or as additional separate booms. However, for simplicity and faster analysis the number of effective longitudinals or booms is generally kept to a minimum number in the idealized structure.

When the idealization is made the functional requirements for the structural components (as mentioned above) can be simplified. These are listed below.

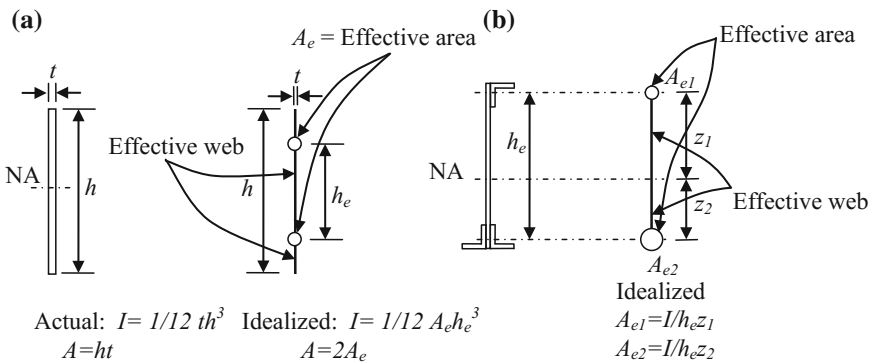


Fig. 12.2 Idealized a skin and b spar

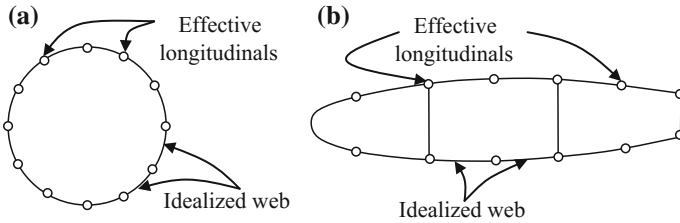


Fig. 12.3 Idealized **a** body and **b** aerodynamic surface structures

1. The longitudinal stiffeners and spar flanges carry only axial stresses.
2. The web, skin, and spar webs carry only shear stresses.
3. The axial stress is constant over the cross-section of each longitudinal stiffener.
4. The shear stress is uniform through the thickness of the webs.
5. Transverse frames and ribs are rigid within their own planes and have no rigidity normal to their plane.

The structures shown in Fig. 12.1 are shown idealized in Fig. 12.3. In general, the fewer the number of longitudinals, the simpler is the analysis. Further, one can lump many longitudinals into a single effective longitudinal for faster analysis. However, for monocoques the structure is idealized into a stiffened shell even if there are no stiffeners. The wall or the skin area is lumped as longitudinals, and the skin between the longitudinals is considered to be effective only in shear.

In thin structures failure may not necessarily be due to tensile, yield, or damage-induced fracture. Instead the loss of form due to compression and shear may be a cause of concern, especially if it occurs at load values that are significantly smaller compared to the failure loads of the material. Therefore the static design of aircraft structures should have a check for form- or buckling-related failures.

12.4.2 Buckling in Aerospace Structures: Design Motivation

The primary aerospace structures, i.e. the fuselage, wings and control surfaces, are thin stiffened structures. The primary building blocks (see Fig. 12.1) are the outer skin, spars, transverse members (frames and ribs), and longitudinal members (longerons, stiffeners, stringers). Each structural building block has a specific role to play. Hence it is prudent to understand the primary loads acting on each of the structural members.

We will focus on the wing structure, with the intention of explaining the role of each load-bearing structural member and the consequent design considerations. In order to understand the loads, look at Fig. 12.4. The resultant lift and drag forces

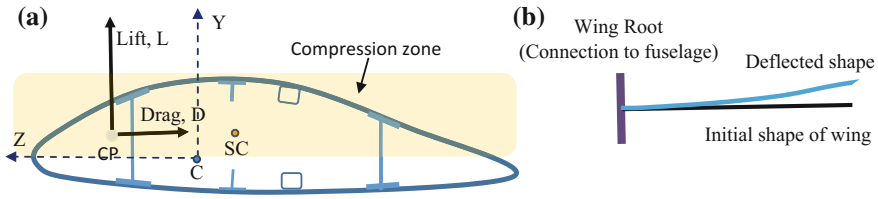


Fig. 12.4 **a** Sectional aerodynamic lift (L) and drag (D), acting at the centre of pressure (CP). The (modulus weighted) centroid of the section is at C , and the shear centre of the section is at SC ; **b** the wing semi-span, with fixed or rigid support at the root and the initial shape and deflected shape due to the bending and twisting loads

about the centre of pressure (CP) of the section give rise to a shear force and twisting (torsional) moment about the shear centre of the section.

It is clear from the loads acting on the cross-section that the following scenarios occur:

1. For the part of the wing structure that has coordinate $y > 0$, the axial stress due to lift-induced bending is $\sigma_{xx} \leq 0$. Hence this part of the wing structure experiences compressive axial stress.

Since the lift is generally much higher than the drag ($L/D \geq 7$), we will ignore the drag contribution to the bending loads for the wing.

2. The part of the wing structure that has coordinate $y < 0$ has an axial stress due to lift-induced bending $\sigma_{xx} \geq 0$. This part of the wing experiences tensile axial stress.
3. The skin experiences significant shear due to the torsional effect.
4. The spar web also experiences significant shear stress due to bending and torsional effects.

12.4.3 Role of the Frames, Spars, and Ribs

The frames, spars, and ribs are relatively more rigid structural elements. They keep the aerodynamic shape of the structure intact and also provide rigidity to the structure—preventing large bending or torsional displacements. The spars, together with the skin, create closed multicelled sections, thus increasing the torsional rigidity of the section tremendously.

Since these structural elements are more rigid, they are considered as length delimiters; i.e. the connections of the skin or the longitudinal elements to the spar or the rib can be assumed to be simple supports for the part of the structure within (see Fig. 12.5). Normally, ribs are separated by 300–400 mm, while the leading edge spar is located at $0.3C$ and the trailing edge spar at $0.7C$ (C is the local chord length).

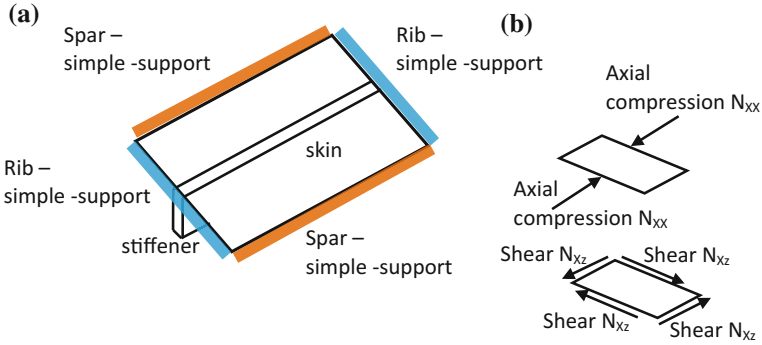


Fig. 12.5 a Stiffened skin structure and b axial and shear loads on the skin structure

Case (a): Buckling of Stiffeners Under Compressive Axial Loads Consider a column subjected to an end compressive axial load P . The column will compress initially as P is increased until it reaches the value of P_{cr} , at which point significant bending deformation will be observed. In order to find the value of this P_{cr} , several approaches can be used. The most accurate will be using the nonlinear analysis of the beam subjected to an increasing value of P , but the analysis requires finite elasticity formulation of the problem. A simplification of the approach is based on the perturbation about an equilibrium position, i.e. by assuming that the beam compresses until the critical value of the load, P_{cr} , and then it develops significant bending deformation. This formulation is based on equilibrium in the deformed (assumed bent) configuration and gives the buckling load

$$P_{cr} = \frac{c EI_{zz}}{L^2},$$

where c is a factor depending on the boundary conditions.

Case (b): Bending-Torsion Buckling of Open-Sectioned Stiffeners For open sections this may not be the lowest buckling load, and the buckled configuration may correspond to a coupled bent and twisted deformed configuration. The detailed analysis of such a section can be obtained from Ref. [1].

Note that the coupled effect is due to the sectional warping and occurs primarily because the torsional rigidity of an open section is very low. For a closed cross-section, on the other hand, the bending-torsion effect will not occur, and the buckling modes will be primarily bending-dominated, since the torsional rigidity will be very high.

Case (c): Buckling of Thin Plate-Like and Stiffened Plate-Like Structures The skin and the spar web are not beam-like elements, but are plate (or shell) elements. These components may buckle not only due to the compressive normal loads but also due to a shear load. This is because the state of pure shear (in a plane-stress problem) leads to two principal stresses that are equal but of opposite signs, i.e.

$\sigma_1 = -\tau_{xy}$; $\sigma_2 = +\tau_{xy}$. The principal stresses are oriented at $\pm 45^\circ$ to the x - y coordinate axes. Hence one sees the buckled profile along a diagonal of a square plate.

Plate buckling analysis can again be done using the perturbation analysis, or via the linearized eigenvalue problem. It should be carefully noted that in this case the in-plane resultant forces may not be constant, and the in-plane problems have to be solved to obtain the spatial distribution of the resultant forces (obtained by in-plane stress multiplied by the thickness of the plate) [21]. In the classical solutions for buckling of plates, the plate is assumed to be unconstrained in-plane, hence leading to constant values of the in-plane forces given by the values applied on the boundary. This is a conservative estimate and leads to lower predicted values of the buckling loads—which is safe from a design viewpoint.

The effect of in-plane constraint is shown in Fig. 12.6, which depicts higher buckling loads if the plate also has simple support in-plane (i.e. the normal in-plane displacement is also fixed along a boundary edge on the unloaded edges).

Again, the buckling load of the skin is typically much smaller than that of a stiffener, and the stiffener is selected such that the buckled mode shape for the skin changes, i.e. the stiffener acts as a simple support. The effect of the stiffener can be seen for the simply supported square plate as follows:

Buckling load for unstiffened plate:

$$N_{xx}^{cr(US)} = \frac{4\pi^2 D}{a^2}$$

Buckling load for plate with axially placed stiffener along the centreline of the plate:

$$N_{xx}^{cr} \approx \frac{\frac{4\pi^2 D}{a^2} + \frac{2\pi^2 E_s I_{yy,s}}{a^3}}{1 + \frac{2A_s}{h \cdot a}} > N_{xx}^{cr(US)}$$

with A_s = stiffener cross-sectional area and $I_{yy,s}$ = stiffener moment of inertia.

Obviously, the location of the stiffener plays an important role in increasing the buckling load. Here the stiffener was placed along the line of maximum bending stress, and hence the effect is maximally seen. If, however, the stiffener is placed perpendicular to the loading direction, then a negligible effect of the stiffener will be felt. Hence optimal location of the stiffener depends on the loading type, direction, and the material used, i.e. for an angle-ply composite laminate the stiffener location will be completely different from that for a cross-ply laminate.

Similarly, for thicker plates buckling may happen post-yielding, and hence the design will be driven by yield (or material failure). The buckling loads for thicker plates can be obtained in terms of those for a thin plate by using an appropriate plastic correction factor [2]. A similar factor can be used for composite laminates.

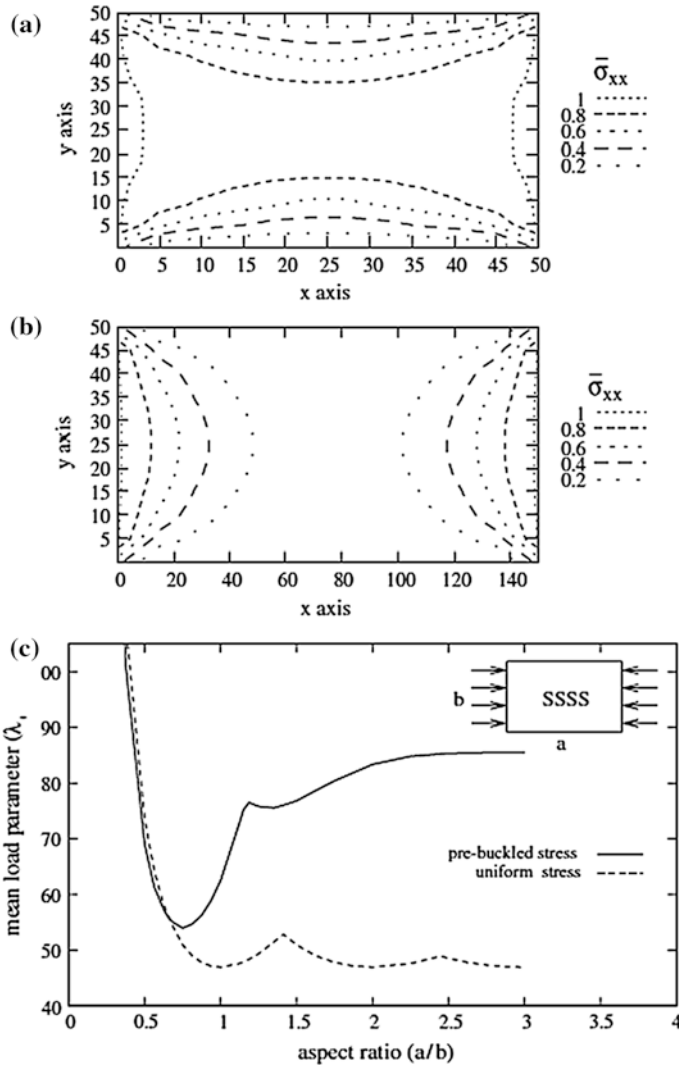


Fig. 12.6 **a** In-plane stress distribution for an isotropic plate with $a/b = 1$ and all edges simply supported, **b** In-plane stress distribution for an isotropic plate with $a/b = 3$ and all edges simply supported, **c** The variation of buckling load (parameter λ_{cr}^0) as a function of aspect ratio for a simply supported plate using the unconstrained (uniform stress) or simply supported in-plane problems [2]

Note on Buckling of Composite Laminates For laminated plates, especially in case of angle-ply, simple von Karman nonlinearity (i.e. the dominant nonlinear term is due to the transverse deflection) cannot be used [22]. Instead all the nonlinear terms should be used. Furthermore, the prebuckled in-plane state of stress (which could

also have nonzero transverse deflection) has to be solved for the buckling analysis to be accurate. Often, a full nonlinear analysis is preferable to find the limit point characterizing the buckling point. Post-buckling analysis may be fruitful for laminates, since the load-carrying capability may degrade less.

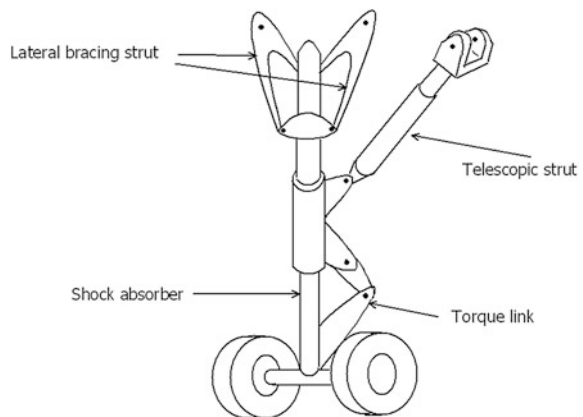
The discussion up to this point focussed on static analysis, i.e. dynamic response was not accounted for in the analysis. The effects of impact and time-varying loads (especially in coupled aerodynamics—structural analysis studies) have to be accounted for when designing structural components. The following sections deal with dynamic analysis based design of landing gears and aeroelastic considerations for lifting and control surface design (e.g. wings and ailerons).

12.4.4 Aircraft Landing Gear Design

Landing gears (undercarriage) are obviously essential subsystems of an aircraft. Their detailed design is taken up early in the aircraft design phase [21, 23–26]. The landing gear in an aircraft provides a suspension system during the ground runs of taxi, take-off, and landing. It is designed to absorb and dissipate the kinetic energy of landing impact, thereby reducing the impact loads transmitted to the airframe. Also, an aircraft oscillates due to the random track unevenness during its ground run. The landing gear design has to keep the oscillations within acceptable limits. The landing gear also houses the wheel braking devices and provides directional control of the aircraft on the ground, using a wheel steering system. The gear is retractable (except in some light aircraft) to minimize the aerodynamic drag on the aircraft while flying. A typical landing gear is shown in Fig. 12.7.

The landing gear design takes into account various requirements of strength, stability, stiffness, ground clearance, and damping under all possible ground attitudes of the aircraft. These requirements are stipulated by the airworthiness

Fig. 12.7 Schematic of a landing gear



regulations to meet operational needs and safety. The gear should occupy minimum volume in order to reduce the stowage space requirement in the aircraft. Further, it should be light in weight to reduce the weight penalty on the aircraft. The service life should be equal to that of the aircraft.

Stages of Landing Gear Design The concept design starts with the study of all design specifications and airworthiness regulations. A concept is then evolved while meeting the functional and regulatory requirements. The landing gear location is worked out, and the type of landing gear is selected. The landing gear geometry is defined. The ground loads are estimated for material selection and preliminary sizing of components. In this preliminary design phase, dynamic simulations are carried out for landing, take-off, and taxi runs on a typical rough runway [27–30]. Retraction kinematics data required for sizing of components are also developed. The initial estimate of the landing loads and shock strut stroke can be made as follows.

The vertical kinetic energy (K.E.) per element = $Wv^2/2g$,
where W is the aircraft weight per landing element.

This energy is stored in the spring and then dissipated over time by the damping (by changing the work into heat). The energy storage/absorption efficiency $n = \text{actual energy stored}/LS$, where L is the load on the landing gear and S is the stroke length. Therefore

$$nLS = Wv^2/2g$$

To keep the stroke length low, L may have to be large. Let the load ratio or load factor be defined as $N = L/W$. This may be between 2 and 5 in practice. Thus,

$$nNS = v^2/2g$$

This relation helps estimate the initial compression in the shock strut. For example, if $N = 3$, $n = 0.6$, $v = 12$ ft/s, then $S \cong 15$ in. This gives an upper bound.

Digital modelling and analysis are used for the landing gear stress analysis. Landing gears are designed as safe-life structures, and low cycle fatigue analysis methods are used for life prediction. This helps in preliminary estimation of impact loads and taxi loads to arrive at the sizing of the landing gear elements for use in geometric modelling and kinematic analysis. The retraction/extension kinematics and actuation are also simulated by dynamic modelling of the hydraulic actuation to arrive at the actuator sizing. The digital analysis is used to arrive at the aerodynamic loads acting on the landing gear during the retraction/extension process.

In the detailed phase, design of all the landing gear components is performed depending on the estimated loads, the size is finalized, and the materials are selected. Dynamic analysis and simulation are carried out to fine-tune certain design parameters for impact energy absorption, taxi and take-off dynamics, shimmy suppression, and retraction/extension. These simulations help in handling a large number of studies in a short time and take into account the hydraulic damping, air

spring characteristics and friction effects, and structural flexibility in the landing gear. Using the computer models developed for this purpose the shock absorber parameters are optimized to maximize the shock absorber efficiency and peak reaction behaviour.

Shimmy oscillations are a perennial problem in design and operation of landing gears, and proper analysis is required to control it. Adequate torsional stiffness and damping are required to ensure a shimmy-free landing gear. Mathematical models are used to predict the onset of shimmy and to design damping devices to control the shimmy oscillations.

Platform drop tests are conducted on rigs to verify shock absorber performance. For structural strength tests of the landing gear, loads are applied through loading actuators in the required directions, and strain data are acquired. Fatigue tests are conducted by block-wise loading via actuators at various amplitudes, simulating loading conditions during service.

The final integration tests of the landing gear are carried out after installation on the aircraft, followed by taxi tests, braking, and steering tests. Fine-tuning of design parameters are done during this phase. This is followed by flight testing in the take-off and landing phases where the full capability of the landing gear is evaluated.

In-service evaluation includes operation under various types of airfield conditions and ambient conditions.

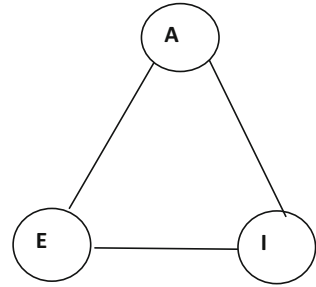
Trade-off studies of strength, stiffness, and costs are needed to finalize the choice of material for a landing gear component. Fatigue and fracture toughness, protection against stress corrosion, wear resistance, reliability in service, etc., are other considerations in the selection of materials.

12.5 Aeroelastic Considerations

Since the successful Wright brothers flight at Kitty Hawk and the failure of Samuel Langley's Aerodrome, the field of aeroelasticity has emerged as an important aspect of design acceptance and airworthiness of aerospace structures. The aeroelastic considerations from Airworthiness Standard FAR 25.629 are quoted in the following to highlight the importance of aeroelastic analysis. FAR 25.629 states that 'The aeroelastic stability evaluations required under this section include flutter, divergence, control reversal and any undue loss of stability and control as a result of structural deformation. The aeroelastic evaluation must include whirl modes associated with any propeller or rotating device that contributes significant dynamic forces. Compliance with this section must be shown by analyses, wind tunnel tests, ground vibration tests, flight tests, or other means found necessary by the Administrator'.

Aeroelasticity is defined as the study of physical phenomena involving the interaction among inertial, elastic, and aerodynamic forces. The influence of this interaction basically creates stability and control problems for the aircraft. If the

Fig. 12.8 Collar triangle [31, 32]



structure were perfectly rigid, there would not be any aeroelastic problem. However, lightweight design means that aerospace structures are also flexible. This structural flexibility is the root cause of various aeroelastic problems. Since structural deformations are caused by aerodynamic and inertia loads acting on the structure, for any aeroelastic analysis one should have good knowledge of the aerodynamics (both steady and unsteady) of lifting surfaces. It is important to recognize that an expert aeroelastician has to be highly knowledgeable about aerospace structures, structural dynamics, unsteady aerodynamics, and control theory (in the case of aero-servo-elasticity). Studies pertaining to aeroelasticity can be best understood by the Collar triangle (see Fig. 12.8) [31, 32].

In Fig. 12.8, the symbols A , E , and I respectively represent aerodynamic force, elastic force, and inertial force. The study of static aeroelasticity pertains to the interaction of aerodynamic and elastic forces only. The various aspects of this study address the problems of (i) divergence, (ii) control effectiveness, (iii) control reversal (or aileron reversal), and (iv) load distribution on a lifting surface owing to elastic deformation. The study of dynamic aeroelasticity addresses the problems involving the interaction of aerodynamic, elastic, and inertial forces. The associated problems are as follows: (i) flutter, (ii) buffeting (due to wake effects), and (iii) dynamic response (due to gust loads, landing loads, stores separation or launching of weapons). In addition, stresses due to thermal variations can play an important role in aeroelastic problems. Inclusion of thermal effects leads to the study of aero-thermo-elasticity. Inclusion of control systems in the analysis may significantly affect the aeroelastic problems and leads to the study of aero-servo-elasticity.

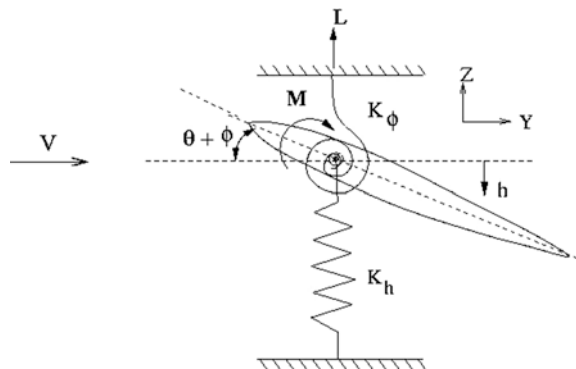
Aeroelastic phenomena have profound effects on the design of aerospace vehicles:

1. **Divergence:** The common divergence problem is wing torsional divergence. For swept wings, bending deformation plays an important factor. The divergence problem is similar to the buckling problem in structures. When the wing or lifting surface is operating at divergence speed, the increment in aerodynamic torsion moment due to an arbitrary increment in twist angle is exactly equal to the increment in elastic restoring moment. When the speed exceeds the divergence speed, the increment in torsion moment is more than the elastic restoring moment, leading to static instability.

2. **Control effectiveness and aileron reversal:** Aircraft can suffer from serious loss of aileron, elevator, or rudder control owing to elastic deformations of the lifting surfaces caused by control surface deflection. Normally, the lift on the wing increases with downward deflection of the aileron (resulting in an increased camber effect). Along with this increase in lift, the aerodynamic nose-down pitching moment also increases. This results in a nose-down twist of the wing, which reduces the lift. Thus elastic deformation of the wing reduces the effectiveness of the control surface, and at a particular speed (known as control reversal speed), the elastic twist due to nose-down pitching moment (effected by the control surface deflection) reduces the increment in lift to zero. However, increasing the torsional stiffness of the wing improves the performance. We note here that in swept-back wing configurations, aileron control reversal is a serious problem: both bending and torsion stiffness have to be increased.
3. **Load redistribution:** Owing to structural deformation, the load on the lifting surface gets redistributed. For structural design the correct load distribution is obviously essential. This problem has to be tackled in an iterative manner in the design of aerospace structures.
4. **Flutter:** Modern aircraft are subjected to many kinds of flutter phenomena. The classical flutter problem is related to bending-torsion coupling (of a wing or lifting surface) in potential flow conditions (see Fig. 12.9). The non-classical types of flutter involve separated flow and dynamic stall. Preventive measures can be undertaken by increasing the torsional stiffness or by mass balancing.
5. **Buffeting:** This phenomenon is related to transient vibrations of the empennage owing to the wake from wing or body. Analysing these problems is difficult. They can be avoided by suitable placement of the structure away from the wake.
6. **Dynamic loads:** External loads due to atmospheric gust or landing loads cause dynamic overstressing.

It should be noted that the types of aeroelastic problems differ for different types of vehicles, e.g. fixed wing and rotary wing. In addition, turbine engine blades also face serious aeroelastic problems. In the following, a list of aeroelastic problems required to be addressed for different configurations is provided for reference.

Fig. 12.9 Idealized model for bending-torsion flutter problem



- i. *Fixed wing aeroelasticity*
 - Subsonic, supersonic, and transonic aeroelastic problems,
 - Aero-servo-elasticity,
 - Aeroelastic issues of highly flexible structures.
- ii. *Rotary wing aeroelasticity*
 - Rotor blade structural dynamic and aeroelastic stability problems,
 - Coupled rotor–fuselage aeromechanical stability problems,
 - Rotor unsteady loads,
 - Rotor noise.
- iii. *Gas turbine aeroelasticity*
 - Blade aeroelastic stability problems,
 - Blade dynamic response problems.
- iv. *Missiles and rockets, re-entry vehicles*
 - Aeroelastic, aero-thermo-elastic problems.

12.6 Conclusions

An overview of several aspects of structural design of aircraft components has been addressed in this chapter. Issues pertaining to structural idealization, material selection, testing methodologies, and static and dynamic instabilities have been addressed. An effort has been taken to give a broad perspective of design procedures. Important topics such as manufacturability and maintenance issues have not been considered.

References

1. Kuhn P (1956) Stresses in aircraft and shell structures. McGraw-Hill Book Company, New York, NY, USA
2. Rivello RM (1969) Theory and analysis of flight structures. McGraw-Hill Book Company, New York, NY, USA
3. Megson THG (2007) Aircraft structures for engineering students, (Fourth edition). Elsevier aerospace engineering series, Elsevier Butterworth Heinemann, Oxford, UK
4. Standard test methods for tension testing of metallic materials, ASTM E8/E8 M-11, ASTM International, West Conshohocken, PA, USA
5. Standard test methods of compression testing of metallic materials at room temperature, ASTM E9-09, ASTM International, West Conshohocken, PA, USA
6. Standard test methods for tensile properties of plastics, ASTM D 638-1, ASTM International, West Conshohocken, PA, USA
7. Standard test method for compressive properties of rigid plastics, ASTM D695-10, ASTM International, West Conshohocken, PA, USA

8. Standard test method for tensile properties of polymer matrix composite materials, ASTM D3039/D3039 M-14, ASTM International, West Conshohocken, PA, USA
9. Standard test method for compressive properties of polymer matrix composite materials with unsupported gage section by shear loading, ASTM D3410/D3410M-03, ASTM International, West Conshohocken, PA, USA
10. Standard test methods for bend testing of material for ductility, ASTM E290-14, ASTM International, West Conshohocken, PA, USA
11. Standard test method for flexural properties of polymer matrix composite materials, ASTM D7264/D7264M-07, ASTM International, West Conshohocken, PA, USA
12. Standard test method for shear testing of aluminum alloys, ASTM B769-11, ASTM International, West Conshohocken, PA, USA
13. Standard test method for shear strength of plastics by punch tool, ASTM D732-10, ASTM International, West Conshohocken, PA, USA
14. Standard test method for in-plane shear strength of reinforced plastics, ASTM D3846-08, ASTM International, West Conshohocken, PA, USA
15. Standard test method for apparent shear strength of single-lap-joint adhesively bonded metal specimens by tension loading (metal-to-metal), ASTM D1002-10, ASTM International, West Conshohocken, PA, USA
16. Azzi VD, Tsai SW (1965) Anisotropic strength of composites. *Exp Mech* 5(9):283–288
17. Tsai SW, Wu EM (1971) A general theory of strength for anisotropic materials. *J Compos Mat* 5:58–80
18. Sih GC (1973) *Handbook of stress intensity factors*. Lehigh University Institute of Fracture and Solid Mechanics, Bethlehem, PA, USA
19. Murakami Y (1986) *Stress intensity factors handbook*. Pergamon Press, Oxford, UK
20. Tada H, Paris PC, Irwin GR (2000) *The stress analysis of cracks handbook*, (Third edition). ASME Press, New York, NY, USA
21. Curry NS (1988) *Aircraft landing gear design: principles and practice*, AIAA education series, AIAA, Reston, VA, USA
22. Onkar A, Upadhyay CS, Yadav D (2006) Generalized buckling analysis of laminated plates with random material properties using stochastic finite elements. *Intl J Mech Sci* 48:780–798
23. Conway HG (1958) *Landing gear design*. Chapman & Hall, London, UK
24. Ravikumar R, Dash PK, Basavaraddi SR (2013) Design and analysis of main landing gear structure of a transport aircraft and fatigue life estimation of the critical lug. *Intl J Mech Prod* 1(4):22–26
25. Divakaran VN, Ravi Kumar GVV, Srinivasa Rao P (2015) Aircraft landing gear design & development—how advanced technologies are helping to meet the challenges. White Paper, Infosys Limited, Bangalore, India
26. White Paper (2008) *Multidisciplinary design of an aircraft landing gear with Altair HyperWorks*, Altair HyperWorks. www.altairhyperworks.de
27. Yadav D, Nigam NC (1985) Reliability analysis of landing gear fatigue life. In: Eggwertz S, Lind NC (eds) *Probabilistic methods in mechanics of solids and structures*. Springer-Verlag, Berlin, Germany, pp 569–557
28. Yadav D, Kapadia KE (1990) Non-homogeneous track-induced response of vehicles with non-linear suspension during variable velocity runs. *J Sound Vibr* 143(1):51–64
29. Yadav D, Ramamoorthy RP (1991) Nonlinear landing gear behaviour at touch down, *Trans. ASME. J Dyn Syst Measur Control* 113(4):677–683
30. Yadav D, Singh CVK (1995) Landing response of aircraft with optimum anti-skid braking. *J Sound Vibr* 181(3):401–416
31. Dowell EH, Curtis HC Jr, Scanlan RH, Sisto F (1980) *A Modern Course in Aeroelasticity*. Sijthoff & Noordhoff, Alphen aan den Rijn, The Netherlands
32. Bisplinghoff RL, Ashley H, Halfman RL (1955) *Aeroelasticity*. Addison-Wesley Publishing Company, Cambridge, MA, USA

Chapter 13

Aircraft Mechanical Systems

R.V. Hulieraj and H.L. Janardhana

Abstract The design process of any aerospace vehicle can be broadly classified into three categories, i.e. structural design, system design and avionics design. This chapter presents the various mechanical systems and sub-systems involved in aerospace platforms with their principles of operation and functional applications in generic form. The major components/equipments involved in each of the systems are mentioned in brief. Finally, the various types of materials, properties, processes and their testing in aerospace mechanical systems design are briefly discussed.

Keywords Mechanical systems · Environmental control · Life support · Anti-icing · Hydraulic systems · Fuel systems · Landing gear · Brakes · Drag parachute · Flight controls · Armaments · Emergency escape systems

13.1 Introduction

Any aerospace vehicle requires a combination of several engineering disciplines, e.g. aerodynamics, electrical, mechanical, metallurgy, electronics and production technology. In this chapter we focus on the mechanical systems in aircraft and the engineering requirements for these systems. The following major systems are considered for a brief explanation:

- Environmental control and life support systems,
- Fuel and hydraulic systems,
- Landing gear, brake and steering systems,
- Anti-icing and de-icing systems,
- Drag parachute system (tactical aircraft),
- Flight control systems, and
- Armament and escape system (tactical aircraft).

R.V. Hulieraj · H.L. Janardhana (✉)
ARDC, HAL, Bangalore, India
e-mail: hulirajrv@rediffmail.com

Each system contains mechanical elements, and some are actuated/controlled with electrical signals. Whatever the system, the physical implementation is mechanical, and the visibility and accessibility of mechanical systems to regular inspections help to maintain their reliability. The use of electrical mechanisms in combination with electromechanical systems enhances the system capabilities.

In the next Sections we shall describe each of the mechanical systems, their contribution to aerospace platforms, and how they have evolved and developed into robust systems ensuring total reliability and comfort for the users.

13.2 Environmental Control Systems

Aircraft environmental control systems (ECS) are necessary to provide a benevolent operating environment to pilots/aircrew, livestock and on-board avionics by conditioning the pressure, temperature and humidity of the air being supplied into the aircraft cabin, cargo compartment as well as on-board avionics racks. An ECS is essential for the following reasons:

1. Modern transport and cargo aircraft typically cruise at altitudes above 11 km. Tactical aircraft can greatly exceed this height, depending on their mission requirements. At this altitude the partial pressure of oxygen (pO_2) is only 4.7 kPa which accounts for about 1/5th that of sea level pO_2 of 21 kPa. This is deemed to be grossly inadequate for sustaining human life. As per Section 25.841 of FAA [1], the minimum pO_2 mandated in an aircraft cabin is about 74 % of the sea level value.
2. Aircraft need to operate in an environment where *external* temperatures vary from -56.5 to $+50$ °C at ground level and as low as -70 to -30 °C at 12 km altitude, as shown in Fig. 13.1.

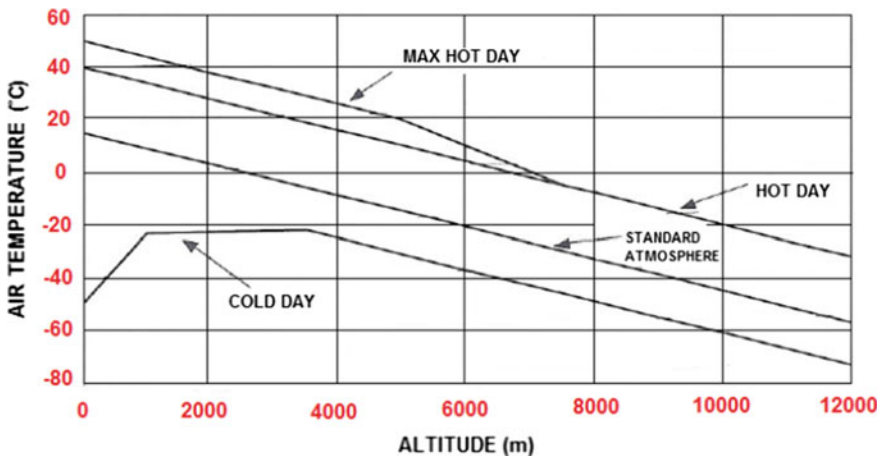


Fig. 13.1 Typical design temperature conditions [1]

3. There is a requirement to restrict the ozone content of the cabin air: ozone has adverse effects on the human respiratory system even at low concentrations. Up to 0.8 ppm ozone in the *external* atmosphere can be encountered at cruise altitudes, and this must be reduced to average and peak levels of 0.1 and 0.25 ppm, respectively [2].
4. The relative humidity (RH) of the cabin air has to be controlled, with both low RH and high RH having adverse effects on passenger comfort. The comfortable range for people is 30–70 % RH. At low altitudes dehumidifiers may, or will, be necessary to remove excess moisture from the *external* air, particularly in tropical regions. At high altitudes the *external* air is dry, so the opposite problem arises. In practice the cabin air at cruise altitude is maintained in the range of 10–15 % RH. This is a compromise, since the ECS has to deliver air into the cabin at a higher temperature than the incoming cold and dry air, and also there should be avoidance of excessive condensation on the *internal* structure of the fuselage (which is cold owing to the *external* surface being exposed to low temperatures).
5. The avionics equipment needs to be maintained within certain ranges of temperature, pressure and humidity. Avionics are the main sources of navigation and communication aids for the pilots and also for the safety of both passengers and aircraft. Excepting light civil aircraft, most other types will have a high density of avionics, and these will often require cooling to avoid too high operating temperatures, as well as protection from too much cooling. An avionics cabinet should be kept within a temperature range of -30 to $+70$ °C for effective operation throughout the flight regime.
6. Transport aircraft must be equipped with an emergency oxygen system to protect the lives of occupants in the case of rapid or explosive decompression at altitude.

13.2.1 Different Types of ECS

There are two types of aerospace ECS systems. These are classified as (i) air cycle systems and (ii) vapour cycle systems. The air cycle system is widely used because of its simplicity, less weight and easy maintainability. However, the combination of air cycle and vapour cycle systems may also be used for different applications on the same aircraft.

Air Cycle Systems are further classified as (a) turbofan and (b) bootstrap systems, which are most commonly used. Bootstrap systems are further categorized into low-pressure and high-pressure systems. In a low-pressure system, the pressure and temperatures at the engine bleed point are typically found to be 1200 kPa and 375 °C, respectively, at maximum levels. However, in this type of system the minimum temperature downstream of the turbine is restricted to 4 °C to reduce an icing threat in

the pipelines. Similarly, in a high-pressure system the pressure and temperatures at the engine bleed point are normally found to be 3200 kPa and 650 °C, respectively, at maximum levels. However, in this system the operating temperature downstream of the turbine varies from -35 to -40 °C at minimum levels. The air at these reduced sub-zero temperatures can be supplied to the avionics since 95 % of the water vapour content gets removed by a high-pressure water separator.

The bleed and operating parameters mentioned above may slightly vary between aircraft depending upon the type of engine and also the ECS system requirements. One such high-pressure ECS system normally used in military aircraft applications is shown in Fig. 13.2.

Some of the important components/equipments involved in bootstrap air cycle systems are heat exchangers, pressure and temperature control valves, cold air unit, flow control and shut-off valves, non-return valves (NRV), sensors and extensive piping networks.

Based on the arrangement of compressor, turbine and fan, the bootstrap systems are classified as 2-wheel, 3-wheel and 4-wheel systems. These systems need to handle huge mass flow rates and also must effect large enthalpy drops. These turbo machines normally operate at a typical speed of 60,000–90,000 rpm [3]. Hence design must take care of all the rotating components and their associated equipment, including optimum balancing for all critical design cases..

Vapour Cycle Systems are closed loop systems and work on the principle that heat is absorbed or lost due to the evaporation of a liquid refrigerant tetrafluoroethane (R-134). They mainly consist of a compressor, a condenser, an evaporator and an expansion valve. The vapour cycle refrigeration systems are five times more efficient compared to air cycle systems in terms of higher coefficient of performance. However, they are high in mass and not environmentally friendly, since the liquids are toxic. Moreover, the maintainability issues are of much concern owing to potential leakage of the refrigerant. Another negative aspect is that the operating temperatures of the liquid refrigerants are quite low [4], in the range of 65–70 °C. Owing to all these issues, vapour cycle systems are not favoured for use in aerospace applications.

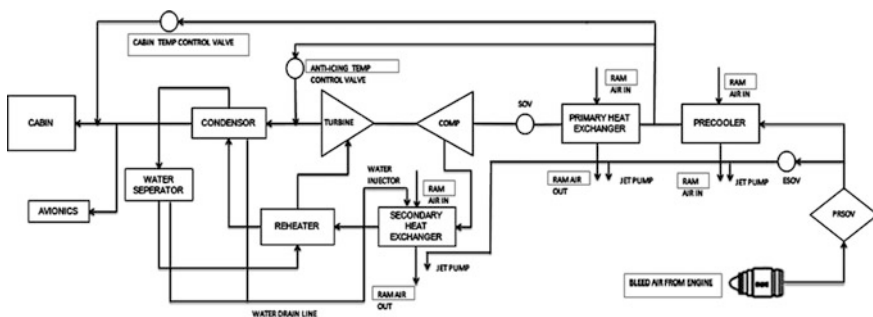


Fig. 13.2 Typical architecture for a high-pressure ECS

13.2.2 Life Support Systems

The life support system provides the oxygen requirements and protects the occupants against hypoxia and toxic agents under all environmental conditions in which a manned aircraft is deployed. The oxygen system also provides pressure for the anti-‘g’ systems needed in high-performance aircraft to sustain the pilots’ operating performances.

Aircraft oxygen systems are broadly classified into (i) gaseous oxygen systems, (ii) liquid oxygen systems, (iii) chemical oxygen systems and (iv) on-board oxygen generation systems. Combinations of these systems are also used in some applications. In commercial aircraft combinations of the systems are required to address the needs of the passengers in case of emergencies (cabin decompression). A short description of these systems is given here:

Gaseous Oxygen is normally stored at 1800 psi in steel cylinders. The systems are simple in construction, leak-proof and easily replenished. However, they are heavy and bulky.

Liquid oxygen (LOX) is stored in a steel container at a pressure ranging from 70 to 115 psi with temperature less than $-183\text{ }^{\circ}\text{C}$. One litre of LOX produces 840 l of breathable gas upon vaporization. From an installation point of view, it occupies about 80 % less volume compared to a gaseous system. Also the weight is approximately 70 % less. However, this system needs regular maintenance and must be replenished after the intended flying hours. The LOX container size may vary (i.e. 3.5, 5, 10 and 25 l) depending upon the aircraft roles and mission requirements.

The sequence of LOX system operation predominantly includes filling, build-up and delivery. The main drawbacks of the LOX system are the continuous loss of oxygen due to imperfect insulation (i.e. $\leq 10\%$ can be lost in 24 h standing after filling), and the extensive care required during handling to avoid fire hazard and frost bite [5].

Chemical Oxygen System This relies on the ignition reaction between sodium chlorate and finely divided iron, resulting in large amounts of pure oxygen. A mainly exothermic reaction is the basis in this system. Most civil aircraft use this system for providing emergency oxygen to the passengers if the cabin ‘altitude’ goes above 20,000 ft due to any technical reasons, e.g. cabin decompression. Oxygen masks are deployed automatically if the cabin altitude exceeds the above limit.

On-board Oxygen System Owing to required increases in endurance of some high-performance aircraft (via aerial refuelling), there is a need for a continuous oxygen supply during the extended missions. An on-board oxygen system is used to overcome this limitation. It generates pure oxygen up to the concentration level of 94–96 % by adsorption of nitrogen by molecular sieve material, and it supplies for unlimited durations.

13.3 Anti-/de-icing Systems

The formation of ice on aerodynamic surfaces, engine cowlings and air intake areas can affect the aerodynamic and engine performances. Additional ice build-up in the engine intake areas can eventually break off and be ingested, potentially damaging the engine. Ice build-up can also affect the operation of an aircraft's probes and fly-by-wire systems, and ice on an aircraft's nose may affect the radar and other electronic warfare equipments and their operations.

The indicative threats mentioned above call for effective anti-icing or de-icing systems to be employed on both commercial as well as military aircraft [6]. Anti-icing systems usually make use of electrical power/bleed air tapped from the engine high-pressure compressor to provide heat energy for precluding/removal of ice-accretion in ice-prone areas. The level of thermal energy extracted from the engine must be adequate for the entire flight operating envelope and for all probable icing accretion conditions.

13.3.1 Ice Protection Systems

An ice protection system can prevent ice building up to an unacceptable level in three distinct ways, namely thermally, mechanically or chemically. Thermal and chemical ice prevention systems can be designed to operate in either anti-icing or de-icing modes. However, mechanical ice protection systems are suitable only for de-icing.

Thermal systems (direct or via electrically induced heating) can provide ice protection either by continuously supplying heat to areas of the airframe where ice formation can occur, or by periodically applying heat to areas where ice has formed.

For medium-sized and large transport aircraft, direct heating via engine bleed air is the most common source of ice protection. The turbofan engines powering such aircraft can supply the required quantities of hot, high pressure air to provide ice protection requirements. The air is typically pressurized at approximately 20 psi [7]. Control is achieved by electrically operated valves, and temperature monitoring is incorporated to prevent overheating.

Chemical ice protection systems operate by lowering the freezing point of water on the aircraft. These systems can act as an anti-icer, preventing any water from freezing, or as a de-icer by acting on the ice next to the airframe surface, weakening the adhesion and causing the ice to slip off: e.g. TKS ice protection liquid or a protective film of glycol preventing ice formation.

13.4 Aircraft Hydraulic Systems

Typical aircraft hydraulic system applications include operation of landing gear (retraction/extension), flight control surfaces (primary/secondary), anti-skid and brakes, and powered flying controls.

Hydraulic systems are extensively used in both safety as well as flight critical operations. Therefore multiple pumps, heat exchangers, filtration systems and accumulators are enabled by these systems. However, in new generation aircraft more electrical systems are replacing hydraulically powered systems, e.g. electro-hydrostatic actuators (EHA) and electromechanical actuators (EMA).

Normally, the operating pressure of hydraulic systems varies from 3000–5000 psi, depending upon the configuration and utilities of the aircraft. Since a single failure may cause failure of the power system, the principle of 2 or 3 redundant circuits is usually applied. A 2-redundant system is used in military aircraft, while in large civil aircraft 3 or more redundancies are used.

Recent research studies have been undertaken by worldwide aircraft industries to raise the system operating pressure from the current level of 5000–8000 psi. This is expected to benefit compact design, thereby reducing the system component mass and installation volume.

A hydraulic system is broadly classified into (i) power generating elements: pump, reservoir, filters, accumulators, etc.; (ii) power transmitting elements: hydraulic fluid, pipes, fittings, hoses, etc.; (iii) power controlling elements: directional valves, non-return valves (NRVs), solenoid valves, etc.; and (iv) power utility devices: hydraulic actuators, jacks, etc.

13.4.1 Hydraulic Fluids

Industries engaged in design and manufacture of hydraulic components for aircraft applications specify the type of hydraulic fluid used. This has to conform with applicable MIL or other contemporary standards appropriate to the operating conditions involved. These include the functionality required, operating temperatures and pressures, and reliability and maintainability. Properties that hydraulic fluids must possess include viscosity, chemical stability, and flash and fire points. The viscosity–temperature characteristics of a given fluid are very important.

The following hydraulic fluids are generally employed:

1. Oil-based minerals, which have low fire hazard properties.
2. Polyalphaolefins, which have good non-flammability characteristics.
3. Phosphate esters, which have good fire-resistant characteristics.

Some of the hydraulic fluids used in military aircraft include DTD 585 (UK), MIL-H-5606 (USA), MIL-H-7644 (USA) and AIR 320 in France. The operating temperature of the fluid is generally limited to about 130 °C (e.g. DTD 585), and components along with associated equipment have to be designed and qualified accordingly. However, the use of MIL-H-83,282 has increased this limit to 200 °C, leading to redesign or requalification of associated components for this higher temperature.

During the operation of hydraulic systems, contamination of the fluid is inevitable. This may be due to internal or external leakages, wear out/damaging of seals, ingress of foreign objects and dust particles during replenishment, ground maintenance checks, etc. However, total shutdown of the system and its associated components depends upon the type and severity of contaminant present, in addition to other technical issues. Different types of contaminants include the following:

- Abrasives, weld spatter, machining chips, rust and particles generated because of friction of reciprocating/rotating machinery.
- Non-abrasives, soft particles worn or shredded from seals and other organic components.

13.4.2 Hydraulic System Components

A typical hydraulic system consists of a pump, reservoir, directional valve, check valve, pressure relief valve, selector valve, actuator and filter.

Pumps The pump is the primary source of energy. It is mounted on the engine accessory gearbox, which in turn is driven by a power take-off (PTO) shaft. However, in the case of engine failure the pump may be driven by an electric motor to cater for emergency control surface actuation. In operation the engine transmits power to the engine gearbox, which transmits it to a hydraulic pump. The pump provides pressurized fluid at a certain value and transfers it to different actuating devices via stainless steel pipes. A reservoir provides the required amount of fluid to the pump under all operating conditions. Some of the recently developed commercial as well as military aircraft are equipped with a ram air turbine (RAT), in addition to batteries, to produce both electrical hydraulic powers to cater for emergency services in case of engine failures. A RAT may produce power from 5 to 15 kVA, approximately.

The pump speed varies depending on the type of engine and the flow demand. A typical speed for a modern military aircraft pump varies from 3000 to 6000 rpm. There is a wide range of low- to high-pressure pumps available for different types of aircraft.

The universal pump used in aircraft hydraulic systems is ‘variable delivery–constant pressure’. The flow rate is variable when the system pressure has to be sustained at a certain value. Generally, a pump is designed to maintain system pressure within 5 % of nominal, except during short transient cases from low to high flow. The different types of pumps normally used in aircraft applications are as follows:

- Constant displacement pumps,
- Piston pumps,
- Vane pumps, and
- Variable displacement pumps.

Hydraulic Reservoir Reservoirs store and supply the required amounts of fluid to the pumps and also compensate for fluid contraction or expansion. The reservoirs are pressurized to provide positive flow of fluid to the pumps. The reservoirs are also equipped with a de-aeration device to prevent cavitations in the pumps. On civil aircraft this pressurization is typically achieved by using the bleed air pneumatic power system to pressurize to 40–45 psi. The pneumatic components of the system are as follows: air relief valves, air bleeder valve, air pressure regulator, air filter, air drier and check valves. Reservoirs are provided with necessary indications for level checks during depot inspection, ground maintenance, etc.

Heat Exchangers (Hx) Heat exchangers are installed in the case drain lines of the hydraulic pumps or main return lines of the system, depending upon the temperature and flow rate of the hydraulic fluid. The purpose of heat exchangers is to cool down the hydraulic fluid temperature, thereby enhancing the service life of the fluid and also the pumps.

Different types of heat exchangers are generally used in aircraft hydraulic systems, such as oil-to-air heat exchangers and oil-to-fuel heat exchangers. However, oil-to-air heat exchangers may impact aircraft drag, while oil-to-fuel heat exchangers may affect fuel system safety issues. For example, fuel is used to cool down the lubrication oil of the engine accessory gearbox, thereby increasing the fuel temperature in the supply tanks. Aluminium-finned tubes are used to transfer heat from the hydraulic fluid to the fuel.

Actuators The main function of an actuator is to transform energy in the form of fluid pressure into mechanical force, or action, to perform work. Action or work may include movement of control surfaces, landing gear retraction/extension and deployment of a braking parachute. An actuator consists of the cylinder housing, one or more pistons and piston rods, and some seals. Inlet and outlet ports are provided through which fluid transforms energy to the piston to effect movement in the desired direction. Inbuilt electrical servo control modules are used to modulate movement of the piston in either direction, based on the output demand.

Actuating cylinders are of two major types: single action and double action. Based on the type of motion, the actuators can be classified as linear or rotary. An actuator is commanded mechanically or electrically by the pilot. A typical actuator used in a military aircraft system is shown in Fig. 13.3.

Fig. 13.3 A typical actuator from a military aircraft



Accumulator This is a steel sphere- or cylinder-type construction partitioned into two compartments by a synthetic rubber diaphragm. The upper compartment is filled with fluid at the system operating pressure, while the lower compartment is filled with nitrogen or air. The main functions include the following:

- Absorption of shocks due to rapid pressure variations in a hydraulic system,
- Helping to maintain a constant pressure within the hydraulic system,
- Helping the hydraulic pump under peak pressure loads, and
- An emergency power source.

Filters As mentioned earlier, different types of contaminants, i.e. system generated as well as outside particles and dust, are carried by the fluid in the form of a suspension. Unless these contaminants are removed they can damage the hydraulic system components leading to catastrophic failures. Hence filters are invariably installed in the pressure, case drain, and return lines.

Filters should be capable of removing contaminants ranging from 5 to 25 μm in size. Contaminants up to 25 μm are removed by case drain filters, whereas return line filters will have capability up to 15 μm , and filters installed in a system line will have the capability to remove contaminants ranging from 5 to 10 μm . Appropriate clogging indications are provided on filters for replacement and maintenance-related activities. The filters must withstand 1.5 times the system pressure.

Unless otherwise specified in the maintenance manuals, the following service life is recommended [7]:

- Pressure line filters—3000 h
- Return line filters—1500 h
- Case drain filters—600 h

Note: the cleanliness class of hydraulic fluids is generally expressed according to NAS 1638 norms.

Valves Valves are very commonly used devices to interconnect or isolate the parts of a system. Some of the valves which are widely used in hydraulic systems may be labelled as flow control valves, NRVs, shutoff valves (SOVs), pressure regulating valves (PRVs) and relief valves. Examples of flow control valves include selector valves, check valves, sequence valves, priority valves, shuttle valves and quick disconnect valves.

Plumbing Network This must be designed in such a way that sufficient fluid flow is supplied to each of the hydraulically powered components at the required pressure. The routing must consider common mode failures and survivability in case of unforeseen emergencies. The designer must consider the pressure drop of each component while establishing pipeline diameters and wall thicknesses by taking into account cases of localized surge.

Pipe mounting schemes should take into account vibrations that may result from system surge, fluid flow reversal and external sources. Also, turbulent flow and pressure losses should be minimized by avoiding sharp bends. Throughout the

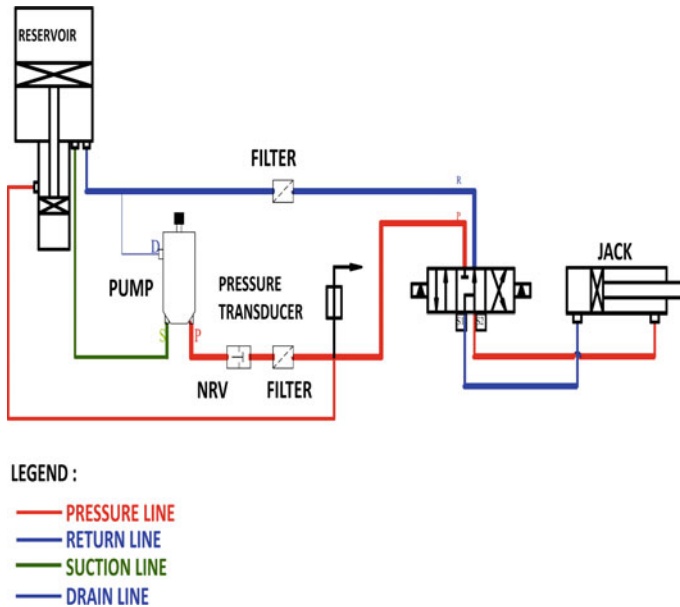


Fig. 13.4 Basic aircraft hydraulic system circuit

system rigid pipelines will be used, made of aluminium alloys or stainless steels or titanium alloys. However, at some points in the system, flexible piping or hose will be used.

One of the basic hydraulic circuits used in aircraft applications is shown in Fig. 13.4. The hydraulic fluid supply to the pump is through a bootstrap hydraulic reservoir, which is pressurized to ensure positive pressure at the pump inlet. The pump is energized by the engine shaft power via a reduction gear mechanism. Pressurized fluid from the pump passes through a non-return valve and filter. Also, the system health is monitored by a pressure transducer. The pressurized fluid from the pump is supplied to a jack for extension or retraction via a command given to the solenoid of the electro-selector. Return fluid coming back to the reservoir is also filtered.

13.5 Aircraft Fuel Systems

The main function of an aircraft fuel system is to store sufficient fuel and deliver the required amount of clean fuel at the right pressure to meet the demands of the aircraft power plant(s). This function is flight safety critical, and consequently the sub-systems and equipment involved should possess a high degree of reliability. Though the basic concept of a fuel system remains the same, it varies functionally between aircraft, based on class, role and type of configuration for which the aircraft are designed.

Fuel tanks are equipped with internal booster pumps, transfer valves, content gauges, venting and plumbing, etc., to feed the engines, allow for refuelling and defuelling, isolate the individual tanks, and in some applications allow for fuel dumping in case of rejected take-off (RTO)/emergency landing or for optimization of an aircraft's centre of gravity. The fuel system should provide positive and reliable fuel flow through all phases of flight including changes in altitude and rapid manoeuvres. Fuel systems should also have continuous monitoring of the pressure, flow, quantity, etc. These systems must be adequately shielded to protect from damages encountered during combat and also from lightning. Appropriate warnings and indications must be provided in the cockpit multifunction displays (MFDs) to initiate necessary actions by the pilots in case of emergencies.

13.5.1 Aircraft Fuels

Aviation fuels are broadly classified into two categories: AVGAS fuels for piston engine aircraft and AVTUR fuels for jet engine aircraft. Some of the significant properties of the aviation fuels include density (as it varies with temperature), vapour pressure, viscosity and freezing point.

Aviation Gasoline (AVGAS) The most important property when specifying an AVGAS is its anti-knock rating. Like all reciprocating internal combustion engines, aircraft piston engines are designed to operate efficiently at a particular knock rating. Another important property is the fuel's volatility to allow successful cold starting. Some types of AVGAS are AVGAS80, AVGAS100 and AVGAS100LL.

Aviation Turbine Fuel (AVTUR) Jet engines can run reliably and efficiently on all AVTUR variants. The main consideration when selecting the properties of AVTUR fuels is that they must be capable of being supplied to the engine over the wide range of operating conditions. AVTUR fuels are all kerosene-based.

Three main types of AVTUR fuels are used presently for both civil and military aircraft applications. The first type is Jet A (freezing point $-40\text{ }^{\circ}\text{C}$), and the second type is Jet A-1 (freezing point of $-47\text{ }^{\circ}\text{C}$), which is used worldwide. The third type is known as Jet TS-1, which has superior low-temperature performance when compared to Jet A-1. However, it has a lower flash point, making it inferior to Jet A-1 from a safety point of view.

Fuel System Contamination Contaminants such as rust and sand could enter the fuel system, which therefore requires filters. Water in the form of ice may also be present in fuel at high-altitude operation, where the fuel will fall below $0\text{ }^{\circ}\text{C}$. Some dissolved water is likely to be present in the fuel itself, and this poses no threat as long as it stays dissolved.

However, water in the form of vapour can enter the fuel system through the vents, some of which may condense during flight on the fuel surface and on other cold surfaces. This may then freeze, forming small ice particles that can lead to filters becoming blocked. Consequently, water can accumulate in the fuel tanks

over a period of time. The build-up of water is also a breeding ground for microbacterial growth, which can attack and corrode fuel system components as well as the aircraft skin.

13.5.2 Fuel System Components

One of the fuel system architectures used in military trainer aircraft is shown in Fig. 13.5. Some of the major components involved in the system have been briefly discussed below.

Fuel Tanks Two types of fuel tanks exist in aircraft: one for storage and one for fuelling the engine. On transport aircraft most of the fuel is carried in integral wing tanks. This has the advantage that the tank boundaries are already in place, providing structural functions (ribs, spars and skins), thus reducing the overall weight of the fuel system. Additional tanks may be located in the fin, tailplane and fuselage. Tanks in the tail can be used to control the aircraft's centre of gravity. In military aircraft additional fuel can be carried externally in drop tanks for accomplishing the intended mission requirements.

The fuel can be transferred from various tanks to the engine supply tank either by pressurization or by employing the fuel pumps. Military aircraft generally use fuel transfer by pressurization. Conditioned air from the ECS system is normally used for pressurization.

Pumps Aircraft fuel pumps can be broadly classified into three main categories: transfer pumps, booster pumps and jet pumps. In general, fuel pumps are typically powered by AC or DC electric motors. However, they may be powered hydraulically.

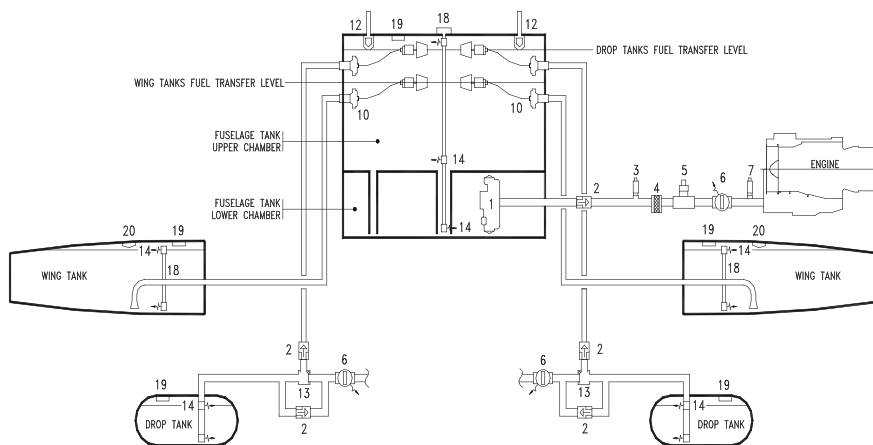
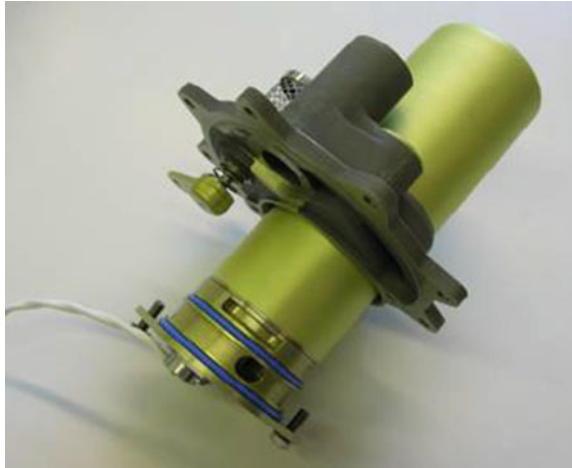


Fig. 13.5 Fuel system of a military trainer aircraft

Fig. 13.6 A typical booster pump from a military aircraft



Transfer pumps: Primarily, fuel is transferred between tanks to ensure that the engine(s) can be continuously supplied with fuel. Additionally, transfer pumps are often used to control the aircraft's centre of gravity. Transfer pumps do not operate continuously.

Booster Pumps: Booster pumps are used to ensure that a sufficient flow of fuel reaches the engine at a sufficiently high pressure. Booster pumps operate continuously throughout the flight. They help to prevent air becoming present in the fuel stream, which can cause engine flameout. They also prevent cavitations due to low fuel vapour pressure and high temperatures. Booster pumps on fighter aircraft are double-ended to ensure operation in both normal flight and inverted flight: one such pump is shown in Fig. 13.6.

Jet Pumps: Jet pumps see extensive use in aircraft fuel system applications. These work on the ejector principle of a high-pressure flow being used to energize a larger flow to an intermediate pressure. They are very reliable, having no moving parts. However, they do require a high-pressure flow from another pump, and their efficiency is low at around 25 %, with the discharge flow limited in pressure.

13.5.2.1 Valves

Fuel system valves control the quantity and direction of fuel flow within the system. The valves are electrically controlled and powered and may be classified under the following categories:

- Non-return valves (NRVs),
- Shut-off valves,
- Refuel/defuel valves,
- Cross-feed valves,
- Fuel dump valves, and
- Fuel vent valves.

In general, a fuel system will include a number of simple non-return (or check) valves in order to prevent fuel flow reversal. Shut-off valves are used to prevent fuel from flowing. This may be from one tank to another, or to the engine. Refuel/defuel valves allow fuel to flow from the refuelling gallery into the fuel tanks. They are controlled to shut once the desired amount of fuel is present in particular tanks. These valves perform a similar function during defuelling.

Cross-feed valves are used to control fuel flow from one side of the aircraft to the other. This may be required, for example, when the port engine has to be shut down and fuel needs to be transferred from tanks on the port side to tanks on the starboard side of the aircraft.

Fuel dump valves are present to allow excess fuel to be jettisoned overboard during an emergency situation. Fuel vent valves serve to vent air and fuel to and from the fuel tanks. During refuelling, air is expelled from the tanks through these valves: in a non-pressurized fuel system, air is allowed to enter the tanks to replace the volume of fuel burned, and this air must later be vented.

13.5.3 Gauging of Fuel

It is important to detect the quantity of fuel when the tanks are full and near-empty, as well as to measure the level of fuel in each of the tanks for effective operation and execution of the intended mission. This can be achieved by using various types of sensors and gauges.

Level Sensors Commonly used sensor types are float-operated, optical and Zener diode. Float level sensors work under the principle that the float position changes as the level of fuel in the tank changes. Zener diode level sensors have no moving parts. They are solid-state electronic devices capable of measuring a particular fuel level in a tank to an accuracy of a couple of millimetres. Typically, some sensors may be positioned to sense when a tank is full and others to detect when a tank is empty. Such probes use positive temperature coefficient directly heated Zener diode heads that have different response characteristics depending upon whether they are surrounded by air or immersed in fuel.

Gauging Probes Fuel gauging probes measure the amount of fuel in a particular fuel tank. This is commonly achieved using several capacitance probes to measure the fuel's capacitance. These probes work on the principle that fuel and air have different dielectric values. The probes must be positioned to cope with the changes in fuel level induced by pitch and roll attitude. Such probes consist of concentric cylindrical metal tubes with plastic cross-pieces to maintain the concentricity.

Fuel System Pressurization Pressurization of the fuel system is to assist in the transfer of fuel around the system. While gravity feed and transfer pumps are sufficient on many aircraft, on others ram air may be used to pressurize the fuel system. Fighter aircraft often require higher pressure than ram air can readily provide, and in such cases pressure-reduced bleed air may be used to pressurize the fuel system. Alternatively, an on-board inert gas generation system (OBIGGS) can

be used, as is done on the F-22. This has the additional advantage of preventing fuel explosion in the tank.

Fuel Jettison For most aircraft the maximum allowable take-off weight is greater than the maximum allowable landing weight. Thus if the planned flight duration is unexpectedly shortened after take-off, fuel jettison may be required to enable a safe landing. Also, in the event of a serious malfunction, such as an engine failure, it may be necessary to jettison fuel and reduce weight, merely to remain airborne. The fuel jettison system will be required to dump large quantities of fuel in a relatively short period of time, of the order of minutes.

13.6 Undercarriage, Wheels and Brakes

Undercarriage is one of the most critical systems in aircraft, in many types of helicopters and also in unmanned aerial vehicles (UAVs) to enable taxiing, take-off and landing. It accounts for 3–6 % of the aircraft by weight. The undercarriage is designed to provide cushioning during landing impacts by absorbing and dissipating kinetic energy, thereby keeping the ground reaction (i.e. dynamic loading) within limits. It must also absorb the effects of irregularities on runway surfaces when operating from unprepared/semi-finished runways in case of emergencies.

Tyres Tyres must be compatible for all sorts of load/speed combinations generally involved. They must have high abrasion resistance and better cooling properties while operating on all kind of runways, and they must possess adequate service life to keep the aircraft maintenance costs as low as possible. Fusible plugs are provided in wheels to deflate the tyres to avoid bursting due to overtemperatures during RTOs. The tyres may be cross-ply or radial in construction.

Brake System An effective braking system is necessary to decelerate and stop the aircraft and also to hold firmly during engine run-up on the ground. Braking is also necessary to stop rotation of the wheels during undercarriage retraction. Different types of brakes are used in aircraft applications, e.g. disc brakes, carbon brakes and tube brakes. The required power for actuation is supplied by the hydraulic system. In modern high-performance military aircraft, brake cooling fans (BCFs) are used for better thermal management of brakes during RTOs and also for enhancing aircraft turnaround time.

Steering Mechanism Nose wheel steering systems are also necessary to facilitate directional control at slow speed and also eliminate overheating of brakes due to differential braking. Steering systems may be manual or power-operated, based on the size and class of the aircraft. The hydraulically operated steering mechanism turns the nose wheel typically up to $\pm 45^\circ$ from the centre. The steering nose wheels are directly connected to the pilot's rudder pedals. A bungee spring is incorporated in both the steering rods to avoid excessive forces created by large movements of the rudder pedals. Shimmy dampers are used to prevent excessive tyre oscillations caused by the steering mechanism and also due to play in the linkage mechanisms.

Shock Absorbers Shock absorbers are an integral part of undercarriage systems. They mainly absorb the vertical component of the aircraft velocity during landing. They avoid rebounding of the aircraft and ensure safe transfer of dynamic loading to the structure. Two types of shock absorbers are used in aircraft, i.e. spring type and oleo-pneumatic type. Oleo-pneumatic shock absorbers are the commonly used type on all sorts of military as well as commercial aircraft because of their good damping capabilities. These shock absorbers have a cylindrical-type construction which is partitioned into two chambers along with an orifice at the middle. The upper chamber is charged with nitrogen or compressed air for absorbing the shock of the aircraft's vertical movement, while the lower chamber is the damping that acts by forcing hydraulic fluid through an orifice, thereby causing friction and slowing the oil.

Anti-skid System In order to protect the tyres and also to preclude incidents on low-friction surfaces or due to pilot error, an anti-skid system is normally provided in which the applied brake pressure is relaxed automatically if an excessive rate of wheel deceleration is detected.

13.6.1 Undercarriage (Landing Gear) Arrangement

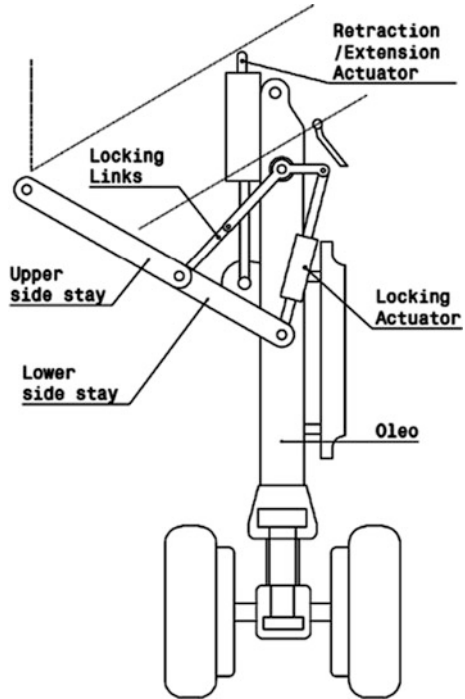
An undercarriage system usually consists of main landing gears and a nose landing gear. The main landing gears are normally designed to carry 90 % of the load, while the nose landing gear is designed to support the remaining 10 % of the load. Tricycle-type landing gear arrangements are commonly used in both military as well as commercial aircraft. This is predominantly due to the following advantages: (i) allowing higher landing speeds, (ii) excellent visibility from the flight deck while landing and ground manoeuvring, and (iii) preventing ground-looping of the aircraft. The main undercarriage may be of single wheel or multiple wheel type, with or without bogies, based on the type and configuration of the aircraft. An example of a main landing gear arrangement on a typical military aircraft is shown in Fig. 13.7.

13.6.1.1 Fixed and Retractable Landing Gears

Two types of landing gear systems are used in aircraft. One is a fixed type and the other one is a retractable type. Fixed landing gear systems are generally used for small and slow-speed aircraft. In this type the landing gears remain extended throughout the flight phase. This type of system induces friction or parasitic drag, imposing some limitations on the aircraft performance. However, this system involves fewer components, giving an overall weight advantage and also being relatively simple in construction.

In order to overcome the limitation of aircraft speeds due to the onset of parasitic drag, retractable landing gear types are used. Since most high-performance military

Fig. 13.7 Main landing gear example



aircraft fly at supersonic speed, it is essential to reduce the drag imposed by landing gears and other structural elements protruding outside the aircraft. Hence mechanisms are provided to retract and stow the landing gear either in the fuselage structure or in wing compartments. Retraction and extension actuators are used for this purpose. The contour surfaces of the follow-up doors of the landing gear are flush with the fuselage or wing surfaces for ensuring a smooth flow of air during flight, thereby reducing the drag. The doors are operated by hydraulic jacks. Suitable up-locks and down-locks are used to hold the landing gear firmly in the retracted and extended modes, respectively. These locks are attached to the airframe surfaces and are operated either hydraulically or electrically. The sequence of landing gear operation is monitored and controlled by an electronic control unit (ECU). This type of system is highly complex in nature and greatly increases the part count. The reliability of this type of system must be very high to avoid catastrophic failures.

Emergency Extension Systems Design must have a provision for emergency extension of the landing gear if the main system fails for any technical reasons. Some aircraft will have a handle inbuilt in the cockpit and connected to the up-locks through mechanical linkages. Upon pulling the handle, it releases the up-locks and allows the landing gear to free-fall to the extended position, which is then firmly held by down-locks. Other means of emergency extension include pneumatic power to unlock the up-locks.

13.7 Drag Parachute Systems

In modern fighter/trainer aircraft, the landing speeds are high and the stipulated landing roll is short. Since the wheel brakes tend to be insufficient when landing on slippery, wet or icy runways, a braking parachute is essential. For normal landings there will be no need for using the parachute. However, in the case of an emergency landing or rejected take-off, the kinetic energy of the aircraft will be very high and the wheel brakes alone will not be able to meet the deceleration requirements, such that the braking parachute must be used.

Braking Parachute Assembly This consists of the main parachute, pilot chute, auxiliary parachute, deployment bag, riser, etc. The main parachute is made from materials which have excellent strength for an adequate life. The strength of the parachute canopy is based on the opening shock encountered at the highest speed at which the parachute is designed to be deployed.

The pilot chute normally has a compression spring and is designed to be rapidly released from the deployment bag in the parachute compartment, quickly inflated, and used to pull out the auxiliary parachute. Once the auxiliary parachute is fully deployed, it pulls the main parachute out of the deployment bag.

The parachutes are classified based on the constructional types: ribbon type, ring slot type and unicross type. Unicross types of parachutes are extensively used in almost all modern aircraft because of good stability, reliability, easy maintainability, low cost and low weight.

Spin Recovery It is mandatory for a combat/trainer aircraft to demonstrate spin recovery capability during the flight test programme. The aircraft must be equipped with a tail-mounted spin recovery parachute system during spin demonstrations, in case an emergency recovery is needed. This is achieved by deployment of the parachute, which then applies an upward force at the rear of the aircraft, bringing the nose down. The effect is to bring the aircraft into a controlled stabilized dive.

13.8 Flight Control Systems

A flight control system is a network of control surfaces, connecting linkages, actuators, operating mechanisms and cockpit controls and displays. All aircraft undergo pitching, rolling and yawing manoeuvres. These actions are performed by using control surfaces which are broadly classified into primary and secondary, depending upon their function and criticality of the operation. The ailerons, elevators and rudder are primary control surfaces; and slats, elevons and trim tabs are secondary control surfaces.

Different types of flight control systems are used in aircraft design: (i) mechanical FCS, (ii) hydromechanical FCS and (iii) fly-by-wire FCS.

Mechanical FCS This is the most basic type, which was used in early aircraft designs. It is currently being used in small airplanes and basic trainer aircraft where the aerodynamic forces acting on the control surfaces are not excessive.

This type of flight control system makes use of mechanical parts such as rods, cables, chains and pulleys to transmit the forces of the cockpit controls to the control surfaces. One such mechanical FCS used on a basic trainer aircraft is shown in Fig. 13.8.

A mechanical FCS is not suitable for bigger aircraft owing to the increase in control surface areas and an exponential increase in the forces needed to operate them.

Hydromechanical FCS As aircraft operating speeds increased, the aerodynamic forces increased beyond those which could allow the pilot to actuate the control surfaces. This led to pilot power being augmented with hydraulic actuators. This power assistance meant that the pilot then lost the ‘feel’ of the aircraft. Thus there was the danger of pulling manoeuvres that would over-stress the aircraft. In order to resolve this problem, limits on control surfaces were imposed and the pilot was provided with artificial ‘feel’ feedback to the cockpit controls.

The FCS basically consists of two parts: a mechanical circuit and a hydraulic circuit. The mechanical circuit provides the link between the control stick and the hydraulic circuits via rods, cables and pulleys, similar to a mechanical FCS. The hydraulic circuit mainly consists of hydraulic pumps, associated parts and actuators. The actuators are powered by hydraulic pressure which is converted into control surface movements: servo valves control the movement of the actuators. Pilot input signals are transmitted via mechanical linkages to the servo controlled valves to power the appropriate actuators and move the appropriate control surfaces.

The main advantage of this type of FCS is that if there is a hydraulic power failure, the pilot can revert back to the manual mode of operation to deflect the control surfaces, albeit possibly with difficulty.

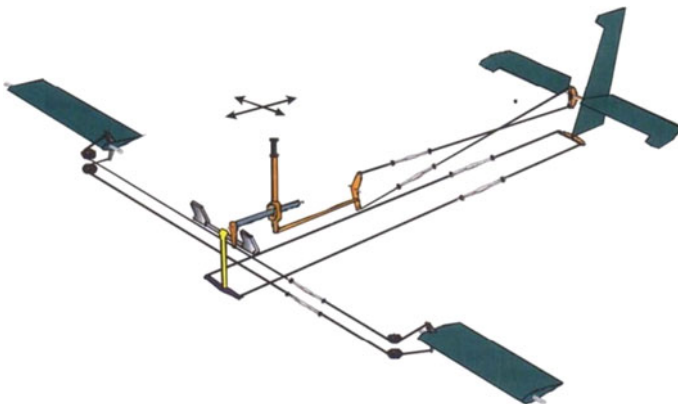


Fig. 13.8 Basic cable-type flight control system [8]

Fly-by-Wire FCS As aircraft operating speeds increased further with the advent of the jet engine, new undesirable aerodynamic effects arose at high subsonic speeds such as roll- and yaw-coupled oscillations known as ‘Dutch rolls’. This led to the requirement for autostabilization systems and the introduction of some computer control to the flight control system. The progress of digital electronics, and consequently computing power, led to the advent of ‘fly-by-wire’ aircraft. Using this technology, mechanical linkages are dispensed with and replaced by actuation controlled by electrical signals. These systems require sophisticated digital flight control computers, a network of air data sensors and essential avionics systems. All modern military and commercial aircraft use this system owing to the robustness of the system and also the reduction of the pilot loads.

In FCS operation the cockpit controls operate signal transducers (sensors) which generate the appropriate commands that are then processed by an electronic controller, which includes the autopilot.

In this system, hydraulic circuits are similar but make use of electrically controlled servo valves that are operated by the electronic controller. In this configuration it is necessary to simulate ‘feel’, and the electronic controller does this also.

Power-by-Wire FCS This system eliminates heavy hydraulic circuits and makes use of electrical power circuits. Electrical actuators are controlled by a digital flight control computer (DFCC). The main advantage of this system is weight saving and closer integration between the aircraft FCS and its avionics systems. A power-by-wire FCS system also greatly reduces the maintenance costs, owing to the absence of hydraulic systems.

13.9 Armament Systems

Typical fighter/trainer aircraft will have weapon stations and pylons for carrying external stores under the wings and fuselage. The stores can be fuel tanks, bombs, missiles, rocket pods, gun pods, target designator pods, fast tactical imagery (FTI) pods, camera pods, etc. Also, typical fighter aircraft will have an integral gun consisting of several sub-systems built into the aircraft structure.

Release of stores from the aircraft stations can be accomplished in several ways. They can be gravity dropped, force dropped, rail launched (missiles) or fired from the reusable pods (like rockets and a podded gun). Also, provision must be made for jettisoning of the external stores to recover the aircraft under emergency conditions.

13.9.1 Armament Construction: Pylons

Pylons are usually monolithic, being machined from aluminium alloy bar stock. This facilitates rigidity, easy assembly, interchangeability, etc. However, composite

pylons are also being used on many of the recently developed military aircraft with supersonic capability.

The pylons and their attachments should have sufficient margin to withstand the change in nominal load factors (G-jump) and fatigue loads that arise from stores release. These loads are mainly due to the combined effects of ejection force, dynamic response and instantaneous decrease in aircraft gross weight.

The main interfaces which are generally provided in the pylons include jettisonable and non-jettisonable stores, wing attachment bolts, ejector release units (ERUs), motorized valves, pylon interface boxes (PIBs), electrical and mechanical fusing units, laser-guided bomb (LGB) hard points, hard points for bomb tailing unit, electrical connectors and junction modules.

Examples of non-jettisonable stores include laser-designated (LD) pylons and guns. Jettisonable stores include missiles, bombs, drop tanks, ammunition, chaff and flares.

Pylons are aerodynamically designed and have quick-release access hatches for easy equipping, inspection and maintenance of equipment installed inside them. Each pylon is provided with a main suspension bolt and rear attachment bolt for interfacing with the aircraft wing.

Ejector Release Units The most important component in a pylon is the ejector release unit (ERU). This can be either a heavy- or light-duty type for the purpose of carrying heavier or lighter stores. The main accessories of ERUs include a ground safety pin, cartridge holder, throttle and cartridge.

Pylon Interface Box The PIB is an electronics box forming the interface between the aircraft and the stores.

Fusing System Pylons are provided with mechanical and electrical fusing units for carriage and release of various types of bomb fuses. Provisions are made for interfaces of both mechanical and electrical fuses at the nose and tail portions of the pylons.

13.9.2 Gun Systems

Gun systems will have several sub-systems, viz. ammunition box, feeder chute, link chute, case ejection chute, hoist system and gun mount installation.

13.10 Emergency Escape System

Military aviation operations normally involve potential risks due to enemy threats, engine flameout, technical failures, loss of control under strong manoeuvring at low altitude, etc. For this reason, most high-performance aircraft are fitted with individual ejection seats or escape capsules.

Emergency seats are equipped with rocket motors to propel the seat with pilot upwards from the aircraft as quickly as possible. Soon after the pilot initiates the ejection, a leg-restraint system avoids injury during ejection. In order to clear the path for ejection seats, the canopy is first severed and shattered by miniature detonating cords (MDCs). These are pasted along the centre line of the canopy to cut it before the seat ejection. MDCs are also pasted along the edges of the canopy for cutting the entire bubble for rapid exit during ground emergency egress cases. An explosive transfer line (ETL) is used to transfer the detonation from the point of initiation to the MDCs.

Upon ejection from the canopy, a drogue parachute is deployed automatically ($\leq 1-2$ s), and deceleration of the seat occurs till a suitable attitude is reached for the main parachute to be deployed.

The main parachute usually gets deployed when the airspeed falls to a maximum of about 250 knots [9]. Then the parachute inflates, stabilizes and reduces the vertical rate of descent to about 7 m/s. The rate of deceleration is limited to about 25 'g' to avoid excessive physiological stress. Upon reaching the safe altitude, a baro-static mechanism ensures that the seat separates from the pilot. This is normally below 10,000 ft.

A typical ejection seat used in military aircraft is shown in Fig. 13.9. Ejection seats have an emergency oxygen supply that caters for a minimum period of 5 min or when the pilot reaches the safe altitude. There is also a personal survival pack which remains attached to the main parachute harness after seat separation and contains a single-seat life raft, rations and survival aids. In general, the escape systems are some of the most complex pieces of equipment of any military aircraft,



Fig. 13.9 Military aircraft ejection seat

and some consist of thousands of parts requiring perfect sequencing of their operations. In the case of twin-seater aircraft the rear pilot ejects first, followed by the front seat pilot with a time delay of approximately 0.54 s for safe separation.

In the secondary mode of ejection, i.e. *ejection through the canopy*, the canopy is broken by ‘canopy-breakers’ fitted to the ejection seat. However, this is considered acceptable only as a backup mode, owing to the risk of head injuries due to high neck loads during impact with the canopy.

13.11 Materials for Mechanical Systems

The materials for mechanical systems include aluminium alloys, steels, titanium alloys, composites, elastomers and textiles. The materials are selected primarily for their functionality and also for saving weight. Other considerations include availability, cost, corrosion resistance and maintainability.

Materials for ECS A variety of materials are used for ECSs. The main criteria involve system operating parameters such as pressure, temperature, flow rates and heat sink medium. Inconel and stainless steel materials are commonly used for high-temperature and high-pressure application lines, e.g. ducting between engine bleed points to pre-cooler and primary heat exchangers. Some of these materials include AISI and AMS standards, i.e. AISI 316, AISI 321, AMS 5599 and AMS 5581.

Aluminium alloys are used in low-pressure and low-temperature pipeline applications, i.e. downstream of heat exchangers, and cockpit and avionics cooling lines. For air-to-air heat exchangers the plates and fins are also usually made of aluminium alloys, which provide high heat transfer efficiency.

Tubing and fittings make up most of the oxygen system plumbing and connect the various components. Most lines are metal in permanent installations. High-pressure lines are usually stainless steel. Tubing in the low-pressure parts of the oxygen system is typically aluminium. Flexible plastic hosing is used to deliver oxygen to the masks; its use increases in permanent installations to save weight. The fittings are typically made of the same material as the tubing. Rubber-bonded cork sheets and O-rings are used for leakage proofing applications.

Materials for Hydraulic Systems The main selection parameters of materials for hydraulic components include the type of fluid used, flow rate, pressure and temperature. Owing to high operating pressures, titanium alloys and stainless steel are extensively used in hydraulic system plumbing lines, e.g. AMS 4944D. However, aluminium alloys are also used wherever operating pressures are less, e.g. MIL-T-7081D.

Appropriate seals, gaskets and hoses must be specifically designated for the type of fluid used. Some of the more common gasket materials are copper, cork and rubber.

Some of the active materials like piezoelectrics, which convert electrical inputs into direct mechanical strokes, are being constantly improved. Since the response

frequency of piezoelectric materials and electrostrictives is in the order of 1000 Hz [10], efforts are being made to use them in the design of very small pumps, servo valves and shut-off valves of actuator systems.

As per MIL-H-5440H, the minimum proof pressure for the pipeline fittings, hoses couplings, etc., for the pressure circuit is 200 % of the operating pressure and 100 % for the return and case drain circuits. Similarly, the burst pressure for the pipeline fittings, hose couplings, etc., for the pressure circuit is 400 % of the operating pressure and 200 % for the return and case drain circuits. The materials used in hydraulic system design should have the capability to withstand and retain their properties within the temperature range of -54 to $+135$ °C.

Materials for Fuel Systems The main governing factors for the selection of materials for fuel system components include the type of fuel used, flow rate demand, operating pressure and temperature of the fuel. In aircraft fuel system design, Al-Cu and Al-Mg alloys, stainless steels and CM steel are used in addition to the materials used in ECS design. Some of them include BSL 63, WW-T-700/6, MIL-T-9047 and MIL-S-6758D4/HT.

Rigid fuel tanks are made from various materials and are installed in the airframe structure. The tanks are often riveted or welded together and can include baffles. They are typically made from aluminium alloy or stainless steel and are riveted and seam welded to prevent leaks. However, composite materials are being used extensively for fuel tank construction in recently developed aircraft. Flexible hoses are used in areas where vibration exists between components, such as between the engine and the aircraft structure.

Materials for Landing Gear and Brake Systems The selection of materials for the landing gear and brake system components is governed by the maximum aircraft all-up mass, maximum landing mass and maximum kinetic energy absorption exerted by the aircraft.

The tyres have a flexible casing constructed of rubber-coated nylon ply cords. The direction of the plies may be bias or radial. They are wrapped around the beads at each edge of the tyre. The core of a bead is a series of steel wires which reinforce the tyre and hold its circular shape. The tyres are inflated with nitrogen/air. The main reason for tyre overheating is heat released from the brake system after kinetic energy absorption. While some heat is released to the atmosphere in the form of radiation, the remaining heat gets transferred to the tyres.

A typical shock strut is usually referred to as an oleo strut. It is constructed of two telescopic cylinders or tubes that are closed at the external ends. Shock struts are equipped with axles for installation of the wheels. The shock strut materials are typically low-alloy high-strength steels.

Aircraft wheels are made from cast or forged aluminium and magnesium alloys for lightness. The materials used for wheel levers and axles include maraging steel with specification MIL-S-46850. The materials used for bush bearing areas include Al bronze with specification DTD197.

The materials for brake systems should have stable and reliable frictional and wear-resistant properties (brake discs) under varying conditions of load, speed,

temperature and environment. There are many factors to consider when selecting a brake disc material. The capability of the brake disc material to endure high abrasive wear, friction and high temperatures is most important. Weight, cost and processing methods also need to be considered.

The frictional heat generated on the rotor surface can influence excessive temperature rises which in turn lead to undesirable effects, such as thermal elastic instability, premature wear, brake fluid vaporization and thermally excited vibrations. The current materials used for aircraft brake discs are carbon-carbon (C/C) composites, carbon-silicon carbide (C/SiC) composites or carbon-carbon-silicon carbide (C/C/SiC) composites.

Carbon/carbon composites perform excellently compared to other materials such as ceramics, metal and plastic. They are light in weight and strong, and can withstand temperatures over 3000 °C without any loss in performance. Carbon reinforced silicon carbide (C/SiC) composite is a new material used for brake systems components such as disc and brake pads. This composite is thought to be more long-lasting than pure carbon-carbon.

Materials for Drag Parachute Systems Nylon is the material used for drag parachute fabrication. The materials for other components include low-alloy steels and aluminium alloys.

13.12 Future Trends in Mechanical Systems and Their Design

Many key technologies are being evolved across the world in the areas of propulsion and on-board airframe systems. It is predicted that there will be an overall 45 % improvement in the fuel efficiency over the next 3 decades, of which 6 % is expected from mechanical system improvements.

The following are some of the recent improvements and breakthrough technologies for mechanical systems. Most of these technologies have either more electric or an all-electric approach:

- Electric ECS/anti-icing/de-icing systems,
- Electric Engine Starter systems,
- Electromechanical/Electrohydrostatic actuators,
- Fault-tolerant Electric Machines,
- Turboelectric/distributive Propulsion systems, and
- Superconducting Generators/Fuel cells.

However, these technologies demand a higher electricity generation capability from the aircraft, and this must come from the on-board propulsion systems. Presently, the A-380 and B-787 aircraft have a power generation capability up to 850 and 1400 kW, respectively. In order to meet this growing power demand, some aircraft have adopted the variable speed and variable frequency (VSVF) and remote

power distribution system (RPDS) concepts. It is envisaged that in the near future the pneumatic auxiliary power units (APUs) will be replaced by the most sophisticated fuel cell APUs for the same class of power densities.

Though the main intent of any electrical system is to generate, distribute and control the electric power required for the functioning of on-board equipments and systems, the fundamental operation of these systems is based on mechanical principles. Thus engine shaft power is extracted via power take-off shafts and speed reduction gear mechanisms before supplying power into the main accessory gearbox. This accessory gearbox in turn supplies the mechanical power at the stipulated rate to the integrated drive generators (IDGs), main engine starter and hydraulic pumps. These deliver electrical, pneumatic and hydraulic power to the different systems on board the aircraft. Furthermore, some of the electrical generators and hydraulic pumps are directly mounted on the engine gearbox as a standby power source to meet emergency requirements. It is evident that all these areas fall under the category of mechanical systems in their basic operation.

While the majority of aircraft systems belong to the category of mechanical systems, their functional and operational effectiveness will be improved only by reinforcing with state-of-the-art solid power electronics in their core design process. Examples include landing gear actuation, operation of flight control surfaces, and control systems with feedback. Thus ideally no system should be purely mechanical or purely electrical.

It is envisaged that over the next few decades some of the new concepts like highly integrated systems, fuel cells, superconducting generators and fly-by-light are going to find a place in aircraft systems applications.

13.13 Summary and Conclusions

It is evident that the mechanical systems used in airborne applications are vital to safety and mission accomplishment. These systems must have high reliability, with multiple redundancies for safe recovery of the aircraft in case of unforeseen emergencies, for example rapid cabin decompression, landing gear extension failure, hydraulic and electrical power failures due to engine flameout, and loss of flight controls.

These mechanical systems are increasingly being combined with fully automatic controls and state-of-the-art solid-state power electronics, following a trend towards more compact and energy efficient systems for effective and highly reliable operations.

In the field of military aviation it is expected that most air confrontations will involve deployment of unmanned aerial vehicles (UAVs), for which mechanical systems are essential to accuracy and performance, endurance, crash survivability and maintainability.

Acknowledgments The authors would like to thank the management of Hindustan Aeronautics Limited, Aircraft Research and Design Centre, Bangalore, India, for facilitating study and extending the wholehearted support with necessary data for writing this book chapter.

References

1. Committee on Air Quality in Passenger cabins of commercial aircraft (2002) The airliner cabin environment and the health of passengers and crew (2002). National Academy Press, Washington, DC, USA
2. Bodha C (2010) Environmental control system and ice protection, MSc thesis. Cranfield University, Cranfield, UK
3. MOET Project Consortium (2009) Electrical environmental control system. Airbus France, Toulouse, France. <http://www.moetproject.eu>
4. Moir I, Seabridge A (2008) Aircraft systems: mechanical, electrical and avionics subsystems integration. 3rd edn. John Wiley & Sons, Inc., Chichester, UK
5. Harding RM (2002) Pressure changes and hypoxia in aviation. In: Textbooks of military medicine - special environments section, environmental stress volume, Office of the US Army Surgeon General & the Borden Institute. Washington, DC, USA
6. Civil Aviation Authority (2000) Aircraft Icing Handbook. Lower Hutt, New Zealand
7. Lawson CP (2012) Environmental control systems requirements and analysis. Cranfield University, Cranfield, UK
8. Airframes & Systems: JAA ATPL Training (JAR Ref 021 01) (2004), Jeppesen Sanderson Inc., Englewood, CO, USA
9. Stoliker FN (2005) Introduction to flight test engineering. RTO AGARDograph 300, Flight Test Techniques Series – Volume 14, Research and Technology Organisation, Neuilly-sur-Seine, France
10. Yoshida H, Sato S (2008) The technology trend and perspective of hydraulics in aircraft flight controls. Paper OS7-2. In: Proceedings of the 7th JFPS international symposium on fluid power, 15–18 September 2008, Toyama, Japan

Chapter 14

Design and Structures of Aircraft Engines

Rajaram Nagappa, Sankarkumar Jeyaraman and C. Kishore Kumar

Abstract Structural integrity and optimal weight configuration of aerospace structures continue to be a challenging task. In the case of aircraft engines, the task poses further complexities relating to rotating components, thermal environment and fatigue considerations. This chapter outlines the engine operating environment, structural design practices, failure modes and some aspects of reliability as applicable to military aircraft engines. A few important structural design methodologies are discussed in detail including the testing and validation aspects. The current design trends and technical challenges involved are also addressed.

Keywords Gas turbine engines · Structural design · Fatigue · Failure modes · Testing

14.1 Background

Piston engine–propeller, turboprop engine, turbojet engine (TJ) and turbofan engine (TF) types are used for powering different categories of aircraft. In all cases, the essential principle is to generate hot gases at high pressure and expand the gases to generate work. In the turbojet and turbofan engines the thrust is produced by the direct expansion of gases.

This chapter discusses the major aspects of high-performance military turbofan aircraft engine design. The flight envelope of military engines includes extreme operating conditions and loads induced by aircraft manoeuvres. This in turn demands a higher degree of structural and performance reliability.

R. Nagappa (✉)
NIAS, Bangalore, India
e-mail: r.nagappa@gmail.com

S. Jeyaraman · C. Kishore Kumar
GTRE, DRDO, Bangalore, India

14.2 Gas Turbine Engine Components and Operating Environment

The gas turbine engine structure consists of rotating and static components. The rotating components are responsible for supplying and extracting work from the working fluid to produce useful thrust/power. The static components support the rotating components and also serve as the flow path. The parts of a modern military turbofan engine parts are shown in the 3-D cutaway view in Fig. 14.1.

Rotating components include fan, compressor and turbine with bladed-discs, all connected together via the shaft. Modern military engines employ a twin-spool configuration, where the low-pressure (LP) spool shaft passes through the high-pressure (HP) spool shaft. The shafts are supported at bearing housings located at axial stations along the length of the engine. The discs of compressor and turbine are attached to the shafts by means of flanges. The blades are mounted on the discs either through axial slots (dovetail type) or circumferential slots. Circumferential slots are preferred for mounting compressor blades and dovetail slots for turbine blades.

Stationary components include stator vanes, casings, combustor, support structures/struts, bypass duct, jet pipe and nozzle. The vanes are mounted on the casings, mostly in a cantilever arrangement. They have a hub platform, which serves as flow path, and in the high-pressure compressor section the disc rim itself serves as the hub for the flow path.

In general the engine is supported by structures such as inlet struts and intermediate casings, which also house the bearings for the rotor support. The bearings are either ball or roller type depending on the type of loads they have to bear. The casings are connected by flanges, and the axial alignment of the engine is maintained by tightly controlling the concentricity of the casings.

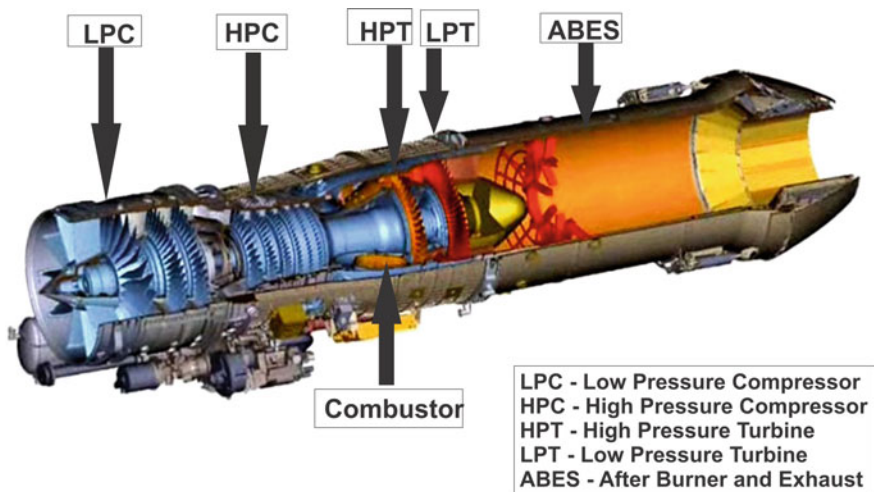


Fig. 14.1 3-D cutaway view of Kaveri engine

The operating environment of gas turbine engine components is extreme and demanding in terms of loads encountered and the required service life. There is a continuing trend towards achieving higher values of overall pressure ratio (PR) and turbine entry temperature (TET) for both civil and military turbofan engines. Overall pressure ratios of 30:1 and TETs of 2200 K have already been attained in military engines.

In supersonic combat aircraft, at Mach 2.0, the first stage fan blades will experience an inlet stagnation temperature of about 400 K and the blade tip speeds are always above 450 m/s. The higher inlet total pressures at supersonic speeds tend to increase the gas bending loads experienced by the blades. In the HP compressor the higher overall pressure ratio results in compressor delivery temperatures in excess of 875 K. The higher temperatures impact adversely on the creep, thermo-mechanical fatigue (TMF) and corrosion characteristics of the components.

In gas turbines the service life reduction caused by TMF largely depends on the number of start–stop mission cycles and not on the service hours. During operation, military turbofan engines are subjected to diverse and demanding conditions. Typically, these include the following [1]:

- Combat rating—2.5 min operation with afterburner (AB) at max condition
- Max dry rating—maximum performance without AB
- Intermediate or Military rating—30 min, without AB
- Max continuous rating.

Typical variations of total pressure and temperature along the engine length for various classes of engines are shown in Fig. 14.2 [1]. Military engine component design tends to be more demanding and challenging (particularly under afterburner, AB, conditions), since, it has to cater to mission cycle requirements when operating in hostile environmental conditions.

14.3 Requirements for Gas Turbine Materials

In aero gas turbines, as in all aerospace structures, the emphasis is on achieving low weight with improved performance, safety and durability. To meet these criteria the materials should be capable of withstanding the combined thermal and mechanical loads. It must also be noted that the hot sections like the turbines operate at temperatures close to the material melting point (T_m). Typically, the material used in the hot section must possess the following characteristics:

- High specific modulus (E/ρ)
- High specific tensile strength (UTS/ρ) at normal and elevated temperatures
- Low coefficient of thermal expansion (α) and thermal conductivity (k)
- Good fatigue strength—both high and low cycle fatigue (HCF and LCF)
- Creep resistance at high temperature (temperature close to $0.8 T_m$)
- Good corrosion, oxidation and wear resistance
- High fracture toughness.

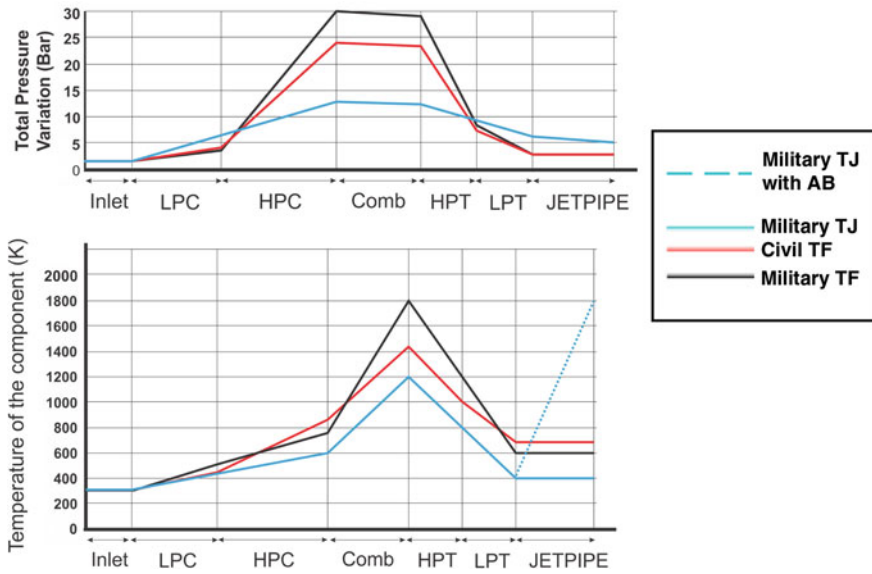


Fig. 14.2 Axial variation of total pressure and temperature

These properties need to be fulfilled individually or in combination, depending upon the component and its functional requirements. Typical operating conditions and materials employed in jet engine components are listed in Table 14.1.

14.4 Engine Design Phases

Aircraft engine design is typically carried out in three distinct phases, namely conceptual, preliminary and detailed design. The design tends to be iterative due to the pronounced interplay of physical (weight and size) constraints, thermodynamic aspects, engine architecture, material availability and manufacturing processes.

Conceptual Design Phase This phase addresses the performance requirements within the constraints of size and weight dictated by the overall aircraft design. Considerations of material availability, cooling system technology and manufacturing capability dictate the choice of TET and PR. In turn, other major performance parameters such as compressor, turbine and combustor component efficiencies, specific fuel consumption (SFC) and bypass ratio (BP) are determined. Design choices such as the number of rotor spools and other aspects, which have a bearing on the mechanical design, are also addressed in the conceptual phase.

Table 14.1 Jet engine components' operating conditions and typical materials

Component	Operating conditions	Alloy base materials
Compressor blades	<ul style="list-style-type: none"> • 0.5–2.36 bar entry • 15–70 bar delivery • 327–875 K 	Steel, Ti and Inconel (nickel-base) alloys such as Ti64, Ti811, Su718, AISI 403, GTD-450
Compressor discs	<ul style="list-style-type: none"> • 0.5–2.36 bar entry • 15–70 bar delivery • 327–875 K 	Steel, Ti alloys, Inconel
Compressor casings	<ul style="list-style-type: none"> • 0.5–2.36 bar entry • 15–70 bar delivery • 327–875 K 	Steel, Ti alloys, Inconel
Combustor liner	<ul style="list-style-type: none"> • Up to 70 bar delivery • Up to 2000 K 	Nickel-base alloys (CM 247)
Combustor casing	<ul style="list-style-type: none"> • Up to 70 bar delivery • Up to 2000 K 	Nickel-base alloys (CM 247)
Turbine nozzle	<ul style="list-style-type: none"> • Up to 67 bar • Up to 1850 K 	Nickel-base alloys (CM 247)
Turbine rotors	<ul style="list-style-type: none"> • Up to 60 bar • Up to 1850 K 	Nickel-base alloys, Su 718
Turbine discs	<ul style="list-style-type: none"> • Up to 60 bar • Up to 1850 K 	Nickel-base alloys, Su 718
Jet pipe	<ul style="list-style-type: none"> • Up to 30 bar • Up to 1000 K (normal) • Up to 2000 K (AB) 	Nickel-base alloys (CM 247)
Bypass duct	<ul style="list-style-type: none"> • Up to 30 bar • Up to 350 K 	Ti alloys, Su 718

Preliminary Design Phase In this phase, the skeletal framework of the engine and its geometric features are realized. The physical dimensions of major components such as the first rotor tip diameter, mechanical spool speeds, number of stages per compressor or turbine spool, number of blades per stage, are determined using the engine cycle parameters. At this juncture the structural design is largely influenced by the overall engine weight budget as well as manufacturing constraints. Major design houses, by virtue of their experience, have evolved empirical relations for engine component design. For example, one such widely used parameter is the product of the annulus area (A) and the square of the rotor rotational speed (N), i.e. AN^2 . Depending on the application and material choice, the AN^2 falls in the range of 0.4×10^{10} to 1×10^{10} ($\text{in}^2\text{-RPM}^2$). This parameter is indirectly related to the maximum possible tip speed for a given material and flow path configuration.

Detailed Design Phase This is the key phase of the design, aimed at achieving the required design targets. In this phase, key design features such as performance and weight as well as reliability and operational features such as manufacturing, inspection, assembly, maintenance, repair and overhaul (MRO) are addressed. Cost aspects also figure in this phase of design.

14.4.1 Engine Structural Design

Various international standards and regulations form the basis for engine structural design. For military aircraft applications the USA brought out MIL-STD-5007D in 1973. A revision of the standard, designated 5007E, came into being in 1983—the standard is mainly applicable for naval application and is in use by the US Navy. MIL-STD-5007D is currently inactive, but in the absence of a replacement standard it is widely followed for design practices [2, 3].

The MIL-STD-5007D is based on the ‘safe-life’ approach and details the requirements for structural life, component tests, inspection and retirement. In 1997 the US Air Force issued the MIL-STD-1783 handbook for structural performance, design development and verification guidance for turbine engines. The handbook states the need for an Engine Structural Integrity Programme (ENSIP) and essentially follows the guidelines of MIL-STD-5007E including both the ‘safe-life’ design approach and ‘damage tolerant’ philosophy [3].

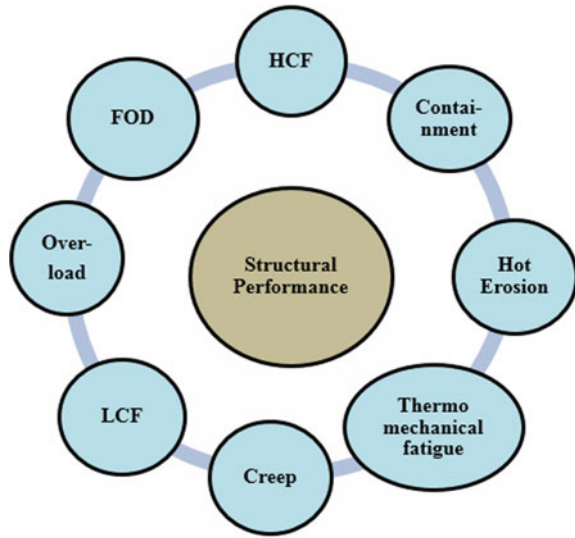
It was indicated in Sect. 14.2 that the gas turbine structure is divided into rotating and static parts. The rotating components are subjected to inherent mechanical and flow-induced vibrations: hence they are designed with sufficient stiffness and adequate fatigue margin. The stiffness consideration is met primarily by the judicious choice of component natural frequencies, whereas reasonable stress margins are ensured to meet the required factors of safety (FoS). All these design requirements are met using structural analysis methods—typically finite element analysis (FEA) and using the candidate material properties (-3σ). These include nonlinear effects, material contact and wear, heat transfer, flutter, buffeting, non-synchronous vibrations (NSV) and fluid–structure interactions. For flow paths, thermo-structural and coupled field analysis finite element analysis (FEA) and computational fluid dynamic (CFD) analysis codes are used. Both in-house developed codes as well as commercial codes are available for carrying out nearly 70 % of the dimensional detailed analyses [4, 5].

Additionally, aircraft engine manufacturers have evolved empirical structural design tools based on their extensive in-house test database. The database has been used to evolve design tools and handbooks for carrying out the basic design and weight estimation. Most handbooks are company proprietary, and consequently it becomes imperative for every design agency to develop their own legacy-based design tools and criteria.

For the structural design of gas turbine components the following operational loads need to be considered:

- Internal pressure
- Centrifugal loads
- Thermal gradients and transients
- Inlet pressure and temperature
- Acceleration and gyroscopic moments
- Unbalance and misalignment
- Manoeuvre
- Flow-induced excitations.

Fig. 14.3 Component failure modes [4]



These operational loads are estimated by the aeromechanical designer using inputs from the performance and material specialists. As part of these estimations the structures are evaluated for the major failure modes shown in Fig. 14.3.

14.4.2 Design Reliability Requirements

The guidelines for reliability assessment are based on the requirement of the mission and follow the ENSIP guidelines. The guidelines are comprehensive and they cover design, testing, inspection and maintenance. The important reliability requirements are detailed below.

In general, the engine structural life is defined in terms of service hours including time for maintenance and repair. Typically, for a given mission requirement, the following duty cycle is considered:

- Zero-Max speed-Zero or
- Idle-Max speed-Idle or
- Cruise-Intercept-Cruise (applicable for combat aircraft).

Structural life is estimated separately for relatively cold parts such as low- and high-pressure compressor (front stages only); and hot parts such as combustor, turbine and exhaust. The intended usage is expected to encompass the mission mix (combination of missions), operating environment, engine attitude conditions, temperature extremes, icing and corrosion requirements, etc. [2].

Structural life requirements are also specified for components in terms of the HCF and LCF cycles separately. The values for HCF range from 1×10^7 and 3×10^7 cycles for steel and non-ferrous parts, respectively, whereas the LCF cycle is obtained as per the user-defined mission cycle. For combat aircraft engines, 0-Max-0 cycles numbering 3200 for cold parts and 1600 for hot parts are suggested [2, 3].

Fan and compressor casings, combustor casings and liners, turbine casings, afterburner casings and liners need to be designed for twice the maximum operating pressure, while ensuring they satisfy the buckling criteria. The hot parts need to be designed for creep resistance in addition to the HCF and LCF requirements.

To ensure rotor integrity containment, over-speed and burst-speed margins need to be estimated for the disc + blades configuration. The over-speed and burst-speed values correspond to 115 and 122 % of the design speed at the maximum allowable gas temperature. The margin demonstration includes a five-minute dwell time at the over-speed condition [2, 3].

Estimation of modal characteristics at different operating speeds for all the rotating and static parts is mandatory, and the prevalent thermal state has to be taken into consideration. The results are used to identify the occurrence of resonance in the operating regime: resonance, if noticed, has to be circumvented through an aomechanical iterative design process.

All the foregoing requirements need component test data as well as measurements from rig and engine tests to validate the design and prove the structural integrity. The test data and results will lead further to the certification and acceptance of the engine.

14.4.3 Component Design Approach

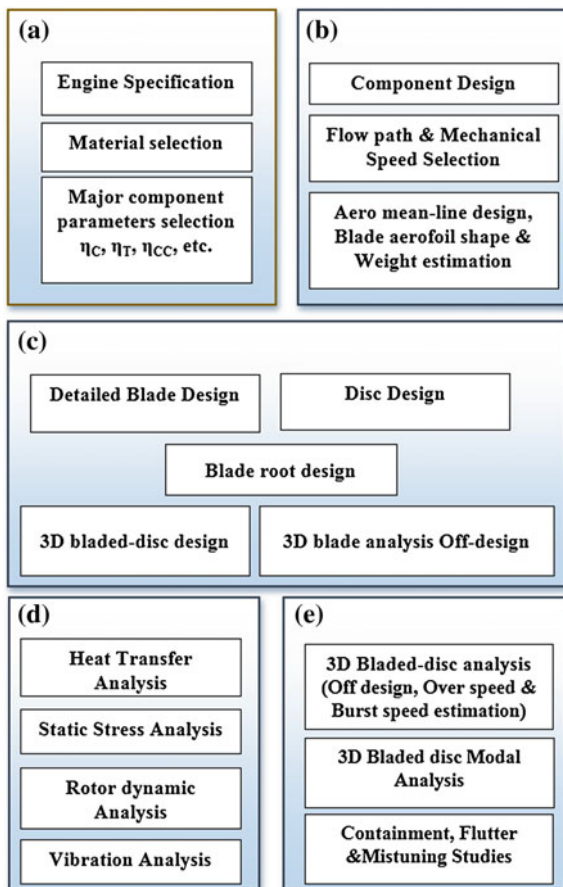
As mentioned in the previous section, a high degree of reliability is mandated in gas turbine design. This implies rigorous theoretical estimations in the early design phase. The gas turbine design community has evolved comprehensive design approaches based on both deterministic and probabilistic methods.

The deterministic approach uses the material property limits to evaluate the design safety factors, but it lacks the potential to cater for real-world uncertainties. Consequently, issues connected with load fluctuations during off-design operation, geometric variations of manufactured component features, and in-service deterioration of component are not addressed. These uncertainties impact the reliability assessment.

The use of a probabilistic-based design method helps in overcoming the lacunae in the above approach. This approach uses the -3σ (sigma) material properties with FEA for design evaluation of components, followed by the HCF and LCF life estimation methodologies.

The conventional disc + blades design is chosen to illustrate the flow of activities involved in various stages of a gas turbine component design. The design approach

Fig. 14.4 Typical conventional blade and disc design



is shown in the block diagram in Fig. 14.4. The design phases as explained in Fig. 14.4 are grouped in separate blocks: a, b, c, d and e. Block a forms the conceptual phase where the complete engine design is initially evolved. In block b, the preliminary component design is taken up; during this phase, the basic architecture and weight are estimated with the 1-D or 2-D through-flow evaluation. In this phase, design choices such as blade height, number of blades, blade airfoil parameters—chord, thickness, stagger and camber—are estimated. Design choices are iterated several times between the aerodynamic and mechanical design choices to obtain the design solution.

In block c, the blade and disc shapes are finalized with the fillets and root angles and locking arrangement with the discs. At this juncture, the design features are carefully evaluated from fabrication and manufacturing considerations.

The main function in block d is finalization of the blade configuration using detailed simulations using 3-D FEA and CFD tools. The analyses include stress evaluation, modal analysis, heat transfer simulation and the rotor dynamic

simulations for operational loads. In this block, the analysis results might lead to an iterative loop with block c and occasionally with block b.

Once the basic design meeting the major operating point structural requirements is completed, the off-design and safety-related issues are addressed. Finally, the design reaches a mature stage in block e and leads to the prototype manufacturing process. The LCF and HCF fatigue lives of the components are evaluated in this phase. Additionally, flutter and bird strike containment requirements are also addressed. Advanced analytical frameworks involving coupled physical domains need to be used. In case of any non-convergence, the design loop might rewind to block b.

The approach described in the preceding paragraphs is applicable to other components of the engine, and the same process is followed for the design of casings, shafts, bearing housings, support frames, mounts and other subsystems.

14.4.4 Specific Design Tools and Methodologies

Some of the important tools/methodologies related to the design of gas turbine components are briefly described in this section [5, 6]:

- Blade lean or untwist compensation
- Campbell diagrams
- Goodman Approach for HCF life
- HCF life estimation using the Palmgren–Miner rule
- Cycle counting techniques
- Creep life estimation using the Larson–Miller parameter (LMP)
- Reduced frequency approach for flutter prediction
- Stiffness estimation of support structures.

Blade Lean or Untwist Compensation Any airfoil placed in the flow is expected to have correct incidence for proper performance. This is applicable to gas turbine blades also. The gas turbine blade can be considered to consist of airfoil profiles stacked radially and twisted as per the design requirement. The cantilevered fan or LPC rotor blade undergoes centrifugal stress combined with pressure and temperature loading and tends to deflect and/or untwist near the tip section. This untwist leads to a change in blade incidence which may result in flow separation, tip stall and performance loss.

The untwist effect is countered by intentionally pre-twisting or re-staggering the blade in the opposite direction. This pre-twist, commonly referred to as ‘blade lean’ allows the blades to revert to their intended incidence under the action of the imposed centrifugal and aero loads. The ‘blade lean’ effect is shown in Fig. 14.5.

Current fan designs employ ‘part-span shrouds/snubbers’ or use wide chord blades [7] to avoid or minimize the blade untwist. This leads to an increase in the

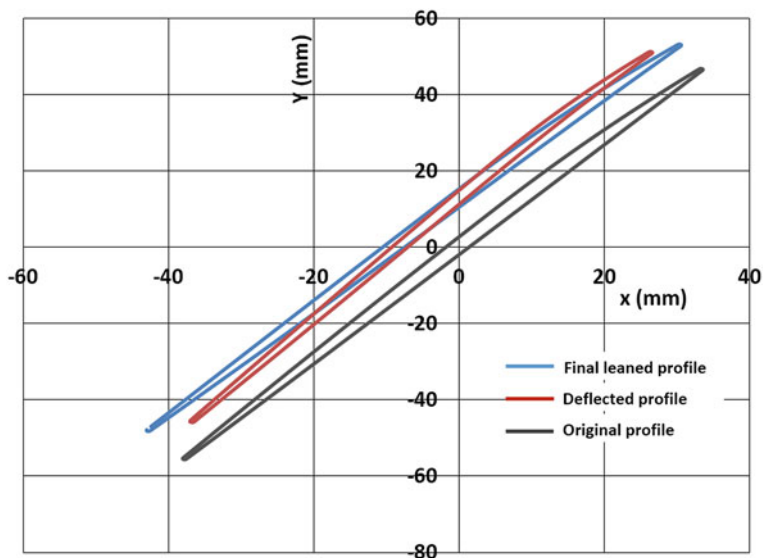


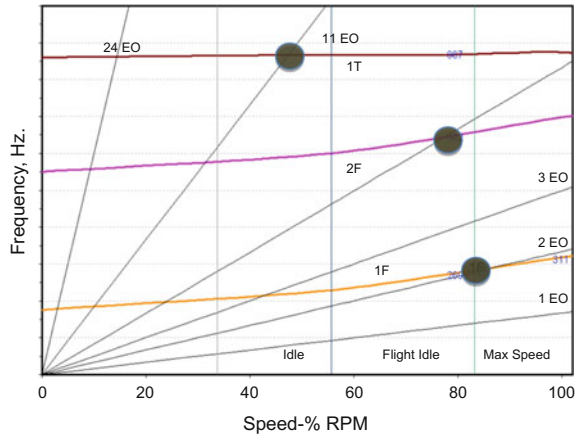
Fig. 14.5 Rotor blade tip profile

blade's fundamental natural frequency and mitigation of blade aeromechanical instability such as blade stall flutter.

Campbell Diagram This is an important design tool widely used in the design of rotating machinery to identify the possibility of resonance. A typical Campbell diagram of a rotor blade is given in Fig. 14.6, which depicts the natural frequencies, excitation or engine order (EO) lines and critical operating conditions. The horizontal lines represent the natural frequencies of the blade arranged in the order of their modes. The modes of a typical rotor blade are termed as first flexure (1F), second flexure (2F), first torsion (1T), etc., and they are arranged in the diagram in their order of occurrence on the vertical axis. The inclined lines are termed the excitation or engine order lines, which correspond to the rotational speed (N) of the component. These EO lines basically depict the possibility of an excitation frequency, which could be an integral multiple of the rotor speed, i.e. $1 \times N$, $2 \times N$, $3 \times N$, etc. The vertical lines represent the speed at which the engine is expected to operate for a considerable time while in service.

While constructing this diagram, the effect of blade loads such as centrifugal force, temperature effects (influencing the blade material property), pressure loads and actual blade fixity conditions are considered. The blade natural frequency tends to increase or decrease depending upon the combination of the loads. For example, in the shown Campbell diagram the 1F and 2F mode natural frequencies increase with speed, whereas the 1T mode does not undergo much change up to the maximum design speed. These features provide crucial information to the designers in the early part of the design about the blade stiffness configuration [8–10].

Fig. 14.6 Typical Campbell diagram for a rotor blade



The filled circles in Fig. 14.6 indicate the possibility of resonance. In the case of the first flexure mode, around 82 % speed, the second engine order (2EO) interferes with an operating point such as cruise. This information alerts the designer at an early phase to critically examine the possibility of the resonance and its likelihood of excitation during service. At present, the rule of thumb is to provide a margin of 10 % of the natural frequency for avoiding a resonance situation. This margin accounts for deviations in manufacturing tolerances, material properties variations, service-related deterioration and in situ minor damage. For example, if resonance cross-over is expected to happen around 500 Hz with a known engine order, say 3EO, the blade frequencies will be chosen either above 525 or below 475 Hz.

This design aspect generates conflict with the other design requirements in rotating machinery and often leads to extended design cycle time. It is also impossible to avoid all the resonance possibilities during the design; hence the decision is largely based on test experience. However, the design information is verified during the test stages of engine development such as component, rig level, subsystem level and engine tests [5, 11– 13].

Goodman Approach for HCF As elucidated in the preceding subsections, engine components experience steady and fluctuating loads during service. The rotating components experience centrifugal loads (steady loads) and superimposed fluctuating gas bending loads (alternating loads) generated by the upstream and downstream excitations.

In a typical mechanical fatigue design approach (proposed originally by Prof. J. Goodman), the effect of mean stress on the allowable alternating stress for a component is studied with the various combinations of stresses, i.e. maximum (σ_{\max}) and minimum (σ_{\min}) values. The conventional Goodman diagram is shown in Fig. 14.7a. The drawback of this approach is that it is not possible to impose any alternating stress (σ_r) on the component when the mean stress value approaches the yield stress (σ_Y) and tensile stress (σ_{UTS}). This characteristic will remain the same

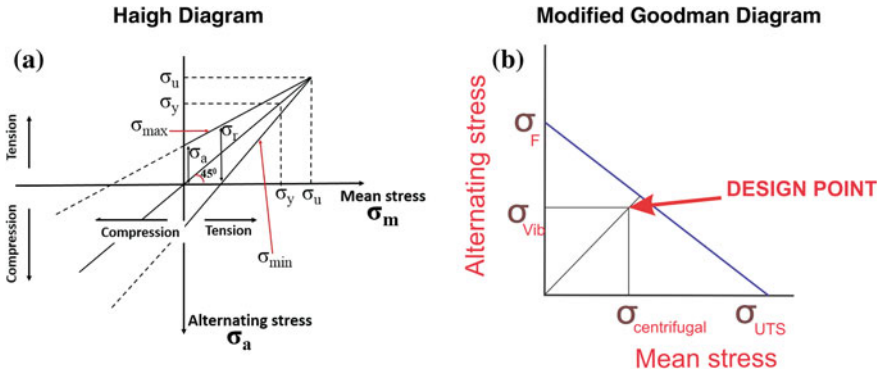


Fig. 14.7 Design approach for HCF life [18]

for tension as well as compression and also for a fully reversed condition, i.e. $(\sigma_{min}/\sigma_{max}) = -1$ [14–17].

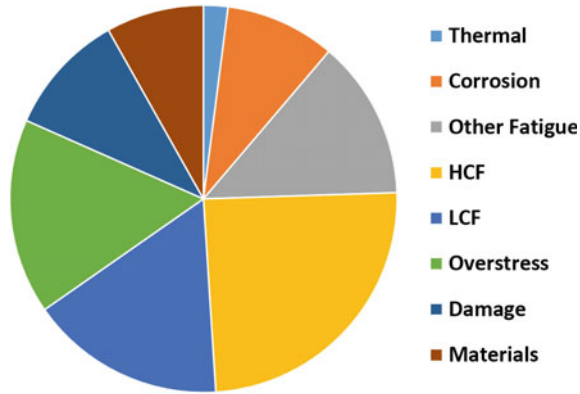
The Goodman diagram was modified in later years as shown in Fig. 14.7b. In this plot, the mean stress is plotted on the horizontal axis up to σ_{UTS} and the alternating stress is represented on the vertical axis till σ_F . To evaluate the allowable alternating stress, the gas turbine component steady stresses due to the thermo-mechanical loads (including gas bending loads) are estimated using the finite element analysis (FEA) method. After estimating the steady or mean stress (σ_{mean}) value, the diagram is used to estimate the allowable alternating stress (σ_{Alt}) for an infinite HCF life, typically 1×10^7 cycles. The operating stress value should lie within the design space indicated in the figure and with sufficient margins from the inclined failure line.

It is important to note that the mean stress values need to be restricted to obtain sufficient margin in the alternating stress range. In general, for gas turbine components to cater to the blade resonance responses and other aerodynamic disturbances, a margin of 100 MPa is provided during the design stage. These stress values are based on the constant amplitude HCF life ranging up to 10^7 cycles. For variable amplitude HCF life considerations, techniques based on the Miner damage rule combined with cycle counting techniques are employed [16, 17, 19–21].

HCF Life Estimation Using Palmgren–Miner Rule The contributory causes to jet engine failure are depicted in Fig. 14.8. It is evident from the figure that HCF accounts for about 25 % of the major engine distress events. This corresponds to around 30 % of the total project cost. Factors such as thermal transients, corrosion, mechanical damage, material inadequacy, manufacturing issues and overstress account for the remaining failure modes.

Considering the higher incidence of HCF-related failures, attempts to establish reliable design criteria have resulted in various HCF-based life assessment approaches. Among them, the ‘Palmgren–Miner’ rule, also called ‘Miner rule’, is commonly used. This rule states that if the cumulative damage of a component

Fig. 14.8 Distribution of failure modes in jet engines



reaches unity after accounting for the various combinations of stress cycles, the component will fail. The rule is expressed as follows:

$$\sum_{i=1}^n \frac{n_a}{N_a} + \frac{n_b}{N_b} + \dots + \frac{n_n}{N_n} = 1 \tag{14.1}$$

where n_a , and n_b represent the number of cycles experienced by the component at the given stress levels (a and b). N_a and N_b represent the maximum number of cycles the component would have withstood at the particular stress levels.

In gas turbine engines all components are subjected to varying stress levels during various phases of a mission. Miner’s rule provides a simple approach, where the fractions related to each stress amplitude can be accounted for. The component is expected to fail once the cumulative damage nears unity [4, 5, 16, 17].

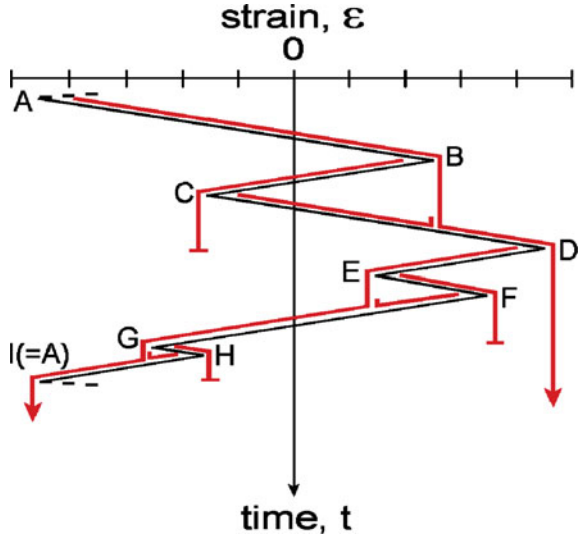
In this approach the uncertainties are considered together in terms of an overall safety factor. This leads to a safe service life, but with considerable weight and cost penalties. Even though this approach is often utilized, it has severe limitations due to its inability to account for factors such as load sequence, component geometry and metallurgical deviations.

Cycle Counting Techniques The Goodman approach, as well as the Miner damage accumulation rule, takes into consideration only a single operating point. In the operation of a military gas turbine, the component endures various stress states such as take-off, climb, cruise, manoeuvres and descent and landing.

The variation in stress levels in the course of a mission can be represented in the form of a mission cycle, and the corresponding life consumption in the process can be evaluated. Fatigue cycle counting methods include range-mean counting, race-track counting and rainflow counting. Among these, the rainflow counting technique is often used to account for the hysteresis effect and variable amplitude mission cycles as illustrated in Fig. 14.9.

Based on the aircraft mission profile, the total number of permissible cycles is established accounting for the load history and hysteresis effects. From this

Fig. 14.9 Rainflow counting pattern



sequence a variable amplitude HCF life can be predicted using the Miner damage accumulation rule.

As per the ENSIP requirement, for any given application such as fighter, bomber, cargo or trainer aircraft, the number of such cycles required will be defined as a requirement and subsequently the number of hours of service will be decided. In the case of the F-22 Raptor aircraft with the PW-F110 engine, the life of hot parts is based on experience and specified as 1487 (0-Max-0) cycles, 10,252 (Idle-Max-Idle) cycles and 11,037 (Cruise-Intercept-Cruise) cycles [2, 5, 17, 20, 21].

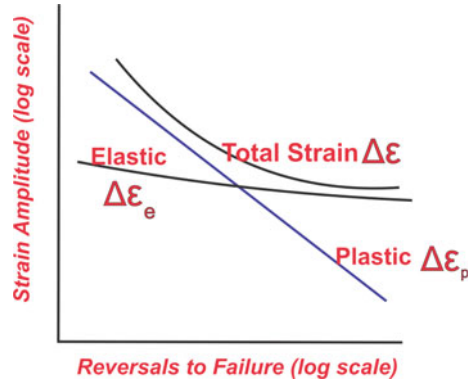
LCF Life Estimation Using Coffin–Manson Relationship As stated earlier, to meet the safety and reliability requirements the gas turbine components such as rotors, casings and shafts have to be designed to perform at 115 and 122 % of design speed. At such off-design conditions, the components experience plastic strain and the entire strain range needs to be considered for the LCF life estimation. The Coffin–Manson relationship given below covers both the elastic and plastic strain ranges:

$$\frac{\Delta\varepsilon}{2} = \frac{\Delta\varepsilon_e}{2} + \frac{\Delta\varepsilon_p}{2} = \frac{\sigma_f'}{E} (2N)^b + \varepsilon_f' (2N)^c \tag{14.2}$$

where

- $\frac{\Delta\varepsilon}{2}$ total strain amplitude
- $\frac{\Delta\varepsilon_e}{2}$ elastic strain amplitude
- $\frac{\Delta\varepsilon_p}{2}$ plastic strain amplitude
- ε_f' fatigue ductility coefficient

Fig. 14.10 Number of fatigue cycles to failure for a given total strain range [$\Delta\varepsilon$, which is the sum of elastic strain range ($\Delta\varepsilon_e$) and plastic strain range ($\Delta\varepsilon_p$)]



- σ'_f fatigue strength coefficient
- b fatigue strength exponent
- E modulus of elasticity
- N number of cycles / reversals to failure

The elastic strain is based on the Basquin relationship with fatigue strength coefficient, whereas the other inputs are obtained from material test data. Using this approach the total strain experienced by the component and hence the number of reversals or cycles to failure can be estimated. The plot depicting all the strain components is given in Fig. 14.10.

It is important to note that the elastic strain can be estimated using FEA, whereas nonlinear elasto-plastic analysis is required to predict the plastic strain.

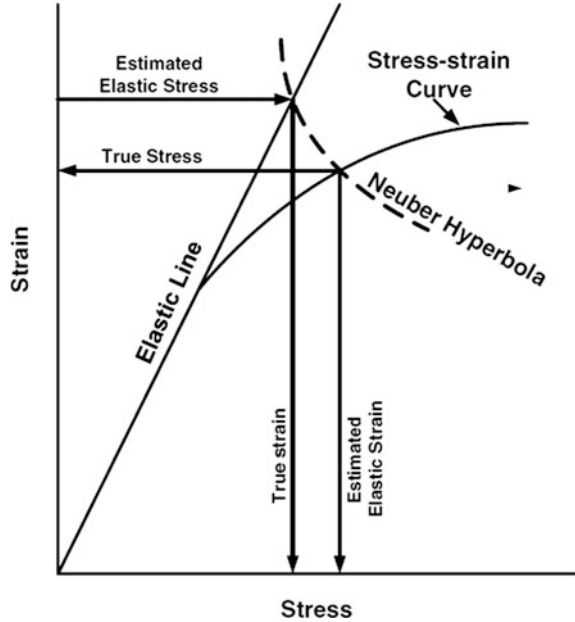
In gas turbine components the holes in the casing flanges as well as locking features in blades and discs are locations of high stress concentration and need to be specifically addressed. The Neuber hyperbola approach shown in Fig. 14.11 provides the means to estimate the true stress-strain state. This technique is mainly used in the design phase, where the result of the linear stress analysis is used to estimate the plastic strain through an iterative approach.

It is important to note that the value of the coefficients used in the Coffin-Manson equation as well as the Neuber approach can significantly influence the LCF life estimation results. It is therefore imperative that the coefficients are generated from representative numbers of material tests simulating the operating conditions of the stress concentration features [19, 22–24].

Creep Life Estimation Hot-end rotating parts of a gas turbine engine experience high temperatures ($\sim 0.8 T_m$) combined with centrifugal loads. For these components, creep and thermo-mechanical fatigue (TMF) are the dominant failure modes. By definition, creep is the progressive failure of a component due to continuous exposure to long-term loading with high temperatures (typically $< 0.5 T_m$) for a long time.

Among the several approaches to predict creep life, the Larson-Miller parameter (LMP) [25] is often employed. The LMP is given by the following equation:

Fig. 14.11 Strain data for LCF estimation [17]



$$LMP = T/1000(\log t_f + C) \tag{14.3}$$

where

- T —component metal temperature, K
- t_f —time to fracture, hours
- C —constant.

The constant, C , is evaluated via tests at different temperatures and is specific to a material [15, 22, 23, 24, 25]. In general, for nickel-base alloys used in gas turbines, the value of C is around 20.

A typical LMP graph for a NIMONIC 80A nickel-base alloy is shown in Fig. 14.12. For estimating the creep life of a turbine blade or disc, the LMP is obtained from the material test curve using the operating stress and the component metal temperature. The stress value is estimated using FEA techniques, and the metal temperature is determined through thermal analysis.

Creep rupture life is highly sensitive to temperature variations. For instance, it can be stated that for a 50 K TET variation, the component life can drop by an order of magnitude from 40 to 5.7 years. Because of this sensitivity, life prediction needs to be evaluated judiciously [4, 15, 17, 26].

Providing thermal barrier coatings (TBCs) and oxidation resistant coatings helps to improve the creep life of turbine blades. TBCs can cause blade metal temperature reduction by 150 K, as shown in Fig. 14.13. This effective temperature containment scheme is responsible for achieving higher TETs and consequently leads to an improvement in the overall engine efficiency. However, TBCs undergo in-service deterioration such as erosion, corrosion, coating peel, spalling and hot corrosion.

Fig. 14.12 LMP graph for Nimonic 80A alloy

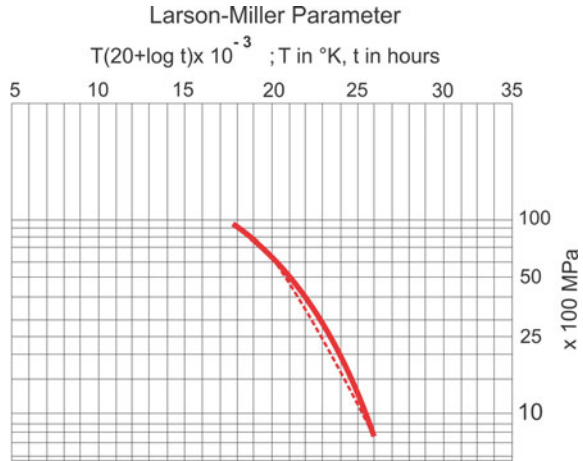
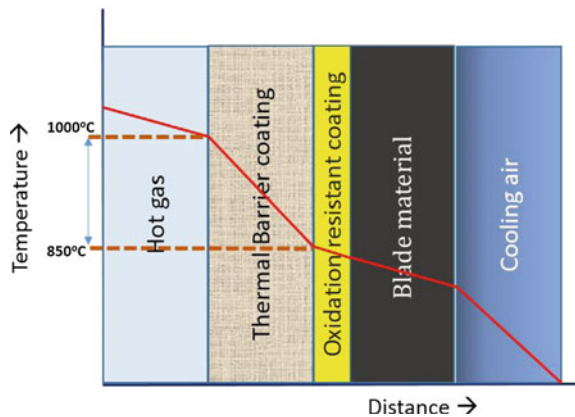


Fig. 14.13 Efficacy of TBC and other cooling systems



Reduced Frequency Approach for Flutter Prediction Engine components are designed to be flutter-free, and this is confirmed by testing.

In addition to the structural design philosophy outlined in the preceding subsections, the reduced frequency is a preliminary aeromechanical empirical criterion. This criterion is used to establish the aeroelastic stability of a blade and is largely based on the test experience of various engine design offices [27].

The reduced frequency relating structural frequency and chord to blade inlet relative velocity is given by the following equation:

$$\text{Reduced frequency, } k = \frac{2\pi fC}{V} \tag{14.4}$$

Table 14.2 Reduced frequency values for different modes [10, 12]

Mode/type of flutter	Reduced frequency (k)
First bending/subsonic	0.3–2.0
First torsion/subsonic and transonic stall	0.8–4.0
Second bending	1.0–6.0
Bending/supersonic	0.2–0.5
Torsion/unstalled supersonic	0.7–1.3

where

f is the blade natural frequency

C is the blade chord (typically 80 % of the blade span and

V is the inlet relative velocity

The value of k quantifies the blade stall flutter characteristics and is applicable for large rotor blades such as the fan and early stages of the LPC. Typical reduced frequency values for different modes are shown in Table 14.2.

Several investigators [10, 11, 28] have provided a detailed physical account for reduced frequency and its relation to the unsteadiness present in the system. Codes coupling finite element analysis (FEA) and computation fluid dynamics (CFD) are being used for research and design iterations [27–31].

Stiffness Estimation of Support Structures Rotor assemblies are supported by frames that house the bearings and also provide the necessary stiffness to the rotors. Modern gas turbines are typically twin-spool engines, where two rotors operate at different mechanical speeds. These rotors have characteristic critical speeds based on their configuration and support stiffness.

The support stiffness values are judiciously chosen based on the dynamic analysis of the rotor configuration. The stiffness values are obtained using the static stiffness analysis while accounting for the bearing load distribution and mounting configuration. However, it is also important to account for the nonlinearity in the joint stiffness between the support frames and bearing housing mounting flanges. These nonlinear effects determine the engine response during the crossing of critical speeds, and hence various damper configurations are used in modern engines.

Typically, the squeeze film damper configuration (SFD) is used in military engines, where highly pressurized lubrication oil is forced through the few hundred microns clearance between the rotor and bearing housings. The pressurized oil absorbs the rotor response during critical crossover and manoeuvres. The design of the damper housings and estimation of their stiffness and estimation of deflections are done using advanced finite element analysis.

Casing Design for Buckling and Overload Unlike the support frames with the load-bearing struts, the fan, combustor and afterburner casings are thin shell-type structures. These shell structures are designed to withstand twice the maximum operating pressure at the peak temperature. These requirements are mandated for reliability demonstration as stipulated in the engine certification programme.

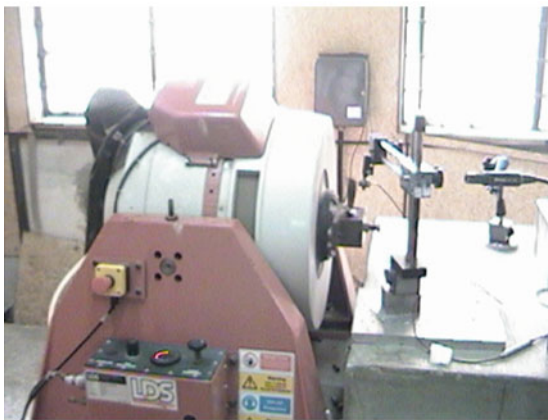
Considering the nature of the loads, the critical failure modes will be buckling and overload. Suitable buckling factors are obtained for the shell-type casing using FEA techniques at different operating conditions. In the case of overload, significant plastic strain is expected and hence the LCF-based life estimation approaches are followed. The Coffin–Manson approach is followed for reliability estimation and subsequently confirmed by testing [2, 3, 32].

Subsystem Design Gas turbines have several subsystems with specific functions. The subsystems include gearboxes, pumps for fuel and lubrication supply and scavenging, full authority digital engine control units (FADECU), actuators and valves. The subsystems are designed to meet the strength and stiffness requirements and are subjected to functional tests and environmental stress screening (ESS) tests as per the MIL-STD-810-F/G for qualification. Modal frequencies and mode shapes of these subsystems are evaluated using finite element analysis and validated through tests.

14.5 Testing and Validation

Gas turbine engine components, as well as the total system prior to acceptance for service, are subjected to a number of qualification tests as mandated by the reliability requirements.

HCF is the predominant mode of failure for blades. Strain surveys are conducted on the blades using electrodynamic or piezo shakers, typically up to 20 kHz, depending on the blade stage. During the strain survey, strain gauges are placed in the response locations (Fig. 14.14) as per the analytically predicted modal



Blade Fatigue Test Facility



Blade Strain survey

Fig. 14.14 Blade fatigue testing and instrumentation

characteristics, and excited using the shakers. The theoretically predicted mode shapes and frequencies are validated by the experimental frequency response function (FRF) using modal shakers.

Spin pits tests are conducted to verify disc structural integrity requirements at the overspeed limit of 115 % and burst-speed level of 122 %. In these tests, dummy blades simulating the weight and centre of gravity position (CG) of the blades are employed. In the case of overspeed the disc will experience plastic deformation, whereas in burst speed the fragments will be contained in the pit. Such tests are prescribed for shafts also. Images are captured via a high-speed camera.

To verify the HCF characteristics of blades, spin pits are operated under high vacuum with the actual blades and sophisticated instrumentation. Test data are transmitted either through the use of slip rings or through telemetry. A blade tip timing technique (BTT) is also used to measure the response.

Casings and pressure vessels are qualified at twice their operating pressure and at the highest operating temperature. The pressure proof test is done in a pressure test vessel.

14.6 Current Trends in Structural Design

The quest and requirements for weight saving and improved reliability are always the design driver for aircraft engines. Advanced materials and improved manufacturing processes aim to address these goals.

Present day engines mostly use conventional rotor configurations of discrete blades and discs that are assembled together. The current trend, however, is towards the use of 'blisks' or integral bladed-disc rotors (IBR), where the blades and disc are welded or machined as a single piece from a forged blank. Figure 14.15 illustrates the conventional bladed-disc and blisk configurations. Weight savings up to 30–35 % can be achieved for 'blisks' using improved manufacturing processes. The advanced manufacturing techniques employed include linear friction welding (LFW), electrochemical machining (ECM) and precision electrochemical machining (PECM). 'Blisks' are used in the fan and compressor stages of modern engines such as the European Consortium EJ200, SNECMA M88-2, General Electric F414 and Pratt and Whitney F119.

Active research is being pursued in the area of 'blings' or bladed rings, with further weight saving potential. 'Blings' are made up of titanium alloy clad layers reinforced with a metal matrix composite (MMC) core in the hoop direction, which offers the requisite tensile strength. Experimental 'blings' are under evaluation in spin pits for structural integrity tests. An example is shown in Fig. 14.16.

In the turbine section, directionally solidified (DS) nickel-base superalloys with thermal barrier coatings (TBC) are already in use. They offer improved creep life over equiaxed grain blades, and further improvement is made possible by the use of single crystal (SC) blades.

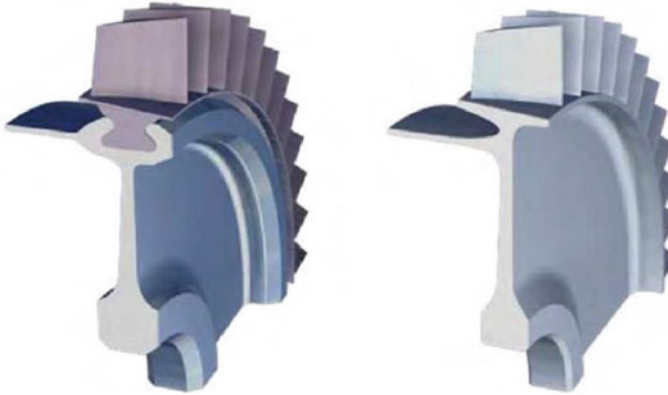


Fig. 14.15 Conventional bladed-disc and blisk [33]

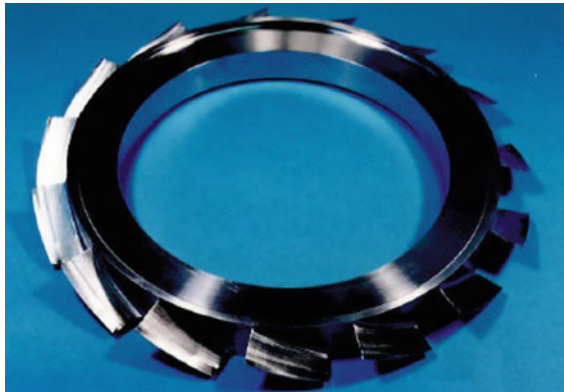


Fig. 14.16 Titanium blisk with MMC core [34]

Generations of SC blades have been produced and are employed in modern engines such as the SNECMA M88-2, General Electric F414, European Consortium EJ200 and Pratt & Whitney F119 and F135. Currently, the fourth generation single crystal blades are used with TBCs, with significant improvement in TET and creep rupture strength. All three different blade materials are illustrated in Fig. 14.17.

Titanium aluminides are being considered for use in the later stages of compressors and also in the low-pressure turbines. These alloys have low density, good tensile strength and good creep and fatigue properties, in addition to enhanced temperature capability up to 750 °C. Major OEMs like Rolls-Royce have already employed titanium aluminides in such applications.

Finally, fan casings, bypass ducts and jet pipe petals are being manufactured from ceramic matrix composites (CMC) and metal matrix composites (MMC). These offer considerable weight savings without compromising the structural integrity.

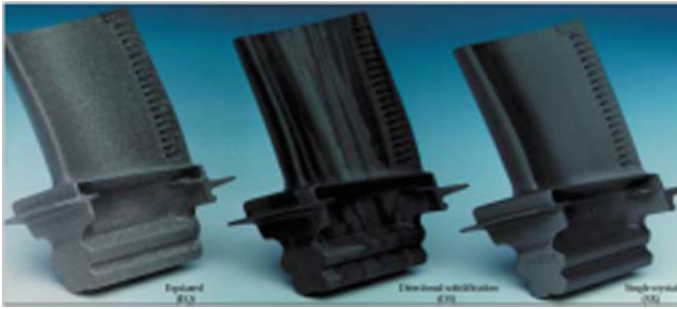


Fig. 14.17 Equiaxed, DS and SC turbine blades (left to right) [35]

14.7 Conclusions

A survey of structural design issues for a military aircraft engine has been presented. Design philosophies and operational constraints are also highlighted along with the iterative nature of the design cycle. Emphasis is placed on the fatigue- and creep-related design methodologies.

Design considerations for the effects of internal flow and high-speed rotation on blade untwist, the corrections required, and aspects of reduced frequency were presented. Current trends in materials, processes and fabrication have also been briefly covered.

Acknowledgments The authors wish to acknowledge the support and encouragement received from the Director, Gas Turbine Research Establishment, Bengaluru. The authors would also like to thank him for permission to reproduce the Kaveri engine and other figures. The authors have benefited from the comments and views of many colleagues at GTRE, especially those from the Compressor, Vibration and Structural Mechanics Groups, for sparing the time to go through the manuscript, and we take this opportunity to thank them heartily.

References

1. Cumpsty N (2003) Jet propulsion. Cambridge University Press, Cambridge, UK
2. Engine Structural Integrity Program (ENSIP), Department of Defense Handbook Mil HDBK 1783B, 1983, Revised in 2002
3. Mil-E-5007D/E, Military specification: engine, aircraft, turbojet and turbofan, general specification, 1973 revised in 1983
4. Meher-Homji CB, Gabriles G (1998) Gas turbine blade failures—causes, avoidance, troubleshooting. In: Proceedings of 27th ‘turbomachinery symposium’, turbomachinery laboratory. Texas A&M University, Texas, pp 177–192
5. Meher-Homji CB (1995) Blading vibration and failures in gas turbines: Part-A—blading dynamics and operating environment, part-b—compressor and turbine distress, part-c—detection and troubleshooting, part d—case studies. Fortieth ASME Gas Turbine and Aeroengine

- Congress. Houston, Texas, ASME paper numbers 95-GT-418, 95-GT419, 95-GT-420, 95-GT-421
6. Meher-Homji CB, Bhargava RB (1994) Condition monitoring and diagnostic aspect of gas turbine transient response. *International gas turbine and aeroengine Congress. Cologne, Germany. ASME paper number 92-GT-100, June 1–4, 1992. Also in *Int J Turbo Jet Eng* 11:99–111
 7. Cumpsty N (1989) *Compressor Aerodynamics*. Addison Wesley Longman Limited, Chicago, USA
 8. Rao JS (1992) *Turbomachine blade vibration*. Wiley, New York, USA
 9. Shannon JF (1945) *Vibration problem in gas turbine centrifugal and axial flow compressor*. H. M. Stationery Office, London, UK
 10. Srinivasan AV (1997) Flutter and resonant vibration characteristics of engine blade. *ASME J Eng Gas Turbine Power* 119(4):742–775
 11. Ewins DJ (1988) Structural dynamics of bladed and bladed discs. In: Platzter M, Carta FO (eds) *AGARD manual on aeroelasticity in axial-flow turbomachines: AG-298, vol-2, Structural Dynamics and Aeroelasticity*, AGARD, Neuilly sur Seine, France, pp 13.1–15.45
 12. Imregun M (1999) *Structural dynamics: basics of disk and blade vibration*. In: *Aeroelasticity in axial flow turbomachines*. von Karman Institute for Fluid Dynamics, Rhode-Saint-Genese, Belgium, pp 1–25
 13. Bendiksen OO (1990) Aeroelastic problems in turbomachines. AIAA paper, vol. AIAA-90-1157-CP, pp 1736–1761
 14. Viswanathan R (1989) *Damage mechanisms and life assessment of high temperature components*. ASM International Press, Metals Park, Ohio, USA
 15. Viswanathan R, Dolbec AC (1986) *Life assessment technology for combustion turbine blade*. ASME international gas turbine conference, Dusseldorf, Germany, ASME paper number: 86-GT-257
 16. Viswanathan R (1989) *Damage mechanism and life assessment of high temperature components*. ASM International, Metals Park, Ohio, USA
 17. Singh MP, Thakur BK, Sullivan WE (2005) *Assessing useful life of turbomachinery components*. In: *Proceedings of 34th 'turbomachinery symposium', turbomachinery laboratory*. Texas A&M University, Texas, pp 177–192
 18. Dieter GE (1986) *Mechanical metallurgy*. In: *Metallurgy and metallurgical engineering series*. McGraw-Hill Book Company, New York, USA
 19. Manson SS, Halford GR (1981) *Practical implementation of double linear damage rule and damage curve approach for treating cumulative fatigue damage*. *Int J Fract Mech* 17:169–192
 20. Singh MP (1985) *Turbine blade dynamics: a probabilistic approach*. *Vibrations of blade disk assemblies*. ASME Book Number H000335, pp 41–48
 21. Singh MP (2001) *Probabilistic HCF life estimation of a mechanical component*. In: *Proceedings of 2001 'ASME international mechanical engineering congress and exposition'*, New York, USA
 22. Manson SS (1966) *Interface between fatigue, creep, and fracture*. *Int J Fract Mech* 2:327–363
 23. Halford GR, Manson SS (1968) *Application of a method of estimating high temperature low-cycle fatigue behavior of materials*. *Trans ASM* 61:94–102
 24. Manson SS, Halford GR (1983) *Complexities of high temperature metal fatigue-some steps toward understanding*. NASA Technical Memo 83507
 25. Larson FR, Miller J (1972) *Transactions of ASME*. 74, p 765
 26. Dundas RE (1985) *Mechanical design of the gas turbine*. In: Sawyer JW (ed) *Sawyer's gas turbine engineering handbook*, vol 1, 3rd edn. Turbomachinery International Publications, Norwalk, Connecticut, USA
 27. Jeffers I, James D, Meece C (1975) *F100 fan stall flutter problem review and solution*. *J Aircr* 12(4):350–357
 28. EL-Aini Y, Capece V (1995) *Stall flutter prediction techniques for fan and compressor blades*. AIAA J AIAA 95-2652(10–12):1–11

29. Fang LC, Li SM (2013) A review of the research on aeroelasticity in aero turbomachinery. *Adv Mater Res* 651:694–700
30. FUTURE, flutter free turbomachinery blades. Available at http://ec.europa.eu/research/transport/projects/items/future_en.htm. Accessed 08 June 2013
31. Kielb RE (1999) Full scale engine testing. In: *Aeroelasticity in axial flow turbomachines*. von Karman Institute for Fluid Dynamics, Rhode-Saint-Genese, Belgium, pp 1–14
32. Surendra Kumar Patel (2010) Structural design analysis of aero-engine components for qualification and development of allied technologies. *DRDO Technology Spectrum* 29–47
33. Ravi Kumar BVR (2013) A review on blisk technology. *Int J Innov Res Sci Eng Technol* 2(5)
34. Moriya K et al (1999) Fabrication of titanium metal matrix composite bling. In: *Research institute of advanced material gas-generator (AMG) 4-2-6*, Kohinata, Bunkyo-ku, Tokyo, 112-0006, Japan
35. Schafrik R, Sprague R (2004) Gas turbine materials. *Adv Mater Process* 5:29–34
36. Dundas RE (1988) Review of design parameters in gas turbine for the prospective users. In: Dalla Betta RA et al (eds) *International gas turbine and aeroengine congress*. The Hague, Amsterdam, The Netherlands
37. Armstrong EK (1967) Recent blade vibration techniques. *ASME J Eng Power* 89:437–444
38. Cohen H, Rogers GFC, Saravanamuttoo HIH (1987) *Gas turbine theory*. Addison Wesley Longman, Chicago, USA
39. *Thermal and high-strain fatigue*. The Metals and Metallurgy Trust. London, UK, pp 154–170

Chapter 15

Missile Propulsion Systems

P. Satyaprasad, M. Pandu Ranga Sharma, Abhishek Richarya,
A. Rolex Ranjit and B.S. Subhash Chandran

Abstract This chapter provides a general description of propulsion systems suitable for missiles. These systems are solid- and liquid-fuelled rockets, liquid-fuelled ramjets, solid fuel ducted rockets (ramrockets), and scramjets. Concise summaries about testing are also given, and mention is made of a scramjet test facility developed by the Defence Research and Development Laboratory (DRDL) in Hyderabad, India. This facility is part of the DRDL hypersonic programme entitled ‘Hypersonic Technology Demonstrator Vehicle’ (HSTDV).

Keywords Missile propulsion · Rockets · Solid fuel · Liquid fuel · Ramjets · Scramjets

15.1 Introduction

The propulsion system in a missile is the prime mover, and in specific cases it also provides flight control. The system contributes to a significant amount of the missile mass (> 50 %). Also, the thrust is a major component of the forces acting on the missile. Hence the design and development of the propulsion system is a critical activity. The propulsion systems used in missiles are rockets, ramjets, scramjets, turbojets, and turbofans.

This chapter discusses rockets, ramjets, and scramjets for use in missiles and explains their operational principles, key subsystems, and testing methods. Turbine-based operational systems are not considered, since they are discussed in Chap. 14 of this Volume.

P. Satyaprasad · A. Richarya · A. Rolex Ranjit · B.S. Subhash Chandran (✉)
DRDL, DRDO, Hyderabad, India
e-mail: subhash_chandran_bs@rediffmail.com

M. Pandu Ranga Sharma
Defence Research and Development Laboratory, PO Kanchanbagh,
Kanchanbagh 500 058, Hyderabad, India

The missile propulsion systems fall into three basic categories:

1. Solid rockets use a solid propellant where the oxidizer and fuel are mixed at a microlevel to form a solid substance.
2. Liquid rockets use liquid fuel and oxidizer kept in separate chambers. These components are injected into the combustion chamber and mixed.
3. Air-breathing systems such as ramjets and scramjets store the fuel in the vehicle but use atmospheric oxygen for combustion. This means that these systems can operate only in the atmosphere (up to 20 km altitude for ramjets and 20–30 km for scramjets).

Rockets have no altitude limitations and can also operate in space and underwater. Another advantage of independence from the atmosphere is that rockets can operate at high combustion chamber pressures. This gives them a high thrust to cross-sectional area ($> 7 \times 10^5 \text{ N/m}^2$), while air-breathing systems are limited by the total pressure and mass of the air ingested and the thrust is limited to $1.5 \times 10^5 \text{ N/m}^2$.

However, since air-breathing systems (ramjets and scramjets) do not carry oxidizers, their propulsive efficiency is high. This is indicated by the specific impulse (I_{sp}), defined as the ratio of thrust to the weight of fuel flow rate (unit in seconds). The typical specific impulses for various systems are shown in Fig. 15.1. Note that rockets have a consistently low specific impulse. This is why solid rockets

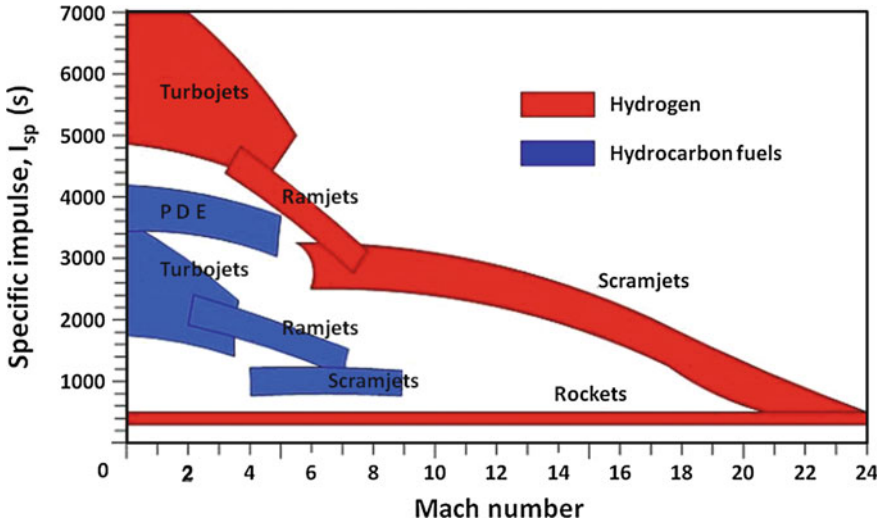


Fig. 15.1 Specific impulse for various propulsion systems: *PDE* pulse detonation engine

are primarily used when large accelerations are required, e.g. boosting to high speed in a short time. On the other hand, air-breathing systems are used when acceleration levels are low, for example in cruise operation.

15.1.1 Operational Principle for Rockets

The principle of operation (thermodynamic cycle) in rockets is the same in all cases. The fuel and oxidizer are burnt in the combustion chamber at high pressure. This converts the chemical energy to thermal energy, which in turn is converted to directed kinetic energy by the rocket nozzle. The momentum with which the gases are ejected through the nozzle provides the thrust reaction that propels the vehicle.

15.1.2 Nozzle Design

The thrust produced by the system is very sensitive to the nozzle design and shape, which is a convergent–divergent tube. This is required to accelerate the flow. The flow is intended to reach Mach 1 at the minimum cross-section (the nozzle throat) and then accelerate to supersonic speeds in the divergent section. This happens for combustion chamber pressures greater than $1.8 \times$ the external atmospheric pressure.

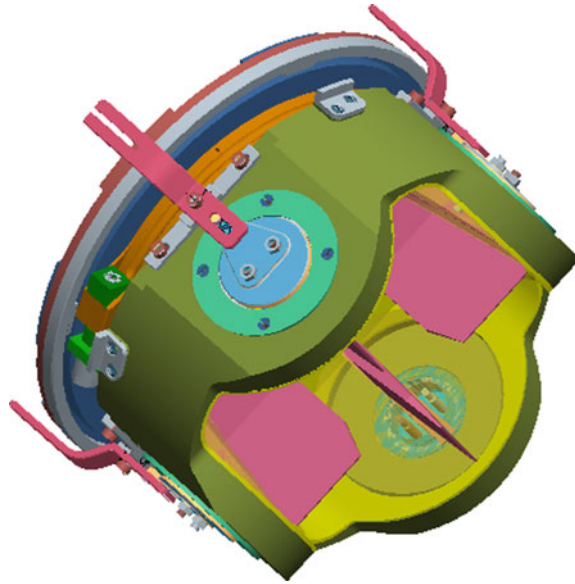
Both the convergent and divergent portions of the nozzle can be conical or curved:

- The convergent part is sometimes curved to project the throat into the combustion chamber. This is called a submerged nozzle.
- The divergent part can be curved to reduce the length (and hence weight) of the nozzle. Sometimes clusters of nozzles are used to reduce the overall length.

Nozzles are designed such that the static pressure of the flow at the exit of the nozzle is not much lower than the atmospheric pressure. Otherwise there is the possibility of flow separation in the nozzle. Another nozzle configuration called a spiked nozzle gives better overall efficiency at varying altitudes (varying ambient pressures).

Owing to the large moments the thrust can create, the nozzle designs must have close control over misalignments and any thrust vectoring. This is done by changing the direction of the exhaust jet by tilting the nozzle or by providing lifting surfaces (vanes) in the jet. An example of using jet vanes is shown in Fig. 15.2.

Fig. 15.2 Jet vane thrust vector control



15.2 Solid Rocket Propulsion System

A typical section of a solid rocket motor with various subsystems is shown in Fig. 15.3. The various subsystems are briefly described in the following subsections.

15.2.1 Rocket Motor Casing

The primary function of the rocket motor is to impart a given propulsive impulse to the flight vehicle and to do this with minimum weight. The mechanical components mainly consist of the motor casing and exhaust nozzle. The motor casing for a solid

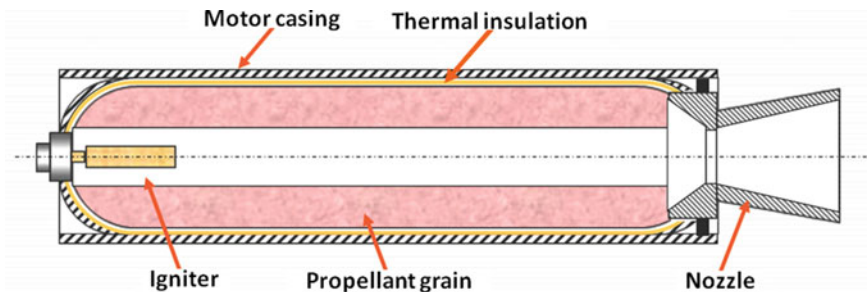


Fig. 15.3 Solid rocket motor schematic

rocket motor serves (i) to protect and ‘store’ the propellant grain (the geometric form of the propellant) until the motor is used; (ii) as a combustion chamber for high-pressure and high-temperature burning of the grain during motor operation; (iii) to mechanically/structurally interface with other motor components such as the nozzle, igniter, internal insulation, and handling/carrying/launch brackets; and (iv) usually as the primary airframe during missile flight, thereby also housing the control actuation systems.

Motor casings may be very large, as for the Space Shuttle solid rocket motors, or small for soldier-portable tactical units. Since the motor casing is essentially deadweight, it should be as light as possible. High-strength steels like maraging steels are the usual choice, but designs utilizing high-strength structural composites (e.g. carbon- or aramid fibre-reinforced plastics) typically result in significantly lower weights than metallic designs. The low mass of composite motor casings makes them suitable for the upper stages of missiles. Aluminium alloys are also sometimes used.

15.2.2 Thermal Insulation

Thermal insulation in a rocket motor is a layer of insulating material placed between the internal surface of the casing and the propellant. The internal profile of the insulation is sized so that the maximum quantity of propellant can be introduced. The main purpose is to protect the motor casing from the thermal environment of the combustion products. The following objectives must also be met:

- Bonding to propellant and casing.
- Inhibition of certain propellant grain surfaces.

Internal thermal insulations use elastomeric materials with various powders or fibres that are designed to enhance the material properties. The most important property requirements are the erosion performance, low thermal diffusivity, and low density.

The design of internal insulation is a function of the combustion geometry. The casing insulation integrity must be maintained during the life expectancy of the motor; that is, the elastomers used for the insulation must maintain their properties during ageing and exposure to environmental conditions.

15.2.3 Nozzle

A solid rocket motor nozzle is the carefully shaped aft-portion of the motor that controls the expansion of the exhaust products so that the energy produced in the combustion chamber is efficiently converted to thrust. Nozzle design is an iterative process in which aerodynamic, thermodynamic, structural, and fabrication considerations are engineered within the constraints imposed by the required nozzle configuration.

The nozzle casing also needs to be protected from internal thermal loads. Carbon- or silica-fibre-reinforced composites are used for this purpose. The throat is made from an erosion-resistant material like graphite, since the performance of the rocket is sensitive to the throat dimension.

15.2.4 Igniter

The function of the igniter is to induce combustion in the propellant in a controlled and predictable manner. The constituents of most solid rocket igniters are (i) an initiation system, (ii) an energetic material in the form of granules or pellets, and (iii) the hardware and other components that house them and provide for mounting the igniters onto the rocket motor.

15.2.5 Grain Design (*Propellant Geometric Form*)

The main aim of the solid propellant grain design is to realize a geometric form of the propellant that will generate the thrust versus time curve required for the mission and also account for other specified constraints. The main steps necessary for grain design are as follows:

- Ballistic performance characteristics (thrust–time variation, total impulse).
- Propellant selection.
- Selection and design of grain configuration.
- Propellant characterization and tailoring.
- Ballistic structural analysis of the design.

The grain design also depends on the design of other motor components. The size envelope and weight constraints (length, diameter, chamber volume available for the propellant, nozzle length, and exit diameter) define the geometric motor design parameters. Also, specified environmental requirements (e.g. temperature range and ambient pressure) must be taken into account. Summarizing, the main factors for selecting the grain configuration are as follows:

- Volume available for the propellant grain.
- Ratio of grain length to diameter.
- Thrust versus time curve: this gives a good idea of what should be the burning area *versus* the web burned curve (neutral, regressive, progressive, dual-level): **N.B:** the web is the internal thickness of the hollow propellant grain.
- Critical loads (thermal cycles, pressure rise at ignition, acceleration, internal flow).
- Manufacturability, which depends on case geometry.

15.2.6 Thrust Vectoring

To provide control of the missile at low speeds or in a rarefied atmosphere, the exhaust jet is directed to produce side forces. Different types of mechanisms are used, such as a flex nozzle (where the divergent portion of the nozzle is turned) and surfaces inserted in the exhaust, i.e. jet vanes, such as already mentioned (see Fig. 15.2).

15.2.7 Motor Static Test

Rocket motors are ground-tested before qualification for flight. The test objectives are grain design validation and margin verifications. Static tests are usually conducted in horizontal test beds, with the standard measurements being chamber pressure and thrust versus time; and in six-component test beds, where measurement of lateral forces is done as well as the standard measurements. The following ballistic parameters are usually evaluated:

- Shape of the pressure/thrust curve compared to prediction.
- Total impulse.
- Full-scale burning rate.
- Variation of burn rate in the propellant grain.
- Erosive burning coefficient.
- Average characteristic velocity.
- Throat erosion.

The experimental data can be compared with the theoretical predictions in order to verify the compliance with specifications and also verify the margins.

15.3 Liquid Rocket Propulsion

A typical liquid propellant engine is depicted in Fig. 15.4.

The rocket system generally consists of one or more *thrust chambers*; one or more *tanks* to store the propellants; a *feed mechanism* to force the liquids into the thrust chamber; a *power source* (a pump or pneumatic pressure) to furnish the energy required by the feed mechanism; suitable *plumbing* or *pipng* to transfer liquids; a *structure* to transmit the thrust forces; and *control devices* to regulate the propellant flow rates.

Liquid propulsion has several advantages:

- Thrust termination as per system demand.
- Multiple start capability.
- Precise thrust control and variable thrust capability.

Fig. 15.4 A liquid rocket engine



- Long duration of operation.
- Highest specific impulse in chemical propulsion.

The liquid propellants, which are the working substances of rockets, constitute the fluid that undergoes chemical and thermodynamic changes. The propellants can be classified as monopropellants and bipropellants:

1. A monopropellant contains an oxidizing agent and combustible matter in a single substance. It may be a mixture of several compounds, or it may be a homogeneous material, such as hydrogen peroxide or hydrazine. Monopropellants are stable under ordinary atmospheric conditions but decompose and yield hot combustion gases when heated or catalysed. They give lower specific impulse (I_{sp}), and so they are used in reaction control systems (RCSs).
2. A bipropellant rocket unit has two separate propellants, usually an oxidizer and a fuel. They are stored separately and are mixed inside the combustion chamber. The majority of successful liquid propellant rocket units have used bipropellants. Bipropellants are further classified as hypergolic and non-hypergolic propellants:

- Hypergolic propellants are propellants which ignite spontaneously upon contact with each other without any external source of energy.
- Non-hypergolic propellants are those which do not ignite upon contact and thus need an external energy source to heat the reactant mixture up to the ignition point. The ignition systems are used only for initial ignition, after which the thermal feedback and flow field will stabilize the flame.

Another classification of liquid propellants is based on the storage conditions: cryogenic and earth-storable propellants. Some liquid propellants are liquefied gases of very low boiling point (-100 to -200 °C). These propellants are defined as cryogenic propellants. The most common cryogenic propellants for rocket applications are liquid oxygen and liquid hydrogen.

In contrast to the cryogenics, earth-storable liquid propellants are stable over a reasonable range of temperature and pressure and are sufficiently non-reactive with construction materials to permit storage in closed containers for periods of a year or more. These propellants permit quick readiness of the rocket engine and may result in greater reliability due to the absence of extremely low temperatures and the need to dispose vapours.

Commonly used liquid propellants are as follows:

Oxidizers

1. IRFNA—*inhibited red fuming nitric acid*
2. LOX—*liquid oxygen*
3. N_2O_4 —*nitrogen tetroxide*
4. H_2O_2 —*hydrogen peroxide.*

Fuels

1. UDMH—*unsymmetrical dimethylhydrazine*
2. G Fuel—*triethylamine + xylidine*
3. Liquid hydrogen
4. N_2H_4 —*hydrazine*
5. MMH—*Monomethyl hydrazine*
6. Hydrocarbon fuels.

15.3.1 Types of Liquid Propulsion Feed Systems

The fuel feed systems transport fuel from the storage tanks to the engine. Because the engine operates at high pressure, the fuel needs to be pressurized. This is done by pneumatic pressurization or by pumps. The high pressure ensures injection at high speeds into the combustion chamber, thereby creating droplets which aid in the combustion. Although there are many types of feed systems available, the basic classification is twofold, namely

1. Turbopump feed system.
2. Pressure feed system.

15.3.2 Turbopump Feed System

The block diagram of a simple turbopump feed system is shown in Fig. 15.5. The turbopump feed system pressurizes the propellants by means of pumps, which in turn are driven by turbines. The turbines derive their power from the expansion of hot gases.

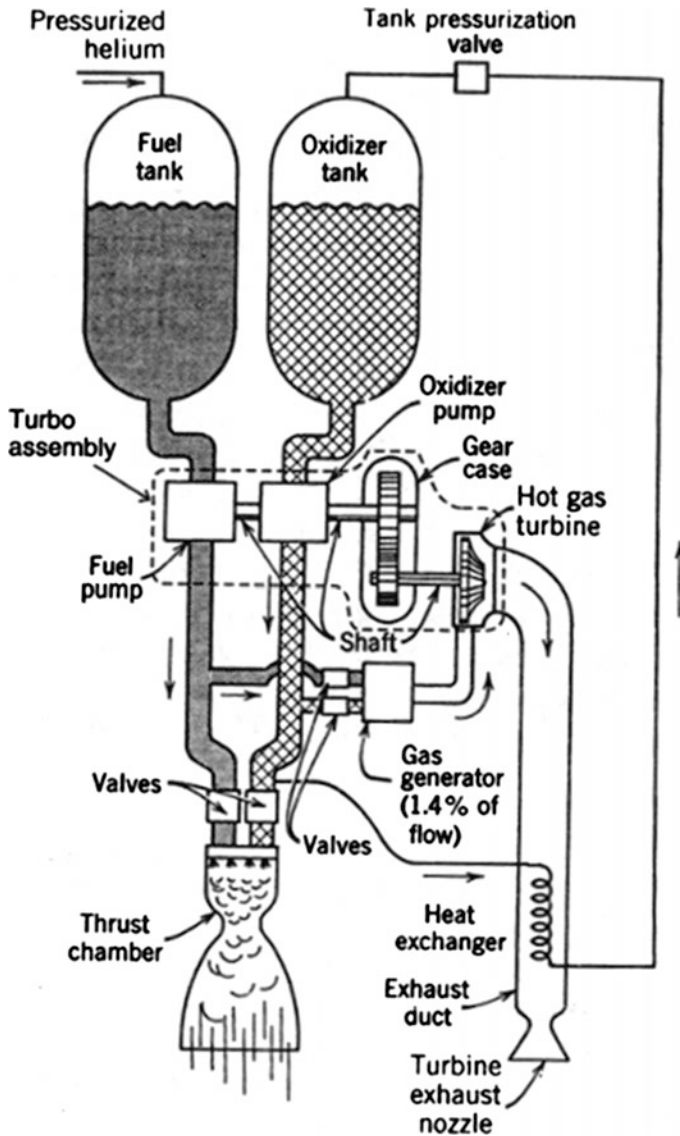


Fig. 15.5 Turbopump feed system schematic

Both the fuel and oxidizer propellant tanks are pressurized to a medium pressure by means of a suitable pressurant, e.g. helium. The propellants are then fed to their respective pumps and pressurized to high pressures, whence they are fed to the thrust chamber. Small quantities of fuel and oxidizer are bled from the pump deliveries and are fed to another combustion chamber called the 'gas generator'. The hot gases produced in the gas generator expand in a nozzle and are fed to the turbine. The turbine in turn drives the propellant pumps. N.B: The mixture ratio in the gas generator will usually be different from the stoichiometric mixture ratio, in order to minimize the temperature of the hot gases going to the turbine.

15.3.3 Pressure Feed System

A simple pressurized feed system is shown schematically in Fig. 15.6. It consists essentially of a high-pressure gas tank, a gas shut-off and starting valve, a pressure regulator, propellant tanks, propellant valves, and feed lines. Additional requirements such as filling and draining provisions, check valves and filters are also often incorporated.

After all tanks are filled, the high-pressure air valve is remotely actuated and admits gas through the pressure regulator at a constant pressure to the propellant tanks. The purpose of check valves is to prevent mixing of fuel and oxidizer when the unit is not in the upright condition. The propellants are fed to the thrust chamber by opening-up valves. When the propellants are completely consumed, the pressurizing gas serves also as a scavenging agent and cleans lines and valves of liquid propellant residue.

15.3.4 Liquid Propulsion Subsystems

The major subsystems of a typical liquid propulsion system are as follows:

1. Thrust chamber,
2. Injectors,
3. Propellant tanks,
4. Air bottle,
5. Turbopump feed system,
6. Valves,
7. Controls.

Some of these subsystems are shown or indicated in Figs. 15.5 and 15.6. They are discussed briefly in Sects. 15.3.4.1–15.3.4.7.

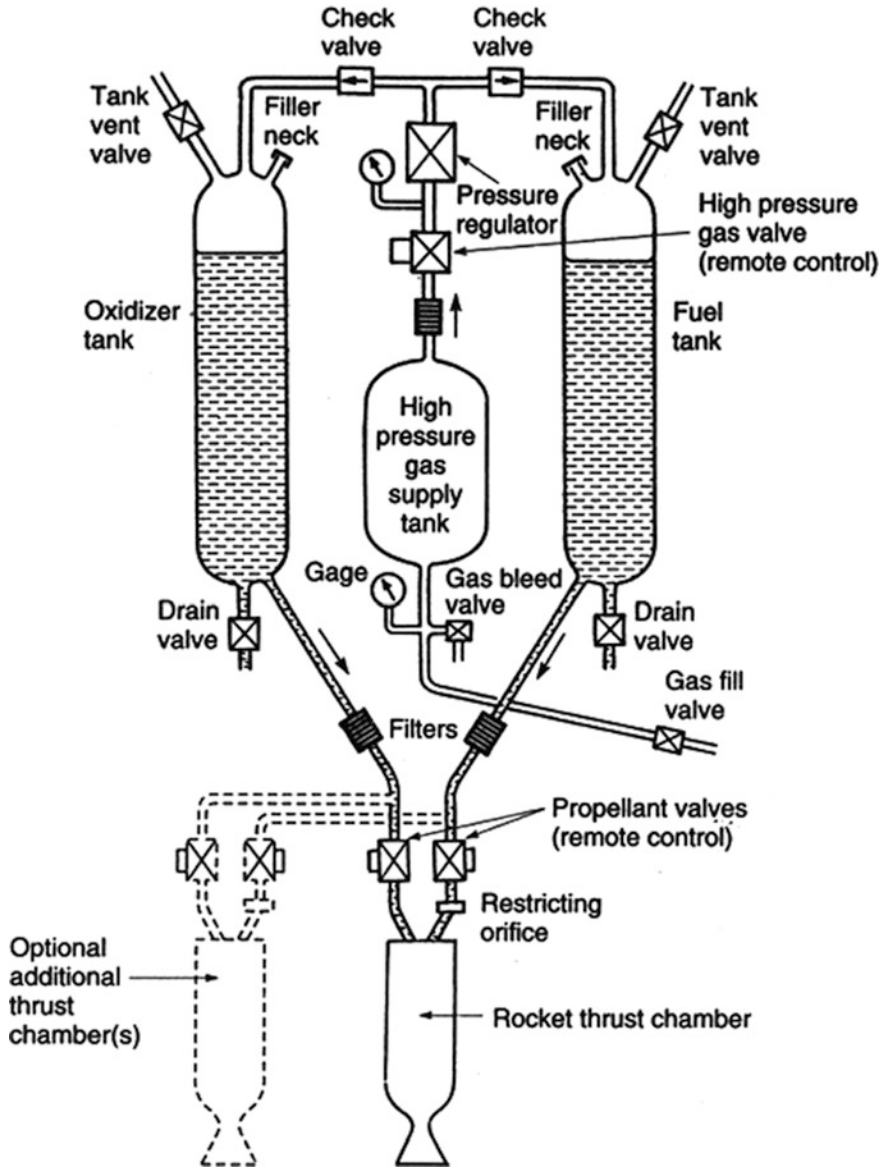


Fig. 15.6 Pressure feed system schematic

15.3.4.1 Thrust Chamber

The thrust chamber is the combustion device where the liquid propellants are metered, injected, atomized, mixed and burned to form hot gases, which in turn are accelerated and ejected at high velocity. A typical rocket thrust chamber assembly consists of the following principal parts: the thrust chamber itself and a nozzle.

The combustion chamber volume is selected with attention to the following:

- The volume has to be adequate to permit mixing, evaporation, and complete combustion of propellants. When the chamber volume is too small, combustion will be incomplete and the performance is poor.
- For prolonged firing durations the wall surface has to be cooled by one of the cooling methods suggested below.
- Since the rockets are airborne, their weight should be minimized.

Selection of Chamber Pressure The chamber pressure is the single most important parameter which governs the system weight and envelope. Higher chamber pressure gives very compact thrusters and thus a compact system. However, there will be a marginal increase in subsystems weight. Also, higher chamber pressures give a slight improvement in performance due to intense mixing and fast reaction rates. For every system there will be an optimum chamber pressure with respect to total weight and total envelope.

Thrust Chamber Cooling Because of high heat transfer rates from hot gases, thermal protection for the rocket motor needs considerable attention. The thrust chamber walls must be kept sufficiently cool to avoid weakening beyond the allowable limit. The following are the usual cooling methods followed:

1. Heat sink. A heavy-walled metal shell is used as the thrust chamber. This absorbs the heat transmitted from the hot gases. This method is limited to ground tests and short duration use.
2. Regenerative cooling. The propellant is circulated through a hollow-walled cooling jacket before injection into the combustion chamber. The cooled propellant absorbs heat by convection while passing through the cooling jacket.
3. Ablative cooling. This is provided by progressive endothermic decomposition of a fibre-reinforced organic surface material. This forms an insulating porous char and protects the outer chamber wall from exposure to high temperatures.
4. Radiation Cooling. Heat is radiated to the surroundings by means of heat-resistant wall material. This cooling method is typically used in space applications.
5. Thermal insulation. Special low-conductivity coatings or ceramic inserts are used to reduce the heat flux to the chamber walls.

15.3.4.2 Injectors

Injectors have to introduce and meter the propellant flow to the combustion chamber and atomize and mix the propellants in such a manner that a correctly proportioned and homogeneous fuel–oxidizer mixture will result, namely one that can readily be vaporized and burned. There are several types of injectors. Their design is very important and is a specialist topic. The reader is referred to the Bibliography references [1–4] for more information.

15.3.4.3 Propellant Tanks

The liquid rocket engine system usually has a fuel tank and an oxidizer tank. However, monopropellant systems have only one tank. Propellant tanks can be arranged in several ways, and the tank design can be used to exercise some control over changes in the centre of gravity during operation.

Cylindrical tanks with rounded ends (see Figs. 15.5 and 15.6) are used for vehicles of relatively large length-to-weight ratios and limited dimensional space envelopes. Spherical tanks may be employed for relatively high tank pressures and less stringent space requirements. The material selections are based on the strength-to-density ratio over a range of temperatures, the ductility and fracture toughness (particularly for cryogenic propellant tanks), and environmental compatibility with the propellants.

In packaged liquid propulsion systems like reaction control systems (RCS), the changing vehicle orientation necessitates a positive expulsion device to prevent pressurizing gas entering the propellant feed system. Frequently used positive expulsion devices are metallic and elastomeric diaphragms, which are highly efficient (97–99 %). Another method is to use moveable pistons in cylindrical tanks.

15.3.4.4 Air Bottles (Pressurized Gas Storage Tanks)

Air bottles need to be lightweight and store gas under high pressure, which is then ready for supply to the propellant feed system at a specified pressure level. Because of these requirements air bottles are generally spherical in shape and made from high strength-to-weight ratio materials such as PH 15-7-Mo stainless steel and Ti-6Al-4V titanium alloy. The bottles may have external filament-wound composite reinforcement layers for added strength.

15.3.4.5 Turbopump Feed System

The principal components in a turbopump feed system are the turbine, pumps, and a gas generator (see Fig. 15.5). There are many different arrangements of turbines and pumps. The selection of any specific turbo pump configuration depends on such

factors as inlet conditions to the pumps and turbine, weight, past experience, performance flexibility, reliability, ease of development, and cost.

The types of turbo pump feed systems and their characteristics are discussed in detail in the Bibliography references [1–4].

15.3.4.6 Valves

Various types of valves are used in propellant feed systems. Although the general design of rocket valves is relatively straightforward, the design details, such as clearance, seat materials, and opening time delay, present development difficulties. The valves in rockets have to be foolproof, for any failure will very often cause a failure of the rocket. Also, a leak in a propellant valve or a delay in opening at an inappropriate time may have disastrous effects. Hence all valves are thoroughly tested for functionality and leakage before installation.

Pressure regulators are special valves used frequently in liquid propellant rockets. Usually the discharge pressure is regulated to a predetermined standard value by continuous throttling of the flow.

15.3.4.7 Controls

All liquid propulsion rockets have controls to accomplish some or all of the following:

1. Start and shutdown of rocket operation,
2. Restart if desired/required,
3. Maintain programmed operation by feed system calibration or by automatic controls,
4. Emergency shutdown when safety devices sense a malfunction or critical condition of the vehicle or the engine,
5. Fill the tanks with propellants,
6. Drain excess propellant after operation.

15.3.5 Engine System Calibration

Each rocket engine has a specified set of performance characteristics, such as thrust, specific impulse, flight duration, and mixture ratio. For accurate performance, the engine characteristics often have very narrow tolerances. Since the internal flow characteristics of an engine can vary with fabrication and control tolerances, the performance of any uncalibrated engine will usually not be exactly equal to the desired performance.

Calibration of an engine is thus necessary to bring the engine performance parameters within the specified tolerance limits. The principal engine performance parameters to be adjusted are thrust, specific impulse, and fuel and oxidizer flow rates.

15.3.6 Testing of Liquid Propulsion Systems

Before rocket engines are put into operational use, they are subjected to several types of tests, some of which are outlined below in the sequence in which they are normally performed:

1. Manufacturing, inspection, and fabrication tests (pressure tests, leak checks, electromechanical tests),
2. Component tests (functional and operational tests),
3. Static tests with complete engine:
 - (a) simulated rocket operation,
 - (b) complete engine test.
4. Static vehicle tests with engine installed in a restrained non-flying vehicle,
5. Flight tests:
 - (a) from a specially instrumented flight test range with special flight test vehicles,
 - (b) with production vehicles.

15.4 Ramjet Propulsion Technology

While a rocket motor carries both fuel and oxygen in the required quantities, ramjet propulsion systems use atmospheric air as the oxidizer. This causes the effectiveness of ramjets, measured in terms of specific impulse (I_{sp}), to be significantly higher than that of conventional rockets (see Fig. 15.1). Depending on the type of fuel, ramjet systems can be classified as liquid fuel ramjets, solid fuel ramjets, and solid fuel ducted rockets (ramrockets). Although the working principle is fundamentally the same, the complexities and enabling technologies are completely different.

In this section, liquid fuel ramjets and solid fuel ducted rockets are briefly described. Solid fuel ramjets have not been used due to the complexity of integrating a booster for practical systems.

15.4.1 Liquid Fuel Ramjets

A simplified schematic of a liquid fuel ramjet, omitting the pressurized fuel tank system, is shown in Fig. 15.7. The cone-shaped spike in the air inlet compresses high-speed air and slows it down before it enters the combustion chamber. This slowing down increases the time for mixing the air with injected fuel and also increases the pressure in the combustion chamber. In turn, this higher pressure increases the propulsive efficiency of burning the fuel with the compressed air.

For this operating system to be effective the speed should be above Mach 1.8; that is, a ramjet-powered vehicle should be boosted to more than Mach 1.8 before the ramjet comes into operation.

15.4.1.1 Ramjet Air Inlet

Air inlets are used to compress the supersonic flow to subsonic flow, as pointed out in Fig. 15.7. The inlets use a combination of oblique shocks and normal shock to reduce the flow velocity with minimum losses in pressure and mass flow rate. Figure 15.8 shows a schematic of shocks in an inlet and a typical Schlieren image of a shock wave emanating from an inlet spike.

Air inlets are designed to minimize the total pressure loss over the whole flight regime while ensuring that the airflow is sufficient to provide the required thrust. The inlets may have various shapes, including circular, semi-circular, or rectangular; and there may be multiple inlets, depending on the overall configuration of the vehicle.

Each geometric parameter affects the performance of air inlets. Professional computational fluid dynamics (CFD) software packages are very effective in

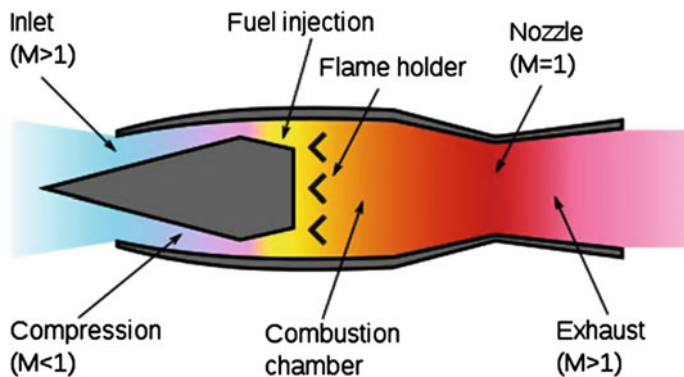
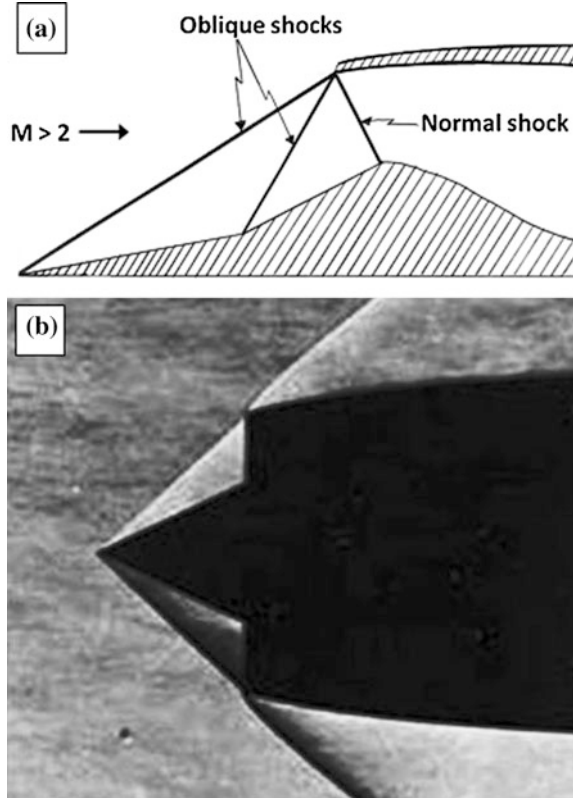


Fig. 15.7 Simplified schematic diagram of a liquid fuel ramjet showing the air/gas flow and Mach number regimes

Fig. 15.8 Inlet shock system
a schematic and **b** Schlieren
 image from a wind tunnel test



estimating the performance and analysing various configurations. Design verification and validation are done, respectively, in wind tunnel and flight tests.

15.4.1.2 Ramjet Fuel Tank

Typical ramjet liquid fuel tanks use a rubber bag to ensure that fuel is always fed to the fuel controller even under high lateral acceleration, since a rubber bag prevents sloshing during flight. Prediction of the rubber bag shape while being emptied under lateral forces is a challenge that requires the development of special analysis tools. At the tank outlet a colander-shaped fitting prevents the bag from blocking the outlet.

15.4.1.3 Ramjet Combustion Chamber

A ramjet combustion chamber is a critical subsystem that requires much testing and analysis for estimating its performance. There are no well-defined methods for

designing the combustion chamber. In the first instance, the combustor size is determined by external design factors such as the overall length and weight of the propulsion system in relation to the vehicle.

The primary design criterion is to ensure complete combustion of the fuel within the chamber. This requires stringent design of the fuel injectors and flame holders and an optimum flow pattern in the combustion chamber.

15.4.1.4 Ramjet Insulation

Silicon-based resins, silicon cloth, and other silicon-based compounds are used for insulation to protect the motor casing. Firstly, the silicon reacts with oxygen to form silicon dioxide, which is an endothermic reaction. Secondly, a silicon-based insulation system does not ablate, but provides a tough char that protects the casing much longer than ablation would.

The char needs to be held to the motor casing, and this is achieved by the provision of hooks fixed to the casing. For very long duration missions, a film cooling system is used: baffles in the motor create a cold air layer between the combustion chamber gases and the casing.

15.4.2 Solid Fuel Ducted Rockets (Ramrockets)

Instead of the pressurized fuel tank system required for a liquid fuel ramjet, solid fuel ducted rockets use fuel-rich grain in the motor casing in front of the ramjet. A schematic example is given in Fig. 15.9. An interstage valve controls the flow rate of fuel-rich grain combustion products into the ramjet combustor, where these products are brought to complete combustion by the ducted inlet air.

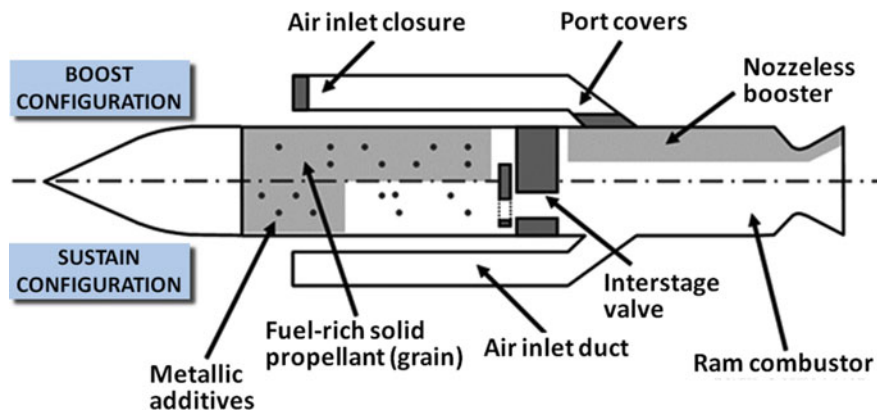


Fig. 15.9 Simplified schematic diagram of a solid fuel ducted rocket

N.B Fig. 15.9 shows two flight configurations: (i) the boost configuration with air inlets closed, when the vehicle is accelerating to the required velocity for ramjet operation and (ii) the sustain configuration with the air inlets open and the ramjet operating.

15.4.2.1 Solid Propellant (Grain)

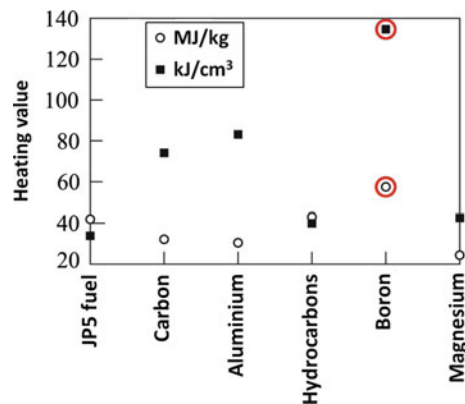
As stated above, the grain is fuel-rich. Common fuel constituents are aluminium- and magnesium-based powders and nitroglycerin; a common oxidizer is nitrocellulose. There has been much research to use boron as an additive, since it has the highest heat of combustion compared to other fuels and fuel additives (Fig. 15.10). However, the achievement of optimum combustion conditions for boron-containing fuels is difficult.

A typical fuel-rich grain contains the main fuel, an oxidizer, binder, burn rate (ballistic) modifier, curing agents, and plasticizers. Development of a fuel-rich grain is challenging since there are several important criteria, namely the burn rate, pressure index, calorific value, and expulsion efficiency. The actual processing is also difficult, for example the handling of fine oxidizer particles and their incorporation into the grain.

15.4.2.2 Ducted Rocket Fuel Flow Control Valve

The fuel flow controller for a solid fuel ramjet is called a hot gas valve (the interstage valve in Fig. 15.9). This valve controls the flow rate of partially burnt combustion products from the fuel-rich motor. Development of hot gas valves is a challenge since they need to cope with high temperatures and particle-laden combustion products and must sometimes operate for long durations.

Fig. 15.10 Heats of combustion of some fuels and additives: after Bibliography reference [5]



The configuration of a hot gas valve is critical for its performance, and each has its own advantages and disadvantages. The mission requirements, e.g. vehicle size, fuel type, and flight duration, also influence the selected configuration. This is a specialist topic, and the readers are referred to the Bibliography references [1–4] for more information.

15.4.3 Ramjet Testing

Ramjets are ground-tested to estimate their performance under varying flight conditions. Different test methods with varying levels of fidelity are used:

Connected-Pipe Tests Combustors are initially tested in connected-pipe mode, where hot subsonic air is ducted directly into the combustor. These tests demonstrate the combustor design integrity and performance.

Semi-Free Jet Tests This is the next test level. The engine, including inlets, is supplied with supersonic air from nozzles in front of each inlet. This simulates the interaction between the intake flow and the combustor, but does not simulate the effects on the airflow of the vehicle body in front of the intake.

Full-Free Jet Tests These are the best simulations because the entire vehicle is surrounded with supersonic airflow, as in flight. However, such tests are very expensive, and only a few countries can do them.

15.5 Scramjet Propulsion

There is worldwide interest in the development of air-breathing hypersonic vehicles and technologies for the space, civil, and military aerospace sectors. In the military sector these technologies would enable hypersonic cruise missiles, which are ideal weapons against time-critical targets and buried and/or hardened targets. The engine of choice for all the potential applications is the Supersonic Combustion Ramjet (scramjet).

15.5.1 System Description

As the name suggests, a scramjet is a type of ramjet. Like a ramjet, a scramjet consists of a supersonic diffuser that compresses the incoming air to higher pressures by a ram effect. However, there is a major difference:

- In ramjets the air is delivered to a combustion chamber at *subsonic* speeds, where it mixes with injected fuel. This mixture is ignited and burns with the aid of a flame holder that stabilizes the flame.
- In a scramjet, the air enters the combustion chamber at *supersonic* speeds, where combustion with the injected fuel occurs at much higher velocities than in a ramjet.

Figure 15.11 is a simplified schematic of the operation of a scramjet engine integrated into a hypersonic cruise vehicle.

Advantages Maintaining supersonic flow throughout the engine avoids excessive losses that result from decelerating the flow to subsonic velocities, as in a ramjet. Also, the supersonic flow inside the combustor allows a simple divergent nozzle to be used instead of a throat nozzle.

Disadvantages The high speed of flow in the combustor makes flame-holding and sustained combustion in scramjets difficult. The high speed also means that the temperature rise from combustion will dissociate the combustion products, resulting in reduced energy for conversion into thrust.

Other Considerations (see Fig. 15.11) Owing to the high drag at hypersonic speeds and large losses in total pressure of the airflow, only an integrated configuration can deliver sufficient thrust to overcome the drag. The front part of the vehicle (the forebody) acts as part of the inlet, reducing the flow speed before it enters the scramjet. There the flow speed is further reduced before the air enters the combustor. N.B: The isolator section acts as a buffer between the inlet and combustor to ensure proper functioning of the inlet.

The slowed-down airflow mixes with injected fuel in the combustor, and the combustion product gases are accelerated through the diverging part of the combustor and the rear portion of the vehicle (the aft-body), which forms part of the engine.

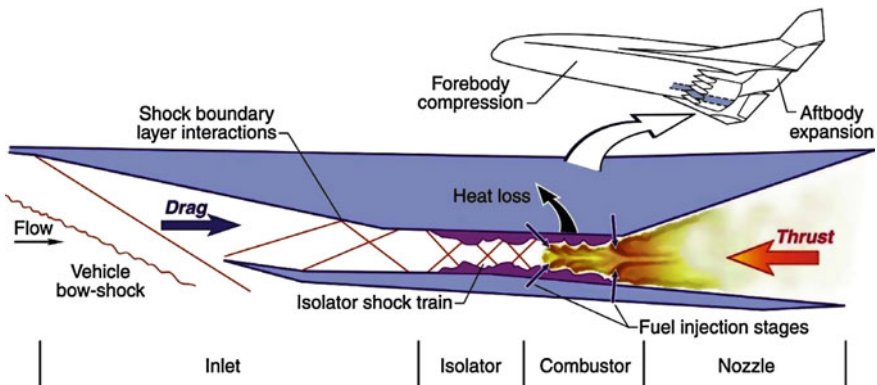


Fig. 15.11 Simplified schematic diagram of a scramjet engine

15.5.2 Subsystems

As indicated in Fig. 15.11, a scramjet engine basically consists of an inlet, an isolator, a combustor, and a nozzle.

Inlet The air inlet is a critical component. It must deliver air to the combustion chamber for a wide range of Mach numbers and with the desired rate and flow conditions. This delivery must be accomplished with as little pressure loss and drag as possible. At high Mach numbers the air compression process is accomplished by a succession of oblique shocks generated both ahead (external compression) and inside the converging part of the inlet (internal compression). Hence the inlet is called a mixed compression inlet (see Fig. 15.12).

An important problem demonstrating the criticality of the inlet and its geometry is ‘unstarting’. This occurs when the area ratio of the throat (minimum area region in the inlet duct) and the capture area is too low for a given Mach number. In the unstarted condition the incoming flow will spill outside via a separated shock, resulting in a mass flow rate lower than the design value. This is an extremely undesirable situation, since besides flow distortion it is accompanied by *low* pressure recovery and *high* pressure drag.

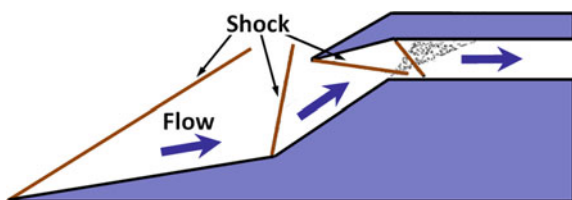
Isolator The isolator is a diverging area duct separating the inlet from the combustion chamber. Pressure disturbances due to combustion are contained within the isolator and prevented from moving upstream into the inlet. This is essential: uncontained shock waves resulting from combustion pressure rises will (also) cause an unstart.

Combustor Supersonic mixing and combustion control is the key technology for the scramjet engine. The operational flight speed range of the scramjet engine is from about Mach 6 to Mach 12 or higher, and within this range very rapid and efficient fuel/air mixing and combustion must occur. This is achieved by various fuel injection methods that also enhance the mixing of the fuel and air.

The fuel injection is staged (see Fig. 15.11), and this together with a *diverging area* combustor prevents the pressure rise in the combustor from becoming too high such that it can also cause an unstart.

Nozzle The nozzle also has a diverging area. The aft-body of the hypersonic vehicle is itself sometimes used as the engine nozzle. This reduces the vehicle drag.

Fig. 15.12 Mixed compression inlet for a scramjet



15.5.3 Other Critical Areas

The other critical areas associated with scramjet engine development are engine–airframe integration, thermal management, and ground testing and performance evaluation:

Engine–Airframe Integration Unlike most other air-breathing engines, a scramjet engine is tightly integrated with the vehicle airframe. The forebody of the airframe acts as the external compression inlet for the engine, and the aft-body acts as part of the engine nozzle. Since the thermal loads on the engine and airframe are very different, it is a major challenge to integrate them.

Thermal Management A scramjet engine operating at Mach 6 experiences temperatures as high as 2500 °C. This requires combinations of strong and creep-resistant high-temperature materials, regenerative cooling techniques, endothermic fuels with high heat capacities, thermal protection coatings, and ceramic tiles.

Ground Testing Scramjet operating conditions are typically to fly at Mach 5–8 and at altitudes between 25 and 35 km. The typical combustor entry conditions are Mach number ~ 2.5 , total temperature ~ 1500 °C, and static pressure ~ 0.5 bar.

Ground testing requires these conditions to be simulated. A preheater is used to increase the air temperature, and a supersonic nozzle accelerates the flow to the desired Mach numbers. Heating can be achieved either by an electric arc or by chemical means (burning hydrogen or a hydrocarbon fuel with air).

There are various modes of ground testing, similar to those for ramjets (see Sect. 15.4.3). Connected-pipe tests are used for small-scale and component-level testing, whereby the combustor is directly connected to an $M \sim 2.5$ nozzle. In free-jet tests the whole engine, together with the vehicle forebody, is placed in front of a Mach 6–8 nozzle and tested.

15.5.4 Development at DRDL in India

The Defence Research and Development Laboratory (DRDL), Hyderabad, is the nodal agency for developing scramjet technology for future hypersonic air-breathing missiles. DRDL is pursuing the hypersonic programme entitled ‘Hypersonic Technology Demonstrator Vehicle’ (HSTDV), see Fig. 15.13.

The objective of the HSTDV programme is to demonstrate autonomous hypersonic flight of an airframe-integrated scramjet propulsion system using hydrocarbon fuel. The flow path of the HSTDV vehicle consists of the forebody (external compression surface), an intake (internal compression surface), scramjet combustor, and a single expansion ramp nozzle. A critical technology in this programme is supersonic combustion, which has been successfully demonstrated in ground tests using the test facility shown in Fig. 15.14.

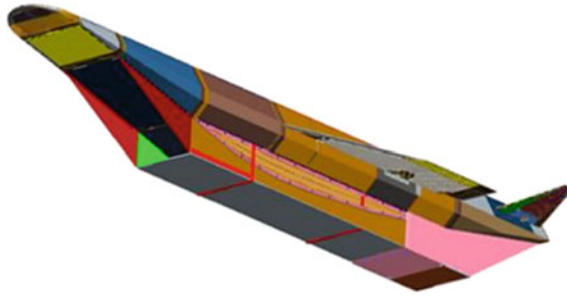


Fig. 15.13 Schematic of the Indian Hyperonic Technology Demonstrator Vehicle (HSTDV)

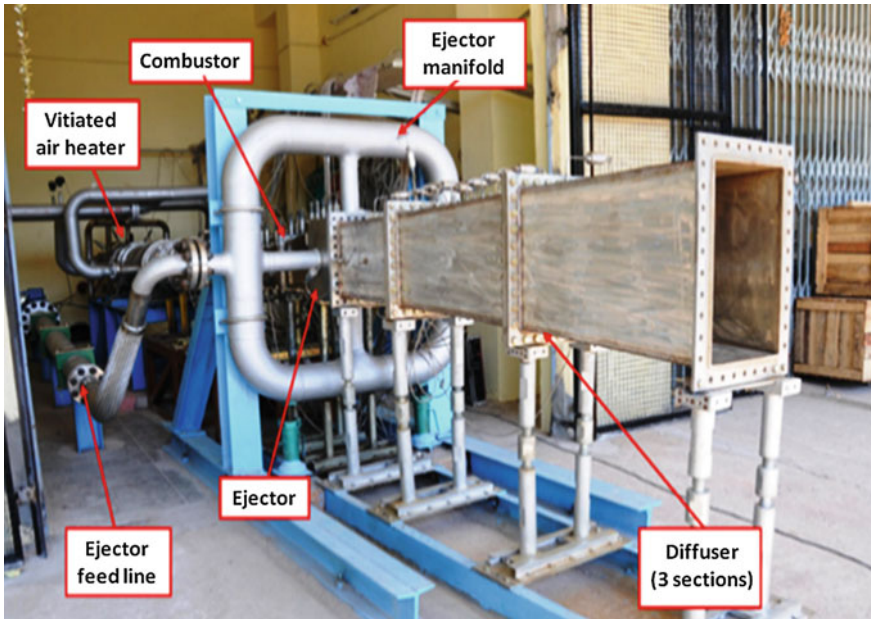


Fig. 15.14 Scramjet test facility at DRDL, Hyderabad

The scramjet propulsion system for the HSTDV has the major subsystems of mixed compression intake, supersonic combustor, and single expansion ramp nozzle.

The entire lower surface of the vehicle is part of the engine. The forebody and air inlet combination compress the external flow from ambient conditions corresponding to 30–32.5 km altitude to about 0.5 bar at the supersonic combustor entry. The combustion products expand through the single expansion ramp nozzle.

The ground test facility shown in Fig. 15.14 has a connected-pipe, hydrogen-fuelled vitiated air heater developed at the DRDL. This has been used to test the HSTDV combustor. The facility has been upgraded to cater to the testing

requirements for a full-scale (two-module) combustor. Two-dimensional convergent-divergent nozzles have been developed to simulate combustor entry conditions. An ejector system has been developed to enable simulating high-altitude conditions.

15.6 Summary

There are several possible propulsion systems for missiles. These are solid- and liquid-fuelled rockets, liquid-fuelled ramjets, solid fuel ducted rockets (ramrockets), and scramjets. This chapter has given overviews of all these systems and some of the most important subsystems. The testing requirements have been summarized also. This includes a scramjet test facility developed by the DRDL as part of the Indian HSTDV programme.

Acknowledgments The authors thank Dr. RJH Wanhill profoundly for his extensive corrections and rewrite as well as a comprehensive review of the chapter contents.

Bibliography

1. Sutton GP, Biblarz O (2001) Rocket propulsion elements, 7th edn. John Wiley & Sons Inc., Hoboken, NJ 07030-5774, USA
2. Mukunda HS (2004) Understanding aerospace propulsion. Interline Publishing, Bengaluru, Karnataka 560032, India
3. Huzel DK, Huang DH (1992) Modern engineering for design of liquid-propellant rocket engines, Revised Edition, Progress in astronautics and aeronautics, vol 147. American Institute of Aeronautics and Astronautics, Inc., Washington, DC 20024, USA
4. Barrere M, Jaumotte A, Fraeijs de Veubeke B, Vandekerckhove J (1960) Rocket propulsion. Elsevier Publishing Company, Amsterdam, The Netherlands
5. Haddad A, Natan B, Arieli R (2011) The performance of a boron-loaded gel-fuel ramjet. Prog Propul Phys 2:499–518

Chapter 16

Fatigue Requirements for Aircraft Structures

R.J.H. Wanhill

Abstract This chapter first summarizes the evolution of fatigue design requirements for aircraft structures. For metallic (mainly aluminium alloy) structures these requirements have developed since the 1950s. Composite materials (notably carbon fibre reinforced plastics) present a relatively new challenge. There follows a concise discussion of the several possible methods for assessing the fatigue lives of aircraft structures. The emphasis is on requirements, but design and operational issues are also addressed.

Keywords Fatigue design • Requirements • Lifting methods • Lifting analyses • Damage tolerance • Testing

Nomenclature

ANN	Artificial neural network
ASIP	Aircraft Structural Integrity Program
ASTM	American Society for Testing and Materials
BB	Building block
CA	Constant amplitude
CFRP	Carbon fibre reinforced plastic
DSG	Design service goal
DSTO	Defence Science and Technology Organisation
DT	Damage tolerance
EIFS	Equivalent initial flaw size
EPFM	Elastic plastic fracture mechanics
EPS	Equivalent precrack size
FAA	Federal Aviation Administration
FCG	Fatigue crack growth
FSFT	Full-scale fatigue test(ing)
GLARE	GLASS REinforced aluminium laminates

R.J.H. Wanhill (✉)
NLR, Emmeloord, The Netherlands
e-mail: rjhwanhill@gmail.com

HELIUM	HELicopter Usage Monitoring database
HOLSIP	HOListic Structural Integrity Process
HUMS	Health and Usage Monitoring System
IDS	Initial discontinuity state
JSF	Joint Strike Fighter
LBW	Laser beam welding
LCA	Light Combat Aircraft
LEFM	Linear elastic fracture mechanics
LOV	Limit of validity
MLB	MegaLiner Barrel
MSD	Multiple site fatigue damage
MY, MZ	Vertical and horizontal bending loads
NDI	Non-destructive inspection
NLR	Nationaal Lucht- en Ruimtevaart Laboratorium
NRC	National Research Council Canada
ODAT	Operational Damage Assessment Tool
OEM	Original equipment manufacturer
QF	Quantitative fractography
QZ	Ground loads
RAAF	Royal Australian Air Force
R.H.	Right hand
RUL	Remaining Useful Life
SHM	Structural health monitoring
S–N	Stress versus number of cycles
USAF	United States Air Force
VA	Variable amplitude
WFD	Widespread fatigue damage
XWB	Extra wide body
ΔP	Pressurization differential
ϵ –N	Strain versus number of cycles

16.1 Evolution of Fatigue Requirements

Since the early 1930s the evolution of aircraft structural integrity has been concerned largely with the service behaviour of high-strength metallic materials, particularly aluminium alloys. Taking a (very) broad view, the history of this evolution is as follows [1, 2]:

1930–1940 Development of all-metal aircraft for public transport. Design and analysis emphasized static strength, with little consideration of fatigue.

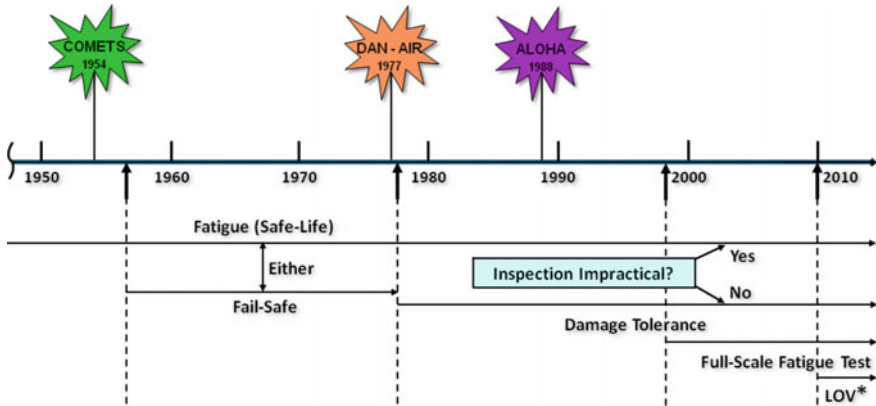


Fig. 16.1 Milestone civil aircraft accidents and evolution of civil aircraft fatigue requirements [2, 8]: *LOV Limit of validity

1940–1956 Increasing awareness, notably for civil aircraft, of the importance of fatigue for airframe safety. Materials with higher static strengths were developed. However, aluminium alloys did not—and still do not—show corresponding increases in fatigue strength (see Chap. 2 in Volume 1 of these Source Books). Design of *civil* aircraft became based on both static and fatigue strengths (safe-life fatigue design) in 1956.

1956–Today Development of fail-safe and damage tolerance (DT) design methods for both civil and military aircraft. These methods recognize that airframe structures must withstand service loads even when damaged or cracked. Safety should be ensured by fatigue and fracture testing and analysis of damaged structures; preservice and in-service inspections; and eventual repairs, replacements, or retirement.

Service failures have greatly influenced these developments. In particular, there are six case histories that may be regarded as ‘milestones’ in the aerospace industry’s approach to structural integrity [3–7]. By happenstance, these case histories are evenly divided between civil and military aircraft, see Figs. 16.1 [2, 8] and 16.2 [2, 9, 10]. The significances of these accidents are discussed in Sects. 16.1.1 and 16.1.2.

16.1.1 Civil Aircraft Milestone Accidents

De Havilland Comets In January and April 1954, two comets suffered pressure cabin disintegration resulting from fatigue. Investigation and follow-up gave a general awareness of finite fatigue lives, the significance of fail-safety and the usefulness of full-scale fatigue testing (FSFT).

Fail-safe design principles mean that major parts of the structure are (were) designed firstly to achieve a satisfactory fatigue life with no significant cracking.

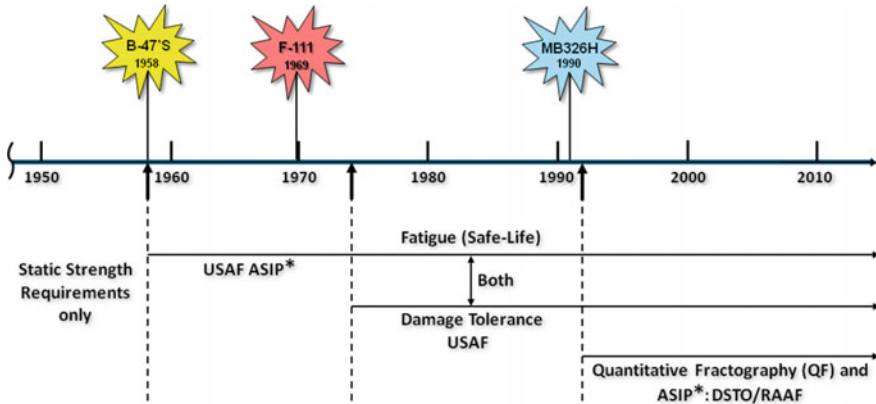


Fig. 16.2 Milestone military aircraft accidents and the evolution of military aircraft fatigue requirements [2, 9] and techniques [10]: *ASIP Aircraft Structural Integrity Program(mes)

Secondly, the structure is (was) also designed to be inspectable in service and able to sustain significant and easily detectable damage before safety is compromised. These latter requirements were met mainly by structural design concepts having multiple load paths and *established* residual strength (fracture) requirements in the event of complete or obvious partial failure of one structural element.

These fail-safe design principles were adopted in 1956, with some exceptions, notably including landing gears, which are not amenable to fail-safe design. However, as yet there was no *requirement* to conduct full-scale fatigue tests, see Fig. 16.1. Although FSFT has generally or often been done since the Comet accidents, the requirement for FSFT became mandatory only in 1998, see the last paragraph about the ALOHA Boeing 737 accident.

DAN-AIR Boeing 707 In May 1977 a Boeing 707 freighter lost the R.H. horizontal stabilizer owing to fatigue in a *supposedly* fail-safe spar. There were several contributing factors:

- inadequate inspection for detecting *partial* failure of the spar upper chord,
- inadequate residual strength after *complete* failure of the upper chord,
- unanticipated high service loads,
- stabilizer modification not checked by FSFT.

This accident prompted (i) reconsidering the problems of ageing aircraft: it became clear that some inspection methods and schedules were inadequate and required supplementary programmes; and (ii) the need for DT, which replaced the fail-safe design principles in 1978.

In civil airworthiness terms, DT means that fatigue cracks will be detected before the safety is compromised, but unlike fail-safety there is no premise that cracking will become obvious before it reduces the residual strength below the required safety level [8].

ALOHA Boeing 737 In April 1988 a Boeing 737 suffered explosive decompression with loss of part of the pressure cabin, subsequently landing safely. The physical manifestation of the accident was multiple site fatigue damage (MSD) along a critical rivet row of the upper skin lap splice. There were several contributing factors:

- skin splice design relied on cold-bonding as well as riveting,
- bonds susceptible to corrosion and disbonding,
- neglected inspections and repairs.

This accident led to recognition that widespread fatigue damage (WFD), of which MSD is one aspect, can cause loss of fail-safety. It also prompted more actions to ensure the safety of ageing aircraft, and corrosion control programmes for both civil and military aircraft.

Other instances of WFD led eventually to *mandatory* FSFT from 1998 onwards and in 2011 the limit of validity (LOV) concept for aircraft above 34,000 kg. The LOV concept requires FSFT to determine the onset of WFD [11], and as such effectively sets a safe-life equivalent for this category of aircraft.

16.1.2 Military Aircraft Milestone Accidents

Boeing B-47s In March and April 1958, *four* Boeing B-47s suffered fatigue failures resulting in wing losses. After the fourth accident, a fleet recovery programme was initiated. This required development of a structural integrity programme that included FSFT. This programme was completed in 1959.

Also in 1959, the US Air Force (USAF) adopted safe-life fatigue design principles and a permanent Aircraft Structural Integrity Program (ASIP), see Fig. 16.2, that included FSFT. This became a *formal* requirement (mandatory) in 1969.

It should be noted that all ASIPs, including those introduced by the Royal Australian Air Force (RAAF) after the MB-326H accident in 1990 (see below), involve much more than fatigue issues [12].

General Dynamics F-111 In December 1969 a General Dynamics F-111A lost the left wing after only 107 airframe flight hours and at less than half the design limit load. Failure occurred by fast fracture after a small amount of fatigue from a large manufacturing flaw in the lower plate of the L.H. wing pivot fitting. The plate was made from a high-strength steel with *limited* fracture toughness.

This failure and FSFT fatigue and fracture problems led to a fracture control programme for the F-111 critical steel components [13]. Furthermore, the F-111 problems and early fatigue cracking and WFD in Lockheed C-5A wing boxes [14] resulted in the USAF abandoning the safe-life policy and introducing their DT approach in 1974–1975 [15, 16]. This preceded the civil aircraft DT requirements by 3–4 years, cf. Figures 16.1 and 16.2. There are some differences, the main one being that the USAF DT approach requires that *initial flaws or cracks should be assumed to be present in new structures*.

However, there is no universal acceptance of the USAF DT requirements for military aircraft. For example, the US Navy still uses the safe-life approach.

Aermacchi MB-326H In November 1990, an Aermacchi MB-326H lost the left wing owing to fatigue failure in the wing spar at only 70 % of the safe-life derived from FSFT. Investigation showed that fatigue began from a badly drilled bolt hole.

Further investigation revealed the following: (i) manufacturing flaws in many holes, (ii) fatigue cracks growing from bolt hole manufacturing flaws in spars from other aircraft and (iii) fatigue cracks growing from *normal* quality holes and other structural details [17].

A fleet recovery programme based on teardown of several high-life wings, followed by quantitative fractography (QF) of the growth of in-service fatigue cracks, showed that the original FSFT-based safe-life was highly unconservative and that wing replacements were the only feasible option.

In addition, the RAAF's structural integrity policy changed similarly to the USAF's after the B-47 accidents in 1958. Since 1990 the RAAF has established comprehensive ASIPs for each fleet. Some have included QF-based fatigue analyses.

16.2 Continuing Developments

This section highlights some developments in fatigue analyses and airframe materials that have implications for future aircraft structural integrity requirements and ASIPs.

16.2.1 Fatigue Analyses for Conventional Alloys

Ongoing fatigue research aims to improve structural analysis capabilities and methods for fatigue life and crack growth predictions. Two of the main developments are: (i) the study of short fatigue crack growth (FCG) and (ii) the possible and actual effects of corrosion on fatigue and the combined action of corrosion and fatigue.

Short Crack Growth When the USAF DT approach was first introduced, in the early 1970s, there were few actual data for short crack growth. Owing to advances in QF this is no longer the case, particularly since the MB326H accident in 1990. There are now many data for early crack growth in high-performance aircraft [10], including the types and sizes of fatigue-initiating initial discontinuities [18]. Analysis methods have been developed to use these data for life predictions and reassessments, including the use of equivalent precrack sizes (EPS) to represent realistic initial discontinuities [10].

Corrosion and Fatigue Since the ALOHA Boeing 737 accident, there has been much effort to develop life-prediction models combining corrosion and fatigue. However, most of these models have been based on laboratory testing rather than service experience and have assumed that corrosion would not only initiate fatigue but also accelerate it.

Evidence from military aircraft indicates that although corrosion can initiate fatigue, the corrosion contribution is predominantly ground-based, while fatigue occurs mainly during flight [19, 20].

At present, the question whether corrosion and fatigue act in combination or independently requires further investigation per aircraft type and operational conditions. This is important since it can have a major impact on service life management [19, 21].

16.2.2 Airframe Materials

Aluminium alloys have predominated in airframes since introduction of the Boeing 247 (1933) and Douglas DC-2 (1934), but composites (mainly carbon fibre reinforced plastic, CFRP) and titanium alloys provide competition for certain applications. It is also important to note that the choices of materials for different types of aircraft vary greatly:

Transport Aircraft Aluminium alloys still account for about 60 % of the airframe structural weight, with the notable exceptions of the Boeing 787 *Dreamliner* and Airbus A350 XWB, which use 50–53 % composites and only 19–20 % aluminium.

Tactical Aircraft The emphasis tends to be on composites and lesser percentages of titanium, aluminium and steels. For example, the British Aerospace/DASA/CASA/Alenia Eurofighter and Lockheed Martin F-35 both use 35–40 % composites, most of which are in the external skin and substructure.

There are exceptions, notably the Lockheed Martin/Boeing F-22, which uses only 24 % composites and 20 % aluminium. Much of the F-22 structure (42 %) is titanium, which can tolerate the relatively high service temperatures, especially in the aft fuselage.

Helicopters Owing to the importance of weight savings for vertical lift aircraft, even higher percentages of composites are being used, e.g., the Bell-Boeing V-22 Osprey airframe consists of nearly 80 % composites [22] and the NHIndustries NH90 airframe is over 90 % composites.

The modern trend is to design and build hybrid airframe structures, not least because of the availability of 3rd generation aluminium–lithium (Al–Li) alloys. Al–Li alloys provide practical structural efficiencies that can rival those of CFRP composites, resulting in similar weight savings with respect to conventional aluminium alloys (see Chap. 3 in Volume 1 of these Source Books). The Airbus A380 represents an important example of a recent hybrid airframe construction, see Fig. 16.3.

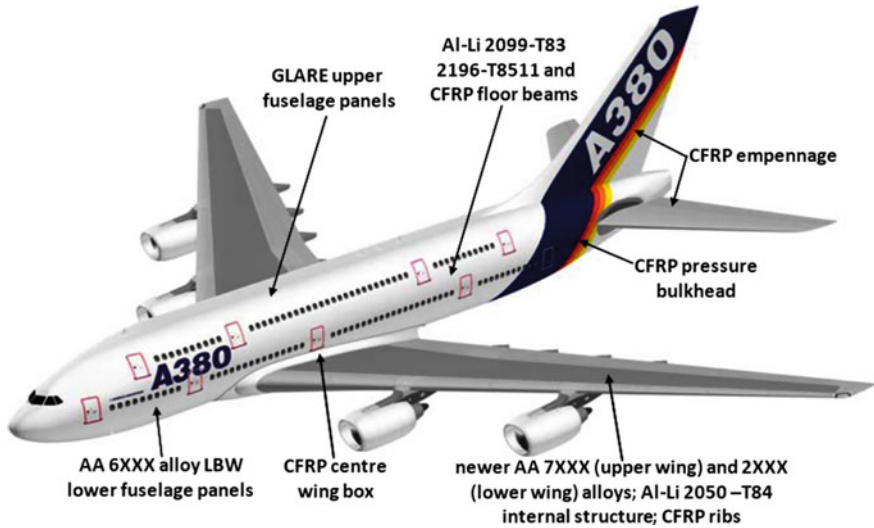


Fig. 16.3 Advanced materials and processing for major structural areas of the Airbus A380 [23]; *CFRP* Carbon fibre reinforced plastic; *GLARE* GLASS REinforced aluminium laminates; AA 2XXX, 6XXX and 7XXX = conventional aluminium alloys; *Al-Li* Aluminium–lithium alloys; LBW = Laser beam welding

The structural integrity implications of using the newer materials are summarised here:

1. Replacement of conventional aluminium alloys by the newer (3rd) generation Al–Li alloys will hardly change the fatigue and fracture structural analysis approaches, since these alloys have reached a similar level of reliability in their engineering properties [23].
2. GLARE (GLASS REinforced aluminium laminates) is a composite used extensively in the Airbus A380 pressure cabin, see Fig. 16.3. (Also see Chap. 13 in Volume 1). GLARE has fatigue and fracture properties amenable to conventional analyses for all-metal airframes, although there are some differences. These have led to a GLARE design ‘toolbox’ to enable compliance with current airworthiness regulations for metallic structures [24].
3. CFRPs have very different properties and design principles. They have high fatigue resistance when free from defects and stress concentrations, but they are susceptible to impact damage and subsequent cracking and delamination. The damage growth—which need not be by fatigue—is difficult to predict. This also makes it difficult to validate repairs. Other related problems are inspection reliability and difficulties in analysing complex components to predict the onset of failure. (More information on these issues is given in Chap. 14 in Volume 1 of these Source Books).

The overall result is that safety is currently ensured by overdesigning CFRPs according to the ‘no growth’ DT principle [25, 26]. However, this does not mean that there are no further developments. The Federal Aviation Administration (FAA) actively sponsors research in several key areas, including structural substantiation, DT and maintenance practices, materials control and standardization, and advanced material forms and processes [27]. These activities continually update the safety and certification requirements for composite structures [27, 28].

Looking to the future, there is a current lack of FSFT programmes for CFRP components under realistic conditions. These include the effects of temperature and humidity on the properties.

16.3 Fatigue Lifting *Methods* for Metallic Airframe Structures

The evolution of fatigue requirements discussed in Sect. 16.1 and illustrated by Figs. 16.1 and 16.2 has meant that several fatigue lifting methods have evolved, see Table 16.1. Some comments on the methods are made here.

Stress–Life (S–N) This method has been used extensively in the safe-life approach. The method relies on simple cumulative damage rules to obtain ‘safe’ fatigue lives under constant amplitude (CA) or variable amplitude (VA) load histories. The safe lives are then factored down using scatter factors based on engineering judgement and experience.

Strain–Life (ϵ –N) This is a common method used to analyse fatigue damage in aircraft fleets, and there are several original equipment manufacturer (OEM) and publicly available tools for doing this.

USAF Damage Tolerance (DT) This method is used for many USAF aircraft. It has been effective in ensuring structural *safety*, whereby the *assumed* initial flaw or crack sizes (see the F-111 discussion in Sect. 16.1.2.) are large enough for fracture mechanics calculations of FCG using models based on well-established macrocrack growth behaviour.

This DT approach has been less satisfactory for analyses of structural *durability*, i.e. achieving an economic life based on FCG. The initial flaw sizes for durability analyses (equivalent initial flaw sizes, EIFS) were set at 0.254 mm for fastener holes (the most critical locations), with smaller sizes allowed by demonstration. These initial crack sizes are well within the *short crack regime*, where until recently there were few relevant data and reliance had to be made on back-extrapolation of long crack growth behaviour using ‘traditional’ analytical modelling. These issues have been addressed by the DSTO approach.

Table 16.1 Survey of methods for fatigue life assessment of metallic airframe structures [10]

- **Stress–life (S–N)**
 - fatigue limits, S_e ; unnotched and notched (K_t); constant amplitude (CA) data
 - modifications to S_e
 - mean stress effects (R)
 - linear damage rule, also for variable R
 - scatter factors

- **Strain–life (ϵ –N)**
 - strain–life equation, unnotched data, $R = -1$
 - cyclic stress–strain curve analysis
 - rainflow cycle counting (closed hysteresis loops)
 - stress–strain at critical location (notch analysis)
 - mean stress effects (R) via equivalent strain equations, leading to equivalent strain amplitudes
 - damage accumulation rule

- **USAF damage tolerance (DT)**
 - specified equivalent initial flaw sizes (EIFS) based on NDI capabilities
 - back-extrapolation of long crack growth data to derive short crack growth
 - LEM long crack growth models (non-interaction, yield zone, crack opening, strip yield) to derive variable amplitude (VA) crack growth from constant amplitude (CA) data
 - possible use of crack opening model for short cracks (FASTRAN); differences in long and short crack thresholds need to be included
 - mainly deterministic: stochastic approach becoming accepted

- **DSTO approach: implemented by the RAAF**
 - actual initial discontinuity/flaw sizes and their EPS
 - actual short-to-long crack growth data using quantitative fractography (QF)
 - data compilations to establish empirical relationships describing crack growth behaviour
 - deterministic (‘upper bound’) estimates of *lead crack* growth
 - scatter factors

- **Holistic approach: proposed**
 - fatigue nucleation mechanisms (also as functions of notch stress concentrations, K_t)
 - fatigue nucleation lives (S–N and/or ϵ –N assessments)
 - evaluation and selection of marker load strategies for quantitative fractography (QF) of short-to-long crack growth
 - actual short-to-long crack growth using marker loads and QF
 - establishment, validation and choice of appropriate crack growth models and ‘laws’
 - deterministic (‘upper bound’) and stochastic approaches
 - environmental effects, notably corrosion

DSTO Approach As mentioned in Sect. 16.2.1, advances in QF since 1990 have provided many data for early crack growth in high-performance aircraft. Analyses have been developed to use these data for FCG life predictions [10].

Holistic Approach This is a broad programme, see Fig. 16.4, and is intended for all aircraft types. The inclusion of corrosion is especially noteworthy: see also the remarks about corrosion and fatigue in Sect. 16.2.1. The programme was first proposed in 2001. Since then it has been under development with participants from the USA, Canada, UK, Poland, Netherlands, Australia and Japan.

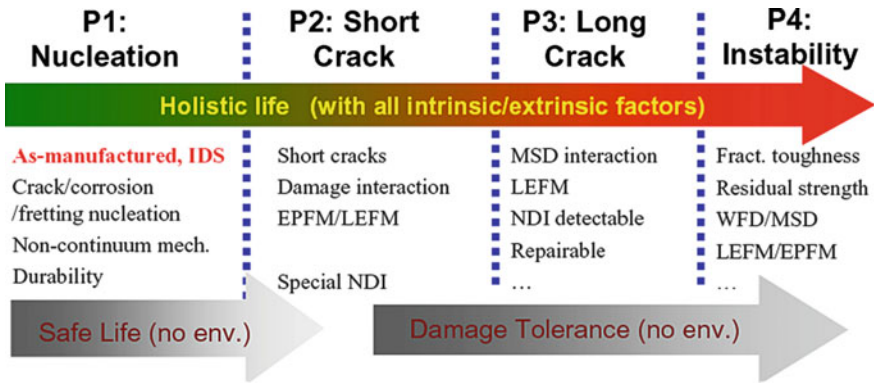


Fig. 16.4 Overview of the HOLSIP programme [29]: *IDS* Initial discontinuity state; *EPFM* Elastic plastic fracture mechanics; *LEFM* Linear elastic fracture mechanics; *MSD* Multiple site fatigue damage; *NDI* Non-destructive inspection; *WFD* Widespread fatigue damage

16.4 Fatigue Lifting Analyses for Metallic Airframe Structures

This section is intended to give generic overviews of fatigue lifting analyses. Much more can be found in specialist books on this topic, for example:

- Bannantine, J.A., Comer, J.J., and Handrock, J.L., 1998, ‘Fundamentals of Metal Fatigue Analysis’, Second Edition, Prentice Hall, Englewood Cliffs, New Jersey.
- Schijve, J., 2009, ‘Fatigue of Structures and materials’, Second Edition, Springer Netherlands, Dordrecht, the Netherlands.

Two especially relevant reports in the present context are as follows:

- Hu, W., Tong, Y.C., Walker, K.F., Mongru, D., Amaratunga, R. and Jackson, P., 2006, ‘A review and assessment of current lifting methodologies and tools in Air Vehicles Division’, DSTO Research Report DSTO-RR-0321, Defence Science and Technology Organisation, Melbourne, Australia.
- Molent, L., Barter, S.A. and Wanhill, R.J.H., 2010, ‘The lead crack fatigue lifting framework’, DSTO Research Report DSTO-RR-0353, Defence Science and Technology Organisation, Melbourne, Australia.

16.4.1 Safe-Life Estimations

Stress-Life Approach This is the traditional basis for safe-life fatigue analysis of aircraft structures. A generic overview of the procedure is shown in Fig. 16.5. Two points require elaboration:

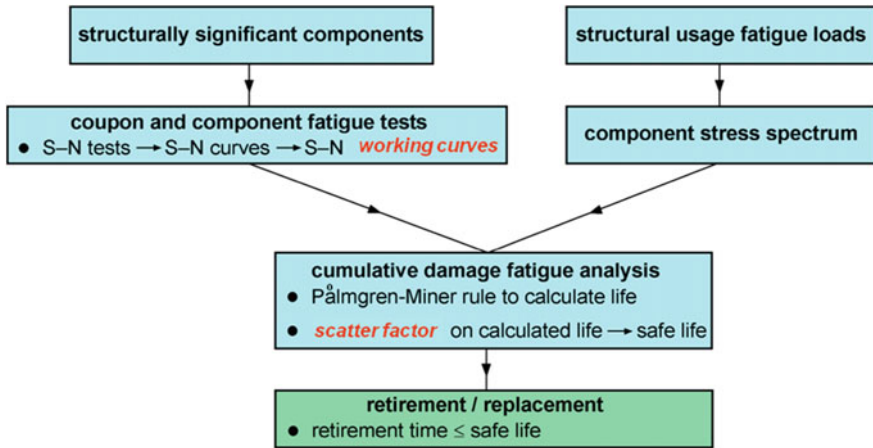


Fig. 16.5 Generic procedure for estimating the fatigue safe-life using the stress-life approach

1. Coupon and component S-N curves are modified into so-called *working curves* with the aid of several adjustment factors that are usually proprietary. These factors account for various influences on service components that are not included or experienced by coupons and components during the laboratory tests.
2. The often-used Pålmgren-Miner cumulative damage rule ignores load sequence effects, and the damage accumulation rate is assumed (incorrectly) to be independent of stress amplitude. The predicted lives can range from $0.3\times$ to at least $3\times$ the actual life [30]. The potential for unconservative life predictions (values >1) is mitigated by using scatter factors based on engineering judgement and experience, as mentioned in Sect. 16.3.

Strain-Life Approach This is commonly used to analyse fatigue damage in aircraft fleets. The damage (loads and accelerations) data are acquired via strain recorders, see Chap. 22 in Volume 2 of this Handbook. There are several OEM and publicly available tools for analysing the data.

Figure 16.6 shows a generic strain-life procedure to estimate safe fatigue lives and remaining lives from fleet data. In practice the test and service data and cumulative damage analyses are integrated into a computer program that includes an algorithm for cycle counting. This is usually ‘rainflow’ counting, which is well-described in Bannantine et al. [31].

16.4.2 Damage Tolerance Estimations

Damage Tolerance (DT) Approach A generic analysis approach based on the USAF DT method is shown in Fig. 16.7. As mentioned in Sect. 16.3, this method is

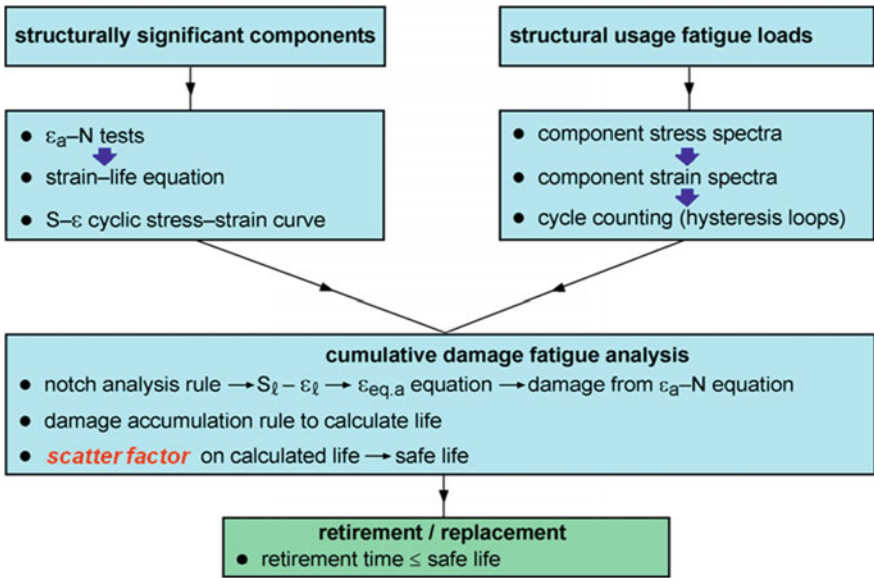


Fig. 16.6 Generic procedure for estimating the safe fatigue life and remaining fatigue life using the strain-life approach

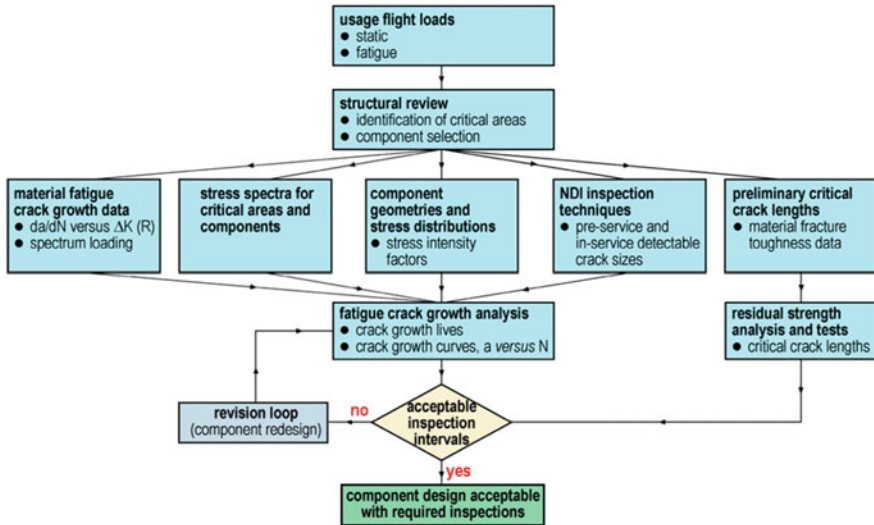


Fig. 16.7 Generic procedure for estimating acceptable damage tolerance (DT) FCG properties using linear elastic fracture mechanics (LEFM) fatigue crack growth models. This procedure is based on the USAF DT fatigue lifing method

used for many USAF aircraft and has been effective in ensuring structural safety. There are two points particularly to note:

1. The FCG analyses use linear elastic fracture mechanics (LEFM) FCG models. These models have difficulties in predicting the behaviour of short fatigue cracks, i.e. cracks with dimensions less than about 0.5 mm [32, 33].
2. Fracture toughness data and residual strength analyses and tests are required to complete the DT procedure. These topics are discussed in Chap. 18 of this Volume.

DSTO Approach This differs importantly from the DT approach with respect to the required input data and the FCG analysis methods, as may be seen from Table 16.1. The following points bear repeating with the addition of some important details:

1. The DSTO FCG analyses begin with EPS representing actual initial discontinuity sizes ('discontinuity' is neutral and covers a variety of fatigue-initiating features, whereas 'flaw' is negative and can be inappropriate). Use of actual initial discontinuity data was also the original intention of the USAF DT approach for *durability* analyses, but until QF advances since 1990 there was a lack of FCG data for (very) early crack growth from initiation sites with EPS values less than about 0.25 mm. Besides being important for durability analyses, service experience has shown the early FCG regime to contribute to improved safety analyses for high-performance aircraft [10, 34]. Also, the importance of WFD (notably in large transport aircraft, see Sect. 16.1.1) is another motivation for QF-based analyses of early FCG and its development [35].
2. The intransigence of the early FCG regime with respect to LEFM modelling has shown the need to develop empirical relationships describing the early FCG behaviour [10, 34]. In turn, this requires QF data compilations of early FCG from service aircraft, FSFT and component and coupon tests.

Hybrid Approaches Notwithstanding the differences between the USAF DT and DSTO approaches, there is much to be said in favour of a *rapprochement*.

The DSTO's position is that both LEFM and empirical FCG modelling can be used where justified by data obtained from service, FSFT and component and coupon tests. Also, the EPS concept for early crack growth has recently [36] been shown to be compatible with the USAF EIFS *durability* concept mentioned in Sect. 16.3.

16.4.3 Operational Damage Estimations

Much effort is being put into structural health monitoring (SHM) systems for rapid damage assessment, see Chap. 22 in Volume 2. The evolution of SHM has the following two main strategies:

1. Developing rapid NDI technologies to reduce the inspection time on the ground, often obtaining help from on-board sensing systems.
2. Monitoring of loads or strains or damage or a combination of these to determine the remaining useful life (RUL) and/or setting up inspection intervals for safe operation of the aircraft. Some of these systems have evolved into Health and Usage Monitoring Systems (HUMS) which use strain sensors extensively.

HUMS began and continues to be the basic system for helicopters, but it is now being used on fixed-wing aircraft, especially tactical aircraft like the Eurofighter and Indian Light Combat Aircraft (LCA). Strain-sensing equipment installed on the aircraft provides operational data that are usually used to estimate the RUL via a safe-life analysis, as shown generically in Fig. 16.6.

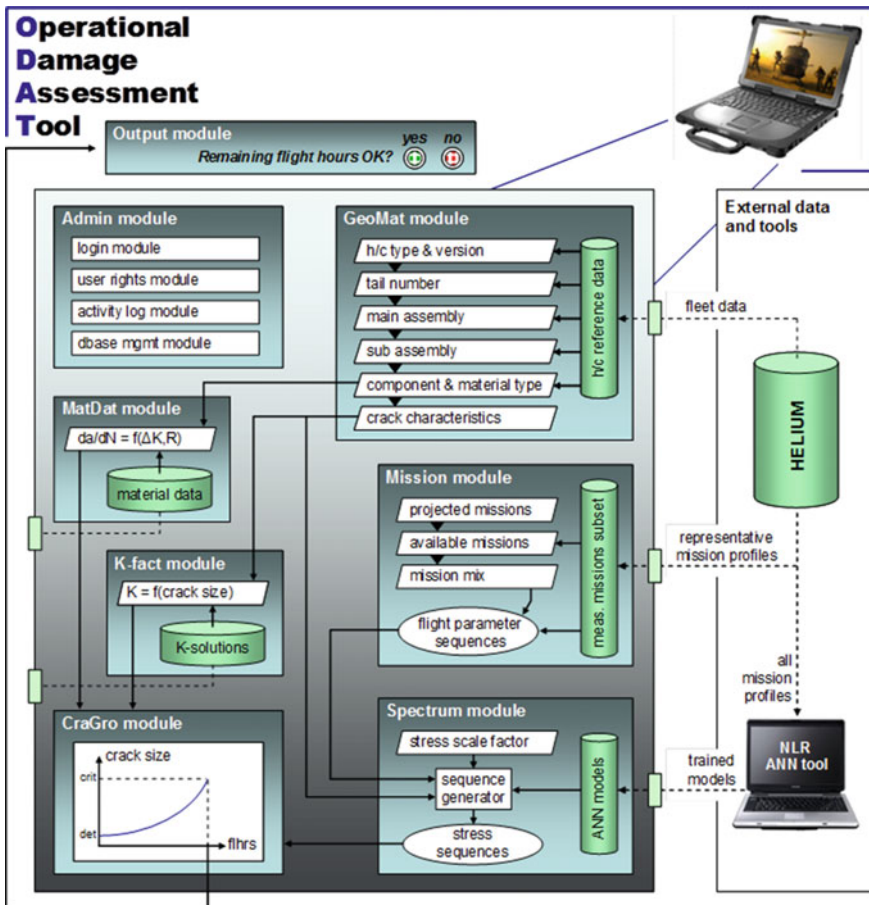


Fig. 16.8 The ODAT system architecture developed by the NLR for a helicopter fatigue life monitoring programme: *HELIUM* HELICOPTER Usage Monitoring database; ANN Artificial neural network. Illustration courtesy of Marcel Bos, NLR

However, it is also possible to use a HUMS system in a DT analysis to calculate a safe crack growth life [37–39]. One such system, developed by the NLR and called ODAT (Operational Damage Assessment Tool), is shown in Fig. 16.8. The architecture reflects the overall procedure for LEFM modelling of FCG to determine the number of flight hours needed to grow a fatigue crack from its detected size to the size at which fast fracture will occur.

The ODAT system requires a reliable FCG model and knowledge of the following parameters:

- the local structural geometry and its effect on the crack driving force (i.e. the so-called β factor in stress intensity factor solutions),
- the type of material and product form and the associated FCG properties,
- the expected operational load history.

Several types of tests, including CA and VA FCG and monotonic and cyclic stress–strain tests, are required for the LEFM crack growth modelling.

Any desired mission history can be assembled by selecting characteristic flights from the HELIUM database, and an artificial neural network (ANN) derives the local stress responses from the relevant flight parameters. The local stress response sequences can then be used as input to the FCG model.

16.5 Testing Requirements

Accurate and reliable estimates of the fatigue lives of metallic airframes present many challenges, particularly for high-performance aircraft and helicopters. There is always a demand for lighter structures with reduced manufacturing and operating costs. This leads to relatively highly stressed and efficient designs where fatigue cracking can occur at features such as shallow radii at the junction of flanges, webs and stiffeners, as well as at holes and tight radii. Consequently, there are usually many areas that need to be assessed for their fatigue and FCG lives and many potential locations at which cracking may occur in service.

Engineering fatigue design relies in the first instance on baseline coupon tests to assess the many locations identified as susceptible to cracking. The coupons may be loaded by CA or representative VA load histories, and they may try to represent some features of a built-up structure. The results of these coupon tests are averaged to give an indication of the structural life for a production aircraft. However, there are significant limitations to this approach:

1. Experience has shown that in high-performance aircraft the components have many features with the potential to crack, and that each of these features is typical of a single type of ‘representative’ coupon. Hence, a component’s average indicated life is equivalent to only the shortest average life from tests on several types of coupons.

- Even when the most critical feature of a component has been identified and assessed by coupon testing, the coupons are rarely fully representative, notably with respect to the surface treatments and finishes required for production aircraft. This is important because the commencement of fatigue cracking is primarily surface-influenced and therefore greatly dependent on small surface discontinuities inherent to component production, as well as any surface-connected discontinuities inherent to the material.

These limitations are addressed by other means. One way, which is mandatory for *all* modern aircraft, is to test actual components and conduct FSFT on part of the structure or even the full airframe, thereby including the effects of component geometry and production. (N.B: FSFT became mandatory for military aircraft in 1969, and civil aircraft in 1998, see Sects. 16.1.1 and 16.1.2.)

Another way is to improve coupon testing by making the coupons optimally representative of the most fatigue-critical details, e.g., by applying surface treatments and finishes used in component production. This may seem obvious, but it is sometimes neglected or overlooked.

16.5.1 ‘Building Block’ Testing Procedure

Figure 16.9 shows a schematic ‘building block’ (BB) approach for testing materials, components and structures as part of an *aircraft certification process*. This is adapted from a schematic for the Lockheed Martin F-35 Joint Strike Fighter (JSF), but is generically valid. The BB approach may be viewed as a pyramid whose base is the initial material evaluation. Each level of the pyramid is the foundation for the

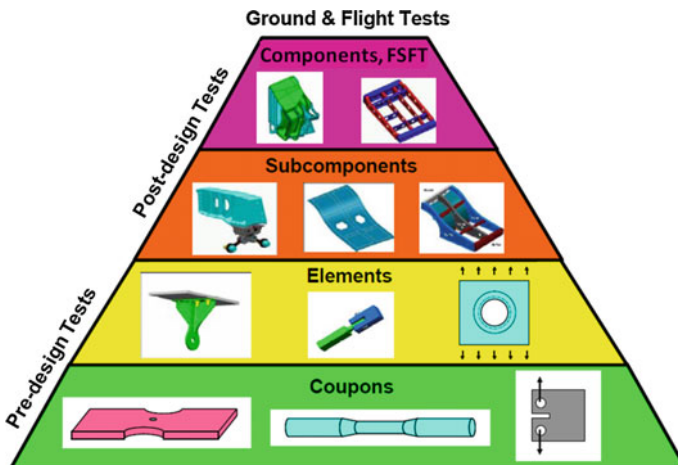


Fig. 16.9 ‘Building block’ fatigue test approach for materials, components and structures: after [40]

next, and the structural complexity and costs increase with each level up to the FSFT(s). The final phase of certification is ground and flight testing of the aircraft.

There are several points to be noted about the testing approach and procedure:

Coupon Testing Level This includes standard and non-standard tests. Examples of standard tests are stress–life (S–N); strain–life (ϵ –N), cyclic stress–strain (S– ϵ) and LEFM FCG. The latter are used to estimate FCG lives according to the USAF DT fatigue lifing method, see Fig. 16.7. An appropriate source for standard tests is ASTM International, see Chap. 9 of this Volume.

Non-standard coupon tests have been developed for the DSTO approach to DT analysis. One type of coupon is a simple flat specimen with an array of laser-induced crack starter slots. These enable QF measurements of FCG from initial discontinuities less than 0.05 mm in size.

However, QF usually requires ‘marker loads’ to be inserted into the fatigue load histories. The types of markers, and the ways in which they are added, can be chosen to ensure negligible influences of the marker loads on the overall FCG [41].

Element to FSFT Levels At all these levels, it is advisable to add marker loads to the fatigue load histories. Sometimes a realistic load history will result in natural crack front markers, but it is better to make sure that they occur. There are comprehensive guidelines for this [41].

Crack front marking is especially relevant to QF analyses of fatigue cracks detected during FSFT teardowns, see Fig. 16.10. Besides being used (and required) directly for certification, the FSFT teardown results are important for possible design modifications, verifying structural analyses, and determining whether retrofits may be advisable or necessary.

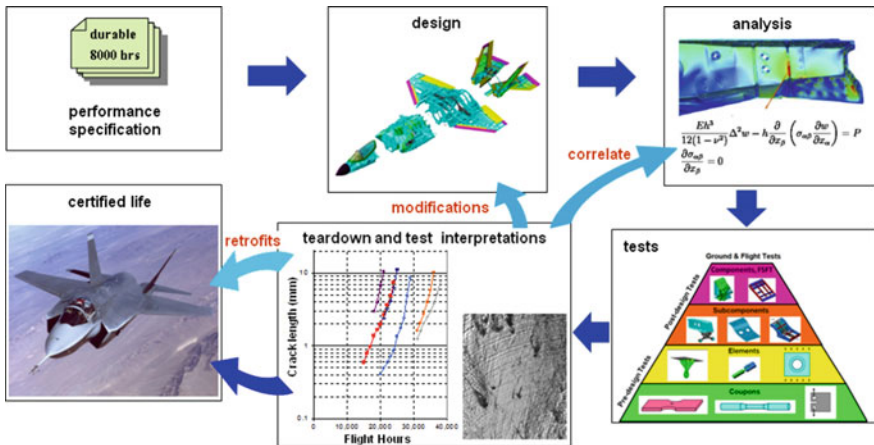


Fig. 16.10 Airframe fatigue certification and the central role of fatigue testing: see Fig. 16.9 also; original illustration courtesy of Madeleine Burchill and Simon Barter, DSTO, Melbourne

FSFT Types It is important to note that FSFT does not imply testing of the entire airframe. This may be done in some instances, but the available space and testing equipment often dictate that major parts of the airframe are tested separately.

An example of part-structure FSFT is the Airbus A380 MegaLiner Barrel (MLB) fatigue test, in which candidate fuselage skin materials were tested. Figure 16.11 shows (i) the MLB; (ii) the types of applied loads, namely fuselage pressurization (ΔP) and bending (M_Y , M_Z) and ground loads (Q_Z); and (iii) the number of simulated flights applied during testing. This is slightly more than twice the nominal Design Service Goal (DSG) of 20,000 flights.

FSFT Requirements As mentioned in Sect. 16.1.1, cases of WFD in civil transport aircraft led eventually to *mandatory* FSFT from 1998 onwards; and in 2011 the LOV concept for aircraft above 34,000 kg. The LOV concept requires FSFT to determine the onset of WFD [11].

These changes were reflected in the FSFT requirements, or rather *expectations*. From 1998 to 2011, the expectation was that an FSFT would be done to a minimum of 2 DSGs followed by specific inspections and analyses [8]. With introduction of the LOV concept, it is recommended that the FSFT is run to 3 DSGs, followed by residual strength testing [8].

The USAF has followed a similar evolutionary path in its DT approach. Thus MIL-STD-1530C [43], which predates the LOV concept, suggests that the FSFT be extended beyond 2 DSGs because the onset of WFD does not always occur within the two-lifetime test period [6].

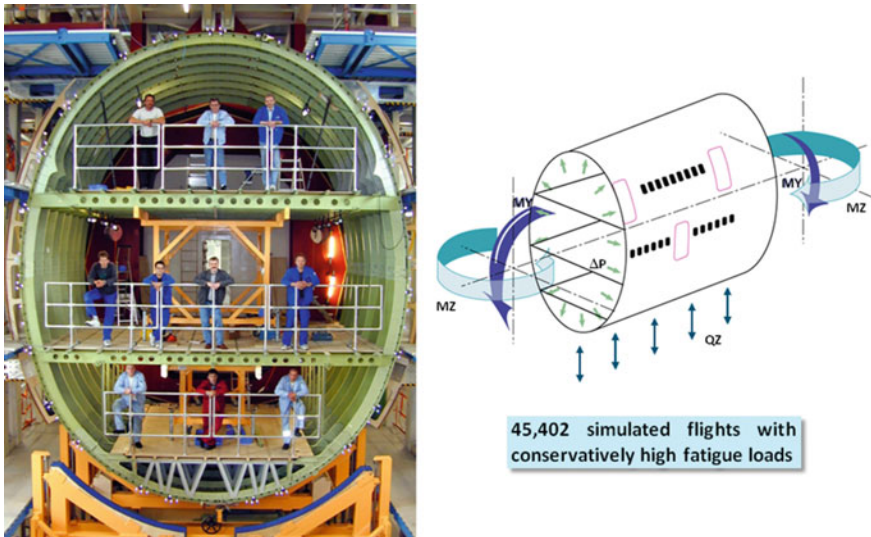


Fig. 16.11 Airbus A380 MegaLiner Barrel (MLB) full-scale fatigue test ‘specimen’, the general loading conditions, and the number of simulated flights applied during testing [42]

16.6 Summary

The fatigue requirements for aircraft structures have evolved since the 1950s. However, this has not been a gradual process: ‘milestone’ accidents have caused paradigm shifts for both civil and military aircraft, as may be seen from Figs. 16.1 and 16.2.

The requirements encompass fatigue design and analysis, and verification using several levels of testing. The ‘final’ verification is by FSFT and teardowns, which provide checks on designs and analyses, and can reveal the need for modifications and retrofits.

Besides ‘final’ verification of structural integrity, FSFT and teardowns provide references for any fatigue problems that arise during service. They are also references for investigating whether it is feasible to extend the service life beyond the original design life. This is a not-infrequent issue.

Acknowledgments Thanks are due to Simon Barter, Lorrie Molent and Madeleine Burchill, DSTO, Melbourne, Australia; and Marcel Bos, NLR Emmeloord, the Netherlands.

References

1. Niu MC-Y (1988) Airframe structural design. Conmilit Press, Wanchai, Hong Kong, p 3 (Chapter 1.0)
2. Safarian P (2013) Fatigue and damage tolerance requirements of civil aviation, lesson 01—introduction, winter 2014. University of Washington, Seattle, Washington
3. Schijve J (1994) Fatigue of aircraft materials and structures. *Int J Fatigue* 16(1):21–32
4. Blom AF (2002) Fatigue science and engineering—achievements and challenges. In: Rouchon J (ed) ‘ICAF’ 2001: Design for durability in the digital age, vol I. Cépaduès-Éditions, Toulouse, France, pp 3–64
5. McEvily AJ (2002) Metal failures: mechanisms, analysis, prevention. Wiley, New York, pp 6–8, 13–15 (Chapter 1)
6. Tiffany CF, Gallagher JP, Babish CA IV (2010) Threats to aircraft structural safety, including a compendium of selected structural accidents/incidents. Aerospace Systems Center Technical Report ASC-TR-2010-5002, Wright- Patterson Air Force Base, Dayton, Ohio 45433-7101
7. Wanhill RJH, Molent L, Barter SA (2016) Milestone case histories in aircraft structural integrity. In: Hashmi S (ed) Reference module in materials science and materials engineering. Elsevier Inc., Oxford, UK, pp 1–19. doi:[10.1016/B978-0-12-803581-8.00847-X](https://doi.org/10.1016/B978-0-12-803581-8.00847-X)
8. Eastin RG, Sippel W (2011) “The “WFD rule”—have we come full circle?”, USAF Aircraft Structural Integrity Program Conference 2011, November 29–December 1, 2011. San Antonio, Texas
9. Wilson ES (1995) Developments in RAAF aircraft structural integrity management. In: Grandage JM, Jost GS (eds) Estimation, enhancement and control of aircraft fatigue performance, vol II. Engineering Materials Advisory Services, Warley, UK, pp 959–970
10. Barter SA, Molent L, Wanhill RJH (2010) Fatigue life assessment for high performance metallic airframe structures—an innovative practical approach. In: Ho S-Y (ed) Structural failure analysis and prediction methods for aerospace vehicles and structures. Bentham E-Books, Bentham Science Publishers, Sharjah, UAR, pp 1–17 (Chapter 1)

11. Federal Aviation Administration (2011) Establishing and implementing limit of validity to prevent widespread fatigue damage. Advisory Circular FAA AC 120-104. U.S. Department of Transportation, Washington, DC
12. Gallagher JP (2007) A review of the philosophies, processes, methods and approaches that protect in-service aircraft from the scourge of fatigue failures. In: Lazzeri L, Salvetti A (eds) Durability and damage tolerance of aircraft structures: metals vs. composites, vol 1. Pacini Ed., Pisa, Italy, pp 1–36
13. Buntin WD (1977) Application of fracture mechanics to the F-111 airplane. In: AGARD conference proceedings no. 221 on Fracture mechanics design methodology. Advisory Group for Aerospace Research and Development, Neuilly-sur-Seine, France, pp 3-1–3-12
14. Mar JW (1991) Structural integrity of aging airplanes: a perspective. In: Atluri SN, Sampath SG, Tong P (eds) Structural integrity of aging airplanes. Springer, Berlin, pp 241–262
15. Military Specification Airplane Damage Tolerance Requirements (1974) MIL-A-83444. United States Air Force, The Pentagon, Virginia
16. Military Standard Aircraft Structural Integrity Program, Airplane Requirements (1975) MIL-STD-1530A (11). United States Air Force, The Pentagon, Virginia
17. Athinotis N, Barter SA, Goldsmith NT (1991) Macchi aircraft safety-by-inspection validation program—A7-076 starboard wing tear-down preliminary report. Defect Assessment & Failure Analysis Report No. M21/91, Defence Science and Technology Aeronautical Research Laboratory, Melbourne, Australia
18. Barter SA, Molent L, Wanhill RJH (2012) Typical fatigue-initiating discontinuities in metallic aircraft structures. *Int J Fatigue* 41(1):11–22
19. Barter SA, Molent L (2013) Service fatigue cracking in an aircraft bulkhead exposed to a corrosive environment. *Eng Fail Anal* 34:181–188
20. Molent L (2015) Managing airframe fatigue from corrosion pits—a proposal. *Eng Fract Mech* 137:12–25
21. Molent L, Barter SA, Wanhill RJH (2015) The decoupling of corrosion and fatigue for aircraft service life management. In: Siljander A (ed) ICAF 2015: Structural integrity: embracing the future—respecting the past; supporting aging fleets with new technologies. VTT Technical Research Centre of Finland Ltd, FI-02044, Finland, pp 1062–1073
22. Deo RB, Starnes JH Jr, Holzwarth RC (2003) Low-cost composite materials and structures for aircraft applications. In: Low cost composite structures and cost effective application of titanium alloys in military platforms. RTO Meeting Proceedings 69(II), NATO Research and Technology Organisation, Neuilly-sur-Seine, France, pp (SMI) 1-1–1-11
23. Wanhill RJH (2013) Aerospace applications of aluminum-lithium alloys. In: Prasad NE, Gokhale AA, Wanhill RJH (eds) Aluminum-Lithium alloys, processing, properties and applications. Butterworth-Heinemann, Elsevier Inc., Oxford, pp 503–535
24. Beumler T (2004) Flying GLARE[®], a contribution to aircraft certification issues in non-damaged and fatigue damaged GLARE[®] structures. Doctor's Thesis, Delft University of Technology, Delft, The Netherlands
25. Federal Aviation Administration (2010) Composite aircraft structure. Advisory Circular FAA AC-20-107B, Change 1, August 24, 2010. U.S. Department of Transportation, Washington, DC
26. Military Composite Materials Handbook (2013) Volume 3. Polymer matrix composites materials usage, design, and analysis. MIL-HDBK-17-3F, U.S. Department of Defense, The Pentagon, Virginia
27. Icewicz L (2007) AC 20-107A “Composite aircraft structure” updates, Commercial Aircraft Composite Repair Committee Meeting, Wichita, Kansas, 14 Nov 2007
28. Icewicz L (2009) Updates to AC 20-107B “Composite aircraft structure”, Composite Damage Tolerance & Maintenance Workshop, Tokyo, Japan, 5 June 2009
29. Komorowski JP, Bellinger NC, Liao M, Fillion A (2007) Application of the holistic structural integrity process to Canadian Forces challenges. In: ASIP 2007, USAF Aircraft Structural Integrity Program 2007, 4–6 Dec 2007, Palm Springs, California

30. Schütz W (1979) The prediction of fatigue life in the crack initiation and propagation stages—a state of the art survey. *Eng Fract Mech* 11:405–421
31. Bannantine JA, Comer JJ, Handrock JL (1998) *Fundamentals of metal fatigue analysis*, 2nd edn. Prentice Hall, Englewood Cliffs, New Jersey
32. Anstee RFW (1983) An assessment of the importance of small crack growth to aircraft design. In: *Behaviour of short cracks in aircraft components*, AGARD conference proceedings no. 328. Advisory Group for Aerospace Research and Development, Neuilly-sur-Seine, France, pp 3-1–3-9
33. Anstee RFW, Edwards PR (1983) A review of crack growth threshold and crack propagation rates at short crack lengths. In: *Some considerations on short crack growth behaviour in aircraft structures*, AGARD Report No. 696. Advisory Group for Aerospace Research and Development, Neuilly-sur-Seine, France, pp 2-1–2-12
34. Molent L, Barter SA, Wanhill RJH (2010) The lead crack fatigue lifing framework. DSTO Research Report DSTO-RR-0353. Defence Science and Technology Organisation, Melbourne, Australia
35. Wanhill RJH, Koolloos MFJ (2001) Fatigue and corrosion in aircraft pressure cabin lap splices. *Int J Fatigue* 23:S337–S347
36. Gallagher J, Molent L (2015) The equivalence of EPS and EIFS based on the same crack growth life data. *Int J Fatigue* 80:162–170
37. De Jonge JB, Van Lummel CWJ (1986) Development of a crack severity index (CSI) for quantification of recorded stress spectra. NLR Technical Report NLR-TR-86049, National Aerospace Laboratory NLR, Amsterdam, the Netherlands
38. Lee H, Park S, Kim H (2010) Estimation of aircraft structural fatigue life using the crack severity index methodology. *J Aircraft* 47(5):1672–1678
39. Aeronautical Systems Center Engineering Directorate (2009) Methodology for determination of equivalent flight hours and approaches to communicate usage severity. Structures Bulletin EN-SB-09-001, ASC/EN, Bldg 560, 2530 Loop Road West, Wright-Patterson AFB, Ohio 45433-7107
40. Ball DL, Norwood DS, TerMaath SC (2006) Joint strike fighter airframe durability and damage tolerance certification. AIAA paper 2006-1867, 47th AIAA/ASME/ASCE/AHS/ASC Structures, Structural Dynamics, and Materials Conference, 1–4 May 2006, Newport, Rhode Island
41. Barter SA, Wanhill RJH (2008) Marker loads for quantitative fractography (QF) of fatigue in aerospace alloys. NLR Technical Report NLR-TR-2008-644, National Aerospace Laboratory NLR, Amsterdam, The Netherlands
42. Wanhill RJH, Platenkamp DJ, Hattenberg T, Bosch AF, De Haan PH (2009) GLARE teardowns from the MegaLiner Barrel (MLB) fatigue test. In: Bos MJ (ed) *ICAF 2009: Bridging the gap between theory and operational practice*. Springer Netherlands, Dordrecht, The Netherlands, pp 145–167
43. Department of Defense Standard Practice, Aircraft Structural Integrity Program (ASIP) (2005) MIL-STD-1530C(USAF), ASC/ENOI, 2530 Loop Road West, Wright-Patterson AFB, Ohio 45433-7101

Chapter 17

Full-Scale Fatigue Testing

R. Sunder

Abstract Full-scale fatigue testing (FSFT) forms an integral part of the aircraft development and certification prior to induction into service. The five historical stages of evolution of FSFT are described with a detailed description of present-day requirements including composite structures. The technology used in the FSFT process is explained in detail.

Keywords Full-scale fatigue testing · Aircraft structural integrity programmes · Damage tolerance · Alloys · Composites

17.1 Why Testing and Why FSFT?

Progress of the Industrial Revolution in the nineteenth century led to a quantum increase in speeds and exponential increase in the number of repetitive load cycles on machines and structures. These resulted in periodic catastrophes as in the case of broken railway axles, even though operational stresses were well within the yield limit. The seemingly inexplicable sudden failures may have led to the rather inappropriate term metal “fatigue”.

Painstaking and systematic research by Wöhler [1], the superintendent of a railway depot in Prussia, finally established a systematic relationship between the magnitude of periodic loads applied on a specimen and the number of such “cycles” to its failure. More significantly, Wöhler determined that there is a certain minimum magnitude of cyclic loading below which the material will withstand seemingly infinite cycling. This stress amplitude is termed the fatigue limit. Thus a material constant was finally available in order to design for durability. Wöhler [1] and Bauschinger [2] established that the fatigue limit is extremely sensitive to mean stress.

Unfortunately, service loads are a statistical mix of cycles of diverse magnitude wherein extremely large load cycles can occur, albeit very rarely. Designing to keep

R. Sunder (✉)
BISS, Bengaluru, India
e-mail: rs@biss.in

extreme load cycles below the fatigue limit is not practical. It became necessary to account for the contribution of individual load cycles in a service load spectrum to cumulative fatigue damage eventually leading to failure. Palmgren's and then Miner's linear damage accumulation law finally made this possible [3]. However, Gassner established that cyclic damage accumulation is not linear [4]. Depending on the material, the service load spectrum, and the sequence of loads in the given spectrum, the damage sum at failure can vary over a very wide range, in fact by about two orders of magnitude. Very importantly, Gassner also established that for a given combination of material and service load spectra, the damage sum would not vary significantly. This finding by Gassner essentially underscores the necessity for full-scale fatigue testing (FSFT) of aircraft structures as a means to establish safe service life.

17.2 Evolution of FSFT

One of the requirements to certify any military or commercial transport aircraft is a full-scale fatigue test. The goal is to evaluate the durability of the airframe under conditions that are as close as practically possible to those that will eventually restrict its service life by fatigue damage.

17.2.1 *Initial Approach*

The evolution of full-scale testing over the past century of flight may be broadly divided into five stages. In the first four decades of aviation, airframes, particularly those of military aircraft, were primarily tested under static conditions. Downloads were applied using sand or shot bags, while uploads were applied using hydraulic jacks [5]. Durability of the aircraft was addressed in an indirect manner by confirming the static strengths of airframes that had already seen much service, and also via *repeat* drop tests in order to determine the effect of undercarriage impact on the residual static strength of the airframe [6].

17.2.2 *Hydraulics in FSFT*

Hydraulic actuators made it possible to perform full-scale fatigue tests on airframes by applying repeated loads, limited by pressure relief valves on individual actuator sets to the required peak load. The pressure would be released by solenoid valves. There are records from the early 1950s of full-scale fatigue tests performed using several such actuators, along with hundreds of strain gauges to track structural response [5]. By applying reasonably high repeat loads expressed as a fraction of limit load, it was possible to get a reasonable idea of fatigue-critical areas of the

structure and assign safe intervals of operation between major overhauls. Very soon, through manipulation of hydraulic circuits with multiple relief valves set to different pressures and solenoids to activate them, it became possible to perform multistep programmed loading full-scale fatigue tests on airframes. This may be considered the second stage in the evolution of full-scale testing and the virtual commencement of automated FSFT to characterize airframe durability.

17.2.3 Advent of Servo-Hydraulics and Computer Control

Airframe load spectra are derived from flight data records collected over hundreds or thousands of flights depending on the aircraft type and its mission distributions. As a minimum, these are non-dimensionalized acceleration, “g”, values along with associated airspeed and instantaneous mass. Given the aerodynamic data from either wind tunnel tests or numerical simulation and for a given mass distribution, airframe loads and their distribution can be deduced with reasonable accuracy for each “g” data point. FSFT performed under pseudo-random flight-by-flight loading thus induces fatigue loading across the load frame in much the same manner as real service conditions (with a few deviations from reality such as a compressed timescale, known to have only a secondary effect on the fatigue process). In any case, from an environment standpoint, laboratory conditions are considered less forgiving than flight at cruise altitude.

All of the above were incorporated in the third stage of evolution of full-scale testing, with the emergence of servo-controlled hydraulic actuators, first with punched paper tape control in the early 1970s to programme load levels on individual actuators; and then through real-time computers in the late 1970s [7]. The latter made it finally possible to enforce pseudo-random cycle-by-cycle simulation of actual flight-by-flight and cycle-by-cycle variations in g-levels, the only distortion being in the timescale. One could claim at last that FSFT under laboratory conditions closely simulated actual usage loads.

The first generation of turboprop and turbojet transport airliners and scores of military aircraft were subjected to FSFT in the late 1950s and into the 1960s. Initially, the goal was to understand why unexpected catastrophic failures occurred as in the case of the De Havilland Comet, but later to support certification of the aircraft for a certain minimum safe period of service, to be followed either by major overhaul or by retirement. One may note that a crucial requirement of all these tests was the accurate simulation of service loads, without any scale-up, on a newly assembled airframe conforming to the same manufacturing process as in routine production.

17.2.4 ASIP and Consideration of Damage Tolerance

The 1950s and 1960s also saw the emergence of, and rapid advances in, the discipline of fracture mechanics, stimulated by several catastrophic failures, starting

with the seemingly inexplicable catastrophic failures of Liberty freighter ships towards the end of WWII. These were followed by equally shocking catastrophic explosive failures of the passenger cabins of the first pressurized jet transport aircraft, the De Havilland Comet, and also that of crucial pivoting arrangements on one of the General Dynamics F-111 variable geometry fighters.

All these accidents were traced to cracks in the structure whose growth led ultimately to catastrophic failure. Using fracture mechanics concepts it became possible for the first time, not merely to assess the strength of a structure when “defect-free”, but also to move the discussion to *decreasing residual strength* in the face of growing defect sizes. The latter constitutes a qualitative leap from understanding of the fatigue failure as “an event”, towards utilizing the new comprehension of the airframe as a structure, whose residual strength is gradually eroded by the occurrence and growth of fatigue cracks. See also Chaps. 16 and 18 in this Volume.

The US Air Force was the first to recognize the significance of fatigue cracks not merely as a problem, but as an *opportunity* to enhance the airworthiness and durability of airframes and reduce operational costs. This came about in the form of the Airframe Structural Integrity Program (ASIP), which lays down the guidelines for handling the entire life cycle of an aircraft—from the design stage right into retirement [8], see Fig. 17.1. Central to ASIP is the idea that the condition of an airframe is characterized by the inevitable formation and growth of defects in the form of fatigue cracks that will eventually reduce its residual strength to unacceptably low levels.

This new approach effectively changed the prevailing emphasis on airframe design and development. On the one hand, the new focus was on identification of structural materials and designs that exhibit enhanced resistance to the growth of fatigue cracks and tolerate defects of larger size. On the other hand, ASIP encouraged the development of non-destructive inspection (NDI) techniques that would permit the assured detection of such defects during scheduled inspections, well before they could threaten the structural integrity of the aircraft. ASIP thereby triggered the gradual transformation of the aviation industry towards “Maintenance on Condition” (MOC) and “Retirement for Cause” (RFC). These effectively opened the way for reliable and prolonged operation of aircraft, their life extension if necessary, and their eventual retirement for cause.

17.2.4.1 Five Tasks of ASIP

As shown in Fig. 17.1, the ASIP process consists of five tasks. Of these, the first four form part of the aircraft development programme from design to induction into service. The fifth task covers the management of the fleet right through to retirement, including life extension programmes if any.

Task I of ASIP essentially describes processes that will be followed to achieve the stated goals of a new aircraft design. Task II of ASIP is partly dedicated to the crucial process of defining safety- and fatigue-critical areas of the airframe and designating each one either as a Fail-Safe design or a Safe-Life design.

TASK I	TASK II	TASK III	TASK IV	TASK V
DESIGN INFORMATION	DESIGN ANALYSIS AND DEVELOPMENT TESTS	FULL-SCALE TESTING	FORCE MANAGEMENT DATA PACKAGE	FORCE MANAGEMENT
ASIP MASTER PLAN STRUCTURAL DESIGN CRITERIA DAMAGE TOLERANCE & DURABILITY CONTROL PROCESS SELECTION OF MATERIALS, PROCESSES, & JOINING METHODS	MATERIALS AND JOINT ALLOWABLES LOAD ANALYSES DESIGN SERVICE LOADS SPECTRA DESIGN CHEMICAL/THERMAL ENVIRONMENT SPECTRA	STATIC TESTS DURABILITY TESTS DAMAGE TOLERANCE TESTS FLIGHT & GROUND OPERATIONS TESTS	FINAL ANALYSES STRENGTH SUMMARY FORCE STRUCTURAL MAINTENANCE PLAN LOADS/ENVIRONMENT SPECTRA SURVEY	LOADS/ENVIRONMENT SPECTRA SURVEY INDIVIDUAL AIR VEHICLE TRACKING DATA INDIVIDUAL AIR VEHICLE MAINTENANCE TIMES
DESIGN SERVICE GOAL AND DESIGN USAGE	STRESS ANALYSIS	AEROACOUSTIC TESTS	INDIVIDUAL AIR VEHICLE TRACKING PROGRAM	STRUCTURAL MAINTENANCE RECORDS
MASS PROPERTIES	DAMAGE TOLERANCE ANALYSIS DURABILITY ANALYSIS AEROACOUSTIC ANALYSIS	FLIGHT VIBRATION TESTS FLUTTER TESTS INTERPRETATION & EVALUATION OF TEST RESULTS		WEIGHT AND BALANCE RECORDS
	VIBRATION ANALYSIS	WEIGHT AND BALANCE TESTING		
	FLUTTER ANALYSIS			
	EFFECTS ANALYSIS NUCLEAR WEAPONS			
	EFFECTS ANALYSIS NON-NUCLEAR WEAPONS EFFECTS ANALYSIS DESIGN DEVELOPMENT TESTS			
	MASS PROPERTIES ANALYSIS			

Fig. 17.1 The five tasks of ASIP [8]. Full-scale testing constitutes Task III. It can also be invoked as part of life reassessment under Task V

To qualify for Fail-Safe design, the part must be deemed inspectable and with the ability to operate indefinitely on the consideration that any defect appearing in service will be detected at the next scheduled inspection to enable repair or replacement, i.e. condition monitoring. Such a design demands the availability of suitable inspection techniques, analysis, and testing to demonstrate maintainability on condition. Failure to comply with this requirement leads to categorization as Safe-Life. The proportion of safety-critical components categorized as Fail-Safe effectively determines the degree of compliance with ASIP. If the majority of parts

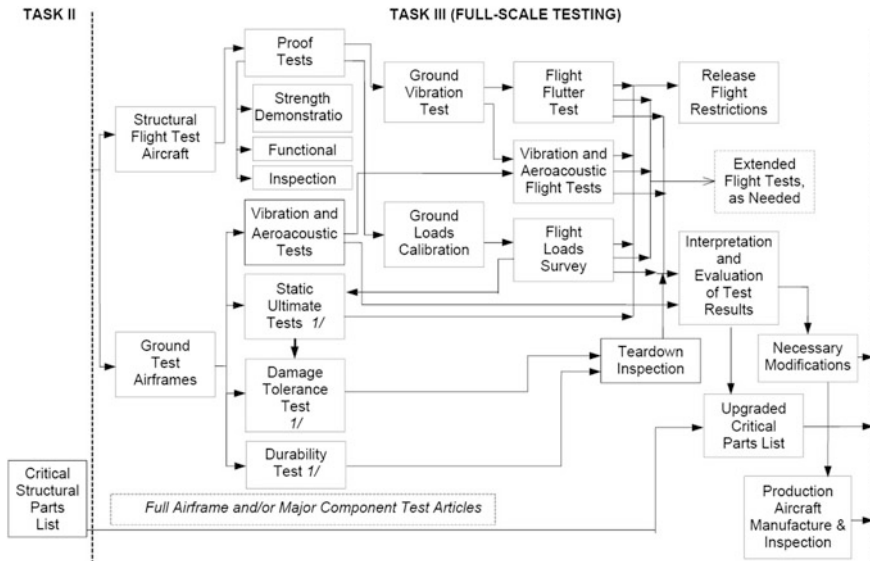


Fig. 17.2 Task III of ASIP [8]. Full-scale fatigue addresses at least three requirements. One to confirm design lifetime, another to validate the inspection intervals, and a possible third to preclude consequences of simultaneous widespread damage at the conclusion of the rated service life. Teardown inspection following a full-scale fatigue test provides quantitative data on fatigue-critical areas for assessment of Fail-Safety as well as Safe-Life. It also yields statistical data amenable to Risk Analysis in planning inspection intervals

on a new airframe are subject to Safe-Life operation, then obviously, strict maintenance will be involved without the benefits of indefinite safe operation of the fleet, and this will lead to escalated life cycle costs.

Full-scale testing constitutes Task III of ASIP, and FSFT forms a major part of this task (see Fig. 17.2). ASIP provides for FSFT to characterize both fatigue-critical areas and proof of design lifetime by testing to two design lifetimes under conditions that closely resemble service usage.

With the advent of ASIP, FSFT entered its fourth stage of evolution. FSFT forms an important part of ASIP but has been extended in order to support new goals. ASIP retains the prevailing requirement of FSFT over two design lifetimes: however, additional elements of full-scale testing address the structural integrity in the presence of defects. This is to confirm the ability of the airframe to withstand a substantial pre-defined extent of cracking (damage tolerance) of safety-critical parts, including wing and fuselage panels. Such testing validates the Fail-Safe design features of the airframe that envisage alternative load paths in the unlikely event of fracture of a safety-critical element such as a stringer or even a bulkhead. Finally, ASIP provides for FSFT of the airframe in the presence of simulated detectable fatigue cracks in order to validate the safe operation between scheduled inspections.

Task V of ASIP describes how aircraft are to be operated through their life cycle. It provides for individual airframe tracking (IAT), whereby flight data records are analysed to build up individual usage history, so-called “personal files”, with details of flight-by-flight load history, along with the records of inspection and maintenance, including part replacement and exchange with other tail numbers. IAT permits flexible scheduling of inspection across the fleet after accounting for the severity of service loads seen by individual aircraft.

The calculations associated with this exercise are based essentially on cumulative damage concepts established in the early work by Gassner. One of the purposes of IAT is to compare actual loads experienced by the fleet with the load spectrum used in FSFT so that corrective action can be taken if required. If differences are insignificant, inspection schedules may be suitably corrected. If they are deemed significant, a repeat FSFT may be called for.

As part of Task V of ASIP, FSFT also provides for the incorporation during service of (i) one or more redesigned structural elements deemed necessary for continued operation or (ii) new ways of operation involving major changes in usage profile, payload, or other such operational necessity. Such a necessity can arise in the event of increasing cost of repair or part replacement after scheduled inspections. In this case, assuming the airframe has already seen much service and if the fleet size is reasonably large, one airframe is “sacrificed” for a complete teardown inspection [9].

Such an exercise provides a number of useful inputs. Fatigue-critical areas found in service are identified. The sheer statistics of hundreds or even thousands of cracks growing from rivet holes form the basis for Risk Analysis to determine how to rework the design and reschedule inspection periods to minimize the risk of failure over continued long-term usage of the repaired aircraft [9]. ASIP provides for additional FSFT either at major subassembly level or on the entire airframe to validate the adopted structural modifications. This procedure has been exercised for a variety of ageing aircraft [9].

17.2.5 Adaptation of ASIP to Composite Structures and Its Impact on FSFT

The concepts and FSFT procedures laid out in ASIP have, over the past four decades, seen widespread acceptance and use by the global aerospace industry. In the meantime, airframe technologies have also evolved. The most significant transformation in this regard is by way of increased usage of composites, particularly carbon fibre-reinforced plastics (CFRP) in safety-critical load-carrying airframe components.

N.B. In addition to the following Sects. 17.2.5.1 and 17.2.5.2, the reader may wish to consult a broadly similar discussion in Sect. 14.5 of Chapter 14 in Volume 1 of these Source Books.

17.2.5.1 Differences in Damage Mechanisms Between Metals and Composites

The fatigue damage mechanics of composites is very different from that of metals. Metals invariably fail due to the growth of fatigue cracks to critical sizes. Alloy sheets used in airframes are inherently damage tolerant and resistant to fatigue crack growth. In thin-walled structures such as airframes, such cracks show up as *through* cracks and are therefore readily detectable once their size becomes comparable with the material thickness.

An invaluable characteristic of fatigue crack growth in metallic materials, particularly under aircraft service loading, is its high degree of reproducibility and low scatter. At the same time, failure mechanisms in metallic airframes are sensitive to the magnitude of loading. Partly for these two reasons, FSFT of metallic airframes is prescribed under load levels that accurately simulate *actual* load levels in service and over just two design lifetimes as an assurance of valid design.

FSFT of composite structures demands a different approach [10]. Carbon fibre is stronger and stiffer than high-strength steel, yet lighter than aluminium, making it an attractive alternative to aluminium alloys that have dominated the aircraft industry for almost an entire century. However, there are a few important features in the manner in which composites fail that seriously affect how FSFT is set up for composite structures.

The basic mechanical properties of aerospace quality carbon fibres, including modulus, ultimate strength, and elongation, are highly reproducible: their data scatter compares favourably with metals. However, damage mechanisms of *built-up* CFRP and other composites are vastly different from metals, particularly in fatigue. CFRP structural elements are sensitive to out-of-plane loads and especially to impact loads. These induce interlaminar separation that is not outwardly visible, but can cause considerable deterioration in residual strength, particularly the compressive residual strength. Thus, although the underwing surfaces of metallic wings attract particular attention during inspection for damage, it is the overwing surfaces of composite wings that pose concern.

Also, unlike metals composites can fail in a variety of ways. In addition, the mechanical properties of built-up composite structures are extremely sensitive to every step in the elaborate process of their manufacture.

17.2.5.2 Statistical Aspects of Fatigue of Composites and Adaptation to FSFT

Over the past three decades much testing has been performed on CFRP coupons with different configurations of practical interest, including different lay-ups [11]. An understanding has emerged about how scatter in fatigue life can vary from case to case, and more importantly about how to model such scatter [12]. These data are used in designing composite structures for durability and damage tolerance. They

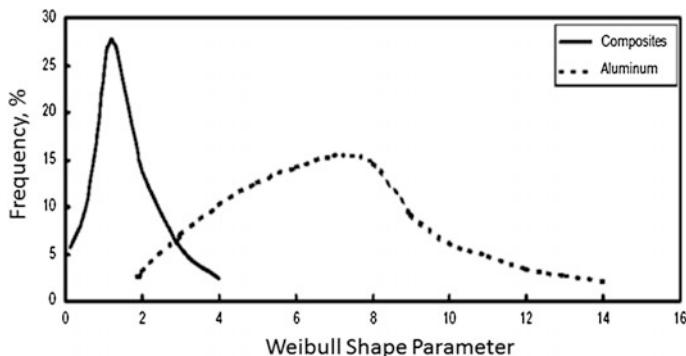


Fig. 17.3 Statistical results of coupon-level fatigue tests performed on composites compared with tests on metals, expressed as percentage frequency of occurrence versus Weibull shape parameter β . Fatigue test results on aluminium alloys and other aircraft quality metallic materials are much more reproducible than those for composites. This is the main reason for serious changes in the manner in which new-generation aircraft containing composite primary structures are designed and tested

also impact the manner in which full-scale test requirements including FSFT are formulated for composite structures.

The Weibull shape parameter provides a reasonable measure of the reproducibility of fatigue life. As shown in Fig. 17.3, large values for metals suggest lower variability as opposed to composites. To determine this parameter, tests need to be performed over the whole range of lay-ups and processes that will be used in manufacturing (e.g. Table 17.1). It follows that in planning FSFT, one needs to account for the fact that statistical parameters describing the residual strength and fatigue responses of composites are vastly different from those of equivalent metallic components.

Reference [10] describes FAA guidelines for full-scale testing of aerospace composite structures. The most important difference between FSFT of conventional metallic structures and that of composite airframes lies in the definition of the load spectrum to be applied during FSFT. Where testing on metallic airframes calls for very faithful reproduction of service load statistics, combined with clipping of extreme tensile loads, the testing of composite airframes is performed with the adjustment of both magnitude and frequency of individual load ranges in the spectrum. These are referred to, respectively, as load and life enhancement factors, and their use is explained schematically in Fig. 17.4.

The rationale behind such adjustment is that given the large scatter in fatigue test results of composites, the required duration of FSFT needs to be increased from two lifetimes (as in the case of metallic structures) to over twelve(!) in the case of composites, which would be impractical. To resolve this problem, guidelines for FSFT of composites call for an increase in the number of large load excursions in the spectrum, but without substantially also increasing their magnitude, since this could cause premature static failure modes, see Fig. 17.5. All the smaller load

Table 17.1 Sample of coupon-level test matrix to be performed on composites in order to characterize the Weibull shape parameter [10]

Laminate	Test method	Loading condition	Standard	Static test environment		Room temp. ambient at three stress levels and at R-ratios:				
				Room temp. ambient	Hot wet	-0.2	0	-1	5	
10/80/10 Laminate	Open hole	Tension	ASTM D 5766	6	6	18	18			18
		Compression	ASTM D 6484	6	6			18		
	Single lap shear, $t = 0.01''$	Adhesive in-plane shear	Modified ASTM D 3165	6	6					
		Single lap shear, $t = 0.06''$		6	6					
Sandwich	Double notched compression	Interlaminar shear	Modified ASTM D 3846	6	6	18	18			18
		Flexure	Modified ASTM C 393	6	6		18			

Numbers indicate repeat test requirements. The results of such testing at coupon- and component-level appear as in Fig. 17.3 and influence the design of FSFT for composite and hybrid airframes

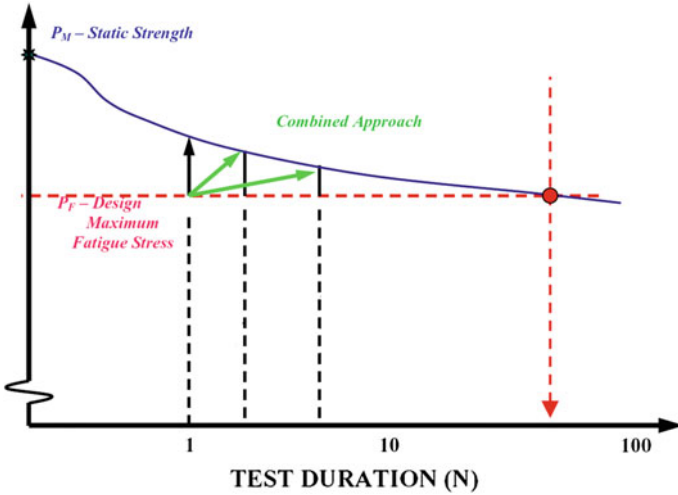


Fig. 17.4 For a given design lifetime the required duration of FSFT will increase with decreasing Weibull shape parameter. It may be reduced through load spectrum enhancement [10]. A judicious approach helps keep the test duration manageable without inadvertently distorting failure mechanisms. The latter problem is particularly critical for hybrid airframes that contain a combination of load-carrying metallic and composite subassemblies

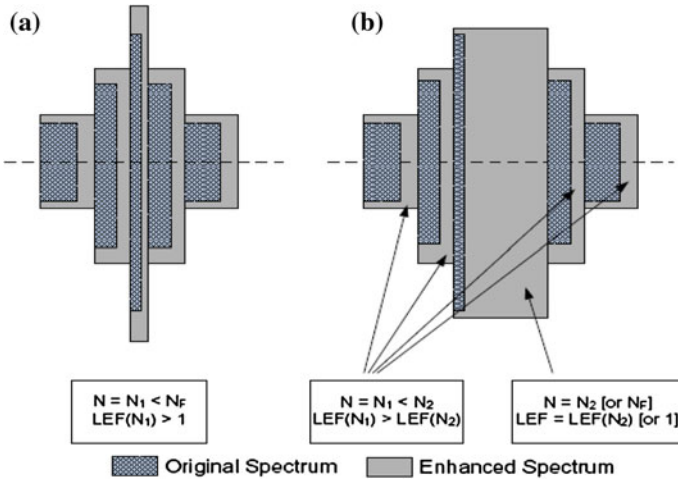


Fig. 17.5 Schematic of FSFT load spectra modified using the approaches described in Fig. 17.4. Option (a) may be suitable for small all-composite airframes that need to be evaluated without fear of failure mechanism distortion. Option (b) is better suited for FSFT on metal-composite hybrid structures such as most large new transports, including the Boeing 787 and Airbus A350 civil airliners as well as military airframes

Table 17.2 Contemporary FSFT programmes are called upon to ensure airworthiness and safety in the light of five different categories of potential damage to the airframe [10]

Category	Examples	Safety considerations (substantiation, management)
<i>Category 1: damage that may go undetected by field inspection methods(or allowable defects)</i>	BVID, minor environmental degradation, scratches, gouges, allowable mfg. defects	Demonstrate reliable service life Retain ultimate load capability Design-driven safety
<i>Category 2: damage detected by field inspection methods at specified intervals (repair scenario)</i>	VID (ranging small to large), mfg. defects/mistakes, major environmental degradation	Demonstrate reliable inspection Retain limit load capability Design, maintenance, mfg.
<i>Category 3: obvious damage detected within a few flights by operations focal (repair scenario)</i>	Damage obvious to operations in a “walk-around” inspection or due to loss of form/fit/function	Demonstrate quick detection Retain limit load capability Design, maintenance, operations
<i>Category 4: discrete source damage known by pilot to limit flight maneuvers (repair scenario)</i>	Damage in flight from events that are obvious to pilot (rotor burst, bird strike, lightning)	Defined discrete-source events Retain “Get Home” capability Design, operations, maintenance
<i>Category 5: severe damage created by anomalous ground or flight events (repair scenario)</i>	Damage occurring due to rare service events or to an extent beyond that considered in design	Requires new substantiation Require operations awareness for safety (immediate reporting)

The FSFT is suitably designed to address each listed category of damage. BVID = Barely Visible Impact Damage; VID = Visible Impact Damage

excursions are enhanced in terms of both magnitude and frequency of occurrence. This leads to a marginal increase in the duration of the FSFT, but in probabilistic terms satisfies the same requirements of design lifetime validation as in the case of metallic structures.

Retention of the magnitude of larger load cycles is an important feature of the manner in which the load spectrum is modified for use in FSFT of hybrid airframes with both composite and metallic parts. Changes in the magnitude of smaller load ranges are unlikely to influence the failure mechanisms of metallic components in the airframe. However, the fatigue test results for these components are likely to be conservative.

Unlike glass fibre-reinforced plastics, damage in CFRP is barely visible because the material is opaque and interlaminar separation can occur deep within the component. Such defects may be present from the time of manufacture and also may be randomly introduced at anytime in service due to impact of tools or equipment. This possibility is taken into account by deliberately inducing barely visible impact damage (BVID) in random impact-prone areas such as the wing upper surface and fairings, prior to commencement of FSFT. By definition, being barely visible, such defects cannot be allowed to propagate to failure during the entire duration of the test. At the very least, once detected during routine ultrasonic C-scan NDI, such defects should not register noticeable growth between two inspection periods, so as to validate the inspection procedure and schedule prescribed for the aircraft.

ASIP guidelines for full-scale testing to qualify a composite airframe for withstanding five different categories of damage severity are listed in Table 17.2. The extension of ASIP requirements to composite airframes to address the validation of safe operation between inspections requires demonstration of no growth of specially induced visible impact damage (VID) over two inspection periods of FSFT under the modified load spectrum previously mentioned.

Under controlled impact velocity, the so-called VID is induced on safety-critical structural subassemblies prior to such testing. The impact energies associated with VID are substantially greater than those associated with BVID. As in the case of metallic airframes, where cracks are deliberately cut into the structure after the main two-lifetime testing is complete, in composite structures VID can be induced subsequent to the FSFT and then testing continued over two inspection periods to confirm no growth conditions.

The requirements for residual strength of damaged composite structures are typically demonstrated after FSFT of the entire structure, as well as on major subassemblies as required.

The use of composites in safety-critical load-carrying elements of airframes is steadily increasing. Their application extends across all types of aircraft, with the Boeing 787 and Airbus A350 projects intended to serve as examples of composite structures designed for widespread and long-term operation much like any other older examples such as the Boeing 747. It would appear that procedures for certification of composite airframes including FSFT represent the state-of-the-art.

17.3 Organization of FSFT

A full-scale fatigue test is an extremely expensive and time-consuming part of aircraft development [13]. Today's total cost for full-scale testing of a 150-seater transport aircraft may add up to about US\$50 million with about 60 % of the cost due to the test article itself, 30 % for the rig, and 10 % for the testing. In the world of experimental testing it is extremely rare for a test article to cost much more than the system required to test it. Nevertheless, this exceptionally high cost is still

negligible by comparison with the value of full-scale testing in terms of ensuring safe operation of an entire fleet over its entire life cycle.

Given the high cost of the test article, the extended duration of the test, and the virtual unacceptability of inexplicable failure of the test article, the requirements for the test system are also exceptionally high by comparison with conventional specimen or component testing. Many of these requirements are listed below:

Load Distribution An airframe may be extremely stiff and strong, but is not designed to offer much resistance to concentrated forces, particularly on the wing. The pressure exerted on the wing surface to lift a transport aircraft is about 5 % of ground atmospheric pressure, or of the order of 500 kg/m^2 of wing surface area.

It would be impossible to exactly reproduce such a load distribution across an airframe under laboratory conditions. Loads are typically applied using innumerable pads adhesively bonded to the wing surface and transferred through whiffletrees leading up from a group of points to a single resultant, and all computed to retain the required load distribution (see Fig. 17.6).

As many as 500 such “hard points” may be required for a fighter aircraft and several thousand for a transport airliner. Given the nature of damage concerns about composites, it may be desirable to leave the upper surfaces of composite wings as “clean” as possible and transfer loads largely through pads bonded to the lower

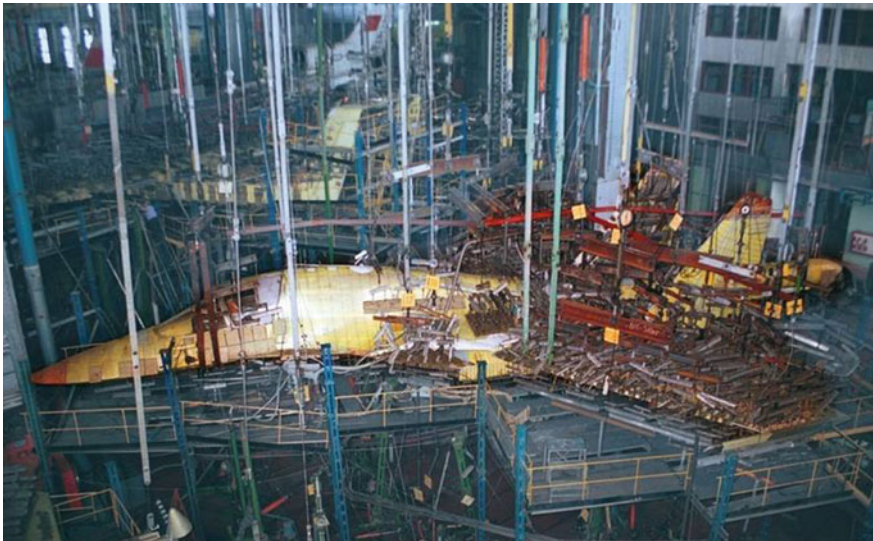


Fig. 17.6 Full-scale fatigue test on a combat aircraft at the Siberian Aircraft Research Institute. The $10,000 \text{ m}^2$ hangar with load-carrying roof, load-carrying floor, and load-carrying columns permits bidirectional loading through actuators positioned appropriately. Innumerable loading points can be seen on the wing surface by way of adhesively bonded straps. These are connected through whiffletree arrangements leading to actuators at top and bottom

surfaces. This would permit ease of periodic NDI of the upper wing surface, in particular those areas that may have been subjected to BVID.

Load Redistribution Stresses on the airframe are sensitive to load distribution across the wing surface. Identical lift in low-speed subsonic flight will be far less damaging than the same lift at higher speed. This is because the centre of pressure tends to move outwards with increasing speed, increasing the bending moment and therefore the stresses in the wing root region.

To make it possible to correctly simulate load redistribution, multiple actuators are used, and the wing area covered by each is suitably chosen to ensure the lowest possible distortion of actual load distribution when switching from one mission configuration to another. With military aircraft it is also essential to reproduce the variations in forces associated with the discharge of stores, firing of missiles, and engagement of air brakes. Testing of variable wing geometry aircraft demands the continued application of aerodynamic loads with variation in wing geometry.

Load axis Reorientation In full-scale tests of transport airliners, take-off and particularly landing loads need to be applied with the appropriate extended positions of leading and trailing edge deployments. These components change their angular orientation with extension, causing the load vector also to rotate. Simulation of this feature demands the loading arrangement also to be mounted on a moving reaction point in order to ensure the required angular reorientation with deployment.

N.B: Since tests are performed on a flight-by-flight basis, the operation of the moving components is simulated appropriately synchronized with the associated load cycles.

Structural Deflections A large wingspan can give noticeable deflections, particularly in the case of large transport aircraft. Thus the Boeing 747 wingtips can deflect over a range of 4 m (4000 mm) under cyclic loading. Obviously, the servo-actuators applying the required forces on the wing must be capable of sustaining very large displacements. This can be achieved using (i) telescopic actuators or (ii) wire ropes guided through pulleys, to take advantage of the leveraging action of a pulley that results in halving its own displacement by comparison with the load point.

A wide variety of solutions is available today to apply forces. The most popular are servo-hydraulic actuators, and in addition to these, today one can find applications of servo-electric drives.

Synchronized Loading and “Crosstalk” A full-scale fatigue test involves continuous synchronized load variation across all the load channels to simulate the specified flight-by-flight load distribution and sequence. State-of-the-art control hardware and software enable highly synchronized digital control waveform generation and data acquisition across hundreds, even thousands, of channels. And they can do so with an update of several thousand times a second. Real-time algorithms

for servo-control use these data to ensure the required degree of synchronous variation in loads across all the load channels.

There are, however, severe limits to the capability of such control, given the nature of structural response to multichannel loading that is associated with a so-called “statically indeterminate” system. The deflection at individual points on an airframe with change in applied load determines its stiffness as perceived by the control system. In linear elastic situations this stiffness may be deemed to be a constant that forms part of the servo-control algorithm and determines the “servo-gain” on individual channels of the test system. However, a load frame connected to multiple loading and anchor points represents a statically indeterminate system, wherein load response at individual points at a given instant of time will be determined by induced deflections and local instantaneous stiffness. Thus even if the airframe may behave as a linear elastic structure, a change in load at any point on the airframe can induce a deflection at (all) other locations on the frame: and it does so even if the set load at those points did not change!

If the loading actuators were to be extremely elastic (flexible), they would, being in load control, readily adapt to any deflection induced by loading at other points. However, loading actuators are designed to be extremely stiff, and this can cause extreme fluctuations in load due to structural response. This shows up as “cross-talk” because loading on one channel begins to induce “unintended” loads on other channels and they begin to correct the error and thereby induce further cross-talk. In the event that cross-talk induced load oscillations are of the same order as one of the natural frequency modes of the structure itself, the consequences can be even worse. State-of-the-art control systems include algorithms to account for “instantaneous stiffness” of individual channels, but even so, there seem to be limits to their capability.

As a consequence, full-scale airframe testing for fatigue proceeds at a very low rate of load variation by comparison with what is achievable on conventional test systems. This is to ensure that loading error on individual channels remains within acceptable limits. The average test frequency in airframe FSFT can be as low as 0.05 Hz. One may note that the problem of cross-talk between individual actuators is practically non-existent in FSFT of ground transportation vehicles. In those cases, ground excitation is the primary source of loading. This is simulated by reproducing displacement time history on the four wheels. Even if ground vehicle dynamics is rendered very complex by the nonlinear and rate-dependent elements introduced by vehicle suspension, the testing requirement itself is simpler because Stroke, rather than Load Control, is involved. And, unlike Load Control, Stroke Control is practically immune to cross-talk.

Cabin Pressurization Cycle This is an essential constituent of FSFT. Given the elastic energy stored, cabin pressurization can lead to uncontained explosive fracture. In fact, it was this concern that determined that the additional FSFT (in 1954) on the De Havilland Comet was done in a water tank. Contemporary practice is to fill as much of the enclosed space in the cabin as possible with “Styrofoam” in order

to reduce the net volume of pressurized air. This also aids quicker pressurization and depressurization between flights.

Air compressors used to impose the required pressurization can deliver pressures enough to cause failure in the event of runaway pressure build-up. Given the potential consequences of such a catastrophe, an extremely simple and reliable system of protection is required. A common practice is to attach an open-ended piping arrangement to the cabin with enough internal water column height to match the maximum pressure likely to be generated in the cabin. Thus, in the unlikely event of runaway pressurization, this water column “hydraulic fuse” is expelled, leading to immediate restoration of atmospheric pressure within the cabin as a guarantee against overload by cabin pressure.

Hardwired Protection Service manifolds on state-of-the-art hydraulic actuators used in FSFT are equipped with mechanically presettable bypass valves for which the highest tensile and compressive loads permissible on the given channel can be independently set. These direction-sensitive hydraulic circuits ensure that the preset load values effectively determine the stall load independently in tension and compression, irrespective of the line pressure and control status. This serves as a fallback option to cater to the extreme possibility of control system or hydraulics malfunction.

Dual-Bridge Load Cells As a rule, all FSFT load cells are of dual-bridge design, i.e. the sensitive element is instrumented with two strain bridges and provides two independent read outs. These two read outs are continuously compared during real-time data acquisition over the entire duration of the FSFT. Should unacceptable deviations be noticed, the test is interrupted and the test specimen unloaded in order to trace and rectify the root cause of the deviation. This scheme serves as a protection against the consequences of malfunction at any stage of movement of the load signal.

Reaction Points Up to six anchor points with load cells are provided to hold the airframe down as it is loaded along all three axes during the FSFT. A pair of anchor points along each axis ensures the measurement of the reaction forces as well as the moment on the frame by solving the equations that balance the sum of all forces and all moments acting on the airframe. An inability to balance forces and moments within an acceptable margin of error also serves as an indication that one or more load cells may be providing misleading read outs or that an unanticipated load transfer is taking place at a location or in a direction that single-axis load cells may be incapable of detecting.

Each loading point on the airframe and each anchor point need to be carefully designed to ensure it exerts force only along the designated axis such that there is no undue force transfer anywhere in the entire system, at any time, and under any loading action. This needs to be confirmed over the entire displacement envelope of the test article.

Structural Response During the entire course of the FSFT the read outs are continuously logged as set points on all the control channels (including cabin pressure), each with its own force and displacement feedback: force feedback from anchor points, and displacement feedback from critical points on the frame, including the extremities.

In addition, read outs are collected from hundreds, even thousands, of strain gauges bonded all over the airframe. Apart from constituting formal test records, these data provide inputs to continuous monitoring of the quality of the test as well as airframe structural response that may reveal the need for (i) fine-tuning the test process for improved quality or (ii) test interruption to investigate the abnormal read outs that might be an indication of damage or malfunction.

Non-contact Measurements An emerging technology that is rapidly transforming the process of displacement and strain measurement in FSFT is non-contact measurements via laser interferometry and digital image correlation (DIC). By positioning high-resolution cameras at different vantage points around the airframe, continuous tracking of deflections becomes possible at all points on a virtual “wireframe” of the test specimen. These can thereby be matched in real time with values computed from finite element method (FEM) analyses.

Real-time Simulation State-of-the-art FSFT test technology provides for simultaneous real-time simulation of structural response, whereby a digital model of the entire test rig operates in real time with the ongoing test, including the airframe and all the loading arrangements, as well as strain sensors attached to the airframe. Continuous improvements in FEM modelling and simulation technology now make it possible also to simulate airframe structural response in the presence of damage such as cracks and delamination of composites.

Thus a state-of-the-art FSFT control room contains a network of computer systems, some involved with the test itself, others analysing collected data, and yet others comparing measured inputs with simulated results. Together these systems provide a holistic environment for efficient conduct of an FSFT, including timely detection of abnormal behaviour of the test article. The latter is an extremely valuable element of an FSFT programme because it enables the possibility of detecting damage before it can assume critical proportions, and can provide for (i) tracking crack growth as a measure of verifying assigned inspection intervals and (ii) timely repairs and design reinforcements as necessary, and, of course, their validation during continued testing.

17.4 Summary

The very nature of metal and composite fatigue makes FSFT an essential and integral part of the aircraft development and certification process. The state-of-the-art FSFT involves integration of the latest digital control techniques and

a variety of drives, primarily servo-hydraulics, along with a vast collection of electronics, transducers, and protection schemes. These ensure that an airframe undergoing testing under laboratory conditions experiences flight-by-flight loading conditions that closely simulate the actual expected usage.

The goal of FSFT is to confirm that the airframe can safely perform its designated functions over its entire design lifetime. The goal of the FSFT programme is also to confirm that the airframe can safely operate up to the next scheduled inspection even in the presence of damage that may have gone undetected during routine in-service inspections.

Special considerations govern FSFT when composites and hybrid structures are tested, with due attention paid to the statistics of fatigue processes in the different materials used on the airframe, as well as to the differences in the nature of damage that may be inadvertently induced in the course of usage.

Additional information about FSFT and about CFRPs is given in Chap. 16 of this volume and Chap. 14 of Volume 1, respectively.

References

1. Wöhler A (1870) Über die Festigkeitsversuche mit Eisen und Stahl. *Zeitschrift für Bauwesen* 20:73–106
2. Bauschinger J (1886) On the change of the elastic limit and strength of iron and steel by tension and compression, by heating and cooling and by frequently repeated loading. Technical Report, Munich Technical University, Munich, Germany (in German)
3. Miner MA (1945) Cumulative damage in fatigue. *Trans ASME J Appl Mech* 12:A159–A164
4. Gassner E (1939) Strength experiments under cyclic loading in aircraft structures. *Luftwissen* 6:61–64 (in German)
5. Hewitt RL (1985) A history of full-scale testing of aircraft structures at the National Aeronautical Establishment. Aeronautical Note NAE-AN-24, NRC No 24089, National Research Council, Ottawa, Canada
6. Cox WJ (1943) Drop test of Cornell aircraft. Report MM-141, National Research Council of Canada, Ottawa
7. Marsh KJ (ed) (1988) Full-scale fatigue testing of components and structures. Butterworth, Cambridge, UK, p 4
8. Aircraft Structural Integrity Program (2002) Department of Defence Handbook MIL-HDBK-1530A(USAF), Washington, DC, USA
9. Lincoln JW (1985) Risk assessment of an aging military aircraft. *J Aircr* 22(8):687–691
10. Determining the Fatigue Life of Composite Aircraft Structures Using Life and Load-Enhancement Factors (2011) Report DOT/FAA/AR-106, National Technical Information Services, Springfield, VA, USA
11. Whitehead RS, Kan HP, Cordero R, Saether ES (1986) Certification testing methodology for composite structures. Report No. NADC-87042-60, Volumes I and II
12. Sendekyj GP (1981) Fitting models to composite materials fatigue data. In Chamis CC (ed) Test methods and design allowables for fibrous composites, ASTM STP 734, American Society for Testing and Materials, Philadelphia, USA, pp 245–260
13. Swanson SR (1974) Handbook of fatigue testing. ASTM Special Technical Publication, ASTM STP 566, American Society for Testing and Materials, Philadelphia, USA

Chapter 18

Residual Strength Requirements for Aircraft Structures

R.J.H. Wanhill

Abstract This chapter is an adjunct to Chap. 16. The present chapter first summarizes the evolution of residual strength design requirements for metallic aircraft structures. There follows a concise discussion of the methods for assessing the residual strengths of aircraft structures, with the emphasis on testing and data requirements.

Keywords Residual strength · Metallic structures · Requirements · Methods · Damage tolerance · Widespread fatigue damage

Nomenclature

AA	Aluminum Association
ASTM	American Society for Testing and Materials
DEF STAN	Defence Standard
DLL	Design limit load
DSG	Design service goal
DT	Damage tolerance
DUL	Design ultimate load
FAA	Federal Aviation Administration
FAR	Federal Airworthiness Regulation
FCG	Fatigue crack growth
FSFT	Full-scale fatigue test(ing)
LEFM	Linear elastic fracture mechanics
L.H.	Left hand
LL	Limit load
LOV	Limit of validity
MED	Multiple element damage
MSD	Multiple site fatigue damage
RAAF	Royal Australian Air Force

R.J.H. Wanhill (✉)
NLR, Emmeloord, The Netherlands
e-mail: rjhwanhill@gmail.com

RCAF	Royal Canadian Air Force
R.H.	Right hand
RNAS	Royal Naval Air Service
RS	Residual strength
SCG	Slow crack growth
UL	Ultimate load
USAF	United States Air Force
WFD	Widespread fatigue damage

18.1 Introduction

As discussed in Chap. 16 of Volume 2 of these Source Books, aircraft structural integrity has been concerned largely with the service behaviour of high-strength metallic materials, particularly aluminium alloys. The emphasis has been on fatigue design and analysis, and their verification by testing.

More specifically, since the mid-1950s there have been developments in fail-safe and damage-tolerant design methods for both civil and military aircraft. These methods recognize that airframe structures must withstand service loads even when damaged or cracked. Safety should be ensured by fatigue and fracture testing and analysis of damaged structures, pre-service and in-service inspections, and eventual repairs, replacements or retirement.

Service failures have greatly influenced these developments. In particular, six case histories may be regarded as ‘milestones’ in the aerospace industry’s approach to structural integrity [1–5], not only with respect to fatigue, but also residual strength. These case histories are discussed primarily with respect to fatigue in Chap. 16. Four of these are also discussed in the next section for the reader’s convenience.

The four milestone case histories and two other cases (EH101 helicopters) are presented along a timeline in Fig. 18.1, and synopses of the cases are given in Sect. 18.2. There then follow surveys of the methods for assessing the residual strengths of aircraft structures. The test data requirements for such assessments are also specified.

18.2 Case Histories

18.2.1 *Civil Aircraft Milestone Accidents*

De Havilland Comets In January and April 1954, two Comets suffered pressure cabin disintegration resulting from fatigue. Investigation and follow-up gave a

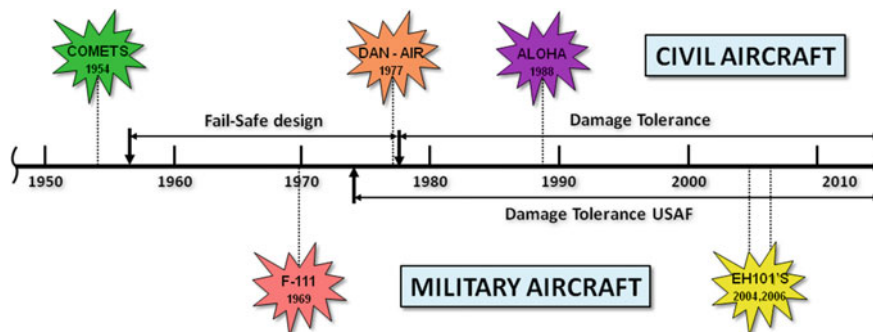


Fig. 18.1 Evolution of fatigue and fracture requirements influenced by *four* civil aircraft accidents and the F-111 military aircraft accident. Two additional accidents (EH101 helicopters) are included for discussion (see text)

general awareness of finite fatigue lives, the significance of fail-safety, and the usefulness of Full-Scale Fatigue Testing (FSFT).

Fail-safe design principles mean that major parts of the structure are (were) designed firstly to achieve a satisfactory fatigue life with no significant cracking. Secondly, the structure is (was) also designed to be inspectable in service and able to sustain significant and easily detectable damage before safety is compromised. These latter requirements were met mainly by structural design concepts having multiple load paths and *established* residual strength requirements in the event of complete or obvious partial failure of one structural element.

These fail-safe design principles were adopted in 1956, with some exceptions, notably landing gears, which are not amenable to fail-safe design. However, as yet there was no *requirement* for FSFT, although it has often been done since the Comet accidents. The requirement for FSFT became mandatory only in 1998, see the last paragraph about the ALOHA Boeing 737 accident.

DAN-AIR Boeing 707 In May 1977, a Boeing 707 freighter lost the R.H. horizontal stabilizer owing to fatigue in a *supposedly* fail-safe spar. There were several contributing factors:

- inadequate inspection for detecting *partial* failure of the spar upper chord
- inadequate residual strength after *complete* failure of the upper chord
- unanticipated high service loads
- stabilizer modification not checked by FSFT.

This accident prompted (i) reconsidering the problems of ageing aircraft: it became clear that some inspection methods and schedules were inadequate and required supplementary programmes; and (ii) the need for damage tolerance (DT), which replaced the fail-safe design principles in 1978.

In civil airworthiness terms, DT means that fatigue cracks will be detected before the safety is compromised, but unlike fail-safety there is no premise that cracking

will become obvious before it reduces the residual strength below the required safety level [6].

ALOHA Boeing 737 In April 1988, a Boeing 737 suffered explosive decompression with loss of part of the pressure cabin, subsequently landing safely. The physical manifestation of the accident was multiple site fatigue damage (MSD) along a critical rivet row of the upper skin lap splice. There were several contributing factors:

- skin splice design relied on cold-bonding as well as riveting
- bonds susceptible to corrosion and disbonding
- neglected inspections and repairs.

This accident led to recognition that widespread fatigue damage (WFD), of which MSD is one aspect, can cause loss of fail-safety. It also prompted more actions to ensure the safety of ageing aircraft and corrosion control programmes for both civil and military aircraft.

Other instances of WFD led eventually to mandatory FSFT from 1998 onwards, and in 2011 the Limit Of Validity (LOV) concept for aircraft above 34,000 kg. The LOV concept requires FSFT to determine the onset of WFD [7].

18.2.2 *Military Aircraft Accidents*

General Dynamics F-111 In December 1969 a General Dynamics F-111A lost the left wing after only 107 airframe flight hours and at less than half the design limit load (DLL). Failure occurred by fast fracture after a small amount of fatigue from a large manufacturing flaw in the lower plate of the L. H. wing pivot fitting. The plate was made from a high-strength steel with *limited* fracture toughness.

This failure and FSFT fatigue and fracture problems led to a fracture control programme for the F-111 critical steel components [8].

Furthermore, the F-111 problems and early fatigue cracking and WFD in Lockheed C-5A wing boxes [9] resulted in the USAF introducing *their* DT approach in 1974–1975 [10, 11]. This preceded the civil aircraft DT requirements by 3–4 years, see Fig. 18.1. There are some differences: one basic difference is that the USAF DT approach required *that initial flaws or cracks should be assumed to be present in new structures*. See Sect. 18.4.2 also.

AgustaWestland EH101s In March 2004 a Royal Naval Air Service (RNAS) AgustaWestland Merlin helicopter crashed just after take-off. The crash was actually a hard landing from a height of about 4–5 m and was caused by a tail rotor malfunction and loss of control.

In January 2006 a similar type of helicopter, a Royal Canadian Air Force (RCAF) Cormorant, crashed into the sea in a nose-low attitude at 69 knots. This crash was subsequently attributed to pilot error.



Fig. 18.2 Disintegration of the Merlin helicopter owing to a fall from 4–5 m [12]

Although neither accident was caused by material or design deficiencies, the damage to the airframes appeared to be (much) more severe than might be expected. For example, Fig. 18.2 shows disintegration of the Merlin [12].

Investigation revealed that major components of the airframes failed by low-energy fracture. These components had been manufactured from a second generation aluminium–lithium (Al–Li) alloy, AA8090, known to be susceptible to low fracture toughness [13]. Furthermore, this low toughness might have been caused or exacerbated by low temperature secondary ageing *during* service [14, 15].

Remedial actions for in-service helicopters are limited: local reinforcements have been used [15]. For new helicopters the Al–Li alloy could be (or has been) replaced by conventional aluminium alloys.

18.3 Residual Strength Definitions

The residual strength limit load (LL) and ultimate load (UL) definitions for airframe structures apply to all possible types of *external* flight and ground loads on the structure. In the first instance these definitions appear to be fairly straightforward:

Limit Load (LL) maximum load to be expected in service.

Ultimate Load (UL) LL multiplied by a historically-based safety factor, $LL \times 1.5$ [16].

However, the 1.5 safety factor is not necessarily ‘hard and fast’. For example:

1. FAR Part 25.303 [17] states ‘*Unless otherwise specified, [author’s emphasis] a factor of safety of 1.5 must be applied to the prescribed limit loads which are considered external loads on the structure.*’ On the other hand, it seems unlikely that this requirement will be relaxed, since there have been cases of commercial

aircraft encountering severe weather and breaking up in mid-air after exceeding LL conditions [16]. (See also the discussion on the Airbus A380 wing test failure [18].)

2. For tactical aircraft the Royal Australian Air Force (RAAF) has an *FSFT* residual strength (RS) requirement of 80 % $UL = 1.2 \times DLL$ without failure [19]. (This specification is derived from the U.K. Ministry of Defence DEF STAN 00-970, which is continually updated.)
DEF STAN 00-970 also states that *calculation* of residual strength should be based on sustaining 80 % design ultimate load (DUL). There is also a requirement for teardown of the test article.
3. To save mass on the Eurofighter 2000 the UL requirement was relaxed to $1.4 \times LL$ for areas of the structure where the loads were controlled by an aircraft system [20].

Thus the $UL = 1.5 LL$ criterion may be relaxed under certain circumstances, notably for tactical aircraft.

N.B The safety factor covers inadvertent service flight and ground loads greater than DLL, structural deflections above LL that could compromise structural integrity, and as-built part thicknesses within tolerance but less than those assumed in the stress analyses. However, the safety factor *does not* cover [16]:

- analysis or modelling errors
- poor design practice
- material property variations
- process escapes (e.g. different materials used than those specified, improperly drilled holes, etc.).

Also, other supplemental safety factors apply to other components, e.g. pressurised lines, fittings and alloy castings (casting factors).

18.4 Residual Strength Methods for Metallic Airframe Structures

As mentioned in Sect. 18.2.1, fail-safe design principles were replaced by DT, which was introduced in 1978 for civil aircraft and a few years earlier for USAF aircraft. Also, WFD in civil transport aircraft led to *mandatory* FSFT (1998) and the LOV concept (2011), which requires FSFT to determine the onset of WFD [7].

The USAF has followed a similar evolutionary path in its DT approach. Thus MIL-STD-1530C [21], which predates the LOV concept, suggests that FSFT be extended beyond 2 design service goals (DSGs) because WFD does not always begin within a two-lifetime test [4].

These changes have been reflected in the residual strength analysis and test methods discussed in Sects. 18.4.1–18.4.3.

18.4.1 Civil Aircraft Fail-Safe Design (1956–1978)

In the civil aircraft fail-safe design period, compliance with the requirements was *relatively* straightforward. Linear elastic fracture mechanics (LEFM) analyses were used to determine whether structural designs with crack arrest features could sustain fast fracture propagating from a single crack. The supporting testing was typically at the coupon and component levels [6], but FSFT was also done on pressurized fuselage sections [22]. Cracking was simulated by artificial damage [6, 22].

Figure 18.3 illustrates the two most important residual strength tests for the Douglas DC-10 pressure cabin [22]. These tests were done with large curved panels in a special test rig. It is important to note that although the ‘crack’ configuration is simple, the panels were not, since they were built-up structures. As an example, a detail of the panel 1 construction is shown in Fig. 18.4.

Analyses of built-up structures are often complex. The most important factor is to decide whether the structure is skin-critical (short crack) or stiffener-critical (long crack), although no clear distinction is possible [23]. It is therefore good practice to

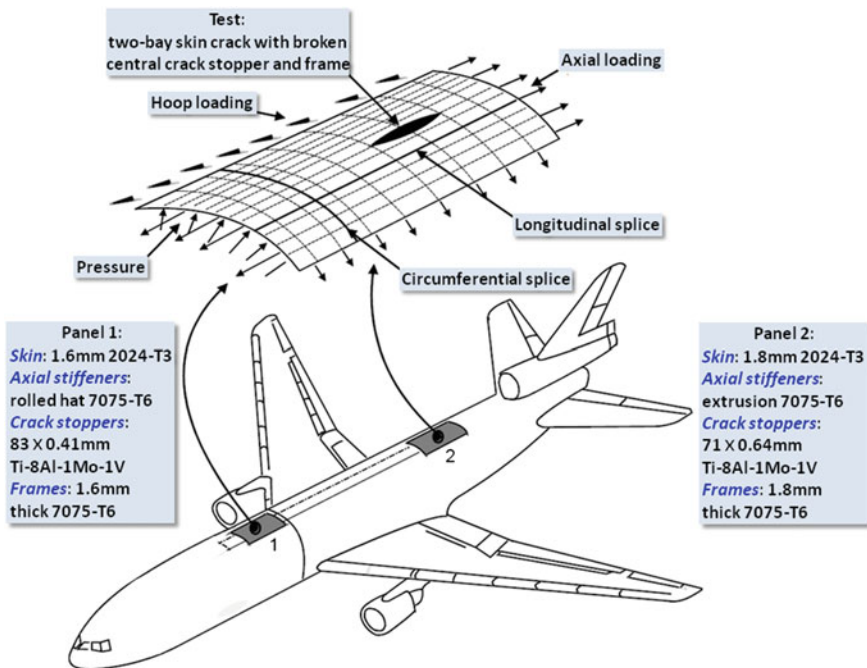
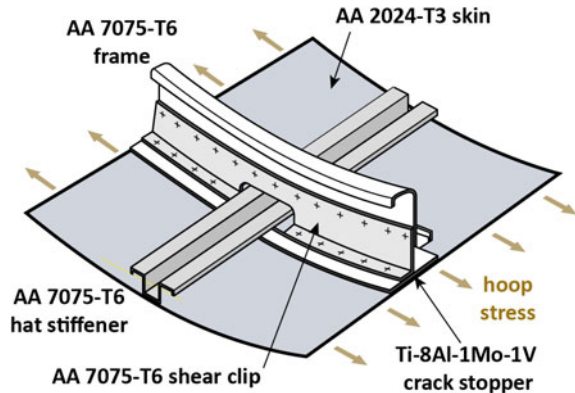


Fig. 18.3 Panel locations for the Douglas DC-10 fuselage fail-safety tests. The tests were done using a curved-panel vacuum fatigue test machine [22]. The tests were designed to demonstrate the two-bay fail-safe crack criterion, whereby the crack is confined (arrested) within the two bays under limit load (LL) conditions

Fig. 18.4 Detail of panel 1 from Fig. 18.3



predict the residual strength based on both skin-critical and stiffener-critical cases. The minimum value should be the governing case [23].

The analysis complexity is due to many factors, including the panel geometry, stiffener type and spacing, attachments (frames and crack stoppers in fuselages; ribs, spar caps and webs in wings), joining methods (mechanical fastening vs. adhesive bonding in the fail-safe design period), fastener flexibility and eccentricity.

In this time period (1956–1978) several LEFM-based computational methods have been developed for fail-safe analysis of built-up structures [23]. Plasticity effects are also incorporated in some methods and have been shown to be necessary [23, 24].

Input fracture mechanics property data for the analyses include fracture toughness (K_{app} , K_c) and crack growth resistance (K_R , J_R) curves. For more details the reader may in the first instance consult Miedler et al. [23], who discuss these methods and provide illustrations of their use. With regard to testing procedures, ASTM International is an appropriate source for standard fracture mechanics tests.



Besides fracture mechanics data, the analyses also require standard mechanical properties of all the materials used, including fastener tensile and shear properties for mechanically fastened structures.

18.4.2 Damage Tolerance Design in the 1970s

The USAF's introduction of DT in 1974–1975 and the civil airworthiness transition from fail-safe to DT principles in 1978 brought about major changes. For civil transport aircraft it was no longer sufficient to design structures to be fail-safe on the basis of obvious cracking, and for USAF aircraft safe-life fatigue design was retained only when necessary, as in the case of landing gears.

The major changes are summarized in Table 18.1. In more detail, these changes are [6]:

Table 18.1 Comparison of fail-safe and damage tolerance design requirements: after [6, 10, 11, 25]

Category	Basic schematics	Design attributes	Substantiation requirements
Civil fail-safe (pre-1978)		<ul style="list-style-type: none"> • Obvious failure or partial failure with continued structural integrity 	<ul style="list-style-type: none"> • Residual strength analyses • Static testing of artificially damaged structure
Civil and USAF damage tolerance		<ul style="list-style-type: none"> • Damage detection by planned inspections • Inspection programmes matched to structural characteristics 	<ul style="list-style-type: none"> • Residual strength and fatigue crack growth (FCG) analyses • Testing to establish basic LEFM-based properties, notably FCG • Inspection programmes

- all fatigue-sensitive areas needing inspection must be properly identified
- the most likely fatigue-cracking scenario(s) for each area must be established
- LEFM-based testing must be done to establish the required properties for FCG and residual strength analyses
- FCG and residual strength must be accurately determined (via extensive analyses covering the cracking scenarios [25])
- inspection methods and capabilities must be well understood, and the requirements must be specified for inspection programmes matched to the structural characteristics.

N.B Besides test data for the plane-stress fracture toughness parameters K_{app} and K_c , the DT approach also requires plane-strain fracture toughness (K_{Ic}) data for DT-cracking scenarios where FCG occurs in thicker-section components.

The two DT approaches have much in common, although as mentioned in Sect. 17.2.2 there are some differences. The main differences are shown in Table 18.2. Civil aviation authorities do not accept non-inspectable structures as damage tolerant [26]. Nor was the starting point for fatigue analysis based on fatigue crack growth (FCG). This changed in 1998 for WFD, see Sect. 18.4.3.

Table 18.2 Comparison of main differences between the civil and USAF damage tolerance approaches introduced in the 1970s

Civil transport damage tolerance (1978)	USAF damage tolerance (1974–1975)
<ul style="list-style-type: none"> • Initial in-service inspection based on safe-life fatigue analysis of ‘defect-free’ new structures • <i>Inspectable structures</i>: <ul style="list-style-type: none"> – DT fail-safety via multiple load paths or crack arrest • <i>Non-inspectable structures</i>: safe-life category only (i.e. not damage tolerant) 	<ul style="list-style-type: none"> • Initial flaws or cracks assumed present in new structures: fatigue crack growth (FCG) immediately from initial damage • <i>Inspectable structures</i>: fail-safety or slow crack growth (SCG): <ul style="list-style-type: none"> – DT fail-safety via multiple load paths or crack arrest. – DT SCG requires initial damage not to reach a critical size within 2 inspection periods • <i>Non-inspectable structures</i>: DT SCG requires initial damage not to reach a critical size within 2 design service lives

18.4.3 Widespread Fatigue Damage (WFD)

Definitions and Occurrence The term WFD came into general use following the ALOHA accident. The Federal Aviation Administration (FAA) defines WFD as follows [27]:

The simultaneous presence of cracks at multiple structural locations that are of sufficient size and density such that the structure will no longer meet the residual-strength requirements of §25.571(b).

(§25.571(b) is from the FAA Code of Federal Regulations on DT and fatigue of transport aircraft structures.)

Examples of WFD are illustrated in Table 18.3. There are two categories:

- multiple site damage (MSD), characterized by the simultaneous presence of cracks in the same structural elements
- multiple element damage (MED), characterized by the simultaneous presence of cracks in similar adjacent structural elements.

Table 18.3 also shows that there are numerous structural locations considered or found to be susceptible to WFD [4, 25]. These include the fuselage and wings.

The WFD Problem The DT approaches introduced in the 1970s relied mainly on safety-by-inspection [6], see Table 18.2. However, owing to the ALOHA accident and other instances of WFD-induced failures in both civil [6] and military [4] aircraft, it became evident that reliance on inspections to detect WFD before it compromised safety was problematic. This problem led the FAA to amend the fatigue requirements for civil aircraft in 1998 [28]. The most significant change was the following requirement:

It must be demonstrated with sufficient full-scale fatigue test evidence that widespread fatigue damage will not occur within the design service goal of the airplane

Table 18.3 Widespread fatigue damage (WFD) categories and structural characteristics

WFD categories and basic schematics	Structural characteristics
<p>The figure contains two schematic diagrams. The top diagram, labeled 'Multiple Site Damage (MSD)', shows a horizontal line representing a skin surface with six vertical U-shaped details. Each detail has a crack. A double-headed arrow below the line indicates the 'maximum allowable skin damage' region, which encompasses all six details. The bottom diagram, labeled 'Multiple Element Damage (MED)', shows a horizontal line with six vertical U-shaped details. Each detail has a crack. A double-headed arrow below the line indicates the 'maximum allowable damage' region, which encompasses all six details.</p>	<ul style="list-style-type: none"> • Similar details and stresses • Structural interactions with reduced allowable damage <p><i>Examples</i> [4, 25]</p> <ul style="list-style-type: none"> • Fuselage skin joints, frames, stringers, tear straps • Stringer to frame attachments • Pressure dome outer ring and web splices • Pressure bulkhead attachments to skin • Centre wing boxes • Wing panels and spanwise splices

This requirement added significantly to the DT certification requirements, since FSFT had not been mandatory (though often done, but not to determine the onset of WFD). The requirement was unilaterally issued by the FAA, and there followed much discussion between various authorities [6].

Since 2011, there is a new civil aircraft requirement, the LOV concept, which mandates FSFT to determine the onset of WFD [7]. Also, safety-by-inspection is no longer allowed for WFD-susceptible areas. Instead the primary strategy is to design and maintain aircraft to minimise the probability of cracking during the service life [6].

An established LOV can be extended (and even re-extended). This requires additional testing, FCG analyses and the use of service experience to determine the inspection and maintenance actions needed to prevent WFD before each extended LOV [6]. But eventually, the inspection and maintenance burdens will become intolerable [4], since without them WFD is inevitable in susceptible structures [6].

As mentioned earlier, the USAF has followed a similar evolutionary path in dealing with WFD. A military standard issued in 2005 [21] suggests extending FSFT beyond 2 DSGs because the onset of WFD does not always occur within a two-lifetime test period [4]. Also, Tiffany et al. [4] recommend teardown inspections of FSFT articles and high time/usage aircraft to aid validation of FCG analyses based on crack growth from initial discontinuities. More information on this aspect is given in Sect. 16.4.2 in Chap. 16 and the literature quoted therein.

Countering WFD The WFD problem is part of the overall DT design process discussed in Sect. 18.4.2. In other words, that process must be gone through, but

with the additional requirement [28] or suggestion [21] that FSFTs be done to determine WFD thresholds in susceptible structures.

18.5 Helicopters: A Short Note

Helicopters present a unique challenge to aircraft structural design. The weight is at a premium owing to the vertical lift requirement, and the main rotor + blade assembly is a source of high frequency vibratory loading that is experienced by major parts of the airframe in addition to low frequency manoeuvre loads.

Helicopter metallic structures are still designed using the traditional safe-life fatigue approach. Although this has important disadvantages (see for example Chap. 16, Sect. 16.4.1), it is capable of substantiating helicopter component fatigue lives equivalent to thousands of flight hours. In particular, the potential for rapidly accumulating damage due to vibratory loading is nullified by using well-established scatter factors to derive S-N working curves and then obtain safe lives from cumulative damage calculations of fatigue lives, again applying scatter factors.

There is (as yet) no consensus on the feasibility of introducing DT design for helicopters. To be successful, DT would have to offer similar or better service life capabilities. Even protagonists admit that the transition from safe-life to DT design will not be easy [29].

On the other hand, situations like those illustrated by the EH101 crashes discussed in Sect. 18.2.2 should not occur when fracture mechanics properties are thoroughly and accurately evaluated, even if only as material screening parameters.

Lastly, there are also developments in operational damage monitoring (Chap. 16, Sect. 16.4.3) that require LEFM-based FCG tests and fracture toughness or residual strength testing.

18.6 Summary

The residual strength requirements for aircraft structures have evolved since the 1950s by paradigm shifts owing to four civil aircraft accidents and the F-111 military aircraft accident.

The requirements encompass residual strength design and analysis and verification using several levels of testing, including standard fracture mechanics tests. The ‘final’ verification is residual strength testing after FSFT.

The problem of WFD deserves special attention. WFD can defeat safety-by-inspection, whereby the residual strength is supposedly restored to a safe level by repair and maintenance after inspection. Hence FSFT is mandated for civil aircraft in order to demonstrate that WFD will not occur during the design service goal (DSG). The USAF suggests extending FSFT beyond 2 DSGs to determine the onset of WFD.

FSFTs should be followed by teardowns, which provide checks on designs and fatigue and residual strength analyses, and can reveal the need for modifications and retrofits.

References

1. Schijve J (1994) Fatigue of aircraft materials and structures. *Int J Fatigue* 16(1):21–32
2. Blom AF (2002) Fatigue science and engineering—achievements and challenges. In: Rouchon J (ed) ‘ICAF’ 2001: Design for durability in the digital age, vol I. Cépaduès-Éditions, Toulouse, France, pp 3–64
3. McEvily AJ (2002) Metal failures: mechanisms, analysis, prevention. Wiley, New York, USA, pp 6–8, 13–15 (Chapter 1)
4. Tiffany CF, Gallagher JP, Babish CA IV (2010) Threats to aircraft structural safety, including a compendium of selected structural accidents/incidents. Aerospace Systems Center Technical Report ASC-TR-2010-5002. Wright-Patterson Air Force Base, Dayton, Ohio, USA
5. Wanhill RJH, Molent L, Barter SA (2016) Milestone case histories in aircraft structural integrity. In: Hashmi S (ed) Reference module in materials science and materials engineering. Elsevier Inc., Oxford, UK, pp 1–19. doi:10.1016/B978-0-12-803581-8.00847-X
6. Eastin RG, Sippel W (2011) The “WFD rule”—have we come full circle? USAF aircraft structural integrity program conference 2011, November 29–December 1 2011. San Antonio, Texas, USA
7. Federal Aviation Administration (2011) Establishing and implementing limit of validity to prevent widespread fatigue damage. Advisory Circular FAA AC 120-104. U.S. Department of Transportation, Washington, DC, USA
8. Buntin WD (1977) Application of fracture mechanics to the F-111 airplane. In: AGARD conference proceedings no. 221 on Fracture mechanics design methodology. Advisory Group for Aerospace Research and Development, Neuilly-sur-Seine, France, pp 3-1–3-12
9. Mar JW (1991) Structural integrity of aging airplanes: a perspective. In: Atluri SN, Sampath SG, Tong P (eds) Structural integrity of aging airplanes. Springer, Berlin, Germany, pp 241–262
10. Military Specification Airplane Damage Tolerance Requirements (1974) MIL-A-83444, United States Air Force, The Pentagon, Virginia, USA
11. Military Standard Aircraft Structural Integrity Program, Airplane Requirements, 1975, MIL-STD-1530A (11), United States Air Force, The Pentagon, Virginia, USA
12. Wanhill RJH, Symonds N, Merati A, Pasang T, Lynch SP (2013) Five helicopter accidents with evidence of material and/or design deficiencies. *Eng Fail Anal* 35:133–146
13. Lynch SP (1991) Fracture of 8090 Al-Li plate: I. Short-transverse fracture toughness. *Mater Sci Eng A* A136:25–43
14. Pasang T, Symonds N, Moutsos S, Wanhill RJH, Lynch SP (2012) Low-energy intergranular fracture in Al-Li alloys. *Eng Fail Anal* 22:166–178
15. Merati A (2011) Materials replacement for aging aircraft. In: Corrosion fatigue and environmentally assisted cracking in aging military vehicles. RTO AGARDograph AG-AVT-140. Research and Technology Organisation (NATO), Neuilly-sur-Seine, France, pp 24-1–24-22
16. Modlin CT, Zipay JJ (2014) The 1.5 & 1.4 ultimate factors of safety for aircraft and spacecraft—history, definition and applications. ntrs.nasa.gov/archive/nasa/casi.ntrs.nasa.gov/20140011147
17. Federal Aviation Administration (1970) Federal airworthiness regulation part 25.303 Factor of Safety, Amendment 25-23, 35 FR 5672, U.S. Department of Transportation, Washington, DC, USA

18. Airbus A380 test wing breaks just below ultimate load target. Retrieved 27 April 2015, from: www.flightglobal.com/news/articles/airbus-a380-test-wing-breaks-just-below-ultimate-load-204716/
19. Royal Australian Air Force (2007) Structural analysis methodology—F/A-18A/B, ASI/2006/1114755 Pt1 (18), Issue 2, AL2, 7 Dec 2007
20. Watson GJ (1997) Eurofighter 2000 structural design criteria and design loading assumptions. In: Loads and requirements for military aircraft. AGARD Report 815. Advisory Group for Aerospace Research and Development, Neuilly-sur-Seine, France, pp 16-1–16-10
21. Department of Defense Standard Practice, Aircraft Structural Integrity Program (ASIP) (2005) MIL-STD-1530C (USAF), ASC/ENOI, 2530 Loop Road West, Wright-Patterson AFB, Ohio, USA 45433-7101
22. Tiffany CF, Swift T (2010) Historical summary of U.S. testing approaches for demonstrating airframe fail-safety. Appendix K in Ref. 4
23. Miedler PC, Berens AP, Gunderson A, Gallagher JP (2002) Analysis and support initiative for structural technology (ASIST). Air Force Research Laboratory Technical Report AFRL-VA-WP-TR-2003-3002, Air Force Research Laboratory, Wright-Patterson Air Force Base, Dayton, Ohio, USA 45433-7542
24. Vliieger H (1977) Prediction of fail-safe strength of realistic stiffened skin aircraft structures. In: Taplin DMR (ed) Fracture 1977—Advances in research on the strength and fracture of materials, vol 3B. Pergamon Press, New York, USA, pp 699–704
25. Goranson UG (2007) Damage tolerance facts and fiction. In: International conference on damage tolerance of aircraft structures (DTAS), Delft, The Netherlands, 25 Sept 2007
26. Swift T (1983) Verification of methods for damage tolerance evaluation of aircraft structures to FAA requirements. In: Labourdette R, Deviller D (eds) Proceedings of the 12th ICAF symposium. Centre d'Essais Aéronautique de Toulouse, Toulouse, France, pp 1.1/1–1.1/87
27. Federal Aviation Administration (2011) Damage tolerance and fatigue evaluation of structure. Advisory Circular FAA AC 25.571-1D, U.S. Department of Transportation, Washington, DC, USA
28. Federal Aviation Administration (1998) Damage tolerance and fatigue evaluation of structure. Advisory Circular FAA AC 25.571-1C, U.S. Department of Transportation, Washington, DC, USA
29. Forth SC, Everett RA, Newman JA (2002) A novel approach to rotorcraft damage tolerance. In: 6th Joint FAA/DoD/NASA aging aircraft conference, San Francisco, California, USA, 16–19 Sept 2002

Chapter 19

Stress Corrosion Cracking in Aircraft Structures

R.J.H. Wanhill and R.T. Byrnes

Abstract Stress corrosion cracking (SCC) occurs, or can occur, in all major alloy systems used in aircraft structures. The consequences of stress corrosion failures may be serious, even leading to loss of an aircraft. This chapter first surveys the types of structures and materials used in aircraft and the environments encountered by them. Case histories from a wide variety of aircraft are used to illustrate the problems caused by SCC in service. Guidelines are given for preventing and alleviating these problems.

Keywords Stress corrosion · Alloys · Primary structures · Mechanical systems · Fluid systems · Case histories · Aluminium alloys · Stainless steels · High-strength steels · Magnesium alloys

19.1 Introduction

Stress corrosion cracking (SCC) in metals and alloys occurs because of the simultaneous presence and interaction of three factors:

1. Metal or alloy susceptibility.
2. An aggressive environment.
3. Sustained (constant) stresses.

Many metals and alloys are susceptible to SCC, including the structural alloys used in aircraft and spacecraft [1]. SCC also occurs in a variety of environments: some are ubiquitous, like salt water, and some are exotic, like liquid fuels for spacecraft launchers.

R.J.H. Wanhill (✉)
NLR, Emmeloord, The Netherlands
e-mail: rjhwanhill@gmail.com

R.T. Byrnes
Defence Science and Technology Group, Melbourne, Australia

The sustained stresses may come from service loads, structural assembly (fit-up stresses), or component manufacture and heat-treatment (residual stresses). Assembly stresses should be minimized by careful design, and residual stresses should be alleviated by stress relief treatments during the manufacturing process. However, residual stresses may still be present, since it may be difficult to eliminate them from thick-section components.

19.1.1 Background to Aircraft SCC

In the 1920s and 1930s metals and alloys gradually replaced wood and canvas in aircraft structures, owing to their higher structural efficiencies, more consistent properties and reliable fabricability. The use of metals also avoided the problems of moisture stability and fungus attack that affected wooden structures. However, many structural alloys were later found to be susceptible to environmental degradation, including corrosion, hydrogen embrittlement and SCC.

Stress corrosion cracking service failures peaked in the late 1960s, mainly due to the widespread use of the aluminium alloys AA2024-T3, AA7075-T6 and AA7079-T6, all of which are highly susceptible to SCC in the short transverse (ST) direction. Improvements in chemistry and processing (aluminium alloys) and control of strength and corrosion protection schemes (high-strength steels) have helped reduce the number of service failures in modern aerospace vehicles.

Service failures of titanium and magnesium alloy components are rare. Titanium alloys require a pre-existing notch or crack to initiate SCC, while magnesium alloys usually undergo general corrosion before SCC occurs. On the other hand, stainless steel components are a somewhat unexpected source of service failures and may even result in aircraft losses, though this is exceptional [2].

Nevertheless, SCC in aircraft is a serious actual and potential problem despite the use of more modern alloys, processing and heat-treatments that are intended to reduce SCC susceptibility. When SCC occurs it causes much downtime owing to extra maintenance, including repairs, replacements (if available) and regular inspections of suspect components. All of these factors incur considerable costs as well as affecting the operational readiness.

19.2 Structures, Materials and Environments

Aircraft structures may be broadly categorized as shown in Table 19.1. Note the mention of fasteners, essential for riveted and bolted assemblies.

Table 19.1 Categories of aircraft structures

Category	Examples
Primary structures	<ul style="list-style-type: none"> • Airframes • Landing gear • Fasteners (rivets, bolts)
Mechanical systems	<ul style="list-style-type: none"> • Gearboxes • Flight controls, actuators • Engine systems
Fluid systems	<ul style="list-style-type: none"> • Hydraulic lines • Fuel and propulsion • Plumbing • Auxiliary and emergency power units

19.2.1 Primary Structures

Because aircraft weight is so important, the choice of materials for primary structures is generally based on high specific strength (strength/density) and high specific modulus ($E/\text{density}$). The corrosion and SCC resistances are important *secondary* considerations, and the design approach in these respects is to use corrosion protection measures (e.g. anodising, cladding, plating, and primer and paint systems), non-susceptible alloys (if possible and feasible) and engineering design changes to improve the distribution of sustained stresses.

Airframes Metallic airframes are constructed primarily of AA2000 and AA7000 series aluminium alloys. Most are used in heat-treatment tempers resistant to SCC, namely the T8XX (AA2000 series) and T7XX (AA7000 series) tempers. These tempers refer to artificial (elevated temperature) ageing heat-treatments.

Important exceptions are the AA2X24 series of alloys, which are used mainly in sheet form (e.g. fuselage skins) and in T3XX tempers, whereby natural ageing occurs at ambient temperatures. These alloys have excellent fatigue crack growth and fracture properties, but have only moderate-to-poor SCC resistance.

Landing Gear Landing gear cylinders and main axles are commonly made from high-strength low alloy steels. The cylinders are sometimes also made from high-strength aluminium alloys. Ancillary components such as torque links, rod-ends, levers and brackets are made from these materials and also high-strength (PH) stainless steels and titanium alloys, e.g. Ti-6Al-4V.

Wheels are usually made from aluminium alloys, but magnesium alloys have also been used. However, the use of magnesium alloys is generally discouraged owing to concerns about corrosion, particularly galvanic corrosion owing to contact with other metals and alloys. The main exceptions are helicopter gearbox housings.

Fasteners Aluminium rivets are commonly used in airframe sheet structures, as are higher-grade low alloy steel and titanium alloy fasteners.

19.2.2 Mechanical Systems

As in the case of primary structures, the choice of materials for mechanical systems is usually based on high specific strength and modulus. Protective coatings are used where necessary to increase the resistance to corrosion and the onset of SCC.

Gearboxes Gearbox housings are castings, often made from aluminium or magnesium alloys, which are used especially in helicopters, since they combine lightness, strength, moderate elevated temperature capability and excellent castability.

Gears are typically made of high-strength low alloy steels. Wear resistance is *the* property requirement for gears, and steels are used because they can be case-hardened.

Other materials suitable for mechanical systems include all grades of stainless steels and nickel-base superalloys, notably for elevated temperature applications.

19.2.3 Fluid Systems

Aircraft require fluid systems, and these rely on the basic compatibility of the alloys and fluids. However, fuel tanks are sealed to prevent leaks; and fuel cells for auxiliary and emergency power units (APUs and EPU) have epoxy coatings owing to the generally aggressive fluids within them.

Stainless steels are used for many applications, including fuel, hydraulic and plumbing lines. These steels generally belong to the “standard” austenitic AISI 300 series, which are essentially Cr-Ni and Cr-Ni-Mo steels to which small amounts of other elements have been added. An important exception is 21-6-9, which is a Cr-Ni-Mn alloy that is generally stronger than the 300 series at ambient and elevated temperatures.

Commercially pure (CP) titanium and Ti-3Al-2.5V tubing are used in aircraft air-conditioning and de-icing systems. Welds in the tubes are (or should be) stress-relieved to avoid hydrogen embrittlement.

19.2.4 Environmental Protection: Corrosion and SCC

The potential and actual environments that may be encountered by aircraft structures include the following that are of most significance for corrosion and the risk of SCC:

1. Air with widely varying humidity, containing environmental pollutants at ground and near-ground levels, and also sea salt aerosols.
2. Potable and waste water from spillages and leaks (galley, lavatories, bilge areas).

3. Water condensate, contaminated by mineral salts.

Airframes As mentioned in Sect. 19.2.1, most airframe aluminium alloys are used in heat-treatment tempers resistant to SCC. Nevertheless, since all *conventional* alloys are susceptible to pitting corrosion, they are often coated with protective oxide films produced by anodising or chemical conversion treatments.

This protection is augmented by inhibitor-containing paint primers and topcoats, and sometimes also by sacrificial aluminium cladding layers that are bonded to sheet and plate products by conjoint rolling operations, vapour phase deposition or electro-deposition.

The latest generation of aluminium–lithium (Al–Li) alloys has generally good-to-excellent corrosion resistance in the commercial T8XX tempers, and this may obviate the need for cladding. However, there are doubts about the SCC resistance in sections thicker than 30 mm [3]. See Chap. 3 in Volume 1 of these Source Books for more information on Al–Li alloys.

Landing Gear High-strength low alloy steels have generally poor resistance to corrosion and SCC, and there may be strength restrictions to reduce the risks of SCC and also hydrogen embrittlement. However, this is not usual for landing gear cylinders and axles. Instead reliance is made primarily on high-quality cadmium, chromium and nickel plating, sometimes in combination. Additional protection is provided by paint systems on external surfaces.

Aluminium alloy landing gear components are susceptible to pitting corrosion, even if nominally immune to SCC, although there have been cases of SCC in older aircraft [2]. The protection against corrosion is similar to that for airframes, i.e. anodising or chemical conversion coatings augmented by inhibitor-containing paint primers and topcoats. (Cladding is not an option, since these components are made from forgings and extrusions rather than sheet and plate, although vapour phase plating has been used to limit exposure to moisture.)

Fasteners Optimum corrosion protection of riveted structures requires wet installation of the rivets using corrosion-inhibiting sealants, but this is not always done.

Low alloy steel fasteners require corrosion protection, which is still often cadmium plating, despite environmental concerns. Several alternative coatings to cadmium have been developed, e.g. tin–zinc and zinc–nickel plating, and ion vapour deposition (IVD) aluminium, but none are completely satisfactory substitutes [4].

Mechanical Systems Magnesium gearboxes may be anodised against external corrosion. The internal environment (oil) is benign. Other components made from aluminium alloys and steels require external corrosion protection systems similar to those for airframes, landing gear and fasteners (*q.v.*).

Fluid Systems Although the alloys in fluid systems are selected for compatibility with the fluids, the external surfaces may require corrosion protection. In particular, stainless steels are susceptible to crevice corrosion that can be a precursor to SCC;

and welded joints, e.g. in tubing, may be inadvertently sensitized to SCC by the heat input from welding. This is discussed further in Sect. 19.3.2.1.

Finally, as mentioned earlier, APU and EPU fuel cells have internal epoxy coatings to protect the alloys from the aggressive fluids (e.g. hydrazine) used to power up the units.

19.3 Aircraft SCC Case Histories

This section surveys a selection of case histories drawn from the authors' experiences. The selection is intended to reflect the variety and importance of the cases for each class of structural alloys and—to some extent—their relative frequency. This can vary markedly, depending on the types of aircraft.

In the survey, there are 33 cases concerning aluminium alloys, 11 for stainless steels, 6 for high-strength low alloy steels and 2 for magnesium alloys. The relatively few cases for low alloy steels compared to stainless steels may be because low alloy steels have to be protected by well-established plating and painting combinations, while stainless steels are often thought to be immune to corrosion and SCC. In any event, all of the cases concern SCC in aqueous or moisture-containing environments.

As far as possible, the cases are treated in groups rather than individually, in order to show commonalities but also to point out significant differences. The measures to alleviate or prevent the recurrence of SCC are listed and/or briefly discussed for each group or case (excepting the magnesium alloy cases, where straightforward replacement occurred). These measures are placed in the most relevant context in Sect. 19.4 of this chapter.

19.3.1 Aluminium Alloys

Table 19.2 surveys the aluminium alloy SCC case histories from the NLR and DSTG archives. The majority are from a variety of military aircraft operated by the Royal Netherlands Air Force (RNLAf) and the Royal Australian Air Force (RAAF).

Most of the cases concerned wing components and landing gear made from AA7000 series alloys. In fact, these were effectively just two alloys, AA7075-T6XX and AA7079-T6XX. There was a similar situation for the AA2000 series alloys, which were either AA2024-T3XX/T4 or AA2014-T6.

The majority of the SCC problems were due to residual tensile stresses introduced during heat-treatment, sometimes aided by prior corrosion pitting. Assembly stresses also contributed, notably tensile stresses introduced by interference fits of bearings or bushings.

Table 19.2 Classification of selected aluminium alloy SCC case histories (DSTG and NLR)

Main parameters		Number	Remarks	
Aircraft types	Combat	14	Most aircraft designed before 1970, pre-dating the late-1960s and early-1970s developments in heat-treatments and alloy chemistry to improve the SCC resistance	
	Transport	11		
	Maritime patrol	7		
	Light trainer	1		
Structural areas	Landing gear	14	Window shield, 3 liquid oxygen fittings, fin pivot-bearing housing, fuselage frame	
	Wing	10		
	Engine/pylon	3		
	Other	6		
Alloy types	AA2000 series	10	See the above remarks on heat-treatments and alloy chemistry	
	AA7000 series	23		
SCC causes	Residual stresses	23–24	7 cases starting from corrosion pitting 4 cases owing to bearing or bushing inserts	
	Assembly stresses	8		
	On-ground tensile stress	1		
	Cold-stamping	1		
Remedial measures	Actual	Repairs	4	1 unsuccessful: incomplete removal of SCC Some cracking allowed (<i>unusual</i>)
		Non-destructive Inspection (NDI)	2	
		Proposed	Fleet-wide replacements	
	Proposed	Replacements using better alloys and/or heat-treatments	9	Only a very few case history reports contained information about whether the proposed remedial measures were taken. However, some are known to have been adopted
		Improved corrosion protection	6	

Two cases were unusual, where the tensile stresses came from (i) component loading while the aircraft was on the ground, and (ii) cold-stamping a groove onto a bearing housing to keep the bearing in place.

The remedial measures obviously included replacing cracked components unless repairs were feasible or—exceptionally—when some cracking was allowed if the components were regularly inspected (NDI). The repair and inspection possibilities are more technically interesting than replacements and are therefore discussed in more detail in Sect. 19.3.1.2.

19.3.1.1 Aluminium Alloy SCC Characteristics

Aluminium alloy SCC can initiate from nominally undamaged smooth or notched surfaces (e.g. fillet radii and holes) as well as surfaces damaged by corrosion and abrasion. The crack path in commercial alloys is intergranular. This is of major importance to the SCC behaviour.

The rolling, forging and extrusion processes used to fabricate half-products and finished components cause the material grains to elongate in the direction of working, resulting in a “pancake” microstructure with elongated grain boundaries. These are usually retained during subsequent heat-treatments and provide easy fracture paths, notably for SCC.

The direction normal to the pancake microstructure is the short transverse (ST) direction. SCC along the elongated grain boundaries (an easy fracture path) occurs when there are tensile stresses in the ST direction. This is often the case for residual stresses introduced during solution heat-treatment followed by the required rapid cooling (quenching).

Macroscopic Characteristics Figure 19.1 shows SCC failure along the flash line of a flap track hinge. The arrows point to the SCC origin, at left, and crack front progression markings. However, progression markings are not always visible.

Microscopic Characteristics Figures 19.2 and 19.3 are fractographs showing (i) a “woody” texture with uplifted grains and (ii) a “pancake” intergranular topography. Both are diagnostic for SCC in aluminium alloys, but uplifted grains can also occur during SCC of other alloys [5].

The uplifted grains are the result of ligament deformation and tearing during the *final* joining of multiple stress corrosion cracks on slightly different levels. This final joining can occur during in-service final failure of a component or when breaking a cracked sample open for laboratory investigation.

Fig. 19.1 SCC fracture in a die-forged AA7079-T651 flap track hinge

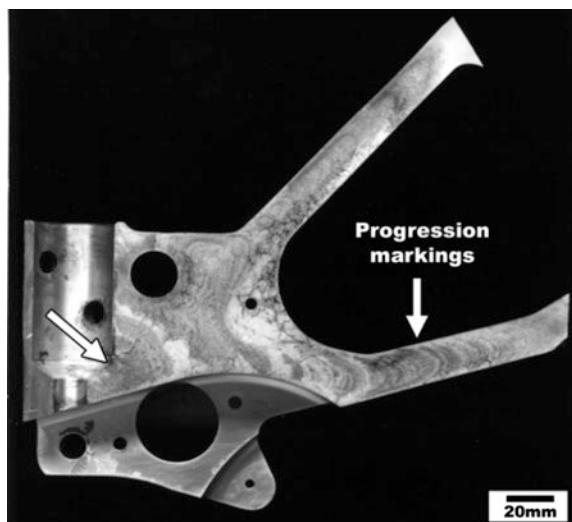


Fig. 19.2 Uplifted grains on an SCC fracture surface from a die-forged AA7075-T6 landing gear linkage arm

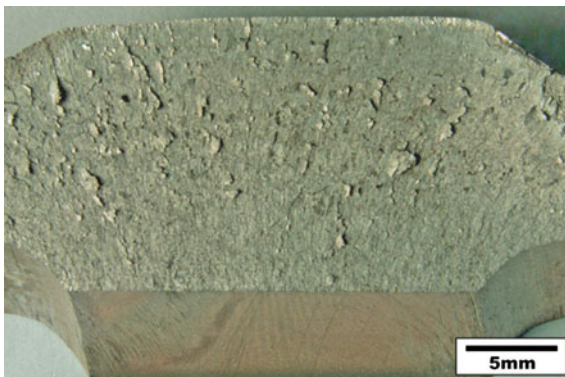
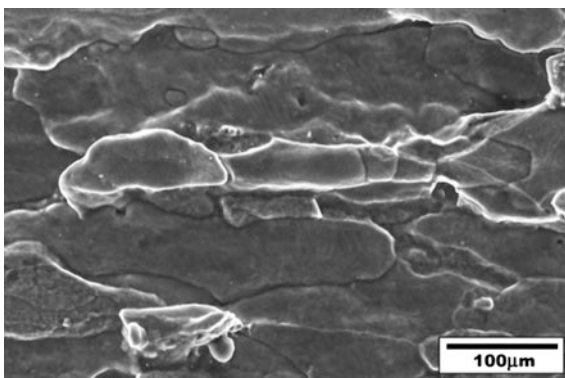


Fig. 19.3 “Pancake” grains on an SCC fracture surface from a thick section AA2024-T3/T4 support strut: SEM fractograph



19.3.1.2 Repair and Inspection Possibilities

Table 19.2 indicates that four case histories involved repairs to SCC-damaged components. Three of these cases concerned main landing gear (MLG) legs, which were large forgings. The fourth was a MLG linkage arm, also a forging.

Table 19.3 summarizes the main aspects of these case histories. The remedial measures all included repair machining, but otherwise there were differences. The reasons lie in the case history details, which are summarized here:

Transport MLG Legs SCC was found in a number of legs in the 1960s. The manufacturer issued a service bulletin for repair machining, which was later repeated. Since this could not go on indefinitely, additional measures were considered. These were shot-peening and an improved paint scheme for existing legs, and changing the heat-treatment for new legs. The changed heat-treatment, from T6 to T7XX, was introduced in the mid-1960s.

Table 19.3 Main aspects of the aluminium alloy cases involving repair and inspection possibilities

Aircraft	Material and component	Problems	Remedial measures
Transport	DTD 5024 MLG legs (AA7075/9-T6 equivalent)	<ul style="list-style-type: none"> • SCC beyond <i>first</i> repair zone 	<ul style="list-style-type: none"> • Further repair machining • Shot-peening • Improved paint scheme • Duplex ageing (T7XX temper)
Maritime patrol	AU4SG-T6 MLG legs (AA2014-T6 equivalent)	<ul style="list-style-type: none"> • Corrosion pits and SCC 	<ul style="list-style-type: none"> • Repair machining • Regular 4-monthly inspections
Combat	AA7079-T6 MLG legs	<ul style="list-style-type: none"> • Small (≤ 4 mm) cracks 	<ul style="list-style-type: none"> • Repair machining and/or regular inspections • Improved corrosion protection
Maritime patrol	AA7075-T6 MLG linkage arm	<ul style="list-style-type: none"> • Incomplete repair machining of bore 	<ul style="list-style-type: none"> • Replacement • Inspect/replace similar parts • Improved corrosion protection

Maritime Patrol MLG Legs Corrosion, sometimes associated with SCC, was found in the late 1960s. The manufacturer issued a service bulletin for repair machining, with the “clean-up” limits based on retaining sufficient static strength. The corrosion damage appeared to occur slowly, and so the repair machining was considered adequate in combination with regular inspections. (Chemical conversion coatings were applied after repair machining, and the external surfaces were also repainted.)

Combat Aircraft MLG Legs Small cracks were detected in two legs in 1985 and subsequently destructively confirmed to be SCC. Since the legs had seen more than 10 years of service and the alloy was the highly susceptible AA7079-T6, it was concluded that the cracks had arrested owing to complete relaxation of residual stresses. Repair machining and improved corrosion protection were proposed for any other legs with small crack indications. None were found, and the problem soon disappeared because new legs made from SCC-resistant AA7075-T73 forgings were introduced in 1986 as part of a major refurbishment.

Maritime Patrol MLG Linkage Arm Four cracks and corrosion pits were detected in the main bore. Two cracks were opened and found to be SCC, with one crack completely through the bore thickness, see Fig. 19.2.

Scratches and abrasion marks were present along the bore, especially at the crack locations. The scratches, abrasion marks and corrosion pits were all chemical conversion coated. This indicated unsuccessful rework to remove the corrosion pits and cracks, followed by reapplying the corrosion protection scheme and returning the linkage arm to service.

In view of these results it was recommended to inspect all other linkage arms and replace any cracked ones. It was also suggested to regularly apply water-displacing compounds (WDCs) to the main bores of undamaged linkage arms to provide improved corrosion protection.

19.3.2 Stainless Steels

19.3.2.1 Background Information

As mentioned earlier, stainless steels are used in mechanical and fluid systems. Applications include fuel and hydraulic tubing, pins, bolts, nuts, clamps, pumps, pistons, bleed air ducts and valves. The alloys include austenitic grades (e.g. 304, 316, 321, 347, 21-6-9 and Nitronic 60), martensitic grades (e.g. 410, 431, 440C) and the precipitation-hardenable grades (e.g. PH 13-8 Mo, 17-4 PH, AM350).

All austenitic stainless steels are susceptible to SCC to some degree [6]. Susceptibility depends on several factors, including the environment, temperature, sensitivity to pitting and crevice corrosion, and metallurgical condition (annealed, cold-worked, welded). SCC initiation can be facilitated by poor design, e.g. sharp corners and crevices, and residual stresses from manufacturing.

An important problem is “sensitization” or “weld decay”. Many austenitic stainless steels are susceptible to sensitization, which occurs when the steels are exposed to certain temperature ranges, e.g. during welding. Chromium carbides precipitate at the grain boundaries and deplete the adjacent matrix of the chromium content needed to maintain corrosion resistance. The steels become susceptible to intergranular corrosion, which in combination with tensile stresses can be considered a type of SCC.

Sensitization can be avoided by using Ti-containing or (Nb + Ta)-containing stabilized steels like 321 and 347, or low carbon (C) grades like 304L and 316L, which can take short-term high temperatures during welding [6, 7]. Any sensitization that does occur can be reversed by post-weld annealing, but if not done correctly, SCC failures can still be expected.

Sensitization can also occur in martensitic and precipitation-hardening stainless steels. Examples are mentioned in Sects. 19.3.2.2 and 19.3.2.3.

19.3.2.2 Stainless Steel Case Histories

Table 19.4 surveys the SCC case histories from the NLR and DSTG archives. All are from military aircraft operated by the RAAF and RNLAf. Most concerned hydraulic and fuel systems tubing made from 300 series and 21-6-9 austenitic steels.

Table 19.4 Classification of selected stainless steel SCC case histories (NLR and DSTG)

Main parameters		Number	Remarks
Aircraft types	Combat	3	2 modern aircraft
	Transport	1	2 modern aircraft
	Maritime patrol	4	
	Light trainer	1	
	Helicopter	2	
Structural areas	Hydraulic system	5	Most of the cases concerned tubing
	Fuel system	2	
	Engine	3	
	Fire extinguisher system	1	
Alloy types	AISI 300 series (austenitic)	5	2 cases of sensitization close to welds
	AISI 400 series (martensitic)	2	
	21-6-9 (austenitic)	2	Sensitized close to welds
	Nitronic 60 (austenitic)	1	Crevice corrosion + SCC
	AM350 (precipitation-hardening)	1	Susceptibility discovered after aircraft loss
SCC causes	Sensitization	5	Possible cause of 1 aircraft loss
	Residual stresses/cold-work	2	1 aircraft loss
	Assembly stresses	1	
	Crevices	3	
Remedial measures	<i>Worldwide</i> replacements with new alloy	1	1 aircraft loss
	Individual replacements	9	(2 aircraft losses)
	Recommended NDI of similar components	9?	Number of recommendations uncertain
	Recommended better alloy	2	
	Recommended corrosion protection	3	Water-displacing compounds (WDCs)

Many of the SCC problems were due to sensitization, and one case may have caused the loss of an aircraft owing to a major fuel leak: the wreckage was too damaged to be certain. Another case definitely led to loss of an aircraft [5]. This case also resulted in worldwide replacement of similar components, using an alloy immune to SCC. Thus stainless steel SCC in aircraft can be a major problem, not just a local inconvenience.

19.3.2.3 Stainless Steel SCC Characteristics

Stainless steel SCC can initiate from nominally undamaged smooth and notched surfaces, although some localized pitting or crevice corrosion always precedes SCC. Besides intergranular cracking owing to sensitization, the SCC can be intergranular in some environments and transgranular in others [8]. SCC in chloride-containing environments occurs at slightly elevated temperatures, typically higher than 50–60 °C [7].

Fig. 19.4 Location of crevice corrosion and SCC in a 21-6-9 hydraulic tube

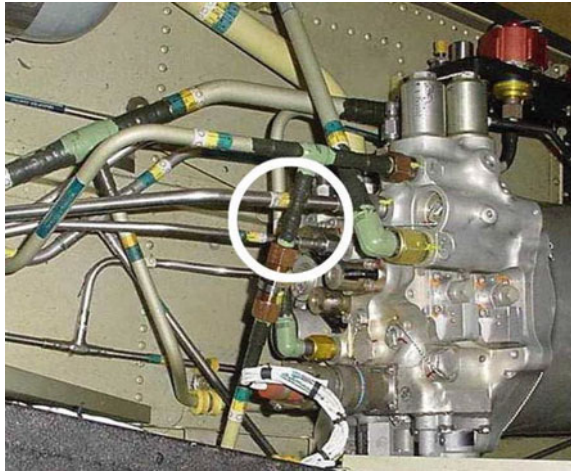


Fig. 19.5 SCC (arrowed) in a 431 nut

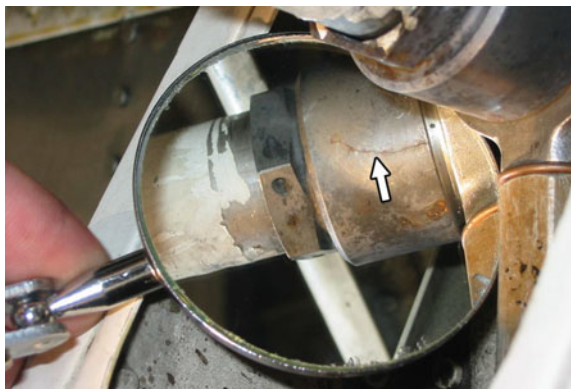
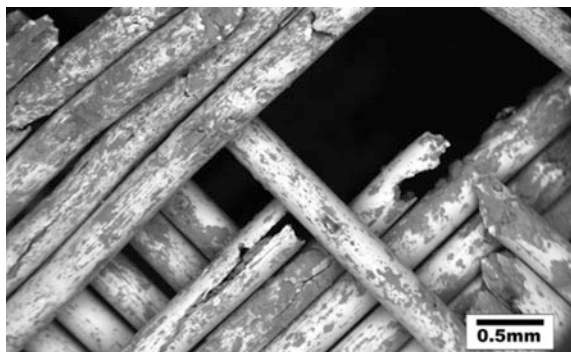


Fig. 19.6 Crevice-induced corrosion pitting and SCC in a 304 wire braid



Macroscopic Characteristics Figure 19.4 shows a typical location (circled) for stainless steel SCC. Usually only an external crack is visible, e.g. Fig. 19.5, but crevice corrosion is sometimes evident. Figure 19.6 shows severe crevice-induced

corrosion pitting and SCC in a wire braid from a hose in an MLG hydraulic system. In this case, loss of system function in service could have had serious consequences.

Figure 19.7 shows a low-magnification fractograph of *intergranular* SCC. The brown discoloration due to fracture surface corrosion is typical, and crack front progression markings are sometimes seen.

N.B. Greenish brown fracture surface corrosion and progression markings were observed for mainly *transgranular* SCC in a 17-4 PH backstay connector from an ocean-going yacht [9]. The green colour probably came from copper (3–5 wt%) in the alloy.

Microscopic Characteristics Figure 19.8 shows a typical intergranular SCC fracture surface from a bolt in a fuel tank coupling.

Fig. 19.7 Intergranular SCC from the 431 nut shown in Fig. 19.5

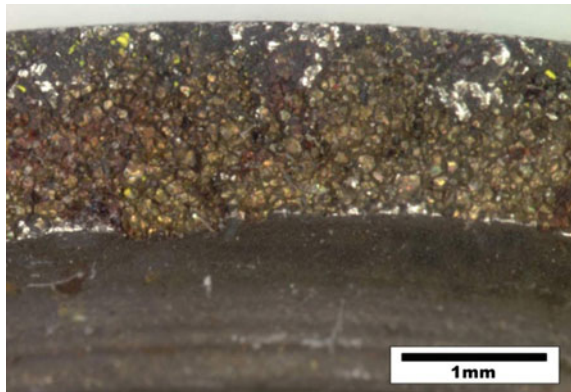


Fig. 19.8 Intergranular SCC from a 431 bolt: SEM fractograph

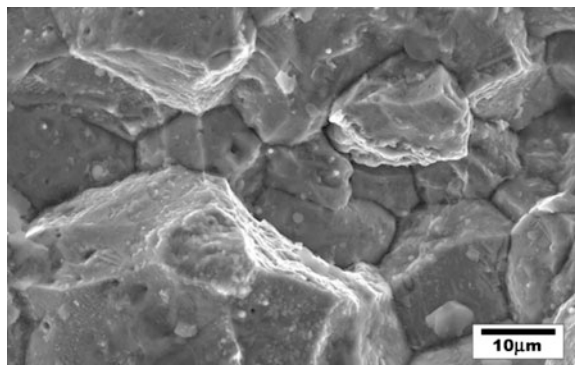


Fig. 19.9 Transgranular SCC from a Nitronic 60 pin: SEM fractograph

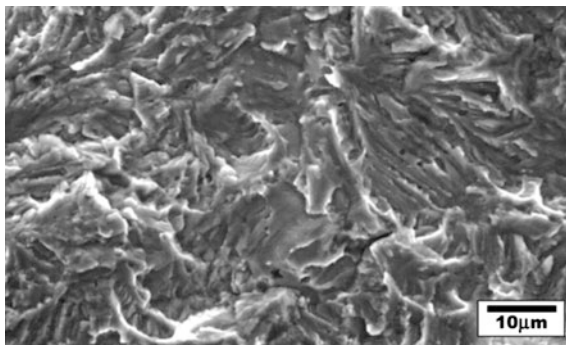


Figure 19.9 shows transgranular SCC in a Nitronic 60 pin from a rear compressor variable vane (RCVV) lever arm assembly in an aircraft gas turbine. The pin failure led to *loss of the aircraft* [5].

19.3.3 High-Strength Low Alloy Steels

19.3.3.1 Background Information

High-strength low alloy steels have a tempered martensite microstructure. The degree of tempering determines the strength range. These steels are used mainly for landing gear, bolts, fittings and mechanical systems, e.g. gears.

The alloys include the AISI grades 4330, 4330M, 4340, 300M, D6ac and H11. All are susceptible to SCC, and also hydrogen embrittlement [10], at yield strengths above 1200 MPa; and they are extremely susceptible at yield strengths above 1400 MPa. Nevertheless, very high-strength steels are generally used for landing gear cylinders and axles to save weight.

It is important to note that SCC in high-strength steels involves hydrogen embrittlement due to hydrogen generated at the crack tips, and that this can occur in moist air as well as aqueous environments. The SCC fracture characteristics are also similar—if not identical—to those of internal hydrogen embrittlement (IHE), which is due to the presence of solute hydrogen in the steel.

19.3.3.2 High-Strength Low Alloy Steel Cases

Table 19.5 surveys the SCC case histories from the NLR and DSTG archives. Five are from military aircraft operated by the RNLAF and RAAF. The sixth was from a commercial transport.

Table 19.5 Classification of selected high-strength low alloy steel SCC case histories (NLR and DSTG)

Main parameters		Number of cases
Aircraft types	Combat	4
	Transport (civil)	1
	Helicopter	1
Structural areas	Landing gear	4
	Wing	2
Alloy types	4340, 4340M	3
	300M	1
	D6ac	1
	H11	1
SCC causes	Removed, damaged and/or worn corrosion protection systems (paint, plating)	4
	Shot-peening omitted during manufacture	1
	Fatigue cracking*	1
Remedial measures	Individual replacements (*1 unnecessary: removal of cracked area sufficient)	5
	NDI of similar components (uncertain)	5?
	Recommended refurbishment of corroded but uncracked components	1

Most of the cases concerned landing gear components, and most were due to damage and deterioration (wear) of the corrosion protection systems. One of these cases is reviewed in Sect. 19.3.3.3, since it well illustrates the characteristics of SCC.

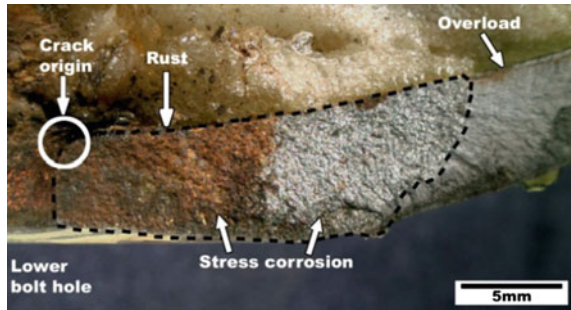
There was one unusual case, where SCC started from an in-service fatigue crack, see Table 19.5. SCC could occur because the aircraft remained on the ground, statically loaded, for about 1 year during major refurbishment. Another unusual aspect was that because the component was very large, the cracking could be removed with careful blending and contouring to enable the component to re-enter service.

19.3.3.3 High-Strength Low Alloy Steel SCC Characteristics: A Case History

Stress corrosion cracking can occur when the corrosion protection systems, paint and/or plating, become damaged or worn. If there is an aqueous environment, then SCC can be initiated and accompanied by corrosion.

SCC usually occurs along the prior austenite grain boundaries, resulting in evident intergranular fracture. However, this is also the fracture mode of IHE. The similar fracture characteristics of SCC and IHE can sometimes make it difficult to determine the failure mechanism, especially in the absence of significant corrosion and black or tinted oxide films on the SCC fracture surfaces [10].

Fig. 19.10 SCC fracture (and overload) in a 300M MLG drag beam



Notwithstanding these interpretative problems, the SCC characteristics of high-strength steels are well illustrated by a case history where a helicopter MLG drag beam made from 300M failed during a routine landing. Investigation showed that failure occurred from a bolt hole owing to corrosion pitting followed by SCC. The following fracture characteristics were observed:

Macroscopic Characteristics Figure 19.10 is a low-magnification view of one of the two cracks from the bolt hole. The bolt hole was severely corroded despite having been cadmium plated, and there was rust on much of the SCC fracture surface. This suggested that the local environment was severe and that the drag beam could have been cracked for a long time in service.

Microscopic Characteristics Figure 19.11 is a montage showing that SCC began from a corrosion pit (upper fractograph) and that the non-rusted fracture was classically intergranular (lower fractograph).

Additional investigation showed that the cadmium plating in the bore of the hole had disappeared and that it was also degrading on the outside of the hole. Besides replacement of the failed drag beam, it was recommended to (i) inspect all other drag beams in the fleet at regular intervals, (ii) replace any cracked ones, and (iii) check the feasibility of refurbishing uncracked but corroded drag beams.

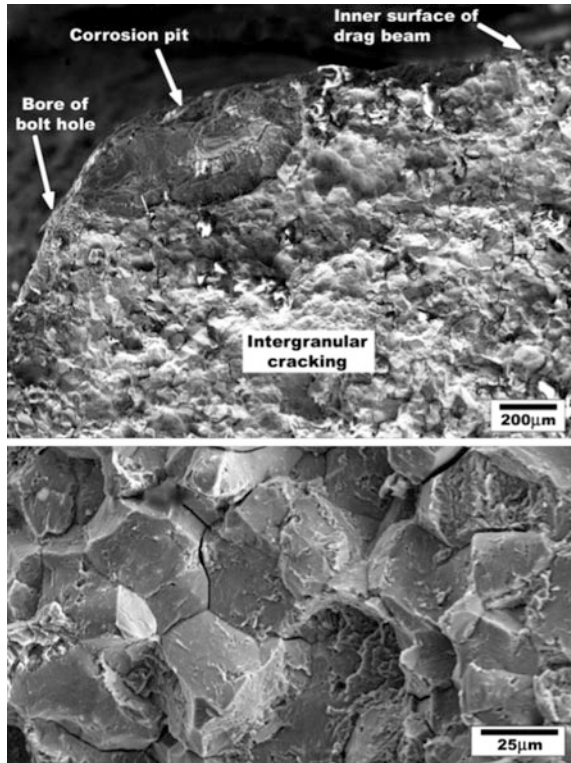
19.3.4 Magnesium Alloys

19.3.4.1 Background Information

As stated in Sect. 19.2, the use of magnesium alloys in aircraft is generally discouraged owing to concerns about corrosion. Protective coating systems are available, and the basic corrosion resistance has been improved by alloy modifications and additions, but the most serious risk is galvanic corrosion in high-conductivity environments, e.g. aqueous salt solutions [11].

Although the corrosion resistance is an issue, magnesium alloys have a long history of use in aircraft components, including wheels, flying controls and

Fig. 19.11 Details of
 Fig. 19.10: SEM fractographs



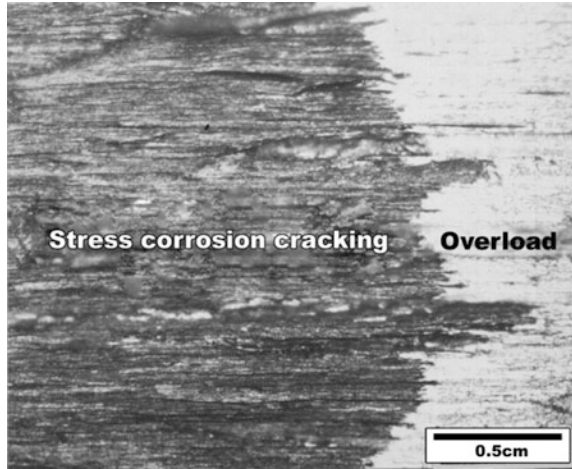
gearboxes. Magnesium alloy gearboxes are more or less standard for helicopters since, as mentioned earlier, magnesium alloys combine lightness, strength, moderate elevated temperature capability (up to about 175 °C) and good castability. Also, the local internal environment (oils and greases) is innocuous.

19.3.4.2 Magnesium Alloy Case Histories

As stated in the introduction to this chapter, magnesium alloy SCC case histories are rare. The NLR and DSTG archives list only 2 SCC failures. These were a nose-gear wheel and a gearbox case in an engine system, from two combat aircraft. The components were sand castings made from the MgAlZn alloys AZ91C and AZ92A, respectively.

For the wheel the sustained stresses enabling SCC were attributed to the tyre pressure, and for the gearbox to a misaligned attachment bolt. The remedial actions were straightforward replacements.

Fig. 19.12 Transgranular SCC fracture in a magnesium alloy gearbox case: optical fractograph [14]



19.3.4.3 Magnesium Alloy SCC Characteristics

Magnesium alloy SCC can be initiated by corrosion pitting, as was the case for the nose-gear wheel mentioned above. The cracking can be both intergranular and transgranular [12, 13], but transgranular SCC is the intrinsic type [13].

Transgranular SCC has a complicated cleavage-like and stepped fracture topography that distinguishes it from magnesium alloy fatigue fracture, which is flatter and often shows fatigue striations and well-defined crack front progression markings [14]. Another distinguishing feature is that magnesium SCC crack fronts can be irregular and jagged, e.g. Figure 19.12, unlike fatigue crack fronts [14, 15].

19.4 Preventative and Remedial Measures to Avoid SCC

Preventative and remedial measures to avoid SCC in aircraft alloys have been discussed throughout the previous sections of this chapter. In this section, we shall place these measures within the context of overall guidelines.

19.4.1 Preventative Measures

SCC of aircraft materials is confined to local aqueous environments and possibly high humidity air for high-strength low alloy steels. Furthermore, the majority of problems concern aluminium alloys, high-strength low alloy steels and stainless steels.

For aluminium alloys, it is primarily the *older generation* aircraft, using AA7000 series alloys in peak aged T6XX tempers that have SCC problems. A widely used older generation aircraft that still has SCC problems in relatively new models is the Lockheed Martin C-130 Hercules, which retains much of the primary structural design and materials from the early 1950s. These problems are returned to in the discussion on repairs in Sect. 19.4.2.

Based on much experience (not only that of the DSTG and NLR), Table 19.6 presents guidelines for preventing corrosion and SCC in aircraft. The *italicized* additions reflect some aspects of the case histories discussed in Sect. 19.3 of this chapter.

For stainless steels there are some additional aspects to consider with respect to alloy selection. Higher-Cr and especially higher-Mo austenitic stainless steels are more resistant to crevice corrosion [6], and a more recent possibility is the use of duplex (austenite + ferrite) stainless steels.

Duplex stainless steels can substitute for austenitic stainless steels at any strength level and with high resistance to SCC [16]. Duplex steels also have a higher surface hardness, which makes them more resistant to abrasion and wear.

19.4.2 Remedial Measures

There are two basic remedial actions: replacement and repair. Table 19.7 gives guidelines for both of these actions. There are some similarities in these remedial measures, and also similarities with the preventative measures listed in Table 19.6. For example, two generally applicable measures are (i) use alloys and/or heat-treatments more resistant to SCC and (ii) improved corrosion protection.

Repair options are generally limited, and none have been indicated for stainless steel components, which are generally easily replaced. In fact, all components that are simple and easily removed will most likely be scrapped. This avoids the costly auditing, certification and changed inspection schedules associated with repairs. More complex and difficult to remove components will also most likely be scrapped unless repairs can be done in situ or replacements are unavailable.

Older Aircraft The need for repairs is particularly relevant to older aircraft that continue in service well beyond their original target service lives. Table 19.7 shows several guidelines and options for aluminium alloys, some of which were discussed with respect to the MLG case histories in Sect. 19.3.1.2.

The remaining two repair guidelines are the use of composite patches and reheat-treatment. Composite patch repairs have been used, for example, on 7075-T6 extrusions in Lockheed Martin C-130H Hercules aircraft.

The reheat-treatment is called retrogression and re-ageing (RRA). This was invented in the early 1970s for increasing the SCC resistance of thin sheets of 7000 series alloys in the T6 temper [17]. Subsequently, the National Research Council

Table 19.6 Guidelines for prevention of corrosion and SCC in aircraft

Types of structures	General guidelines	Specific guidelines	
		Materials	Coatings
Primary structures and mechanical systems	<ul style="list-style-type: none"> • Restrict strength levels • Protective coatings where necessary for aluminium alloys and low alloy steels 	Al alloys for primary structures and landing gear: <ul style="list-style-type: none"> – AA2000 series in T8XX tempers (<i>if feasible</i>) – AA7000 series in T7XX tempers – <i>Reduce residual and assembly stresses</i> 	Cladding, metallic coatings (IVD); anodising or chemical conversion coatings; paint systems
		Low alloy steels: <ul style="list-style-type: none"> – UTS <1400 MPa (higher for landing gear) – <i>Wear-resistant coatings (whenever feasible)</i> 	Cd, Cr or Ni plating with covering paint systems
		Stainless steels: <ul style="list-style-type: none"> – PH grades \geq H1000 temper – <i>Avoid sensitization and residual stresses</i> – <i>Avoid crevices if possible: use WDCs otherwise</i> – <i>Use alloys more resistant to SCC</i> 	–

Table 19.7 Guidelines for remedial measures against corrosion and SCC in aircraft

Damaged components	Alloy classes	Guidelines
Replace	All	<ul style="list-style-type: none"> • Straightforward replacement • Improved corrosion protection, e.g. use WDCs • Inspect similar components and replace as necessary • Regular inspections of replaced and retained components
	Aluminium alloys Stainless steels	<ul style="list-style-type: none"> • Replace with alloys and/or heat-treatments more resistant to corrosion and SCC
Repair	Aluminium alloys	<ul style="list-style-type: none"> • Repair machining of corroded and/or cracked components • Shot-peening • Improved corrosion protection, e.g. paint systems and WDCs • Re-ageing to SCC-resistant tempers • Composite patches • Inspect similar components, repair (or replace) as necessary • Regular inspections of repaired (and replaced) components
	High-strength low alloy steels	<ul style="list-style-type: none"> • Refurbishment of corroded but uncracked components • Improved corrosion protection, e.g. use WDCs • Inspect similar components: repair (or replace) as necessary • Regular inspections of repaired (and replaced) components

(NRC) in Canada modified the RRA treatment to make it suitable for thicker sections [18] and in situ application on airframes [19].

There is also the potential to RRA-treat replacement components prior to installing on an aircraft so as to forestall recurring problems. The DSTG has used in-house data and information supplied by the NRC to certify the use of thicker section RRA 7075-T6 extrusions on RAAF C-130J aircraft. However, to date this has not been implemented.

19.5 Summary

Stress corrosion cracking is a serious problem for aircraft structures. Its occurrence causes much downtime owing to extra maintenance, including repairs, replacements and regular inspections of suspect components. All of these factors incur considerable costs as well as affecting the operational readiness. SCC can even cause loss of an aircraft, though this is rare.

Aluminium alloy SCC problems occur primarily in older aircraft, but also in new aircraft of older designs, using AA7000 series alloys in T6XX tempers. However, this significant restriction does not apply to stainless steels and high-strength low alloy steels, *which are just as susceptible in modern aircraft*.

DSTG and NLR case histories for a wide variety of aircraft indicate that most SCC problems concern aluminium alloys and stainless steels, followed by high-strength low alloy steels. This rather unexpected ranking for low alloy steels may be due to mandatory protection by well-established plating and paint systems. On the other hand, stainless steels are often thought to be immune and not requiring protection.

Stainless steels are actually far from “stainless”. Many are susceptible to crevice corrosion, leading to SCC; and they can also be sensitized to SCC if fabricated and welded without due regard to material composition and post-weld annealing.

This chapter has presented guidelines for preventing and alleviating SCC problems in all these materials. These guidelines include limited possibilities for repair of components made from aluminium alloys and high-strength low alloy steels.

References

1. Korb LJ (1987) Corrosion in the aerospace industry. Metals handbook, vol 13, 9th edn. Corrosion, ASM International, Metals Park, Ohio, USA, pp 1058–1100
2. Wanhill RJH (2009) Aircraft stress corrosion in the Netherlands. NLR Technical Publication NLR-TP-2009-520, National Aerospace Laboratory NLR, Amsterdam, the Netherlands
3. Holroyd NJH, Scamans GM, Newman RC, Vasudevan AK (2014) Corrosion and stress corrosion of Aluminum–Lithium Alloys. In: Eswara Prasad N, Gokhale AA, Wanhill RJH (eds) Aluminum–Lithium Alloys: processing, properties and applications. Butterworth-Heinemann, An Imprint of Elsevier Publications, New York, USA, pp 457–500
4. Defence Standard 03-36 (2010) Guidance to the use of cadmium alternatives in the protective coating of Defence equipment. Issue 2, 25 June 2010, Defence Procurement Agency, Glasgow, UK
5. Kool GA, Kolkman HJ, Wanhill RJH (1994) Aircraft crash caused by stress corrosion cracking. American Society of Mechanical Engineers Paper 94-GT-298, International Gas Turbine and Aeroengine Congress and Exposition, 13–16 June 1994, The Hague, the Netherlands
6. Washko SD, Aggen G (1990) Wrought stainless steels. In: Metals handbook, vol 1, Tenth edn. Properties and selection: irons, steels, and high-performance alloys corrosion. ASM International, Materials Park, Ohio, USA, p 873
7. Vander Voort GF (1990) Embrittlement of steels. In: Metals handbook, vol 1, Tenth edn. Properties and selection: irons, steels, and high-performance alloys corrosion. ASM International, Materials Park, Ohio, USA, p 707
8. Latanision RM, Staehle RW (1969) Stress corrosion cracking of iron-nickel-chromium alloys. In: Staehle RW, Forty AJ, Van Rooyen D (eds) Proceedings of conference: fundamental aspects of stress corrosion cracking. National Association of Corrosion Engineers, Houston, Texas, USA, pp 214–296
9. Wanhill RJH (2003) Failure of backstay rod connectors on a luxury yacht. Pract Fail Anal 3 (6):33–39

10. Wanhill RJH, Barter SA, Lynch SP, Gerrard DR (2011) Prevention of hydrogen embrittlement in high strength steels, with emphasis on reconditioned aircraft components', Chapter 20 in: Corrosion fatigue and environmentally assisted cracking in aging military vehicles, RTO AGARDograph AG-AVT- 140, NATO Research and Technology Organisation, Neuilly-sur-Seine, France, pp 20.1–20.61
11. Anon (1979) Corrosion resistance of magnesium and magnesium alloys. In: Metals handbook, vol 2, Ninth edn, Properties and selection: nonferrous alloys and pure metals. ASM International, Metals Park, Ohio, USA, pp 596–609
12. Speidel MO, Blackburn MJ, Beck TR, Feeney JA (1972) Corrosion fatigue and stress corrosion crack growth in high strength aluminium alloys, magnesium alloys, and titanium alloys exposed to aqueous solutions. In: Devereux OF, McEvily AJ, Staehle RW (eds) Corrosion fatigue: chemistry, mechanics and microstructure. National Association of Corrosion Engineers, Houston, Texas, USA, pp 324–342
13. Winzer N, Atrens A, Dietzel W, Song G, Kainer KU (2007) Stress corrosion cracking in magnesium alloys: characterization and prevention. *J Met* 59(8):49–53
14. Slater SL, Wood CA, Turk SD (2007) Preliminary failure assessment of T56-A-15 reduction gearbox case cracking. DSTO Contract Report DSTO-CR-2007-0256. Defence Science and Technology Organisation, Melbourne, Australia
15. Lynch SP, Trevena P (1988) Stress corrosion cracking and liquid metal embrittlement in pure magnesium. *Corrosion* 44:113–124
16. Ekman S, Pettersson R (2009) Desirable duplex. *Mater World* 17(9):28–30
17. Cina B, Gan R (1974) Reducing the susceptibility of alloys, particularly aluminium alloys, to stress corrosion cracking. United States Patent 3856584, 24 Dec1974
18. Wallace W, Beddoes JC, deMalherbe MC (1981) A new approach to the problem of stress corrosion cracking in 7075-T6 aluminum'. *Can Aeronaut Space J* 27:222–232
19. Raizenne D, Sjoblom P, Rondeau R, Snide J, Peeler D (2002) Retrogression and re-aging of new and old aircraft parts. In: Proceedings of the 6th joint FAA/DoD/NASA conference on aging aircraft, 16–19 Sept 2002, (CD-ROM). San Francisco, California, USA

Part IV
Special Technologies

Chapter 20

Aero Stores (Materials) Inspection and Quality Assurance

K.K. Mehta and S. Chawla

Abstract Quality assurance (QA) encompassing inspection, testing, evaluation and certification of an aero store provides the guarantee for reliable performance during its operational usage. QA agencies shoulder the prime responsibility for flight safety. Military aircraft are often required to operate in harsher environments than their civilian counterparts. Hence the quality requirements for military aero stores are stringent. In the development phase the primary role of QA is to detect design deficiencies during qualification testing as part of the airworthiness certification. Further, this Chapter discusses (i) the importance of process control during manufacturing of aero stores and (ii) the critical inspection stages and important check points, spot/surprise checks and quality audits for various materials (aluminium, titanium, nickel-based alloys, special steels and composites).

Keywords Aero stores · Inspection · Quality assurance · Aluminium alloys · Titanium alloys · Steels · Superalloys · Composites

20.1 Introduction

The complexity of aero stores presents extreme challenges to the quality assurance agencies during their certification, inspection and clearance, as well as to the designers, manufacturers and materials experts [1]. Aero materials require high specific strength combined with other mechanical and physical properties that can sustain extreme environmental conditions, very high operational criticality and the requirement of stringent tolerance levels for failure and safety.

Although large numbers of aero materials have been developed and type tested/qualified, it is still not possible to guarantee compliance during the full

K.K. Mehta
DGAQA (GW & M), Hyderabad, India

S. Chawla (✉)
DGAQA, New Delhi, India
e-mail: sjccrim@gmail.com

service life, even after fulfilling the complete specification requirements. Strict control of metallurgical process parameters during each stage of processing is required to produce clean aero grade materials [1]. Thus aero materials require a broader umbrella of quality assurance that encompasses not only the important tools of quality control (QC), but also ensures the establishment of a complete quality management system (QMS).

The term “Quality”, defined as “all those planned and systematic actions necessary to provide adequate confidence that a product or service will satisfy the given requirements” is fundamental to the present chapter [2]. Quality cannot be imposed by government through edicts or legislation. It basically results from the management commitment, their systems, culture and the environment within which an organization operates. In view of critical flight safety aspects related to aero materials, inspection/clearance by an independent quality regulatory agency is mandatory, and as such is followed by many countries [3]. The regulatory agency coordinates and ensures establishment of a robust quality system not only by assessing the product testing, but also through controlling the various process parameters, anticipating potential failures during service use, and simulating operational requirements.

This chapter describes in detail the various activities involved during QA, duly covering inspection/testing from raw materials acquisition to the final material/product, critical process control stages, non-destructive testing (NDT), calibration requirements, quality audits, spot/surprise checks, statistical analysis of test data, processing parameters and standard operating practices.

20.2 Importance of QA for Aero Materials

The requirement of an aero store is to execute the requisite mission without hazard to the operator/crew or to the general public. Failure is not an option in an aero system, since the consequences may be grave and catastrophic. The quality requirements are therefore stringent. Quality plans are accordingly put in place to ensure that a defective store is not certified. When the aero store involves material problems the QA scope broadens because of the wide range of processing variables associated with each material. Although different agencies are involved in achieving the desired product quality, the QA group has the prime responsibility for achieving high reliability and flight safety.

20.3 General Categories of Aero Stores

Not all aero stores are highly critical from an airworthiness viewpoint: the stores are broadly divided into the following three categories:

- (i) Flight critical, i.e. airframe and engine components
- (ii) Mission critical, i.e. air armaments (missiles, bombs, etc.)
- (iii) Non-critical, i.e. aircraft internal component parts.

20.4 Quality Management System Requirements for Aero Stores

Manufacturers of aero stores should have QMSs conforming to aerospace specifications AS 9100, EN 9120, etc. [4, 5]. The laboratory testing procedures should be accredited in conformance with NABL requirements [6]. For all special processes, e.g. heat treatment, plating and NDT, the manufacturer ought to establish conformance with NADCAP approval [7]. These guiding requirements provide confidence that the manufacturer's quality system will produce a store that will meet the specifications. At the same time, this provides confidence to the management that the intended quality is being achieved. The principal guiding documents for defence aero stores are described below:

- (i) **DDPMAS-2002** (Procedure for Design, Development and Production of Military Aircraft and Airborne Stores), Ministry of Defence (MOD), Govt. of India, is a document that describes detailed procedures for certification and QA along with the roles and functions of various organizations, including the Directorate General of Aeronautical Quality Assurance (DGAQA), the inspection/clearing authority, and users such as the Indian Air Force, Army Aviation, and Naval Aviation [8].
- (ii) **AFQMS** (Approval of Firm and its Quality Management System). This is a DGAQA document describing the QMS requirements for an approved firm to manufacture aero stores [9]. To deal with the technicality of aero stores along with responsibility of QA officers, firms and subcontractors, an additional DGAQA document called a Technical Standing Order (TSO) is used [10]. The other documents used to develop or produce aero materials/stores are technical specifications (TS), development test schedules (DTS), type test schedules (TTS), release specifications (RS), acceptance test procedures (ATP), quality plans (QP), manufacturing process documents, route cards, log sheets, and test reports.

20.5 Modes of Inspection

Basically, there are two modes of inspection during development and subsequent production phases for aero stores. The first is direct inspection, in which the airworthiness agencies are directly involved in QA activities. The second is called the

surveillance mode, where all inspection and testing activities are carried out by approved QC personnel of the manufacturing agency under the supervision and control of airworthiness agencies. However, all the critical stages of inspection/test/re-verification are checked by the personnel of airworthiness agencies as per respective QP/ATP. The details of the surveillance mode of inspection are indicated in the AFQMS document [9].

20.6 Phases of QA

The production of aeronautical materials is considered acceptable only after satisfactory type certification. During type certification the performances of at least three consecutive heats/batches of the material are analyzed for reproducibility of properties with respect to the development/type test schedule (DTS/TTS). Accordingly, the phases of QA/inspection are categorized as (i) the development phase (qualification testing and type approval), (ii) production phase, and (iii) in-service exploitation phase (i.e. during maintenance, repair, modifications, refurbishment and life extension).

20.6.1 *Inspection and QA During the Development Phase*

During the development phase of an aero store, extensive inspection and testing activities are carried out as part of the QA. For example, the efficacy of the manufacturing process is assessed/analyzed during this phase. The inspection involves stricter analysis of the various process parameters and the consistency of performance. Process consistency is assessed by repeating at least three batches within a similar level of process tolerances.

The important activities as a part of QA are as follows:

- (a) Critical examination of the user requirements and design parameters for finalization of the detailed technical specification of the aero store.
- (b) Examination of various qualification test parameters for satisfying the technical specification requirements, and finalization of the detailed type test schedule accordingly.
- (c) Assessment of the capacity and capability of the manufacturing firm.
- (d) Scrutiny of the process document prepared by the manufacturing agency from the inspectability viewpoint.
- (e) Calibration check of instruments, gauges, furnaces, etc., as per relevant standards: e.g. BS M54 for temperature uniformity in the heat treatment and reheating furnaces; IS 1828 for load calibration of tensile testing machines [11, 12].

- (f) Monitoring of process control from input stage to final product with complete traceability records such as log sheets and route cards.
- (g) Mechanical, metallurgical and NDT testing witness and coordination.
- (h) Coordination of type test results in the type record document.

20.6.2 Inspection and QA During the Production Phase

Once the three type test batches have been assessed and a type-approval certificate has been issued, regular production batches can be taken up after the issue of an RS/ATP document by the QA agency. This document includes various inspection/test stages, a sampling plan and test extraction plans. The tests indicated in the RS or ATP are production level tests. They therefore exclude the special tests which were part of type certification, such as fatigue, long term creep, and high/low temperature tensile and impact tests.

In addition to the critical stages of inspection and testing, the regular and surveillance QA activities (periodic calibration, quality audits and spot/surprise checks) are done during regular production activity. Besides these, statistical quality control (SQC) is used to analyze the large number of materials data generated during the development and production phases of a material. The documentation part is thoroughly checked before the issue of a final inspection note (IN)/clearance letter. The documents include route cards (RCs), inspection/test reports or certificates (TC), marking, packaging, bonded stores details, inspection tags, and records of traceability.

20.6.3 Inspection and QA During the In-Service Exploitation Phase

The activities during this phase relate to the performance shortfalls, failures and defects as reported by the end-user of the aero store. Proper failure and defect analyses are carried out by a joint team comprising the production agency, certification agencies and user representatives. The testing methodology adopted to solve the problem and the complete testing are closely supervised by the QA agency. Based on the findings and recommendations, remedial actions are implemented to avoid any recurrence.

The changes to any operation, including the inspection checklist and testing, are documented and submitted to the certification agencies for their review and approval.

20.7 Inspection/Test Stages for an Aero Material

As part of inspection and quality control of an aero store, the various inspection/test stages checked by the QA agency are as follows:

A. Raw material inspection

- (i) Source of raw material
- (ii) Purity of raw material
- (iii) Scrap quality and quantity
- (iv) Master alloy composition
- (v) Storage condition
- (vi) Raw material inspection and clearance (RMIC) certificates.

B. Primary and secondary melting

- (i) Melt type (virgin or scrap heat)
- (ii) Alloy additions
- (iii) Melting
- (iv) Vacuum leak rate (cold and hot)
- (v) Final chemistry and gas analysis
- (vi) Tapping temperature
- (vii) Conditioning of ingot
- (viii) Identification of ingot (top, bottom)
- (ix) Melt interruption, if any.

C. Processing by forging

- (i) Calibration of reheating furnaces
- (ii) Heating cycles (time–temperature) as per process sheet
- (iii) Degree of reduction per heating cycle
- (iv) Minimum temperature for forging
- (v) Ultrasonic testing (UT) after forging for rough estimation of any cracks.

D. Processing by hot rolling

- (i) Calibration of reheating furnaces
- (ii) Heating cycle as per process sheet
- (iii) Maintenance of furnace atmosphere
- (iv) Maintenance of minimum rolling temperature.

E. Processing by cold rolling, bar and wire drawing

- (i) Condition of rolls (wear and tear),
- (ii) Rolling directions (e.g. unidirectional and cross-rolling),
- (iii) Condition of die for wire drawing,

- (iv) Intermediate pickling or annealing in-between rolling as per process sheet,
- (v) Waviness, flatness, dimensional inspection.

F. Heat treatment

- (i) Furnace temperature uniformity
- (ii) Placement of job thermocouple along with materials during heat treatment
- (iii) Maintenance of proper atmosphere inside the furnace
- (iv) Hydrogen dew point measurement (important for wire annealing furnaces)
- (v) Heat treatment cycle as per process sheet
- (vi) Heat treatment of test samples in calibrated furnaces before testing.

G. Non-destructive Testing (NDT)

- (i) Ultrasonic testing (UT), fluorescent or dye penetrant testing (FPT or DPT), magnetic particle inspection (MPI), radiography and visual examination
- (ii) Tests to be performed by Indian Society for Non-destructive Testing (ISNT)/American Society for Non-destructive Testing (ASNT) level I or level II qualified persons
- (iii) Sensitivity check carried out periodically on DPT/FPT chemicals
- (iv) All NDT equipment should be calibrated and consumables should have valid service life
- (v) All recordable defects properly marked after confirmation
- (vi) All reference blocks used in UT should be of the same material grade as the material being tested and have valid calibrations
- (vii) All NDT reports should be in the proper format and issued by level II or III persons.

H. Metallurgical and mechanical testing

- (i) Macro- and microstructure analysis of ingot/product
- (ii) Grain size, inclusion rating test
- (iii) Hardness, tensile, impact, creep, stress rupture, low cycle fatigue (LCF), high cycle fatigue (HCF), fracture toughness (K_{IC}/J_{IC}): samples are extracted from the product as per QAP and machined to the approved drawings
- (iv) Metrological checks of test samples
- (v) Testing as per standard specifications
- (vi) Each failed specimen test should be repeated with two new specimens. The failure of any one specimen causes rejection of the lot/batch.

I. Final inspection and clearance

- (i) Mobile spectroscopy on each product
- (ii) Visual inspection
- (iii) Dimensional inspection
- (iv) Log sheet/process records verification of all production stages
- (v) All test certificate verification
- (vi) Identification and marking as per applicable scheme
- (vii) Packaging as per specification requirements.

J. Developmental phase additional tests

- (i) High and low temperature tensile,
- (ii) Fatigue (LCF and HCF),
- (iii) Creep/stress rupture test,
- (iv) Fracture toughness,
- (v) Low temperature impact,
- (vi) Impulse testing (viz. tubes),
- (vii) Stress corrosion cracking (SCC) testing,
- (viii) Fatigue crack growth rate (FCGR) testing,
- (ix) Intergranular corrosion resistance (IGCR) test.

20.8 Salient QA Attributes

Production is carried out in accordance with an approved process sheet, ensuring correct sequencing of all suboperations and steps in these operations. Stepwise inspection/testing are carried out as per type test schedule/approved quality plan/ATP/RS.

Unique ingot heat or melt numbers, forging lot number, heat treatment batch number and individual billet/bar/sheet/plate/extrusion/tube/wire/ring serial numbers are generated at respective production stages. Route cards or traveller cards are maintained with complete traceability from the raw material stage to the finished product.

Periodic calibrations of heat treatment furnaces, instruments, gauges, thermocouples and testing machines are monitored regularly. The records of calibration along with product acceptance records, raw material test reports, mechanical and metallurgical reports, gas analysis, NDT and radiographic films are retained for a period of 10 years.

Documentation of all non-conformances is maintained, and internal defect investigation (IDI) is carried out for corrective actions. Articles deemed scrap are clearly identified, separately stored and periodically disposed off. Periodic quality audits and spot checks are carried out for improving overall product quality and yield.

20.9 Important Inspection and Quality Control Attributes

20.9.1 Aluminium Alloys

Many aluminium alloys are used for aero applications in view of their high specific strength. The list of type-approved aluminium alloys is given in Table 20.1. The important inspection and quality test stages for these alloys are as follows:

- (i) The casting of a specific aluminium alloy should be from the similar smelter melt. The casting parameter records for each melt, along with grade identification, is essential. Apart from control of the chemical composition within the specified range, the inclusion control is carried out via PoDFA

Table 20.1 Some of the important type-approved aluminium alloys

Grade of type-approval material	Product	Type-approval number	Type-approved sizes
AA2014, T 652 (HF-15)	Forged bars	1833 dt. 27th Aug 2014 M/s Manjeera forgings	190 mm ϕ \times 900 L 190 mm ϕ \times 500 L
AA2014, T 652 (HF-15)	Forged bars	1705 dt. 18th Jan 2012 M/s DSPL	190 mm ϕ \times 470 L OD 190 \times ID 130 \times 850 L 190 mm ϕ \times 500 L
AA2014, T 652 (HF-15)	Forged bars	Under process, M/s DSPL	190 mm ϕ \times 900 L
AA2014, T 652 (HF-15)	Forged bars	1728 dt. 7th Sept 2012	T W L 20 \times 95 \times 315 20 \times 80 \times 135 20 \times 85 \times 152 75 \times 135 \times 170 95 \times 150 \times 175 95 \times 215 \times 315
AA2219, T8511	Extruded bars	Under process	40 and 85 mm ϕ \times L
AA6082, T651	Extruded bars	Under process	60 and 150 mm ϕ \times L
AA6061	Cold rolled sheets	Under process	1.5, 2.0 and 2.4 mm thickness
Al-356A	Investment cast pedestal unit and gimbal box for light combat aircraft (LCA)	1517	Investment casting

(or any other specified process). Gas content such as hydrogen, oxygen and nitrogen for each melt is ensured to be within the specified limits before further processing.

Developed by Alcan, PoDFA (Trade name) is a method for evaluating the nature and concentration of inclusions. A liquid aluminium sample is taken from the melt pool and poured into a filter crucible under vacuum. When the metal is solidified, the filter along with the residual metal is cut, mounted and polished before being analyzed under a microscope for inclusion contents.

- (ii) Complete homogenization of the cast billet is essential to homogenize the elemental segregation within and around dendritic regions. The rough ultrasonic test (UT) is carried out at this stage to detect major linear/multiple cracks due to solidification shrinkage, segregation and improper homogenization. In the past, high UT rejection has been observed for certain alloys, viz. AA6061 and AA2219 grade, at this stage.
- (iii) The hot working (forging, hot rolling and extrusion) should be performed after proper soaking specified in the process document. The hot reduction ratio should be sufficient to eliminate the cast structure and generate a reasonable degree of work hardening. Working below the recrystallization temperature range is not permissible, since it may cause hot cracking. The grain flow direction during hot working has to be identified and is done by sample extraction.
- (iv) Fine scratch marks, dents and laminations may hamper the formability as well as reducing the structural and mechanical properties. High rejections of low thickness sheets (1.5, 2 mm) of grade AA6061 and AA2219 have been found to be due to scratch marks or roll marks caused by wear and tear of the rolls.
- (v) Heat treatment of aluminium alloys is very important. The heat treatment cycles comprise solution treatment, quenching, controlled stretching/deformation, and natural or artificial ageing as per specified temper designation.

The temperature during solution treatment must be closely controlled: too high temperatures may cause eutectic melting; too low temperatures result in retention of prior coarse precipitates in the final microstructure. Both effects are detrimental to the mechanical properties. Similarly, the ageing treatments also require close control.

The quench delay after solution treatment and the amount of controlled stretching/deformation after solution treatment are important check points. The solution treatment furnace should be of a type where quench delays above 10–15 s are avoided. Controlled stretching/deformation must also be done soon after quenching, generally within 30 min. Longer times can reduce the yield strength, e.g. in AA 2014.

- (vi) Specimen extraction and identification from each heat treatment batch for mechanical testing (destructive and non-destructive) and characterization is very important. Longitudinal specimens are those whose grain flow

direction is parallel to the working direction. The other two main specimen orientations are long transverse and short transverse. There are also tangential and radial orientations for round cross-section products.

- (vii) The microstructure should be free from eutectic melting and segregation. As a result of hot/cold working, the grains are generally elongated in the longitudinal and transverse directions. The grain sizes of these microstructures are measured using the linear intercept method as per ASTM E112. The geometric mean of the grain sizes in three orthogonal planes, such as normal to rolling, long transverse and short transverse directions, is reported as the average grain size. The substructure cell size, if specified, should be measured with precision.
- (viii) During mechanical testing of properly identified specimens the cross-head speed, calibration of the load cell and extensometer, specimen dimensions, gauge length punching and machine alignment should be as per approved test procedure.

For fatigue and stress corrosion specimens the surface finish and fillet radii are very important. For high and subzero tensile testing, proper soaking should be done at the test temperature before testing.

The hardness records after solutionizing and ageing should be maintained and correlated to thermal conductivity: a linear relation between hardness and thermal conductivity is an indication of material homogeneity [13].

- (ix) Aero grade aluminium alloys are generally qualified to A1 class (AMS 2630C) of ultrasonic testing [14, 15]. Care should be taken while drawing the distance amplitude curve (DAC). The DAC should represent a 1.2 mm flat bottom hole (FBH) reference defect for single as well as multiple 0.8 mm FBHs and linear discontinuities. During ultrasonic inspection the defect crossing 50 % of DAC should be recorded. Dye or fluorescent penetrant inspection to detect surface defects should be pre-verified with standard panels having standard size surface discontinuities.

20.9.2 Titanium Alloys

Titanium alloys have high specific and fatigue strengths, and they can also be processed to have high toughness. These alloys are used primarily in aero engines, and also in high load density airframe structures, particularly in high performance aircraft. The list of type-approved titanium alloys is given in Table 20.2. The important QA attributes are as follows:

- (i) The selection of raw materials used to produce titanium alloys is very important. The raw materials should be obtained from approved sources. The oxygen content and purity of Ti sponge are of prime importance. Most of the α or β stabilizers should be added in the form of master alloys, since adding

Table 20.2 Type-approved titanium alloys

Grade and name of type-approval material	Product	Type-approval number	Minimum type-approved size
BT 3-1, $\alpha + \beta$ alloy	Forged and hot rolled bars	639	100 mm forged bars, 30 mm hot rolled bars
BT -9, $\alpha + \beta$ alloy	Forged and hot rolled bars	646	φ 28 h bars
Titan 31A (GTM-Ti-6-4) $\alpha + \beta$ alloy	Forged and hot rolled bars	907	30 φ h bars
Titan 31A (triple melted) $\alpha + \beta$ alloy	Forged and machined bars	908	180 mm φ
Titan 31A (double melted) $\alpha + \beta$ alloy	Feed stock for forging	909	180 φ
BT 5-1, α alloy	Forged and hot rolled bars	733	φ 20 mm h bars, φ 100 forged bars
Titan 23A (GTM-Ti-OT4-1) Near- α alloy	Cold rolled sheets	906	1 mm thick cold rolled sheets
Titan 23A (GTM—Ti-OT4-1) Near- α alloy	Forged and hot rolled bars	910	φ 50 h bars
Titan 26A, Near- α alloy	Forged and machined bars	1293	160 φ machined bars

Fe, Mo, V, etc., in powder form may lead to oxygen pick-up if the powder is exposed to air for too long.

- (ii) Compaction of sponge into briquettes and welding them together should not cause additional contamination. Vacuum arc remelting (VAR, double or triple) is done as specified for particular alloys. The melt rate, arc distance, feed rate, cold leak rate and melt control mechanism specified in the process sheet should be strictly followed. Hot-topping to avoid pipe formation should be performed in the last stage of remelting.
- (iii) The reheating cycle and forging reduction schedule should be followed as per specified process sheet. The heating rate, soaking time/temperature, cooling rate, furnace atmosphere and minimum working temperature are important check points. The macrostructure should reflect no segregation, flakes, ring patterns, freckles, etc. Rough UT should be done after forging to avoid the carrying-forward of defects into the downstream process.
- (iv) Hot or cold forming should be done as per strict reheating and hot/cold working schedule.
- (v) In general, the product supply conditions are annealed and machined, but it is to be noted that for alloys to be used in the heat-treated condition, all

properties should be subsequently evaluated on specimen blanks (sometimes on the product also) to ensure the desired properties.

In $\alpha + \beta$ titanium alloys, UT can be done without any problem. However, the β titanium alloys (under development and yet to be type approved) show very poor UT response [16].

- (vi) Since, titanium alloys tend to have anisotropic (textured) mechanical properties, the orientations of specimens for tensile, fracture toughness and fatigue testing are very important. The longitudinal, long transverse, short transverse, tangential and radial samples should be identified properly. The specimen designation given in ASTM E 399 is followed for fracture toughness testing. Titanium alloys are also deformation (strain)-rate sensitive, so the rate of straining during mechanical testing is very important.
- (vii) The microstructural characterization should be performed with utmost care, since the properties are highly dependent on the amounts and morphologies of the constituent phases, notably for $\alpha + \beta$ alloys. These quantities and parameters have to be checked against the specifications.

20.9.3 Nickel/Iron-Based Superalloys

Nickel-based and some Fe/Ni-based superalloys are the mainstay of the turbine sections of aero engines. The list of type-approved alloys is given in Table 20.3. These alloys contain many additional elements, which have to match with close specifications. Consequently, all the processing requires very close control, and no scrap metal additions are permitted.

The QA requirements for nickel-based superalloy components are very strict:

- (i) Mechanical tests (room temperature tensile, high temperature tensile, creep, low cycle fatigue, high cycle fatigue and stress rupture); metallurgical tests (grain size, γ' as well as γ'' size and shape, the nature of carbides and their distribution, directionality of grains, γ' depleted region, volume fraction of eutectic and other undesirable phases); and physical properties should be evaluated with due care [17, 18].
- (ii) The solution and ageing treatments as well as cooling and heating rates are very important parameters that must be as specified during regular production.
- (iii) The ceramic die size, mould design and other investment casting parameters for cast components (turbine blades and vanes) are established before commencement of production batches.
- (iv) The dimensional tolerances and profiles of components should be strictly followed.

Table 20.3 Type-approved nickel-based and iron/nickel-based alloys

Grade and name of type-approval superalloy	Product	Type-approval number	Minimum type-approved size
Superni 75A, Ni-based	Billets and bars	495	36 φ hot rolled bars
Superni 75A, Ni-based	Forged bars	546	
AE 435, Ni-based	All forms	566	0.3 thick strips, 1.0 thick sheets, 16 φ hot rolled bars
AE 868, Ni-based	All forms	762	0.8 mm cold rolled sheets, 15 φ hot rolled bars, 2.5 φ wire, 70 φ forged bars
AE 437B, Ni-based	Forged, hot and cold rolled sheets	1008	15 φ and 32 φ hot rolled bars
AE 602, Ni-based	Hot rolled and cold rolled sheets	1006	0.9 and 1.2 thick cold rolled sheet
Superni 263A, Ni-based	Hot rolled bars	904	20 φ hot rolled bars, 180 φ forged bars
Superni 263A, Ni-based	Cold rolled sheets	929	1.2 mm thick cold rolled sheets
AE 437A, Ni-based	Hot rolled bars	1007	20 φ and 30 φ , hot rolled bars
ZS6YVI, Ni-based	Remelt stock	1292	80 φ
BZL12Y—VI, Ni-based	Remelt stock	1416	80 φ
Super cast 247A, Ni-based	Remelt stock	1489	80 φ
Superni 718, Fe–Ni based	Cold rolled sheets	1291	2 mm thick cold rolled sheets
Superni 718A, Fe–Ni based	Forged and hot rolled bars	905	160 φ forged bars
Superni 718A, Fe–Ni based	Feed stock for compressor blades	922	20 φ hot rolled bars
Superfer 696 M, Fe-based	Hot rolled and billets	1005	14, 27, 40 φ bars

- (v) Wrought products (forgings, forged bars, hot rolled, hot drawn bars, cold drawn bars and cold rolled sheets) should be hot/cold worked and heat treated strictly as per approved schedule.
- (vi) The UT, DPT and radiography checks require utmost care to ensure sound and defect-free materials.

20.9.4 Steels

Steels with exceptional mechanical as well as physical properties are covered in this category. The list of type-approved special steels is given in Table 20.4. Production and QA of such steels requires special attention, which is enumerated here:

Table 20.4 Type-approved steel alloys

Grade and name of type-approval steel	Product	Type-approval number	Minimum type-approved size
MDN 321A austenitic stainless	Billets and forged bars	322	120 φ forged bars
MDN 321A austenitic stainless	Annealed wires	619	0.5 mm wire
MDN 321A austenitic stainless	Cold rolled sheets	693	1.5 thick cold rolled sheets
MDN 321A austenitic stainless	Cold drawn wires	991	0.35 φ -5 φ wire
MDN 321A (Virgin) austenitic stainless	Hot rolled bars	732	40 and 33 φ bars
MDN 347A austenitic stainless	Hot rolled and forged bars	556	75 φ forged bars and 45 φ mm hot rolled bars
MDN 347 austenitic stainless	Sheets	713	1.2 thick, 3.2 thick
12X18H10T austenitic stainless	Bars, sheets and wires	626	65 φ forged bars, 3.0 mm hot rolled sheets, 0.8 cold rolled sheets, 15 φ hot rolled bars, 0.2 mm φ wire, 0.1 strips
AE 961W martensitic stainless	All forms	614	Forged bars 66 φ , hot rolled bars 12 φ
MDN 431A martensitic stainless	Forged and hot rolled bars	903	125 mm φ forged bars, 20 mm φ hot rolled bars
MDN 431A martensitic stainless	Hot rolled flats	928	6 mm flats hot rolled
MDN 15-5PH precipitation hardening martensitic stainless	Forged and hot rolled bars (non-weldable)	1166	90 φ forged bars, 35 φ hot rolled bars
12X2H4AW low-alloy	Hot rolled bars	640	15 φ hot rolled bars, 56 φ forged bars

(continued)

Table 20.4 (continued)

Grade and name of type-approval steel	Product	Type-approval number	Minimum type-approved size
MDN LA1 (12X2H4AW) Cr Ni case carburizing	Forged bars	992	Forged bars 60, 65, 125 φ
E16NCD13 low-alloy	Forged bars	1294	125 mm φ , forged bars
30XGCN2A high strength low-alloy	Bars and sheets	642	28 φ hot rolled bars, 4 mm cold rolled sheets, 110 φ forged bars
30KHGSA high strength low-alloy	Hot rolled bars	1165	24, 42, 65 φ hot rolled bars
MDN 132A high strength low-alloy	Forged bars	927	180 mm, forged bars
MDN 127A low-alloy	Hot rolled plates and cold rolled strips	1453	9.5 mm thick, hot rolled plate and 3.5 mm cold rolled strip
16XCH (MDNLA2) low-alloy	Cold drawn wires	682	3.4 mm φ wire
MDN 250A maraging	Forged bars	694	215 φ forged bars
MDN 300A maraging	Hot rolled strip	1710	10 mm thick

- (i) The primary melting and/or secondary melting process should ensure strict control over chemical composition as well as homogeneity.
- (ii) The cleanliness of such steels is very important. Also, the gas contents, particularly hydrogen, oxygen and nitrogen, have to be well within the specified limits. The vacuum induction melting (VIM), electro slag remelting (ESR) or vacuum arc remelting (VAR) process parameters are accordingly controlled.
- (iii) The forging temperature and time of soaking is strictly followed as per established process sheet to eliminate the cast structure of the ingot in order to achieve chemical homogeneity throughout the product. Some grades are considered hot transfer grades, wherein the hot ingot from the melt shop is directly transferred to the forge shop for immediate hot working. If the hot transfer of such grades is not feasible, the ingot should be kept at the required temperature as per process sheet requirement until the forging starts.
- (iv) The identification and the grain flow direction are recorded at every stage of forging. The macrostructure test and rough UT is performed at the initial forged-down stage, and defective portions are discarded. This avoids further processing of any existing inhomogeneities.
- (v) Further working (hot rolling, cold rolling, extrusion and wire drawing) as well as heat treatment is carried out within the specified close processing

windows adopted for these special steels. Major deviations are recorded and discussed by a salvage board. Sometimes a few additional tests are suggested for clearance of materials with deviations.

- (vi) Some additional tests are generally required for special steels besides the regular destructive and non-destructive tests, e.g. impact at subzero temperatures, stress corrosion cracking (SCC), intergranular corrosion resistance (IGCR), reverse bend fatigue, fracture toughness (K_{IC} , J_{IC}), grain flow direction and cleanliness.

20.9.5 Composites

Composites can be made from mixtures of three categories of materials, namely metals, ceramics and polymers. A composite structure consists of a matrix material and a reinforcement material, in which the components act together to give the desired characteristics. These materials are extensively used for aerospace applications.

Some applications of these materials are for airframe structural components (carbon fibre reinforced plastics (CFRPs); aircraft brake pads (metal matrix composites and carbon-carbon composites providing elevated temperature strength); and steel wire reinforced rubber tyres and hoses). The important inspection and testing attributes for these materials are given below.

- (i) Each batch of reinforcement material is tested for mechanical properties (tensile strength) and physical properties (density, size, electrical and thermal properties), chemical composition and purity level.
- (ii) Perishable materials (notably adhesives) are checked for their shelf life, storage conditions, and release certificates from the manufacturers prior to their usage.
- (iii) Monitoring of process control from input stage to final product, with complete traceability records such as log sheets, route cards as per the laid down/approved process specification, time-temperature thermograms, vacuum levels, hydraulic pressure checks, working environment, and inspection and clearance of moulding and sintering dies.
- (iv) Inspection and testing of final composite materials, including mechanical properties at room and elevated temperatures, compressive and flexural strength, interlaminar shear strength, microstructural examination, density, thermal conductivity, specific heat, porosity, weight, adhesion test, and functional tests (e.g. friction tests for brake pads).
- (v) Non-destructive testing: UT, CT scans, radiography, for finding flaws, voids and delaminations.

20.10 Summary

Strict Quality Assurance results in defect-free exploitation of aero stores throughout their assigned life. The material costs are only a fraction of the total aircraft costs, so no compromises on quality requirements are permissible. Material production is a process-oriented activity, requiring complete control (e.g. during melting, processing, thermo-mechanical working and heat treatment) from the input stage to the final product. This means close monitoring of critical process parameters with in-process inspections/testing for each batch of material. Since different materials have different characteristics, each will require a specific quality plan for ensuring the final product quality.

Acknowledgments The authors are grateful to DGAQA, Ministry of Defence, Government of India, for constant encouragement.

References

1. Gupta B, Krishna VG (1996) Aerospace materials. S. Chand and Co., Ltd., New Delhi, India
2. Storey A, Briggs R, Jones H, Russell R (2000) Monitoring bathing waters—a practical guide to the design and implementation of assessments and monitoring programmes. In: Bartram J, Rees G (eds) E & FN Spon, New York, USA, pp 49–67
3. European Aviation Safety Agency (EASA) (2014) Acceptable means of compliance (AMC) and guidance materials (GM). www.easa.europa.eu
4. Quality management systems—requirements for aviation, space and defense organizations, Standard AS9100C (2009), SAE International, Warrendale, PA, USA. www.sae.org
5. EN 9120: BS EN 9120:2010, Quality management—requirements for aviation, space and defense distributors. British Standards Institution, London, UK, 2010
6. NABL ISO/IEC 17025: Quality management system (QMS) and technical requirement of energy measurement. Geneva, Switzerland, 2005
7. NADCAP Audit Criteria for Chemical Processing NADCAP AS7108 (1990), National aerospace and defense contractors accreditation program, SAE International, Warrendale, PA, USA. www.sae.org
8. DDPMAS-2002: Procedure for design development and production of military aircraft and airborne stores, (Supersedes DDPMAS-75). Ministry of Defence, Govt. of India, New Delhi, India. ISB: CEMILAC/6003, Aug 2009
9. AFQMS: Approval of a firm and its quality management system. Directorate General of Aeronautical Quality Assurance (DGAQA), New Delhi, India, 2011
10. TSO: Technical Standing Order. Directorate General of Aeronautical Quality Assurance (DGAQA), New Delhi, India, 2002
11. Specification for temperature control in the heat treatment of metals, BS M 54:1982
12. Metallic materials — verification of static uniaxial testing machines, Indian Standard, Part 2: Tension creep testing machines — verification of the applied load, IS 1828 (Part 2): 2002, Bureau of Indian Standards, New Delhi, India
13. ASM International Committee (1990) Properties and selection: nonferrous alloys and special-purpose materials, metals handbook, vol 2, 10th edn. ASM International, Materials Park, OH, USA
14. Inspection, ultrasonic, of thin materials 0.50 inch (12.7 mm) thick, Standard AMS 2630B (1995): SAE International.

15. Inspection, ultrasonic, of thin materials 0.50 inch (12.7 mm) and under in cross-sectional thickness, Standard AMS 2632A (1995): SAE International, Warrendale, PA, USA. www.sae.org
16. Titanium and titanium alloy bar and billet, Standard AMS 2631B (1995): SAE International, Warrendale, PA, USA. www.sae.org
17. Davis JR (ed) (2000) ASM specialty handbook: nickel, cobalt, and their alloys. ASM International, Materials Park, OH, USA
18. Sims CT, Stoloff NS, Hagel WC (eds) (1987) Superalloys II: high-temperature materials for aerospace and industrial power. John Wiley & Sons Ltd, New York, USA

Chapter 21

Fatigue Life Enhancement for Metallic Airframe Materials

L. Molent and S.A. Barter

Abstract This chapter briefly summarises some of the life enhancement and repair techniques available to locally increase the fatigue lives of metallic airframe structures. The chapter concentrates on a broad review of those methods as applied to aluminium alloy aircraft structures, for which most of the techniques have been developed. Although aimed at aluminium alloys, most of these methods are equally applicable to the other metallic airframe structural materials, i.e. steels and titanium alloys. To round out the descriptions of each of the methods, the pros and cons are also briefly discussed based on the experience of the authors in maintaining the structural integrity of several aircraft types.

Keywords Fatigue life enhancement · Residual stresses · Stress concentration reduction · Repairs

21.1 Introduction

Aircraft require highly efficient and durable structures to meet performance and life goals. To achieve this, it is not unusual for manufacturers to rely to some degree on fatigue life enhancement techniques (i.e. methods to increase the fatigue resistance of local and highly stressed details). The locations for these enhancements may be chosen in the design phase or may be identified during testing; or, indeed, during service. It is usual that full-scale fatigue testing (if such a testing has been carried out) reveals locations prone to fatigue cracking that require remedial action and that cannot be easily redesigned, nor can redesign changes treat some problem locations where unanticipated in-service cracking has occurred.

L. Molent (✉) · S.A. Barter
Aerospace Division, Defence Science and Technology Group, Melbourne, Australia
e-mail: Lorrie.Molent@dsto.defence.gov.au

In this chapter several of the more common fatigue life enhancement techniques are briefly summarised and their relative merits discussed. These enhancement methods fall into two broad classes, namely those that are aimed at inducing a local beneficial compressive residual stress field, and those that are aimed at reducing the local operational stresses.

21.2 Life Enhancement via Residual Stress Application

It is well known that fatigue is dominated by the magnitude and range of positive stress excursions, and to a secondary degree the mean stress level of those excursions [1]. Therefore any technique that can reduce the positive stress range and/or mean stress will have a beneficial effect on fatigue (i.e. all other factors being unchanged, an increased fatigue life will result).

One way of achieving this is to induce compressive residual stresses in a material in the region of any potential fatigue crack path, such that the effective tensile cycles that are subsequently experienced are lower and the range is reduced by part of that range becoming negative (i.e. occurring in compression and therefore non-damaging).

Several of the techniques that are used in the aviation industry based on induced residual compressive stresses for the fatigue life enhancement of airframe components are given in Table 21.1 along with their perceived benefits and drawbacks.

It is well known that in most cases, and particularly for the wrought aluminium alloys used extensively in aircraft airframes, fatigue is predominantly a surface phenomenon [1]. Thus many of the compressive residual stress techniques aim to produce a surface layer of compressive residual stress at the location that is considered to be most at risk of cracking.

While these surface residual compressive stresses are well known (as will be shown later in this chapter) to be very good at resisting fatigue crack growth, these stresses are balanced by a tensile residual stress field within the component. This tensile stress region has been sometimes cited as a concern since it may be an area where unexpected fatigue cracking could initiate. To counter this concern, it should be noted that these balancing tensile stresses are usually considerably lower (in their peak) than the reciprocal peak of the compressive stresses and are spread over a larger region of the material than the compressive residual stresses. This is shown schematically in Fig. 21.1, which is a typical residual stress profile for a peened aluminium surface.

Nevertheless the tensile region would appear to give the possibility that cracks would favourably initiate and grow more rapidly within this region than through material with no residual stresses. This is generally not the case for several reasons, two of which are environmental (for the possibility of internal cracking the cracks would grow at a slower rate) and geometry (the cracks would be either fully or partially embedded; or the crack-containing region is remote from any K_t effect, such as from a hole).

Table 21.1 Summary of life enhancement techniques relying on compressive residual stresses

Technique	General description	Pros	Cons	References
1 Shot peening	Small diameter media (e.g. glass, ceramic or metal) with typical diameters from 0.25 to 1 mm are accelerated in a compressed gas to impact a metal's surface and induce deformation and residual stresses that are approx. 0.25–0.5 mm deep. Alternatively, the peening media may be adhered to a rotating flapping wheel	Simple. Portable. Amenable to robotic control. Cheap	Operator dependent. May induce fatigue initiating discontinuities such as laps and folds or embedded media, e.g. broken glass beads in the surface. Can result in a rough surface finish, particularly on softer materials such as aluminium alloys. Such rough surfaces can mask existing cracking. Can lead to unintended part distortion. Edges can be folded over (preventing peening of the covered region) or these may split (producing crack initiators)	[2–11]
2 Split sleeve cold expansion of holes	Plastic deformation through radial expansion (cold working 3–5 % for aluminium alloys) of a hole by sleeving and drawing through an oversized mandrel. Induces a zone of residual compressive stress that may extend radially to about one radius distance around the hole, so typically >1 mm deep	Portable and controlled. Effective even if a small crack less than a radius long exists in the treated hole	Only applicable to holes. May not be applicable to holes with short edge distances since the material between the hole and the edge may yield through the section leaving a complex stress field that can include tensile residual stresses at the edge. Leaves a “pip” at the split in the sleeve that needs to be removed	[11–21]
3 Laser shock peening	A thin liquid layer on a metal's surface is rapidly heated by a high-energy laser pulse, causing it to be vaporised into plasma at temperatures in excess of 10,000 °C. This generates a high-pressure pulse	Controlled and repeatable, usually requiring robotic control. The surfaces of the regions treated retain a smooth finish	Expensive and generally requires the component to be brought to the apparatus. Thin items need to be shocked from both sides at the same time to prevent distortion. Poor control can lead to local melting of	[22–25]

(continued)

Table 21.1 (continued)

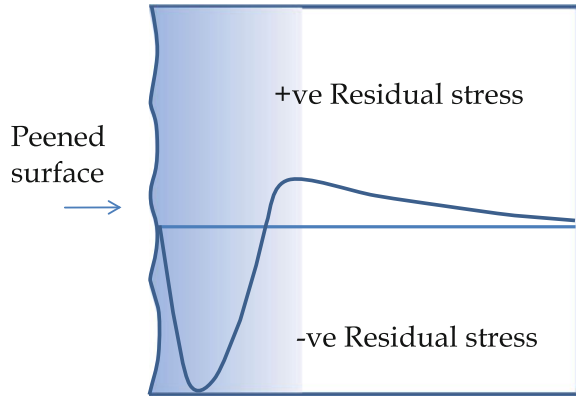
	Technique	General description	Pros	Cons	References
4	Cold burnishing (deep surface rolling)	A high-pressure fluid is used to float a metallic rolling ball in a socket which is hydraulically pressed against the workpiece and rolls freely along a surface to induce plastic deformation and a residual stress layer that is typically at least 1 mm deep. Other simple rolling methods are available	Automated and amenable to robotic control. Excellent surface finish after rolling	<p>the surface of the components. The generation of excessively powerful pulses or the interaction of these pulses when applied from opposite sides of a component can result in internal bursting of materials with poor short transverse strength properties</p> <p>Requires component to be brought to apparatus. Thin items need to be rolled from both sides at the same time to prevent distortion. Shapes other than very simple ones are difficult to treat. Edges are difficult to treat and may be damaged if the roller gets too close or they have a small radius</p>	[11, 26, 27]
6	Interference fit fasteners and bushings	The fastener insertion/locking process induces radial compression (typically 5 %) as well as supporting the hole (i.e. reducing the stress concentration factor under cyclic loads)	Controlled and repeatable and in very common practice	<p>More production intensive and expensive than neat-fit fasteners. For bushes, sensitive to application technique. Holes in soft materials, such as aluminium alloys, may be broached by bush insertion. This can lead to loss of the pressure that the bush applies to the hole surface to impart the compressive stress, and hole surface damage that can initiate cracking, e.g. see [33]. Inspection may be difficult</p>	[28–34]

(continued)

Table 21.1 (continued)

Technique	General description	Pros	Cons	References
7 Shrink fit fasteners or bushings	Similar to interference fit, but achieved by inserting the fastener or bushing as-cooled and allowing it to expand on reaching room temperature to achieve the radial compression	Effective if carried out correctly. Bush can be made of a material more durable than the hole itself, i.e. capable of bearing loads	Sensitive to application technique as in the case of interference fit fasteners or bushings	
8 Cold coining	A hole is straddled by two dies with raised rings (ring thickness may be ≈ 1 mm) which are squeezed to produce deformation rings adjacent to the perimeter of a hole. This produces a ring of residual stresses adjacent to the hole	The process is simple and can be positively identified through the visibly compressed surface rings	Requires access to both sides of the item. Non-concentric (to the hole) rings may be produced due to final hole placement in stack-ups. Cracking may be detected in the bore of the hole since balancing tensile stresses may be formed there. However, this cracking will (by design) be retarded when it grows into the compressive rings	
9 Cold expansion of bushings in holes	Cold expanding a bush that has been placed in a hole via drawing a mandrel through it in a similar manner as the split sleeve process. The bush induces radial compression in the wall of the hole as well as supporting the hole (i.e. reducing the stress concentration factor under cyclic loads)	Controlled and repeatable. Broaching is avoided. Large holes can be treated. The bush can be made of a material more durable than the hole itself	More production intensive and expensive than neat-fit bushings or fasteners. Bushing covers the surface of the hole, making inspection difficult. The bushing may not cover all the hole's surface owing to end chamfers, and cracking can develop at these locations	[19, 34]

Fig. 21.1 Schematic diagram of residual stress distribution below a peened surface. With traditional bead peening techniques this compressive layer generally extends to between 0.2 and 0.5 mm below the surface in most materials



Environmental Considerations For internal subsurface initiation, which is an insidious form of cracking that is sometimes possible, an environmental effect on fatigue is absent in several structural alloys, fatigue crack growth can be very sensitive to the environment, particularly from hydrogen that has been dissociated from moisture in the air by the newly formed surface produced by a growing fatigue crack. As an example, fatigue crack growth in aluminium alloys (and others) is accelerated by the presence of atmospheric moisture. However, for a subsurface crack, initiation and growth will occur *in vacuo*. For aluminium alloys the lack of moisture in an embedded crack will considerably slow crack growth, typically by about ten times the rates observed for surface initiating cracks.

Geometrical Considerations In addition to atmospheric considerations, geometry is also influential on initiation and crack growth. For instance, an embedded crack has two ends and is therefore effectively half the size of a crack of the same length where one end of the crack is at the free surface of, say, a hole. Additionally, for initiation, surface discontinuities (e.g. pits from manufacturing chemical processes, marks, scratches and tears from machining) tend to be larger and more numerous than internal discontinuities (inclusions, porosity in wrought material etc.), promoting surface initiation.

Finally, should a crack initiate in the region of the peak of the balancing tensile residual stress, it will still be retarded in its growth from the end that is growing towards the compressive residual stress field, and this will retard its overall growth rate.

21.2.1 Application of Residual Stresses

Choice of Techniques The choice of the most applicable technique will consider many factors: accessibility to the area of interest and possible contamination (e.g. by peening media) of the surrounding areas, cost, repeatability/reliability, the area

or feature to be treated, the material, local configuration of the component, the cyclic stresses that will be applied in the region of interest, the principal tensile direction, the effect that any residual stresses may have on the corrosion resistance of the component (particularly stress corrosion resistance), the scatter in the required life improvement factor ($LIF = \text{Enhanced life}/\text{Original life}$) and its relationship to the expected service stresses and the depth of the residual stresses produced. More information on LIFs is given in Sect. 21.4.

Incomplete Removal of Cracks Care must be taken when using residual stress methods to ensure correct application and that any fatigue cracks present (typically those below non-destructive detectability thresholds) are accounted for: i.e. they have been removed prior to the application of the method, or are at least no deeper than the effective depth of the compression induced by the method (preferably much shallower than this).

Assurance of this is, in itself, very difficult when these techniques are applied retrospectively to structure that has already seen service loading. This leads to a preference for methods that produce deep compressive stress layers such as hole cold expansion, laser shock peening and surface rolling (low plasticity burnishing), that produce residual compressive layers of similar sizes (depths) to the crack sizes at the non-destructive inspection (NDI) detection limits for aircraft in service.

When cracking below the NDI detection limit is a possibility, i.e. a crack could be missed when one of these methods is applied, and the crack tip is within or near the final compressive residual stress layer, it may not be as detrimental as could be expected from its size alone. During the application of some methods, most notably hole cold expansion, the region with the compressive residual stress field is first stretched and if a crack is present and not very large, its tip may also be stretched to form a strong plastic zone around it that on relaxation may form a strong compressive zone about the crack tip. This highly localised stress field can be stronger than the surrounding material's compressive stress field, and so produce a strong local retardation effect at the crack tip even if it extends a little further than the residual stress zone formed around the remainder of the hole. As a result of this, there are several reports of good fatigue enhancement of cracked holes by cold expansion, Refs. [16, 38, 39]. Notwithstanding all the above considerations, it must be noted that maintenance authorities and aircraft operators are reluctant to leave cracks in holes treated by cold expansion.

21.3 Life Enhancement via Stress Concentration Reduction

It is not uncommon for fatigue cracks to initiate at stress concentrations or geometrical discontinuities. Therefore these potential sources of fatigue crack initiation are normally eliminated during design by the control of local geometry. However, some unanticipated cracking at local details may often occur during full-scale

fatigue testing or service. This is normally rectified through further design changes, or retrofit or modification programmes to address these locations in aircraft already in service.

Some techniques for reducing stresses to enhance fatigue life are summarised in Table 21.2 and Refs. [2, 11]. One means of repair is through re-profiling the shape of a location. Such repairs aim at improving the local geometry by optimisation of the shape of any blend (to remove a crack, corrosion or other damage), thereby leading to lower stress peaks at the detail and improved fatigue resistance, even though the *overall* stress has been increased in the local section.

Table 21.2 also provides some details on the means of optimising local geometry, including those where mechanical blends are required. The latter are common repair solutions for surface corrosion, scratches and dents.

21.4 Life Improvement Factors for Residual Stress Methods

A LIF is usually established for each of the life enhancement techniques summarised in Table 21.1. The LIFs are used in design as well as establishing new lives for in-service modifications. All of the techniques listed in Table 21.1 can produce significant LIFs when applied correctly, for example see Figs. 21.2, 21.3 and 21.4.

However, it must be stressed that the LIFs quoted in the literature are related to a specific technique and are only applicable to the material, spectrum and stress level cited. Therefore for many applications a series of coupon tests may be necessary to develop the appropriate LIF for a specific application. It should also be noted that for techniques that rely on induced compressive residual stresses for fatigue life enhancement, the LIFs can be reduced if the local stresses exceed yield, since the residual stresses can be lost through this yielding.

By way of example, a series of simple “dogbone” (waisted flat plate) coupons of aluminium alloy (AA)7050-T74511 were peened and tested with a wing root bending moment spectrum at different peak stress levels. The mean LIF (compared to unpeened coupons) for the four stress levels is plotted in Fig. 21.5 and a curve has been fitted. This shows that for this particular case the LIF would drop to 1 when the spectrum peak stress is equal to the yield strength of this material.

Further, while it is not uncommon to have fatigue life enhancement techniques applied to production aircraft and, importantly, to the fatigue certification test article, to the authors’ knowledge no aircraft regulatory agency will allow the use of LIF values for in-service applications unless the repeatability and quality of the application can be assured. For peening this may mean that there will be a requirement for the process to be automated by such a method as “robotic peening” since hand peening of complex shapes can produce high scatter in the results.

Table 21.2 Summary of life enhancement techniques relying on stress peak reduction

Technique	General description	Pros	Cons	References
1 Reshaping, and/or adding material during design	Conventional design practice if any location is suspected to have inadequate fatigue life. Includes machining of shallow radii, thickening local regions (i.e. around holes) and introducing doublers as part of the design	Ideally all structures and particularly structural details are based on good design practices and assumptions, and the aircraft is operated not longer than its design life	Unfortunately, not all structural details may be adequately designed. Manufacturing may introduce local features that are not fatigue resistant or contain discontinuities. Service loading may be found to be different from the design cases. The aircraft's life may exceed the design goals	[35, 36]
2 Conventional fastened doubler repair	Doublers are simple and often effective at reducing stresses in a location of a component that is highly stressed or contains cracking, corrosion or mechanical damage. Such doublers are usually fastened in place by bolts or rivets	Simple and applicable in many cases	Requires a good understanding of the loading. Introduces new stress-raising details in the form of additional fastener holes. Covers up critical areas and makes these difficult to inspect. May give a false sense of security through the assumption that any damage under the doubler will not grow. Fastened doublers can also lead to corrosion problems due to poor sealing of the interface	[35, 37–41]
3 Bonded repair	Alternative to conventional fastened doubler that does away with the fasteners and the holes that these require	More efficient. No new stress concentrations due to additional fasteners. Doubler stiffness and strength can be more easily tailored to local loading by using tailored composites. Boron and aluminium oxide composites are non-conductive so that eddy current inspection is possible through them. The sealed interface limits any corrosion under the doubler	Very process- and surface finish-dependent. Often requires heat to cure the adhesive and pressure/vacuum to remove air bubbles from the bond line. Bond line effectiveness difficult to qualify non-destructively. Thermal mismatch may lead to undesirable residual stresses. Stress concentrations may exist at the ends of the doubler if it is not suitably tapered	[42, 43]

(continued)

Table 21.2 (continued)

Technique	General description	Pros	Cons	References
4 Laser cladding	A form of additive manufacturing where a high-powered laser is used to melt metallic powder (about 50 µm diameter) carried in an inert gas (e.g. argon) to produce a layer/s that is welded to a surface	Can restore geometry of damaged component or can build-up areas to reduce local stresses	Produces a heat-damaged zone and introduces residual stresses that are usually tensile at the surface and therefore can be damaging by fatigue. Usually requires the component to be brought to apparatus. Potential for subsurface defects, e.g. lack of fusion, cracking, brittle zones and soft zones. Yet to be adequately qualified for aircraft aluminium materials	[44-47]
5 Reshaping a critical detail by material removal (including optimisation of the shape)	Mechanical blending is often used to remove damage such as surface cracks and corrosion. The shape of the blend can be optimised to minimise the resulting stress concentration using iterative computational techniques	Simple. Can be used to remove damage (e.g. cracks, corrosion and other damage types) while also reducing peak stresses by tailoring the final shape	Even when extending the blend to cover the expected depth of non-detectable cracks, the possibility of a crack existing still remains, which usually requires an additional "confidence cut". Simple radial blends may produce a significant stress concentration if not optimised. Blending removes any surface protection. Limited to locations where the new shape does not compromise residual strength. Optimisation requires complex models of the geometry and representative loads for design, and specific tooling for application	[9, 48, 49]
6 Stop drilling	A small hole is drilled a few millimetres ahead of a crack. It is good practice to ream and cold work the hole. It should also be plugged before reinforcing the area with a doubler.	Does not require the crack to be removed, thus facilitating a simpler repair	Risk that the hole will not remove the tip of the crack and the cracking will continue unretarded. The hole may not be applied at the crack tip and the crack can then run around it. The time for	[15, 50, 51] (continued)

Table 21.2 (continued)

Technique	General description	Pros	Cons	References
7 Other	<p>(Note: a bonded composite doubler provides an alternative approach [42])</p> <p>Welding: many types but only appropriate in specific cases and rarely for the high strength aluminium alloys used in airframes</p>	<p>Welding is well understood, easy to apply and can be automated</p>	<p>re-initiation of the crack from the other side of the hole may be similar to the time that it would have taken for the crack to grow to that position, giving no advantage</p> <p>Many welding difficulties with airframe materials are well known, and post-weld heat treatments are usually required as a minimum. High strength aluminium alloys are generally unsuitable for weld repair unless the process is very tightly controlled or the heat input (FSW) is relatively low. Besides the heat-affected zones, the residual stresses may cause problems</p>	[52]
	<p>Friction-stir welding (FSW)</p> <p>Supersonic particle deposition (SPD) or cold spray: A relatively new process for depositing metal by accelerating metallic particles to high speed in an inert gas and impacting them on the surface of the part to be built up</p>	<p>FSW has potential to address some of the drawbacks of conventional fusion welding for high strength aluminium alloys</p> <p>SPD is automated with limited mobility. Deposition rates are very high and the heat input very low. Adhesion, when good, allows load transfer to the coating</p>	<p>FSW has greater potential than conventional methods for surface build-up, welding-up cracks and surface modification.</p> <p>SPD is currently useful for surface build-up but not for fatigue enhancement. The adhesion is yet to be proven as adequate in highly stressed regions. The equipment for these processes remains bulky and generally requires robotic manipulation of the process head</p>	[53]

Fig. 21.2 Crack growth from unpeened (*open symbols*) and peened surfaces (*solid symbols*) of flat plate AA7050-T7451 specimens tested under an aircraft wing spectrum (*block*) at a peak stress level of 390 MPa. Note the increased initiating discontinuity size and the decreased growth rate in the peened specimens [7]

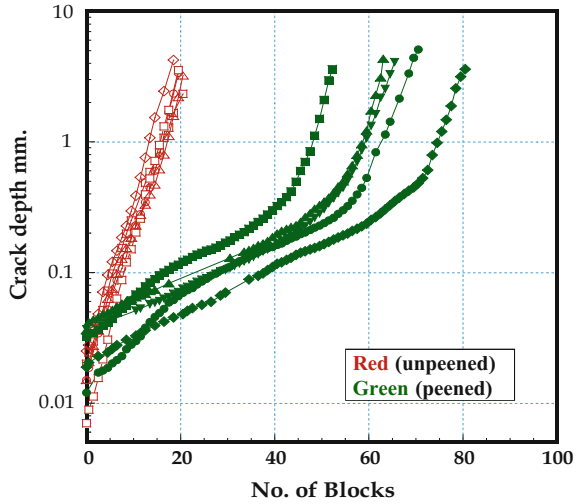


Fig. 21.3 Fatigue life improvement in AA2024-T851 specimens tested under constant amplitude loading [19]

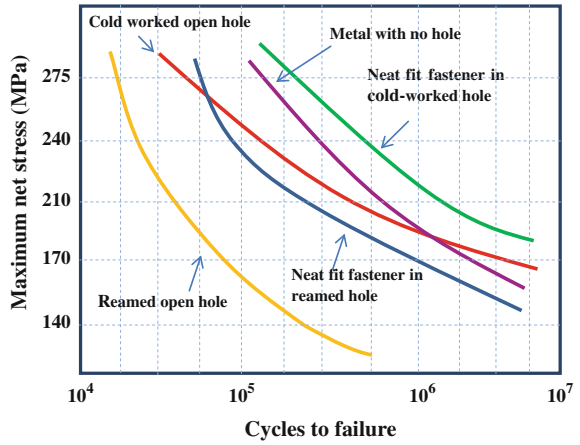
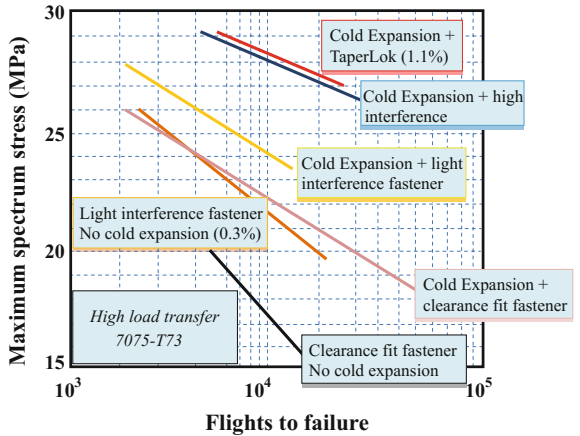


Fig. 21.4 Cold expansion with interference fit fasteners in a AA7075-T73 high load transfer joint [19]



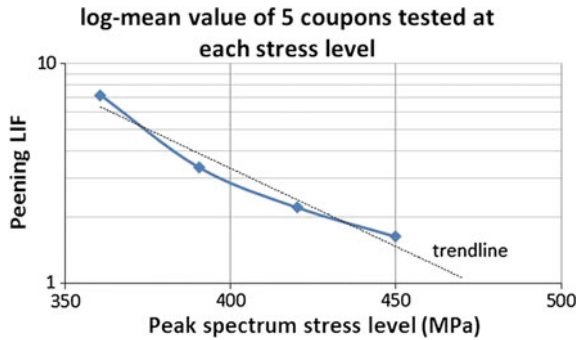


Fig. 21.5 A plot of the LIF versus the peak stress for a wing root bending moment spectrum applied to flat dogbone test coupons with peened versus unpeened surfaces. The material was aluminium alloy AA7050-T74511 with yield strength of 470 MPa. The exponential fit (trendline) indicates that the LIF would drop to about 1 if the peak stress equalled the yield stress of the material

21.5 Conclusions

The many fatigue enhancement methods available to the designer and the service engineer can enable the control of fatigue cracking in aircraft airframes while maintaining a light and efficient structure capable of resisting high service stresses for long lives. However, poor application of these methods can have the opposite effect. Thus a thorough understanding of the pros and cons of these methods is required, as is an understanding of the potential for fatigue cracking in a structure, and what the driving issues are.

It is important to treat each application of fatigue life-enhancing methods on a case-by-case basis, having weighed the pros and cons of the method being considered and the many issues associated with the location to be treated. The reader is referred to some aircraft accidents where, amongst other causal factors, it was found that poor repairs or poor application of life enhancement methods contributed to the accidents, see for example Refs. [33, 35–41].

References

1. Schijve J (2003) Fatigue of structures and materials in the 20th century and the state of the art. *Fatigue* 25:679–702
2. American Society for metals shot peening and other surface working process. Metal Progress, Cleveland, OH, USA, 1947
3. Sharp PK, Clayton JQ, Clark G (1994) The fatigue resistance of peened 7050-T7451 aluminium alloy—repair and re-treatment of a component surface. *Fat Fract Eng Mater Struct* 17(3):243–252

4. Sharp PK, Liu Q, Barter SA, Baburamani P, Clark G (2001) Fatigue life recovery in aluminium alloy aircraft structures. *Fat Fract Eng Mater Struct* 23:S31–S37
5. Barter S (2003) Fatigue crack growth in 7050T7451 aluminium alloy thick section plate with a glass bead peened surface simulating some regions of the F/A-18 structure. DSTO-TR-1477, Melbourne, Australia
6. Sharp PK, Clark G (2001) The effect of peening on the fatigue life of 7050 aluminium alloy. DSTO-RR-0208, Melbourne, Australia
7. Forgues S, Brosseau J (2005) Evolution of Shot peening on the CF-18: from OEM to Robotic. In: *Proceedings of ICSP9*, Paris, France
8. Martin P (1999) Use of shot peening to improve fatigue life of the CF-18 life limited locations. CASI conference, Montreal
9. Molent L, Barter S, Main B (2008) Life assessment and repair of fatigue damaged high strength aluminium alloy structure using a peening rework method. *Eng Fail Anal* 15:62–82
10. Zupanc U, Grum J (2010) Effect of pitting corrosion on fatigue performance of shot-peened aluminium alloy 7075-T651. *J Mater Process Technol* 210(9):1197–1202
11. McClung RC (2007) A literature survey on the stability and significance of residual stresses during fatigue. *Fat Fract Eng Mater Struct* 30(3):173–205
12. Finney JM, Evans RL (1995) Extending the fatigue life of multi-layer metal joints. *Fat Fract Eng Mater Struct* 18(11):1231–1247
13. Finney JM, Niessen C, Absolom N, Lemm K (1996) Strength and fatigue life enhancements of cracked metal. DSTO-TR-0434, Melbourne, Australia
14. Finney JM (1993) Cold expansion and interference for extending the fatigue life of multi-layer joints. ARL-RR-17, Melbourne, Australia
15. Callinan RJ, Wang CH, Sanderson S (1998) Analysis of fatigue crack growth from cold-expanded/interference fitted stop drilled holes. DSTO-TR-0704, Melbourne, Australia
16. Clark G, Pell RA (1992) Experimental and theoretical analysis of fatigue crack growth at fastener holes in an aluminium alloy. *Trans Multi-Discip Eng Aust GE16*(2)
17. Evans RL (1996) Effect of plate thickness on the in-plane and through thickness stresses at a hole. DSTO-TR-0330, Melbourne, Australia
18. Heller M, Evans RL, Allan RB (1999) Cold expansion tests for plates containing elongated holes. DSTO-TN-0233, Melbourne, Australia
19. Reid L (2008) Answers to hole cold expansion working questions you were afraid to ask. In: *Proceedings of 11th Joint NASA/FAA/DOD conference on aging aircraft*, Phoenix Arizona, USA, 21–24 April 2008
20. Ozelton MW, Coyle TG (1986) Fatigue life improvement by cold working fastener holes in 7050 aluminum. In: *Fatigue in mechanically fastened composite and metallic joints*. ASTM STP 927, pp 53–71
21. Heller M, Jones R, Williams JF (1991) Analysis of cold-expansion for cracked and uncracked fastener holes. *Eng Fract Mech* 39(2):195–212
22. Gujba AK, Medraj M (2014) Laser peening process and its impact on materials properties in comparison with shot peening and ultrasonic impact peening. *Materials* 7(12):7925–7974
23. Polin L, Bunch J, Caruso P, McClure J (2011) F-22 program full scale component tests to validate the effects of laser shock peening. In: *Proceedings of ASIP conference 2011*, San Antonio, TX, USA
24. Montrose CS, Wei T, Ye L, Clark G, Mai YW (2002) Laser shock processing and its effects on microstructure and properties of metal alloys: a review. *Fatigue* 24(10):1021–1036
25. Rankin J, Heidenberger T, Campbell J, Hackel L, Mills T (2013) Laser peening for enhanced fatigue lifetime of Navy aircraft. In: *Proceedings of 4th international conference on laser peening and related phenomena*, Madrid, Spain, 6–10 May 2013
26. Zhuang W, Liu Q, Djugum R, Sharp PK, Paradowska A (2014) Deep surface rolling for fatigue life enhancement of laser clad aircraft aluminium alloy. *Appl Surf Sci* 320:558–562
27. Prev y PS, Cammett JT (2004) The influence of surface enhancement by low plasticity burnishing on the corrosion fatigue performance of AA7075-T6. *Int J Fat* 26(9):975–982

28. Mann JY, Machin AS, Lupson WF, Pell RA (1983) The use of interference-fit bolts or bushes and hole cold expansion for increasing the fatigue life of thick-section aluminium alloy bolted joints. ARL-Structures Note-490, Melbourne, Australia
29. Carey RP (1972) Experimental determinations of strain fields resulting from interference fit tapered pins. ARL-Structures and Materials Note-377, Melbourne, Australia
30. Champoux RL, Landy MA (1986) Life enhancement and high interference bushing installation using the ForceMate bushing installation technique, In the proc of Fatigue in Mechanically Fastened Composite and Metallic Joints. ASTM STP 927:39–52
31. Finney J (1993) Cold expansion and interference for extending the fatigue life of multi-layer metal joints. DSTO ARL, Research Report 17, Oct 1993
32. Petrak GJ, Stewart RP (1974) Retardation of cracks emanating from fastener holes. *J Eng Fract Mech* 6:275–282
33. Viscount 720C aircraft VH-RMQ near Port Headland Western Australia, 31st Dec 1986, Dept of Civil Aviation, Air Safety Investigation Branch, Melbourne, Australia, Sept 1969
34. Reid L (2001) Applying the damage tolerance approach to expanded bushing and rivetless nut plate installations. In: Proceedings of 26th ICAF symposium, Montreal, 1–3 June 2001
35. Aviation Safety Council report: Aviation Occurrence Report: In-Flight Breakup Over the Taiwan Strait Northeast of Makung, Penghu Island, China Airlines Flight Ci611, Boeing 747-200, B-18255, May 25, 2002, Published in two volumes in 2005
36. Wanhill RJH, Molent L, Barter SA (2015) Milestone case histories in aircraft structural integrity. Reference module in materials science and materials engineering, Elsevier Inc., 2016
37. Anon, Aircraft Accident Investigation Report Japan Air Lines Co., Ltd. Boeing 747 SR-100, JA8119 Gunma Prefecture, Japan Aug 12, 1985
38. Update on Investigations of Firefighting Airplane Crashes in Walker, California and Estes Park, Colorado, National Transportation Safety Board, Sept 24, 2002
39. Visick J (1991) Damage tolerance/maintenance of airworthiness—an operator’s viewpoint. In: Proceedings of international conference on aircraft damage tolerance assessment and repair, Melbourne 26–29 Aug 1991
40. Tiffany CF, Gallagher JP, Babish CA (2010) IV. Threats to aircraft structural safety, including a compendium of selected structural accidents/ incidents. ASC-TR-2010-5002, AFBWP, OH, USA
41. Aircraft Accident Report-Aloha Airlines, flight 243, Boeing 737-200—N73711, near Maui, Hawaii, 28 April 1988
42. Baker A, Rose F, Jones R (2002) Advances in bonded composite repair of metallic aircraft structure, vol 1. Elsevier Science Ltd., Amsterdam
43. Jones R, Barter S, Molent L, Pitt S (2005) Crack patching: an experimental evaluation of fatigue crack growth. *Compos Struct* 67:229–238
44. Liu Q, Janardhana M, Hinton B, Sharp K (2011) Laser cladding as a potential repair technology for damaged aircraft components. *Struct Integrity* 2:314–331
45. Liu Q, Elambasseril J, Sun S, Leary M, Brandt M, Sharp PK (2014) The effect of manufacturing defects on the fatigue behaviour of Ti-6Al-4V specimens fabricated using selective laser melting. *Adv Mater Res* 891–892:1519–1524
46. Sexton L, Lavin S, Byrne G, Kennedy A (2002) Laser cladding of aerospace materials. *J Mater Process Technol* 122(1):63–68
47. Steffen N, Siegfried S, Eckhard B, Karl-Hermann R (2007) Laser beam build-up welding: precision in repair, surface cladding, and direct 3D metal deposition. *J Therm Spray Technol* 16(3):344–348
48. Burchill M, Heller M (2003) Optimal notch shapes for loaded plates. *J Strain Anal* 39(1):99–116
49. Schnack E (1979) An optimization procedure for stress concentrations by the finite element technique. *Int J Numer Meth Eng* 14:115–124
50. Chen GX, Heller M, Wang CH (2002) An alternative stop drilling method for life extension of fatigue cracks. In: Hu DS (ed) *Structural integrity and fracture*. Pub Swets & Zeitlinger B.V. Lisse, The Netherlands

51. Finney JM, Neissan C, Absolom N, Lemm K (1996) Strength and fatigue life enhancements of cracked metal. DSTO, Technical Report DSTO-TR-9434, Oct 1996
52. Fratinia L, Zuccarellob B (2006) An analysis of through-thickness residual stresses in aluminium FSW butt joints. *Int J Mach Tool Manufac* 46:611–619
53. Jones R, Molent L, Barter S, Matthews N, Tamboli D (2014) Supersonic particle deposition as a means for enhancing the structural integrity of aircraft structures. *J Fatigue* 68:260–268

Chapter 22

Structural Health Monitoring

Prakash D. Mangalgiri and Kota Harinarayana

Abstract This chapter describes and discusses the evolution of structural health monitoring (SHM) technologies for aircraft. The introduction gives the importance of SHM, its application potential and the principal constituents. This is followed first by a description of strain monitoring systems and HUMS and then of damage monitoring systems. Two major classes of techniques—namely acoustic waves and fibre optics—are described and reviewed. A few applications are also highlighted. Issues and strategies for implementation of SHM are discussed, indicating the path forward.

Keywords Structural health monitoring · Health and usage monitoring systems · Damage monitoring · Sensing · Acoustics · Fibre-optics · Interferometry · Fibre bragg gratings · Certification

22.1 Introduction

Structural health monitoring (SHM) has evolved as a strategy to ensure safety and availability of a structure for intended operations at an economical cost of servicing and maintenance. The emphasis in SHM is on damage assessment and involves both “Diagnosis” and “Prognosis” (D&P).

In aircraft parlance, the assessment of damage may be direct or indirect but is usually aimed at assessing “consumed life” or “residual life” or “residual strength”,

Prakash D. Mangalgiri—Currently, Private Consultant, Bangalore.

P.D. Mangalgiri
Aeronautical Development Agency, Bangalore, India
e-mail: pdmgiri@yahoo.com

K. Harinarayana (✉)
IIT Bombay, Powai, Mumbai 400076, India
e-mail: hnkota@yahoo.com

or similar parameters that aid in decision-making about the safety of operation and/or the period of safe operation.

Recent advances in the understanding of complex damage mechanisms in materials and in mechanics of structures, along with developments in sensor technology, smart materials and electronics; and even more so, the advances in computational and computer technology have given SHM a high position. These advances are enabling development of SHM systems that can be capable of complete assessment of “health” and integrity of the structure (i.e. diagnostics), with an assessment of residual life or strength (i.e. the prognostics), and with or without continuous monitoring.

Some of the specific application scenarios for SHM of aircraft include:

- life extension of ageing aircraft with monitoring of multiple site damage (MSD) and widespread fatigue damage(WFD)
- reduction of maintenance downtime through optimal scheduling of inspections and use of rapid non-destructive evaluation (NDE) techniques on the ground
- incorporating an SHM system in a new aircraft to ensure structural integrity on a much more economical scale and providing condition-based maintenance rather than a scheduled one
- ensuring structural integrity of composite structures through detection of hidden damage.

A typical SHM system has the following components:

- (i) A *Sensing* system which collects information about the structure from certain parameters.
- (ii) A *Diagnoser*, which analyses the information from the sensors through a built-in knowledge base and a reasoning system, and assesses the damage condition.
- (iii) A *Prognosis unit* which makes predictions about the damage growth or remaining useful life or residual strength, via analyses of the damage information and a built-in knowledge base and reasoning system.
- (iv) A *Supervisory system* which oversees the operation of the SHM system and acts as a decision aid for the user.

In advanced versions, one may incorporate “learning” based on the damage and its growth in service, thus leading to more accurate D&P.

Over the years, the evolution of SHM in aircraft has followed two main, often complementary, strategies:

- (i) Monitoring of loads or strains or damage or a combination of some or all of these with the intention of arriving at Remaining Useful Life (RUL) and/or residual strength, and/or setting up inspection intervals for safe operation of the aircraft. Some of these systems have evolved into health and usage monitoring systems (HUMS) which currently use strain sensors extensively.
- (ii) Developing rapid NDE (RNDE) technologies to reduce the inspection time on the ground, often obtaining help from on-board sensing systems.

In recent years, with evolution of the new paradigm of Integrated Vehicle Health Management (IVHM) encompassing all or several of the aircraft systems, SHM is becoming a part of the IVHM strategy and issues alerts. These alerts serve as early warnings or notifications to take suitable actions “in-advance”, thereby ensuring mission readiness and safety rapidly and economically.

A good account of developments in SHM in general, and for aircraft in particular, can be found in several conference proceedings, monographs and books, see for example Refs. [1–6]. In what follows, the current state of the art is reviewed, especially in the context of the Indian aerospace scenario. The discussion is focussed on major constituents of an SHM system as mentioned above, namely sensing systems and the D&P methodology. A few related aspects from the viewpoint of practical application of SHM technology are also discussed.

22.2 Health and Usage Monitoring Systems (HUMS)

Actual operation of an aircraft usually differs significantly from that assumed at the design stage, particularly for tactical aircraft owing to several reasons such as mission-mix changes, flight envelope expansions, equipment and payload changes or enhancements, mass and configuration changes, and increased engine thrust. Load monitoring therefore assumes great significance in determining the actual “life” consumed (or used or expended) or actual “damage” caused, and consequently arriving at remaining useful life (RUL).

In the case of aircraft (or their structural components) designed on the basis of the safe-life fatigue design philosophy, the damage calculations will directly influence the life-extension strategy (should life extension be feasible). For damage tolerant designs the knowledge of actual loads and usage influences the calculation of (safe) crack growth intervals and determination of conservative inspection schedules.

Traditional load monitoring systems have used on-board g-meters. The g-excursions are then related to expended fatigue life by analytical means, relying often on a simple cumulative fatigue damage rule, e.g. the Palmgren-Miner rule.

The next step was to use several other recorded flight parameters to estimate the loads and/or local stresses at critical locations on the aircraft, and use this information to arrive at the expended life at these locations. The fatigue damage analyses also became more refined, using advanced theories of damage accumulation and extensive material and component test data. However, the conventional analysis methods have been generally time-consuming and cannot be implemented in a real-time or concurrent time scenario.

An improvement on such methods is to use flight history data and create a database mapping the flight parameters into local stresses at critical locations, using methods such as artificial neural network or Gaussian regression, for example see Refs. [7, 8]. Further, as newer technologies became available, the strains at the

critical locations could be directly measured and monitored. These strains could then be converted to stress cycles to derive expended life using cycle counting techniques such as “Rainflow” [9] and an appropriate cumulative damage rule [10]. These more advanced methods have given rise to the HUMS philosophy.

HUMS has its origin from helicopters, where vibratory data were used to assess rotor blade life. HUMS continues to be a basic system on helicopters, but it is now being implemented on fixed-wing aircraft, especially fighters. A good historical review of usage monitoring in helicopters and other aircraft can be found in [11]. It has recently been reported that the Eurofighter uses a HUMS system: strain sensors at 20 points in the airframe send data, collected 16 times a second, to a central processing and data storage unit [12]. In India the Light Combat Aircraft, Tejas MkI, has a HUMS system with 13 strain monitoring locations, as shown in Fig. 22.1.

Contemporary SHM technology has made several strain sensing techniques available. Of these, the two most popular are (i) electrical resistance strain gauges and (ii) Fibre Bragg Gratings (FBGs) etched on optical fibres.

A major inconvenience in using electrical strain gauges is the associated wiring: two wires are required for each sensor. The FBGs offer a much more elegant solution, being lightweight and passive, and having low power utilization, immunity to electromagnetic interference, high sensitivity and bandwidth, long lifetimes and low cost. Also, with the advent of optical data transmission, an FBG solution looks very attractive: FBG sensors can be multiplexed, and hundreds can be put on a single optical fibre, Fig. 22.2 [13].

Apart from strains, FBGs can also monitor temperatures. Their main disadvantage appears to be their fragility and reparability. However, significant R&D

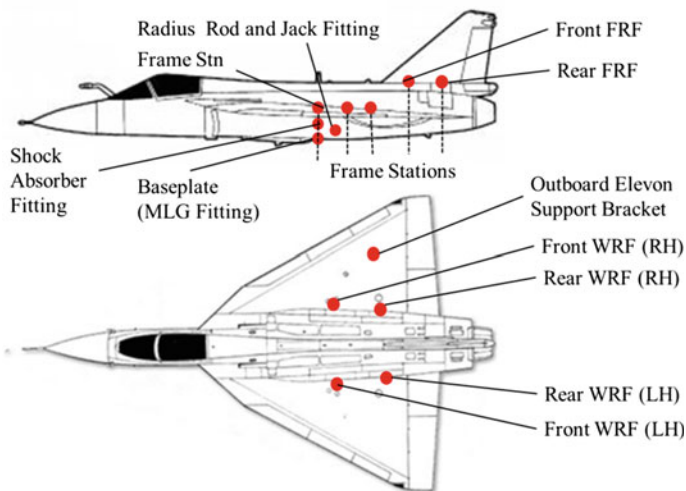
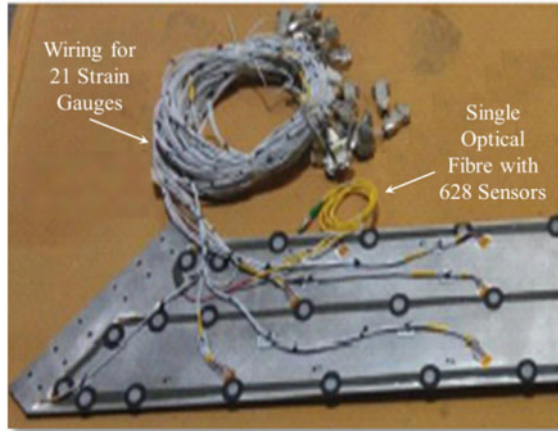


Fig. 22.1 HUMS using resistance strain gauges in the Indian light combat aircraft (LCA), Tejas. Source ADA, Bangalore

Fig. 22.2 Resistance strain gauges and Fibre Bragg Gratings on an optical fibre.
 Source [13]



efforts are being put into the fibre optics technology to overcome such limitations, and FBG-based strain sensing systems are likely to be the most preferred in the near future.

22.3 Damage Monitoring

In the traditional HUMS approach outlined above, the concept of damage is subsumed in the concept of “expended life”. However, the knowledge about damage in its physical sense can give much more ability to handle the lifing and safety issues in a more systematic and cost-effective manner through proper prognosis, optimal repairs and maintenance.

Such damages can occur in various forms: fatigue damage, cracks, cuts, dents and corrosion in metallic materials; delaminations, porosity, fibre cuts, matrix cracks and impact damage in fibre reinforced composites. Conventional approaches focused on metallic materials have mostly dealt with fatigue cracks and their growth, but other forms of damage (like corrosion or damage in composites) have also been receiving significant attention in current SHM developments.

The essential aspect of damage-tolerant structures in aircraft is to take advantage of the period of damage growth (conventionally, fatigue crack growth) while the damage is not critical and will not lead to any disastrous consequences. This advantage comes with a penalty in terms of inspection costs needed to keep track of the damage so that due repairs (or other alternative actions) can be undertaken at a proper time.

It is to be noted that while well-established techniques exist for predicting the growth of fatigue cracks in metals and alloys, no such methods are available for corrosion or for damage growth in composites. Currently, the design of composite structures is based on the “no growth” damage tolerance principle [14, 15]. However,

this does not rule out the occurrence of incidental impact damage and its growth or the possibility of undetected manufacturing flaws leading to damage growth.

Notwithstanding the above considerations, recourse is generally taken to inspection intervals based on test data, and any damage is repaired when found. This makes a good case for event-based detection of damage like an impact on composites, or regular/continuous monitoring in the case of corrosion. These would then provide condition-based replacements for frequent scheduled inspections, thereby avoiding unnecessary downtime and maintenance costs.

Central to damage monitoring is the development of sensing systems, consisting of the sensor elements, the signal processing, and the associated signal-damage correlation, which basically constitute the “Diagnosis” part. Subsequently, it is required to assess the damage criticality and growth: this is the “Prognosis” part.

22.4 Sensing Systems: An Overview

As discussed in Sect. 22.2, the information about the state of health of the structure is gathered through a scheme of sensors. Based on the physics or the physical parameters of sensing, the techniques can be classified as follows:

Strain Sensing

- (a) Electrical strain gauges: resistance wire/foil strain gauges, semiconductor strain gauges.
- (b) Optical fibre based: Various types, the most common being Fibre Bragg Gratings (FBGs).

Damage Sensing

- (a) *Wave-based techniques*: These are based on stress waves passing through the materials. These include ultrasonics (U/S), acoustic emission (AE) and acousto-ultrasonics (AU), developed originally as NDE techniques and now becoming very relevant in SHM. They include all kinds of longitudinal, shear and Lamb waves, guided waves (GW) or any combinations of them, and span a wide range of frequencies from a few Hz (structural modes) to several MHz or even GHz.
- (b) *Electromagnetics*: These include methods such as eddy current, infrared (IR) and X-ray radiography.
- (c) *Thermal techniques*: These include techniques such as thermography.
- (d) *Other Special*: Mechanical gauges like crack gauges, shearography, comparative vacuum monitoring (CVM).

Amongst the several sensing systems listed above, the most promising and relevant systems in the SHM context are the wave-based techniques (such as guided acoustic waves) and fibre-optics-based techniques. Sections 22.5 and 22.6 will focus the discussion on these two systems.

22.5 Acoustic Waves for Damage Detection

Use of acoustic waves for assessment of damage or its growth can be seen to have taken two major directions:

(1) *Ultrasonic (U/S) Non-destructive Testing (NDT) and Inspection* Ultrasonic waves from an external source are passed through the material, usually in the thickness direction, and information about the damage/defect is sought from the resulting signal parameters (e.g. attenuation, time of transit). This can be repeated at several points along the planar dimension of the structure, constituting a “scan” of the entire structure.

As a non-destructive testing and inspection tool, the use of U/S is well established over six decades [16] and the techniques and instrumentation have been refined over the years to a high level of sophistication [17]. Significant advances have made these techniques applicable to composite structures, solving issues such as frequencies to be used, design of probes, couplants, and signal analysis to arrive at damage definition.

Ultrasonic C-scan is basically a mapping of attenuation of U/S signals through the thickness over a planar (or moderately curved) area. C-scanning has become a standard inspection tool for composite structures in the aerospace industry. This is often supplemented by (i) A-scan (received signal amplitude as a function of time of flight of U/S signals due to defects, etc.) in local regions in order to get a depth-wise location of defects and some other information, and (ii) B-scan, which is a side-view of analysis of A-scans along several lines.

Use of ultrasonic bond-testers has also become common in the composites industry. A useful description of many such devices can be found in standard texts and handbooks such as [16, 17] and this topic will not be discussed further here.

The advent of SHM has spurred further developments in U/S systems towards creating Rapid NDE (RNDE) systems. These developments have resulted in portable rapid scanning systems using phased arrays, air-coupled transducers and Lamb waves or guided waves with advanced analytical techniques that correlate the signals to damage [18–21]. Some of these developments carried out at IIT Madras are shown in Fig. 22.3.

(2) *Monitoring of Damage via Acoustic Waves* There are two main categories depending upon the source of acoustic waves:

- (a) Acoustic emission, where acoustic waves are generated from an internal source in the material, and
- (b) Acousto-ultrasonics, where acoustic waves generated from an external source (at specific locations) are propagated through the structure or a structural component and are captured at the surface at the same or different locations.

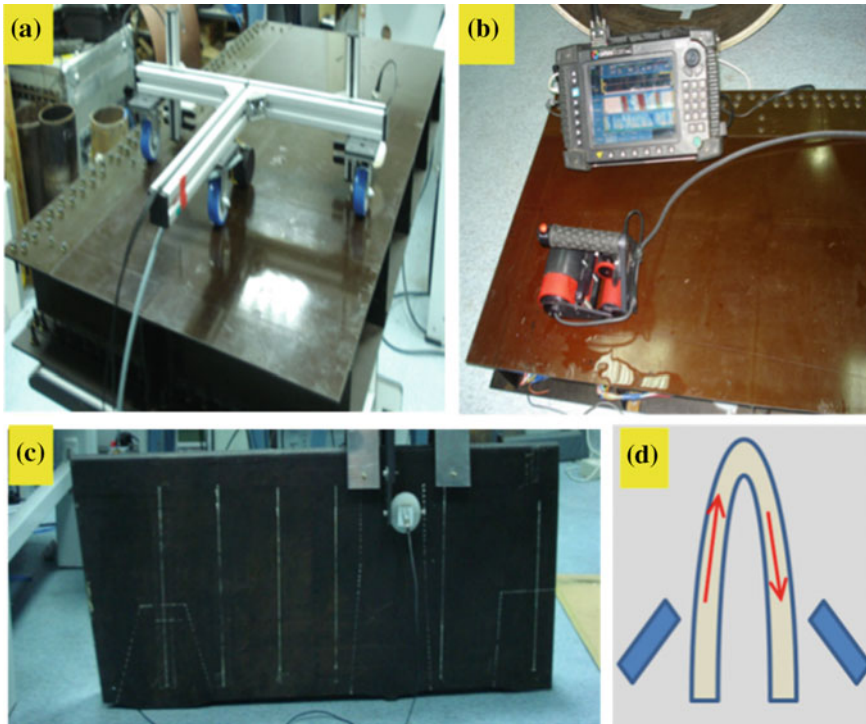


Fig. 22.3 Rapid NDE (RNDE) developments at IIT Madras. **a** Air-coupled transducers, **b** phased array rapid scan, **c** techniques for curved parts and **d** schematic of a curved part

22.5.1 *Passive Acoustic Techniques: Acoustic Emission (AE)*

Microstructural changes in metallic materials (such as plastic deformation, micro cracking, crack growth, grain boundary fracture, void growth) and several types of micro- and macro-failures in composites (such as delamination, matrix cracking, fibre pull-out, fibre-breaks) result in release of energy with generation of transient elastic waves (stress waves) that propagate through the material. This is called acoustic emission (AE).

The SHM interest in AE arises from the fact that such microstructural events take place at very small loads, and the incremental micro-failures are too small to cause any “structural damage”. Thus under actual service conditions (external loading) the AE due to micro-failures can be continuously monitored to provide information about internal damage long before it becomes critical. Extensive literature is available on AE and its correlations with damage in various kinds of materials (see for example, Refs. [22–24]). Hence the discussion here will be limited to its relevance and usage in SHM.

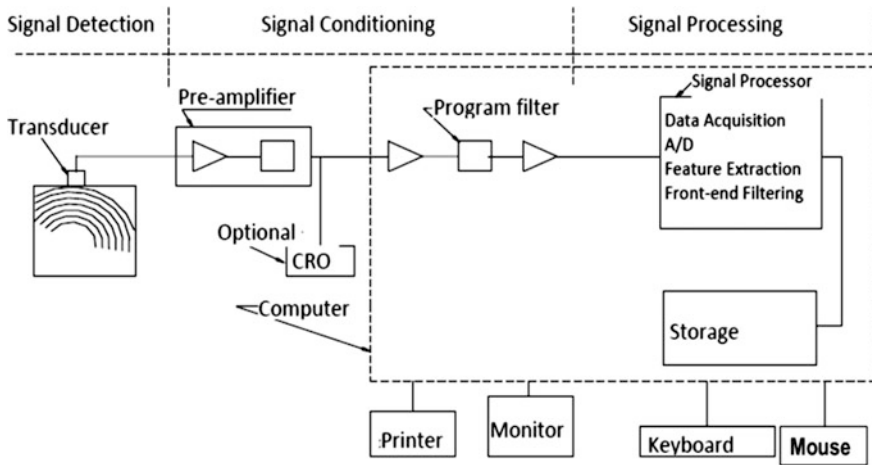


Fig. 22.4 A typical set-up for acoustic emission [6]

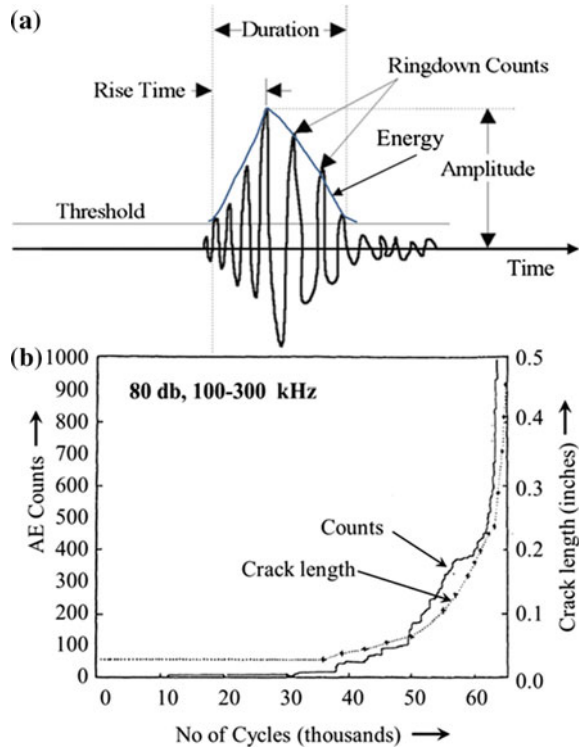
A typical AE set-up is schematically shown in Fig. 22.4 and consists of a transducer (sensor) mounted on the surface of a structure and acoustically connected to it via a couplant, a preamplifier and a filter connected to a signal analyser. Generally, several sensors are required for a large structure, and multi-channel signal analysers are commonly used.

Although AE covers a wide range of frequencies (from a few Hertz to about 10 MHz), practical difficulties limit the measurement of AE in the range of 50–2000 kHz [24]. The piezo-based AE transducers can be designed to respond to a band of operating frequencies: a resonant transducer has high sensitivity and is useful when the frequency content of the AE is known, while a broadband sensor can be used to capture AE signals for frequency analysis. The broadband sensors have low inherent sensitivity and need good electronic preamplifiers to generate useful signals.

The choice of operating frequency and the corresponding transducer depends largely on the purpose of AE examination. Other factors that influence the choice are as follows: the material, its thickness, the expected attenuation, background noise, and environmental conditions, e.g. temperature and humidity. Standard practices have been evolved for selection and calibration of transducers: see for example, ASTM E750-10 dealing with instrumentation, ASTM E1106-07 for calibration of sensors and ASTM E2374-10 for system performance verification. A good summary of AE related standards can be found in Ref. [25]. The need for better AE sensors for SHM with low footprint and the advances in fibre optics have resulted in FBG-based AE sensors [26–29], which are discussed in Sect. 22.6.

The couplant is generally a thin layer of water-soluble paste, wax, grease, oil or an adhesive and is used to provide continuous contact between the transducer and structure surface. Light clamping or spot-adhesive bonding is generally provided to aid contact and prevent undue relative motion.

Fig. 22.5 Acoustic emission: **a** typical burst signal and its parameters **b** increasing AE activity with fatigue damage



Traditional AE work and signal analysis has mostly relied on resonant transducers (for good sensitivity) and single or multi-parameter analysis using time domain parameters, see Fig. 22.5a. The AE activity monitored during loading gave a qualitative picture of the damage progression, as seen in Fig. 22.5b. This was later enhanced by using broadband transducers and the inclusion of frequency-domain parameters in the analysis.

With further advances in electronics, instrumentation, computational techniques and real-time computing power, more options have now become viable, so that much more information contained in an AE signal can be put to use. Many of these approaches are common with other acoustic wave-based techniques, such as Wavelet analysis [30, 31] and Quantitative Acoustic Emission analysis [32, 33] including the modal AE [34–36]. Similarly, several techniques of signal processing and pattern recognition have been developed and are in use, with some using artificial neural networks to obtain inferences about the damage [37–39].

The main aspects of applying AE are listed here:

- Source location, i.e. identifying where damage is occurring
- Identifying the type of damage (e.g. plastic deformation, crack growth, corrosion in metallic materials; matrix cracking, delamination, fibre-breaks in composites)

- Identifying damage initiation versus damage progression
- Identifying the size or criticality of damage.

A good description of all these aspects can be found in [22, 23]. For various research aspects one may refer to [24–41].

With respect to SHM, the AE technique offers a good passive method, since it can locate the source of damage and often assess the criticality of its growth. However, there are some concerns that must be addressed, particularly since the system must operate in an actual service environment. These include:

1. A significant number of false alarms from non-damaging events. Development of noise rejection techniques or homing on to AE signals would be important.
2. Limited ability to discriminate damage mechanisms and damage extent. Also, the data processing is complex and takes much time. This becomes an impediment to “real time” or on-line prediction.
3. Acoustic emission is triggered by very brief events. Although these can be recorded and analysed for information, it is not possible to re-create or reproduce the event. The reliability of the technique thus needs to be re-established for every application.

22.5.2 Active Acoustic Techniques: Acousto-Ultrasonics and Guided Waves

In contrast to passive techniques, where the source of acoustic waves is uncontrolled and cannot be manipulated at will, it is also possible to use “active” methods in which acoustic waves are transmitted into the structure by an externally controlled source. The essence of such techniques is to investigate the modification of signals by damage or defects in the wave paths.

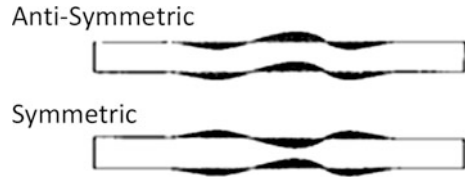
The signals are analysed (often in conjunction with reference signals from an undamaged component) to derive information about the damage. Many variations of these techniques are well developed:

- The waves are often propagated in a planar manner and, depending upon the type and mode of the waves used, such techniques can be variously classified, e.g. as *Lamb Wave* or *Guided Wave (GW)* techniques.
- Another variation of these techniques is *Laser Vibrometry*, where a laser is used to detect wave undulations over the surface, thus facilitating rapid scanning of a large area.

There is a significant amount of commonality with passive AE in the theoretical foundations and sensing technologies. The acoustic signals are sensed by capturing surface undulations or movements due to wave propagation.

The most common sensors and transducers have been piezoelectrics, which can be used both as actuators and sensors. However, non-contact sensing using lasers

Fig. 22.6 Representation of anti-symmetric and symmetric flexural guided wave (GW) modes in a plate



with Doppler effect (LDV: laser Doppler vibrometry) [42–47], and fibre-optic-based sensing using Fibre Bragg Gratings (FBGs) [26–29, 48, 49] have been under development in recent times, and some of them have also become commercially available, for example [49]. Additionally, MEMS (Micro-Electro-Mechanical-Systems) technology-based surface acoustic wave (SAW) sensors have been developed and have found use in niche applications [50, 51]. Most of the present commercial systems operating with piezoelectric transducers are able to operate over the entire acoustic frequency spectrum with reasonable sampling rates (~ 20 msp/s) [52], and are in use for monitoring several types of structures including aerospace structures.

The most significant applications have been developed using the guided waves (GW) technique. Guided waves can be classified in many ways (e.g. plate waves, cylindrical waves and rod waves) or based on the nature of the vibration (e.g. extensional or longitudinal waves, shear-horizontal waves, flexural waves and torsional waves). Also, the wave modes can be broadly classified into symmetric and anti-symmetric modes, based on the type of symmetry of the displacement profile exhibited by the wave during propagation, see Fig. 22.6. Finally, for a given type of guided wave there are many orders of modes that can exist.

The GW technique is becoming popular in the SHM and NDE community. A major merit of the technique is its potential to have a global, long-range inspection technique which can interrogate even some inaccessible regions and is able to discriminate amongst damage features together with structural features. On the other hand, the technique demands a high level of understanding of guided waves and associated phenomena (such as dispersion and multi-modality) on the part of the user. With the development of advanced mathematical tools that can assist in devising computer-aided systems, the technique is poised to have widespread applications. More detailed information may be found in Refs. [53–58].

22.5.3 *Emerging Applications of Acoustic Waves for SHM*

A number of applications of guided waves in NDE and SHM are emerging. Some of the developments towards rapid NDE using GW ultrasonics were already depicted in Fig. 22.3.

Perhaps one of the most significant developments is the SMART layer application initially developed by Stanford University [59] and now commercialised by

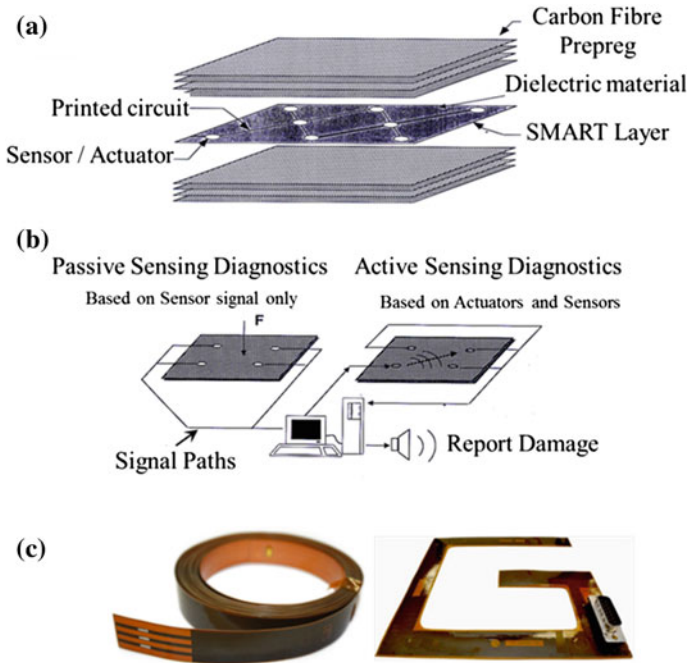


Fig. 22.7 a SMART layer developed using piezo-discs and printed circuit board technology, b the schemes of passive and active diagnostics, and c commercial products by Acellent Technologies [59, 60]

Acellent Inc [60]. The SMART application is shown in Fig. 22.7. Piezo transducers (discs) are embedded in thin layers of a polymeric (dielectric) film, which forms a single patch or “smart layer”, which can then be mounted on the structure or could be embedded in a laminated composite during fabrication. Compatible instrumentation and signal processing software have been developed to predict (a) the location and energy of an impact event occurring on a composite plate structure and (b) the damage in the composite plate.

Figure 22.8 shows a laboratory set-up at the IISc Bangalore, demonstrating the use of Piezo Wafer Active Sensing (PWAS) for locating delamination or disbonding in a stiffened composite plate [58]. The wafer is directly bonded to the structure and serves as both actuator and sensor [55–58].

Another example is shown in Fig. 22.9. Defects in T-joints in integrally stiffened composite plates for aircraft structures continue to be of concern. Figure 22.9 depicts a laboratory set-up using Laser Doppler Vibrometry for detecting delamination in such a T-joint [46]. It is to be noted that extensive analytical treatment is required to arrive at a suitable detection algorithm.

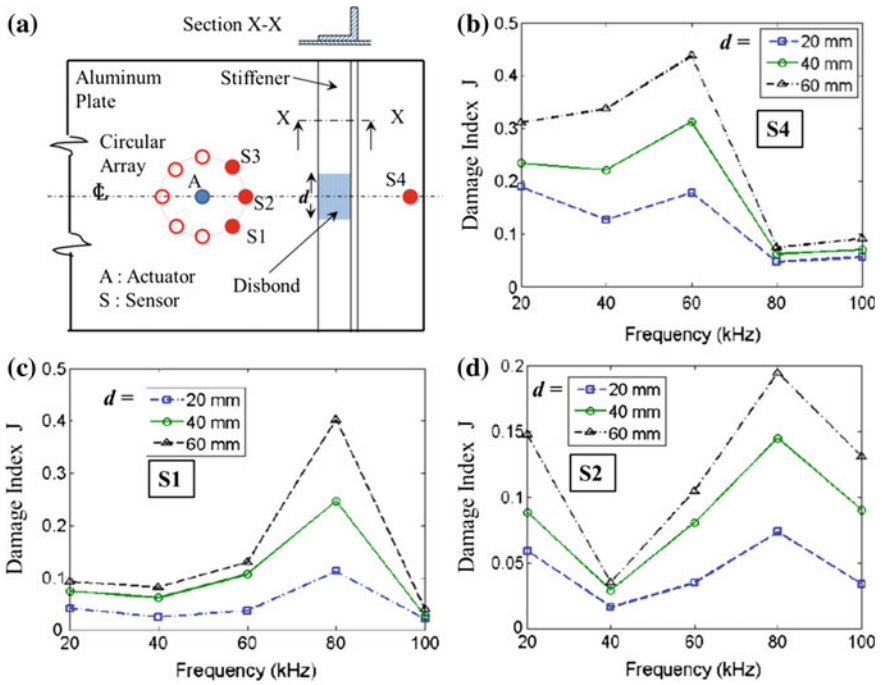


Fig. 22.8 Illustration of piezo wafer active sensing (PWAS) development for disbond detection in a stiffened plate with bonded stiffener. Note the use of a damage index (J) based on various modes [58]

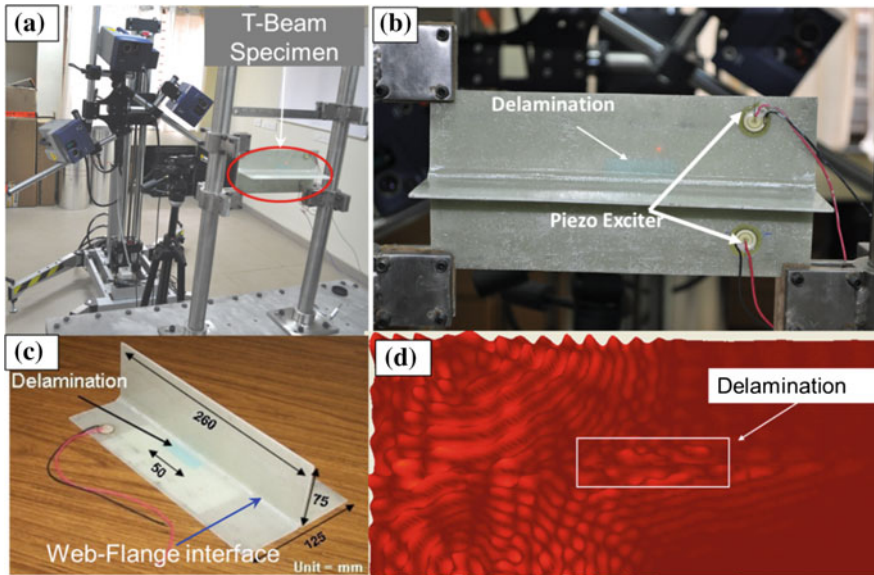


Fig. 22.9 A laboratory set-up to demonstrate use of Laser Doppler Vibrometry for detecting defects in a composite T-joint. The lower right corner shows the image of the propagating wave pattern disturbed by a delamination near the web-flange interface [46]

22.6 Fibre Optics for Damage Detection

In the last couple of decades, advances in fibre-optic sensors and instrumentation have opened up new and elegant options for SHM. These developments have been encouraged by two different considerations:

- For aircraft composites the optical fibres seem to be a natural choice that can be embedded and can provide vital information about in situ strains
- The demand for improved disaster prevention systems for large scale civil infrastructure needing sensing over large distances and distributed areas.

For aircraft applications, fibre-optic (FO) sensors have several advantages such as low weight, high sensitivity, immunity to electromagnetic interference (EMI) and multiplexing capability. Several types of FO sensors have been developed based on various optical effects such as interference, frequency shift due to gratings or reflectometry.

Advances in opto-electronics have helped in developing compact instrumentation required to quantify the above-mentioned effects with high precision and sensitivity. Figure 22.10 is a schematic representation of various types of FO sensors that have been developed. Many of these (highlighted in the figure) have been developed sufficiently for commercialisation: e.g. the extrinsic Fabry–Perot interferometer (EFPI), low-coherence interferometry (commercially called SOFO),

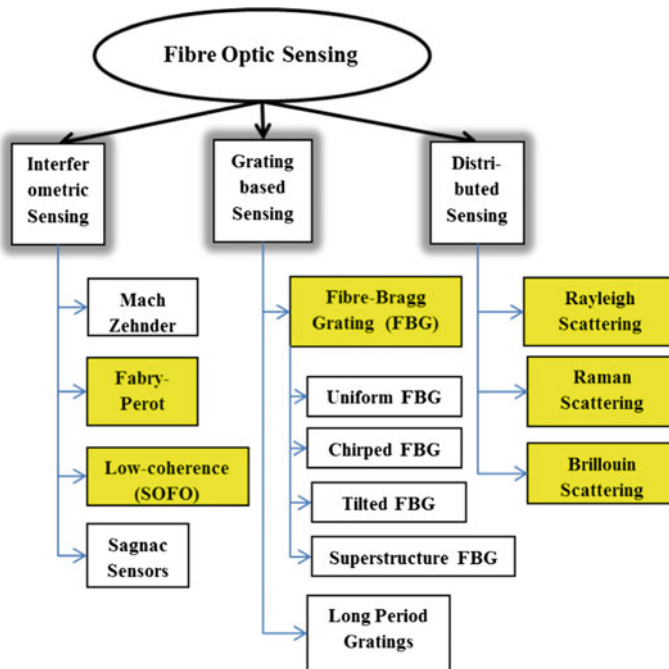


Fig. 22.10 Various types of fibre optic (FO) sensors. Sensors already in the commercial domain have been highlighted [62]

the French acronym of “Surveillance d’Ouvrages par Fibres Optique”), Fibre Bragg Gratings (FBGs) and a few others.

Amongst these, the FBGs, which can act as point sensors for strain and temperature, have become popular and preferred for aircraft SHM applications, owing to ease of handling and the capability for dense multiplexing using optical frequency-domain reflectometry (OFDR).

More recently, significant advances have also been made in grating-less sensing technology using optical scattering and optical time domain reflectometry (OTDR), which can provide large scale distributed sensing. A good review of FO sensors can be found in [61, 62] and features of various FO-based sensors based on [62] are summarised in Table 22.1.

22.6.1 Interferometric Sensors

Interferometric sensors make use of the optical interference obtained from a reference signal and a signal shifted due to strain on a structure. Various schemes have been investigated, amongst which the extrinsic Fabry–Perot interferometric sensors (EFPI) (see Fig. 22.11, and [61–63]) and low-coherence sensors have been successfully used for practical strain measurements. EFPI sensors have good sensitivity and are quite compact, but they cannot be multiplexed. The low-coherence type sensors measure strain over a large gauge length, and even though successful for gross strain measurements in large civil structures they are not favoured for SHM of aircraft, since large strain gradients may be present.

22.6.2 Grating-Based Sensors

The grating-based sensors, amongst which the Fibre Bragg Gratings (FBGs) have been found to be most useful, use the change in wavelength caused by a grating etched on an optical fibre. This wavelength change depends on the period (pitch, spacing) of the grating lines, which changes due to straining caused by loads or temperature changes. A good review of FBG technology and status can be found in Ref. [64].

Figure 22.12 shows the principle of the FBG sensors. Broadband light is passed through the fibre with the grating. Interference between the individual grating planes results in a narrow wavelength range of light being reflected. The remaining wavelengths are transmitted through the grating. The reflection wavelength, the Bragg wavelength λ_B , of the FBG, is determined by the spacing between the individual grating planes as:

$$m \cdot \lambda_B = 2nA$$

where A is the grating period, n is the effective refractive index of the fibre core and m is the diffraction order. Theoretically, considering different values of m , there

Table 22.1 Features and comparison of various fibre optics based sensors [62]

Features	Fabry–Perot interferometric sensors	SOFO interferometric sensors	OTDR	ROTDR	BOTDR	Fibre Bragg Grating sensors
Sensor type	Point	Long gauge	Distributed	Distributed	Distributed	Point; semi-distributed
Main sensing parameters	Temp.; strain; rotation; pressure	Deformation; strain; force	Fibre loss; break location	Temp.	Temp; strain	Temp; strain; rotation; pressure
Multiplexing	Parallel; time-division	Parallel; time-division	Distributed	Distributed	Distributed	Quasi-distributed, wavelength; division
Measurement point on one line	1	1	Depending on the range and resolution	Depending on the range and resolution	Depending on the range and resolution	10–50
Typical resolution strain (μ strain); Temp. ($^{\circ}$ C)	0.15; 0.1	1; N/A	N/A; N/A	N/A; 0.1	20; 0.2	1; 0.1
Capability for large wavelength shift detection (\sim 10 nm)	Yes	No	No	No	No	Yes
Spatial resolution	0.1	0.1	1–10	1	1	0.1
Fast response for acoustic signal detection >100 kHz	Yes	No	No	No	No	Yes
Advantages	High sensitivity; accurate	Long gauge; high spatial resolution	Wide spread applications	Infinite sensing points; fibre integrated	Infinite sensing points; fibre integrated	Linearity in response; accurate; high resolution; inherent WDM encoding
Disadvantages	Single point	Low speed (10 s)	Detection limitations	Temp only; high cost	Cross-sensitivity	Cross-sensitivity

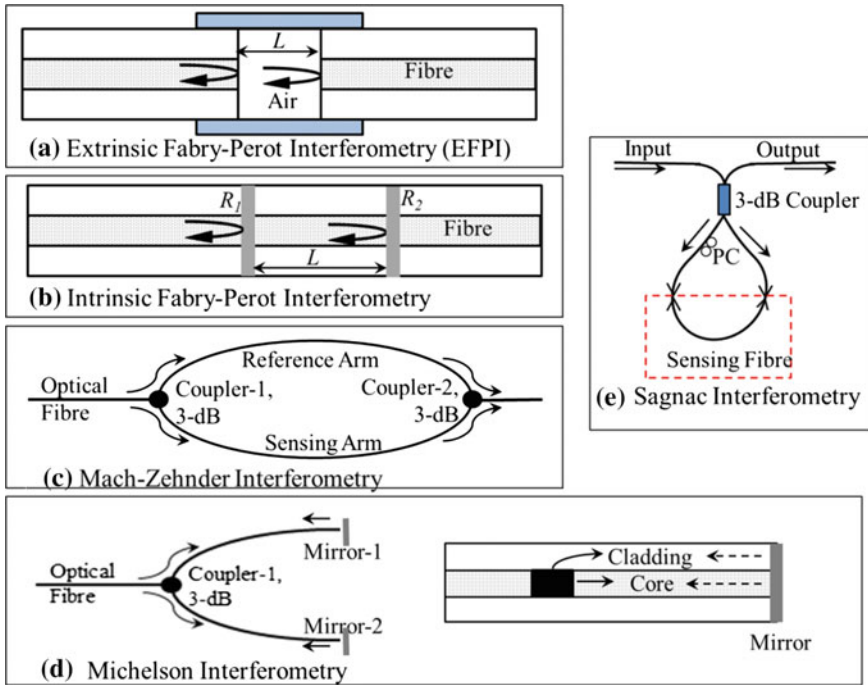


Fig. 22.11 Fibre optic sensors: Interferometric sensing [63]

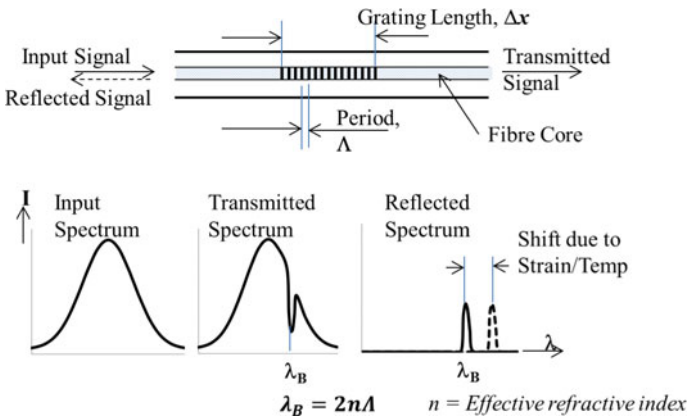


Fig. 22.12 Principle of Fibre Bragg Grating sensor

exist an infinite number of Bragg wavelengths. However, these are separated by quite a large spectral range and in practice only the first Bragg resonance wavelength (1550 nm, $m = 1$) is often used. The reflection can be observed as a peak in the reflected spectrum; correspondingly, a gap is seen in the transmission broadband spectrum. The Bragg wavelength changes because of the strain (ε) or the temperature (T) and the shift $\Delta\lambda_B$ can be described as

$$\frac{\Delta\lambda_B}{\lambda_B} = C_\varepsilon\varepsilon + C_T\Delta T$$

where C_ε and C_T are coefficients (often experimentally determined) for strain and temperature change respectively.

As noted earlier, an important feature of FBGs from the SHM point of view is that they can be multiplexed. For example, in one demonstration by NASA, several hundred FBGs have been multiplexed to monitor an airframe structure [65]. The system is based on the principle of optical frequency domain reflectometry (OFDR) and essentially eliminates the bandwidth limitations.

22.6.3 Distributed Sensing

Optical time domain reflectometry (OTDR) has been in use for some time to determine fibre loss and breakage locations, as well as to evaluate splices and connectors in fibre optic sensors. This technique is based on an attenuation profile generated by measuring the Rayleigh back-scattered light when an optical pulse is introduced into an optical fibre line.

In recent years, advances in instrumentation and opto-electronics have made measurements of other scattering effects possible, leading to the use of optical fibres as grating-less sensors capable of distributed sensing. Raman scattering and Brillouin scattering phenomena have been used in developing the ROTDR and BOTDR techniques [66]. However, both these techniques have large spatial resolution (~ 1 m to a few metres) and even though good for large structures like bridges and pipelines, they have limited applications so far in aircraft. A typical application in aircraft could be loss of a bolt in a large bolted structure, as demonstrated in [67, 68].

On the other hand, recent experiments to use Rayleigh scattering for strain measurements using OFDR has shown excellent promise, with spatial resolution of about 5–10 mm or even less, with an acceptable accuracy of strain measurement [69–72].

22.6.4 Practical Examples

An outstanding example of several multiplexed FBG sensors is provided by the fibre optic strain and shape (FOSS) sensing system developed by NASA and used on predator aircraft [65]. The system boasts 32,000 sensors on 8 optical fibres (4000 each) with maximum length of 80 ft (~25 m) and a sampling rate of 100 sps. In another interesting application, using commercial systems, 17 FBGs were used to monitor strains and temperatures on a personal aircraft [73]. Various trials of strain and damage monitoring using FO sensors have been attempted, particularly on Unmanned Air Vehicles (UAVs) [74–78]. Figure 22.13 shows an FBG sensors system developed in India by NAL being tested on a UAV, in a joint effort by ADE and NAL in India and IAI of Israel. Four sensors on each fibre were mounted on tail-booms of the UAV. Using an artificial neural network (ANN) based algorithm, load estimations were carried out. Also, through interrogation on the ground it was possible to detect damage [77, 78].

Another interesting application of FBGs studied by NAL, Bangalore, is to detect and identify impacts on composite structure and the associated damage by means of a network of FBGs, see Fig. 22.14. While the location of impact could be identified within a reasonable error band, the energy of the impact could not be assessed very

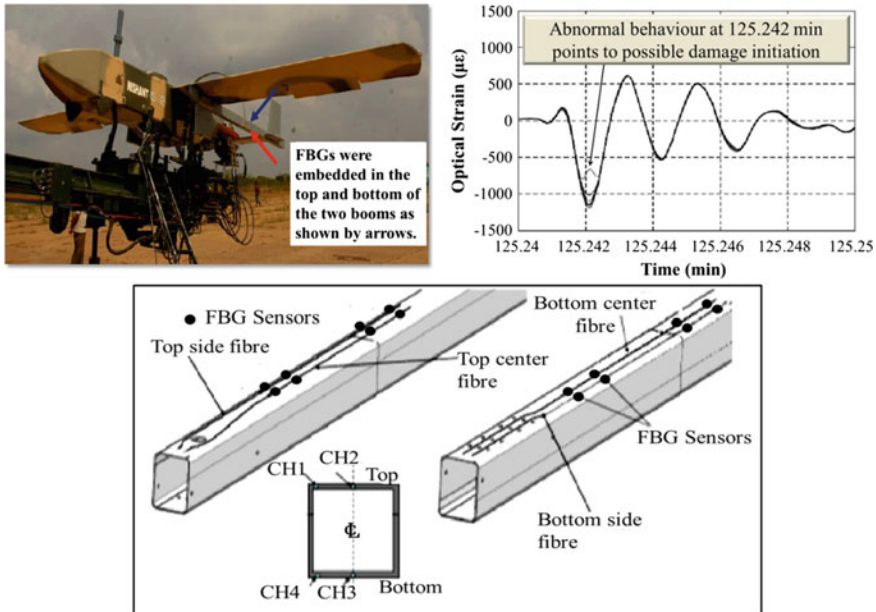


Fig. 22.13 FBG sensors on a UAV to monitor strains as well as damage [77, 78]

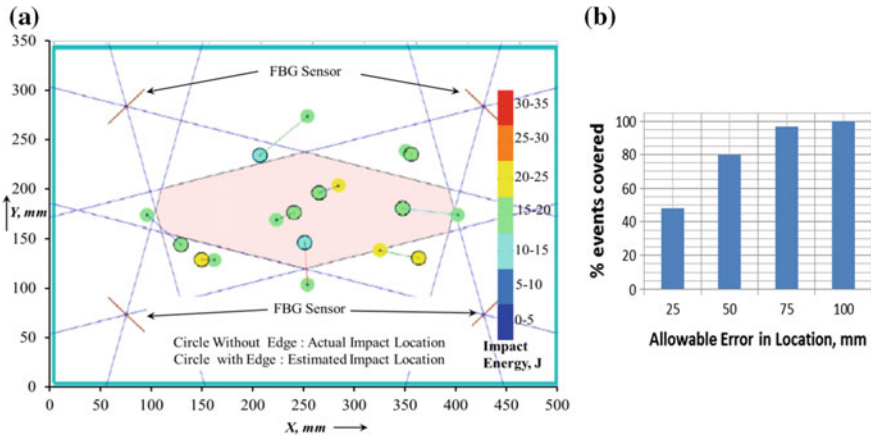


Fig. 22.14 Identifying locations of impacts on composites using FBGs: **a** layout of impact events, energy and sensors, **b** location error bands. *Source* ACECOST project, NAL, Bangalore

accurately. However, this would be improved with newer techniques and a denser network.

22.7 Fibre Optics and Acoustic Sensing

FO-based systems have been basically developed for strain monitoring. However, with novel strategies they can also be used for damage monitoring—especially when used as acoustic sensors [26]. Realising this in practice presents major challenges in the required instrumentation. For example, several FBG sensors may have to be multiplexed, and this makes a demand on fine resolution of wavelength. Further, when used for detecting acoustic waves—from a few kHz to several hundred kHz—the strain to be detected is very small and this needs further refinement of wavelength resolution. Also, such interrogation systems need to be robust and immune to stray sensing in spite of high sensitivity.

Several types of FO-based acoustic sensors are reviewed in [26]. Further developments have led to phase-shifted FBG [27]. The AE sensors using FBG look very promising from experiments on identifying transverse cracking and delaminations in composites [28], as well as for defect identification in aluminium plates [29]. A typical set-up as used in [29] incorporates a specially designed interrogator and is shown in Fig. 22.15.

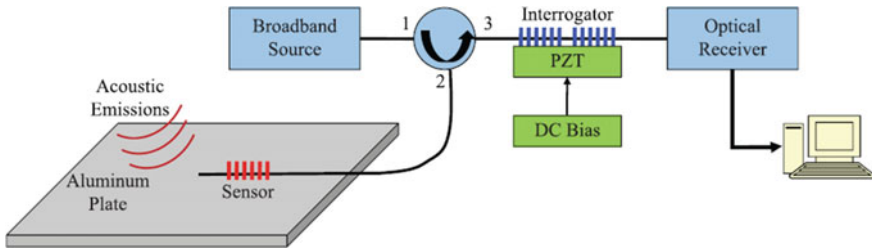


Fig. 22.15 A typical set-up using an FO-based acoustic sensor [26]

22.8 Issues and Strategies

22.8.1 *Metallic versus Composite Structures*

It is well recognised that for a conventional metallic (basically aluminium) aircraft structure, the main issue in structural integrity is fatigue damage and corrosion, where damage progression is cumulative and continuous. On the other hand, composites are laminated materials, and the central issue is impact damage, which is a random event in time.

Thus while the strategies for metallic structure may be formulated on the basis of identified hot-spot monitoring (such as HUMS), strategies for composites may need more of a “field” approach. Zoning of the structure in terms of criticality and perceived probability and severity of impact can help in optimising the number of sensors. Such considerations also lead to strategies with emphasis on point-based or local techniques, such as strain sensors, crack gauges and comparative vacuum monitoring (CVM) for metallic structures; and emphasis on “field” (such as GW-based) techniques for composites.

22.8.2 *Online versus Offline*

At the present time, damage monitoring algorithms do not appear to have reached the stage of reliably monitoring damage directly online. Two approaches appear to be considered as practical at this stage: (i) use of various sensing techniques to create a rapid NDE system (such as Laser (non-contact) scanners, ground-based GW scanners) and (ii) use of on-board sensors, and off-board interrogation systems and data analysis for rapid detection of damage.

22.8.3 SHM as a Part of IVHM

Another issue connected with online monitoring (or just sensing) is the data architecture and its implementation into an Integrated Vehicle Health Management (IVHM) system. Figure 22.16 shows a typical scheme to be used as described in [79]. The data are collected from each zone using a scheme of multiple remote data concentrators (RDCs), and processed to assign “fault codes” signifying the presence of damage within each local region. Additional damage attributes may be obtained by doing a local area analysis so that detailed information becomes available to the ground maintenance personnel as well as the pilot, if necessary.

One of the developments that is being eagerly awaited, and may soon be in practice, is the use of wireless transmission of data and information about various sensor networks, both within the aircraft as well as to ground stations. Already there has been considerable success in using wireless communication technology for SHM applications in civil engineering [80]. A major factor for aircraft applications appears to be the availability of sufficient on-board power to enable successful and persistent deployment [81].

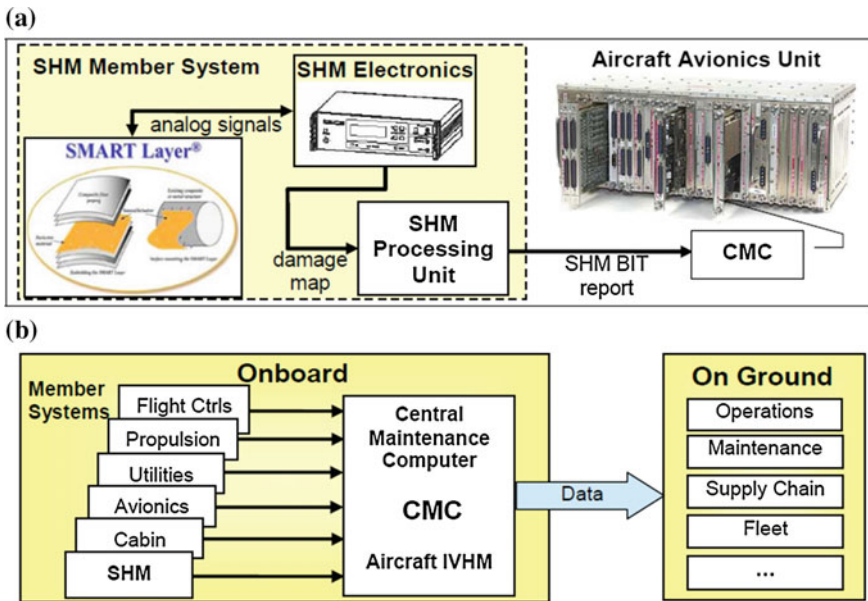


Fig. 22.16 SHM as a part of an IVHM system on an aircraft: **a** SHM data may be collected from various zones, **b** SHM unit in conjunction with various other units of IVHM [79]. <http://web.stanford.edu/~gorin/papers/HonAcell05.pdf>

22.8.4 *Diagnosis versus Prognosis*

While the major emphasis in SHM “techniques” seems to be focused on detection of damage via various sensing systems, there is also a significant effort in studying damage progression and in assessing its criticality. Fracture mechanics-based models for fatigue crack growth in metallic materials have matured quite well, and some of these algorithms are already in use with HUMS systems: see for example Sect. 16.4.3 in Chap. 16 of this Volume.

On the other hand, damage growth in composites and progression of corrosion in metals need further efforts to achieve a maturity level sufficient for practical use. At the present time, fatigue in composites is considered to be sub-critical due to highly reduced design allowable strains [82]. However, with material advances and better SHM systems, higher allowable strains are likely to be used in future. This means that fatigue growth in composites would have to be incorporated into the health management systems. There is much R&D work on damage growth prediction in composites, and this should pave the way for better prognoses.

22.8.5 *Certification*

A major hurdle in implementing several of the SHM developments is the issue of certification. Establishing reliability of an SHM system involves several complex issues ranging from the reliability of sensors to validation of algorithms.

A consensus amongst various stakeholders, including aerospace manufacturers, suppliers and operators, is gradually evolving, as may be seen from the efforts of the SAE [83] and other similar forums. This should allow wider implementation and use of SHM technologies in the near future.

22.9 *Concluding Remarks*

Structural health monitoring (SHM) is considered to be a major advance in aircraft structural technology for obtaining significant economic benefits in operation as well as in improving safety.

SHM will also influence the way structures are designed, through better utilisation of the capability of materials without compromising safety, thus leading to lighter, more efficient structures. Already, the use of HUMS and large area strain monitoring are in place, and several systems are nearly ready for implementation.

Amongst the sensing systems, fibre-optics-based and guided-acoustic-wave-based systems show much promise, and many have reached the maturity to become commercial products. Current strategies are mostly aimed at rapid NDE and off-board analysis of on-board or embedded sensors.

Further advances in terms of Diagnosis and Prognosis of damage will strengthen the case for a much more advanced SHM. Already, a few consensus standards have evolved for implementation. The near future should see SHM systems becoming indispensable parts of aircraft.

References

1. Chang F-K (ed) (2013) Structural health monitoring: a roadmap to intelligent structures. In: Proceedings of the 9th international workshop on structural health monitoring, 10–13 Sept 2013, DEStech Publications Inc., Lancaster, PA, USA
2. Farrar CR, Worden K (2012) Structural health monitoring: a machine learning perspective. John Wiley & Sons, Chichester, UK
3. Gopalakrishnan S, Ruzzene M, Hanagud S (2011) Computational techniques for structural health monitoring. Springer-Verlag London Limited, London, UK
4. Huston D (2010) Structural sensing, health monitoring, and performance evaluation. CRC Press, Boca Raton, FL, USA
5. Dattaguru B, Mangalgiiri PD, Selvarajan A (eds) (2004) Structural health monitoring, ISSS monograph. Institute of Smart Structures and Systems, Bangalore India
6. Proceedings of the 7th European workshop on structural health monitoring (2014). <https://hal.inria.fr/EWSHM2014>
7. Tuck A, Kekoc V (2011) KC-30A structural health monitoring system verification and validation. In: AIAC14, 14th Australian international aerospace congress & 7th DSTO international conference on health & usage monitoring (HUMS 2011)
8. Fuentes R, Cross E, Halfpenny A, Worden K, Barthorpe RJ (2014) Aircraft parametric structural load monitoring using gaussian process regression. In: EWSHM-7th European workshop on structural health monitoring, 8–11 July 2014, Nantes, France
9. ASTM E 1049, 85 (2005) Rainflow counting method, 1987
10. Schijve J (2008) Fatigue of structures and materials. Springer Science & Business Media, Berlin, Germany
11. White DJ (2013) Five decades of developing aircraft usage technology. In: 15th Australian international aerospace congress (AIAC15) & 8th DSTO international conference on health & usage monitoring (HUMS 2013), Melbourne
12. http://www.aviationtoday.com/av/military/Typhoon-Europes-Finest_917.html#VBITD5SSxqU
13. http://www.nasa.gov/pdf/625715main_3-5-C_Chan.pdf
14. Composite Aircraft Structure (2009) Advisory circular FAA AC-20-107B, federal aviation administration. US Department of Transportation, Washington, DC, USA
15. Composite Materials Handbook (2002) Volume 3. Polymer matrix composites materials usage, design, and analysis, MIL-HDBK-17-3F, US Department of Defense, The Pentagon, Virginia, USA
16. Briks AS, Green RE Jr, McIntire P (1991) Ultrasonic testing. In: Non-destructive testing handbook, vol 7, American Society for Non-destructive Testing, Columbus, OH, USA
17. Tittmann BR, Crane RL (2000) Ultrasonic inspection of composites. In: Kelly A, Zweben C (eds) Comprehensive composite materials, vol 5. Elsevier Ltd, Amsterdam, The Netherlands, pp 259–320
18. <http://www.olympus-ims.com/en/webinars/pacomp/>
19. Freemantle RJ, Hankinson N, Brotherhood CJ (2014) Rapid phased array ultrasonic imaging of large area composite aerospace structures. In: World conference on NDT. http://www.ndt.net/article/wcndt2004/pdf/aerospace/551_freemantle.pdf

20. Satyanarayan L, Krishnamurthy CV, Mohan KV, Balasubramaniam K (2007) Simulation of ultrasonic phased array technique for imaging and sizing of defects using longitudinal waves. *Int J Pres Vessels Piping* 84:716–729
21. Rajagopalan J, Balasubramaniam K, Krishnamurthy CV (2006) A phase reconstruction algorithm for Lamb wave based structural health monitoring of anisotropic multilayered composite plates. *J Acoust Soc Am* 119:872–878. <http://dx.doi.org/10.1121/1.2149775>
22. Grosse CU, Ohtsu M (eds) (2008) *Acoustic emission testing*. Springer-Verlag, Heidelberg, Germany
23. Kalyanasundaram P, Mukhopadhyay CK, Subba Rao SV (eds) (2007) *Practical acoustic emission*. Indian Society for Non-destructive Testing, Chennai, Tamil Nadu, India
24. Wevers M, Surgeon M (2000) Acoustic emission and composites. In: Kelly A, Zweben C (eds) *Comprehensive composite materials*, vol 5. Elsevier Ltd, Amsterdam, The Netherlands, pp 345–357
25. Carlos MF E07.04—overview of current and developing ASTM acoustic emission standards. <http://www.diapac.ru/Articles/ASTM.pdf>
26. Wild G, Hinckley S (2008) Acousto-ultrasonic optical fiber sensors: overview and state-of-the-art. *IEEE Sens J* 8(7):1184–1193
27. Wu Q, Okabe Y (2014) Novel real-time acousto-ultrasonic sensors using two phase-shifted fibre bragg gratings. *JIMMS* 25(5):640–646. doi:10.1177/1045389X13483028
28. Wu F, Wu Q, Okabe Y, Kobayashi S, Saito K (2014) Identification of damage types in carbon fibre reinforced plastic laminates by a novel optical fiber acoustic emission sensor. In: 7th European workshop on structural health monitoring (7th EWSHM), Nantes, France
29. Srinivasan B, Harish AV, Balasubramaniam K (2014) Elastic wave sensing using fibre bragg grating—based sensors and dynamic interrogators. *J IISc* 94(3):329–339
30. Staszewski W, Boller C, Tomlinson GR (eds) (2004) *Health monitoring of aerospace structures: smart sensor technologies and signal processing*. John Wiley & Sons, Wiley Online Library: doi:10.1002/0470092866.index
31. Subba Rao SV, Subramanyam B (2008) Analysis of acoustic emission signals using wavelet transformation technique. *Def Sci J* 58(4):559–564
32. Muravin G, Adams CW, Muravin B, Turkel E, Lezvinsky L (2004) Quantitative acoustic emission NDI for analysing dynamic fracture. *World Conf NDT*. http://www.ndt.net/article/wcndt2004/pdf/reliability/513_muravin.pdf
33. Wilcox PD, Lee CK, Scholey JJ, Friswell MI, Wisnom MR, Drinkwater BW (2006) Quantitative structural health monitoring using acoustic emission. In: Matsuzaki Y (ed) *Smart structures and integrated systems*, proceedings of SPIE, vol 6173, 61731K. doi:10.1117/12.658510
34. Dunegan HL (1997) Modal analysis of acoustic emission signals. *DECI newsletters and reports*. <http://www.deci.com/oct97.htm>
35. Prosser WH (1998) Waveform analysis of AE in composites. In: *Proceedings of the 6th international symposium on acoustic emission composite mater*. San Antonio, pp 61–70. <http://ntrs.nasa.gov/archive/nasa/casi.ntrs.nasa.gov/20040095919.pdf>
36. Waller JM, Saulsberry RL, Nichols CT, Wentzel DJ (2010) Use of modal acoustic emission to monitor damage progression in carbon fiber/epoxy tows and implications for composite structures. *QNDE conference*, San Diego, CA. <http://ntrs.nasa.gov/archive/nasa/casi.ntrs.nasa.gov/20100026035.pdf>
37. Bhat C (2001) Artificial neural network approach for characterization of acoustic emission source from complex noisy data. PhD thesis, Department of Aerospace Engineering, Indian Institute of Science, Bangalore, India
38. Bhat C, Bhat MR, Murthy CRL (2008) Characterization of failure modes in CFRP composites—an ANN approach. *J Compos Mater* 42(3):257–276
39. Ramasamy P, Sampathkumar S (2014) Prediction of impact damage tolerance of drop impacted WGFRC composite by artificial neural network using acoustic emission parameters. *Compos B Eng* 60:457–462

40. Bhat MR, Majeed MA, Murthy CRL (1994) Characterisation of fatigue damage in unidirectional GFRP composites through acoustic emission signal analysis. *NDT and E Int* 27(1):27–32
41. Gagar DO (2013) Validation and verification of the acoustic emission technique for structural health monitoring. Ph.D thesis, Cranfield University, UK. https://dspace.lib.cranfield.ac.uk/bitstream/1826/8402/1/Gagar_D_O_Thesis_2013.pdf
42. Kim HC, Park HK (1984) Laser interferometry system for measuring displacement amplitude of acoustic emission signals. *J Phys D Appl Phys* 17:673–676. doi:10.1088/0022-3727/17/4/006
43. Enoki M, Watanabe M, Chivavibul P, Kishi T (2000) Non-contact measurement of acoustic emission in materials by laser interferometry. *Sci Technol Adv Mater* 1:157–165. doi:10.1016/S1468-6996(00)00017-6
44. Staszewski WJ, Jenal RB, Klepka A, Szewedo M, Uhl T (2012) A review of laser Doppler vibrometry for structural health monitoring applications. *Key Eng Mater* 518:1–15
45. Pohl J, Mook G (2013) Laser-vibrometric analysis of propagation and interaction of lamb waves in CFRP-plates. *CEAS Aeronaut J*. doi:10.1007/s13272-012-0057-5
46. Kolappan GG, Mahapatra DR, Gopalakrishnan S (2012) Guided-wave-based damage detection in a composite T-joint using 3D scanning laser Doppler vibrometer. In: *SPIE smart structures and materials—non-destructive evaluation and health monitoring*, International Society for Optics and Photonics, Bellingham, WA, USA, pp 83481Q1–83481Q12
47. Staszewski WJ, Jenal RB, Klepka A, Szewedo M, Uhl T (2012) A review of laser Doppler vibrometry for structural health monitoring applications. *Key Eng Mater* 518:1–15
48. Betz DC, Thursby G, Culshaw B, Staszewski WJ (2003) Acousto-ultrasonic sensing using fiber bragg gratings. *Smart Mater Struct* 12(1):122–128
49. Mendoza E, Prohaska J, Kempen C, Esterkin Y, Sun S, Krishnaswamy S (2013) Distributed fiber optic acoustic emission sensor (FAESense™) system for condition based maintenance of advanced structures. *Optical sensors, SM4C-4*. Optical Society of America, 2013 (also in 6th EWSHM). <http://ndt.net/article/ewshm2012/papers/th3c4.pdf>
50. Malocha DC, Gallagher M, Fisher B, Humphries J, Gallagher D, Kozlovski N (2013) A passive wireless multi-sensor SAW technology device and system perspectives. *Sensors* 13(5):5897–5922. doi:10.3390/s130505897
51. Chin T-L, Zheng P, Oppenheim IJ, Grevec DW (2010) Surface acoustic wave devices for wireless strain measurement. In: *Proceedings of SPIE*, vol 7647, pp 764743-1
52. [http://www.mistrasgroup.com/products/company/publications/2\\$Acoustic_Emission/PCI-2_Board.pdf](http://www.mistrasgroup.com/products/company/publications/2$Acoustic_Emission/PCI-2_Board.pdf)
53. Balasubramaniam K, Sekhar BV, Vishnu Vardan J, Krishnamurthy CV (2006) Structural health monitoring of composite materials. *Key Eng Mater* 321:759–764
54. Su Z, Ye L (2009) Identification of damage using Lamb waves: from fundamentals to applications. Springer Science & Business Media, Berlin, Germany
55. Giurgiutiu V (2014) Structural health monitoring with piezoelectric wafer active sensors, 2nd edn. Academic Press, Cambridge, MA, USA
56. Giurgiutiu V, Zagrai A, Bao JJ (2002) Piezoelectric wafer embedded active sensors for aging aircraft structural health monitoring. *Struct Health Monit* 1(1):41–61
57. Gresil M, Giurgiutiu V (2013) Guided wave propagation in composite laminates using piezoelectric wafer active sensors. *Aero J* 117(1196):971–994
58. Rathod VT, Mahapatra DR (2010) Lamb wave based monitoring of plate-stiffener debonding using a circular array of piezoelectric sensors. *Int J Smart Sens Intell Syst* 3(1):27–44
59. Chang FK (1999) Built-in structural health monitoring. In: *Proceedings of ISSS-SPIE'99*, international conference on smart materials, structure and systems, Bangalore, Jul 1999, Allied Publishers, New Delhi, India, pp 44–49
60. <http://www.acellent.com/blog/1/products/sensors/>
61. López-Higuera JM, Incera AQ, Cobo A (2011) Fiber optic sensors in structural health monitoring. *J Lightwave Tech* 29(4) (15 Feb 2011)

62. Guo H, Xiao G, Mrad N, Yao J (2011) Fiber optic sensors for structural health monitoring of air platforms. *Sensors* 11:3687–3705. doi:[10.3390/s110403687](https://doi.org/10.3390/s110403687)
63. Lee BH, Kim YH, Park KS, Eom JB, Kim MJ, Rho BS, Choi HY (2012) Interferometric fiber optic sensors. *Sensors* 12:2467–2486. doi:[10.3390/s120302467](https://doi.org/10.3390/s120302467)
64. Majumder M, Gangopadhyay TK, Chakraborty AK, Dasgupta K, Bhattacharya DK (2008) Fibre bragg gratings in structural health monitoring—present status and applications. *Sens Actuators A Phys* 147(1):150–164
65. Lance Richards W, Madaras E, Prosser WH, Studor G (2013) NASA applications of structural health monitoring technology. Keynote lecture in 9th international workshop on structural health monitoring, Stanford University. http://structure.stanford.edu/workshop/IWSHM2013/documents/Keynote%20presentations/IWSHM%202013%20Keynote_Richards.pdf
66. Adachi S (2008) Distributed optical fiber sensors and their applications. In: SICE annual conference, the university electro-communications, Japan, Aug 20–22, 2008, pp 329–333. <http://ieeexplore.ieee.org/stamp/stamp.jsp?tp=&arnumber=4654674>
67. Hotate K, Kashiwagi M (2003) High spatial resolution reflectometry for optical subscriber networks by synthesis of optical coherence function with measurement range enhancement. *IEICE Trans Electron* E86-C(2):213–217
68. Hotate K (2006) Fiber sensor technology today. *Jpn J Appl Phys* 45(8B):6616–6625
69. Bergman A, Ben-Simon U, Schwartzberg A, Shemesh NY, Glam B, Burvin J, Kressel I, Yehoshua T, Tur M (2014) Evaluation of a UAV composite wing spar repair using an embedded optical fiber rayleigh back-scattering distributed strain sensing. EWSHM—7th European workshop on structural health monitoring, Nantes, France. <https://hal.inria.fr/hal-01020351>
70. Sundaram R Personal communication
71. Renee Pedrazzani J, Castellucci M, Sang AK, Froggatt ME, Klute SM, Gifford DK (2012) Fiber optic distributed strain sensing used to investigate the strain fields in a wind turbine blade and in a test coupon with open holes. *SAMPE Tech*. http://lunainc.com/wp-content/uploads/2013/04/Pedrazzani-et-al-SAMPE-Tech-2012_FINAL.pdf
72. Song J, Li W, Lu P, Xu Y, Chen L, Bao X (2014) Long-range high spatial resolution distributed temperature and strain sensing based on optical frequency-domain reflectometry. *IEEE Photonics J* 6(3)
73. Chandler K, Ferguson S, Graver T, Csipkes A, Mendez A (2008) On-line structural health and fire monitoring of a composite personal aircraft using an FBG sensing system. *Proc SPIE* 6933–6939. doi:[10.1117/12.783125](https://doi.org/10.1117/12.783125)
74. Yu M (2008) Fiber optic sensor technology. IMAC XXVI, Orlando, FL. https://sem.org/PDF/fiber_optic_sensor_technology.pdf
75. Kressel I, Balter J, Mashiach N, Sovran I, Shapira O, Shemesh NY, Glamm B, Dvorjetski A, Yehoshua T, Tur M (2014) High speed, in-flight structural health monitoring system for medium altitude long endurance unmanned air vehicle. In: EWSHM-7th European workshop on structural health monitoring, pp 274–280. <https://hal.inria.fr/hal-01020352/document>
76. Nicolas MJ, Sullivan RW, Richards WL (2013) Fiber bragg grating strains to obtain structural response of a carbon composite wing. In: ASME 2013 conference on smart materials, adaptive structures and intelligent systems, paper no. SMASIS2013-3265, American Society of Mechanical Engineers, pp V002T05A012-V002T05A012
77. Gupta N, Augustin MJ, Sathya S, Jain S, Vishwamurthy SR, Gaddikeri KM, Sundaram R (2013) Structural health monitoring of composite aircraft structures using fiber bragg grating sensors. *J IISc* 93:4. <http://journal.iisc.ernet.in>
78. Kressel I, Handelman A, Botsev Y, Balter J, Guedj P, Gorbatov N, Tur M, Pillai ACR, Prasad MH, Gupta N, Joseph AM, Sundaram R (2012) Evaluation of flight data from an airworthy structural health monitoring system integrally embedded in an unmanned air vehicle. Paper Tu.4.A.4. In: 6th European workshop on structural health monitoring, Dresden, Germany

79. Gorinevsky D, Gordon GA, Beard S, Kumar A, Chang F-K (2005) Design of integrated SHM system for commercial aircraft applications. In: 5th international workshop on structural health monitoring, Stanford, CA, USA
80. Arun Sundaram B, Ravisankar K, Senthil R, Parivallal S (2013) Wireless sensors for structural health monitoring and damage detection techniques. *Curr Sci* 104(11):1496–1505
81. Boyle D, Magno M, O’Flynn B, Brunelli D, Popovici E, Benini L (2011) Towards persistent structural health monitoring through sustainable wireless sensor networks. In: Seventh international conference on intelligent sensors, sensor networks and information processing (ISSNIP). IEEE Pub, Adelaide, pp 323–328. doi:[10.1109/ISSNIP.2011.6146587](https://doi.org/10.1109/ISSNIP.2011.6146587)
82. Mangalgiri PD (2013) Design allowable considerations for use of advanced composites in aircraft structures. *J IISc* 93(4):571–592
83. Guidelines for implementation of structural health monitoring on fixed wing aircraft, SAE ARP6461 (2013). Society for Automotive Engineers, Warrendale, PA, USA

Chapter 23

Failure Analysis and Prevention

K.P. Balan and A. Venugopal Reddy

Abstract This chapter first reviews the fracture and fractography of metals and alloys, with examples of typical fractographs. Then the tools and techniques used in failure investigations are briefly described. The second main part of the chapter is devoted to three case studies on aeronautical component failures. Each case study is described with background information, followed by experimental results consisting mainly of visual examination, fractographic examination, metallographic examination, hardness measurements, and chemical analysis. The results are then discussed and conclusions are drawn. Wherever possible, suitable remedial measures are suggested.

Keywords Failure analysis • Techniques • Case histories • Fracture • Fatigue • Hydrogen embrittlement • Stress corrosion • Wear • Defects • Overloads • Overheating

23.1 Introduction

An engineering system is expected to meet certain functional requirements over the total technical life with a specified reliability. When the system fails to perform its function, deficiencies in design, manufacture, assembly or maintenance, and also unexpected operational conditions (in-service loads, environmental effects) may or might be suspected. A systematic and scientific failure analysis can often find the cause(s) of failure. Remedial measures can help in preventing similar occurrences in future.

Background information and circumstantial evidence are also important—and even vital—in failure analysis. A failure analyst should acquire background

K.P. Balan
DMRL, Hyderabad, India

A. Venugopal Reddy (✉)
ARCI, Hyderabad, India
e-mail: aramadaka@hotmail.com

information, obtain access to or information about any other suspect components, take samples (if possible) and make standard specimens for required/diagnostic tests, and record and document the evidence and test results. The interpretation of the evidence and results should lead the analyst to arrive at the most probable cause of failure.

23.2 Fracture of Metals and Alloys

Understanding the mode of fracture is an important step in any failure analysis of a broken or cracked component. There are different types of fracture in metals and alloys. These can be broadly classified as ductile or brittle, and transgranular or intergranular, whereby transgranular fracture can be either ductile or brittle, and intergranular fracture is usually brittle.

Each type of fracture leaves characteristic and diagnostic fracture features on the fracture surfaces. Actual diagnosis is a task for specialists and can be difficult. However, knowledge of the (probable) type of fracture is essential for determining the cause of failure.

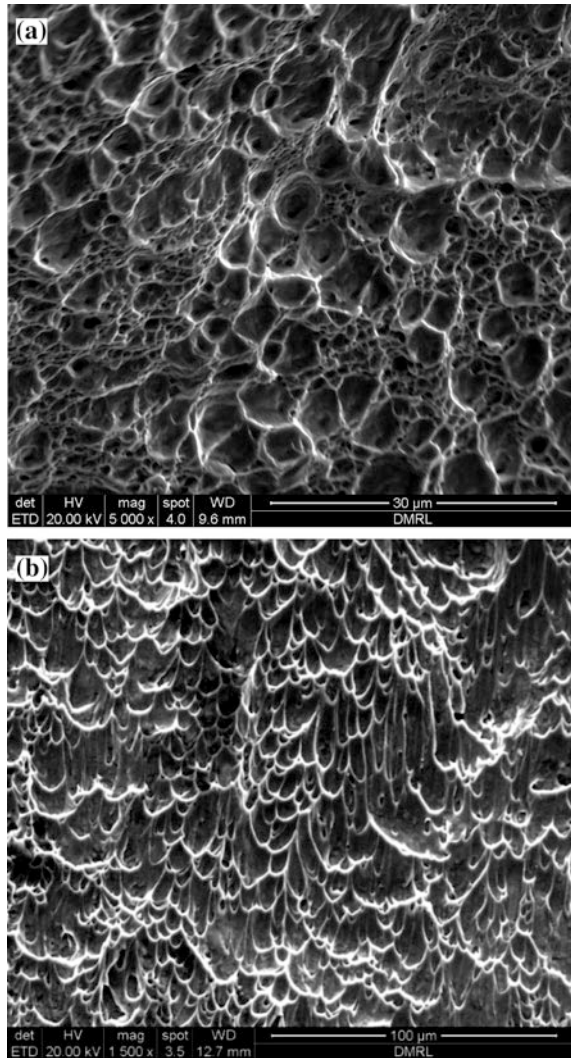
23.2.1 Ductile Fracture

Plastic deformation of a metallic part precedes a ductile fracture, and hence the fractured part shows a change in dimensions in the form of increased length or a (local) decrease in cross-section. A typical example of severe plastic deformation is the cup-and-cone fracture in a tensile test. In actual components the plastic deformation preceding fracture may be more localized, depending on the state of stress (plane strain or plane stress) during fracture. Plane strain fractures occur in thick components, e.g. heavy-section forgings such as large bulkheads and landing gear, and plane stress fractures occur in thin components, e.g. aircraft fuselage and wing skins.

Fractography of Ductile Fracture The fracture surface of a ductile fracture shows a dull and fibrous appearance when examined visually or under a stereomicroscope. Fracture surfaces that show a 45° shear fracture or shear lip formation are usually due to ductile fracture.

In a scanning electron microscope (SEM), ductile fracture reveals a dimpled appearance owing to the coalescence of microvoids during the fracture process. The microvoids can be equiaxed or elongated depending on the mode of failure: tensile fracture (equiaxed); bending and shear fractures (elongated). Examples of equiaxed and elongated microvoids are shown in Fig. 23.1.

Fig. 23.1 SEM micrograph showing ductile fracture
(a) equiaxed microvoids and
(b) elongated microvoids



23.2.2 Brittle Fracture

Brittle fractures are characterized by little or no dimensional changes in the fractured parts. Brittle fractures in aircraft metals and alloys are uncommon and usually the result of unexpected problems such as hydrogen embrittlement or stress corrosion cracking (SCC).

Brittle fractures have a bright and faceted appearance. For fast brittle fracture the fracture surface sometimes shows macroscopic and submacroscopic chevron patterns that help in locating the fracture origin.

Fig. 23.2 SEM fractograph showing fatigue a transgranular cleavage fracture

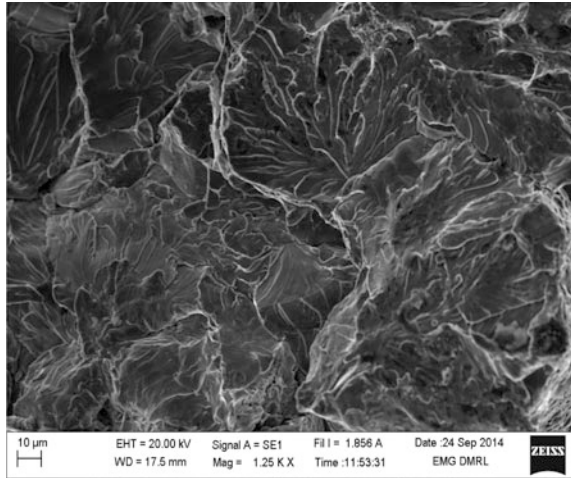
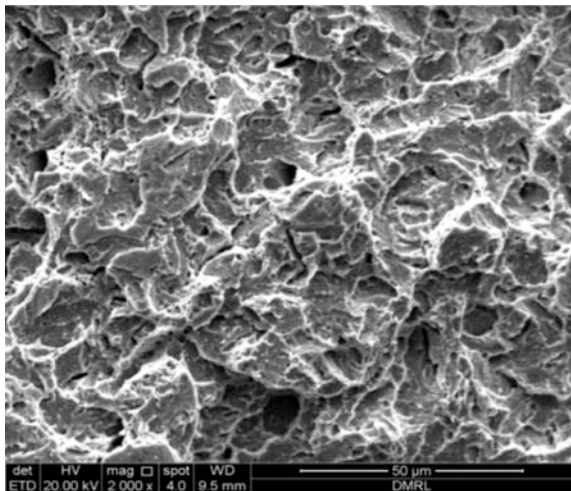


Fig. 23.3 SEM fractograph showing a ‘quasi-cleavage’ fracture

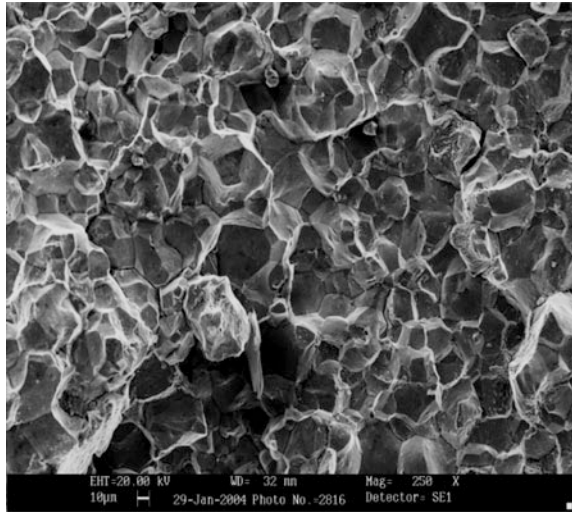


Fractography of Transgranular Brittle Fracture In the SEM a transgranular brittle fracture reveals cleavage or cleavage-like features, namely crystallographic facets with so-called river markings or feathery patterns. An example is given in Fig. 23.2.

As mentioned above, a normally ductile metal can fail in a brittle manner owing to problems such as hydrogen embrittlement and SCC. When failure is transgranular, there may be a mixture of ductile and brittle fracture features, sometimes referred to as quasi-cleavage, as in Fig. 23.3.

Fractography of Intergranular Brittle Fracture In the SEM this type of fracture usually shows polygonal grain facets and sometimes intergranular secondary

Fig. 23.4 SEM fractograph showing an intergranular fracture



cracks, e.g. Figure 23.4. Metallurgical abnormalities and environmental factors are generally responsible for a metal to fail in an intergranular mode: the exception is creep rupture, which is a normal failure mode for high-temperature alloys.

23.2.3 Fatigue Fracture

Many failures of components used in engineering systems occur by fatigue, which takes place under conditions of cyclic loading. The fractured parts do not show any gross deformation in a fatigue fracture. However, a part that has failed by fatigue finally separates due to fast fracture.

Fractography of Fatigue Fracture A part that has failed by fatigue shows a macroscopically smooth fracture that may extend over most of the entire fracture surface. The fatigue fracture, although macroscopically smooth, can show progression markings that delineate the growth and shape of the fatigue crack (see Fig. 23.5). These markings represent significant variations in the cyclic load history, and they can be helpful in tracing back to the origin of the fatigue crack.

In the SEM, the smooth fracture may reveal fatigue striations (Fig. 23.6). Each striation represents one significant load excursion. This can be most important for further analysis. Aluminium alloys and stainless steels often show well-defined striations; titanium alloys also show striations, though mixed with other, rather complex features; and steels and nickel-base superalloys often show features that—although characteristic of fatigue—do not resemble striations. Thus the fractographic determination of whether a fracture is due to fatigue may have to rely on other clues besides striations, e.g. progression markings.

Fig. 23.5 SEM fractograph showing fatigue progression markings

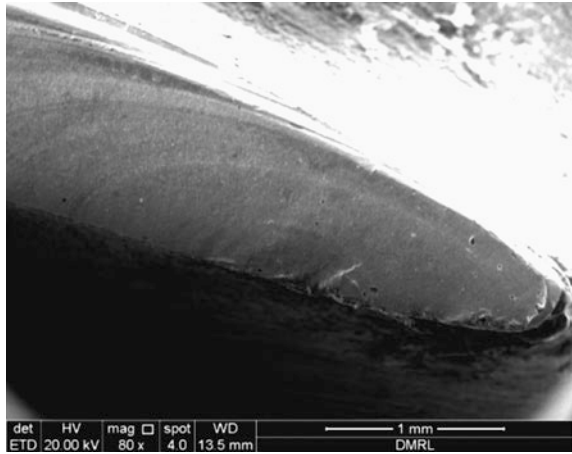
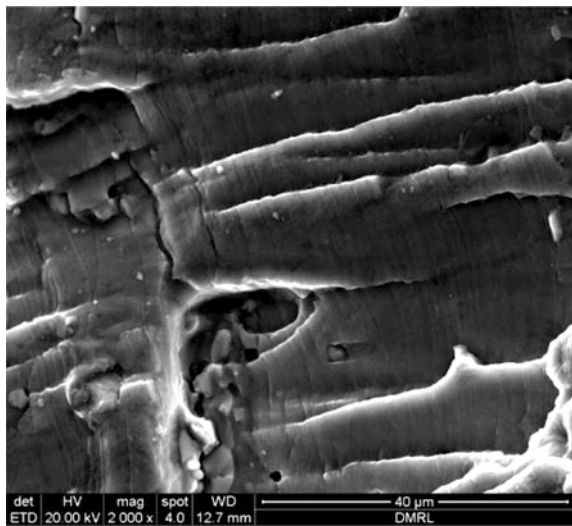


Fig. 23.6 SEM fractograph showing fatigue striations (direction of crack propagation is from *left to right*)



23.3 Major Causes for Component Failures

23.3.1 Poor Material Quality

Improper selection of material for a specific application is found to be the cause of a number of failures. Proper selection of materials for a desired application demands consideration of not only material cleanliness, composition, properties and corrosion and oxidation resistance, but also factors such as fabricability, availability, service life, and cost. It also has to be borne in mind while selecting a material that the properties are influenced by the service conditions. Imperfections in the form of

Fig. 23.7 Fractured nut received for examination

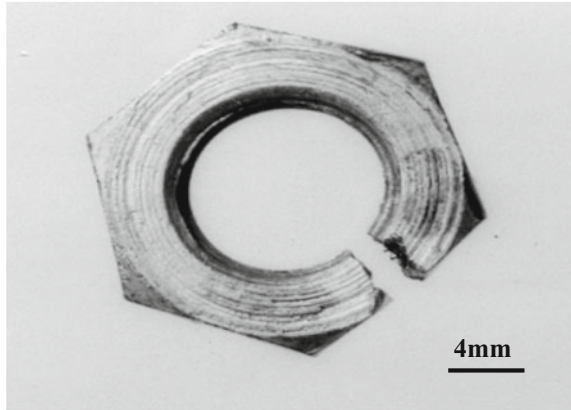
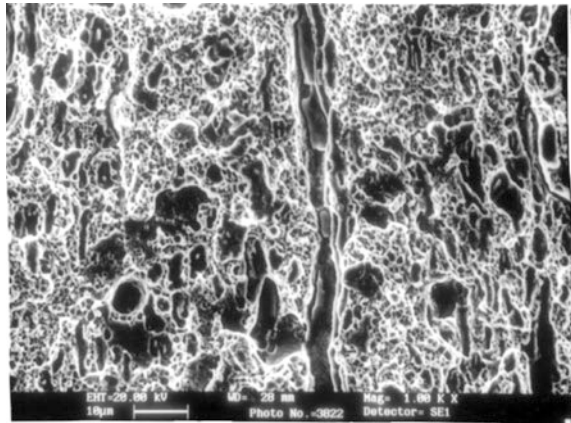


Fig. 23.8 SEM fractograph showing tearing around and along MnS inclusion stringers and microvoid coalescence (dimpled rupture) (1000 \times)



non-metallic inclusions, porosity, voids and cracks can be responsible for many failures.

A steel hexagonal lock nut used for fastening fins with M8 screws onto a missile cracked during application of a torque of 20 Nm [1]. The nuts were made using a low-alloy Ni–Cr–Mo steel, hardened at 860 °C and tempered at 550 °C. The manganese sulphide (MnS) inclusion content of the nuts was abnormally high, but the users did not specify any limit in the quality plan. Fracture of the inclusions and tearing around them, together with microvoid coalescence (dimpled rupture), indicated that the failure was by overload initiating from the inclusions (Figs. 23.7 and 23.8).

23.3.2 Manufacturing Defects

Surface discontinuities such as seams, laps, and folds formed during metal working can act as stress raisers in service. Discontinuities such as shrinkage cavities,

Fig. 23.9 Cracked lock washer received for examination



porosities, blow holes, voids and pipes formed during ingot solidification are known sources of weakness during subsequent fabrication, since these defects serve as sites for crack initiation. Insufficient mechanical reduction while forging from ingot to bars can leave an as-cast structure in a wrought product.

Imperfections and discontinuities occurring in castings, if undetected, can initiate failures during service. Cold shuts, gas porosity, hot tear, shrinkage cavities, inclusions, seams, cracks, etc., are some of the commonly found defects in castings. A sound foundry practice coupled with mandatory non-destructive testing of castings can help in avoiding the use of defective castings.

Heat treatment is one of the important steps carried out in the manufacture of components, to achieve the correct microstructure in order to get the optimum properties. Many component failures are the results of improper heat treatments imparted to the components.

Lock washers used with lock nuts in the transmission system of a helicopter cracked in service, see Fig. 23.9 [2]. The low-carbon steel lock washers contained cracks at the fillets between the tabs and bodies of the washers, as in Fig. 23.10. These cracks were attributed to cold working during manufacturing. The cracks grew under fatigue loading to cause failure of the washers in service.

Fig. 23.10 Fillet between tab and body of the lock washer showing cracks due to cold working

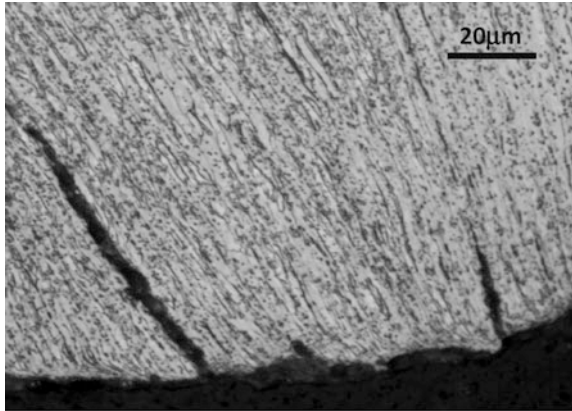
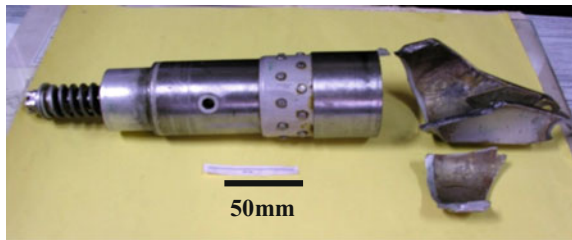


Fig. 23.11 Failed portion of nose wheel lug assembly received for examination



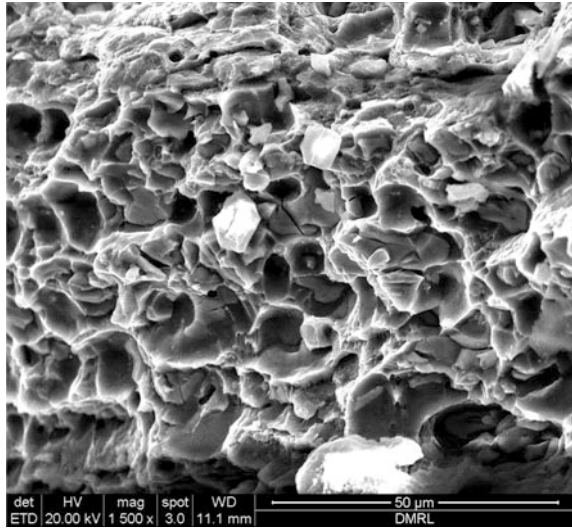
23.3.3 Operational Overload/Abuse

Under service conditions a component may be subjected to stresses that may exceed the design stresses, causing fast fracture (overload) and failure.

A trainee pilot, while landing an aircraft, touched down on the main wheels followed by the nose wheel (as is normal). However, the aircraft thereafter did a mild bounce of 1–2 ft and landed on all three wheels in a 3-point touchdown. This was followed by bouncing to a height of 4–6 ft and landing on the nose wheel [3]. During this third landing the nose wheel lug assembly of the self-centering mechanism broke and the nose wheel collapsed. Figure 23.11 shows the failed part of the assembly.

The failed component was made of AA 2014 grade aluminium alloy in a solution-treated and precipitation-hardened condition. Analysis revealed that the lug had failed due to impact overload, as evidenced by the fracture surface appearance, see Fig. 23.12.

Fig. 23.12 SEM fractograph showing microvoid coalescence due to fast fracture (overload) of the nose wheel lug



23.3.4 Fatigue

Failures occurring under the conditions of cyclic loading are called fatigue failures. Fatigue is the most important mode of failure in aircraft structures and engines. Many engine components are subjected to repeated loading and vibrations.

Unlike failures under static or quasi-static loads, fatigue failures occur at stresses that are lower than the yield strength of the material. Fatigue failures are generally found to start at or near a surface where there is a local stress concentration. A stress concentration can occur at (a) fillets, holes, grooves, keyways, and other geometrical changes, (b) rough surfaces, tool marks, and machining marks, and (c) surface and near-surface discontinuities or defects in the material such as non-metallic inclusions, porosity, and decarburized layers in steels.

A forged and machined aluminium alloy grade L77 Brake Unit calliper fractured in service unexpectedly. The failed part is shown in Fig. 23.13 [4]. Detailed examination showed that fatigue cracks originated at deep scratches/machining marks on a fillet radius and propagated to about two-thirds of the section thickness, see Fig. 23.14. The remaining section could no longer withstand the applied load and failed due to fast fracture.

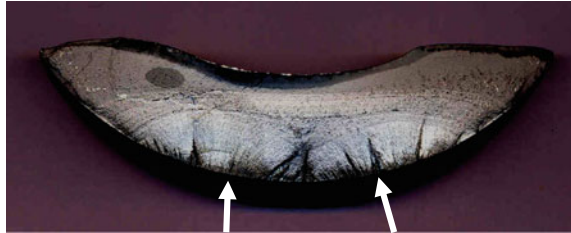
23.3.5 Corrosion

Corrosion is defined as the deterioration of a metal due to chemical or electrochemical reactions with its environment. There are different types of corrosion:

Fig. 23.13 Failed aircraft Brake Unit component received for examination



Fig. 23.14 Fracture surface of the failed Brake Unit part showing multiple fatigue origins and progression markings (0.25×)



uniform corrosion, pitting corrosion, crevice corrosion, intergranular corrosion, stress corrosion, and hot corrosion.

Uniform Corrosion This is the most common variety of corrosion. Suitable surface protection measures such as painting, coating, anodizing, cladding and cathodic protection are commonly used for preventing uniform corrosion.

Pitting Corrosion This is a form of extremely localized attack that results in the formation of a pit, leading eventually to perforation of the metal. Most pitting is associated with halide ions, with chlorides, bromides, and hypochlorites being the most prevalent. Selection of a material more resistant to pitting corrosion is the most important method of prevention. Any damage caused to a passive surface film has to be prevented in order to improve the pitting resistance of the material.

Crevice Corrosion Small volumes of stagnant solution of a corrosive nature cause crevice corrosion when they become trapped under gaskets, bolt, and rivet heads, and between lap joints. Metals that form a passive oxide film on their surfaces are particularly prone to crevice corrosion, e.g. stainless steels and aluminium alloys. Preventive measures that could be beneficial are as follows: avoid stagnant conditions owing to too-close proximity of metal surfaces; sealants around and within joints; and solid non-absorbent gaskets wherever possible, etc.

Fig. 23.15 SEM macrograph showing corrosion debris near the compressor blade leading edge and fatigue progression markings (10×)

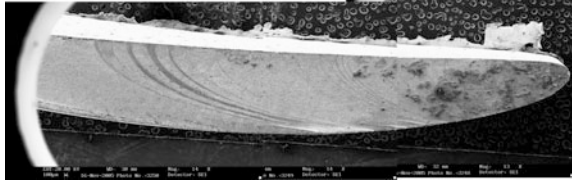


Fig. 23.16 SEM fractograph showing pitting corrosion at the leading edge of the blade (two irregular pits just on the 'nose' of the leading edge) (200×)



Intergranular Corrosion Grain boundaries depleted of critical alloying elements and the formation of less noble grain boundary films are prone to intergranular corrosion. For example, Cr_{23}C_6 carbides preferentially precipitate along grain boundaries in austenitic stainless steels (18-8 type) when the steels are heated or slowly cooled through the temperature range 400–900 °C; and this precipitation depletes the chromium content in the areas adjoining the grain boundaries, lowering the corrosion resistance. The steel is then 'sensitized' and susceptible to intergranular corrosion.

A first-stage compressor blade made of AISI 414 martensitic stainless steel failed in service after a life of 677 h since the last overhaul, while the life between overhauls should have been 1500 h [5]. Examination of the blade showed that pitting corrosion had occurred on the leading edge of the blade, and that this led to fatigue cracking followed by fast fracture. Figure 23.15 shows an overview of part of the failed blade, and Fig. 23.16 shows the corrosion pitting at the leading edge.

23.3.6 Hydrogen Embrittlement and Stress Corrosion Cracking (SCC)

Absorption of excessive amounts of hydrogen in a metal together with the presence of residual or applied tensile stresses can cause hydrogen embrittlement,

particularly in high-strength steels. The sources of hydrogen pickup are various, including furnace atmospheres during heat treatment, pickling, electroplating, environmental water, moist air, acids, hydrogen sulphide, and hydrocarbons. Hydrogen embrittlement from the environment can be prevented by heat treating *in vacuo*, using liners or coatings impervious to hydrogen, and using inhibitors. There are also strict guidelines for avoiding/alleviating hydrogen pickup during electroplating.

The simultaneous presence of tensile stresses and a specific corrosive medium causes stress corrosion cracking (SCC) in susceptible metals and alloys. The cracking pattern of SCC may be intergranular or transgranular, or mixed. SCC is generally environment-specific for a specific alloy system. For example, brasses crack in an ammonia-rich environment but not in chlorides, whereas stainless steels behave in the opposite way.

Preventive methods in combating SCC can be avoiding or removing residual stresses, adding inhibitors to the environment (if liquid), applying cathodic protection, and changing the material. In practice, it is best to change the material or its metallurgical condition, such that there is little or no susceptibility in the service environment.

Socket head cap screws M14 × 1.5 were used to assemble an intermediate dome to the nozzle end dome flange before proof pressure testing a Stage II rocket motor case [6]. The proof pressure level was 6.6 MPa, but the screws failed already at a pressure of 6 MPa.

The screws were made of cadmium-plated high-strength low-alloy steel with a hardness level of 450 HV. Investigation revealed that the screws had failed due to hydrogen embrittlement, since they had not been baked properly after plating. Evidence for the hydrogen embrittlement is given in Fig. 23.17, which shows that fracture was a mixture of intergranular cracking and microvoid coalescence.

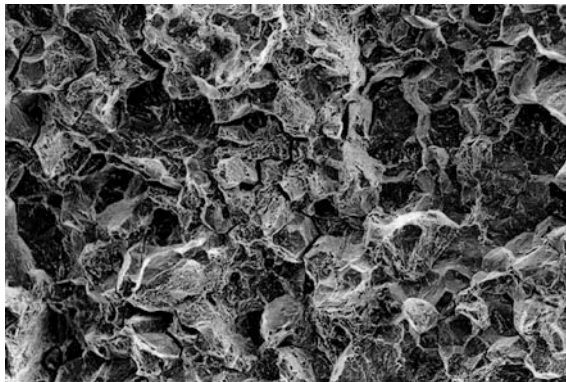


Fig. 23.17 SEM fractograph showing failure of a cap screw by intergranular fracture and microvoid coalescence. This also shows that interpretation of hydrogen embrittlement can be difficult: in most high-strength steels hydrogen embrittlement is almost entirely intergranular, while in others *unembrittled* failure may be partly intergranular (1000×)

23.3.7 Wear

There are different types of wear, for example abrasive wear, erosive wear and adhesive wear. Lubricants are used to avoid premature wear in engineering devices, such as bearings, gears, axles, shafts, pistons and cylinders.

Lubricating oils, grease, and solid lubricants like molybdenum disulphide are commonly used for lubrication. Failure of lubrication can cause dry running conditions of moving parts, resulting in frictional overheating and subsequent failure of the parts and the component.

A high-pressure compressor rotor (HPCR) case-hardened steel gear of an aeroengine failed in service, see Fig. 23.18 [7]. The failure was due to premature wear-out of the internal splines of the gear: the middle region of the splines was completely worn out, see Fig. 23.19.

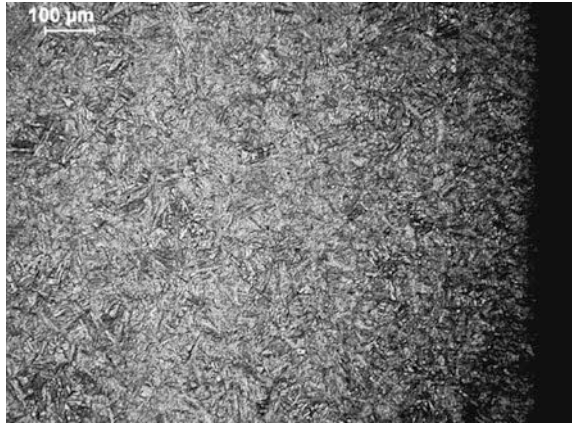
Fig. 23.18 The failed HPCR gear received for examination



Fig. 23.19 The two halves of the HPCR gear central splined region, showing worn-out splines



Fig. 23.20 Etched metallographic cross-section of an intact spline near the surface, showing the absence of case hardening (no white-etching surface layer)



Metallography showed that the splines were not case-hardened, see Fig. 23.20. This was confirmed by hardness measurements: the hardness of the surfaces and cores of the splines was almost the same, about 380 HV. Thus the HPCR gear had failed by wear because case hardening was omitted.

23.3.8 *Overheating*

The major types of elevated temperature failures are creep deformation and stress rupture, which is also due to creep. Creep usually begins in metals and alloys at temperatures slightly above their recrystallization temperatures. However, for the class of alloys known as superalloys, creep is postponed to high temperatures, typically above 650 °C (see Chap. 9 in Volume 1 of these Source Books).

A helicopter engine was received with a complaint about fracture and failure of a second-stage turbine blade made from a nickel-base superalloy [8]. The broken blade was suspected to have damaged other rotating parts downstream of the gas flow path. The blade-operating temperature was about 900 °C. The engine had completed 593 h since last overhaul and 5111 h since new, while the intended service life was 12,000 h.

Blueing of the aerofoil region, as in Fig. 23.21, confirmed that the blade had suffered overheating. Failure of the blade had occurred near the tip, and half of the fracture surface from the leading edge revealed intergranular fracture (see Figs. 23.22 and 23.23). The remaining fracture was fast fracture (overload), as evidenced by microvoid coalescence.

The cracking of the blade near the leading edge was attributed to creep and stress rupture owing to an increase in operating temperature.

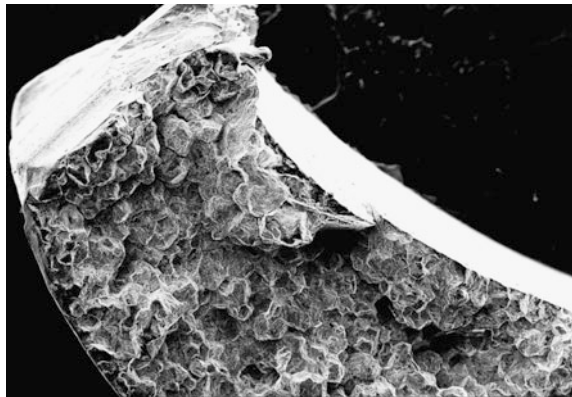
Fig. 23.21 Failed turbine rotor blade as-received. Note the blueing discoloration of the aerofoil and tip breakage



Fig. 23.22 Blade fracture surface showing a rough oxidized (*dark*) region over half the chord, beginning from the leading edge ($7.5\times$)



Fig. 23.23 SEM fractograph near the leading edge of the blade, showing an intergranular and oxidized fracture ($150\times$)



23.4 Tools and Techniques of Failure Analysis

Acquisition of Background Information An account of the circumstances that led to a failure needs to be obtained from the operators and users. Information like the intended service life and actual life at failure will assist the failure analyst in the investigation.

The service loads and types of stresses (static or dynamic), operating environments and temperatures, and the material specifications are some of the essential background data.

If failure occurred in a nominally defect-free component and under the expected service conditions, then the design safety factor may need to be checked. This is

often difficult to do and usually requires cooperation from the component manufacturer.

Selection of Samples It is always better for the analyst to visit the accident site in order to get first-hand information and request and collect suspect components for analysis. Unfailed components may also be requested for comparison. However, it is often the case that a failed component will be delivered to the failure analyst. This makes it all the more important that background information is obtained.

Photographic Records Photographs of the accident site and suspect/failed components in the as-received condition, with suitable scale markers, must be taken and recorded, with dates, times, and signatures. While taking photographs of failed parts, several images from various angles and orientations should be made. Making sketches of a failed part is also a good practice.

Preliminary Examination This requires much care and skill. The failed component must be visually examined to begin to understand the failure. Any foreign substances such as soil, oil, grease, embedded particles, and corrosion debris near or at the failed location should be recorded and samples taken for eventual analysis. Visual examination should be done firstly without magnification aids and subsequently or contemporaneously using a 10× magnifying glass and a stereo microscope (up to 50×). For fracture surfaces this should be done under diffused light conditions, avoiding sharp reflections. The component nominal and actual dimensions should be measured and checked against design drawings and specifications.

Non-Destructive Testing (NDT) NDT tests help in checking for defects and cracks. Surface-connected narrow and tight cracks exposed to the surface are revealed using a dye-penetrant test. Surface and shallow defects in electrically conducting materials, i.e. metals, can be detected using eddy current probes. Surface and subsurface cracks in magnetic materials may be detected using magnetic crack detection techniques. X-ray radiography is also useful to detect subsurface flaws. Ultrasonic testing may be used to determine and locate internal flaws in wrought products (this is a standard technique during forged component production). Much more on NDT techniques is given in Chap. 11 of this Volume.

Chemical Analysis This can check whether the material of a failed component has the specified composition. There are different techniques for chemical analysis. The technique is chosen based on the element(s) to be analysed and the available component size. Suitable samples are to be prepared before analysis, since different techniques demand different sample sizes and shapes. The sampling technique requires the removal of surface contaminants before chemical analysis.

Optical Microscopy Samples are prepared for metallographic examination by standard techniques. In the as-polished condition, defects such as voids, cavities, porosities, and secondary or pre-existing cracks are noted. Non-metallic inclusions and their size and distribution density are recorded in the case of steels and alu-

minium alloys. After etching with a suitable reagent, a sample is examined to view constituent phases and grain shapes and sizes. Defects such as alloy segregation and banding (in steels) can also be observed. The microstructure near and remote from the failure location may reveal whether any microstructural anomaly could have contributed to the failure and whether such an anomaly was the result of service use or was present from manufacturing.

Scanning Electron Microscopy (SEM) The scanning electron microscope has the advantages of high resolution and good depth of focus and is an established cornerstone of failure analysis of fractured parts. Secondary electrons (SE), backscattered electrons (BSE), and X-rays are all generated during SEM, and these can be detected and analysed for specific contributions to the examination. SE and BSE are used for fractographic and metallographic analysis, and these can be combined with X-ray analysis in spot- and line-scan element analyses. Quantitative and semi-quantitative chemical analyses can be made using energy-dispersive analysis of X-rays (EDX).

Electron Probe Microanalysis (EPMA) The wavelength-dispersive X-ray analysis technique (WDX) is used in EPMA. This is more accurate than EDX. EPMA is used mainly for spot- and line-scan element analyses. However, modern scanning electron microscopes also can have WDX facilities. Examples of the use of WDX analyses are as follows:

1. Determination of concentration gradients at phase boundaries, grain boundaries, diffusion couple interfaces, and in welded sections.
2. Identification of phases and inclusions.
3. Analysis of coatings.
4. Determination of segregation within a single phase.

X-Ray Diffraction (XRD) In contrast to chemical analysis for elemental composition of the alloy, phase analysis by the XRD technique determines the presence and compositions of the phases or compounds. In failure analysis, XRD is used to determine

1. The volume fraction of retained austenite in steels.
2. Residual stresses in a component.
3. The composition(s) of service-induced deposits and contamination.

Mechanical Properties Hardness and tensile tests are (sometimes) done to check the mechanical properties of alloys, particularly steels. Tensile tests are also used for checking the strengths of wires and wire cables. Microstructural and mechanical strength nonconformity due to improper heat treatment or degradation during service can be determined from hardness measurements, including the presence or absence of case hardening for steels (see the earlier discussion of an HPCR gear failure).

For steels the impact toughness is important when checking for embrittlement effects such as strain-age embrittlement, quench-age embrittlement, tempered martensite embrittlement, temper embrittlement, and general behaviour at low temperatures. Fracture toughness, fatigue, and stress corrosion tests may also be useful for checking the properties of steels as well as other alloys, depending on the type of failure encountered.

23.5 Case Studies

23.5.1 Steel Inner Gear of an Aeroengine

Background A cargo aircraft was reported to have ‘autofeathered in air’. Preliminary inspection showed damage of a steel inner gear of an aeroengine [9]. This component was stated to have an approximate working speed of 8620 RPM, a service temperature of 65–80 °C, and an operating pressure of 6.5–7.0 MPa.

Experimental Results The failed inner gear is shown in Fig. 23.24. Three gear teeth on either side of the fracture were found to be badly worn, with less damage away from the failure location. There was also general rubbing on the inner surface of the gear.

The fracture surfaces showed a smooth fracture feature originating at a tooth root fillet at one end (see the arrow in Fig. 23.25). This was a quarter-elliptical crack that grew in the gear radial direction. Beyond this smooth area the fracture surface was rough and fibrous.

The fracture surface was cleaned and examined by SEM. The smooth area showed that the origin of the crack was at the tooth root fillet, and faint progression markings emanated from this region, see Fig. 23.26. The smooth fracture region

Fig. 23.24 Failed steel inner gear received for investigation

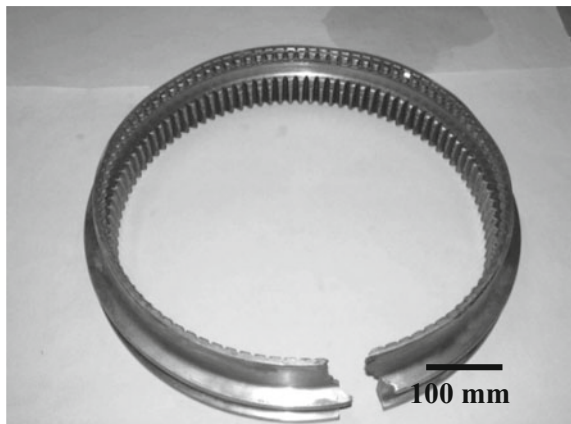


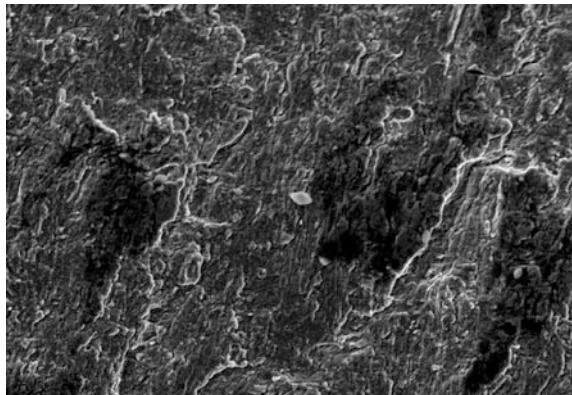
Fig. 23.25 Fracture surface of the failed inner gear showing the fracture profile characteristics and the origin (arrowed)



Fig. 23.26 SEM fractograph of the fracture surface showing the origin at the tooth root fillet and (very) faint progression markings (50 \times)



Fig. 23.27 SEM fractograph of the smooth fracture region showing ill-defined fatigue striations (750 \times)



showed ill-defined fatigue striations, as in Fig. 23.27. The fibrous fracture region revealed equiaxed dimples, characteristic of microvoid coalescence.

A sample adjacent to the fracture surface and perpendicular to the teeth was sectioned and prepared for metallographic examination. In the unetched condition

Fig. 23.28 Unetched section of a gear tooth, showing cracks at the tooth root fillet

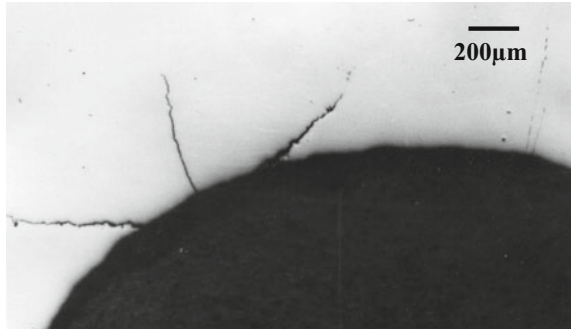


Fig. 23.29 Etched cracked sample showing a more or less white-etching case-hardened surface layer about 550 μm deep (see the main text)

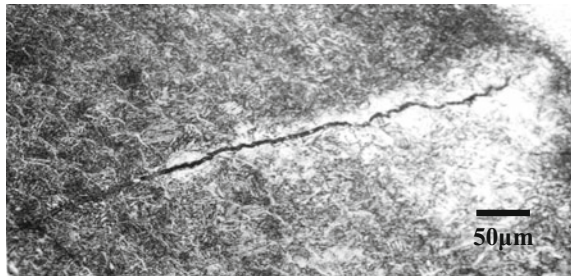
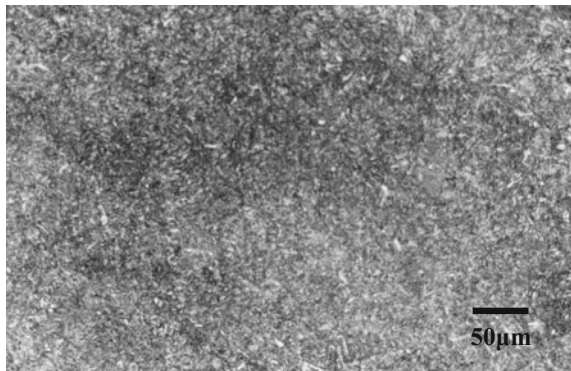


Fig. 23.30 Micrograph of the etched sample showing tempered martensite in the core



the sample showed a few cracks originating from the root of a tooth (see Fig. 23.28). This tooth was the second one from the failure location. On etching with 2 % nital, the sample revealed a case-hardened structure, see Fig. 23.29. The average case depth was 550 μm. The crack in this figure was mainly transgranular. The crack did not show any decarburization around it or oxidation products within it. The case showed a tempered martensitic structure with a white-etching network along the prior austenite grain boundaries. The core of the sample showed a tempered martensite structure, as in Fig. 23.30. The average Vickers hardness of the core and case was 350 and 750 HV, respectively.

Chemical Composition The chemical composition of the steel is given in the following table:

Element	wt%
C	0.41
S	0.002
P	0.013
Si	0.19
Mn	0.40
Cr	1.30
Ni	0.13
Mo	0.15
Al	1.20
Fe	Remainder

Discussion Chemical analysis, microstructure, and hardness suggested that the failed inner gear was made of a low-alloy steel conforming to Russian grade 38XMHOA, specification MTY 1-950.70, and used in the tempered and case-hardened condition.

The opening out of the failed gear (see Fig. 23.24) indicates that there were significant circumferential residual stresses. The severe damage of the tooth profiles over the entire gear suggested that the gear had suffered destructive wear, which is generally associated with excessive tooth loading for the lubricant being used [10].

Cracks at a tooth root fillet, see Fig. 23.28, could have been generated during final grinding. This is inferred from the facts that the cracks are small and did not show decarburized layers around them or oxides within them: cracking during heat treatment would probably have resulted in some decarburization and oxidation of the crack surfaces.

Conclusions From the fractographic evidence, see Figs. 23.25, 23.26 and 23.27, it is concluded that one of the (probable) grinding cracks propagated under fatigue loading, eventually leading to fast fracture and failure of the gear. This would have caused the gear to try to open out, leading to severe wear of the teeth close to the failure location.

Remedial Measures These include the following:

1. NDT of other gears for grinding cracks.
2. Replacing the failed gear with a new crack-free gear.
3. Reporting the cracking problem to the gear manufacturer.

23.5.2 Inner Flange of Flame Tube

Background The inner flange of a flame tube was found to have cracked during disassembly/inspection of an aeroengine which was received by a base-repair depot for defect investigation [11]. The flame tube was reportedly made from a nickel-base superalloy of grade XH60BT (Russian specification). It was also reported that the maximum working temperature of the component was 1300 °C and it had completed a service life of 1289 h.

Experimental Results Figure 23.31 shows the cracked flame tube after engine disassembly, and Fig. 23.32 shows front and back views of a sample taken from the cracked area. It was noted that after cutting to remove this sample, the flame tube had opened out by about 150 mm.

The dark U-shaped areas visible at the bottom of the flame tube in Fig. 23.32a are locations where the flame tube protective coating was absent. Cracking passed through the centre of one of these dark areas. Optical stereomicroscopy indicated that these dark areas had probably been welded and subsequently ground for levelling. The grinding was prominent on the back of the cracked region, see Fig. 23.33. The reason for the welding (repair) was unknown.

The flange showed another crack from a similar U-shaped area adjacent to the primary cracked area, see Fig. 23.34. The main cracked portion was cut out and removed, and the fracture surface is shown in Fig. 23.35.

On cleaning and examining under a stereo microscope, the fracture surface revealed faint progression markings emanating from the U-shaped area, see Fig. 23.36. The fracture surface was cleaned and examined by SEM. The fracture origin showed narrow terraces of fatigue striations and some secondary cracking: Fig. 23.37 shows an overview, Fig. 23.38 shows a detail showing the striations, and Fig. 23.39 shows the secondary cracking.

Sections from the primary cracked area and the U-shaped area containing the primary crack were prepared for metallography. On etching with Kalling's reagent, the region adjacent to the cracked area showed columnar grains, as in Fig. 23.40.

Fig. 23.31 Inner flange of the flame tube showing the damage and cracking

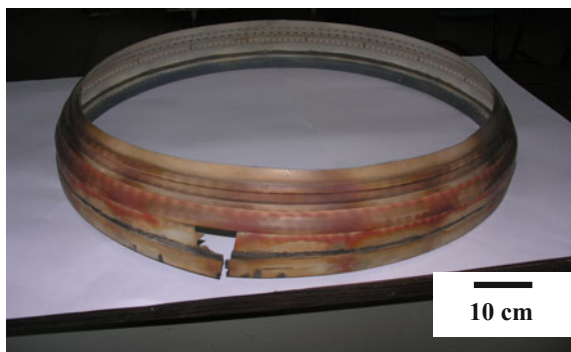


Fig. 23.32 A piece cut from the inner flange showing front (a) and back views of the cracked area (0.25 \times) (b). Note in (a) the several dark U-shaped areas at the bottom of the flame tube

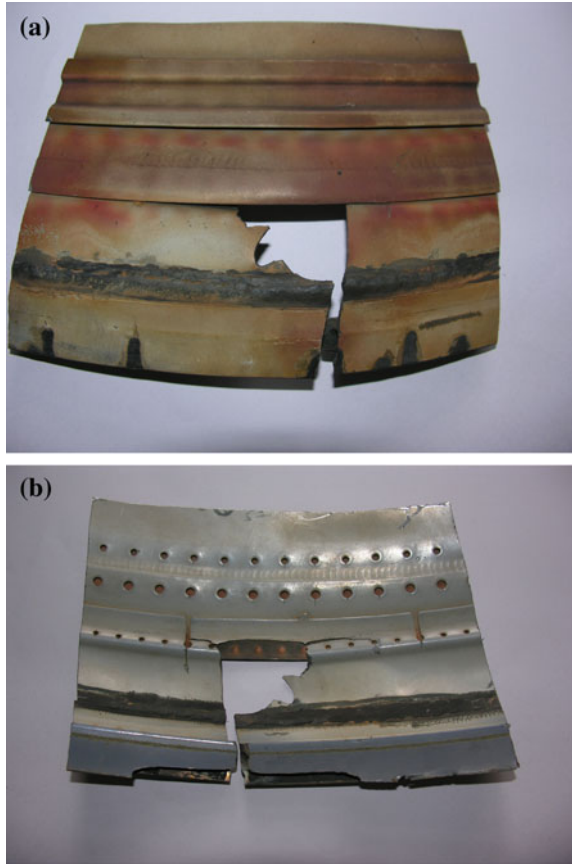


Fig. 23.33 Prominent grinding marks on the back of the cracked area (0.5 \times)

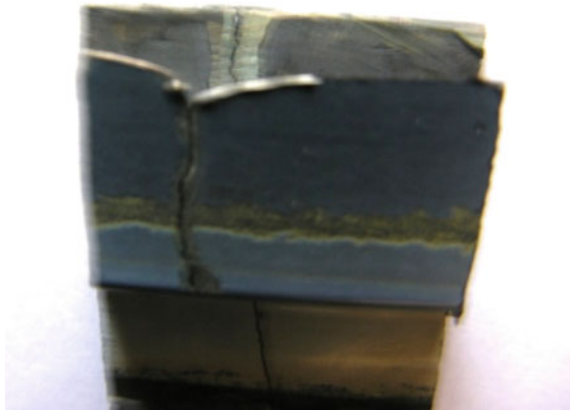


Fig. 23.34 Another crack seen on a U-shaped area near the primary crack (2×)

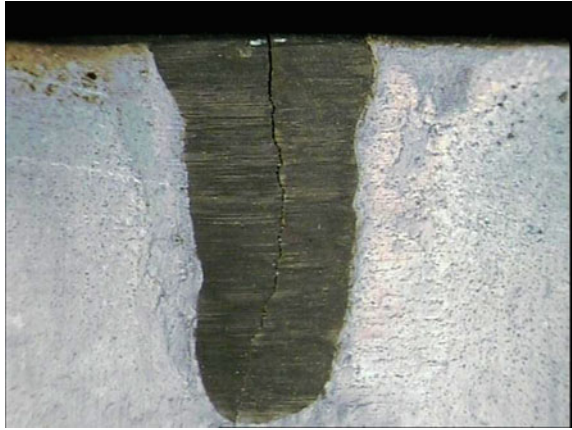


Fig. 23.35 Fracture surfaces after opening the primary crack (0.5×)



Remote from the cracked area, the alloy revealed equiaxed grains of γ with undissolved carbides and carbides precipitated along grain boundaries, as in Fig. 23.41.

The section from the U-shaped area containing the primary crack showed a weld and cracks at the weld –parent alloy interface: An example is given in Fig. 23.42. The weld showed columnar grains near the interface and fine dendrites within coarse grains.

The average Vickers hardness on the inner flange sample was found to be 250 HV for the parent alloy and 220 HV for the weld at the U-shaped area containing the primary crack.

Fig. 23.36 Primary crack fracture surface showing faint progression markings which emanated from the U-shaped area (4 \times)

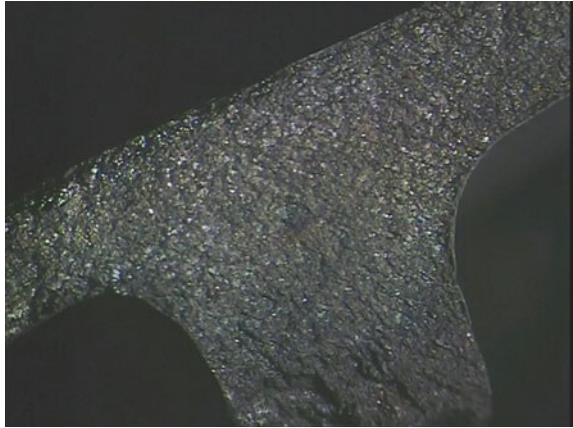


Fig. 23.37 SEM fractograph (overview) of the fracture origin showing narrow terraces of fatigue striations and some secondary cracking (750 \times)

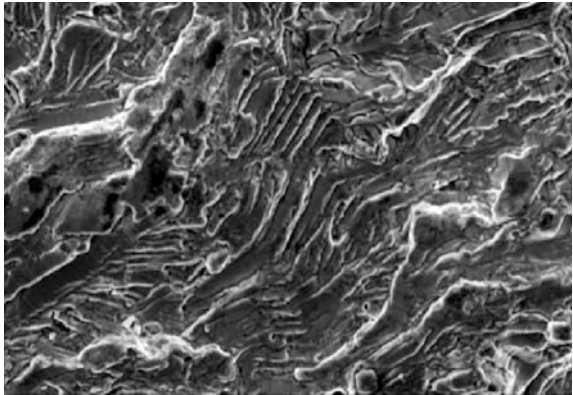


Fig. 23.38 SEM fractograph detail showing fatigue striations (1500 \times)

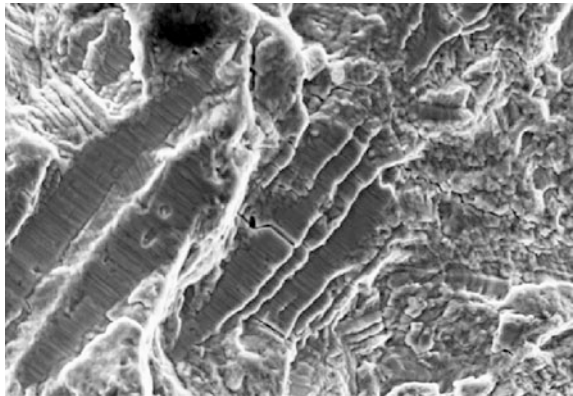


Fig. 23.39 SEM fractograph of the fracture origin showing predominantly intergranular secondary cracks. The irregular grain boundaries indicate a cast microstructure (500 \times)

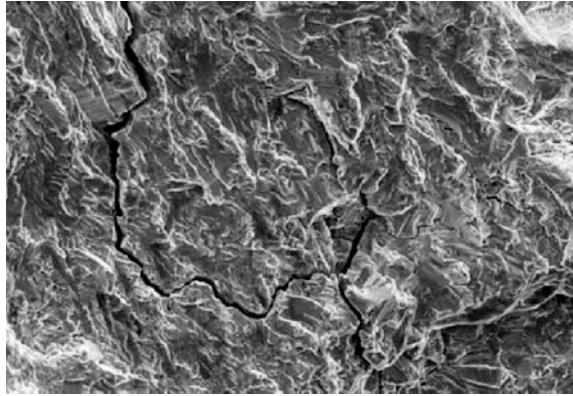


Fig. 23.40 Microstructure of a section adjacent to the cracked area showing columnar grains (etchant: Kalling's reagent)

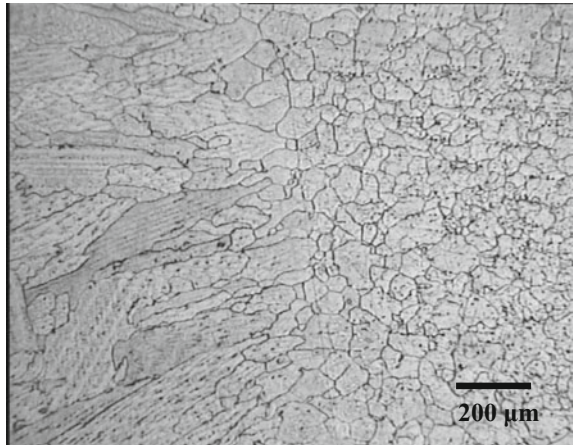


Fig. 23.41 Microstructure of a section remote from the cracked area showing equiaxed grains of γ with undissolved carbides and carbides precipitated along grain boundaries (etchant: Kalling's reagent)

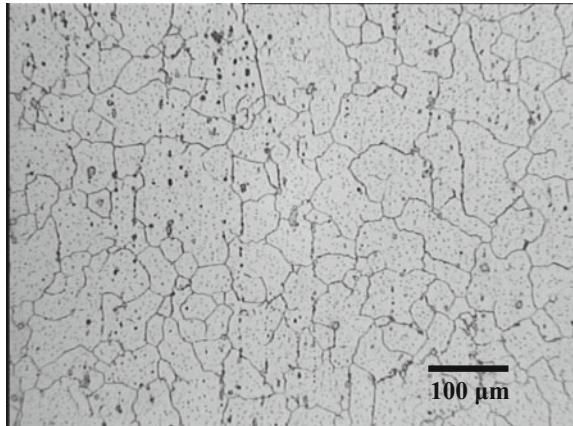
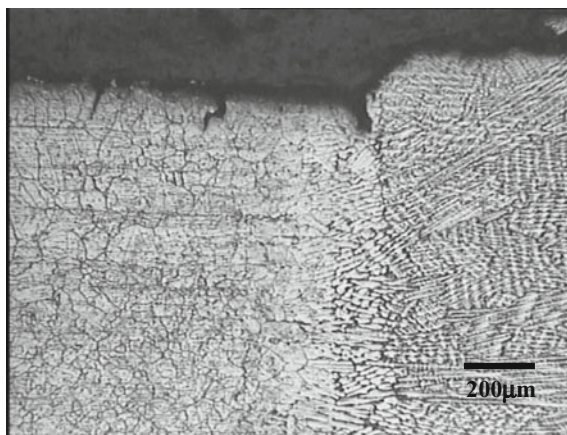


Fig. 23.42 Microstructure of a section from the U-shaped area adjacent to the primary crack, showing a weld and a crack at the weld–parent alloy interface (etchant: Kalling’s reagent)



Chemical Composition Chemical analysis of the flame tube is as given below.

Element	wt%
Cr	24.0
W	12.30
Fe	0.78
C	0.05
Mn	0.26
Si	0.43
Ti	0.32
Ni	Remainder

Discussion The chemical composition indicated that the inner flame tube was made of a nickel-base superalloy with the approximate composition of grade XH60BT of GOST 5632-72, the specified material.

The microstructure and hardness revealed that the alloy was used in a solution-treated condition. The opening-out of the ring to about 150 mm on cutting a portion from it indicated that the flange had contained significant circumferential residual stress.

Metallography showed that the five U-shaped areas corresponded to repair welds and that these had been coarsely ground. EPMA indicated that the chemical compositions of the parent alloy and the welds were similar.

Crack initiation at the weld and propagation into the flange in a U-shaped area adjacent to the primary crack revealed the cracking sequence, which would have been the same for the primary crack. The circumferential residual stress in the component probably induced the cracking of the welds. Subsequently, the cracks propagated by fatigue. The fine striations shown in Fig. 23.38 had spacings less

than 1 μm , indicating high-cycle fatigue (most probably due to vibrations caused e.g. by fluctuations in gas pressure).

Conclusions Weld repairs (including coarse grinding) and residual manufacturing stresses in the inner flange of the flame tube most probably led to crack initiation at the weld(s). Examination of the primary crack indicated that it then propagated by high-cycle fatigue.

Remedial Measures :

1. Repair welding of small areas should be avoided if possible.
2. Inner flange components should be stress-relieved after fabrication.

23.5.3 Centre Main Bearing of an Aeroengine

Background The centre main bearing (CMB) of an aeroengine failed 163 h after last overhaul [12]. Disassembly of the aeroengine revealed that the CMB was damaged and the rollers were worn down to approximately half of the original diameter. The working temperature of the bearing was less than 80 °C.

Experimental Results The failed CMB is shown in Fig. 23.43. The outer surface of the inner race was badly worn, see Fig. 23.44. The rollers were also worn and deformed badly. The bearing races showed blueing indicating overheating. The cage was damaged in a few places.

Sections of the failed components were observed by optical metallography. On etching with 2 % nital, both the inner and outer surfaces of the inner race showed a white-etching layer (Figs. 23.45 and 23.46). In the remaining area the sample

Fig. 23.43 Components of the failed CMB showing bearing races, rollers, and cage



Fig. 23.44 Badly worn outer surface of the inner race of the bearing (1.25 \times)



Fig. 23.45 Micrograph of the inner surface of the inner race, showing a white-etching layer and a crack initiating from it (etchant: 2 % nital, 200 \times)

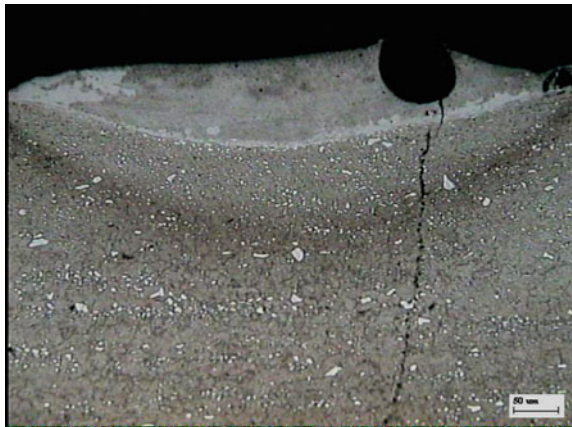


Fig. 23.46 Micrograph of the outer surface of the inner race showing a white-etching layer (etchant: 2 % nital) (100 \times)



Fig. 23.47 Micrograph of a section of the inner race showing a tempered martensite structure with undissolved carbides (etchant: 2 % nital, 500 \times)

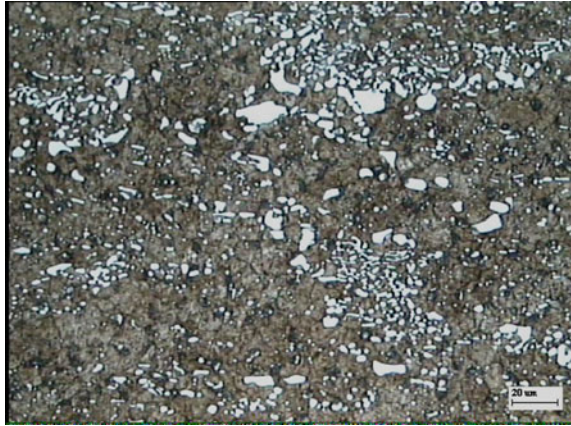
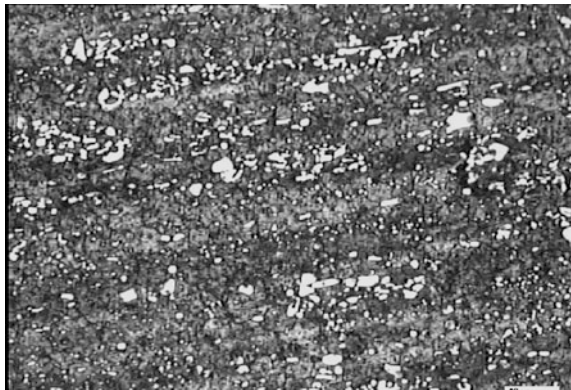


Fig. 23.48 Section of the outer race showing tempered martensite with undissolved carbides (etchant: 2 % nital, 500 \times)



showed a tempered martensite structure with undissolved carbides, see Fig. 23.47. The outer race also showed a tempered martensite structure with undissolved carbides, see Fig. 23.48.

A transverse section of a roller showed a wide white-etching layer on the surface, see Fig. 23.49. In the remaining area the sample showed a tempered martensite structure with undissolved carbides, see Fig. 23.50.

The average Vickers microhardness measured in the white-etching region of the inner race and roller and the average Vickers hardness measured on the cores of the components are given in the table following Fig. 23.50.

Fig. 23.49 Transverse section of a roller showing a white-etching layer on the surface (etchant: 2 % nital, 50×)

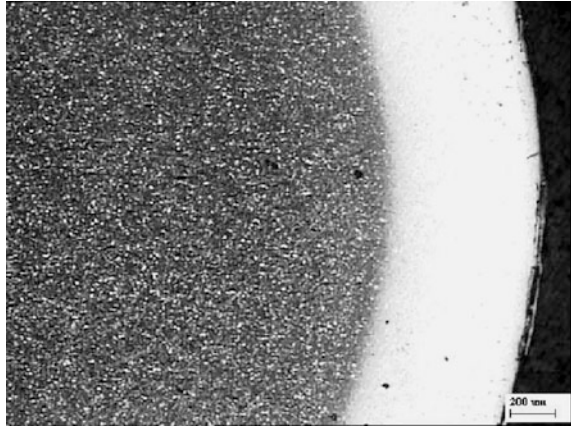
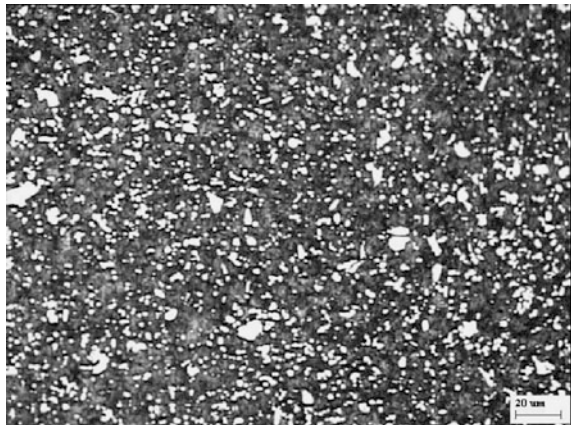


Fig. 23.50 Section of the roller sample showing undissolved carbides in tempered martensite (etchant: 2 % nital, 500×)



Hardness: Average Vickers microhardnesses for the CMB components

Part	Hardness (HV)
Inner race surface	811
Core	760
Outer race	756
Roller surface	806
Core	544
Cage	219

Chemical Composition The CMB component chemical compositions are given in wt% below.

Element	Inner race	Roller	Cage
C	0.73	0.74	1.0
W	17.5	18.3	–
Cr	4.90	4.16	1.25
V	1.10	1.10	–
Mn	0.26	0.26	0.30
Si	0.14	0.21	0.24
Fe	Remainder	Remainder	Remainder

Discussion Chemical analysis, microstructural studies, and hardness suggested that the races and rollers nearly conformed to 17W-4Cr-1V-0.7C steel and were used in a hardened and tempered condition. Chemical analysis of the cage showed that it was made of 1.0C-1.2Cr low-alloy steel. Microstructure and hardness suggested that the cage was used in a spheroidized annealed condition.

There was a significant difference between the hardness of the cores and the surfaces of the rollers and inner race, which suggests that they had experienced high service temperatures and then self-quenched, resulting in the formation of a white-etching layer of untempered martensite.

The low hardness of the roller core (544 HV) could be due to self-tempering during the experience of high temperatures: this suggestion is made because the hardness of rollers is generally maintained at similar levels to that of the races, or slightly higher [13].

All the metallographic evidence for the races, and rollers points to the CMB becoming distressed due to overheating, most probably owing to a lack of lubrication. The damage to the cage would have been due to the deformation of the rollers.

Conclusion The CMB most probably failed owing to a lack of lubrication.

Remedial Measures

1. Replace the CMB bearing, ensuring proper lubrication.
2. Inform the maintenance depot of this problem.

23.6 Concluding Remarks

Failure analysis is an essential discipline in engineering. Knowledge of the causes of failures helps in understanding their occurrence and in preventing additional failures. Proper utilization of available tools and techniques helps the failure analyst

in acquiring enough data while analysing a problem. Expert interpretation of the analysis results and circumstantial evidence will help in arriving at the most probable cause of a failure.

A failure analyst should be unbiased and is expected to possess a high degree of professional ethics. Besides analysing failures, it is important to suggest remedial measures and ensure their implementation.

Acknowledgments The authors would like to thank Dr. Russell Wanhill for his excellent review of this book chapter and also for his numerous inputs which have become integral parts of the text. The authors are thankful to Dr. Amol Anant Gokhale, distinguished scientist and director, Defence Metallurgical Research Laboratory Hyderabad, India, for his support and encouragement for the failure analysis activities. The authors also acknowledge with gratitude the help and support given by their colleagues in DMRL, Hyderabad, in the experimental work associated with the case studies presented in this chapter.

References

1. Balan KP (1998) Technical Report, DMRL/MIG/32/98
2. Balan KP, Narender Y (2014) Technical Report, DMRL SFAG 2014_46
3. Sambasiva Rao A, Balan KP (2012) Technical Report, DMRL/FR/2012_41
4. Balan, KP, Narender Y (2011) Technical Report, DMRL/FR/2011_24
5. Kolla HH, Jagtap NB (2005) Technical Report, DMRL/FR/2005_41
6. Balan KP (2002) Technical Report, DMRL/FR/2002_14
7. Balan KP, Narender Y (2009) Technical Report, DMRL/FR/2009_25
8. Srinivas M, Balan KP, Sai Madhav A (2007) Technical Report, DMRL/FR/2007_34
9. Balan KP (2003) Technical Report No. DMRL/FR/2003-34
10. ASM Metals Handbook (1986) Vol 11, 9th ed. American Society for Metals, Metals Park, OH 44073, USA, pp 598–599
11. Balan KP, Narender Y (2006) Technical Report No. DMRL/FR/2009_03
12. Balan KP, Narender Y (2005) Technical Report No. DMRL/FR/2005_01
13. ASM Handbook (2002) Failure analysis and prevention, vol 11. ASM International, Materials Park, OH 44073-0022, USA, p 2401

Bibliography

1. Tawancy HM, Ul-Hamid A, Abbas, NM (2004) Practical engineering failure analysis. Marcel Dekker, New York, NY 10016, USA
2. Wulpi DJ (2001) Understanding how components fail. ASM International, Metals Park, OH 44073, USA
3. IITRI Fracture Handbook (1979): Failure Analysis of Metallic Materials by Scanning Electron Microscopy, Metals research Division, Illinois Institute of Technology Research, Chicago, IL 60616, USA
4. Ross B (1995) Investigating mechanical failures. Chapman and Hall, London, UK
5. Unterweiser PM (1979) Case histories in failure analysis. ASM, Metals Park, OH 44073, USA
6. Jones DRH (1993) Materials failure analysis. Pergamon Press, London, UK
7. Hutchings FR, Unterweiser PM (1981) Failure analysis: The British engine technical reports. ASM, Metals Park, OH 44073, USA

8. Colangelo VJ, Heiser, FA (1987) Analysis of metallurgical failures, 2nd ed. Wiley, Hoboken, NJ 07030-5774, USA
9. ASM Metals Handbook (2002) Failure analysis and prevention, vol 11. ASM International, Materials Park, OH 44073-0002, USA
10. ASM Metals Handbook (1992) Fractography, vol 12, 9th ed. ASM International, Materials Park, OH 44073-0002, USA
11. Baldev R, Jaykumar T, Thavasimuthu M (2002) Practical non destructive testing, 2nd ed. Woodhead Publishing Limited, Cambridge, UK
12. McMasters RC (1963) Nondestructive Testing Handbook, Vol. II, Ronald Press, New York, USA
13. McCall JL, French PM (1978) Metallography in failure analysis. Plenum Press, New York, NY 10013, USA
14. Vandervoort GF (1979) Metallography as quality control tool. Plenum Press, New York, NY 10013, USA
15. ASM Metals Handbook (2004) Metallography and microstructures, vol 9. ASM International, Materials Park, OH 44073-0002, USA
16. Kiessling R (1968) Non-metallic inclusions in steels, Part III. Iron and Steel Institute Publication, London, UK
17. George K (1990) Steels: Heat treatment and processing principles. ASM International, Metals Park, OH 44073, USA
18. Paul MU, Howard BE, James K (1985) Heat treater's guide standard practices and procedures for steel. ASM International, Metals Park, OH 44073, USA
19. Vijendra S (2004) Heat treatment of metals, 2nd ed. Standard Publishers Distributers, Delhi, India
20. ASM Metals Handbook (1991) Heat treating, vol 4, 10th ed. ASM International, Materials Park, OH 44073-0002, USA
21. Brooks CR, Choudhury A (1993) Metallurgical failure analysis. The McGraw-Hill Companies, Inc., New York, NY 10121, USA
22. Barer RD, Peters BF (1970) Why metals fail. Gordon and Breach, New York, USA
23. Pilkey WD (1997) Peterson's stress concentration factors, 2nd ed. Wiley, Chichester, UK
24. Fontana MG, Green ND (1978) Corrosion engineering, 2nd ed. The McGraw-Hill Companies, Inc., New York, NY 10121, USA
25. Chawla SL, Gupta RK (1993) Materials selection for corrosion control. ASM International, Metals Park, OH 44073, USA
26. Ugiansky GM, Payer JH (1979) Stress corrosion cracking—the slow strain-rate technique, ASTM STP 665, ASTM International, West Conshohocken, PA 19428, USA
27. Cotterill P (1962) The hydrogen embrittlement of metals. Progress in materials science, vol. 9, Pergamon Press, London, UK
28. Harris TA (1991) Rolling bearing analysis, 3rd ed. Wiley, Chichester, UK
29. Rexnord Industries (1978) Failure analysis gears-shafts-bearings-seals. Milwaukee, WI 53208-4200, USA
30. Szeri A.Z (1980) Tribology: friction, lubrication and wear. Hemisphere Publishing Corporation, New York, NY 10036, USA
31. Bernasconi G, Piatti G (eds.) (1978) Creep of engineering materials and structures. Ed., Applied Science Publishers Ltd, Barking, Essex, UK

Chapter 24

Airworthiness Certification of Metallic and Non-metallic Materials: The Indian Approach and Methodologies

M. Sai Krishna Rao, P. Rambabu, Ch.V.S. Murthy, B. Jana, B. Saha, N. Eswara Prasad, P. Jayapal and K. Tamilmani

Abstract The Indian scenario of airworthiness certification and philosophy of certification of metallic and non-metallic materials and approach, the classification of materials based on their criticality of application and agencies involved in certification activity, and their roles and responsibilities are briefly described in this chapter. Appropriate examples and case studies for each class of materials are also discussed.

Keywords Airworthiness · Certification · Aluminium alloys · Titanium alloys · Carbon composites

Nomenclature

ADA	Aeronautical Development Agency, Bengaluru
AMS	Aerospace material specification
APL	Antenna platform (casting)
ASL	Advanced Systems Laboratory, Hyderabad
ASTRA	Name of the beyond-visual-range air-to-air missile (BVRAAM)
BALCO	Bharat Aluminium Company, Korba
BF	Bharat Forge, Pune
BVRAAM	Beyond-visual-range air-to-air missile
CABS	Centre for Airborne Systems, Bengaluru

M.S.K. Rao · P. Rambabu · Ch.V.S. Murthy · B. Jana · B. Saha
RCMA (Materials), CEMILAC, Hyderabad, India

N. Eswara Prasad (✉)
DMSRDE, DRDO, Kanpur, India
e-mail: nep@dmsrde.drdo.in

P. Jayapal
CEMILAC, Bengaluru, India

K. Tamilmani
Office of DG (Aero), DARE, Bengaluru, India

CEMILAC	Centre for Military Airworthiness and Certification, Bengaluru
CTE	Coefficient of thermal expansion
DGAQA	Directorate General of Aeronautical Quality Assurance
DMRL	Defence Metallurgical Research Laboratory, Hyderabad
DRDL	Defence Research and Development Laboratory, Hyderabad
DRDO	Defence Research and Development Organisation, New Delhi
DS	Directional solidification; <i>also</i> , directionally solidified
DSPL	Deccan Smiths Private Limited, Hyderabad
DT	Destructive testing
DTS	Development test schedule
ECIL	Electronics Corporation of India Limited, Hyderabad
FI/FISCL	Firth India Steel Company Limited, Nagpur
GIL	Graphite India Limited, Bengaluru
GOST	Russian Acronym for GOSUDARSTVENNYY STANDART (State Standard)
HAL	Hindustan Aeronautics Limited
HAL (F&F)	Hindustan Aeronautics Limited, Foundry and Forge Division, Bengaluru
HAWK	Name of an advanced jet trainer
HCF	High-cycle fatigue
HPTB	High-pressure turbine blade
HPTV	High-pressure turbine vane
HT	Heat treatment
HTCC	High Temperature Composites Centre of ASL
IAF	Indian Air Force
ID	Inner diameter
INDALCO	Indian Aluminium Company, Alwaye
IPCL	Investment and Precision Castings Limited, Bhavnagar
KMML	Kerala Minerals and Metals Limited, Kollam
L	Length; <i>also</i> , longitudinal
LCA	Light combat aircraft (Also named <i>TEJAS</i>)
LCF	Low-cycle fatigue
LPTB	Low-pressure turbine blade
LRU	Line replaceable unit
LTCC	Local type certification committee
MIDHANI	M/s Mishra Dhatu Nigam Limited, Hyderabad
MMBL	Manjeera Machine Builders Private Limited, Hyderabad
MMR	Multi-mode radar
MU	Mahindra Ugine Steel Company Limited, Colaba
NDT	Non-destructive testing
NFC	Nuclear Fuel Complex, Hyderabad
OCT	A Russian avionic specification
OD	Outer diameter

OFA	Ordinance Factory, Ambajheri
PC	Provisional clearance
QA	Quality audit; <i>also</i> , Quality assurance
QC	Quality control
R&D	Research and development
RCMA	Regional Centre for Military Airworthiness
RD	Regional Director
RDAQA (GM&W)	Regional Director, Aeronautical Quality Assurance (Guided Missiles and Weapons)
RPS	Revised process sheet
RS	Release Specification
RT	Room temperature
RTO	Resident Technical Office
SIFL	Steel and Industrial Forgings Limited, Thrissur
SMPL	Senor Metals Private Limited, Jamnagar
SOFT	Safety of flight test
TA	Type approval
TC	Type certification
TET	Turbine entry temperature
TR	Type record
TTS	Type test schedule
TY/TU	Russian abbreviation for technical conditions
UT	Ultrasonic testing
UTS	Ultimate tensile strength
VIM	Vacuum induction melting
YS	Yield strength
ZTQE	Zero time quantitative evaluation

24.1 Introduction

The requirements of low probability of failure versus a hostile service environment, high stresses, restrictions on weight and size indicated by users/designers, and stringent operational requirements necessitate a high degree of consistency in the behaviour of aerospace materials [1]. To minimize variability and maintain a high degree of consistency within a narrow range of property requirements, a systematic approach/method has been adopted and practiced. This is generally called “airworthiness certification/type testing/type evaluation” [1, 2].

Once a system, material, manufacturing process and component fabrication technique has undergone airworthiness certification, it can be assumed that the system/material/component will perform as per requirements under the intended operational conditions and fulfil the intended purpose for the desired period of time [3, 4].

24.2 Aeromaterial Production in India

The Indian aerospace industry was established in 1940. Since then, it has been serving the Indian Air Force by meeting the requirements for several types of military aircraft and helicopters. Most of the aircraft and their engines are being manufactured under licence agreement with various foreign partners. The materials required for these projects were being imported and stocked on a three- to five-year requirement basis.

Owing to limited off-take, a large variety of involved specifications, numerous mill forms and sizes, mandatory stringent airworthiness evaluation norms, and huge investment needed for sophisticated advanced production and testing facilities, in the majority of cases it was rather difficult to enthruse Indian material manufacturers to develop and produce their own patented alloys.

Furthermore, before establishing MIDHANI as a public sector undertaking under the Ministry of Defence, the metallurgical plants which existed in India were also limited; and wherever they existed, they were not well equipped with the necessary facilities and expertise essential for manufacturing aerospace materials. Import from the partners' approved sources has therefore been the most economical alternative [4].

Indigenization for self-reliance in the aerospace material industry becomes all the more untenable since some of the requirements are only a few kilograms of each mill form per year. It also provokes negative reactions from material producers towards aerospace customers who buy only a small quantity but demand extremely high quality. Thus the responsibility to solve material problems shifts from the material producer to the aircraft manufacturer [5–7].

The DMRL established in Hyderabad, India, is one of the leading laboratories under the DRDO, an arm of the Ministry of Defence. DMRL specializes in the development of high-temperature, high-performance materials, namely:

- (a) primary material products, such as titanium sponge, rare earth metals, hard and soft magnets;
- (b) high-temperature, high-performance materials, such as Ti and Ni alloys, and their components;
- (c) composites and their preforms and structures;
- (d) high temperature, wear resistant and abradable coatings; and finally
- (e) new and sophisticated material manufacturing, production and joining technologies.

These activities are all done on a laboratory to pilot plant scale. Following successful development, upscaling to industrial levels is done. Contributions to the development of materials and material technologies, especially those related to carbon and polymer matrix composites, and special fabrication methodologies by the ASL and DRDL of DRDO are also significant.

Import substitution and indigenization on a production scale is done by MIDHANI for many strategic materials like titanium alloys, superalloys and special

steels, some of which are based on DMRL developments. The integrated facilities at MIDHANI have been catering to the country's metallic materials requirements for aircraft, missiles, space and atomic energy industries. Over 50 strategic aerospace materials in various mill forms have already been successfully developed, type approved and supplied to the aircraft and aeroengine divisions of HAL, and many more are "in the pipeline".

Titanium sponge is being produced at KMML. Seamless tubes for hydraulic piping are being produced at NFC. Other industries both in public and private sectors, including INDALCO, BALCO, OFA, FI, MU, DSPL, MMBPL and SML, have also contributed to indigenization efforts for aerospace alloys. Conversions to the required shapes and sizes are normally carried out by HAL (F&F) Division; NFC; BF, SIFL; and IPCL, Bhavnagar, if required [8].

24.3 Airworthiness Regulators in India

The Indian organization of airworthiness regulations began with the formation of an RTO in Bengaluru, India, in 1958. More RTOs were established across the country to meet the regulatory demands of various certification disciplines. In 1995 the CEMILAC was founded in Bengaluru to coordinate and consolidate the activities of the RTOs [9]. CEMILAC currently has 14 RCMAAs (previously the RTOs), each with unique core competence. These competences include the following [9, 10]:

1. Ability to devise qualification requirements for airworthiness certification at the component, systems, subsystems, equipment and whole aircraft or engine level.
2. Capability to undertake certification of fully fledged combat aircraft, helicopters, engines, systems, equipment, materials and software programs.
3. Knowledge base to assess performance and evaluate designs after identifying the implications of technology advances in aerodynamics, structures, systems and equipment.
4. Security and impartiality to safeguard the intellectual property rights of customers by ensuring confidentiality of information.

24.4 Certification Methodology

The certification of a new or existing material for aerospace applications is a necessarily complex and thorough procedure, consisting of many steps and stages. Whenever there is (or appears to be) a new material requirement for the Indian Air Force or any aerospace development agency, the general procedure is as follows [9, 10]:

1. The aircraft operator/agency approaches an RCMA, and based on the RCMA's advice the operator selects a potential supplier or manufacturer. After assessing their capabilities, the RCMA circulates a "DTS/TTS" for an LTCC meeting chaired by the RD of the RCMA. Members of the LTCC include the relevant agencies and the supplier or manufacturer and operator. After the LTCC meeting the RCMA finalizes the DTS/TTS, which is the final qualification document for the material/component.
2. There are two stages involved in the approval of a supplier or manufacturer: approval of the supplier or manufacturer, and approval of the material. Both tasks are carried out by teams from CEMILAC and the DGAQA. Approval of the material requires satisfactory conformance to tests typically from three batches of material and verification of compliance with the DTS/TTS. The RCMA then issues PCs for each batch.
3. After the issuance of a suitable number of PCs, depending upon RCMA requirements, the supplier or manufacturer and the RCMA prepare the TR. The RCMA then forwards the TR along with a recommendation to CEMILAC, in order to obtain the TA. Once the TA is issued, the DGAQA and RCMA prepare the RS and issue it to the supplier or manufacturer. The production route is also sealed by the RCMA.
4. During regular production all material and component batches processed according to the sealed production route are released by the DGAQA, as per RS, and copies of the test certificates are forwarded to the RCMA.
5. Any deviations encountered during the series production are to be referred by the supplier or manufacturer to the DGAQA, and via the DGAQA to the RCMA. Based on the RCMA's advice about the production modifications, the supplier or manufacturer prepares RPSs for approval by the RCMA.
6. The TA issued to the supplier or manufacturer is renewed periodically by CEMILAC, contingent upon a mandatory reapplication from the supplier or manufacturer and a subsequent recommendation from the RCMA.

For aerospace usage the approval of materials to aid the designers is carried out to provide the following categories of properties, even for known materials produced at a second source:

- ZTQE of materials based on available national/international standards, mainly to evaluate mechanical properties: tensile strength, impact strength and fracture toughness.
- Real-time static properties: creep strength, rupture strength and structural stability.
- Real-time dynamic properties: high-cycle and low-cycle fatigue and crack propagation behaviour.

A detailed illustration of the certification methodology is given in Fig. 24.1 [10].

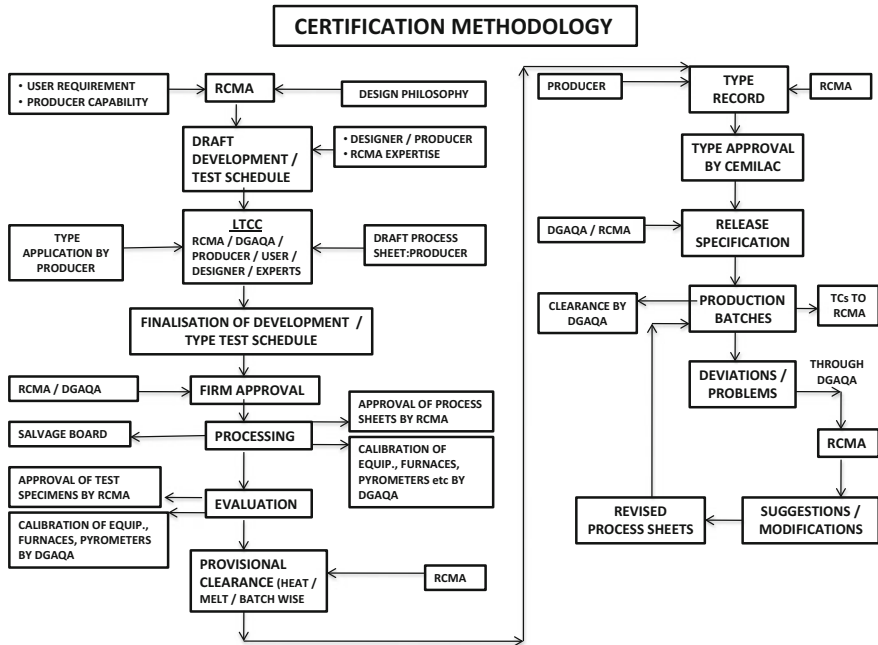


Fig. 24.1 Detailed illustration of the Indian certification methodology for aerospace materials

24.5 Airworthiness Certification Methodology

The design philosophies developed for the aircraft industry are based on well-established safety factors that are less conservative than those of other industries. This is essential because aircraft must have lightweight and highly efficient structures. In turn, this demands the use of high-strength materials with verified consistent performance.

Furthermore, the relatively high costs of manufacturing and the thrust for military aerial supremacy have stimulated a competitiveness that has brought airworthiness requirements into ever sharper focus [4]. Initiation of approval of a new supplier gets consideration when the tender is either essential for engineering purposes or commercially attractive. Tenders concerning essential aspects are mainly associated with selection of materials for initial design or design modifications. Approval of an additional supplier is also considered in the following cases:

- Approved supplier unable to meet new demands,
- Problematic supplies from an approved source,
- Mandatory buy-back clause in the licence agreement.

In all these cases, the involvement of the end-user in terms of time, technique and money is full and complete. However, in the case of material manufacturers, these are accepted as alternative or additional suppliers based on commercially attractive terms, after verification of all technological aspects. Also, approval is mostly at the cost of the manufacturer [4].

Approval of suppliers: There are two distinct stages involved in the approval of a new supplier/manufacturer. Firstly, there is a QA of the supplier's organization. This begins with the supplier submitting detailed documents about the organization, emphasizing the technical aspects. After scrutiny of these documents, a team of quality and engineering experts from the airworthiness regulatory bodies (CEMILAC/DGAQA) and representatives from developing and user agencies visit the organization and investigate its facilities in detail, in particular:

- Personnel and their technical backgrounds.
- Production facilities.
- Performance of equipment and system of monitoring.
- QC and its check system.
- Discipline of check system and checks on equipment and control systems.
- Handling of nonconformity in production.
- Systems of studying specifications and filing.
- Laboratory and R&D facilities (if any).

The team prepares a report after being satisfied about the supplier's capability of manufacturing aerospace materials and/or components. This report is submitted to the regulatory body's quality assurance agency for approval of the supplier's organization as a potential manufacturer. Only after this approval has been obtained, is the second stage of approving the materials and components undertaken.

Approval of materials: In the first instance the supplier provides general data to indicate competence in making a particular material or component, together with a declared procedure/process from start to finish. This is followed by several evaluation stages. For any Class A (i.e. primary and premium quality) metallic component there are three distinct stages of evaluation for ensuring consistent behaviour in service [4, 9, 10]:

- Material evaluation
 - Semi-product (mill form) evaluation: bars, sheets, plates, etc.
 - Raw part cut-up testing: forgings, extrusions, castings, etc.
- Product evaluation
 - Components testing and their validation.
- Performance evaluation
 - Full-scale structural unit and complete airframe tests.
 - Ground and flight testing of the aeroengine/aircraft.

Material evaluation: There are two distinct stages of material evaluation for each Class A component, namely evaluations of mill products and raw parts:

1. **Mill products:** Evaluation of mill products could be either for ab initio development or second-source approval. In the case of ab initio development, the material is tested for all possible properties. From the results the use of the material for specific applications is assessed. If a second source for an already known material is to be approved, then only the properties that depend on processing are checked. The list of properties includes tensile and compression strengths, elastic moduli, mechanical anisotropy, fatigue, crack growth and fracture.

A major aspect of the evaluation is correlation of the properties with processing variables, microstructures and chemical composition. Repeat tests are done by the customer/certification authority to check the properties. If satisfactory, then the supplier is requested to provide raw parts from 3 to 5 batches of material for evaluation. For Class A components the usual number of batches is 5. For Class B (secondary) components 2 or more batches may be evaluated. The supplier also has to provide details of processing factors and procedures that, if changed, would significantly affect the final product.

2. **Raw parts:** Evaluation of raw parts (also termed cut-up testing) is different in emphasis from mill product evaluation. The cut-up specimen tests are designed to determine the material performance under the load and environmental conditions representative of service.

As an example, Table 24.1 shows comparisons between metallurgical evaluation (ab initio and second suppliers) and production clearance specifications for Nimonic 263 sheets used in combustion chambers [1].

The number of tests conducted for approval of some typical aerospace alloys developed under collaboration and evaluated to the partner's type certification documents is compared in Table 24.2 with the number of tests specified in GOST/TY/OCT specifications: the large numbers of tests reflect the criticality involved in metallurgical evaluation for TC [12].

24.6 Metallic Materials Case Studies

24.6.1 *Aluminium Alloy Investment Castings for an Antenna Platform (APL)*

India has the smallest lightweight multi-role supersonic combat aircraft (LCA) in the world. The APL of the MMR is the primary LCA sensor and provides data for navigation, guidance and mission effectiveness.

Table 24.1 Extent of metallurgical evaluation during ab initio development, second-source approval and series production of a typical nickel-base superalloy (Nimonic 263) in sheet form for use in combustion chambers

Initial development	Second-source approval	Series production clearance
Chemical analysis <ul style="list-style-type: none"> • Raw material • Raw product • Trace elements 	Chemical analysis <ul style="list-style-type: none"> • Raw material • Raw product • Trace elements 	Chemical analysis <ul style="list-style-type: none"> • Raw product
Mechanical properties <i>Short-term properties</i> <ul style="list-style-type: none"> • UTS (plain and notched) at RT and HT • Hardness • Single bend test • Reverse bend test • Erichsen cupping test 	Mechanical properties <i>Short-term properties</i> <ul style="list-style-type: none"> • UTS (plain and notched) at RT and HT • Hardness • Single bend test • Reverse bend test • Erichsen cupping test 	Mechanical properties <i>Short-term properties</i> <ul style="list-style-type: none"> • UTS (plain) at RT and HT • Hardness • Single bend test
<i>Long-term static properties</i> <ul style="list-style-type: none"> • Stress rupture from 500 to 900 °C at intervals of 100 °C • Creep for 50 to 5000 h (700, 750, 800, 850 and 900 °C) 	<i>Long-term static properties</i> <ul style="list-style-type: none"> • Stress rupture at 550, 700 and 800 °C • Creep for 50 to 300 h (700, 750, 780 °C) 	<i>Long-term static properties</i> <ul style="list-style-type: none"> • Creep for 50 h at 780 °C)
<i>Long-term dynamic properties</i> <ul style="list-style-type: none"> • Fatigue (HCF and LCF) • Thermal fatigue 	<i>Long-term dynamic properties</i> <ul style="list-style-type: none"> • Fatigue • Thermal fatigue 	
Metallographic examination <ul style="list-style-type: none"> • Micro • Macro • Non-metallic inclusions 	Metallographic examination <ul style="list-style-type: none"> • Micro • Macro • Non-metallic inclusions 	Metallographic examination <ul style="list-style-type: none"> • Micro • Macro
Weldability test	Weldability test	
Oxidation resistance	Oxidation resistance	
Physical properties <ul style="list-style-type: none"> • Density • Modulus of elasticity • Dynamic moduli • Specific heat • Thermal conductivity • Coefficient of thermal expansion • Electrical properties • Magnetic properties 	Physical properties <ul style="list-style-type: none"> • Density • Coefficient of thermal expansion (CTE) 	
Size and tolerance check	Size and tolerance check	Size and tolerance check
Defects <ul style="list-style-type: none"> • Surface • Internal (NDT) 	Defects <ul style="list-style-type: none"> • Surface • Internal (NDT) 	Defects <ul style="list-style-type: none"> • Surface • Internal (NDT)

Table 24.2 Number of tests conducted for approval of three typical aerospace alloys developed under collaboration

Engine disc materials	Number of tests during certification	Number of tests as per GOST/TY/OCT
AE 961 W (HR steel)	140	19
BT 9 (Ti alloy)	99	21
AE 435 (Ni-base superalloy)	107	18

In 2004 the ECIL approached IPCL for development of gimbal box and pedestal unit castings for use in the LCA’s APL. This task has paved the way to the indigenization and development of APL castings for the LCA.

With active technical support and guidance from RCMA (Materials), RDAQA (GW&M), ADA and ECIL, IPCL not only succeeded in developing these critical castings with a quality and yield that are of truly international standards, but also provided a comprehensive technological base in India for such complicated precision castings.

The APL mechanical assembly (Fig. 24.2) consists of three major subassemblies: a 650-mm flat plate antenna, gimbal box and pedestal unit. The gimbal box and pedestal units (Figs. 24.2c, d) are investment cast and precision-machined components made from aerospace-grade aluminium alloy Al 356A.

The design and finalization of drawings for the castings and machining were completed based on a critical study of two imported castings. The metallic moulds were then designed and fabricated from these drawings. M/s IPCL later made certain trials for manufacturing these castings, based on their in-house R&D expertise. This enabled them to gain adequate experience and familiarity to handle

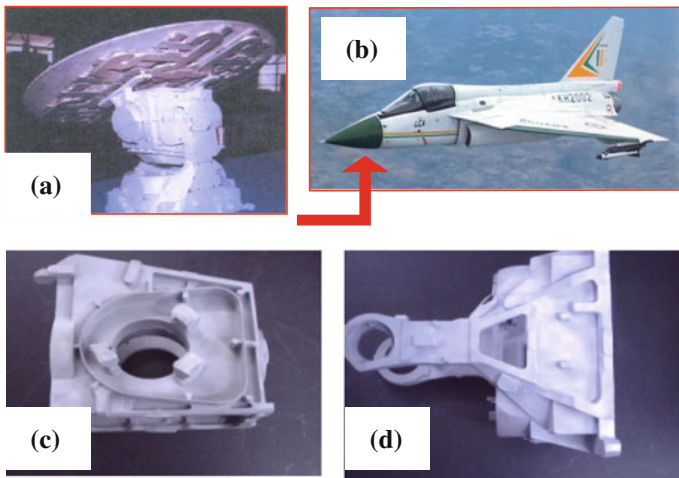


Fig. 24.2 a APL assembly for b the LCA; c gimbal box and d pedestal unit castings of the APL

such activities prior to the actual developmental trials. To approve the company and for quality audit, a team of airworthiness agencies personnel from RCMA (Materials), DGAQA and representatives from M/s ECIL visited M/s IPCL. The team examined mainly the following:

- The quality of the raw materials, such as waxes, ingredients for slurry preparation, quality of aluminium alloy for melting.
- Raw material storage and in-house analysis facilities for the material.
- Investment casting production facilities.
- HT facilities.
- Performance of equipment and calibration status.
- System for monitoring operations.
- Testing, chemical analysis laboratory and NDT facilities.
- QC systems.
- Discipline of checks on equipment and control systems.
- Handling of nonconformity in production.
- System of studying the specifications/standards and its implementation.
- Data recording system.

For providing the final TA to the gimbal and pedestal castings it was decided to process a minimum of three batches, since the APL unit is part of the MMR, which is “mission critical”, and the component is categorized as “Class II” by the designer.

Since the international best-reported yield of this type of investment castings is generally about 50 %, it was decided to cast 10–15 sets of castings in each batch, allowing for rejections during various stages of processing and also to provide castings for cut-up characterization. From these considerations it was assumed that three type test batches would deliver a minimum of 14 sets of castings (gimbal and pedestal) to the programme, as per the order placed on IPCL for the project.

Subsequent to the quality audit of IPCL and scrutiny of the process documents and procedures to be followed for manufacturing of these two castings, an LTCC discussed and finalized the certification requirements.

After considering the mandatory requirements based on the AMS 4260 specification and design requirements, a list of tests was identified to form part of the DTS (RCMA (M)/104 dated 12.04.06) for qualifying the casting during type testing. Following this, a cut-up plan for specimen extraction was worked out, covering the maximum and minimum cross-sections of the castings.

The castings were then developed and manufactured under type testing mode. A specified number of melts were taken and grouped into type test batches for characterization as per the development test schedule. The obtained yield in the first batch was very low (20 %). RCMA (Materials) studied the test reports, analysed the results, and suggested some modifications/improvements to the IPCL’s investment casting process. Evaluation of subsequent batches, and incorporating further suggestions by RCMA (Materials), the yield improved substantially (up to 65 %), as shown in Table 24.3.

Table 24.3 Batch-wise yield of investment castings during certification

Batch no.	I	II	III	IV	V
Yield (%)	20	50	43	65	61

The following results were achieved after successful completion of type certification:

1. Three sets of APL castings (gimbal and pedestal) were selected for engineering mock-up applications.
2. Three sets of development APL castings were given a clearance. These APL units have successfully cleared a SOFT test and also undergone HAWK aircraft integration trials at CABS, Bengaluru. To date, 50 sets of APL castings have been supplied after successful airworthiness certification.
3. Immense efforts were made to improve the castings yield from 20 % to around 60 % during the certification activity. It is concluded that a successful investment casting technology has been established for the first time in the country for producing these APL units to be used in the LCA's MMR.
4. The user feedback has been—"the performance of the APL castings is found to be satisfactory during the flight trials along with other LRUs for checking the functionality of the radar (in all the modes)".
5. After successful completion of airworthiness activities and user trials, TA (No. 1517) was accorded for aluminium alloy Al 356A investment castings (gimbal box and pedestal unit), to IPCL vide letter no. CEMILAC/5070/TA—1517 Dated 28.09.2010.

24.6.2 Aluminium Alloy HF 15 Forgings

ASTRA is an active radar homing BVRAAM developed by the DRDL of DRDO. DRDL required a forged aluminium alloy material for fabrication of critical components of the ASTRA airframe and avionics packages. ASTRA has four airframe sections, namely the radome (Section I), seeker section (Section II), warhead section (Section III) and avionics section (Section IV). These are classified as Class "A" components (see Fig. 24.3).

DRDO is developing these ASTRA missiles to arm IAF aircraft. This means the missiles have to function in severe environmental conditions; and this poses stringent quality requirements for qualification of feed stock material required for fabricating the missile components.

Since the missiles have IAF aircraft as launching platforms, it was mandatory to type certify the material to be used for fabrication of certain critical components. RCMA (Materials) was given the responsibility of qualifying and fulfilling the certification requirements of the feed stock material, which was aluminium alloy HF 15 forged stock.

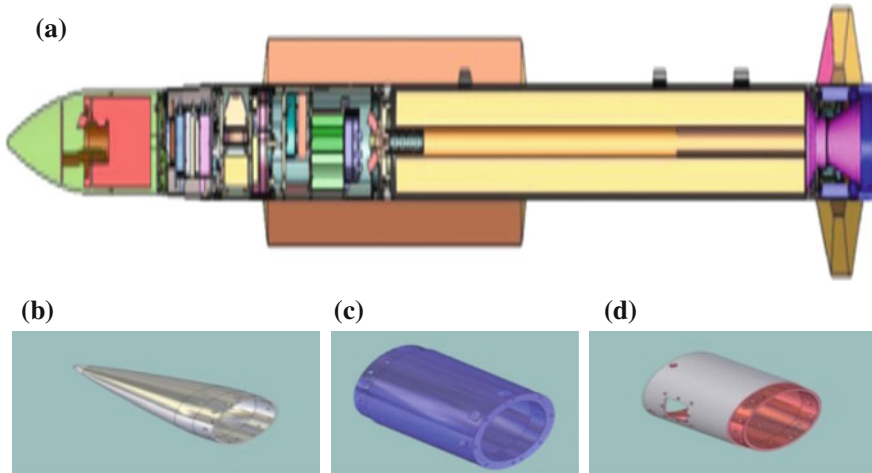


Fig. 24.3 a ASTRA aeromissile; b–d components fabricated from HF15-T652 aluminium alloy

Based on the material processing capabilities and fabrication facilities, DSPL was identified for production of aluminium alloy HF 15 forgings for fabrication of the components required for the ASTRA missile. The selection of M/s DSPL for this activity was further based on (i) their experience in manufacturing aerospace-grade materials, specifically forgings, and (ii) the technical audit carried out by the airworthiness agencies for accessing their technical know-how, equipment availability, quality control parameters, man power capabilities, etc.

DRDL placed an order with DSPL to carry out the processing and supply of three sizes of forgings (viz. $\phi 190 \times 470$ mm L, $\phi 190$ OD $\times \phi 130$ ID $\times 850$ mm L, and $\phi 190 \times 500$ mm L) made from aluminium alloy HF 15 in the T652 temper condition, and after complete type testing/type evaluation from airworthiness agencies.

Subsequent to the quality audit of DSPL and scrutiny of the process documents and procedures to be followed for manufacturing of these forgings by the airworthiness agencies, an LTCC meeting was conveyed between the designer (Project ASTRA), manufacturer (DSPL) and airworthiness agencies, i.e. RCMA (Materials) and RDAQA (GW&M), and external experts to finalize the certification requirements.

After considering the mandatory requirements based on the AMS 4133D specification and design requirements, tests were identified to form part of the type test schedule (TTS) for qualifying the forgings during type testing. Accordingly, the TTS was issued by RCMA (Materials) vide No. RCMA(M)/111 dated 04.02.08 covering all the tests and other relevant details. A summary of the tests included in the TTS is given below:

1. Chemical composition
2. Non-destructive testing
 - Visual inspection.
 - Dimensional inspection.
 - Dye penetrant inspection.
 - UT.
3. Mechanical testing
 - Tensile properties (longitudinal and transverse)
 - at room temperature.
 - at $-40\text{ }^{\circ}\text{C}$, $+50\text{ }^{\circ}\text{C}$ and $+250\text{ }^{\circ}\text{C}$.
 - Hardness.
 - Impact strength
 - at room temperature.
 - at $-40\text{ }^{\circ}\text{C}$.
 - Shear strength.
 - Fatigue strength.
4. Stress corrosion cracking
5. Metallographic examination
 - Microstructure.
 - Macrostructure.
 - Grain flow check.

All the specifications and procedures required for conducting these tests were provided in the TTS, along with the specimen drawings approved by the airworthiness agencies.

Project ASTRA had indicated their requirements of HF 15-T652 feed stock for fabricating the components. The feed stock was procured and manufactured under type testing mode and characterized and qualified as per the certification requirements laid down in the TTS.

For the type certification exercise, two sizes were rationalized. First, Section I (OD $190 \times$ L 470 mm) and Section IV (OD $190 \times$ L 500 mm), as a single size for certification; and secondly, Sections II and III (OD $190 \times$ ID $130 \times$ L 850 mm) were classified as a single size. Approved drawings for the rough forgings were enclosed along with the TTS. After finalizing the qualification requirements for these forgings as per the TTS, and then deriving the sample extraction plan, test specification/test parameters and specimen drawings, the certification activity for these two sizes of forgings was commenced.

For providing the final TA for these two sizes of forgings, it was decided to process a minimum of three batches from each size (a total of 6 batches) to ensure consistency and integrity. Accordingly, it was decided to forge a specific number of

blocks in each batch and to designate one forging from each batch for cut-up characterization (in other words, these six batches constituted the three type testing batches of the two section sizes). They were then forged, heat treated to the T652 condition, proof machined and tested as per TTS No. RCMA (Mat)/111, dated. 04.02.2008 under type testing mode at M/s DSPL.

Presently, the ASTRA project requires 40 forgings for Sections I and IV, and 80 forgings for Sections II and III, in addition to the forgings required for cut-up evaluation in each batch as per the TTS. After the technical audit the vendor, DSPL, was fine-tuned to meet the airworthiness activities, specifically fulfilling requirements like a high standard of QC during processing, characterization and testing. The following were the achievements after successful completion of type certification.

1. Based on the project requirements, two sizes of forgings were delivered after qualifying for all the test requirements as per the TTS.
2. The successful development and type certification of aluminium alloy HF 15 in the T652 condition provides a significant value addition to indigenization of missile materials for India.
3. M/s DSPL was approved as one of the indigenized sources of supply of airworthiness quality aluminium alloy HF 15 in the T652 condition.
4. After successful completion of airworthiness activities and user trials, Type Approval TA No. 1705, dated 18.01.2012 was accorded for aluminium alloy HF 15 forgings in the T652 condition to M/s DSPL, Hyderabad, vide letter no. CEMILAC/5070/TR-1705, dt. 18.01.2012.

24.6.3 Nickel-Base Cast Superalloy Supercast 247A

(A) Remelt Stock:

Supercast 247A is an advanced nickel-base cast superalloy suitable for turbine blades and vanes. The alloy has been developed successfully in the form of remelt stock by DMRL and MIDHANI under the airworthiness coverage of RCMA (Materials).

Supercast 247A is similar to the Western alloy CM 247 LC. It contains Cr, Co, Mo, W, Al, Ti, Ta, Hf, C, B, Zr, and nickel as base. There are 8 trace elements and 9 low melting-point elements that are to be controlled at ppm level, since they otherwise reduce the strength of the alloy drastically. This alloy mainly attains its strength from gamma prime (γ') precipitates. Solid solution and carbide strengthening are the other strengthening mechanisms.

Process Definition: Three consecutive melts have been recommended for type certification activity, with vacuum induction melting (VIM) as the melting route in view of the criticality of the applications, the narrow tolerances of alloying elements, and required cleanliness of the melt.

Issuance of TTS: Specified mechanical properties for these components have been drawn up after a thorough survey of recent advancements in the fields of material development and testing methodologies. A TTS has been issued comprising of chemical composition (with tolerances) to be aimed at, melting/casting techniques to be followed, heat treatments to achieve maximum strength and test methods to be followed with relevant national/international specification standards [TTS No. RCMA (Mat.)/131/Dt. 09.03.2010].

Batch Production: MIDHANI has been approved by the airworthiness agency for taking up the development of Supercast 247A, owing to the firm's vast experience in the development of aeronautical-grade materials for defence applications. Raw materials for the purpose have been permitted to be procured from approved sources to minimize the impurity contents.

Property Evaluation: Since this alloy is characterized by an extremely narrow range of compositional limits, extremely low levels of gaseous impurities (particularly nitrogen and oxygen, which are to be controlled to below 10 ppm), a round robin test methodology was adopted to assess and certify the chemistry of the remelt stock. The obtained chemistry was found to be comparable to the specification requirement, as stipulated in the type test schedule issued by the airworthiness agency. Tensile properties at room temperature and high temperature stress rupture properties at 760, 870 980 and 1040 °C were evaluated. These properties satisfied the specification requirements, and CEMILAC has approved this alloy under the recommendations of RCMA (Materials), Hyderabad, as a direct substitute for the imported version.

(B) Aerofoil Castings

The turbine entry temperature (TET) is one of the important factors that influence the efficiency of an aeroengine. The higher the TET, the higher is the efficiency. Keeping this in mind, efforts have been made globally to develop newer materials to withstand higher TETs. However, there is a limitation to the extent that the TET can be increased, since it requires materials that can cope with the higher temperatures.

As part of the indigenization activity, DMRL in Hyderabad has taken on the development of HPTV, HPTB and LPTB aerofoil components, in association with RCMA (Materials) to accord airworthiness certification. The CM 247 LC/Supercast 247A alloy, intended for casting by the DS technique, was chosen for casting these components. This alloy acquires its strength after solution treatment and two-step ageing that results in a bimodal γ' precipitation.

RCMA (Materials) was involved from the development stage to ensure implementation of airworthiness requirements in establishing the technology for consistency among the batches and integrity within the batch of components. A development test schedule (DTS) was issued by RCMA (Materials) after finalization of acceptance criteria for master heats and components in an LTCC meeting.

Three successive shell mould batches, with 12 shells in each batch, for each type of component have been identified for type certification. These shell moulds were

prepared by investment casting technology using wax patterns (which were replicas of the components) and ceramic materials to build up the shell. Besides the hollow (cored) components, each shell was supplied with a minimum of two solid components for cut-up evaluation, and two integral test bars were used for heat treatment batch qualification.

After dewaxing and firing the shells, components were cast by VIM. 100 % NDT was conducted on these components. After solutionizing and two-step ageing of the solid components and the integral test bars, the correctness of the heat treatment was checked by stress rupture testing of the bars at 980 °C.

Macrostructure studies of the components were done to assess porosity levels and grain orientation. Subsurface defects were assessed by X-ray radiography. Test specimens machined from solid components were tested for high-temperature tensile and stress rupture strength. The microstructures were studied to assess residual gamma prime, microporosity and eutectic gamma prime levels.

Since the test results met the specification requirements, provisional clearances have been issued by RCMA (Materials) to the manufacturer for supply to the user for further processing.

24.6.4 Titanium Alloy—Ti 1023

This case study deals with indigenization and certification of a beta titanium alloy, Ti 1023, with intent to use this alloy in the aerospace industry. The alloy Ti 1023 (Ti-10V-2Fe-3Al) is a beta titanium alloy which has a reasonable share of the market for aerospace applications. In the Boeing 777 the replacement of steel landing gear components by Ti 1023 resulted in weight savings of 270 kg per aircraft. Presently this alloy is intended for applications like slat and flap tracks of the LCA wings. The LCA currently uses 12 slat tracks made of maraging steel. Use of this beta titanium alloy in place of maraging steel in the slat tracks, as well as components of the landing gear, is expected to result in considerable weight

Fig. 24.4 Landing gear of the LCA

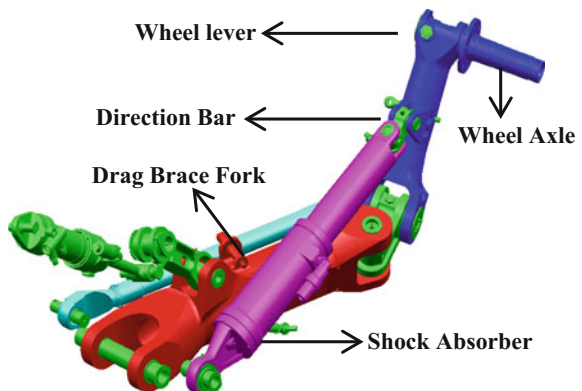


Table 24.4 Mechanical properties of Ti 1023 alloy

Properties	0.2 % YS (MPa)	UTS (MPa)	% El	% RA	K _{Ic} (MPa√m)
Specified	1103	1193	4	–	≥ 44
Properties obtained					
Specimen 1	1148	1226	6	12	67
Specimen 2	1142	1217	10	24	61
Specimen 3	1149	1225	6	12	75

savings. Figure 24.4 is a schematic of the landing gear for which the existing maraging steel will be replaced by Ti 1023.

Certification Methodology: The methodology adopted for certification of this alloy was similar to the procedure mentioned in Sect. 24.1 of this chapter.

Since the alloy is to be used for critical applications, RCMA (Materials) made a detailed in-depth study of the processing, the properties characterization techniques, the structure–property correlations and the related aerospace qualification specifications.

This information was used during finalization of the DTS/TTS during the LTCC meeting held between the designer, manufacturer, user and airworthiness agencies. M/s. MIDHANI was the approved manufacturer of the alloy. As per the standard procedures, the manufacturing agency provided all the process documents to the airworthiness agencies, and after approval the first batch/heat of 1.4 ton was made in the presence of the airworthiness agencies and developing agencies.

In this effort a concurrent certification approach was adopted. It was decided that once the heat/batch met the DTS requirements, an airworthiness clearance should be accorded on a heat-by-heat basis. Based on the encouraging results from the first type test batch (Table 24.4), a second type test batch was made to ensure that certain issues were solved. These heats were processed into forgings and hot rolled bars for subsequent manufacturing of components.

The flow chart in Fig. 24.5 shows the process followed for the processing and certification of this new alloy. Detailed characterization of this second type test batch is being done, and the preliminary results are very encouraging.

24.7 Airworthiness of Non-metallic Materials and Certification Methodology [Case Study on Carbon–Carbon Composite Brake Discs for TEJAS]

LCA-TEJAS is designed and developed by ADA in partnership with HAL. Both ADA and HAL are supported in this national effort by various DRDO and other national laboratories, academic institutions, and private and public sector

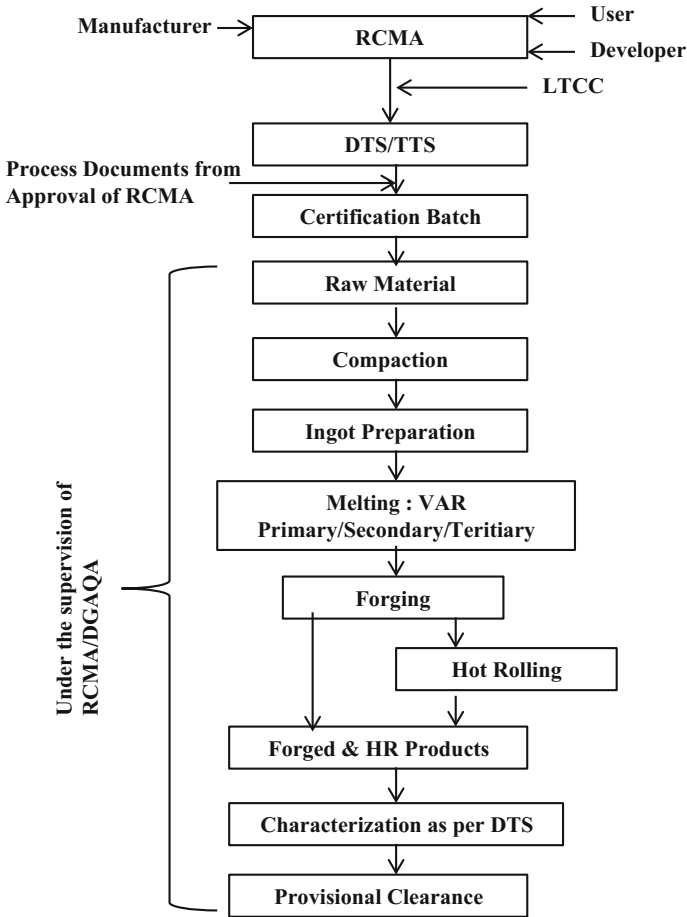


Fig. 24.5 Flow chart for the certification process of beta titanium alloy Ti 1023

industries. In order to make the aircraft light so as to enhance its combat mission capability, the *TEJAS* aircraft contains approximately 45 wt% polymer-based composites. The material for its braking system is also a composite, namely a carbon-carbon (C-C) composite.

The two main wheels of *TEJAS* use multiple disc brakes. Each brake consists of three rotating discs (rotors) sandwiched between four stationary discs (stators), as shown in Fig. 24.6. The two stators positioned at either end have only one surface that experiences rubbing and are therefore called single stators. The others are called double stators. The rotors are keyed to the aircraft wheel and rotate with it. When braking is applied the stators are brought into contact with the rotors, and these contacts provide the braking action.

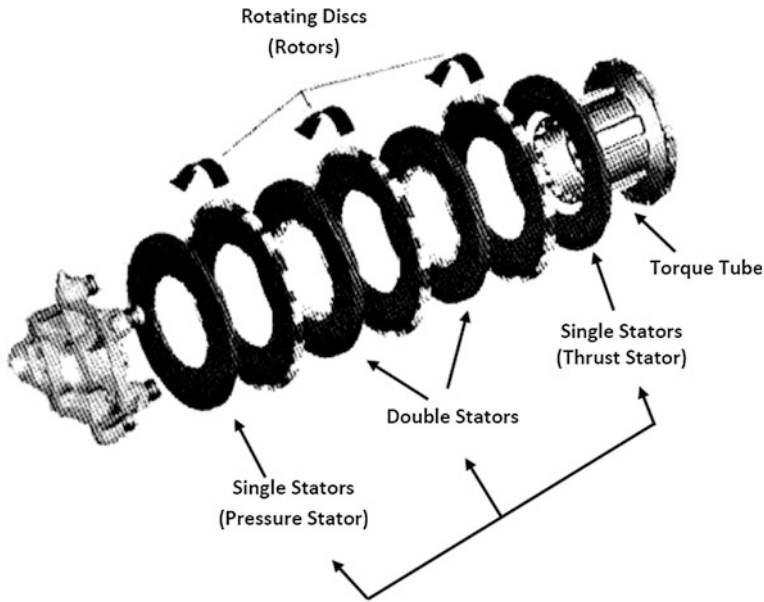


Fig. 24.6 Exploded view of C-C composite brake discs stack in *TEJAS* aircraft wheels

Aircraft brakes are required to provide frictional torque to stop the aircraft and to hold it stationary against its engine thrust. As the kinetic energy of the aircraft is absorbed, a considerable amount of heat is generated due to the friction between the rotor and stator discs. This causes the bulk temperature of the discs to rise over 600 °C with surface temperature reaching more than 2000 °C. Thus aircraft brakes must be capable of absorbing a considerable amount of heat, of the order of several hundred MJ.

Further, the brakes should withstand the most hostile condition, which is when take-off of a fully loaded aircraft is aborted, i.e. the brakes should have a rejected take-off (RTO) capability. C-C composites have this capability, unlike other known braking materials such as ceramic pads fitted onto metal (copper or steel) discs; and they also provide considerable weight savings and longer service life (40 % lighter and more than double the service life compared to their steel counterparts). C-C composites accordingly emerged as a popular structural single-piece brake material which can fulfil the above requirements.

The High Temperature Composites Centre (HTCC) of ASL, located in Hyderabad, has established state-of-the-art facilities and process technologies for C-C brake disc composites based on multiple cycles of liquid pitch impregnation and pyrolysis. Graphite India Limited (GIL), Bengaluru, is the identified production agency and has been manufacturing C-C brake discs employing the ASL process technology. RCMA (Materials) fully participated right from the stage of raw materials selection through each stage of processing and testing, to certify the material to fulfil the airworthiness requirements.

The developed process technology is being continuously revised to improve the performance of the process (in terms of increased yield by nullifying the rejection rate) as well as the brake discs (in terms of increased service life, i.e. number of landings, by reducing wear rate). The results of the improvement programme yielded development of Mark-II (expected no. of landings ~150–250), Mark-III (expected no. of landings ~300–350), Mark-IIIA (expected no. of landings ~400–450) and Mark-IV discs (expected no. of landings ~700). Presently, the *TEJAS* aircraft are fitted with Mark-III discs. The production and evaluation of Mark-III and Mark-IV discs are in progress. Moreover, a process is under consideration for upscaling to make mark-V discs (expected no. of landings ~1000).

With the participation of ADA (user), HAL (designer of the brake unit), ASL (process designer), DGAQA (production controlling authority) and technology experts, RCMA (Materials) devised an extensive testing programme by issuing a TTS in order to qualify the brake discs for service use. The testing programme included the following product evaluations:

- A. Carbon–carbon brake discs
- B. Non-destructive testing
 - Visual inspection.
 - Dimensional inspection.
 - Through transmission ultrasonic inspection.
- C. Evaluation of C–C material by cut-up testing
 - Physical properties
 - Density.
 - Open porosity.
 - Mechanical properties
 - Flexural strength at RT.
 - Inter-laminar shear strength (ILSS) at RT.
 - Compressive strength at RT and 950 °C.
 - Thermal properties
 - Coefficient of thermal expansion (RT–1000 °C).
 - Specific heat (RT–600 °C).
 - Thermal conductivity (RT–1500 °C).
 - Mass loss rate (RT–1000 °C).
- D. Metallic attachments to C–C Discs (clips and rivets)
 - Chemical composition.
 - NDT—DPT and UT.
 - Tensile strength.
 - Hardness.
 - Microstructure.

E. Performance evaluation

- Disc-on-disc brake dynamometer (normal energy and overload).
- Full-scale brake dynamometer (normal, overload and RTO).
- Aircraft level testing.

Based on the above evaluations of the discs produced by HTCC and GIL, the Mark-II brake discs were first issued type approval by CEMILAC, vide TA No. 1407 dated 16.04.2014, for usage in the LCA (Air Force version). Mark-III brake discs were later issued type approval by CEMILAC for both Air Force (vide TA No. 1712 dated 22.03.2012) and Navy (vide TA No. 1734 dated 30.10.2012) versions of the LCA.

To date, the supply of 27½ aircraft sets of Mark-II discs (385 nos.) and 35½ aircraft sets of Mark-III discs (497 nos.) was made for usage in *TEJAS* flights, resulting in considerable foreign exchange savings.

24.8 Type Clearance Process

On declaration by the material manufacturers that their products meet all the requirements stipulated in the approval specifications, the user conducts repeat tests to check the claims. In many cases the user also keeps certain test data in-house and verifies these data before placing development orders for three to five melts/batches, based on the class and end use. Details of significant factors that, if changed, will affect the final product, are also supplied by the manufacturer. These include but are not limited to the following:

- Processing parameters.
- Processing controls.
- Technical team employed.
- Quality control checks.
- Handling of bonded stores.

Evaluation of minimum number of melts/batches: For materials to be manufactured into Class A components, most users ask for characterization of five different melts/batches before giving approval. Initially one to two heats are completely used for testing the alloy and the products. Based on the results another three heats are ordered. Final clearance is given only after satisfactory performance of the product of the five heats. However, for Class B components about two to three melts are checked. For example, two heats are considered enough for sheet products to be used in non-critical applications [1, 4].

24.9 Significance of Metallurgical Evaluation

Metallurgical evaluation is the first step in the type certification. The success of certification therefore mostly depends on the consistency of properties that determine the safety limits when designing a component. Value-wise, the cost of a complete metallurgical evaluation is relatively inexpensive compared to the testing of the components. And full-scale testing is much more expensive than component testing.

Since each stage of evaluation during the certification is progressively costly, it is vital that repetition of type certification be kept to a minimum. Seen in this light, it is clear that metallurgical evaluation is of primary importance in certification and documentation, since it is the first deciding factor, at a significantly lower cost [1, 4].

General engineering versus aerospace material specifications: Aerospace materials have tighter ranges of alloying elements, better control of a large number of impurity and trace elements, lower acceptance limits of detrimental elements, higher mechanical property limits, stringent metallographic acceptance norms, and comprehensive checks on real-time (both static and dynamic) properties (tensile, fracture toughness, fatigue, etc.).

24.10 Summary and Conclusions

The main objective of the airworthiness regulator in India (CEMILAC, Bangalore) is to achieve and ensure a high level of safety and reliability. The functions and responsibilities of this organization are summarized in this chapter. This was followed by a discussion on the airworthiness certification methodology for materials. Case studies have been given to illustrate the extent of the evaluations that are required.

Since its inception in 1982, RCMA (Materials), CEMILAC has certified more than 100 materials in different mill forms, castings and forgings, components covering the entire gamut of high-temperature materials, special steels, titanium alloys, carbon-carbon composites and NDT products developed by central PSUs and the private sector. Details can be obtained by contacting the corresponding author of this chapter.

Acknowledgments The authors would like to thank the support from CEMILAC, Bangalore, especially from Shri G Gouda, GD (propulsion) and Dr. VK Varma, GD (TCS). They also would like to thank their colleagues and associates from DMRL, ASL, MIDHANI and BDL. Funding from DRDO is gratefully acknowledged.

References

1. Gupta B, Gopala Krishna V, Kumar Ashok, Yadav JS, Saha B (1996) Certification of aerospace materials: a global concept. *Aerospace materials—with general metallurgy for engineers*, vol 1. S. Chand & Company Ltd., New Delhi, India, pp 1–35
2. Bradley EF (1979) “Introduction”, source book on materials for elevated temperature applications. ASM, Metals Park, Ohio, USA
3. Baillie ILG, Soper WPC (1978) Design philosophy for airframes. Proceedings of conference on ‘forgings & properties of aerospace materials. The Metals Society, London, UK, pp 08–23
4. Gupta B, Yadav JS, Krishna Rao MS (1991) *IE(I) Journal* 72:07–13
5. Megson THC (1972) Aircraft structures for engineering students. Edward Arnold Ltd., London, UK, pp 410–415
6. Aerospace structural metals handbook (1981) Mechanical properties data centre. Battelle Columbus Laboratory, Ohio, USA, 3:26
7. Alexander JD (1979) Design philosophy for engine forgings”, In: Source Book on Materials for Elevated Temperature Applications, ASM, Metals Park, Ohio, USA, pp 1–7
8. Gupta B, Gopala Krishna V, Saha B, Yadav JS (1989). *HTS Digest*, vol. 35
9. Tamilmani K (2012) Indian military airworthiness approval process by CEMILAC. *Aeromag Asia*, VI, pp 24–26
10. Saha B, Wanhill RJH, Eswara Prasad N, Gouda G, Tamilmani K (2013) Airworthiness certification of metallic materials. In: Eswara Prasad N, Gokhale AA, Wanhill RJH (eds) *Aluminium-lithium alloys: processing, properties and applications*. Butterworth-Heinemann an Imprint of Elsevier, Oxford, UK and Waltham, USA, pp 537–554

Bibliography

The following documents and publications have aided in drafting the Indian material certification specifications, methodologies and approvals, and hence serve as general references and guideline volumes:

1. Procedure for Design, Development and Production of Military Aircraft and Airborne Stores (DDPMAS)—2002, Ministry of Defence, DRDO, India.
2. European Aviation Safety Agency (EASA) Regulations and Certifications (Undated).
3. Defence Standard 00-970, Design and Airworthiness Requirements for Service Aircraft, Ministry of Defence, UK (Undated).
4. Federal Aviation Administration (FAA) Federal Aviation Regulations, FAR (Undated).
5. International Civil Aviation Organization (ICAO) Standards, Recommended Practices and Procedures, Safety Management Manual (SMM), DOC 9859-AN-460, 2007.
6. Joint Aviation Authorities: Joint Aviation Requirements, JAR (Undated).
7. Military Specification Airplane Damage Tolerance Requirements, MIL-A-83444 (USAF), 1974.
8. Military Handbook MIL-HDBK-5H: Metallic Materials and Elements for Aerospace Vehicle Structures, US Department of Defence, Cancelled May 2004.
9. MMPDS-01, Metallic Materials Properties Development and Standardization (MMPDS), DOT-FAA-AR-MMPDS-01, US Department of Transport, January 2003.
10. Av.P.970: Design Requirements for Military Aircraft.
11. Av.P 32: Design Requirements for Guided Weapons.
12. Indian Standards, India.
13. Aerospace Material Specifications (AMS), USA.
14. American Society for Testing Materials (ASTM), USA.

15. British Standards (BS), UK.
16. Turbomeca and LA Specifications, France.
17. DIN Standards, Germany.
18. GOST, TY and TU Standards, Russia.

Chapter 25

Lightweight Ballistic Armours for Aero-Vehicle Protection

Arun Kumar Singh, R.J.H. Wanhill and N. Eswara Prasad

Abstract This chapter surveys the materials and technologies involved in the development of armour for aircraft, especially helicopters. The materials suitable for these applications are a mixed family of armour-grade ceramics and polymer matrix composites, and transparent armour laminates. These materials are tailored to specific requirements based on mission profiles and threat assessments, which are discussed first. Some examples of armour in helicopters are given to illustrate the applications. Finally, the qualification test requirements are summarised. The following books are important and useful reference sources: (1) Bhatnagar, A. (Ed.), 2006, 'Lightweight Ballistic Composites', Woodhead Publishing Limited, Abington, Cambridge, UK. (2) Hazell, P.J., 2016, 'Armour: Materials, Theory and Design', CRC Press, Taylor & Francis Group, Boca Raton, FL 33487-2742, USA.

Keywords Ballistic armour · Aero vehicles · Ceramics · Composites · Helicopters · Testing

25.1 Introduction

The survivability and safety of aircraft, particularly helicopters, on low-level missions is a continuing issue. Helicopter losses or damage in combat is a serious problem, since they are relatively slow moving, noisy, and often in close proximity to hostile ground forces. Also, insurgents and other groups undergo training in targeting helicopters using light machine guns (LMGs) and other small arms fire.

Ballistic armour technology will become increasingly important in the coming years, and the emphasis is always on lightweight solutions. This applies especially

A.K. Singh (✉) · N. Eswara Prasad
DMSRDE, DRDO, Kanpur, India
e-mail: singhak@rediffmail.com

R.J.H. Wanhill
NLR, Emmeloord, Marknesse, The Netherlands

to helicopters, owing to their vertical take-off and landing capabilities, which demand maximum weight savings for the overall aircraft as well as any armour.

25.2 Threats to Helicopter Structures

This section is based on a comprehensive literature review [1] of the impact vulnerability of basic helicopter structures manufactured from polymer matrix composites (PMC).

During missions in combat zones, helicopter structures may be subjected to extremely concentrated impact loads from various types of projectiles, fragments from high-explosive warheads, and jets from shaped charge warheads. In large scale conflicts there is a relatively high probability of sustaining a hypervelocity impact. On the other hand, ballistic threats are more likely from local conflicts and peacekeeping missions. These latter threats are the primary consideration in the present chapter.

25.2.1 Ballistic Threats

Ballistic threats include bullets from hand-held weapons and high-explosive incendiary (HEI) projectiles from shoulder weapons. Typical examples of ballistic range threats are small calibre projectiles, such as 5.56–7.62 mm armour-piercing incendiary (API), and large calibre 12.7–14.5 mm API projectiles. HEI projectiles present a more complex threat because they combine a high concentration of impact energy with less-concentrated (but wider distributed) energy due to the detonation of the high explosive.

Low-energy impacts can also be ballistic threats, notably for PMC structures. For example, secondary fragments such as ricochet projectiles, and even stones or inspection/repair tools hitting the airframe external surfaces, can be classified as low-energy/low-velocity threats [1].

N.B: Carbon fibre PMC susceptibility to impact damage is discussed in Chap. 14 in Volume 1 of these Source Books.

A number of factors play a role in the severity and lethality of any of the threats against helicopters. These factors include the type of weapon, the impact velocity, the mass and shape of the projectile, and the angle of attack. However, for ballistic threats to PMC structures the key parameters are usually considered to be the projectile's diameter, mass and its nose shape [1].

25.3 Armour Systems

Armour systems for ballistic protection can be classified into three main categories according to the way threats are dealt with. These categories are passive, reactive and active armours [2]. They are discussed briefly here.

25.3.1 *Passive Armour Systems*

Passive armour systems are designed to absorb the kinetic energy of a projectile or a shaped charge jet. Special layered combinations of high-strength steels, ceramics and polymeric materials are used to absorb and diffuse the damage. The material combinations and the layering depend on the type of threat and the weight and volume constraints of the vehicles to be protected. Steel and ceramic armours are applicable mainly to ground and marine vehicles, while lightweight composite armour is more appropriate for aircraft.

To absorb more energy, the armour surfaces are placed obliquely, *if possible*, thereby (i) increasing the path the projectile must travel, and (ii) causing kinetic energy (KE) threats to ricochet when the angle of incidence is high (typically $>55^\circ$). These benefits of obliquely placed armour provide greater protection for the same weight of armour. In other words, to meet a given threat the use of obliquely placed armour can save weight.

Sometimes the armour includes a space between two layers. This is done to defeat jets from shaped charges and to dissipate shock waves generated by certain types of ammunition.

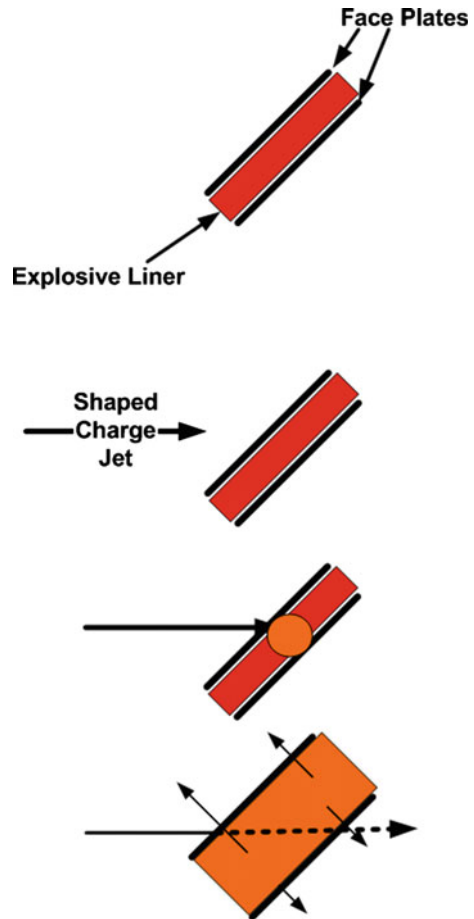
25.3.2 *Reactive Armour Systems*

Reactive armour systems consist of special constituents placed between two metal plates. These constituents react energetically when impacted by a projectile. These types of armours can be classified as explosive reactive armours and non-explosive reactive armours.

Explosive Reactive Armours (ERAs) In this type, a layer of high explosive (HE) is placed between two plates of identical or different materials. An ERA reduces the total penetration of a shaped charge jet, because when the jet penetrates into the explosive layer the resulting explosion creates a high-pressure zone that spreads the jet laterally [2]. An open-source schematic is shown in Fig. 25.1.

Non-explosive Reactive Armours These are analogous to ERAs, but the HE layer is replaced by an ‘energetic’ material. This reacts less violently than detonation, such that lower pressures are generated.

Fig. 25.1 Explosive reactive armour



Non-energetic Reactive Armours These use elastomeric interlayers that absorb the impact energy by expanding and causing local bulging of the metal plates.

25.3.3 Active Armour Systems

Active armours use sensors to detect incoming threats and are designed to respond to intercept, disrupt or deflect these threats. Held [3] classifies different active defence concepts according to the intercept ranges:

- Close range: < 2 m
- Medium range: 2–10 m
- Long range: > 10 m.

The working principles of these three concepts are as follows [3]:

Close Range (i) Sensors fire shaped charges to trigger the high-explosive content of an attacking shaped charge warhead, thereby preventing good jet formation; (ii) sensors trigger impactors to destroy or disrupt an incoming penetrator such that its fragments will hit a larger area on the armour and have less penetrative capability.

Medium Range Sensors determine the direction, velocity and distance of a threat and fire a suitable fragmenting charge from an array. The fragments hit the incoming projectile and destroy it.

Long Range Sensors launch a highly manoeuvrable mini-missile with a homing head.

25.3.4 Summary

The foregoing review of armour systems is very brief. This subject is immense: a convenient and authoritative source is Hazell's book [4], already mentioned at the beginning of this chapter. Most of the interest in armour is for ground and marine vehicle protection, where weight is not a primary consideration. However, as already mentioned in Sect. 25.1, the added weight is crucial for helicopters and other aircraft. Thus the most suitable solutions for countering ballistic threats are lightweight passive armour systems. The systems that best meet these requirements for air vehicles are non-metallic, discussed in the next section.

25.4 Lightweight Armour Materials

Metals have very good ballistic efficiency, but their generally high density (e.g. steels and titanium alloys) is a major disadvantage. Aluminium alloys provide relatively light armour and are generally used in light armoured ground vehicles. Even so, the necessary material thicknesses for adequate protection of air vehicles make them unsuitable.

Ceramic materials have low density and can be used for lightweight armour but only in combination with other materials, since they are brittle and tend to shatter with low-energy dissipation. The remaining options are PMCs, which are usually combined with ceramics, see Sect. 25.4.3.

25.4.1 Ceramics for Armour

The high hardness and low density of ceramics make them ideal candidates for armour materials. They are generally used in the form of tile shapes for impact surfaces of composite armour. The functions of ceramic impact surfaces are blunting, breaking and erosion of the projectile, and absorption of kinetic energy from the impact [5].

Figure 25.2 shows the relative ballistic efficiencies (resistances) of several ceramics to impact from a 7.62-mm AP projectile [6]. It is evident that denser materials provide greater resistance to penetration. Thus compromises with respect to weight are likely or inevitable.

In practice, the generally preferred ceramics are alumina (Al_2O_3), zirconia-toughened alumina (ZTA), silicon carbide (SiC), boron carbide (B_4C), titanium diboride (TiB_2), and aluminium nitride (AlN), with a short list of Al_2O_3 , SiC and B_4C [7]. The choices represent compromises or ‘tailoring’ for specific applications, see Sect. 25.4.3, since Fig. 25.2 shows wide differences in the properties of some materials, notably boron carbide compared to titanium diboride and various aluminas.

Some further considerations about these materials are given here and in Table 25.1:

1. Aluminas. These are the most widely used ceramics for armour, ranging in content from 85 to 99.9 % Al_2O_3 : the higher percentage is generally preferred. These ceramics have moderate hardness, strength and toughness.
2. ZTA. Addition of zirconia to alumina greatly increases the fracture toughness. However, ZTA has a somewhat higher density.
3. Silicon carbide. SiC is hard and corrosion resistant, with moderate toughness and density.

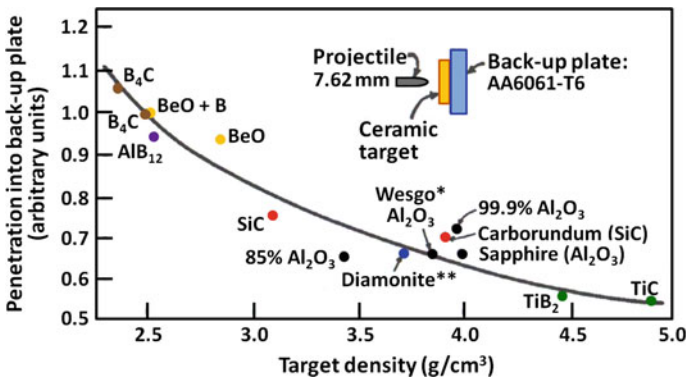


Fig. 25.2 Relative ballistic efficiency of various ceramics as a function of their density: *asterisk* Wesgo is a subsidiary of Morgan Technical Ceramics; *double asterisk* Diamonite = yttrium aluminium garnet. Data source is Ref. [6]

Table 25.1 Mechanical properties of ceramic materials for armour [2, 8]

Material	Density (g/cm ³)	Hardness (GPa)	Young's modulus (GPa)	Fracture toughness (MPa√m)
Al ₂ O ₃	3.6–3.8	16–20	380	3.2–3.5
ZTA	4.1	16	360	8.0
SiC	3.2	27	370	4.38
B ₄ C	2.5	30	400	2.5
TiB ₂	4.5	33	570	6.2–8.0
AlN	3.25	11–13	330	2.5–3.7

4. **Boron carbide.** B₄C is a hard and lightweight material, with high erosion resistance, but the toughness is relatively low. Nevertheless, the low density favours its use in composite armour for helicopters and other aircraft (besides its proven worth for body armour). Typical applications are for integrated seating and floor and side panels, and engine and tail drive shaft protection.
5. **Titanium diboride.** TiB₂ has not only high hardness and very high modulus, but also a significantly higher density, see Fig. 25.2 and Table 25.1.
6. **Aluminium nitride.** AlN has very high corrosion resistance and thermal conductivity, a moderate density, low-to-moderate toughness and the lowest modulus.

25.4.2 PMCs for Armour

PMCs have become important for lightweight armour consisting of several layers of different materials [9–14]. Although this topic is complex, as may be concluded from a recent review [14], the consensus appears to be that armours consisting of layers of different materials—notably ceramics and PMCs—offer the most effective resistance to damage. More information on this topic is given in Sect. 25.4.3.

In the present subsection, the focus is on the PMC reinforcement fibres and textiles. A survey of the open literature, including advertising brochures, shows that the most often-mentioned reinforcements are aramid (aromatic polyamide) fibres, frequently referred to as Kevlar[®]: there are several trade names for this type of fibres.

Other popular fibre types are E-glass, S- or S-2 glass, and UHMWPE (various grades of ultra-high molecular weight polyethylene with trade names Dyneema[®] and Spectra[®]). Carbon fibres are also sometimes selected.

Specific Strength and Stiffness A survey of these properties for the several fibre types is given in Fig. 25.3. This has been prepared using data in manufacturers' brochures and the open literature.

N.B: Figure 25.3 is only a guide, since the original data show considerable variation and are not standard design allowables. However, this survey is a touchstone for comparison with manufacturers' information. For example, the rankings in Fig. 25.3 are similar to those from independent data on the specific strengths and moduli of glass, aramid, Dyneema and carbon fibre yarns [15].

The data envelopes in Fig. 25.3 show large differences between the specific strength and stiffness properties of the fibre types. This is partly owing to significant differences in material densities, see Table 25.2.

The UHMWPE fibres Dyneema and Spectra have especially low densities, and from Fig. 25.3 would seem the best choice for strong and lightweight PMC armour. However, the popularity of glass and aramid fibres makes it obvious that other considerations can prevail. These are discussed next.

Other Properties While the specific strength and stiffness are the basis for manufacturing strong and lightweight PMCs, other properties are important for the service performance in armour applications:

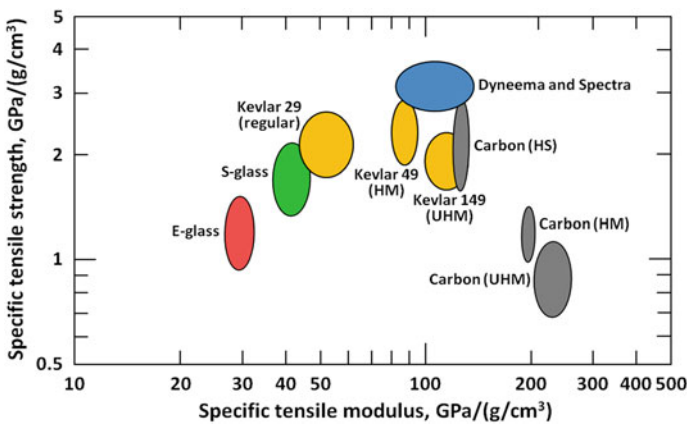


Fig. 25.3 General survey (see text) of specific tensile strengths and stiffnesses for fibres used in PMC lightweight armours: *HM* high modulus; *HS* high strength; *UHM* ultrahigh modulus

Table 25.2 Fibre densities: several sources

Fibre type	Density (g/cm³)
E-glass	2.54–2.60
S-glass	2.40–2.50
Kevlar	1.44–1.47
Dyneema and Spectra	0.97
Carbon	1.80–2.10

1. **Ballistic performance.** This is a complex topic that tends to be over-simplified by PMC armour manufacturers. Hogg [11] pointed out that the relative performance of different materials is difficult to judge from literature data, mainly because the assessment methods vary, but also because the type of projectile is important.

Nevertheless, there are some general trends. The energy absorption is greater for (i) fibres with greater failure strains, (ii) PMCs with greater areal density (higher volume fractions of fibres) and (iii) ballistic tests as compared to drop-weight tests. Furthermore, the influence of the PMC resin matrix is minimal [11].

Another aspect worth mentioning is that hybrid PMCs can have enhanced ballistic performance [13].

2. **Miscellaneous properties.** These include corrosion resistance, moisture absorption, temperature resistance and fire–smoke–toxicity (FST) performance. Unfortunately, armour manufacturers’ information about these properties can be conflicting, and it is usually not clear whether comparisons refer to the fibres themselves or the PMCs.

This distinction is important: for example, sensitivity to moisture and temperature effects may be more a problem of the resin matrix, as in the case of carbon fibre PMCs, see Sect. 14.4 of Chap. 14 in Volume 1 of these Source Books.

Costs Differences in PMC costs can be broadly classified as follows: E-glass (low), S-glass and aramid (medium); UHMWPE and carbon (high). Cost differences are important and are included in the performance drivers for PMC armours [16].

25.4.3 Ceramic—PMC Armour

Ceramic—PMC armours consist basically of an outer ceramic tile layer that blunts or fractures the impacting projectile, and a PMC backing layer that captures the

Fig. 25.4 Schematic illustration of defeat of a bullet by ceramic—PMC armour: adapted from Refs. [17, 18]

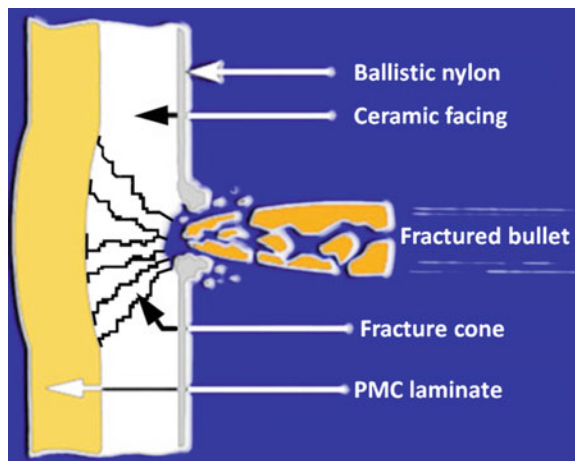
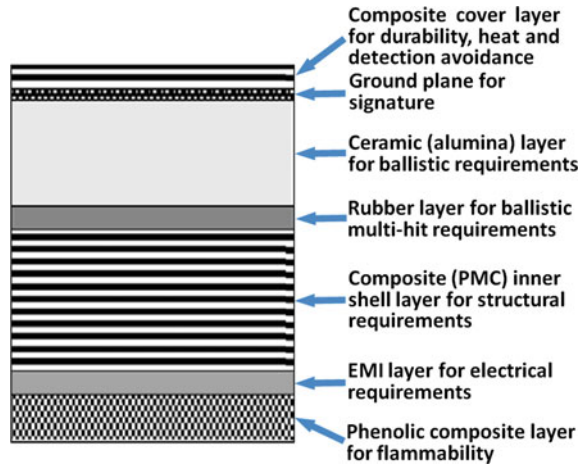


Fig. 25.5 Example of a lightweight multifunctional ceramic—PMC armour [11, 20]



slowed remnants of the projectile, and continues to support the undamaged ceramic layer, see Fig. 25.4. Extensive fracture of the ceramic behind the projectile is ideal [11], but lateral cracking should be limited. This is achieved partly by constraint from the PMC backing layer and also by limiting the sizes of the ceramic tiles. These are often hexagonal-shaped [11].

Most ceramic—PMC armours have a thin external composite layer to suppress spalling [19] and protect the ceramic surface from minor damage. However, this surface layer can be multifunctional; also the entire system can be much more elaborate and multifunctional. An example is shown in Fig. 25.5 [11, 20].

Complex armour systems such as that illustrated in Fig. 25.5 necessarily cost much more, not only because of the material costs, but also because of the number of manufacturing stages needed to produce and assemble the components into the finished armour.

Design and Performance Drivers Table 25.3 gives a summary of these requirements, adapted from Ref. [16].

A key consideration is the threat level, already discussed in Sect. 25.2. All armours are ‘tailored’ to meet the operational threat levels. NATO classifies and standardises threats into five levels [21]:

Table 25.3 Design and performance drivers for lightweight aircraft armours

Design drivers	Performance drivers
<ul style="list-style-type: none"> • Weight • Space constraints • Structural role • Environment^a • Projectile type(s) • Single or multi-hit capability 	<ul style="list-style-type: none"> • Protection against blast and fragmentation • Higher survivability at affordable costs • Minimal effect on aircraft (helicopter) operational capabilities

^aIncludes corrosion, FST and temperature effects

- Level 1: assault rifles; ball ammunition
- Level 2: assault rifles; API steel core ammunition
- Level 3: assault and sniper rifles; AP tungsten carbide (WC) core
- Level 4: heavy machine gun; API ammunition
- Level 5: automatic cannon; armour-piercing discarding sabot (APDS) projectiles.

Ceramic—PMC armours are added to helicopters (and other aircraft) to meet threats up to level 3. Levels 4 and 5 require integral armouring of the airframe, for example the Boeing AH-64 Apache helicopter [22], since the addition of armour would result in unacceptable weight penalties.

A more specific example is given by Hogg [11]: ceramic—PMC composites meeting level 2 threats would require tiles about 8 mm thick and PMC layers about 12 mm thick, but for level 4 the tiles would need to be up to 25 mm thick and the PMC layers up to 60 mm thick.

It is obviously essential to assess the threat levels from the operational requirements, which were mentioned briefly at the beginning of Sect. 25.2. The main distinction is between combat zone operations (high threat levels) and local conflicts and peacekeeping missions (lesser threat levels).

25.4.4 *Transparent Armour*

Glass/plastic transparent armour for helicopters has a long history. One of the earliest investigations was for the Bell UH-1 helicopter [23]. Recently, in 2011, the *general* topic of transparent armour has been extensively reviewed [24]. The interested reader should consult this review for all the strategical considerations and technical aspects, which include design principles and material selection charts.

Nevertheless, it is worthwhile to mention the legacy and newer concepts of transparent armour systems, see Figs. 25.6 and 25.7 [24]. **N.B:** these illustrations are primarily relevant to ground vehicles, but the principles are similar.

Legacy transparent armour systems use laminates of soda-lime glass and polycarbonates adhesively bonded by polymeric interlayers [23, 24]. For helicopters the total number of glass and polycarbonate layers would probably be only three: two outer glass layers and one inner polycarbonate layer.

The newer concepts consist typically of three functional layers [24]:

1. Strike face. This is glass, glass-ceramic or a transparent ceramic. Its function is to fracture/blunt/erode a projectile.
2. Intermediate layers. These are glass or polymethylmethacrylate (PMMA). They arrest cracks and absorb energy and can also mitigate thermal expansion mismatch between layers.
3. Backing layer. This is polycarbonate, which is tough and ductile [23]. Its main functions are to reduce spalling (fragmentation) of the armour system and prevent debris entering the vehicle.

Fig. 25.6 Legacy transparent armours [24]

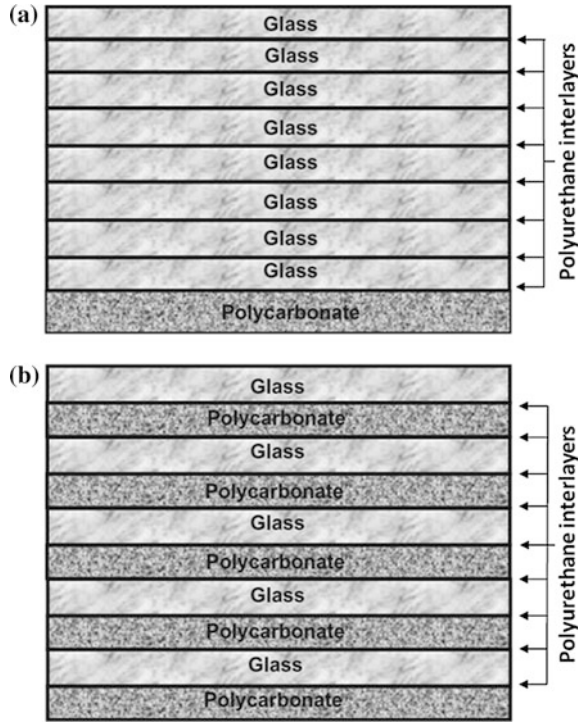
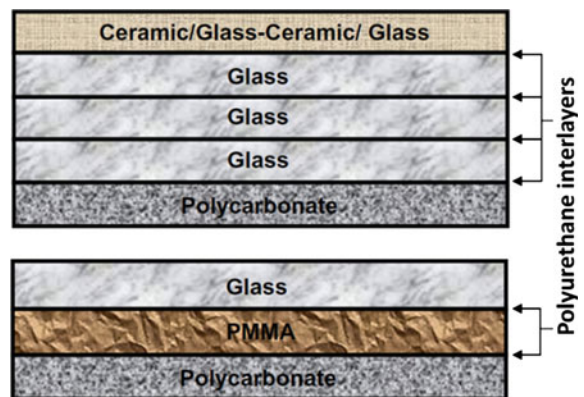


Fig. 25.7 Newer three-functional layer transparent armour concepts [24]



25.5 Examples of Ballistic Armour for Helicopters

Ballistic armour for helicopter protection is used selectively and may be both internal and external. Only the vital parts of the aircraft are protected. These include the cockpit, passenger or cargo areas, engine, tail drive shaft, and special equipment bays.

A generic example of armour locations is shown in Fig. 25.8. While this is informative, manufacturers tend to be unrevealing about the actual materials and construction of the armour. This is understandable for strategic and commercial reasons. However, there are exceptions [17, 26].

A particularly informative exception is the description of armour added to the Mil Mi-17 transport helicopter [26]. A summary for the cockpit area is given in Table 25.4, and examples are shown in Fig. 25.9. Note the use of steel plates as well as composite panels for the floor.

The other exception is a description of the cockpit and cabin floor armour in helicopters used by the German Border Police [17]. Figure 25.10 shows (a) an example of the armour and (b) the armour materials and assembly. The tiles are especially noteworthy, since they are made of carbon fibre reinforced SiC, which is itself a composite.

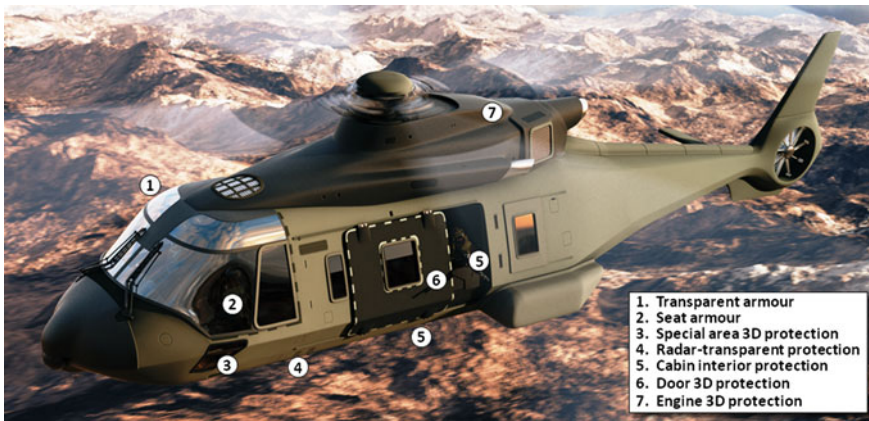


Fig. 25.8 Illustration of composite armour applications for helicopters: adapted from Ref. [25]

Table 25.4 Mi-17 cockpit ballistic armour [26]

Armour type	Threat level	Material
Steel plates (floor)	3+	Armox 500 steel
Bulletproof glass (front)	3	Multilayer glass
Composite side panels	3+	SiC/aramid
Dyneema floor and overhead panels	3+	Dyneema HB26/HB50
Composite overhead panels	3+	SiC/aramid

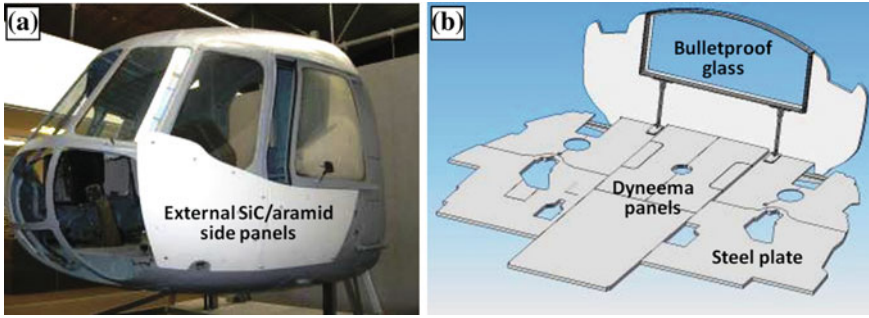


Fig. 25.9 Examples of external (a) and interior (b) armour installed on Mil Mi-17 helicopters [26]

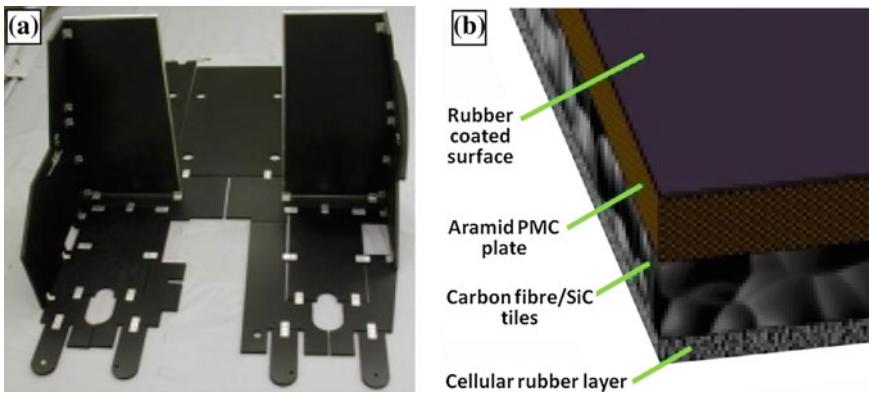


Fig. 25.10 Example of cockpit seat and floor armour for German Border Police helicopters [17]

25.6 Test Requirements for Ballistic Armour Protection Systems

The test requirements for ballistic armour may be broadly classified as follows:

- Ballistic performance (threat levels and ammunition calibres; single or multi-hits)
- Environmental resistance (temperature; humidity; weathering; exposure to aqueous, fuel and oil environments over a range of temperatures)
- Fire–smoke–toxicity (FST).

There are several US Military and NATO Standards that cover or partially cover the test requirements. The main ones are given here.

Ballistic Performance The current US Military Standard is MIL-STD-662F [27]. The NATO equivalent is AEP-55, Volume 1 [28], and is more detailed.

Dateraksa et al. [7] provide an excellent illustration of the use of MIL-STD-662E, the predecessor to MIL-STD-662F, for evaluating different ceramic—PMC combinations: Al₂O₃, SiC and B₄C tiles backed by an S-2 glass PMC.

Another useful example is given by Nayak et al. [13], who tested the ballistic performance of ZTA tiles backed by aramid PMCs.

Environmental Resistance The current US Military Standard is MIL-STD-810G [29]. This is encyclopaedic in scope and includes references and links to international standardization agreements (NATO) as well as overlapping US Department of Defense Standards.

Fire—Smoke—Toxicity (FST) This is the subject of a US Navy Military Standard MIL-STD-1623E [30]. This Standard covers a large number of materials, referring to other Department of Defense Standards and also to several ASTM Standards. However, MIL-STD-1623E does not directly address composite armour, and it is not clear from manufacturers' brochures and the open literature which Standards and/or tests are used to qualify ceramic—PMC armours with respect to FST.

25.7 Concluding Remarks

The design, manufacturing and qualification of ballistic armour are complex processes carried out by specialist suppliers. The demands made on armour for aircraft, especially helicopters, are severe, as may be seen from the design and performance drivers.

Ceramic—PMC composites have become established as best meeting the requirements for lightweight armour to be added to existing airframes, and when the threat levels are limited to portable weapons (assault and sniper rifles). However, there may be exceptions, for example, the armoured steel base plates used in Mil Mi-17 helicopters [26].

A variety of composite armour materials are available, and there is no general solution, despite individual manufacturers' information. Indeed, different armour materials may be used for the same aircraft. This is also demonstrated by the Mi-17 armour.

References

1. Resnyansky AD (2006) The impact response of composite materials involved in helicopter vulnerability assessment: literature review—part 1, DSTO technical report DSTO-TR-1842 Part 1, Weapons Systems Division, Defence Science and Technology Organisation, Edinburgh, South Australia 5111, Australia
2. Roopchand J (2013) Integrated survivability concept—a hybrid protection system for AFVs—a literature survey report. *Int J Eng Innov Technol (IJEIT)* 3(6):228–233

3. Held M (1993) Armor. In: Proceedings of the 14th international symposium on ballistics, 26–29 Sept 1993. Quebec City, Canada, (National Defense Industrial Association, Arlington, VA 22201-3601, USA), pp 45–57
4. Hazell PJ (2016) Armour: materials, theory and design. CRC Press, Taylor & Francis Group, Boca Raton, FL 33487-2742, USA
5. Savage G (1990) Ceramic armour. *Met Mater* 6(8):487–492
6. Meyers MA (1994) Dynamic behavior of materials, first edition. Wiley, New York, NY 10158-0012, USA, pp 597, 598
7. Dateraksa K, Sujirote K, McCuiston R, Atong D (2012) Ballistic performance of ceramic/S₂-glass composite armour. *J Metals Mat Min* 22(2):33–39
8. Madhu V, Balakrishna Bhat T (2011) Armour protection and affordable protection for futuristic combat vehicles. *Defence Sci J* 61(4):394–402
9. Navarro C, Martinez MA, Cotes R, Sanchez-Galvez V (1993) Some observations on the normal impact on ceramic faced armours backed by composite plates. *Int J Impact Eng* 13 (1):145–156
10. Gama BA, Bogetti TA, Fink BK, Yu CJ, Claar TD, Eifert HH, Gillespie JW Jr (2001) Aluminum foam integral armor: a new dimension in armor design. *Compos Struct* 52:381–395
11. Hogg PJ (2003) Composites for ballistic applications. Department of Materials, Queen Mary University of London, London
12. Ünaler E (2005) Development and characterization of light-weight armor materials, M.Sc. thesis, Izmir Institute of Technology, 25 July 2005, Izmir, Turkey
13. Nayak N, Banerjee A, Sivaraman P (2013) Ballistic impact response of ceramic-faced aramid laminated composites against 7.62 mm armour piercing projectiles. *Defence Sci J* 63(4):369–375
14. Akella K, Naik NK (2015) Composite armour—a review. *J Indian Inst Sci* 95(3):297–312
15. <http://www.toyobo-global.com>
16. Owens Corning [Company name] (2010) Lightweight composite armor: an industry transformation opportunity. Presentation at the armored vehicles India conference, 22–24 Nov 2010, New Delhi, India
17. Papenburg U (2005) Ultra-lightweight ballistic protection systems for aircraft and helicopters. IBCOL Composites GmbH, Munich, Germany
18. ‘Admin’ (2005) Lightweight armor protection for combat vehicles, defense update. 25 Oct 2005. defense-update.com
19. Horsfall I, Austin SJ, Bishop W (1999) Structural ballistic armour for transport aircraft. *Mater Des* 21(1):19–25
20. Qiao P, Wang J (2007) Hybrid composite structures for ballistic protection, United States patent application publication no. US 2007/0068377 A1. 29 Mar 2007
21. NATO Standardization Agency (NSA) Standardization Agreement (STANAG) (2012) Protection levels for occupants of armoured vehicles, STANAG 4569 (Edition 2), Haren, B-1110 Brussels, Belgium
22. Edwards MR (2002) Materials for military helicopters. *Proc Inst Mech Eng, Part G: J Aerosp Eng* 216:77–88
23. McDonald WC (1977) Glass/plastic transparent armor for the UH-1 helicopter, AMMRC final report AMMRC CTR 77-27. Army Materials and Mechanics Research Center, Watertown, MA 02172, USA
24. Grujicic M, Bell WC, Pandurangan B (2012) (online 2 Aug 2011) Design and material selection guidelines and strategies for transparent armor systems. *Mat Des* 34:808–819
25. ‘Advanced Armour’, TenCate Advanced Composites bv, Nijverdal, The Netherlands. <http://www.tencateadvancedarmour.com>
26. ASU Baltija Ltd. (2011) Armor set for Mi-17 helicopter, modification description. <http://www.asubaltija.com>
27. MIL-STD-662F (1997) Department of defense test method standard ‘V₅₀ Ballistic Test for Armor’, US army research laboratory, weapons & materials research directorate, Aberdeen proving ground, MD 21005-5069, USA

28. NATO/PfP (2005) Procedures for evaluating the protection level of logistic and light armoured vehicles, AEP-55, volume 1 (Edition 1), Haren, B-1110 Brussels, Belgium
29. MIL-STD-810G (2008) Department of defense test method standard, 'Environmental engineering considerations and laboratory tests'. Aeronautical Systems Center ASC/ENFS, Wright-Patterson AFB, OH 45433- 7101, USA
30. MIL-STD-1623E(NAVY) w/Change 1 (2010) Department of defense design criteria standard, 'Fire performance requirements and approved specifications for interior finish materials and furnishings (naval shipboard use), naval sea systems command, SEA 05S, Washington Navy Yard, DC 20376-5160, USA